THE UNIVERSITY OF NOTTINGHAM

AN ASSESSMENT OF DUST GENERATION FROM ORES

By

EVAGGELIA PETAVRATZI Meng, MSc

School of Chemical, Environmental and Mining Engineering

May 2006

To D.F.

"Εν μόνον ἀγαθὸν εἶναι, τὴν ἐπιστήμην, καὶ ἓν μόνον κακόν, τὴν ἀμαθίαν·"

Σωκράτης

"The only good is knowledge, the only evil is ignorance"

Socrates

Abstract

Dust from mining activities is produced from several unit operations and is often a serious problem to the industry, due to the influence it can have on human health and the safety record and productivity of a mine. So far, legislative parties and the industry have approached dust as an issue that needs to be controlled, only when a mining operation or process generates undesirable particulates. Nevertheless, new legislation and standards, such as the EU IPPC directive (Integrated Pollution Prevention and Control) and air quality strategies aim to drive mining companies to incorporate dust assessment planning that will be implemented through the whole life cycle of the mine. Mitigation and monitoring practices as well as health surveillance programs will need to be clearly defined.

This project's purpose is to understand how mining processes and in particular how the mechanisms inherent within common unit operations (i.e transfer processes using haulage roads or conveyor belts, the tipping, loading and stockpiling process, the screening process etc) result in the generation of dust. If the operation of unit operations could by optimized to produce less dust, then a "fit-for-purpose" strategy for dust minimisation could be developed to follow exploitation, processing and production demand.

The literature on dust from mining operations identified that generation of fines/dust occurs due to the presence of the mechanisms of abrasion and impact. Based on this logic, an experimental methodology was developed, which aimed to assess how dust was generated for each different mechanism and for a variety of ores of different mineralogy. Five different ores were tested, a limestone, talc, an iron ore, a lamproite and a copper ore and the same experimental methodology was followed for each.

Experimentation using the HSE-WSL tumbling mill test determined that under the effect of abrasion, ores yielded higher dustiness values during longer tumbling times, whilst parameters such as the sample mass and the particle size distribution of the feed sample could also influence the dust generation patterns. The findings of the computational modelling (discreet element modelling) and experimentation (high speed video recording) suggested that control and optimisation of operational parameters (e.g mill velocity, or tumbling time) within processes that involve

abrasion, such as the use of conveyor belts, mills, and screens could minimise the potential of dust generation by this mechanism.

The use of a novel impact test determined a positive relationship between the energy input and the particle size distributions of the broken particles, as well as the accumulation of fine particulates in the range of dust (<75μm). Also an increase in the bulk volume of ores resulted in larger quantities of fine particulates. These observations suggest that it is possible to reduce dust in processes that involve drop from heights and impaction (i.e transfer points in conveyor belts, tipping, loading) by adjusting the energy input and the bulk volume of ore at impact to as low a level possible.

Particle size analysis of the produced dust fractions were found to be material dependent and varied considerably for the different ores. Almost all materials produced significant amounts of ultra fine particles below 10μm and 2.5μm, both under impact and abrasion, which reveals the potential adverse impacts to the environment and human health. Quantitative mineralogical analysis using the mineral liberation analyser determined that the dust fraction presents a different composition to that of the ore. Comparison of the results collected for the five different ores using the HSE-WSL mill and the impact test identified that certain materials yielded high dust levels under abrasion and low under impact. Therefore it would be expected that dust control approaches for such materials would differ according to the mechanisms of the involved process and the mineralogy of the sample.

According to the findings of this study a reduction in dust produced from mining unit operations could be possible by optimising the involved processes either by altering their operating parameters (drop height during tipping, velocity of conveyor belt) or by optimising the design of processes so as to reduce abrasion or impact. New legislation such as the EU IPPC directive has already started considering such an approach as important, and newly developed Best Available Techniques documents refer to this as the primary step companies should follow to minimise dust. Additional advantages of this approach are that it can reduce cost for dust control by making use of less conventional mitigation practices, and in the long term it could also minimise the utilization of energy and water going to suppression, extraction and dust collection systems. In certain cases the proposed route could also optimise the production chain, especially where the generation of fines is undesirable (e.g iron ore processing or aggregates production).

Affirmation

The work reported in this thesis is solely the work of the author and has not been published elsewhere except for the following publications.

Conference Proceedings:

Petavratzi, E., Kingman, S., Lowndes, I., & Cunningham, D. 2004, "Understanding dust produced in mineral site processes", in *1st International Conference on Advances in Mineral Resources Management and Environmental Geotechnology*, Z. Agioytantis & K. Komnitsas, eds., Heliotopos Conferences, Hania, Greece, pp. 721-726.

Petavratzi, E., Kingman, S., Lowndes 2004, "Dust issues within the mineral industries-A review", in *JKMRC 2004 Student Conference,* M. Daniel & David Goeldner, eds., JKMRC, pp. 339-358, Brisbane, Australia

Published Journal Publications:

Petavratzi, E., Kingman, S., & Lowndes, I. 2005, "Particulates from mining operations: A review of sources, effects and regulations", *Minerals Engineering*, vol. 18, no. 12, pp. 1183-1199.

Submitted Journal Publications:

Petavratzi, E., Whittles, D., Kingman, S., & Lowndes, I. 2005, "An investigation into the mechanism of dust generation in a tumbling mill", submitted in *Powder Technology*

Petavratzi, E., Kingman, S., & Lowndes, I. 2006, "Assessment of the dustiness and dust liberation mechanisms of limestone quarry operations", submitted in *Chemical Engineering and Processing*

Proposed Journal Publications:

Petavratzi, E., Kingman, S., & Lowndes, I. 2006, "Compositional characterisation of mineral dust using the Mineral Liberation Anaysis system", to be submitted in *Journal of Minerals & Materials Characterization and Engineering*.

Petavratzi, E., Kingman, S., & Lowndes, I. 2006, "Assessment of the dust generation potential of ores under the effect of impact mechanism", to be submitted in *Minerals Engineering.*

Acknowledgments

I would like to acknowledge the financial support and assistance of my industrial sponsor Rio Tinto Technology and the Engineering and Physical Sciences Research Council (EPSRC).

I would like to personally thank my supervisors, Dr. Ian Lowndes and Dr. Sam Kingman for their guidance, support and encouragement throughout my PhD. Also I would like to thank Dr. David Whittles for his assistance with computational modelling, Dr George Rice for his helpful advice in particle size experimentation and Louisa Groves for her help with the Mineral Liberation Analyser. Also I am grateful to the EPSRC Engineering Instrument Pool for providing a high speed video recording system.

Special thanks go to all technical staff of the School of Chemical, Environmental and Mining Engineering, who assisted to the development and maintenance of apparatus as well as with experimental work. Many thanks go also to all my colleagues from L4 and L3 that made work and time spent in the school much happier.

Finally I would like to thank my family for their support and last but not least my partner Dimitri for his infinite patience and encouragement during all these years.

CONTENTS

Contents of Tables

Contents of Figures

Chapter 1. Introduction

Many of the extraction and downstream processing activities found in mining sites are associated with the production of dust that can represent a minor problem, a nuisance or an environmental and occupational health hazard.

Mitigation practices are often employed by mining industries to control, capture and avoid the produced dust from entraining into the air. Research so far associated with the problem of dust emissions from mining sites has focused on the development and evaluation of dust control practices. Dust control measures may be successful, but they may be expensive to use and require large amounts of water and energy. Especially from large mining operations the production of dust is inevitable and the need for mitigation methods, plus the use of water, chemicals and energy for dust mitigation is continue, which can add significantly to the mining cost. Also incorrect planning, use and maintenance of dust control methods could result in reduced dust capture efficiencies and the dust emission from fugitive dust sources.

Dust is generated during many stages of a mining operation from the extraction, loading, haulage and downstream processing of the minerals. To minimise dust and fines production and design effective dust mitigation strategies requires a fundamental understanding of the mechanisms that influence dust formation for a particular ore. For a particular mining operation the following questions need to be considered:

- How do the various processes influence the generation of dust?

- Do the operating parameters of a process affect the dust production profile of an ore?
- How do different mechanisms associated with common industrial processes influence the generation of ore particulates?
- Are the physical properties of the particulate matter, namely the particle size and mineralogy, influenced by the different industrial processes and involved mechanisms?
- Is there some relation between the various process mechanisms and the generation of dust from an ore and if so, could it be possible to minimise the production of particulates by altering operating parameters of the industrial processes?

The aim of this project was to conduct a series of laboratory scale experiments, to provide answers to all the above questions and to make recommendations of some alternative routes that could also assist to the reduction of dust. However, this does not imply that these findings will replace the existent dust control practices, but they will contribute to them by providing in depth understanding of how dust is generated from mining activities. Hence it would be possible for engineers to design a dust assessment plan that will satisfy their particular needs. Nevertheless, under specific circumstances it could be possible to reduce the amount of mitigation practices in use. The following paragraphs of this chapter present the background to the problem, its aim and objectives and an outline of the thesis.

1.1. Background to the problem

Particulate emissions comprise a problem in almost all forms of mining. They are produced through a range of processes starting from blasting to transporting, sample preparation, processing and handling (Arup Environmental 1995). Dust is potentially hazardous to human health, the environment, the working conditions as well as the productivity of a mine (Department of the Environment - Australian Government 2005). The production of the primary and secondary fine particulates in 2002 by sector in the European Union can be seen in Figure 1 (European Environment Agency 2006). Emissions from mines contribute to more than one industrial sectors represented on this diagram. For example, the coal mines are included to the energy industries sector, whereas other types of mines are described under the industry-processes and other-non energy categories. As the US Department of Energy states, dust emission from mines is high priority-high profile issue for the industry and improvements of both active and passive methods for dust control are needed to

further reduce dust emissions (US Department of Energy 2000). According to a survey conducted by the Mineral Planning Authorities in the U.K. to evaluate the potential for dust generation and emission from a range of surface mines, the proportion of "problematic" sites varied considerably between different mineral types (Figure 2)(Arup Environmental 1995). There are a number of factors that account for this variation. These are the scale of operation, the nature of the rock, the colour and opacity of the rock, the length of operation and the type of activities undertaken within a site (Arup Environmental 1995).

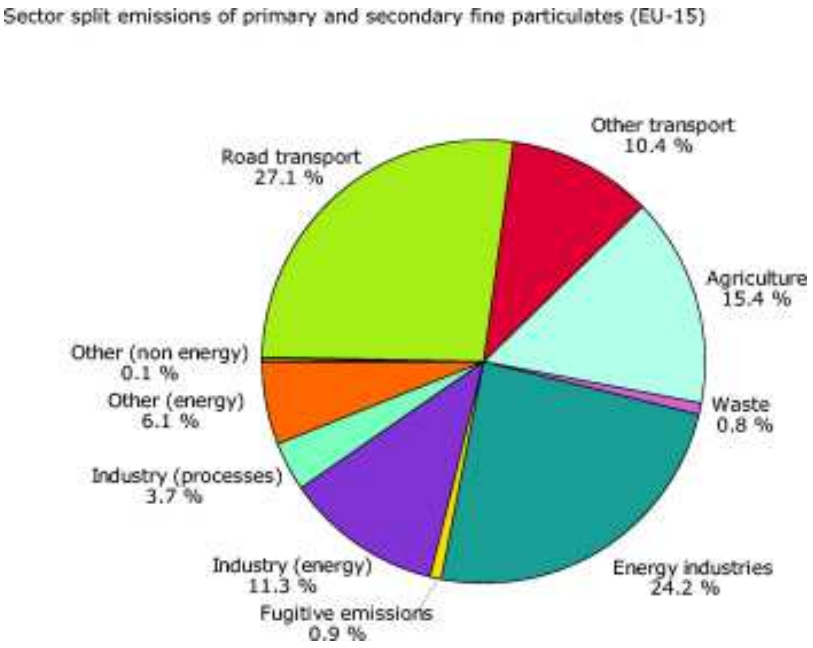

Figure 1: Sector split of EU15 emissions of primary and secondary fine particulates in 2002 (European Environment Agency 2006).

Countries with strong mining background are aware of the potential danger particulate emissions can cause in the short term and long-term, leading to introduction of new guidelines, roadmaps, regulations or even standards (Department of the Environment - Australian Government 2005; US Department of Energy 2000). Exemplarily, the US mining industry scope for the future is to reduce dust emissions in mineral preparation by 15 percent in near term and by 90% over long-term (11 to 20 years) (appendix I) (US Department of Energy 2000). To do so, they propose that dust conditioning processes and efficiencies have to be improved and dust reduction needs to be implemented in all aspects of rock disintegration (US Department of Energy 2000).

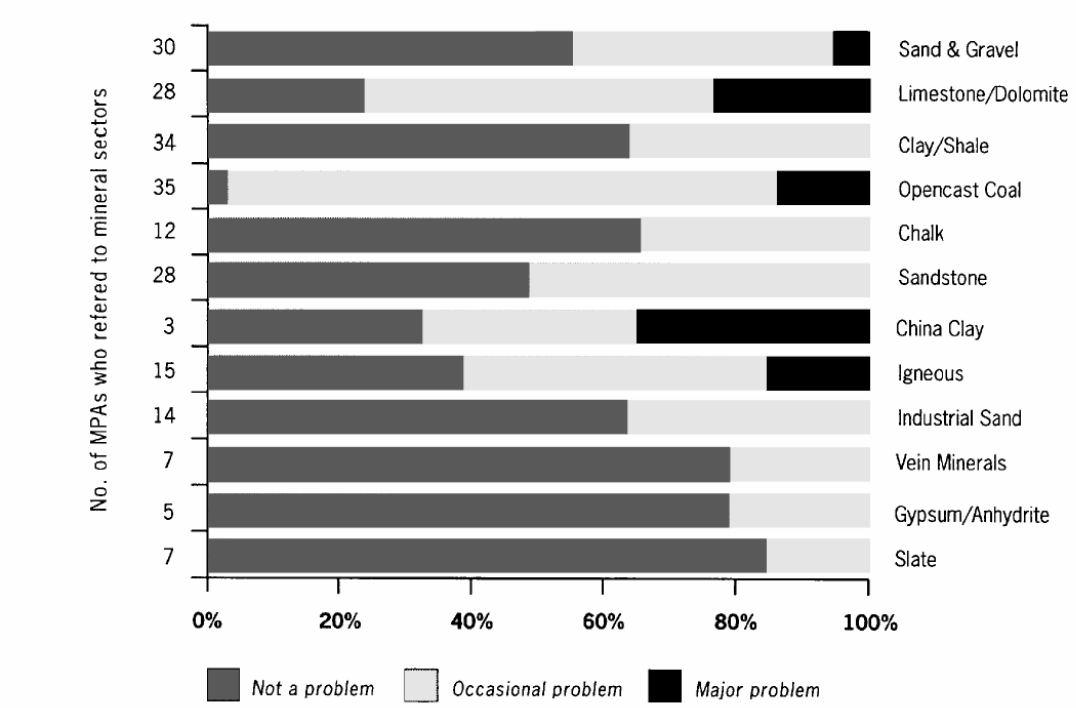

Figure 2: Mineral Planning Authorities perception of dust as a problem in England and Wales, (Arup Environmental 1995)

In Europe the development of the Integrated Pollution Prevention and Control directive aims to minimise the pollution arising from various industrial processes including from mining and from a variety of pollutants such as air emissions. Companies need to comply with the directive through their whole life cycle and they need to introduce emission limit values based on Best Available Techniques (BAT) reference documents (BREFs) (EIPPCB 2006). For instance, the BREF document on "emissions from storage and handling of bulk material" clearly outlines the need for a well defined dust assessment plan developed from each industry that adequately minimise the production and emission of dust in the environment and the exposure to humans (European Commission 2005). This reference document provides guidelines on "Best practice" for various storage and handling processes and the proposed approaches are commonly classified into primary and secondary. What is interesting in the approach followed by this BREF document, is that the primary Best Available Techniques propose to minimise dust emissions by altering or adjusting parameters of the storage and handling processes, for instance the drop heights from conveyor belts, or the velocity of conveyors, rather than introduce dust control practices such as extraction and suppression systems, which are considered as secondary approaches. Nevertheless the discussed BREF document is the first to be introduced (in 2005) (European Commission 2005).The aim of this project fits well with the proposed dust minimisation approaches of this BREF document and provides a scientific justification and case study of how control upon industrial processes could assist to the reduction of generated dust.

In conclusion, the particulate emissions from mining operations have started to concern legislative authorities, and mining companies will need to comply with any newly introduced regulations and guidelines. However the introduction of new legislation or standards from legislative parties or mining companies should be based upon accurate results from field data or laboratory based experiments and it is the research's role to provide this information.

1.2. Aims and objectives

The aim of this project is to understand measure and evaluate how dust is produced from industrial processes that take place in a mine. Commonly the creation of dust is the result of the effect of a mechanism, associated with an industrial process.

Looking close to common processes, for instance the transfer of material by conveyor belts, or the haulage, the tipping of ore or the stockpiling, it is observed that dust will be produced due to the presence of abrasion caused by interparticle or particle-surfaces contacts or due to impact, which is mainly associated with drop from heights. Hence this project's purpose is to identify how these two different mechanisms may generate dust.

Several sub-objectives were identified in support of this aim and they are presented at the bullet points below.

- To determine an experimental methodology that will accurately simulate the mechanisms of impact and abrasion.
- To identify the influence of the operational parameters and ore characteristics (i.e particle size) upon dust generation for both mechanisms.
- To characterise the particulates produced by impact and abrasion through particle size analysis and mineralogical identification techniques, in order to reveal if the effect of the different mechanisms and various operational parameters affect the dust characteristics.
- To perform studies for various ores and to identify how the dust generation process differs between materials.
- To compare the results obtained from the various ores and to identify their critical differences.

1.3. Thesis outline

The thesis consists of ten chapters. Chapter 1 presents an introduction to the project. The aims and objectives of the project together with a brief background to it are given.

Chapter 2 outlines a critical review of the previous research studies on dust from mining activities found in the literature. The chapter starts by providing simple definitions and terminology that relates to dust and follows by presenting the impacts of dust, information relevant to legislation and occupational exposure, common dust sources and the behaviour of particulates. The chapter concludes with a discussion of some more technical issues that refer to monitoring techniques, prevention and control methods and work practices.

Chapter 3 focuses on an outline of the characterisation methods that have been used by previous research workers to investigate dust. A large part of the chapter refers to previous research with dustiness tests. Results and trends that have been obtained by past trials are presented and discussed.

Chapter 4 explains the experimental practices that have been followed by this study. The methodology implemented is described step by step, whereas the analytical techniques used are outlined.

Chapters 5 to 9 comprise the core of this thesis as they present the findings of the investigation that took place for five different mineral ores. Hence each chapter corresponds to a different ore. Their structure is very similar and it is based on the adopted methodology that has been presented earlier in Chapter 4. In each one of these experimental chapters, the results obtained are discussed and conclusions are drawn for the dust generation potential of the individual ores from representative mineral processing and materials handling processes. Chapter 5 describes the experimental steps and results that have been obtained during work with Tunstead limestone quarry. Most of the preliminary testing and the set up of experimental procedures have been determined through work with limestone obtained from this quarry. The limestone as a rock it presented a much more homogeneous composition than any of the other samples and this was thought to eliminate any variation present during preliminary testing that could be attributed to a complex mineralogy. Chapters 6 to 9 describe and discuss the outcomes of the investigations that took

place for Talc de Luzenac, Hamersley iron ore, Argyle lamproite and the Kennecott copper ore respectively.

Chapter 10 compares and discusses the outcomes of Chapters 5 to 9. The comparative studies aimed to identify some overall trends and to determine if it is possible to classify materials according to their dust generation potential associated with different processes. The comparative studies also allowed the identification of the effect that different mechanisms of industrial processes have on the generation of dust from an ore, in order to determine if a certain material presents a higher potential to produce particulates under one category of processes but not in others. A summary of the results of this project together with recommendations for future research work are also presented.

Additional information and results that are not presented within the thesis can be reviewed in appendices I-VI, found in the PDF files of the attached Compact Disk (CD). Appendix I provides supplementary data from Chapters 1, 2, 3 and 4. Appendices II to VI correspond to Chapters 5, 6, 7, 8 and 9 respectively. Research papers produced during this project (published and submitted) can be found as PDF files in the attached CD. Finally two movies from the high speed video recording of the tumbling mill are also included in this CD.

Chapter 2. Dust from mining operations – A review

2.1. Introduction to mineral dust

Dust is a generic term used to describe fine particles that are suspended in the atmosphere. A range of definitions may be found in the literature which discriminates between different particulate characteristics.

According to ISO and British Standard Institute (BSI 1994); (ISO. 1995), dust is defined as small solid particles, conventionally below 75μm in diameter, which settle out under their own weight but which may remain suspended for some time. Aerosol scientists on the other hand, describe dust as a solid particle aerosol formed by the mechanical disintegration of a parent material, such as during crushing or grinding processes. Dust particles from rock samples range in size from sub micrometer to more than 100μm and are usually irregular (Hinds 1999).However dust for the mining industry is not considered only the fraction of the particles that entrains into the air, but also the fine material, which is produced from processing and handling operations (Maxwell 1999;Wilkinson et al. 1989). Fines are transferred together with the ore, which often diminish the value of the commodity or comprise spillage sources and under certain conditions can introduce the generation of airborne dust (Maxwell 1999;Wilkinson et al. 1989). Also within some branches of the mineral industries, for example the aggregate industries, dust can have even a wider definition including small material under 2mm in size (Arup Environmental 1995). Of

course this sort of definition corresponds to a commercial fine product fraction and not to an airborne nuisance solid state. So, different definitions can be used in different circumstances.

Mine dust is quite different compositionally to other types of dust. In an urban environment, dust derives from industry, transport, land clearing and wood smoke. Mine dust is typically less complex in its composition, consisting mainly of particles from exposed soil and rock (Department of the Environment - Australian Government 2005).

Particle size, concentration and chemical composition are the most critical properties of dust, because they can reveal the hazardous potential of dust to human health and the environment (Friedlander 2000). In industry (e.g mining, chemical, pharmaceutical), particles are collected to recover a desirable product or reduce emissions and occupational exposure. The chemical composition of a particle is of toxicological concern, as certain categories of dust may be toxic. Both particle concentration and chemical composition are reflected in occupational exposure limits, air pollution emission standards, and ambient air quality standards (Friedlander 2000).

The particle size is probably the most important physical property of dust (Figure 3). The efficiency of mitigation methods (Friedlander 2000), the generation and deposition potential as well as legislative standards and guidelines primarily depend on particle size. Dust particle size is described by the diameter of the particle. The most frequently used diameters are the aerodynamic and Stokes diameter (Figure 4). They are both equivalent diameters, which define the size of a particle in terms of its aerodynamic behaviour rather than its geometric properties. The aerodynamic diameter (*da*) is the diameter of a hypothetical sphere of density 1g/cm3 having the same terminal velocity as the particle in question (Hinds 1999). The aerodynamic diameter is used as a descriptor of the motion of particles in collection devices such as cyclone separators and impactors (Friedlander 2000). The Stokes diameter (*ds*) is the diameter of a sphere that has the same density and settling velocity under similar conditions as the particle (Allen 1997). The two equivalent diameters are expressed mathematically with regard to the terminal velocity by Equation 1.

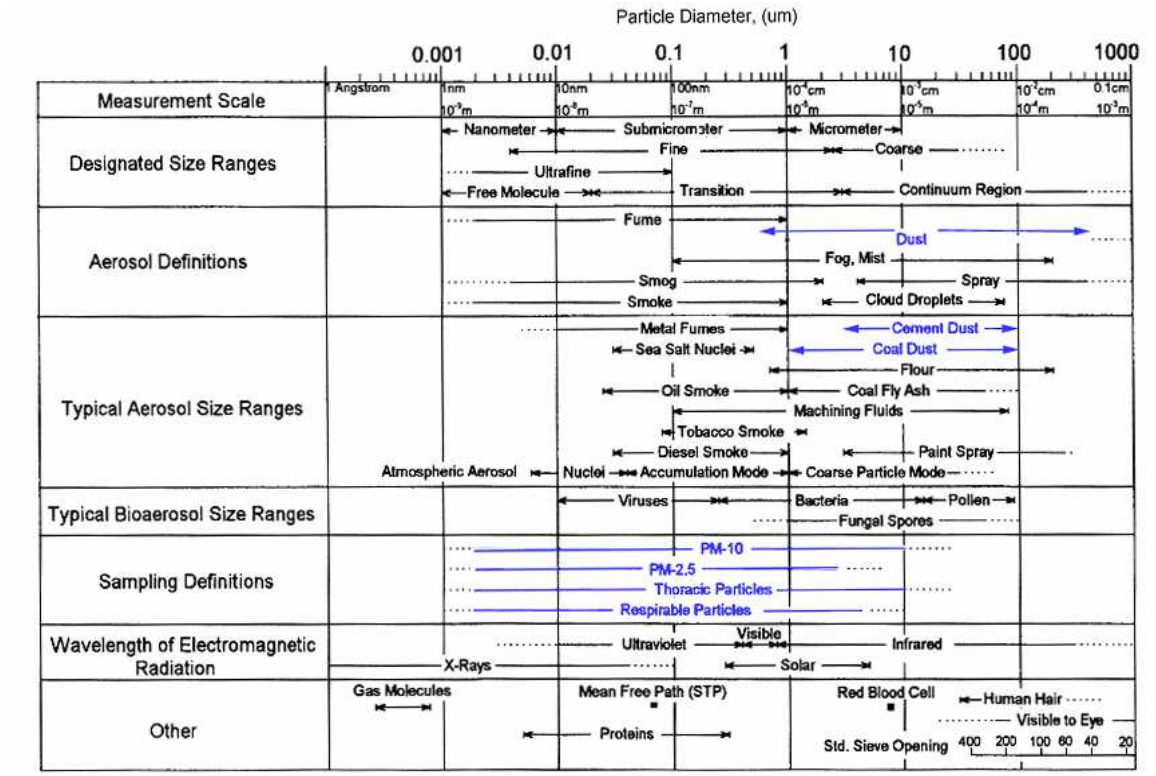

Figure 3: Particle size ranges and definitions of aerosols, (Hinds 1999)

$$[\text{Equation } \mathbf{1}] \quad V_{TS} = \frac{\rho_b d_s^{\,2} g}{18\eta} = \frac{\rho_0 d_a^{\,2} g}{18\eta} \qquad \text{(Hinds 1999)}$$

(ρb: particle density (g/cm^3),, ρ0: unit density 1g/cm^3, ds: Stokes diameter (cm), da: aerodynamic diameter (cm), g: acceleration of gravity (g/cm^2), η: viscosity (poise))

Both Stokes and the aerodynamic diameter need to be used with care as in certain circumstances, like in shear flows, the motion of irregular particles may not be characterized accurately by an equivalent diameter alone. This is due to the complex behaviour of irregular particles compared with spheres (Allen 1997).

2.2. Impacts of particulate emissions produced from mining activities

The adverse impacts of dust are mainly associated with human health and the environment. However, safety and productivity might also be influenced by high concentrations of dust. The impacts of dust are discussed in detail in the following sections.

2.2.1.. Impacts on the environment

Dust emissions from mineral sites can affect the environment, the agriculture and ecology of a region. The principal cause of dust emission at mineral workings is wind blow, which lifts dusts from the surfaces, disperses them and deposits them away from the source. Weather conditions (i.e. rainfall patterns, atmospheric turbulence, seasonal changes etc.) and topography are also determinative parameters to the dust emission process (Office of the Deputy Prime Minister 2005). Materials related properties like moisture content and rock type can significantly affect uncontrolled emission levels (US EPA 1998b).

Dust deposition is one of the major environmental impacts resulting from particulate emission from mineral sites. Deposition rates are related to the size of the airborne particles. Research has shown that large particles (> 30μm) deposit within 100m of sources of dust, intermediate sized particles (10 – 30μm) are likely to travel up to 200 – 500 m whereas smaller particles (<10μm) can travel up to 1 Km. Dust deposition is greatly influenced by weather conditions and topographical characteristics (Office of the Deputy Prime Minister 2005).

Nuisance from surface soiling is determined by the colour contrast between the deposited dust and the surface, "the cleanness" of the surface prior to settlement, public opinion and any other special characteristics of the area (MIRO 2005).

The effects of dusts on the agriculture and ecology of an area are determined by the concentration of dust particles in the ambient air, their size distribution, the deposition rates and the chemistry of the dusts. These factors can influence the chemistry of the soil and health of surrounding plants, the meteorological and local microclimate conditions, as well as the penetration rate of dust into vegetation (Arup Environmental 1995). Apart from vegetation, dust deposition can affect animal communities and woodlands (Balkau 1993).

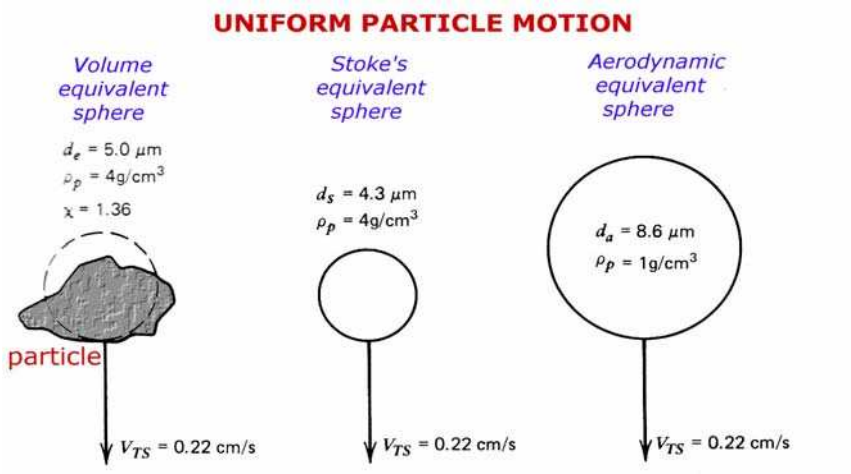

Figure 4: The equivalent spheres of an irregular particle (modified by (Hinds 1999)).

2.2.2. Effects of dust in human health

Dust is one of the largest occupational hazards and it has been one of the largest occupational killers through the years. Whenever materials are handled or broken down, dust is liable to be produced (Trade Union Congress 2001).

Exposure to any dust in excessive amounts can create respiratory problems. Different dusts may affect the body in different ways and may cause harmful effects through skin or eye contact and ingestion, as well as by inhalation (depending upon the individual physical and chemical properties of dust) (Health and Safety Executive 1997). Dust can also cause many diseases, the commonest of which associated with mining activities and individuals, are (Trade Union Congress 2001;World Health Organization 1999):

- Lung damage such as pneumoconiosis and in particular silicosis, asbestosis, CWP (coal workers pneumoconiosis) etc as well as cancer
- Damage to the nose, throat and eye.
- Damage to the skin: Dust may cause various types of dermatitis, which are a widespread and often serious problem or even skin cancer (e.g cement)
- Systematic poisoning and skin absorption: It can occur if water-soluble materials dissolve in sweat and pass through the skin into the bloodstream, (e.g lead).
- Gastrointestinal tract irritation through ingestion: It is likely when poor hygiene allows eating, drinking or smoking in contaminated or dirty workplaces.

- Ischaemic heart diseases
- Irritation and inflammatory lung injuries. Certain dusts may cause chronic bronchitis, which can lead to chronic emphysema (e.g chromium compounds and manganese)
- Allergic reactions like occupational asthma or in the skin like rashes and eruption. (e.g. cobalt, platinum, chromium, nickel etc)

A comprehensive list of natural materials associated with human diseases can be seen in Table 1.

2.2.3.Effects on safety and productivity

Dust can affect safety at work leading to reduced visibility in the workplace and therefore the nuisance value of such concentrations should not be underestimated (SIMRAC 2003).

In addition certain dusts, for example from coal and sulphide ores can cause explosions (Field 1982;Trade Union Congress 2001). The explosiveness of a dust depends on five major parameters. These are the presence of combustible dust in a finely divided form, availability of oxidant, presence of an ignition source, some degree of confinement and a state of mixed reactants (Liu and Katsabanis 1992;Soundararajan R. et al. 1996).

From these five factors, three of them which comprise the ignition force, the oxidant and the fuel (inflammable dust) are often illustrated in explosion triangles, which show that all of them are needed to start an explosion (Brunius and Brunius 1995). In dust clouds particles are surrounded by oxygen found in the air, which is available for the inflammable material. An explosion occurs when enough dust particles are exposed to enough oxygen and they are close enough to maintain the combustion of surrounding particles (Brunius & Brunius 1995;Eckhoff 1995a;Field 1982).

Table 1: Natural materials associated with human disease, (Banks and Parker 1998)

Rock type/ore	Human health implications
Chrysotile, crocidolite, anthophyllite etc	Used as asbestos. Asbestosis, lung cancer; cancer of the gastrointestinal tract; pleural, mesothelioma
Mica group minerals	Pulmonary fibrosis; silicosis; strong association with free silica, likely a major factor in producing fibrosis
Feldspar	Silicosis; often attributed to the included crystalline silica
Fullers earth – Bentonites	Pneumoconiosis without massive fibrosis and nodules; mottled X-ray appearance; some related silicosis
Granite, quartzite, sandstone, slate	Silicosis; silico-tuberculosis; nodular silicosis; fibrosis; enlarged and hardened lymph glands
Limestone, marble, dolomite	Bronchitis, emphysema, some scarring reported; calcinations increases toxicity; caustic burns; dermatitis
Silica, quartz, flint, crystobalite, tridymite	Silicosis; silicotic nodules in spleen; silico-tuberculosis; progressive pulmonary fibrosis; cristobalite-tridymite are more fibrogenic
Talc	Talcosis; talc pneumoconiosis
Bauxite ore; corundum	Aluminosis; lung scarring; pneumoconiosis; emphysema
Chromite	Lung cancer; ore may be associated with crhysotile asbestos
Iron ore (hematite, magnetite, taconite)	Siderosis; reports of increased lung cancer among taconite ore
Lead ore (galena, cerussite, anglesite)	Pneumoconiosis; diseases of the central nervous system; nephritis; anemia
Uranium, thorium and vanadium ores	Excess lung cancer
Tin; titanium	Severe X-ray changes in miners; tin pneumoconiosis; severe lung scarring; titaniosis

The inflammable risk of dust increases with the degree of fineness and dryness. Dust particles between 200μm and 500μm are considered explosive, whereas dust of particle size below 30 microns is considered highly explosive (Brunius & Brunius 1995). A minimum concentration of dust is needed for an explosion to happen, which varies for different types of materials. Commonly a few tenths of g/m^3 are enough to cause an explosion. Therefore adequate dust explosion prevention and control in practice mush be based on in depth understanding of the physical and chemical phenomena involved (Brunius & Brunius 1995;Eckhoff 1995a;Eckhoff 1995b;Hume 1993).

Dust can also minimize productivity and cause product damage. It adheres on machinery and products reducing the life cycle of equipment, modifying the properties and minimising the value of the commodities (Maxwell 1999). For instance, dust that contains high concentrations of silica can be abrasive, leading to wear of equipment (Wilkinson et al. 1989). Also dust-laden air, which is transported through duct systems with high velocity often cause a "sandblast" effect and for that reason continuous maintenance is required for a system to keep operating (Binzen 1985).

2.3. Dust terminology

Dust may be sub classified with regard to its environmental, occupational health and physiological effects (Figure 5).

The environmental impacts of dust are due to both airborne and non-airborne particulate matter. Generated dust is produced by mechanical processes in which solid material is broken into smaller fragments, not all of which become airborne although is capable of entraining into the atmosphere.

Total suspended dust is the generated dust that is entrained in the air. The nominal size of this fraction has particles with a diameter up to 50 μm (Department of the Environment - Australian Government 2005). Nuisance dust mostly describes coarse particles that can result in the reduction of environmental amenity or may damage machinery, diminish visibility or become an irritant substance in the atmosphere (SIMRAC 2003). Fugitive dust refers to dust derived from not easily defined source or more than one sources (Office of the Deputy Prime Minister 2005). Fugitive dust is one of the larger problems in mines as it often generates from unconfirmed sources and avoids capture. Fugitive dust is often found deposited outside mine boundaries or far away from major dust sources (Office of the Deputy Prime Minister 2005).

Potential occupational health hazards have established a classification on airborne particulate matter. The inhalable, thoracic and respirable fractions (fig.6) are determined by the European Committee for Standardization (CEN) and British Standard Institution on the BS EN 481:1993 (CEN 1993).

The total inhalable dust is the fraction of airborne material, which enters the nose and mouth during breathing and is therefore available for deposition anywhere in the respiratory tract (CEN 1993), (ISO. 1995). When sampling of the inhalable fraction

takes place, the percentage Ei of airborne particles of aerodynamic diameter D in micrometers, is given by [Equation 2 (CEN 1993):

[Equation 2] $Ei=50\ (1+\exp[-0.06D])$

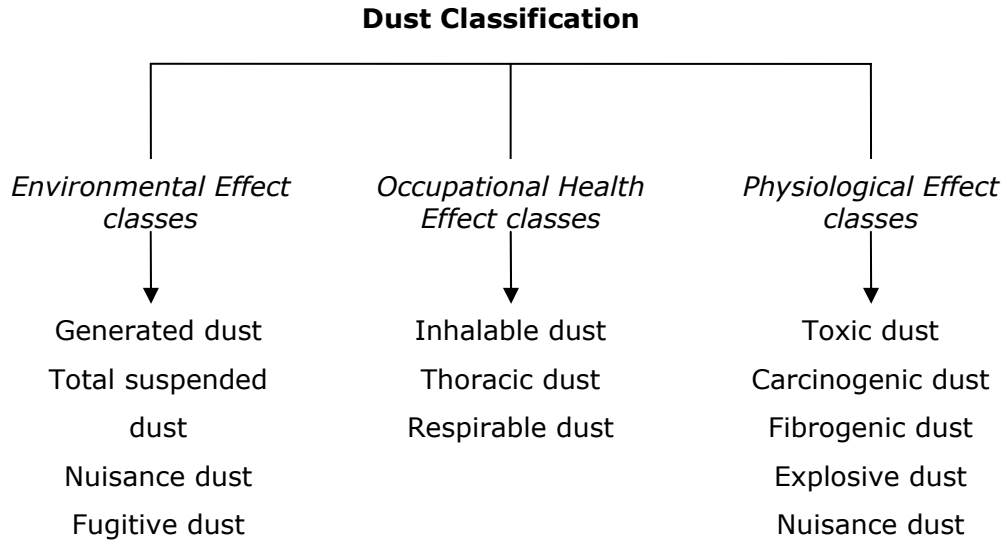

Figure 5: Classification of dust (Petavratzi et al. 2005).

Thoracic dust is defined as the fraction of inhaled particles that penetrate beyond the larynx. This fraction varies from individual to individual as well as with breathing pattern. The thoracic fraction conforms to the percentage of the inhalable convention, which is to be collected at an aerodynamic diameter D in micrometers, given by a cumulative lognormal distribution, with a median size of 11.64 μm and a geometric standard deviation of 1.5 (CEN 1993). Respirable dust represents the fraction, which penetrates to the gas exchange region of the lung. Similarly to the thoracic fraction, the respirable fraction varies according to individual characteristics and breathing pattern (Health and Safety Executive 1993). Respirable fraction is the percentage of the inhalable fraction convention, which is to be collected at an aerodynamic diameter D in micrometers, given by a cumulative lognormal distribution with a median diameter of 4.25μm and a geometric standard deviation of 1.5 (CEN 1993). The inhalable, thoracic and respirable conventions are shown in Figure 6

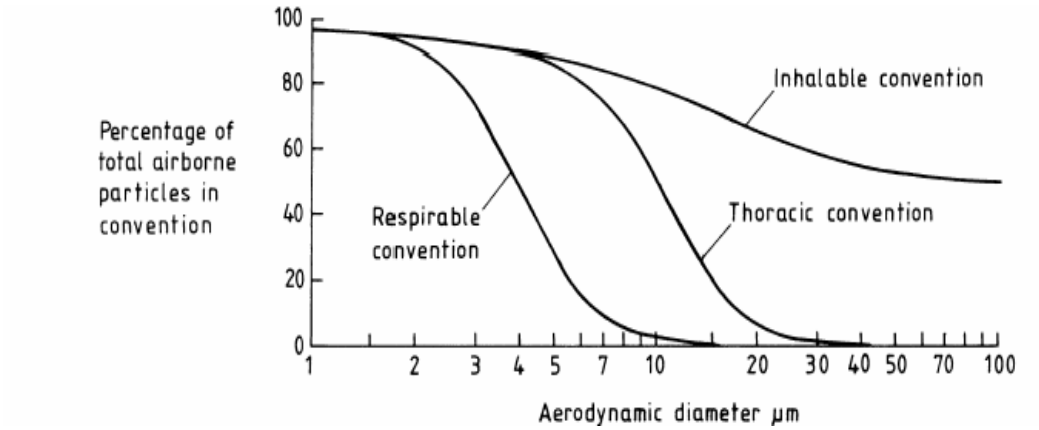

Figure 6: The inhalable, thoracic and respirable convention as percentages of total airborne particles (CEN 1993)

The physiological effect of dust on human health is another major issue in any mining operation. Certain types of dust can negatively affect the health and safety of working conditions. For example, toxic dusts can cause chemical reactions with the respiratory system or allow toxic compounds to be absorbed into the bloodstream through the alveolar walls. Examples of such hazardous dusts are lead, arsenic, uranium and other radioactive minerals, tungsten, silver and nickel (SIMRAC 2003). Carcinogenic dust, like uranium, asbestos, arsenic or quartz dust can cause cancer. Many other dusts cause microscopic scarring of lung tissue (fibrogenic dust). Over long periods this can produce a fibrous growth of tissue resulting in loss of lung elasticity and a greatly reduced area for gas exchange. Silica, asbestos, mica, talc are some of the most hazardous of the fibrogenic dusts and may also produce toxic and carcinogenic reactions (SIMRAC 2003).

2.4.Legislation and standards on dust

The legislation, which applies to dust issues and emissions from mines internationally, is not specific. It is particularly difficult and complex to define dust standards, as particulate emissions give rise to a variety of nuisance and other impacts (Office of the Deputy Prime Minister 2005). General air quality standards and legislation that applies to any industry also apply to the mining industry. Indicators like the PM10 (particles with an aerodynamic diameter less than or equal to a nominal 10 micrometers) and PM 2.5 (particles with an aerodynamic diameter less than or equal to a nominal 2.5 micrometers) are commonly used to determine standards and limits (US EPA 1997).

For the nuisance effects of mineral dust the use of guidelines or standards relating to health effects (i.e PM 10, PM 2.5) is recommended to be used with care, as they might be inappropriate. Nuisance effects in mines are predominantly caused by deposition or coarse particles (> 30 μm), whilst health effects may result from inhalation of PM 10, PM 2.5 (Office of the Deputy Prime Minister 2005).

2.4.1. The legislative framework within the U.K

Throughout the UK, the Pollution Prevention and Control (PPC) regime applies, which implements the EU Integrated Pollution Prevention and Control (IPPC) Directive in the UK (UK Environment Agency 2005). Special emphasis is placed on the application of Best Available Techniques (BAT) to reduce the environmental impact of the process (UK Environment Agency 2003). The affected sectors of the mining industries are the ferrous and non-ferrous metal industries and the mineral industries (cement, glass, ceramics, bricks).Part B of the PPC regulations refers to Air Pollution Control, which is regulated by Local Authorities. These regulations also apply to mines and quarries. For the nuisance impacts of mineral dust in U.K. there are no agreed standards or guidelines. In relation to health effects of PM10 the U.K. National Air Quality Strategy (DEFRA 2000) has adopted an air quality standard of 50 $\mu g/m^3$ (Office of the Deputy Prime Minister 2005).

2.4.2. Legislation and standards in Europe

In Europe and with regard to the EU environmental legislation, EU Directives govern the impacts of the extractive industry on waste, water, air quality and the nature conservation (Commission of the European Communities 2000). The Sixth Environment Action Programme (EAP), "Environment 2010: Our future, Our choice" includes Environment and Health as one of the four main target areas and air pollution is one of the issues included under the Environment and Health (European Commission 2006). The development and implementation of the thematic strategy for air pollution under the Sixth Environment Action Programme (EAP) is underpinned by the Clean Air for Europe (CAFE) programme, which was introduced in March 2001 (Commission of the European Communities 2005). The overall strategy on ambient air quality is summarised in the Framework Directive 96/62/EC on ambient air quality, assessment and management. This Directive covers existing legislation and new air quality standards. Particulate matter is one of the pollutants included, which is relevant to the mining industry. Daughter Directives followed the Framework Directive, which set the numerical limit values and target values for the various

pollutants. The first Daughter Directive 1999/30/EC introduced target values of the particulate matter (PM10) and some of them can be viewed in Table 2.

Table 2: Limit values for particulate matter below 10μm (PM_{10}) as given in Annex III of Council Directive 1999/30/EC (The Council of the European Union 1999).

	Averaging period	Limit value	Date by which limit value is to be met
STAGE 1			
1. 24-hour limit value for the protection of human health	24 hours	50 μg/m^3 PM_{10}, not to be exceeded more than 35 times a calendar year	1 January 2005
2. Annual limit value for the protection of human health	Calendar year	40 μg/m^3 PM_{10}	1 January 2005
STAGE 2 (1)			
1. 24-hour limit value for the protection of human health	24 hours	50 μg/m^3 PM_{10}, not to be exceeded more than 7 times a calendar year	1 January 2010
2. Annual limit value for the protection of human health	Calendar year	20 μg/m^3 PM_{10}	1 January 2010

Permissions for industrial installations in EU are given by the Integrated Pollution, Prevention and Control (IPPC) Directive of 1996 (The Council of the European Union 1996), as industrial production processes still contribute considerable share of pollution to Europe. The permits are based on the concept of Best Available Techniques (BAT). All installations covered by Annex I should obtain an authorisation permit. Annex I of IPPC Directive includes only specific industries of the mining sector such as cement and lime, ceramics, asbestos, glass and coal, as well as smelting roasting and sintering installations (The Council of the European Union 1996). The Best Available Techniques (BAT) is documented in BAT Reference Documents (BREFs) (EIPPCB 2006). References of BAT techniques to minimise dust from the above mining related sectors can be found in the appropriate documents (BREFs) (EIPPCB 2006). BAT Reference documents do not only correspond to industrial sectors, but also to processes that prevention and control needs to be implemented, such as the BREF on "Emissions from storage of bulk or dangerous materials", which is also applicable for the mining industry (European Commission 2005). This document provides one of the most detailed references to techniques and approaches that can be adopted to reduce dust from storage, handling and transfer processes. The approaches presented state that the production and extraction process should reduce material's tendency to make dust before it leaves the production plant, whilst the behaviour of operations and the construction of techniques that prevent dust formation should carefully be examined and implemented (European Commission 2005).

2.4.3. North America legislation and air quality standards

The US Clean Air Act (CAA) and its Amendments of 1990 define the legislative framework around air matters. It consists of six sections known as Titles, which direct the Environmental Protection Agency (EPA) to establish, implement and enforce national standards for ambient air quality (US EPA Office of Compliance 1995a;US EPA Office of Compliance 1995b). Under the Title I of the CAA, EPA has established national ambient air quality standards (NAAQS) to limit levels of criteria pollutants including particulate matter. Fugitive dust emissions from mining activities are regulated under the National primary and National secondary standards (US EPA 1997).

The Clean Air Act regulates the processes of various metal and non-metal mining operations. New Source Performance Standards (NSPS) applicable to metallic mineral-processing plants have been established (40 CFR 60 Subpart LL). These standards regulate emissions of particulate matter in metal mining operations in crushers, conveyor belt transfer points, thermal dryers, product packaging stations, storage bins, truck loading and unloading stations, and rail car loading and unloading. Standards of Performance for Non-metallic Mineral Processing Plants (40 CFR 60 Sub-part OOO) and Standards for Performance for Calciners and Dryers in Mineral Industries require these industries to control or reduce emissions of particulate matter, apply specific monitoring, record keeping and reporting requirements (US EPA Office of Compliance 1995b;US EPA Office of Compliance 1995a).

The U.S. Environmental Protection Agency has also introduced the "Compilation of Air Pollutant Emission Factors" (AP-42). Emission factors and emission inventories are fundamental tools for air quality management. They are emission estimates, which are important for developing emission control strategies, determining applicability of permitting and control programs, ascertaining the effects of sources and appropriate mitigation strategies (US EPA 2005b). An emission factor is a representative value that relates the quantity of a pollutant released to the atmosphere with an activity associated with the release of that pollutant. These factors are usually expressed as the weight of pollutant divided by a unit weight, volume, distance or duration of the activity emitting the pollutant (Table 5). There is an extended list of emission factors for several mineral processing routes produced by EPA (US EPA 2005d). They are neither EPA-recommended emission limits, nor standards and they should not be used for such a purpose. They have been given a rating from A to E with A being the best to indicate the reliability and robustness of a factor. Air pollutant emission

factors can be retrieved from the Factor Information Retrieval System (FIRE) database (US EPA 2005c)

2.4.4.Legislation and standards in Australia

The environmental legislation enacted in Australia covers the impacts of dust emissions from the mining industry. The National Environment Protection Council has established a National Environment Protection Measure relating to the National Pollutant Inventory (NPI) (Department of the Environment - Australian Government 2005). The National Pollutant Inventory has produced a database presenting comprehensive information on the pollutants released into the environment and substances including the mining industry (National Environment Protection Council 2005). Similar to the United States the NPI guide has developed emission factors estimates for fugitive emissions in mining (National Pollutant Inventory 1999).

2.5. Occupational health limits

Occupational exposure limits are set to prevent or limit the exposure of workers to dangerous substances in workplaces and to protect them against risks from such substances. Occupational exposure limits can work either in a form of a standard, in which case industry needs to comply with them, or as guidelines and reference material to prevent exposure and adverse effects to human health. Most countries have their own occupational exposure limit system set by the appropriate authorities.Other countries (e.g from Eastern and South Europe) adapt well-established systems (e.g. the ACGIH limits) for their own use. Some of the different occupational exposure limit systems followed around the world can be seen in Table 3.

2.5.1.Occupational exposure limits in the U.K

In 2004, the UK Health and Safety Commission introduced a single type occupational exposure limit, called the Workplace Exposure Limit (WEL). For substances, which can cause cancer, the law requires that their amounts in workplace air must be reduced as much as possible. This imposes a single duty on employers to ensure that the amount of hazardous substance in their workplace air must not exceed the WEL (Health and Safety Commision 2003).

Table 3: Summary of the most distinct occupational exposure systems internationally

Occupational Exposure Limit Authorities	Occupational Exposure Limits	Information Source
Scientific Committee on Occupational Exposure Limits – European Union	Indicative limit value Binding limit value	http://europe.osha.eu.int/good_practice/risks/ds/oel/notes.stm#prep
National Institution for Occupational Safety and Health (NIOSH) – United States	Recommended Exposure limit (REL)	http://www.cdc.gov/niosh/npg/npg.html
American Conference of Governmental Industrial Hygienists (ACGIH) - United States	Threshold limit values (TLVs) Biological exposure indices (BEI) (both represent guidelines)	http://www.acgih.org/TLV/
International programme on chemical safety (WHO/IPCS/ILO/EU)	International chemical safety cards. Use of ACGIH and MAK limits (German system)	http://www.cdc.gov/niosh/ipcs/icstart.html

The UK Health and Safety Executive normally use two reference periods (Health and Safety Executive 2002):

- The 8-hour reference period relates to the procedure whereby the exposures in any 24-hour period are treated as equivalent to a single uniform exposure for eight hours. This is referred to as the 8-hour time-weighted average (TWA).
- Alternatively, exposures may be averaged over a 15-minute period, referred to as the short-term limit (STEL).
- For substances where no short-term exposure limit is specified, it is recommended that a figure of three times the long-term limit should be used as a guideline for controlling short-term exposure.

2.5.2.Occupational exposure limits in Europe

The list of occupational exposure limit values in Europe (EC 2005) is limited and it is in a primary stage of development. Only a few of the substances included are relevant to mineral products. The following directives endorse European occupational exposure limits (European Agency for Safety and Health at Work 2005):

- Council Framework Directive 89/391/EEC on the introduction of measures to encourage improvements in the safety and health of workers at work
- Council Directive 98/24/EC on the protection of the health and safety of the workers from the risks relating to chemical agents at work

- Commission Directive 2000/39/EC establishing a first list of indicative occupational exposure limits (for 63 agents).

Two different types of occupational limit values take place in Europe (EC 2005):

- The Indicative limit value (ILV/IOELV) is set by the European Commission following evaluation of the relationship between the health effects of hazardous substances and the level of occupational exposure.
- The Binding limit value, which reflects scientific data as well as socio-economic considerations (BOELV).

The Scientific Committee on Occupational Exposure Limits (SCOEL) has recommended a first list of 63 indicative occupational exposure limit values (EC 2000), which are supplemented by further notations and information such as routes of absorption, as (European Agency for Safety and Health at Work 2005):

- The eight-hour time weighted average (8h-TWA)
- Short-term exposure limits (STEL) and
- Biological limit values (BLVs)

When seeking information on occupational exposure limits relevant to the mining sector, it is advisable to search the established legislation and health and safety regulations of the host country, as national legislation (most of the time) is better developed. However, trans-national occupational exposure limit values will be introduced in the near future (European Agency for Safety and Health at Work 2005).

2.5.3. Occupational exposure systems in U.S.A

Occupational systems used in North America can possibly be characterised as the most advanced around the world and for that reason other countries have adopted them.

Occupational exposure limits in North America are determined by more than one source. The National Institute for Occupational Safety and Health (NIOSH) currently classifies hazardous substances using one exposure limit called the Recommended Exposure Limit (REL). It is based on risk evaluations using human or animal health effects data, and on an assessment of what levels can be feasibly achieved by engineering controls and measured by analytical techniques (NIOSH 2005).

The American Conference of Governmental Industrial Hygienists (ACGIH) provides another system of occupational exposure limits, which is commonly used. Many countries and industries around the world have adopted the American Conference of Governmental Industrial Hygienists (ACGIH) system as their main occupational limit provider or for comparison reasons. The American Conference of Governmental Industrial Hygienists have established threshold limit values (TLVs) and biological exposure indices (BEI) for an extended list of substances, which are reviewed very often. TLVs and BEIs are not standards. They are guidelines designed for use by industrial hygienists in making decisions regarding safe levels of exposure to various chemical substances and physical agents found in the workplace (American Conference of Governmental Industrial Hygienists (ACGIH) 2005).However threshold limit values (TLVs) do not adequately define the fine line between safe and dangerous concentrations of hazardous chemicals. For this reason the US ACGIH system attracted much criticism once it took on a degree of federal regulatory significance (Health and Safety Commision 2003).

In terms of mineral related substances and limits on dust, the NIOSH and ACGIH systems do provide certain information especially for substances with adverse effects on health, like silica, asbestos and coal. They are not fully detailed including references on all physical substances, as the effects on health for many of mineral related substances are still unknown.

2.5.4.Occupational exposure limits elsewhere

Australia and South Africa are two countries with strong and active mining industries. In Australia, the National Occupational Health and Safety Commission determines occupational exposure standards. Limit values are provided through an online database, which includes many mining related substances with hazardous effects on health (National Occupational Health and Safety Commission 2005). Occupational exposure limits and standards in South Africa are provided by the Association Societies for Occupational Safety and Health (ASOSH) (ASOSH 2005).

2.6. Sources of dust

Dust usually originates from larger masses of the same material through some mechanical breakdown processes. In mineral sites dust can be generated during a range of site preparation, stockpiling, loading, transportation and mineral processing operations (Table 4). It is influenced by material properties, like hardness, particle

size distribution, particle density and moisture and by process parameters, such as mechanical breakdown process, energy spent on the process, drop from height, solids mass flow rate and the extent of handling (Liu et al. 1999;World Health Organization 1999). The composition of generated dust is not necessarily the same as that of a parent rock, since different minerals might break down or be removed, due to the effect that various processes have upon rocks, at different rates (World Health Organization 1999).

Dust emission is the process whereby dust is lifted from a surface to become suspended in the atmosphere. Energy is required to overcome the gravitational and cohesive forces that bind dust particles to the surface (Office of the Deputy Prime Minister 2003). The ability of suspended particles to disperse is determined by the capacity of the dust particles to remain airborne. This may be influenced by both the weight of particles and the inter particle forces and the drag, lift and movement imparted by the flow of air on the particles, (Liu et al. 1999).

Table 4: Dust sources in mineral sites. (adapted from (Arup Environmental 1995) and (Mohamed et al. 1996)) Legend: ((+) signifies a major source, (-) signifies a minor source, (0) signifies a negligible source.)

Operation & Equipment	Emission Mechanism	Relative Potential Contribution to Total Site Dust Levels	Primary Source	Secondary Source
Drilling & Blasting	Air flush from drilling and from force of blast	Small	+	-
Loading and dumping	Dropping material from height	Moderate	-	+
Draglines	Dropping material from heights	Large	-	+
Crushing and Preparation	Impact, abrasion and dropping from heights	Large	+	-
Conveyors	Dropping from heights	Small	0	-
Haulage roads	Raised by tyres, exhaust and cooling fans	Large	0	+
Storage piles	Wind blow, high wind speeds	Small	0	-

The emission of dust is also greatly influenced by the prevalent weather conditions (Arup Environmental 1995). Apart from the emission potential due to weather conditions or particulates suspension capacity, the mineralogy of the rock is an additional parameter to be considered. Different mineral types develop different generation patterns and emission rates (Arup Environmental 1995). Typical dust emission sources from a range of mining and mineral processing operations, as reported by the AP42 emission factors documentation of USA Environmental Protection Agency (US EPA) are shown in Table 5 (US EPA 2005b).

Table 5: Common emission sources for a variety of mining and mineral processing operations.(constructed by AP42 emission factors documentation (US EPA 2005b))

Processing	Materials	Operations	Factors affecting emissions
Crushed stone processing	Limestone, granite, dolomite, sandstone, quartz, quartzite, sand and gravel, lightweight aggregates	Crushing, screening, size classification, material handling and transfer, storage	Topography Climate surface moisture particle size throughput rate operating practice type of equipment mineralogical and chemical composition blasted area drop from heights etc.
Pulverized mineral processing	Calcium carbonate, talc, barite	Grinding, screening, size classification	
Coal mining	Coal, overburden	Blasting, truck loading, bulldozing, dragline, vehicle traffic, storage piles, grading, topsoil removal etc.	
Talc processing	Talc	Drilling, blasting, crushing, screening, grinding, drying, calcining, classifying, materials handling, transfer operations, packaging, storage	
Feldspar processing	Alkaline feldspars, plagioclase series, feldspathic rocks and sands	Crushing, grinding, screening, drying, materials handling, transfer operations	
Clay processing	Kaolin, ball clay, fire clay, bentonite, fuller's earth, common clay and shale	Crushing, screening, grinding, materials handling, transfer operations	
Metallic mineral processing	Hard ores: copper, gold, molybdenum, iron and soft ores: uranium, bauxite, titanium, zirconium ores	Crushing, dry grinding, material handling and transfer, drying ores	

2.6.1.Mobility behaviour of dust

The mobility behaviour of dust is quite complex as it consists of different phenomena acting on different sized dust particles. For a particle to become airborne it must have an aerodynamic drag force larger than the sum of the particle weight and the interparticle forces (Liu et al. 1999)). Smaller particles will behave as a gas and they will be influenced by molecular forces, while larger particles will be affected by gravitational and inertial forces (SIMRAC 2003).

Particle size, shape, chemical composition, mass concentration and density are important parameters for characterizing the behaviour of dust (Arup Environmental 1995). The chemical composition, the shape and the dust mass concentration are considered critical properties from a health and safety point of view (SIMRAC 2003).

The main forces acting upon emitted dust particles are gravitational settlement, Brownian motion, eddy diffusion and agglomeration. Other mechanisms like impaction, re-entrainment, interception (Figure 7) and deposition, are also important. Particulate control systems use these behaviour characteristics to achieve particle collection (US EPA 2005a). The gravitational force applied to dust particles will tend to let the dust settle under its own weight. Stokes' Law normally describes gravitational settlement (Hinds 1999). Stokes' Law applies well to particles that are above the respirable size range (SIMRAC 2003).

Quite often suspended dust particles follow irregular motions, scientifically attributed the Brownian diffusion characterisation, which is shown in Figure 7. Brownian motion applies to very small particles (0.01 to 0.1 μm) where Stokes' law breaks down due to bombardment by gas molecules. This causes the particles to move about in random manner. Displacement in all directions takes place, which exceeds the displacement due to gravity settling ((Allen 1997); (US EPA 2005a)).

Eddy diffusion is present predominantly in ventilating air due to turbulence. Agglomeration results when particles collide with one another due to a relative motion between them and adhere to form larger particles (Hinds 1999). Agglomeration is considered the most important interparticle phenomenon for airborne particles. Impaction (Figure 7) results due to the inertia of a particle at higher velocities impact onto an object and adhere to it, or to re-entrain it into the air

(SIMRAC 2003). Dust deposition is highly dependant upon the prevalent weather conditions, as well as the particle size (Office of the Deputy Prime Minister 2003).

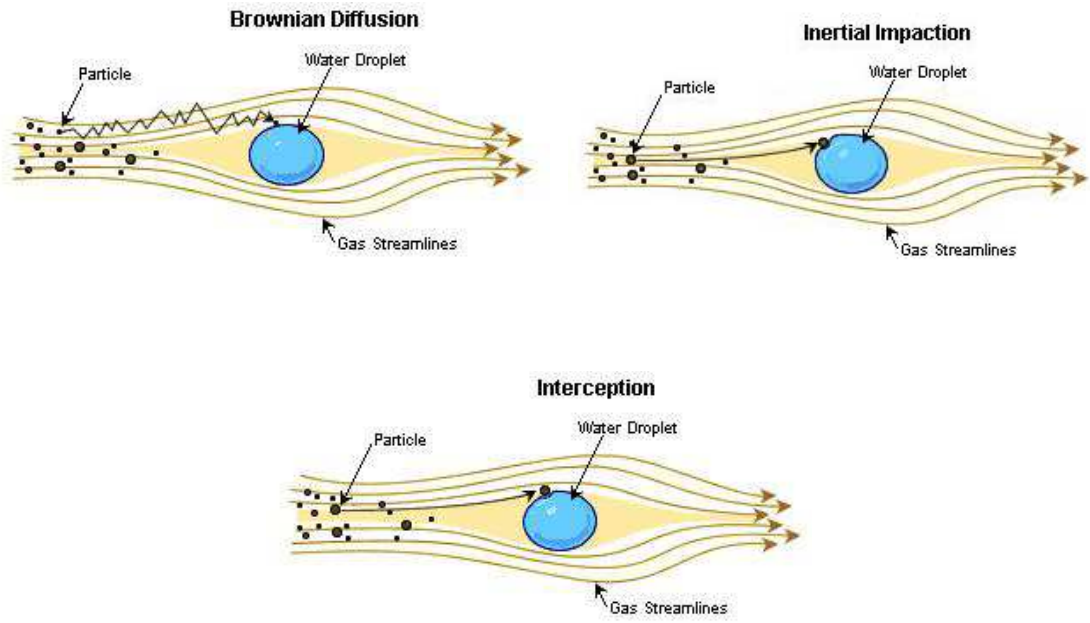

Figure 7: Examples of (a) Brownian motion of a small particle. The particle is captured by a water droplet as a result of its random movement; (b) Inertial impaction of a particle. Due to inertia, the particle moving in a gas stream impacts the water droplet; (c) Interception. The obstacle-target (water droplet) is offset slightly from the direct path of the moving particle. As the particle approaches the edge of the obstacle is collected by a process called interception (US EPA 2005a).

2.6.2. Research tools for the determination of dust sources

Dust dispersion modelling is now widely used by mining operations as a means to identify dust sources, to understand the behaviour of mineral particulates and to assess dust control-planning methodologies. Dispersion modelling of dust is a process where a physical system is represented by a series of mathematical procedures in a computer program. Predictive models (Figure 8) exist which allow the inclusion of both point and non-point dust sources. Algorithms are available that estimate dust contribution from a variety of sources. By combining these sources and local meteorological data, the models build a picture of dust deposition rates over the area surrounding the mine (Department of the Environment - Australian Government 2005). The model must represent as realistically as possible the physical processes that are taking place including the generation of the dust, the transport of dust by the wind, the deposition of dust from the plume by gravitational settling, and the trapping of dust within a pit. Computer modelling relies on the use of standard Gaussian dispersion models and considers climatic factors such as rainfall, temperature and winds, which can have a significant influence on the levels of dust produced from a specific mine. Past trials have found that similar mines in different

climatic regimes may generate totally different profiles (Department of the Environment - Australian Government 2005). The results of a number of validation studies indicate that dispersion modelling can provide reasonably accurate predictions of annual average deposition rates if properly constructed emission inventories are used and appropriate meteorological data are provided (Department of the Environment - Australian Government 2005). An example of such a model, developed for Tunstead limestone quarry in Derbyshire (U.K), is shown in Figure 8.

Another developing area of modelling currently being used to assess dust emission and control is the use of computational fluid dynamics (CFD). Computational fluid dynamic modelling is mainly used as a tool to examine possible solutions to a problem. It is both used as a predictive (Figure 9) and design tool and it is fast, accurate and cost effective. A CFD model is constructed in a number of steps. Firstly the correct and complete geometry of the situation to be modelled must be defined. Secondly, the properties of the fluid involved in the problem including viscosity, density, temperature and other thermodynamic properties are specified. Once the geometry and the properties of the flow situation are known the solution procedure can be commenced (SIMRAC 2003). It can find application on numerous circumstances like ventilation design and implementation or a combination of mining processes (e.g. tipping-crushing process) or even focus on a particular equipment specifications (i.e crushers).

Modelling cannot replace experimental work, but if properly validated it can show trends and it can help gaining better understanding of the dust generation processes involved.

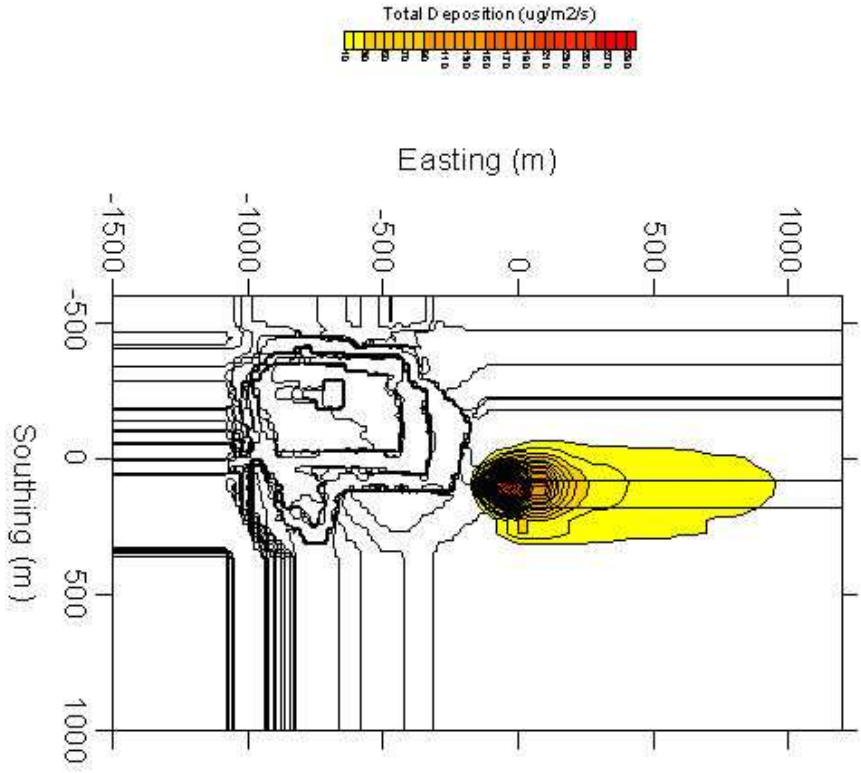

Figure 8: The use of dispersion modelling. The example shown was constructed using the Atmospheric Dispersion Modelling System (ADMS software), for the Tunstead limestone quarry in Buxton, U.K. The concentration and depositional behaviour of dust particulates produced by blasting is presented. Wind direction 270^0, stability class G (Appleton et al. 2003).

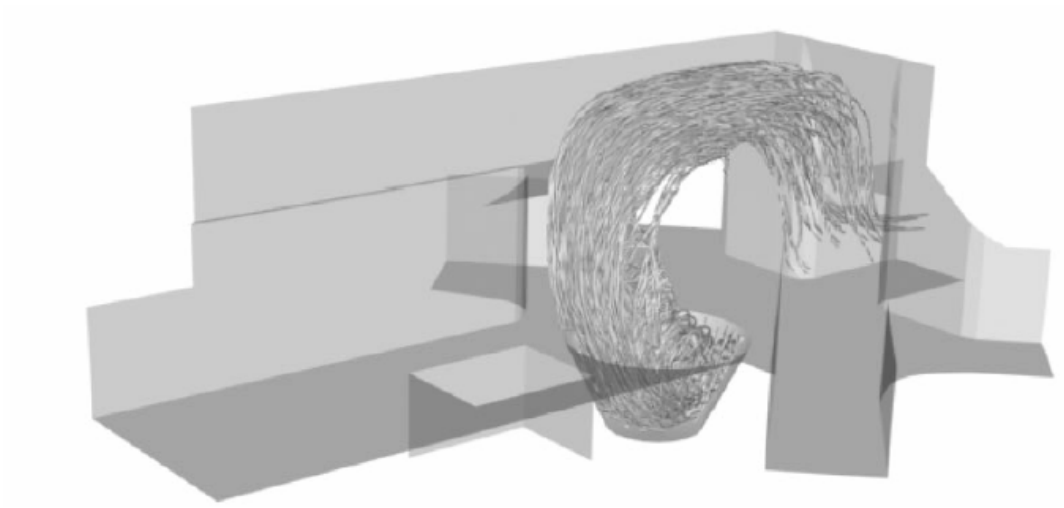

Figure 9: The use of computational fluid dynamic modelling (CFD) as a prediction tool of the dust generation process. The 3-D CFD model simulates the production of dust caused during tipping of granular material to a crusher (Silvester et al. 2004).

2.7.Monitoring

Monitoring methods are often used in industrial operations to assist the evaluation of dust generation and help to set more pragmatic objectives for dust prevention and control. Samples of dust are normally obtained for regulatory purposes to ensure that exposure is adequately controlled or to determine certain issues like dust behaviour or dust properties (Trade Union Congress 2001).

The types of samples that are normally obtained are (Hinds 1999;Martin Marietta Corporation 1987):

- Process/source samples to measure airborne dust concentration deriving from the source emissions.
- Ambient/ background samples to measure the contribution of other sources to dust levels
- Occupational health related samples of the inhalable, respirable and thoracic fraction
- Real-time dust measurements to determine the dust profile over a time period.

2.7.1. Sampling and measuring techniques for particulate matter

There are numerous factors to be considered before establishing a dust monitoring strategy. Some of the most important are the sampling period and duration, the sampling location, the sampling and analytical end method, the data handling and data analysis and finally any supplementary data collection, which might be relevant to the study (UK Environment Agency 2000). Most of the time, all these issues, are addressed by the initial objective for monitoring, although there might be extra points of concern. For example if the aim of the study is air quality monitoring, then the averaging period of the relevant air quality criteria with which the data will be compared need to be considered (UK Environment Agency 2000). Secondly, different data handling and analysis procedures will be required for real time results taken for public health warnings or routine results for authorisation compliance monitoring where several weeks turnaround may be adequate (UK Environment Agency 2000).

The most commonly used sampling and measurement techniques are summarized below and in Table 6.

Table 6: Common monitoring techniques and instrumentation ((UK Environment Agency 2000); (US EPA 1998a)).

Sampling – Measurement techniques	Instrumentation
Filter paper technique	Glass fibre filters, membrane, nylon, PVC, PTFE
Particulate sampling trains	Hi-Vol samplers (i.e Anderson), Medium-flow samplers (i.e. LIS/P Aerosol samplers), Low-flow samplers (Eight port samplers)
Automatic paper tape instruments	Beta gauges, Light attenuation monitors
Continuous microbalance instruments	TEOM, piezo-electric microbalance
Light scattering systems	Optical particle counter
Size selective techniques	Cascade impactors, selective inlet systems, electron mobility analysers, elutriators
Deposit gauges	Non-directional dust gauges, directional dust gauges

- Isokinetic sampling method, where a sample is taken from a moving stream. The sampling can be extractive i.e. when a sample is taken from an active stream of a duct or stack or direct, when the sample is taken in a windy environment. One of the main problems that can arise is anisokinetic sampling, which results when failure to sample isokinetically. Anisokinetic sampling often happens because of particle inertia in the region of curved streamlines near the inlet (Hinds 1999). The isokinetic sampling technique is not widespread in ambient air monitors (UK Environment Agency 2000).

- Sampling from still air. This method is similar to the isokinetic sampling, but the sampled air remains still. Two sources of error are associated with sampling from still air, one due to the settling velocity of the particles and one due to particle inertia (Hinds 1999).

- Mass concentration measurements. Measurements can be direct or indirect. Gravitational analysis (i.e cascade impactors) is an example of direct measurements, whereas light scattering (i.e optical counters) is an indirect method of determining the particle mass. Many categories of personal sampling equipment and air monitoring instruments fall into this category (Hinds 1999).

- Continuous real-time monitoring, where real-time measurements are obtained. These are mainly applied for air quality monitoring purposes. Automatic paper tape instruments (Beta gauges, light-attenuation monitors), continuous

microbalance instruments (TEOM, piezo-electric microbalance), light scattering systems and electrical mobility methods are some of the common direct reading techniques used (US EPA 1998a).

- Personal sampling provides the essential information on occupational health and human exposure patterns, which is beneficial for prevention and controlling of dust and employers exposure (Martin Marietta Corporation 1987). Different instruments are needed according to whether respirable or inhalable dust is to be collected ((Health and Safety Laboratories 2000). The personal sampling apparatus need to facilitate on the breathing zone of the human. The essential features of all systems are a collection substrate such as a filter and a pump for pulling the air through it (Health and Safety Laboratories 2000).

2.8.Prevention and control of dust in the mineral sites

Dust generation leads to the development of dust control measures to avoid environmental and health related impacts. There are several available mitigation strategies and techniques and they correspond to different cost and efficiency levels. To follow a definite dust control strategy is not always straightforward due to the complexity of the dust generation process, the materials behaviour and the working conditions, as well as the cost. Dust control in mining is mainly achieved through containment, ventilation, suppression and collection (Goldbeck and Marti 1996). A summary of the different strategies available is shown in Table 7.

Different types of mining use different combinations of dust control processes that suit their circumstances. Table 8 shows some of these dust control methodologies used in a variety of mining applications as well as particular processes.

Common dust collection systems such as cyclones, baghouses and scrubbers remove only the fine material that becomes airborne at each collection site. Nevertheless it has been estimated that 95 % of the dust stays with the material (i.e attached on the surface of particles). Hence, at each transfer point new fugitive dust is released, which needs to be collected. Also often dust is deposited back onto the product creating once more additional dust (Eslinger 1997).

Table 7: Basic dust control strategies and methods (Mohamed et al. 1996)

Strategy	Method	Expense	Efficiency
Prevention	Water/steam infusion	High	Moderate
	Foam infusion	High	Moderate
	Wet drilling	Low	High
Removal	Dust collectors – wet	Moderate	High
	Dust collectors – dry	Moderate	High
Suppression	Water sprays	Low	Moderate
	Wet cutting	Low	Moderate
	Foam	Moderate	Moderate
	Cutting variable optimisation	Low	Moderate
	Descent chemicals	Moderate	Moderate
	Water – jet assisted cutting	High	Moderate
Isolation	Enclosed cabs	Moderate	Moderate
	Enclosed dust generation	Moderate	Moderate
	Exhaust ventilation	Low	Moderate
	Blasting off-shift	Low	Moderate
	Control of air flow	Low / Moderate	Moderate
	Control of personnel location	Moderate / High	Moderate
Dilution	Main ventilation stream	Moderate	Moderate
	Local ventilation dilution	Low	Moderate

Control of dust could be implemented not just by common mitigation methods, but also by automating physical separation processes (US Department of Energy 2000). As the US Department of Energy states, systems that increase automation will benefit employee health and safety in the industry as well as it will increase plant efficiency (US Department of Energy 2000). This will require smart systems that adjust to material properties. The development of inexpensive full-scale simulators of processing plants can be another tool to further assist the integration of the physical separation process. Although this trend has been little followed by the industry in the past and present, it will be a definite objective for the long- term.

A good example illustrating the need for dust control is the Heavy Mineral Sand Industries (HMS). The flowsheets of Figure 10 present the various mining and processing steps and associated emissions.

Table 8: Mining processes and associated dust control methods, ((Kissel 2003); (SIMRAC 2003))

Mining techniques and processes	Common Dust control methods
Underground mining and tunnelling	Ventilation, suppression by water and additives, dust collectors
Continuous mining	Effective spray systems, modified cutting cycle, regular bit replacement
Longwall mining	Use of high water and airflows, avoid dust from walkway, move workers upwind, reduce dust from the stage loader-crusher, use gob-curtain and shearer-clean system
Surface mining	Drill control with wet or dry systems, haul road dust control, containment of mobile equipments
Ore pass	System of stopping and airtight doors, isolate tipping locations, wet rock prior to tipping and while falling into the pass
Drilling	Water suppression, dry collection using an enclosure and a dust collector
Haulage roads	Wetting, salts, surfactants, soil cements, bitumens, films
Conveyor belt	Wetting, containment, belt cleaning Wetting, containment, belt cleaning
Transfer points and crushers	Enclosures, exhaust ventilation, water sprays

Heavy mineral sand operations are considered highly hazardous due to the generation of dust that contains radioactive elements (Hewson and Hartley 1990). Heavy mineral sand deposits (i.e Western Australia) contain up to 10% heavy minerals of which 1-3% is monazite. Monazite is a rare earth phosphate that in turn typically contains 5 to 7 % radioactive thorium and 0.1 to 0.3 % uranium (Hewson & Hartley 1990). Often mineral sand deposits also include xenotime, which contains yttrium (i.e Murray Basin deposits). Radiation hazards due to inhalation of dust started being a problem when monazite and rare earth oxides containing thorium became a valuable by-product (Uranium Information Centre 1998).When the radioactive material is concentrated, during the separation and production of monazite, the radiation levels are increased.

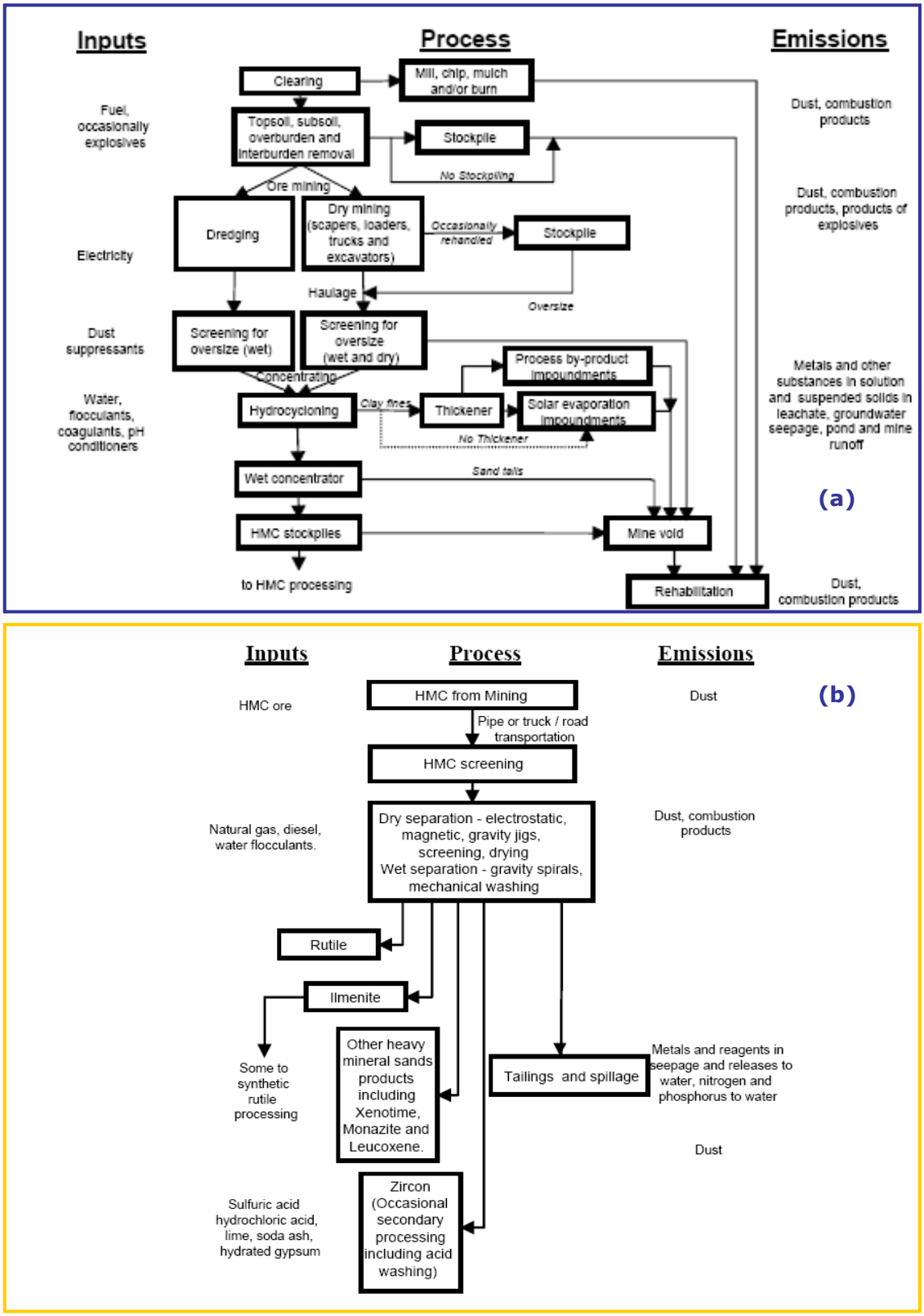

Figure 10: Likely emissions from mineral sand operations ,from (a) mining and concentrating processes and (b) heavy metal concentrate separation processes (dry plant) (Environment Australia 2001).

The hazard is greater at the secondary plant or "dry plant" as many of the processes taking place are dry (Hewson & Hartley 1990;Uranium Information Centre 1998). The need for special control in the dry separation plants is high, thus dust control is the most important objective in radiation safety for the heavy mineral sand industries. In

Australia permissible exposure limits were introduced to control exposure, whereas the industry invested in engineering programs to reduce airborne dust as well as in research to improve industry knowledge about airborne radiation (Uranium Information Centre 1998). A variety of mitigation techniques are currently used, from very simple ones like enclosures to more advanced ones like dust collectors (i.e electrostatic precipitators). Investment on improved dust control methods has been beneficial for the Western Australia companies as they managed to reduce the average radiation levels by 70 percent (Uranium Information Centre 1998).

2.8.1. Containment and ventilation solutions

Containment is a cheap and easy way to implement dust control. It is used to avoid entrainment of dust into the atmosphere either as an isolating method or in combination with others (Goldbeck & Marti 1996). Often other methods do not manage to control dust and the use of enclosures is the only choice. Containment is mainly used in mineral processing operations such as crushers and bunkers. Examples of the application of containment to a variety of equipment are shown in Figure 11.

Local exhaust ventilation (LEV) methods in underground mines provide the best use of air in the vicinity of workers and in the vicinity of dust sources. Ventilation air reduces the dust concentration by dilution and by displacement. The principle behind dilution ventilation is the provision of air so to dilute and remove dust. However, in contrast, displacement ventilation confines the dust source and keeps it away from workers by putting dust downwind of the workers. It is far more effective than dilution ventilation, but it is harder to implement (Kissel 2003). A typical local exhaust ventilation system consists of four major components, an exhaust hood to capture dust emissions at the source, the duct work to transport the captured dust to a dust collector, a dust collector to remove the dust from the air and a fan and motor to provide the necessary exhaust volume and energy (Martin Marietta Corporation 1987).

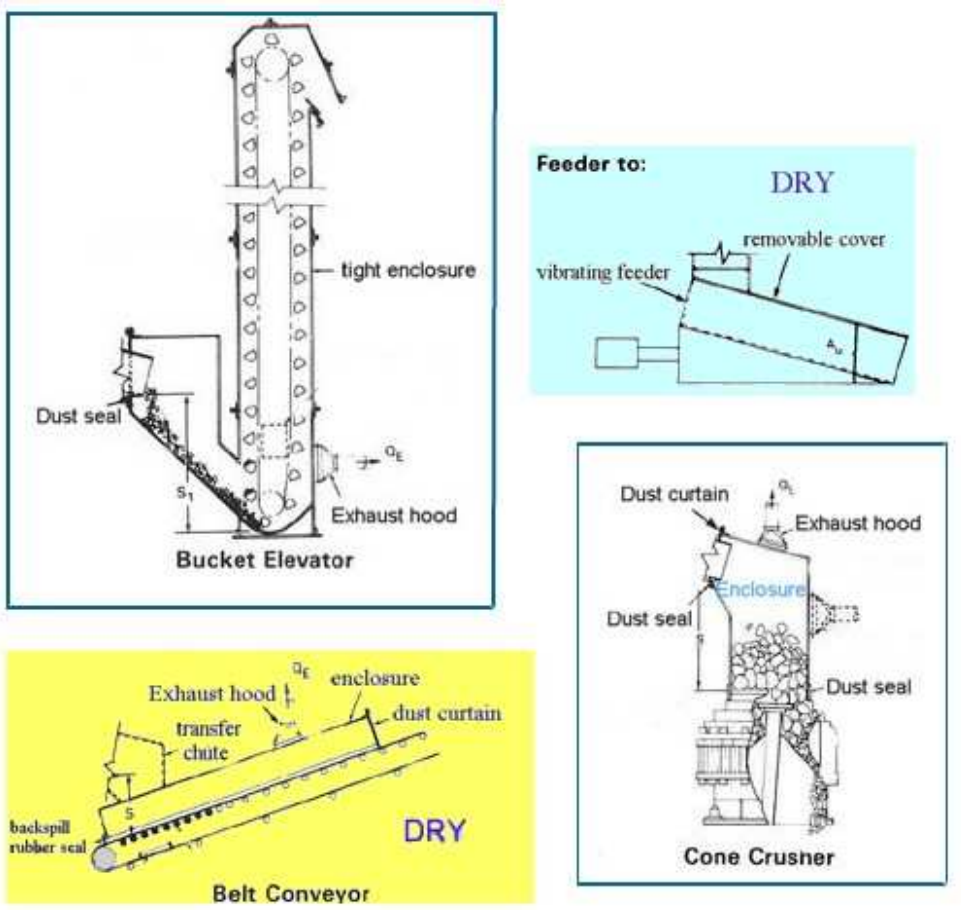

Figure 11: Examples of containment in mineral processing operations (Martin Marietta Corporation 1987).

2.8.2.The use of water sprays

Dust suppression is the use of water or chemically treated water in the term of a spray, fog or foam to prevent the generation of airborne particulates (Goldbeck & Marti 1996). There is a large variety of different mechanical systems used for this purpose. Most of these systems fall into one of the four main groups, which include atomised water sprays, electrostatically charged fogs, high-pressure sprays and sprays that use foam or wetting agents (Kissel 2003;Martin Marietta Corporation 1987). Examples of typical spray nozzles are shown in Figure 12.

The most frequent method of dust suppression is the use of water (Herrmann and Evensen 1994). Suppression is achieved by adding to the moisture content of the material and thus increasing the weight/mass ratio and cohesiveness of the material (Goldbeck & Marti 1996). The majority of dust produced during breakage stays attached to the surface of the broken material, so wetting ensures that dust particles will remain there. Wetting systems can provide static spreading and dynamic

spreading. During static spreading the material is wetted while stationary, whereas dynamic spreading wets the material while moving (Martin Marietta Corporation 1987). Impaction, droplet size-particle size relation and electrostatic forces affect the wetting - collision process between the particle and the droplet (Kissel 2003).

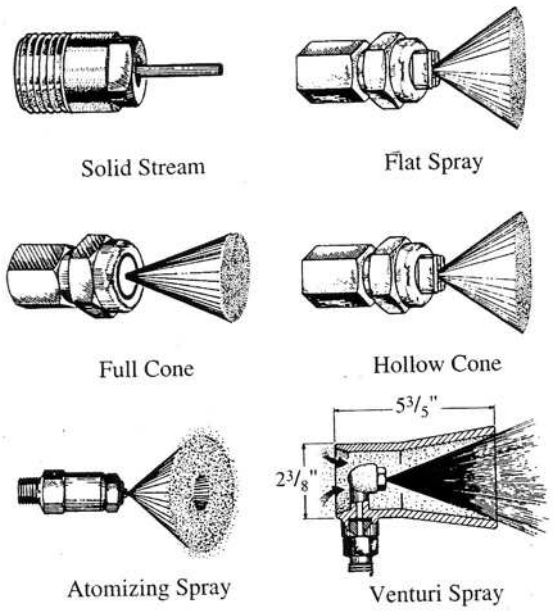

Figure 12: Typical spray nozzles used in dust suppression systems (Mohamed et al. 1996).

Certain disadvantages are associated with the use of water. In conveyor belts for example excess water may promote belt slippage, may leave conveyor belts awash with water and reduce the effectiveness of conveyor cleaning systems (Gibor 1997;Goldbeck & Marti 1996). Also the use of water can increase the possibility of wet and hence sticky fines accumulating within chutes and around transfer points, alter material's performance (i.e increased moisture content on coal is undesirable (Herrmann & Evensen 1994)), complicate its flow dynamics, block screens with mud as well as drench the product material on the belt (Gibor 1997;Goldbeck & Marti 1996). Weather conditions might greatly influence the water spraying process (i.e. during summer spraying need to be more frequent), whereas high wind speeds might make the water suppression process impossible. Water is not an effective binder so dust particle might become loose and released back to the air (Herrmann & Evensen 1994). The volume of water applied is typically in the range of 0.5% to 4% moisture added to the material (Goldbeck & Marti 1996).

The use of chemical additives and dust binding agents can increase the efficiency of the suppression process (Gibor 1997;Herrmann & Evensen 1994). Wetting agents enhance the ability of water to attract and hold dust particles. Chemical additives such as the Ciba Alcotac 1235 (polymeric) are added to water to reduce its surface

tension and thus form droplets easier, whilst dust binders like the Ciba Alcotac DC range (polymeric) have been designed to provide an adherent film to the surface of materials, preventing this way the creation of airborne dust (i.e from stockpiles) (Ciba Specialty Chemicals 2006). Drawbacks of the use of chemical additives include the additional and continuing cost and the impact of the chemicals on the end-use of the material (Goldbeck & Marti 1996).

Fog suppression systems are an improved version of the water suppression systems (Goldbeck & Marti 1996). They produce ultra fine mist which agglomerates the very fine particles. Fog suppression is based on the principle that droplets have a similar size to the dust particles and thus effectively combine them. Dry fog dust suppression works similar to a wet scrubber – fabric filter combination. The fog generated acts like a fabric filter and dust particles are urged to pass through it, colliding with the droplets. Since it is water based, the particle becomes wet similarly to a wet scrubber (Gibor 1997). Figure 13 shows the interaction of water droplets (small, large size) and dust particles. Less than 0.1% moisture is added to the product (Gibor 1997).

Water sprays produce air currents, which blow away much of the dust cloud (Kissel 2003). The effectiveness of the dust suppression can be improved by slowing the air movement within the loading zone. If the air velocity is too high, particles avoid collision with the water droplets (slipstreaming). If, however, the movement of air is slowed down (ie by increasing the size of an enclosure) then impaction takes place and particles are more efficiently wetted (Goldbeck & Marti 1996).

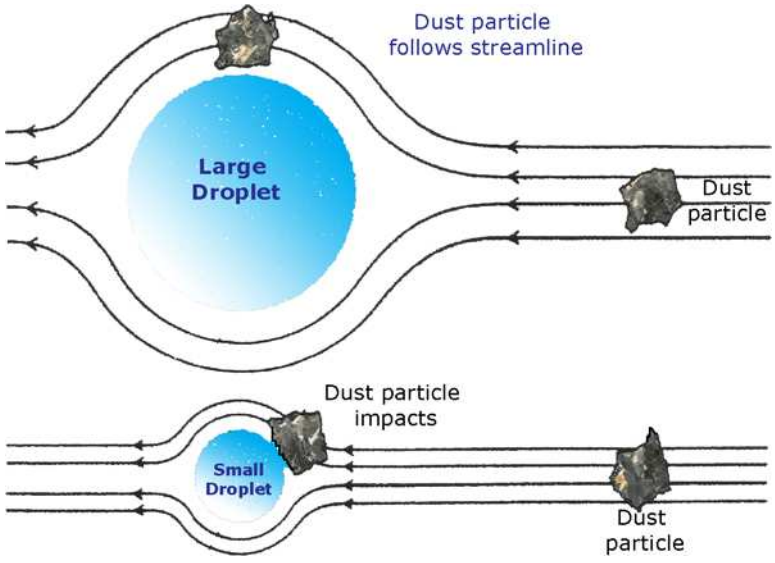

Figure 13: Interaction of water droplets and dust particles. The air currents and the ratio of droplet size to dust particle size play a major role. (Gibor 1997)

2.8.3. Dust collectors

Dust collectors play a valuable role in dust reduction. They mechanically capture the airborne material from the air stream and discharge cleaned air either into the atmosphere or back into the workplace. Dust collectors (Figure 14) are passive systems and most of the times represent the final piece of a dust control system pyramid (Goldbeck & Marti 1996). The efficiency of a dust collector is the filtration efficiency of the unit multiplied by the capture efficiency of its inlet (Kissel 2003). The selection of a dust collector should be based on the following factors (World Health Organization 1999); (Martin Marietta Corporation 1987):

• Dust concentration and particle size: Both vary considerably in mining operations

• Degree of dust collection required. Dust collection depends on the potential of dust to become a health hazard or public nuisance, regulations and established emission rates as well as the plant location and the nature of dust.

• Characteristics of air stream and atmospheric condition.

• Characteristics of dust, like composition, abrasion or hygroscopicity.

• Methods of dust disposal

Four types of industrial dust collectors are commonly used; inertial separators, fabric collectors, scrubbers, and electrostatic precipitators.

Inertial separators use a combination of centrifugal, gravitational and inertial forces to distinguish dust from the gas stream. Dust is subsequently moved by gravity into a hopper where it is temporarily stored (Dorman 1974). The primary types of inertial separators are settling chambers, baffle chambers and centrifugal collectors (Martin Marietta Corporation 1987).

Centrifugal collectors use the cyclonic action to separate dust particles from a gas stream. Barrel cyclones, multi-tube multi-type cyclones and axial flow cyclones are some of the two commonest in use types (Gibor 1997). Their efficiency increases with increasing particle concentration. One of the main disadvantages of the majority of cyclones is their low efficiency for very fine particles (below 5μm) (World Health Organization 1999).

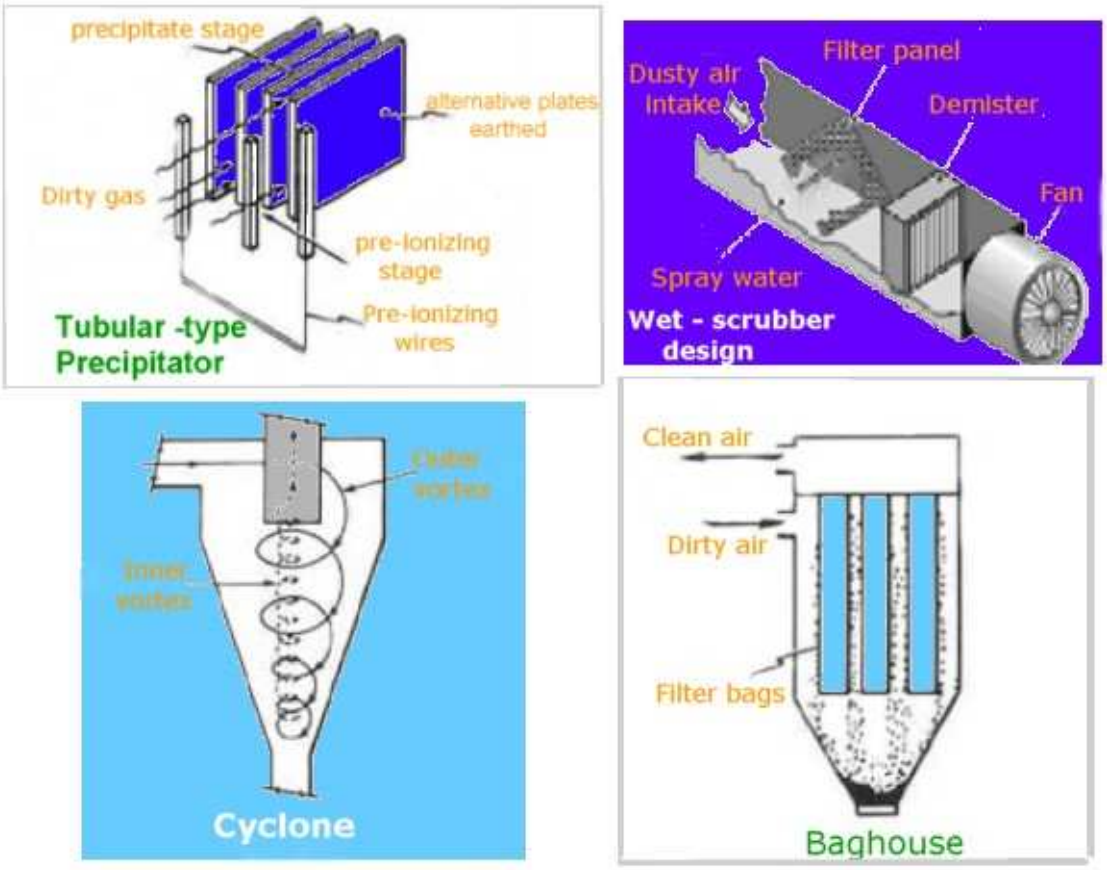

Figure 14: Typical dust collectors used in the mining industry (Kissel 2003;Martin Marietta Corporation 1987)

Fabric collectors, also known as baghouses, remove airborne particulates from carrier gas streams through filtration (Martin Marietta Corporation 1987). Bag houses are highly efficient for fine particle collection easy to operate and maintain, but they need relatively high installation and operation costs and they present limited use in high temperatures or in handling of sticky materials (World Health Organization 1999).

Wet scrubbers use a liquid phase (commonly water) to ensure collection of dust particulates. When operated the scrubbing liquid comes in contact with the dust laden stream. The degree of contact achieved between the liquid and the solid particles determines the dust removal efficiency (Martin Marietta Corporation 1987). Wet scrubbers require low initial cost, they can collect both particles and gaseous pollutants, they do not produce secondary dust sources and they are able to operate under high temperatures and with high humidity gas streams. Where fire and explosions is an issue (i.e coal mines), wet scrubbers exhibit minimum hazards. Nevertheless adequate arrangements need to be done for disposal of waste liquid. Also extra power consumption is necessary to collect finer particles (World Health

Organization 1999). Common types of wet scrubbers used in the mining industry are the dynamic self-induced spray scrubber, the multi-wash scrubbing tower and the venturi scrubbers. The latter are popular for the collection of fine dust (Gibor 1997).

The operation of electrostatic precipitators is based on the use of electrostatic forces to separate dust particles from gas streams. A high potential electric field is established between discharge and collecting electrodes of opposite polarity. The dust-laden gas stream passes through the field (Martin Marietta Corporation 1987). Particles acquire charges in the strong electric field and are deposited on an opposite charged electrode (Dorman 1974). The collected material on the electrodes is removed by rapping or vibrating the electrodes (Martin Marietta Corporation 1987). Electrostatic precipitators exhibit high efficiencies (over 99%), low operating pressure drops and dry disposal of solid material. They also require large spaces, high cost and skilled operation and maintenance (World Health Organization 1999).

2.8.4. Dust control through alternative engineering solutions and good practice

Dust control cannot only be implemented through existing mitigation techniques, but in some degree it can achieved by considering the generation of dust in equipment and process design. The US Occupational Safety and Health Administration states that the use of alternate equipment, improved equipment design or sometimes even the change in process can greatly reduce dust emissions, whereas reverse engineering can be applied on the malfunctioning parts of the industrial processes that are liable for the dust production (Martin Marietta Corporation 1987).

Coal handling applications is a good example of how alternative engineering solutions can reduce the amount of dust produced. Generating dust during coal handling is unavoidable and quite often the maintenance of dust equipment (i.e sprays) is not a high priority. On one occasion redesigning transfer chutes greatly improved the performance of the handling operation as well as minimized the levels of dust ((Schimmelpeennig 2004); (Schimmoller 2003)). So far, the objective of transfer chutes design was to simply move material from point A to B without considering as a design factor the minimum dust generation. Engineered systems that control material's behaviour at the end point of a conveyor belt and keep the material tightly together through the drop chute can minimize air entrainment dust generation and belt wear. In Powder River Basin (PRB) coal mine in Wyoming, Martin Engineering has tested a redesigned chute system with promising results. At the coal mine the system was installed on a belt-to-belt transfer where 4,200 tonnes per hour (tph)

moved from 72-inch belt to a 60-inch belt receiving conveyor with a drop height of 15.5 feet. The results of measured dust levels before and after installing the redesigned chute revealed that fugitive dust loads fell 76% and respirable dust loads fell 25%, while material handling tonnage increased (Schimmoller 2003).

Another example of a coal mine process with high dust levels is drilling. The blasthole drilling machine generates high concentrations of respirable dust from several sources. A cost effective solution implemented by the National Institute for Occupational Safety and Health (NIOSH) in the drill's dust collector fines dump was to attach a piece of brattice cloth around the dust collector dump point. This simple solution of creating a dust collector dump shroud reduced the respirable dust levels from 0.16 to 0.24 mg/m^3, succeeding an overall respirable dust reduction of 63% - 88% (Reed et al. 2004).

In free falling powder streams dust is generated during the transfer process that moves the dust particles outside the powder stream. This is due to the effect of particle's momentum, induced airflow during the falling movement and impaction of the particles on the surface of the receiver. When designing processes of powder transfer the particle velocity could be reduced by keeping the drop height of the powder stream as low as possible, producing internal physical barriers to slow the velocity of particles and providing de-entrainment space (extra- space) for particles to return into the process (Johnson 2003). For instance when a powder is transferred through a chute, then its velocity could be minimized by using a zigzag chute. The transfer of powder from one conveyor to another could also result to the production of dust. However the reduction of drop height to the highest degree possible reduces the powder velocity and the amount of induced air to the powder stream. The use of physical barriers such as lay-on guides between the chute and the belt's surface, skirtboards to keep the powder on the belt and belt scrapers to clean residual dust and fines could also assist to the minimisation of particulates (Johnson 2003)

An alternative engineering design of equipment, which was developed to minimise the generation of dust was the cascade chute system. Conventional loading chutes allow bulk material to free fall the full length of the chute. The induced air through the free falling action and the high impact velocity of the discharge material creates dust, as well as degradation and segregation of the product (Maxwell 1999;PEBCO 2006). The cascade chute consists of a series of opposite inclined cones supported by flexible straps and surrounded by a wind shroud. A fabricated carrier at the end of the chute is lifted or lowered by wires from a hoist (appendix I). When lifted, the

carrier supports the cones, which automatically stack into one another. Material detection probes inside the carrier prompt the winch to lift as the discharge product increases in height (Maxwell 1999). The cascade chutes have found application during ship-loading activities (i.e kaolin - Imerys Minerals, calcined petroleum coke – Conoco etc), silo loading and transfer points (i.e Cleveland Potash Ltd) (PEBCO 2006).

The use of stacker conveyors could also help to the reduction of dust. Stacker conveyors reduce the absolute drop height by moving an adjustable boom that may be raised or lowered to the height of the pile. By adjusting the height of the conveyor belt the breakage of soft ores can be eliminated and thus the dust produced is minimized (European Commission 2005). This method can be ideal for the transfer and stockpiling of soft ores such as coal and talc.

Nowadays engineering solutions and mitigation techniques are included in "Good Practice" (Figure 15) guidelines produced by legislative, occupational health and health and safety authorities like the US Occupational Safety and Health Administration, the National Institute for Occupational Safety and Health (NIOSH), the Integrated Pollution Prevention and Control directive (IPPC – EU) and other. A summary of good practice examples can be found in appendix I.

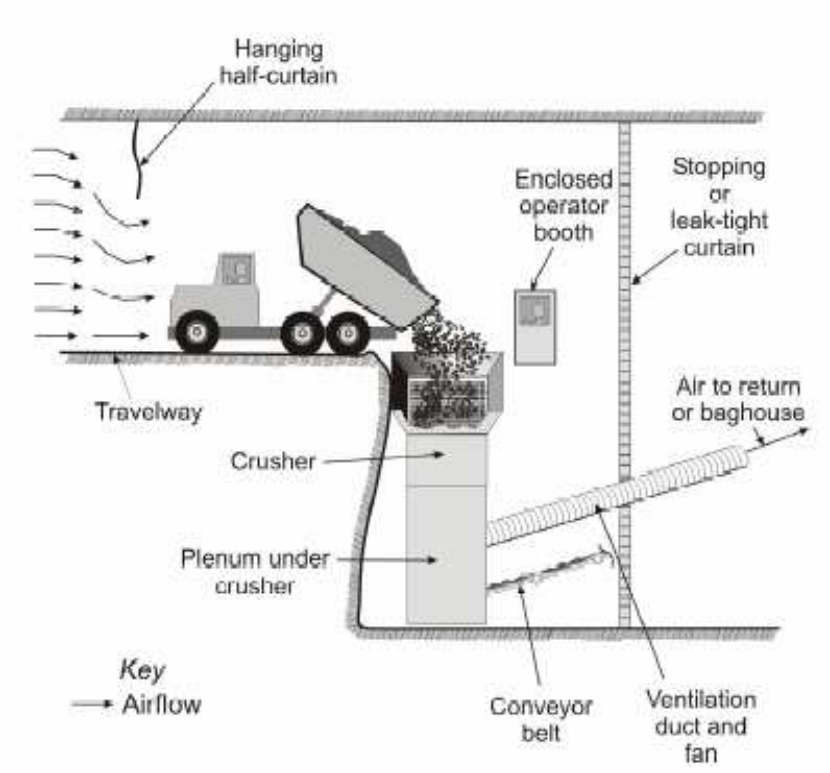

Figure 15: Good practices example of the tipping process to a crusher (Kissel 2003)

2.9. Work practices

Work practices are particularly important whenever the tasks performed influence the generation and release of hazardous agents into the work environment. Work practices depend a great deal on worker response and collaboration. Adequate training will allow workers to perform tasks safely and if it is well implemented might prove to be one of the key elements of preventive strategies (World Health Organization 1999). Good housekeeping, good work practices and careful hygiene must be the aim of any health and safety strategy.

Personal protective equipment should be used when all control possibilities have been explored but they do not provide adequate protection. Personal protective equipment (PPE) includes respiratory protective equipment, protective clothing and other accessories used in workplaces. It is mainly provided for welfare purposes and it should not be considered as a control measure except as a last resort (Trade Union Congress 2001). When considering personal protective equipment, the dust characteristics need to be taken into account. The use of personal protective equipment requires hazard awareness and training on the part of the user. Employers and employees must understand the equipment's purpose and limitations (US Department of Labour and Occupational Safety and Health Administration 1998). Maintenance and replacement shall take place at a right time or otherwise their use will not provide maximum protection.

Mineral dusts in workplaces are often responsible for the development of various diseases. Screening and surveillance are two complementary tools, which can be used to identify problems and to plan appropriate interventions. Screening is the administration of a test or series of tests to individuals in order to detect any diseases. Surveillance aims to continuously watch and evaluate over the distribution and trends of incidence through the collection and consolidation of mortality reports and other data (Wagner 1996). Serious concerns have been reported on the usefulness of mortality statistics, as lately it is believed that death certificate data significantly underestimate the prevalence of chronic occupational illnesses in the population (Banks & Parker 1998).

2.10.Summary of Chapter 2

This chapter reviewed the literature findings associated with the production of dust from mining activities. The generation of dust produces adverse impacts to human

health, the environment and the safety and productivity of a mine. Legislation around the world aims to ensure air quality and for that reason ambient air standards are employed, which the industry has to adopt. Additionally occupational exposure standards are used to define safe exposure limits in the working environment for all substances that can be hazardous to humans. Reference to common dust sources, the mobility characteristics of dust and research tools that can be employed to determine potential fugitive dust sources have been presented. Monitoring techniques and dust mitigation techniques that are used by the mining industry have also been reviewed. Dust control could also be achieved through different routes to the conventional methods that could prove to be cost effective and easy to implement. Alternative dust mitigation techniques commonly incorporate the design of such equipment, or the optimisation of industrial processes that can reduce the generation of dust. The objective of this project is to provide in depth understanding of the relationship between the process of dust generation and the mechanisms of different industrial operations, which would assist to the development and the accurate determination of potential alternative solutions for the mitigation of dust. However, this objective could not be implemented without the use of experimentation. The following chapter (Chapter 3) presents a review of experimental techniques that have been used for the characterisation of dust and which would assist the development of this project.

Chapter 3. Characterisation of mineral dust

3.1. Introduction to characterisation of mineral dust

As it noted in the previous chapter, dust is a very general term that has different meanings and significance within different industrial or scientific sectors. Although, the literature and research findings relevant to the characterization of dust generated from mining activities are not as well documented as particulate matter from ambient and urban sources, nevertheless the same principles and techniques are applicable. So far, experimental techniques aim to investigate dust through qualitative and quantitative procedures. Compositional analysis, particle size characterisation techniques, and dustiness determination techniques are normally used. This chapter reviews the different directions that can be followed to experimentally characterize dust.

3.2. Compositional analysis of the particulate matter

Compositional analysis of dust is required when the adverse impacts to human health and the environment are investigated. Qualitative analytical procedures, such as mineralogical characterisation techniques, identify the various compounds of the particulate fraction, but they can also provide morphological characterisation data. Quantitative techniques, such as chemical analysis, determine the exact amounts of the various dust compounds. Commonly, chemical analysis techniques, x-ray

diffraction analysis, optical microscopy (transmitted or reflected light), scanning electron microscopy and x-ray microanalysis are employed. The combination of the referred analytical techniques can give a versatile result. Elemental maps are constructed by chemical analysis and X-ray microanalysis (SEM/EDX) (Adachi and Tainosho 2004;Kasparian et al. 1998). A qualitative mineralogical profile can be assembled using X-ray diffraction (XRD) analysis, optical microscopy (transmitted, reflected light) and scanning electron microscopy (Davis 1984;Fukasawa et al. 1983;Gregurek et al. 1998;Queralt et al. 2001). Morphological characterisation, particle size and shape measurements are also an option through the use of optical microscopy and scanning electron microscopy (SEM) (Adachi & Tainosho 2004).

Research so far, aimed to characterize urban particulate matter from a specific region (e.g within a city area) (Davis 1984;Fukasawa et al. 1983;Ganor et al. 1998;Kasparian et al. 1998;Sturges et al. 1989), or distinguish a particular component of the dust fraction (e.g heavy metal particles) (Adachi & Tainosho 2004;Puledda et al. 1999), or identify the potential sources of dust and subsequently analyse them (e.g industrial emissions from mining works) (Gregurek et al. 1998;Kupiainen et al. 2003;Tervahattu et al. 2005). Therefore it becomes obvious that compositional analysis techniques have been used to assess air quality and the effects of particulate matter emissions to air pollution, which in their turn reflect potential hazards to human health.

Mineralogical examination methods were used to identify dust sources in complex situation, where emissions of particulates cannot clearly be related to particular processes (e.g. transport, industry) (Gregurek et al. 1998). Past research findings have shown that the coarse fraction of urban aerosols, which occupies the highest concentrations of their composition correspond to mineral compounds (Davis 1984;Fukasawa et al. 1983). It has also been revealed that particulate phases emitted are a characteristic fingerprint of the industrial processes from which they originate (Gregurek et al. 1998). Such an approach could prove favourable for the mining industry, in particular when issues of fugitive dust sources arise which need to be tackled. If the composition of dust could be matched to specific processes, then the identification of potential sources could become easier.

The compositional analysis techniques presented in this section are already used by mineral industries for ore/ product examination. Nevertheless they can also be applicable for characterisation of the particulate matter produced by mining activities and identification of dust sources. Compositional analysis results are of great

importance for identification of the hazardous potential of dust to the environment, the human health and industrial applications.

3.3.Determination of the dustiness of a sample

The term dustiness is used as a measure of the stages through which dust originates. It refers to the tendency of dry materials to liberate dust into the air when handled under specified conditions (British Occupational Hygiene Society Technology Committee 1985). It should be stated that the terms dust and dustiness refer to the estimation of particulates liberation potential of products and not to occupational hygiene concept of concentration of airborne dust in the work places (British Occupational Hygiene Society Technology Committee 1985). It is a measure of the ease of liberation of fine particles from a bulk source to form dust clouds (Higman 1986). The dustiness of a material depends on both the parameters that influence the dust generation process and emission process, thus is empirical and the results are greatly method dependent (Breum 1999). A measure of the dustiness of a material is obtained from a dustiness test.

3.3.1. Dustiness Tests

Throughout the years a wide variety of dustiness tests have been produced and used to compare the propensity of different materials to release dust into the air. Potentially these tests are of interest to both industrial producers and hygienists (Heitbrink 1990).The range of their application is very wide and could cover not only the mining sector, but the rubber, chemicals, pharmaceutical products, dry foods and pigments industries. A preliminary assessment of some of these methods has been carried out by the British Occupational Hygiene Society Technology Working Party on Dustiness Estimation (U.K.) and has been published in BOHS Technical Guide No 4 (British Occupational Hygiene Society Technology Committee 1985).

Dustiness tests usually consist of two parts: a generator and a sampler (Schneider and Hjemsted 1996). Most of the tests available follow three common principles for dust generation (British Occupational Hygiene Society Technology Committee 1985;Higman 1986;Lyons and Mark 1994) ;(Schneider & Hjemsted 1996):

- Impact or single drop methods. The test material falls from a certain height onto a metal surface in an enclosed chamber.

- Fluidization methods. A current of air passes through a bed of coarse particles mixed with the test material at a sufficient velocity to overcome the interparticle bed forces and to cause dispersion.
- Rotating drum methods. The test material is repeatedly lifted by a series of blades and dropped into the drum chamber as it rotates.

The chosen dustiness procedure should most closely simulate the operation under investigation (Higman 1986). Also the flow behaviour of the material to be tested must be taken into consideration when choosing a dustiness test method. The relevance of the test methods to various material handling operations is shown in Table 9. Recommendations on the optimum test method with respect to the materials properties are given in Table 10.

Table 9: Dustiness test methods and industrial processes (Higman 1986). (√: indicates that good results can be expected, x: indicates unsatisfactory results, !: indicates that reasonable results should be obtained with care)

	Impact tests	Rolling drum	Fluidized bed
Dustiness ranking	√	√	√
Effectiveness of dedusting	!	√	√
Effects of attrition	X	!	!
DUST GENERATION IN			
Screening – classification	!	!	√
Mixing, granulation, coating	X	√	!
Pneumatic drying, conveying	X	√	√
Loading-unloading	√	!	!
Mechanical conveying- elevating	!	√	!
Bagging	√	!	√
Vehicle movement	√	√	√
Losses from stockpiles	!	!	√

Table 10: Recommendations on dustiness test methods and materials properties (Higman 1986). (√: indicates that good results can be expected, x: indicates unsatisfactory results, !: indicates that reasonable results should be obtained with

care, o: indicates that good results can be expected provided that material can be fluidized.)

Material property	Impact tests	Rolling drum	Fluidized bed
Fine, free flowing	√	√	√
Fine cohesive	!	√	√
Fine, with additives	X	√	√
Coarse	√	√	o
Coarse, with additives	X	√	o
Sticky material	X	!	X

3.3.1.1. *Single drop tests*

A variety of gravity dispersion methods can be found in the literature. The British Occupational Hygiene Society has summarized the most significant ones in Technical Guide No 4 (British Occupational Hygiene Society Technology Committee 1985).

The gravity dispersion methods allow a defined mass of product to fall into an enclosed space, i.e a chamber, or to be tipped from a container within the chamber. The dust cloud produced is evaluated through mass determination, light obscuration and visual inspection (British Occupational Hygiene Society Technology Committee 1985). The drop height varies between 0.5 to up to 3m and the sample mass varies between 5g and 3 kg, although usually a sample of 30g to 100g is tested (Hamelmann and Schmidt 2003).

Mass determination methods are achieved by drawing air through a filter media and thus having sampling dust on its surface or by collecting fine dust that has settled onto a surface for subsequent weighing (British Occupational Hygiene Society Technology Committee 1985).

One of the earliest methods developed is that of the National Coal Board (Figure 16), in which coal samples are tipped down a duct (0.465m square section, 2.4m height). Air is drawn at an adjoining long horizontal duct at 113 l/min and dust is deposited on a filter attached at the end of this duct. Glass slides at the bottom of the duct collect dust for microscopy examination (National Coal Board 1957).

An interesting large scale experiment is described by Sutter et al. (1982), in which the environmental impacts of large spills of radioactive materials are assessed (Figure 16). The experiment was carried out in a stainless steel tank (height: 3m,

diameter: 2.9m), where material was released from a variety of drop heights (1-3m) and masses (25-1000g) (Sutter et al. 1982). The materials chosen were TiO_2 powder traced with uranine, depleted uranium powder, uranine and uranium solutions. Sampling of dust took place at various locations by high volume filters and impactors. These samplers collected dust for 30 minutes and achieved a 99% collection of airborne material. The conclusions made pointed out that source quantity and spill height were important parameters in aerosol generation, whereas all spills produce a fraction of particles of 10 µm aerodynamic diameter and smaller (Sutter et al. 1982).

Two more recently developed well reported single drop tests include the MRI dustiness test produced by the Midwest Research Institute (Kansas City, U.S.A.)(Heitbrink 1990) ;(Cowherd and Grelinger 1992) and the Roaches Dust Particle Apparatus (DPA) produced by Roaches Engineering Ltd. (U.K.) (Figure 17) (Lyons and Mark 1992). Both tests simulate the pouring / dumping operation of a finely divided test material (Cowherd & Grelinger 1992). The suspended particles generated during the test are captured on filters mounted in the chamber lid (Heitbrink 1990;Lyons & Mark 1992). In the MRI test the powder is poured out of a metal beaker, which starts rotating until it is completely inverted. Dustiness is calculated as the total number of milligrams of dust generated per kilogram of powder tested. The parameters that can easily be varied by the user are the flowrate, the vibrator setting and the bulk density of the material being tested (Heitbrink 1990). In the Roaches dust particle apparatus, 10g of test material are placed in the conical hopper at the top of the cylindrical tower fitted with a trap door. The experiment is initiated when the trap door opens and the material falls to the bottom of the chamber. With the help of a vacuum pump the dust cloud is collected onto a pre-weighed glass fibre filter (Lyons & Mark 1992).

In the light obscuration tests (Figure 17), the dust concentration is assessed by the reduction of intensity of a laser beam. The reduction opacity is transformed into a dustiness index (British Occupational Hygiene Society Technology Committee 1985;Hamelmann & Schmidt 2003).

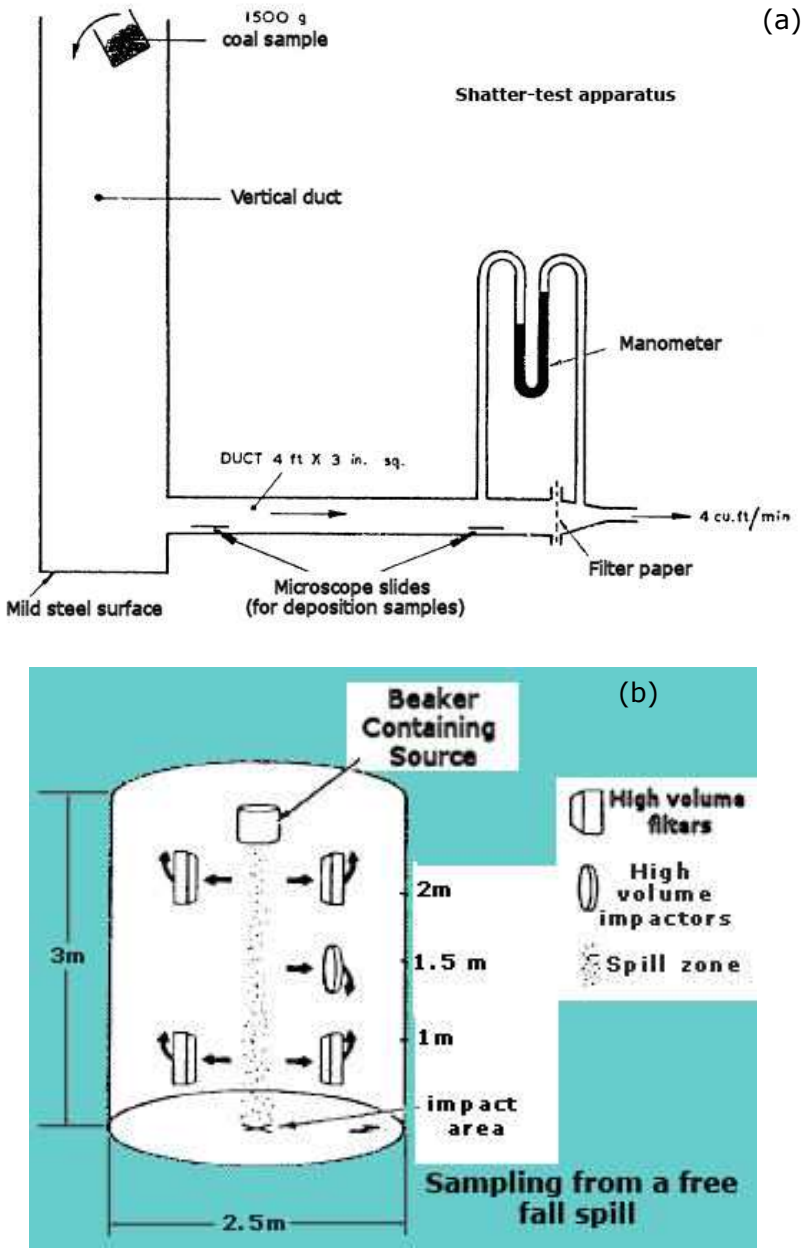

Figure 16: (a) The shatter-test apparatus (British Occupational Hygiene Society Technology Committee 1985) and (b) the free falling testing process (Sutter et al. 1982).

A slightly different method has been developed by Castor et al. (1990), in which rather than striking a surface with a powder, a surface strikes a powder by putting the sample at rest on a floor and jolting the floor upwards from below (Castor and Gray 1990). Similarly to the rest of the light obscuration methods the dustiness measurement is taken by monitoring the dust cloud with a laser beam (Castor & Gray 1990).

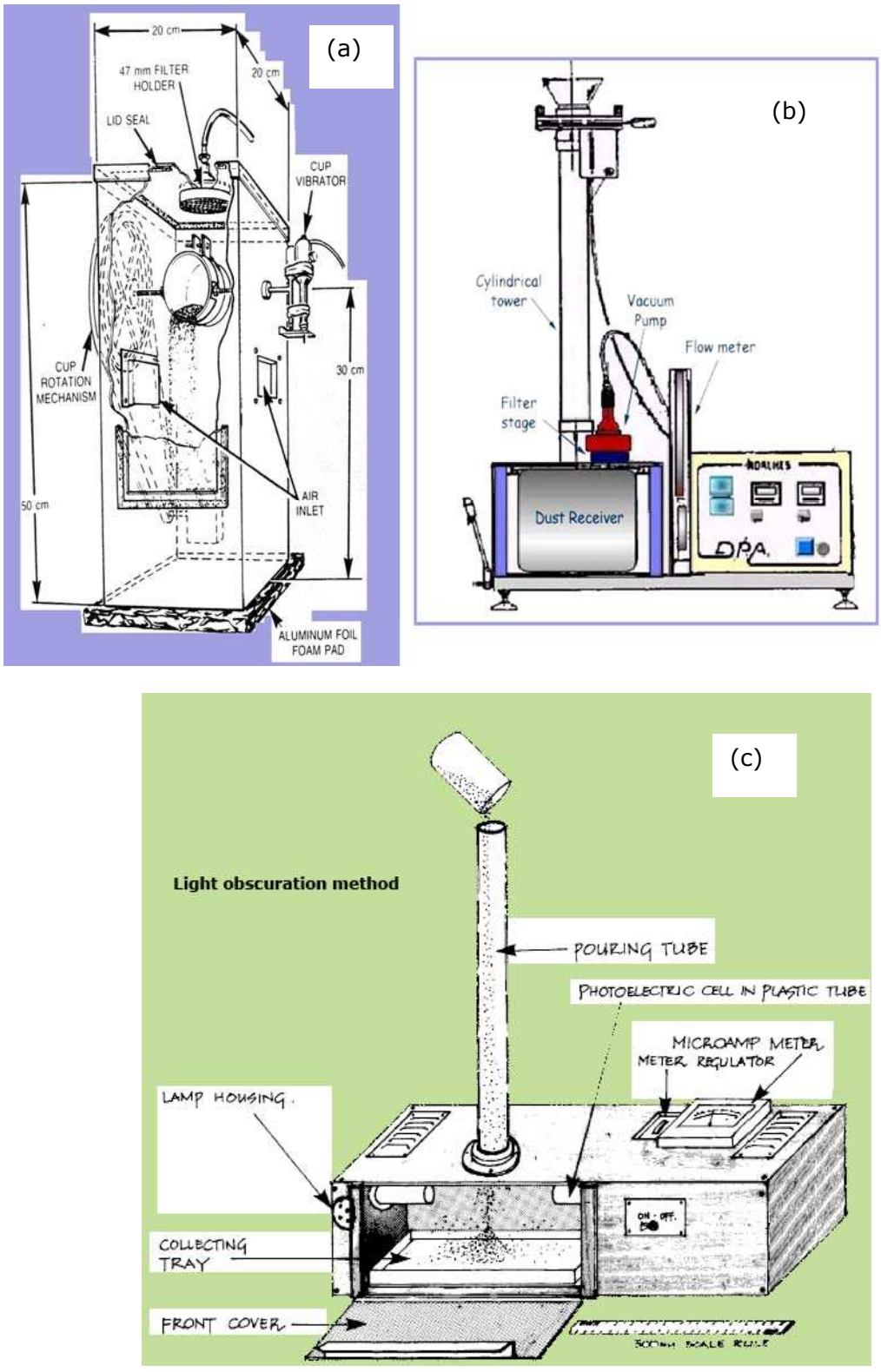

Figure 17: (a) The MRI dustiness test (Heitbrink 1990), (b) the Roaches dust particle apparatus (Lyons & Mark 1992) and (c) A single drop- light obscuration apparatus (Monsanto Europe S.A.) (British Occupational Hygiene Society Technology Committee 1985)

Single drop methods simulate processes from mineral processing operations that are associated with drop from heights such as tipping, loading and dumping, transfer

points (i.e between conveyor belts), stockpiling and other. They have the advantage of being fast, easy to handle and easy to clean. They can produce both gravimetric and optical measurements. Nevertheless, the single drop methods developed so far have only tested the dustiness of powders, whereas mineral processing operations more often handle coarse rock particles. Unfortunately, the physical dimensions of most of these single drop tests do not allow experimentation with coarse particles. Dust is produced from mining processes that involve drop from heights due to the presence of fine particles that accompany the rock samples, but also due to the degradation of rock particles, therefore it is essential that single drop methods will be altered to permit testing of coarse particle fractions as well. The majority of the existent single drop tests conducted experiments using a sample mass below 100g. For materials that exhibit high compositional variability, the use of a small mass might not represent well a bulk sample and this could affect dustiness. During the pouring of the powder, dust deposits on the walls of the apparatus before it reaches the filter, causing loss of dust that otherwise would have deposited on the sampling media. Finally it has been reported that the measured dustiness index from single drop methods is usually below those assessed by other methods (Hamelmann & Schmidt 2003), although this could be attributed to the different mechanisms of the various tests. Consequently, for all the above reasons, the use of single drop tests should carefully be determined in accordance with the project objectives and the physical characteristics of the materials to be tested (composition, particle size). Furthermore, there is need for development of single drop techniques that will allow the use of a range of particle size fractions as well as sample masses, which will simulate handling and processing operations that involve drop from heights other than the ones used only for powders.

3.3.1.2.*Fluidization dustiness tests*

In this class of method dust is liberated by the action of a gas passing through the sample (British Occupational Hygiene Society Technology Committee 1985). The devices often consist of a vertical stainless steel cylinder and glass modules. The sample is placed onto a sintered plate at the bottom end of the tester and it is continuously subjected to an upward air stream. Some sort of agent (i.e. sand) is added to cohesive materials in order to achieve homogeneous fluidization (Hamelmann & Schmidt 2003;Sethi and Schneider 1996). The dust cloud is captured by a collection device (i.e. filters, Andersen collector, cyclone etc) found on the top of the cylinder and the dust yield is determined (Hamelmann & Schmidt 2003).

Typical examples of fluidization dustiness tests include the Warren Spring Laboratory fluidized bed dustiness tester (Figure 18) (British Occupational Hygiene Society Technology Committee 1985) and a gas fluidization dustiness tester produced by the National Institute of Occupational Health in Denmark (Figure 18) (Sethi & Schneider 1996). In the WSL fluidized bed dustiness test the sample is loaded at the bottom of a glass tube on a porous metal bed, where air is passed at a fixed rate to fluidize the bed and liberate the dust. Dust particles are sampled isokinetically and pass into an Andersen cascade impactor for particle size distribution analysis. The weights collected in a given time period are a measure of the test material's propensity to emit dust (British Occupational Hygiene Society Technology Committee 1985). The gas fluidization dustiness test is a modified version of the fluidized bed dustiness tester produced by the Warren Spring Laboratory. In this case the airborne particles are measured in situ as a function of time by an optical particle counter and a tapered element oscillating microbalance (TEOM) along with gravimetric measurements (Sethi & Schneider 1996).

Fluidization dustiness tests should be used when the occupational hazards of dust are of research interest. This is because such tests cannot utilize other materials than fine powders. Fluidization tests do not simulate directly a specific category of industrial processes, therefore it is often difficult to relate dustiness results with applications. Also it has been reported that such tests subject particles to higher stressing than other dustiness methods. This intensive stressing of the sample avoid conclusions to be made for a wide arrange of applications (Hamelmann & Schmidt 2003). Material properties, like the density and particle size, play an important role to the dustiness determination (British Occupational Hygiene Society Technology Committee 1985;Hamelmann & Schmidt 2003). According to research findings, the dust index increases as the median diameter decreases (Sethi & Schneider 1996).The repeatability and accuracy of the measurements taken with these tests depends not only upon the physical properties of dust, but also upon the homogeneity of fluidization bed. A heterogeneous fluidization bed might result to high variations in dustiness, whilst the assessment of its homogeneity is often very difficult. The fluidization test approach does not fit with the objectives of this project which tries to relate the generation of dust with mineral processing operations.

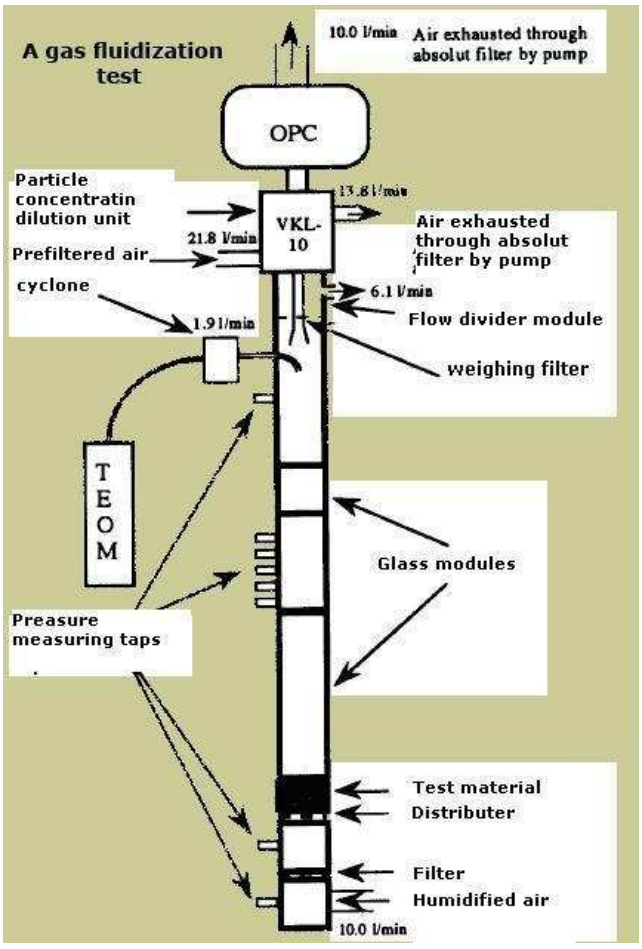

(a)

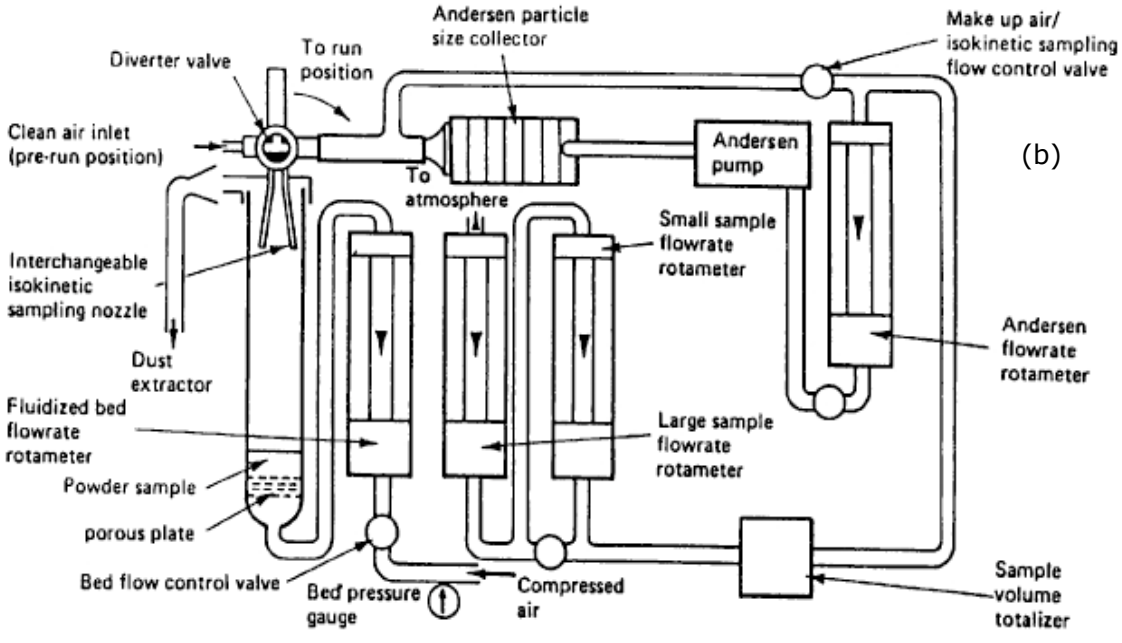

(b)

Figure 18: (a) A gas fluidization test (Sethi & Schneider 1996); (b)The Warren Spring Laboratory fluidized bed apparatus (British Occupational Hygiene Society Technology Committee 1985)

3.3.1.3. *Rotating drum methods*

In this class of method the sample is dispersed in a rotating drum (British Occupational Hygiene Society Technology Committee 1985). Lifter bars enable the mixing of the sample. Dust generated is transferred to a measurement unit like an impactor, an optical counter or it is collected on a filter media (British Occupational Hygiene Society Technology Committee 1985;Hamelmann & Schmidt 2003).

Characteristic rotating drum methods comprise the Warren Spring Laboratory (WSL) rotating drum, and the Heubach dustiness test (Figure 19).

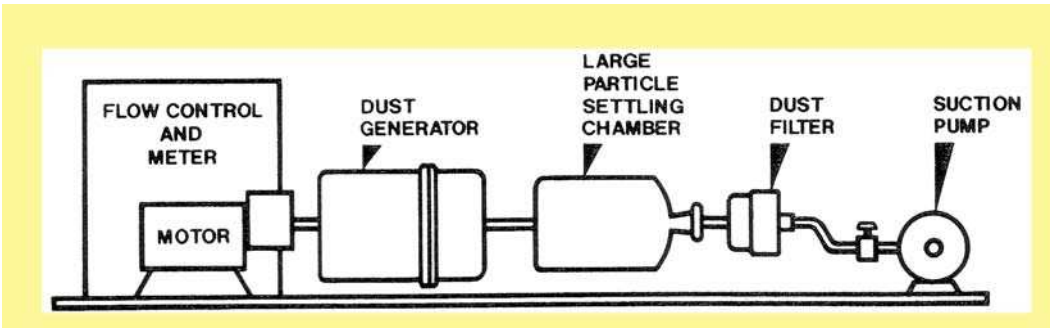

(a)

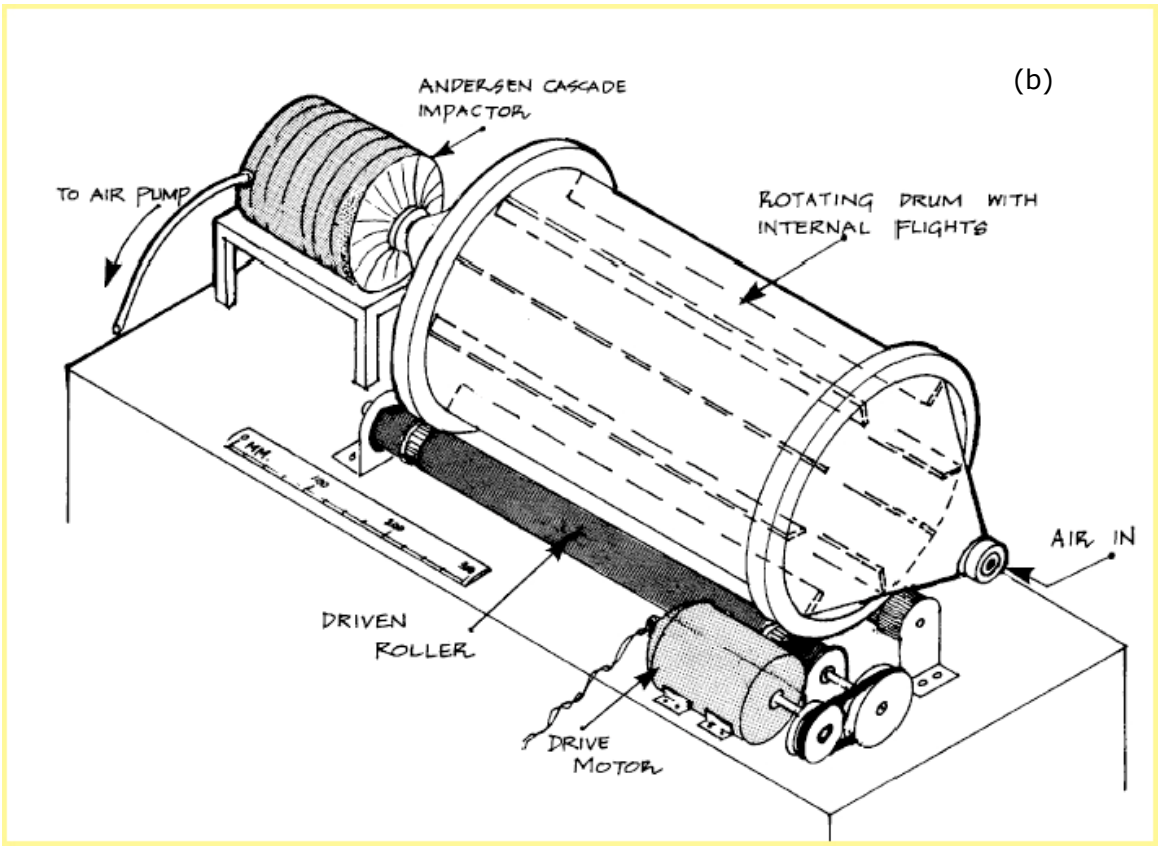

Figure 19: (a)The Heubach dustiness test (first apparatus) and (b) the Warren Spring Laboratory rotating drum (British Occupational Hygiene Society Technology Committee 1985;Heitbrink 1990)

The initial WSL (Warren Spring Laboratory) rotating drum dustiness test designed by Higman et al (1984) consists of a large drum with vanes attached on the inner of the drum and an Andersen size selective sampler with a backup filter where all airborne particulates are captured (Higman et al. 1984;Lyons & Mark 1992). Any airborne particulates produced from the tumbling action were drawn through a modified Andersen sampler, which consists of three stages. The pre-separator stage has a 50% cut point (d50) at an aerodynamic diameter of 10 µm. The impaction stage has a d50 of 9 µm, whereas the backup filter collects all particles, which penetrate the impaction stage (Lyons & Mark 1992). The dustiness measurements obtained are for particles below 9 µm, for particles above 9 µm and for all particles (Lyons & Mark 1992).

A second approach to produce a practical dustiness test method, which will determine the health related dustiness of powders and materials the HSE-WSL dustiness test has been developed (Health and Safety Laboratory 1996); (Lyons & Mark 1994). The main difference of this method in comparison to the old WSL test is the different selection stage. The HSE-WSL test comprises of a series of foam filters and paper glass filter, which capture and separate the particulates to the three CEN/ISO (CEN 1993) health related fractions (Lyons et al. 1992). Further information on the method is given in Chapter 4.

A modified version of the WSL method has been used by the Danish National Institute of Occupational Health (Schneider & Hjemsted 1996); (Breum 1999). The drum is built similar to the WSL drum. The dust collection system consists of 90 mm diameter filter placed in a vertical filter holder (Schneider & Hjemsted 1996). The ration of mass of dust collected onto the filter to the mass of material under testing determines the dustiness of a sample. In advance, an isokinetic probe, samples a fraction of the air, which is driven to a TEOM (tapered element oscillating microbalance) Series 1200 ambient particulate monitor (Schneider & Hjemsted 1996). The TEOM monitor is used to record dust concentration versus time at the outlet of the drum (Breum 1999). The oscillating frequency change determines the filter weight gain and real-time mass concentrations are obtained (Schneider & Hjemsted 1996).

The Heubach test also comprises a rotating drum test, which works similar to the WSL rotating drum test. The Heubach apparatus has been the first commercial dustiness estimation device manufactured by Heubach GmbH of Langelsheim, West Germany (British Occupational Hygiene Society Technology Committee 1985). A

mass of sample is placed in the dust generator, a drum which rotates at 30 rpm. Three vanes enable mixing of the sample. Air flows into the dust generator and transports the dust through the particle settling chamber onto a filter, which collects the airborne particulates. The mass of dust generated equals the weight gain on the filter after blank correction (Heitbrink 1990).

The Lubbock Dust Generation, Analysis and Sampling System is another rotating drum dustiness test, which has been developed to simulate and measure characteristics of particle generation by wind erosion and collection of aerosols by a filter sampler in dusty environments. It consists of three sections: a controlled-energy dust generator, a dust transport/measurement zone, and a dust settling / aerosol collection chamber (Gill et al. 1999). A schematic presentation of Lubbock apparatus is shown in Figure 20.

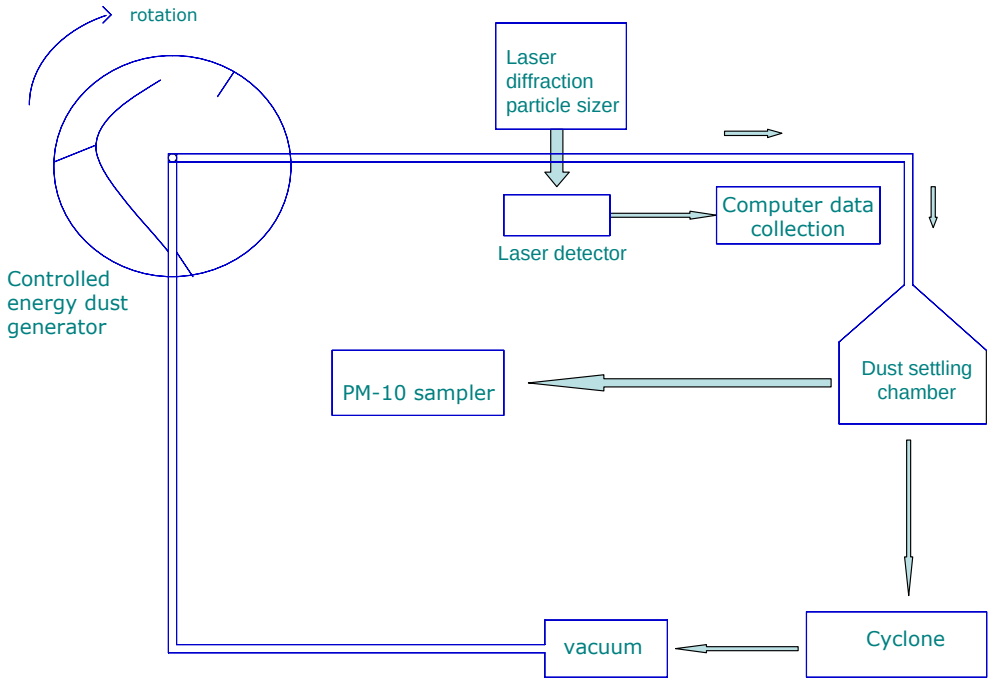

Figure 20: Schematic representation of Lubbock dust generation, analysis and sampling system (Gill et al. 1999).

The controlled energy dust generator consists of a rotating drum. Four rollers enable the rotation action. Three baffles are fixed to the interior drum surface as well as a half-barrel section (fixed to frames outside the barrel) (Gill et al. 1999). The drum is capped with a Plexiglas shield. Test samples are placed inside the barrel, which rotates at a pre-selected rate. The fixed half barrel holds the sample against the baffles until the sample reaches the top of the drum, from where it falls (Gill et al. 1999). Air is blown into the drum by a wet-dry vacuum and the dispersed dust is entrained into a pipe in the centre of the drum to exit the dust generator. Dust is

transported through a pipe in which it is analyzed for particle size by laser diffraction spectroscopy. Afterwards, dust enters a settling chamber. A fraction of the dust laden air is removed during the entrance to the settling chamber to collect the PM_{10} fraction. PM_{10} is collected using a low- volume impaction aerosol sampler (MiniVol). Most of the remaining dust particles that exit the settling chamber are collected by a cyclone (Gill et al. 1999).

The various rotating drum methods present only small differences in their design, which are attributed to the different sampling approaches. Similar to other categories of dustiness tests (i.e single drop methods, fluidization tests), they have been developed to assess the occupational adverse impacts of the particulate matter and it is for this reason that different sampling methods have been used. Often these sampling methods try to provide apart from dust mass concentration results, particle size analysis data. Therefore particle sizing techniques are combined with the various dustiness tests (e,g the use of an Andersen impactor in the old version of the WSL apparatus). However, particle sizing methods require their own control measures (e.g specific flowrate levels) thus adjustments with the dustiness test should take place. In certain cases, such adjustments might limit the capabilities of dustiness tests, for instance, testing might not be possible beyond a specific range of flowrate.

The tumbling action is considered representative of many material handling processes, like mixers, conveyors, and mills. Nevertheless research so far has not proved, how well dustiness tests relate to industrial processes, or what are the parameters (e.g specific mechanisms) of these operations being simulated by dustiness tests. According to Gill et al. (1999), a rotating drum method may also be appropriate for laboratory simulations of a dust monitor down wind of a field undergoing wind erosion (Gill et al. 1999). In comparison to other methods the rotating drum tests operates under a continuous lifting-falling action. Rotating drum methods are thought to be more versatile than the single drop and fluidized bed dustiness tests. The size of the tumbling mill, of any of the different rotating drum test versions, allows a variety of samples with different physical characteristics to be tested, such as fine powders, or granular materials, dry or damp materials. Fine, lumpy, dry or damp material can easily be tested. According to previous researchers the tumbling action simulates more realistically the effect of particle attrition and the break up of aggregated particles (Lyons & Mark 1994). However this is a statement that has not been accurately justified by experimentation. If the mechanisms of the tumbling action in the rotating drum test were investigated, then it would be possible

to explain what industrial processes the dustiness results relate to and thus to identify potential dust sources or even propose mitigation practices.

3.3.2. Dustiness tests and past research findings

Dustiness tests have been used so far to evaluate and measure the dust generation potential of several types of materials like mineral related samples (i.e. calcium carbonate, talc, coal), animal feed (various grades), wood, plaster, garden peat and other (Breum 1999;Higman 1986;Lyons & Mark 1994;Schneider & Hjemsted 1996).

Powder producers use dustiness tests as routine quality control procedures to determine the dustiness of their products as well as investigation tools so as to fabricate materials with the minimum possible dust effects (Heitbrink 1990). Higman (1986) reported that the addition of 2% oil in a chemical blowing agent had a greater than six-fold reduction in the total dust emission, whilst the addition of 1.5% glycelor in a talc powder resulted to a 30 times reduction of total dust emissions (Higman 1986). Dustiness testing provides an objective and quantitative assessment of a material in relation to its ability to generate dust under varying circumstances. Thus dustiness tests can be very useful for the industrial sector (Higman 1986). Some of the main considerations associated with the use of tests are shown in Table 11.

The evaluation of the effects of the test parameters upon material dustiness is one of the main research points of interest (Breum 1999;Cowherd & Grelinger 1992;Heitbrink 1990;Lyons et al. 1996;Schneider & Hjemsted 1996). The variables for a single drop method and a rotating drum method could involve the mass of test material, the type of release (i.e single, repeated), rate of release, fall height, the sampling time, the position of sampling media, the air flow rate plus the rotation speed for the rotating drum methods only (Carlson et al. 1992). Both rotating drum tests and single drop tests have been investigated. The variability of dustiness with mass of test material, flow rate, testing time, air relative humidity, rotation speed (for rotating drum tests) has been assessed for different tests and material types. All alterations to test parameters affect the amount of dust and the size distribution of dust generated during these tests. According to previous research findings the test parameters of dustiness tests need to be carefully controlled in order to have reproducible dustiness results (Breum 1999;Heitbrink 1990).

The dependency of the physical properties of the test materials on the dust yield values has been examined only to a small extend and further research work is required to determine the relationship between dustiness and the properties of the material under examination. According to Hjemsted and Schneider (1996), physical properties like the moisture content, the particle shape and size and the bulk density can affect the dustiness of a material (Schneider & Hjemsted 1996). As an example, they observed that two different kinds of copper powder had a two orders of magnitude difference in dustiness index. The highest dustiness index corresponded to a powder consisting of flaky shaped particles, whereas the lowest dustiness index was yielded from a powder with spherical particles (Table 16) (Schneider & Hjemsted 1996).

The influence of a range of factors, both test variables and materials' physical properties, as recorded by various researchers can be seen in Table 12, Table 13, Table 14, Table 15, and Table 16. . According to these result (Table 12, Table 13, Table 14, Table 15, and Table 16), the majority of previous studies concluded that an increase in flowrate, sample mass or dust dispersion time resulted to a subsequent increase of total dust yield. Nevertheless the level of increase is dependent upon the material properties, whereas there were occasions that materials (i.e investigation of the flowrate effect on fused alumina (Table 12)), did not satisfy the above statement.

The correlation between dustiness test results and dust exposures has been examined by Heitbrink et al. (1990) at two bag dumping and bag filling operations (Heitbrink et al. 1990). The dustiness tests used during these studies were the Heaubach dust measurement appliance and the MRI dustiness tester. At one bag dumping and bag filling operation, there was evidence of a relationship between dustiness test results and dust exposure, whereas at the remaining two operations no correlation was observed. The authors concluded that the relevance of dustiness tests and occupational exposure levels need to be evaluated at each site. Also they stated that laboratory based results should be validated by field measurements (Heitbrink et al. 1990).

Table 11: Argumentation associated with the use of dustiness tests (Breum 1999;Heitbrink 1990;Heitbrink et al. 1990;Higman 1986).

Advantages	Comment
Estimation of product loss	Handling applications are liable for product loss
Estimation of emissions into the working environment	Assessment of the severity of the situation can be achieved
Assessing the relative dustiness of a material	Very important especially when the handling of toxic dusts is involved
Assessment of the effectiveness of dust suppression techniques	Materials with suppression agents and without can be tested
Quality control	Standardized dust measurement techniques can be used to monitor and improve products
Determination of need for dust control	The likelihood of a material to create dust problems and hence the need for dust control can be assessed.
Disadvantages	**Comments**
Test operating parameters need to be controlled	Control over the operating parameters of dustiness tests helps to achieve test reproducibility, comparative results and low standard deviations.
Dustiness tests are empirical.	Dustiness tests cannot guarantee that they adequately simulate dust generation in actual powder handling operations. Dustiness test results must be correlated with personal dust exposures at the operation of interest.
Dust exposure might be influenced by a plethora of extra variables	Variables like the work practices, the operation of the plant, equipment maintenance, process leakage and others might have a great effect upon dust exposure, making correlation with dustiness test results impossible.
The choice of dustiness test must be based on the principles followed by the powder handling operation	The mechanisms of dust generation in the dustiness tester must not differ from the mechanisms of dust generation in the process of interest.

On another occasion a comparison study of two dustiness evaluation methods, the rotating drum Heubauch device and the Laboratory Dust Disperser (LDD) (gravitational method) aimed to identify the effect that the air flow rate variance has on the dustiness index and the inhalable dustiness index values (Carlson et al. 1992). The test materials consisted of two animal feed additive premixes. Particle size analysis using a cascade impactor assisted the determination of the inhalable dustiness index. The fraction of the aerosol that has an aerodynamic equivalent particle diameter below or equal to 15 μm, multiplied by the dustiness index was used to define the inhalable dustiness index. One of the main conclusions of this study was that particle size measurements should be incorporated into dustiness measurements that an estimate of the inhalable dustiness index can be made (Carlson et al. 1992).

Table 12: The effect of flow rate upon the dustiness of materials as derived from rotating drum tests and single drop tests (Carlson et al. 1992;Heitbrink 1990;Lyons & Mark 1994;Schneider & Hjemsted 1996).

Parameter	Test method	Material	Results	Reference
Flow rate	Rotating drum test	fused alumina	↑ flowrate ⇨ ↑ dustiness index	(Schneider & Hjemsted 1996)
	Rotating drum test	aloxite	↑ flowrate ⇨ ↑ dust yield	(Lyons & Mark 1994)
	Heubauch drum test and MRI test	limestone	↑ flowrate ⇨ ↑ cumulative mass of dust	(Heitbrink 1990)
	Heubauch drum test and LDD test	Animal feed additives premixes	↑ flowrate ⇨ ↑ dustiness index	(Carlson et al. 1992)

Table 13: The effect of sample mass on the dustiness of materials as derived from rotating drum tests and single drop tests (Breum 1999;Heitbrink 1990;Lyons & Mark 1994;Schneider & Hjemsted 1996)

Parameter	Test method	Material	Results	Reference
Sample mass	Rotating drum	Fused alumina	↑ mass ⇨ ↓ dustiness index (50 to 200g)	(Schneider & Hjemsted 1996)
	Rotating drum	Aloxite	↑ mass ⇨ ↑ dust yield (25 to 400g)	(Lyons & Mark 1994)
	Heubauch drum test	limestone	↑ mass ⇨ ↑ dustiness index until a plateau is reached	(Heitbrink 1990)
	MRI test	limestone	↑ mass ⇨ ↑ dustiness index	(Heitbrink 1990)
	Rotating drum test	Several materials (i.e bentonite, talc, coal etc)	↑ mass ⇨ ↑ dustiness index (within one material)	(Breum 1999)

In the HSE-WSL rotating drum dustiness test dustiness index is expressed in terms of the health related dust fractions defined by ISO-CEN. Whilst the use of the health related dust fractions do not guarantee that the results are closely related to personal exposure data monitored by field measurements, it was considered a step forward (Lyons et al. 1996;Lyons et al. 1992;Lyons & Mark 1994). More information on this test is given in Chapter 4.

Table 14: The influence of sampling time on the dustiness of a range of materials as derived from rotating drum and gravitational test methods. (Hjemsted and Schneider 1993; Lyons & Mark 1994; Schneider & Hjemsted 1996; Heitbrink 1990)

Parameter	Test method	Material	Results	Reference
Sampling time	Rotating drum test	MMVF (animal feed)	↑ sampling time (up to 30 sec) ⇨ ↑ dustiness index. After 30 sec dustiness index decreases	(Hjemsted and Schneider 1993)
	Rotating drum test	Feed for pigs	↑ sampling time ⇨ ↑ dustiness index (initially). Dust continues to generate during the whole test period, but at lower rates.	(Hjemsted & Schneider 1993)
	Rotating drum test	Aloxite	↑ sampling time ⇨ ↑ dust yield (up to 20 sec.). Further increase on dust dispersion time does not cause any extra increase on dust yield.	(Lyons & Mark 1994)
	Rotating drum test	Fused alumina	↑ sampling time .(3 to 10 minutes)⇨ ↑ dustiness index; except with the test conditions 50g, 60rev/min, 80 lpm, where the difference in dustiness index between 3 to 10min. is neglidgible	(Schneider & Hjemsted 1996)
	Heubauch drum test	limestone	↑ sampling time ⇨ ↑ cumulative mass of dust	(Heitbrink 1990)
	MRI test	limestone	↑ sampling time ⇨ ↑ cumulative mass of dust. After 10 minutes a plateau is reached	(Heitbrink 1990)

Table 15: The influence of surface adhesion on rotating drum dustiness methods (Breum 1999;Lyons & Mark 1994;Schneider & Hjemsted 1996)

Parameter	Test method	Material	Results	Reference
Surface adhesion	Rotating drum test	Several materials (i.e bentonite, talc etc)	It depends on material properties. For example bentonite exhibits low adhesion compared to coal	(Breum 1999)
	Rotating drum test	Aloxite, two different grades (fine and coarse)	Coarser grade did not deposit on the walls, whereas fine grade adhere to the inner drum surface	(Lyons & Mark 1994)
	Rotating drum test	Fused alumina	The largest change in amount of deposited dust on the drum walls from 50 lpm to 80 lpm is found at the conical ends	(Schneider & Hjemsted 1996)

Table 16: The effect of a range of different factors apart from the dustiness test operating parameters, on the dustiness of a range of materials (Higman 1986;Hjemsted and Schneider 1996;Schneider & Hjemsted 1996).

Parameter	Test method	Material	Results	Reference
Air humidity	Rotating drum test	coal	↑ air humidity⇨ ↑ dustiness index	(Hjemsted & Schneider 1996)
Particle shape	Rotating drum test	Copper powder; type I: with flaky particles; type II: with spherical particles	Copper powder with flaky particles exhibited much higher dustiness index from powder with spherical particles	(Schneider & Hjemsted 1996)
Additives	Rotating drum test	Chemical blowing agent	Addition of 2 % oil ⇨ ↓ dust rate (factor of 6), further add of oil ⇨ ↓ particles ≤ 9 µm.	(Higman 1986)
Process	Rotating drum test	Animal feed; Feed 1: ground in a rolling mill, moisture content 20%; Feed 5: ground in a hammer mill, moisture content 13%	Dustiness index of Feed 1 was reduced by a factor of 100 compared to feed 5	(Schneider & Hjemsted 1996)
Particle size	Rotating drum test	30 mixtures of coke	Dustiness is dependant upon the proportion of fines (<50µm). Maximum dustiness when around 15% of material under 50µm.	(Higman 1986)

Cowherd (1992) correlated the dustiness levels obtained from the MRI dustiness tester with the US Environmental Protection Agency AP-42 fugitive dust emission factor model. Experimentation took place for a variety of materials including sodium chloride, portland cement, activated carbon and hydrated lime (14 different samples with more than one order of magnitude in range). In one of their studies, this project investigated the dust releases from the handling of several finely divided materials and airborne particulate concentrations were monitored in a room-size-chamber. They found out that the particulate emission rate in the room ventilation air stream was found to correlate nearly 1:1 with the dustiness of the material determined using the MRI tester. In a separate study of the dustiness of crushed limestone, the measured dustiness agreed closely with the AP-42 emission factor for materials handling operations. The authors discovered a close relationship between the AP-42 prediction model for fugitive dust emissions and the results obtained from the MRI dustiness tester. Thus, it was concluded that the MRI dustiness test was a suitable device for generating source profiles for modelling of fugitive dust source contribution to ambient particulate levels (Cowherd & Grelinger 1992). Nevertheless, it should be stated that the AP-42 fugitive dust emission factors are prediction tools and can only

find use as guidelines, thus they do not always simulate with accuracy real conditions.

The Lubbock apparatus followed a different approach to the other dustiness tests. Research with this test tried to identify how dust is generated from wind erosion, which was considered a function of the kinetic energy that dust particles travel. The kinetic energy of the soil particles in the laboratory test was calculated from the height the particles drop to the bottom of the drum. Thus, the impact velocity of the soil particles was found to be equal to 3.12 m/sec (Gill et al. 1999). According to authors, this value of impact velocity is considered to simulate well the saltation of dust particles, during impact with rocks in moderate to strong wind erosion events (Gill et al. 1999). The calculation of kinetic energy and impact velocity do not explain what is the exact dust generation mechanism. Do the soil particles break when they impact at the bottom of the drum? What trajectories do the particles follow during the rotation of the drum? What is the effect of friction upon the particles? Answers to these questions are not given in detail. Nevertheless, the approach followed with the Lubbock system is much more appropriate than conventional dustiness tests, because it describes the fundamentals of the dust generation process. On the contrary, conventional dustiness tests did not proceed to experimentation beyond the measurement and classification of emitted dust and this is considered a great disadvantage. Research using typical dustiness tests did not accurately indicate the mechanisms that generate dust and thus to consider that rotating drum tests simulates well common handling processes is nothing more than a hypothesis. Dustiness testing research could benefit in many ways from the rational followed using the Lubbock system. As Heitbrink et al. (1990) states, in many cases the mechanisms of dust generation in the dustiness tester differs from the mechanisms of dust generation in the process of interest. As a result the correlation between laboratory based dustiness measurements and field – personal exposure data is very poor. Thus, these tests need to be carried out on a more scientific basis. This will require fundamental research into the nature of dust generation by powder handling operations (Heitbrink et al. 1990).

The development of empirical models could also help the scientific progress in the development of better dustiness tests. Mathematical models that produce consistent dustiness results can be used as prediction tools and they can assist the standardization of the dustiness test methods. An attempt to produce a three-parameter multiplicative model for dustiness potential was developed by Breum (1999) for two test materials (bentonite and baryte) (Breum 1999). The model used

surface adhesion, time and mass of test material as the main parameters that can predict dustiness potential and it is described by Equation 3. An analysis of multiple linear regression was used to explain the variation in D_N from the three predictors (M_N, MT_N, SA_N) and the data for bentonite and barium sulphate were fitted to the model.

$$\text{(Equation 3)} \qquad D_N = \alpha \times M_N^{\beta} \times MT_N^{\delta} \times SA_N^{\lambda}$$

(D_N: dustiness for a given material; M_N: actual mass normalized to the maximum of mass under testing, 200g; MT_N: the median time normalized to the test period, 180 sec) and SA_N: surface adhesion (%); the α, β, δ, λ represents coefficients of the multiplicative model)

The model proved useful to predict dustiness, but it was sensitive to the type of test material (Breum 1999). For one material (barium sulphate) only one of the variables (mass) turned out to be statistically significant, while for the second material (bentonite) two variables (mass, median time) were considered significant predictors. The surface adhesion parameter was not significant for any of the two materials, however depending on the material in test, it is expected that surface adhesion is of importance to dustiness. The results suggested that a model to be significant needs to embody all the variables that influence the dustiness of a material, including rotation speed, air flow rate in the drum and humidity of the air delivered to the drum.

Research so far investigated the dustiness of powders, for a large variety of materials. In the mining industry however, dust is generated not only due to the handling of powders and for this reason work should try to identify the dustiness potential of coarser rock fractions as well. The development of dustiness tests did not consider the parameters of industrial processes that are liable for the generation of dust and for this reason it is difficult to make any direct associations between the two. Some previous studies (Cowherd & Grelinger 1992) tried to relate the dustiness results from various apparatus with airborne particulate concentrations (monitoring data), in order to investigate what category of dustiness test provides the best match. However different industrial processes might follow different dust generation patterns and thus the use of dustiness tests should fit the process characteristics, as not the same mechanisms will be liable for the production of dust. Therefore more than one category of test could be used depending on the process under investigation. For instance, if the dust emission of rock during tipping is investigated,

then it might be more appropriate to use a single drop test, than a fluidization or rotating drum test. Nevertheless prior to such correlations, the mechanisms that are liable for the production of dust in the various dustiness tests, as well as the dependency of their operating parameters upon dust yield should be identified.

The future steps of dustiness research need to work on a plethora of different sectors, so as to scientifically evolutes and standardizes. Understanding of the handling processes and the dust generation mechanisms within them, in depth investigation of the materials' physical properties, and test operating parameters and mathematical modelling practices for the prediction of dustiness potential should be some of the future trends for dustiness research.

3.4. Particle size measurement techniques for particulate matter and fine material

This section summarizes common particle size measurement techniques that are often used for the characterization of particulate matter. Particle size is considered the most important parameter for characterizing the behaviour of particulate matter (Griffiths et al. 1998). Many of the dust properties depend on particle size. The nature of the laws governing these properties may change with particle size (Hinds 1999). Legislation, occupational health and air quality standards are based on particle size. Therefore, particle size determination is fundamental so as to understand the dust properties.

In general mineral dust is in the micrometer size range and can exhibit complex particle shape. Shape is another important physical property of the particulate matter, which is closely related to particle size and the physical characteristics of the material that dust originates from. For example talc particles often exhibit an acicular or flaky shape, thus dust will possibly present a similar shape.

In the development of particle size measurement techniques it is usually assumed that particles are spherical (Hinds 1999). Particle size measurement techniques commonly use equivalent diameters for non spherical particles (Washington C. 1992). An equivalent diameter is the diameter of the sphere that has the same value of a particular physical property as that of an irregular particle. Some commonly used equivalent diameters are shown in appendix I.

Particle size measurement techniques can be grouped into two different categories. These are the direct particle size measurement techniques and the indirect methods. Direct measurement of particle size is achieved through microscopic observations (Hinds 1999). In contrast, indirect methods estimate particle size from the measurement of a property related to size. Common indirect methods include sedimentation techniques, impaction, mobility analysis and light scattering (Hinds 1999). A summary of common particle sizing techniques in accordance to their particle size range is shown in Figure 21.

3.4.1.Direct measurements of particle size

Microscopy permits direct measurement of the physical dimensions of the particles (Griffiths et al. 1998;Hinds 1999). It is useful not only for particle size measurement, but also for morphology evaluation (Allen 1997). For each particle a size is assigned based on its two-dimensional projected image. For a sphere this is the diameter of the circular silhouette. For irregular particles the use of equivalent diameters is made. The projected area diameter is commonly used (Hinds 1999). The projected area diameter is measured using sets of circles of standard area printed on an eyepiece graticule or reticule (Hinds 1999;Washington C. 1992). Hence, particles are grouped into ranges defined by successive circle sizes. A size analysis by number is normally performed than by mass (Allen 1997).

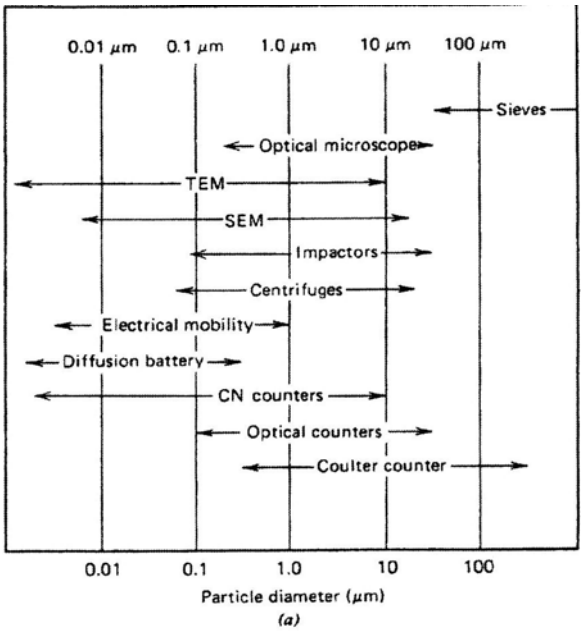

Figure 21: Particle sizing techniques and their particle range (Hinds 1999).

Optical microscopy and electron microscopy (scanning electron microscopy- SEM and transmission electron microscopy – TEM) is normally used in direct methods for particle sizing (European Commission 1996). Light microscopy can determine the measurement of particles in the size range from 3 μm to 1 mm. Scanning electron microscopy (SEM) from 20nm to 1 mm and transmission electron microscopy (TEM) from 2 nm to 10 μm (Allen 1997). Preparation of samples for microscopy observation has to be done with great care since the measurement sample is small and it is difficult to make it representative of a bulk (Allen 1997;Washington C. 1992). Undesired aggregates and agglomerated material might be present in the sample, which might need special treatment. Further, the sample needs to disperse uniformly as usually only a small region is examined (Allen 1997). Microscopy techniques are labour intensive, tedious, slow, require skills and careful preparation and are subject to operator errors or bias (Griffiths et al. 1998;Hinds 1999).

Nowadays direct particle size measurements have been revolutionized by the introduction of computerized methods of image analysis, which have become very popular (Hinds 1999;Washington C. 1992). Automated image analysis systems have virtually eliminated manual methods. Image analysis systems use scanning techniques for converting images into electrical signals, which are processed to yield data on the image (Allen 1997). The image may be from an optical or electron microscope or a photograph. Particle size and shape are interpreted from arrangement of continuous dark pixels on light background or vice versa. The computer can then calculate a variety of geometric diameters. The accuracy, speed and versatility are some of the advantages of the automated image analysis techniques. Automated image analysis works best with a high contrast image. If particle images have low contrast with fuzzy, grey edges, the size of the particles measured is controlled by instrument settings. In this case the sizing process must be calibrated to yield accurate results that are free from bias (Hinds 1999).

Automated image analysis systems could be considered more versatile than conventional microscopy techniques, nevertheless there are several barriers to be taken under consideration for the use of this technique for dust particle size analysis. Hence, the accuracy of the measurement depends on the software – user capabilities. Old versions of image analysis software require a greater expertise from the user, who will need to adjust parameters, such as image's contrast, to a level that the measurement can be taken without eliminating essential characteristics of the sample. Most of the time, mineral dust consists of several particles with different sizes ranging from a few microns to up to a few hundred microns. Scanning electron

photomicrographs, or microscopy photos might not be able to present clearly the small particles and this will eventually introduce errors to the measurement. The quality of the initial data (photographs, SEM photomicrographs), as in the case of conventional microscopy techniques depend on the accuracy of the sample preparation method that should represent well a bulk sample and it should avoid the presence of aggregates – agglomerates. For all the above reasons, automated image analysis is not considered an appropriate method for dust particle size analysis.

In the past few years automated image analysis has been evolved by combining the progress in microelectronics, such as frame grabbers with advanced image analysis algorithms (Xu and Di Guida 2003). This new technological trend is called dynamic image analysis (DIA) (Figure 22). The sample is injected between two hydrodynamic sheath flows (wet process), which cause the sample to narrow and become planar. This way the sample is retained at the plane of focus of the instrument. Particles are dispersed homogeneously in the medium and circulated constantly. Particles are imaged individually and images are stored (Malvern Instruments 2005a;Xu & Di Guida 2003). Up to 300,000 particles can be measured. The size range of dynamic image analysis varies between different instruments, but as a general rule it can range from sub-microns up to a few thousand microns (Malvern Instruments 2005a;Xu & Di Guida 2003). Apart from particle size, particle shape and other morphological parameters can be obtained (Malvern Instruments 2005a).

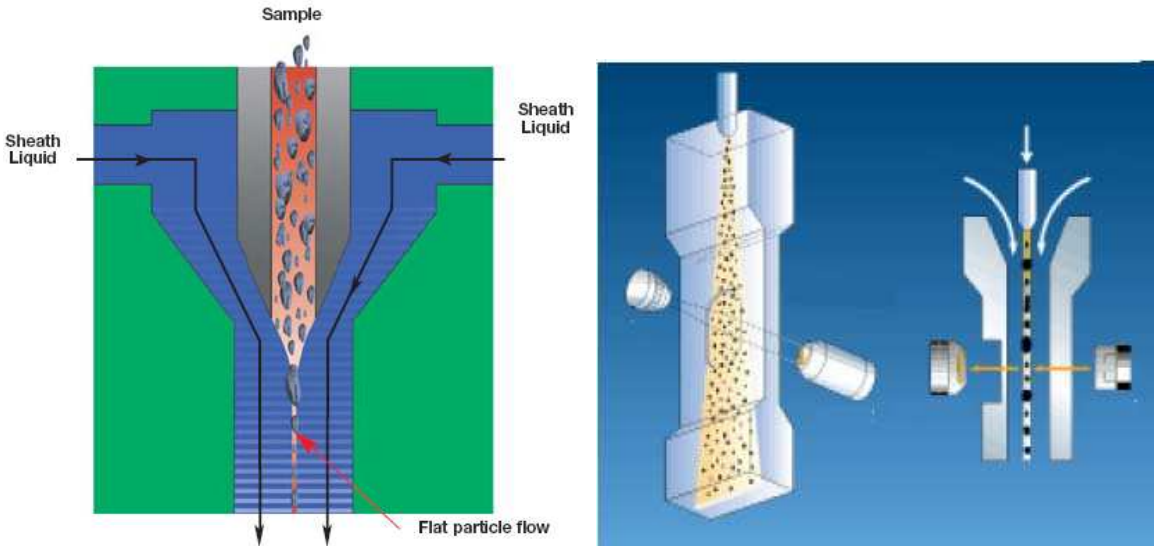

Figure 22: The instrumental set up and process of the dynamic image analysis method (Malvern Instruments 2005a).

Dynamic image analysis as all microscopy based techniques measures the two-dimensional projected area diameter of particles. In order to achieve accurate particle size and shape analysis results, the particles need to be favourably oriented with the flow of the dispenser, adopting their most mechanically stable state (Malvern Instruments 2005a). If the orientation of particles changes during measurement, then this will affect the particle size distribution results introducing errors. For example acicular shaped particles or flakes, might produce large differences in particle size distributions if the particles do not retain the same orientation during measurement. For very fine particles the dispersion of the sample should be efficient, so as to break up any aggregates or agglomerates present. When samples consist of a wide particle size distribution, then the focusing on the very fine fractions (a few microns) might produce some fuzzy images of the particles and thus the particle size of them could be underestimated or overestimated. The dynamic image analysis system is a useful apparatus when particle shape characterisation is required.

3.4.2.Indirect methods for measurement of particle size

During the years several different indirect methods have been developed for the estimation of particle size. Indirect methods determine the particle size through measurement of a property related to size. The most common methods used for particle size measurements of the particulate matter are sedimentation, impaction, mobility analysis and light scattering. The particular characteristics of each one of these methods are presented on the following paragraphs.

3.4.2.1. *Sedimentation techniques*

Sedimentation methods rely on gravitational settling to measure particle diameter. Settling of the particles depends on the difference in specific gravity between that of the settling media (i.e liquid, air) and the particle material (European Commission 1996). Sedimentation methods follow the principles of Stoke's Law (Allen 1997). Sedimentation practices are used for particle size measurement purposes in general and some of the most common techniques in use are the Andersen pipette, sedimentation balances, photosedimentation, x-ray sedimentation and centrifugal sedimentation. These techniques have been reviewed elsewhere (Allen 1997;Washington C. 1992).

The particle size of particulate matter by sedimentation methods is estimated using instruments such as the sedimentation cell and elutriators. In the sedimentation cell the particulate matter is introduced into a small volume (smaller than 1 cm^3) and particles are illuminated through windows by an intense light beam (Griffiths, Mark et al. 1998;Hinds 1999). The particles are observed by a horizontal microscope in a direction perpendicular to the light beam (Griffiths et al. 1998;Hinds 1999). The time taken for particles to settle through a well defined distance between two lines of reference is recorded and used to determine particle settling velocity and diameter. The sedimentation cell technique allows the determination of the aerodynamic diameter. The method is appropriate for particles with an aerodynamic diameter in the range of 0.3 to 5 μm (Griffiths et al. 1998;Hinds 1999). Brownian motion of very fine particles (below 1μm) causes significant variation in the measured settling velocity and such particles might often be found out of the field of view (Hinds 1999). For larger particles (5 – 50μm) the aerodynamic diameter can be measured using a settling tube. This is a vertical glass tube (diameter 7 mm, length 0.3-0.8 m) illuminated along its axis by a low power laser (Hinds 1999).

Elutriator relies on particle settling through a fluid flow to determine their diameters and they can be either vertical or horizontal. Horizontal elutriators are commonly used for particle sizing. Two flow streams are used: a clean air stream and the aerosol stream. A horizontal laminar flow is established in a horizontal duct of rectangular cross-section. Aerosol is introduced as thin stream along the upper surface of the duct and particle settling occurs perpendicular to the gas streamlines. These devices produce satisfactory results for rough estimation of large particles (above 1 μm), whereas smaller particles are completely removed by the laminar gas flow. The operational characteristics of elutriators make them suitable to be used for respirable dust sampling, although to achieve a precise cut off size is difficult. Particles of different sizes, settle at different rates and locations along the duct floor (Griffiths et al. 1998;Hinds 1999), and this way it is possible to determine particle settling velocity and particle diameter. An elutriator spectrometer utilizes under similar principles (Hinds 1999).

Sedimentation techniques for particle sizing purposes are considered labour intensive and tedious, provide rough estimations of particle sizing, and they require careful handling during experimentation. However they could be consider as an alternative collections dust system or as occupational dust sampling devices, as they require low capital cost and they are easy to construct.

3.4.2.2.*Inertial techniques*

Inertial impaction techniques have been extensively used by aerosol scientists for the measurement of particle size distribution by mass. Inertial systems measure the aerodynamic diameter of the particulate matter (Burgess et al. 2004;European Commission 1996).

Cascade impactors are often used for particle size analysis purposes. All inertial impactors operate on the same principle. The dust or aerosol stream is passed through a nozzle and directed onto a flat plate (impaction plate). The impaction plate deflects the flow of the stream lines on a 90^{o} bend. Particles whose inertia exceeds a certain value collide on the flat plate, whereas smaller particles follow the streamlines (Hinds 1999). A series of impaction stages are used to produce a size distribution (Mitchell and Nagel 2004). The mass of the particles collected on the impactor plate and of those collected on the back up filter are determined by weighing them before and after sampling (Griffiths et al. 1998;Hinds 1999). Each impactor stage separates the mass of particulate matter into the particles larger than the cut off size and the particles smaller than the cut off size. The impactor stages are assumed to have the ideal cut off sizes, which implies that the mass of oversized particles testing through each stage equals the mass of the collected undersize ones (Hinds 1999). Nevertheless, this cannot always be true and if it is not, it can cause distortion to the particle size distribution. Particles are assumed to stick to the impaction plate surface when they strike it. However, particles may adhere and subsequently blow off, or they might bounce. If bouncing of particles takes place, then some of the dust mass might end up in smaller size range (Friedlander 2000;Hinds 1999). Additionally, particles may deposit in the passage ways between stages, resulting to loss of material. Finally, as particles deposit on the impaction plate, they form conical mounts of particles, which can influence the flow geometry and the cut off size (Friedlander 2000;Hinds 1999). All the above drawbacks reduce the efficiency of cascade impactors to produce accurate and reproducible particle size analysis results.

Time-of-flight instruments provide real-time, high resolution measurements of aerodynamic particle size (0.5 to 20μm) and size distribution over a wide size range (Hinds 1999;Mitchell & Nagel 2004). Real-time aerodynamic particle sizers separate particles on the basis of the inertia. Particles are accelerated through a well defined flow field (Burgess et al. 2004). Particle time-of-flight is measured across a split laser beam, and it is subsequently converted to aerodynamic diameter through a function derived from calibration with particles of known diameter (Griffiths et al. 1998).

When the particle passes through the first laser beam, it creates a pulse of scattered light detected by the photomultiplier tube. The same happens when the particle meets the second beam. For the time interval between the two pulses, the average velocity of the particle as it passes through the timing zone is calculated (Hinds 1999). Two of the most well know real time particle sizers are the TSI Aerodynamic Particle Sizer and the API Aerosizer (Griffiths et al. 1998;Petters 2003). Coincidence errors may occur as a result of incomplete separation of particles (Burgess et al. 2004). More information on inertial techniques can be found elsewhere (Burgess et al. 2004;Griffiths et al. 1998;Hinds 1999;Mitchell & Nagel 2004). Several limitations exist in time-of-flight instruments that are mainly attributed to particle motion, as it is outside the Stokes region due to operation under high velocities. Particle related properties such as density and shape and apparatus disadvantages reduce the efficiency of particle size analysis. Particles of different density, but of same aerodynamic diameter and settling velocity can have different lag times. Therefore a particle with higher density will have a lower velocity in the timing region, which will be interpreted by the instrument as a larger particle (Hinds 1999). Also non-spherical particles, they go through the timing region faster and thus the apparatus consider them of smaller in size. When a particle arrives just after one that has not completed its time-of-flight, then instrument's electronics might be confused and interpret these two particles of smaller size. Finally when the instrument operates at a pressure different to the one calibration took place (i.e ambient pressure), then misinterpretation of particles' velocities can take place, which will eventually affect the particle size distribution results (Hinds 1999).

3.4.2.3.*Electrical mobility analysers*

Electrical sensing zone instruments are commonly used for the estimation of aerosol and particulate matter particle size. Differential mobility analyzers (DMA) are used to determine the particle size of particulates below 10μm. Main disadvantages of these instruments are the relative slow response time and the complicated handling (Hinds 1999). These instruments would be unsuitable for particle size measurements of mineral dust, which commonly consist of particles above the cut off size of 10μm.

Instruments like the Coulter Counter series can be used for particle sizes ranging from 0.3 to 200μm and they can be more appropriate for the measurement of dust. They make use of electrical resistance to measure particle size distributions in liquid suspensions (Griffiths et al. 1998;Xu & Di Guida 2003). Particles are forced to pass

through a small orifice (10 to 400μm), across which an electrical current is maintained by placing electrodes in the liquid on either side of the orifice (Hinds 1999). Due to different resistance of the particles to that of the liquid, a momentary variation in the current is created and displaces the electrolyte. This change is proportional to the volume of the particle and can be converted into a measure of the particle diameter. Accumulation of these data can produce a size distribution of the particles weighted by volume (Griffiths et al. 1998). However the range of particle sizes is limited to 2-40% of the orifice diameter. Therefore polydispersity might require the use of a variety of different aperture tubes to be used. Furthermore, particle shape, porosity, air bubbles or dirt might affect the particle size measurements (Hinds 1999).

3.4.2.4.*Light interaction techniques*

Light scattering provides a dynamic and sensitive tool for the determination of particle size. Light scattering instruments may be divided into four systems which are widely used. These are the optical particle counters, the laser diffraction analysers, the laser doppler techniques and the light intensity deconvolution analysers (Griffiths et al. 1998). They are all based on the principle that even a very small particle (submicron size) produces a detectable scattered light signal (Hinds 1999).

Optical particle counters (OPC) measure the quantity of light scattered by individual particles as they pass through a beam of intense monochromatic or white light. The relationship between the intensity of scattered light and particle size is calculated by applying Mie theory (Griffiths et al. 1998;Xu & Di Guida 2003).

A range of instruments based on the principle of laser light diffraction (low angle laser light scattering) has been developed through the years. Laser diffractometers are field scattering systems that determine the size distribution of a population of particles simultaneously during the course of a single measurement sweep (Griffiths et al. 1998;Xu & Di Guida 2003). The principle of the laser diffraction method is also described by an international standard (ISO 1999). The interaction of light is converted to particle size by applying either the Fraunhofen approximation or the Mie theory (ISO 1999). The Fraunhofen and Mie approximations used by light scattering techniques are discussed further in Chapter 4. Typical examples of modern and well established laser diffraction instruments include the Mastersizer series of Malvern

instruments (Malvern Instruments 2005b). More information on the laser diffraction method is given in Chapter 4.

Laser phase-Doppler analysers are non-invasive systems and can be utilized to obtain simultaneous information about particle size and velocity. Laser intensity deconvolution analysers are single-particle counters where the particle size is estimated by measuring the absolute intensity of light scattered by particles traversing a focused laser beam (Griffiths et al. 1998).

A disadvantage of light-scattering instruments is that the scattering may be sensitive to small changes in the refractive index, scattering angle, particle size and shape (Hinds 1999). The advantages – disadvantages of light scattering techniques are discussed in detail in Chapter 4.

3.4.2.5.*Alternative particle sizing techniques*

Apart from the particle size techniques that have been presented in the previous paragraphs, a new trend has been observed where more than one sizing methods are combined together to produce a new one, which fits best the research circumstances and objectives.

For example, regarding the size classification of airborne particles Madler et al. (1999) produced a new device that collects and classifies (aerodynamic size classification) the dust generated under lab-scale simulation of mechanical released processes (i.e re-suspension, powder handling, break up of solids). The technique combines an elutriator, a centrifugal classifier and a conventional cascade impactor (Madler et al. 1999). The release process takes place within a vertical elutriator, where the airborne particles are separated from the non-airborne material. The airborne fraction is subsequently classified in situ in the size range between 0.1 and 100 μm by a combination of a centrifugal classifier and a conventional cascade impactor (Madler et al. 1999). The in situ aerodynamic classifier could also be described as a dustiness test due to its intention to simulate mechanical release processes. The main difference between the presented technique and common dustiness tests is that the latest do not report on size analysis in the size range above 20μm (Madler et al. 1999).

Another example of an alternative particle sizing technique comprises a new sizing technique for fine powders dispersed in air, which combines a boiling method with a DMA (differential mobility analyser) – CNC (condensation nucleus counter) system. The boiling method enables particle aggregates to break up into their system. This method is suitable for fine dry powders with coagulated particles, whilst good results were obtained for non-spherical particles as well (Kousaka et al. 1998).

These techniques are commonly developed to fit the requirements of specific projects. The combination of different particle sizing techniques aims to eliminate the deficiencies of individual methods. However this is not always possible, making control upon the parameters that introduce errors to results complicated.

3.4.3. Conclusions on particle size measurement techniques

A variety of particle size measurement techniques for the characterization of particulate matter have been reviewed. Depending upon the research objectives different methods might be used to fulfill the requirements. Particle sizes are usually viewed in terms of geometrical (i.e surface, volume) or behavioral (i.e sedimentation) equivalence (Burgess et al. 2004). Quite often particulate matter is classified using the aerodynamic equivalent diameter, for example when human exposure or air quality is the main research focus points. Hence, inertial techniques are commonly used.

Light interaction techniques have recently become very popular, as they are easy to use, quick, accurate and have good reproducibility. No matter which technique has been chosen for particle size analysis, caution should be taken during the sampling and preparation process, as these are often a source of error and concern (Allen 1997;Burgess, Duffy et al. 2004).

There is a need for standards for calibration of all sizing methods (Burgess et al. 2004). These should include both size and parameters affecting the classification process like the refractive index or even particle shape. These standards should be sensitive, accurate and reproducible (Burgess et al. 2004). The size distribution of anisometric particles depends strongly on the particle shape and it is essential to study the effect of particle shape on size measurements. Particle shape also influences calibration of almost all particle sizing instruments (Bumiller et al. 2005;Endoh et al. 1998). To control and eliminate the effect of particle shape on particle size measurements it was suggested the development of an instrument,

which will combine the image analysis and the light scattering methods (Burgess et al. 2004).

3.5. Summary of Chapter 3

A large number of dust characterization techniques have been presented that focus into different critical sectors of particulate matter research. In addition, reference is made to methods that can potentially enhance common research procedures. Compositional analysis techniques, dustiness testing, particle size classification methods are some of the mainstream particulate matter characterization steps. This project aims to identify the potential of a range of rocks to generate dust under different processes, therefore under different mechanisms. The experimental procedure followed, incorporates techniques from each characterisation sector presented in this chapter and for this reason it was considered critical to review techniques and finding of other researchers. Discussion of the advantages and disadvantages of the reviewed characterisation techniques has already identified the methods that could be used for the characterisation of mineral dust. Chapter 4 presents in detail the experimental route and techniques utilised for the completion of this study. The selection of these techniques was based upon the literature findings presented in this chapter.

Chapter 4. Experimental Procedures and Analytical Techniques

4.1. Introduction

This chapter presents the experimental processes and analytical techniques that have been used to assess the propensity of different ores to produce dust. The methodology followed aimed to investigate the mineral dust generation potential that resulted from different fracture mechanisms. Experiments were performed on a variety of rock types including limestone, talc, lamproite, iron ore and copper ore. The dust generation process was characterised by a series of analytical techniques including mineralogical characterisation, dustiness testing and particle size analysis. Both qualitative and quantitative analytical methods have been utilized and they are described in detail in the following sections.

4.2. The experimental procedure

Previous research (Arup Environmental 1995;Mohamed et al. 1996), concluded that common industrial processes such as the transport of material with conveyors, tipping processes, the use of haulage roads, comminution and others have a propensity to generate dust by two main mechanisms, impact and abrasion-attrition. These two mechanisms can act individually or in combination. Therefore, for the purposes of this project, an experimental methodology was established, with the aim

to improve the understanding of how these two mechanisms influence the production of dust/fines.

The structure of the experimental methodology adopted is shown in Figure 23.

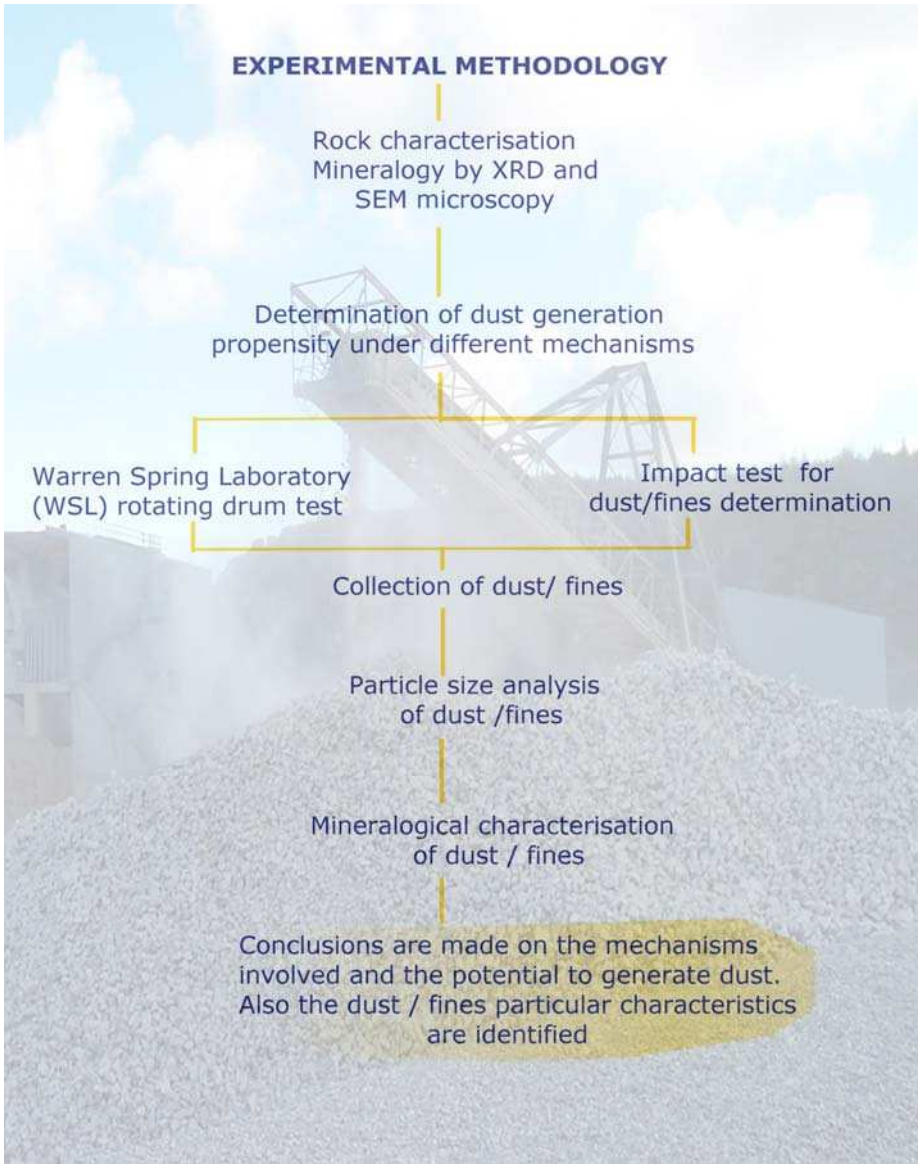

Figure 23: Schematic diagram of the experimental methodology followed by the project.

Firstly, the mineralogy of the primary rock test samples was identified. The mineralogical characterisation took place both by x-ray diffraction analysis and scanning electron microscopy (SEM). In addition, the mineralogical composition of the Kennecott copper ore and Argyle lamproite was quantified using the mineral liberation analyser (MLA) technique. (Jk Technology Centre 2005) Determining the mineralogy of the primary rock samples was of great importance for the following

steps of experimental work, because it provided the essential compositional analysis background and thus allowed comparisons to be made with the dust mineralogy results. Detailed information on the mineralogy related analytical techniques are given at the appropriate paragraphs later in this chapter.

Following the mineralogical characterisation two different tests were employed, which aimed to simulate the mechanisms found in operations related to minerals handling and processing. These were the last version of the Warren Spring Laboratory rotating drum test (HSE-WSL test) and the impact test. The latter comprised a modified version of the JK drop weight test. The two tests also attempted to quantify the dust produced, whereas the dust generation process was investigated for a range of operational parameters and test fractions. The rotating drum test simulated processes where the abrasion-attrition mechanism is dominant, such as transfer of materials by conveyor belts, haulage roads, mixers, grinders and others. On the other hand, the impact test simulated industrial applications where the major mechanism is impact, like processes that involve drop from heights (i.e transfer points, stockpiling and others). Further details on the testing procedure of each test can be found at subsequent paragraphs in the chapter.

The particulate fraction was collected separately from each test sample and testing procedure (WSL test or impact test), and additional analysis was carried out. Particle size measurements and advanced mineralogical studies on the dust fraction comprised the next step of the experimental methodology. The particle size of both the coarse fraction of the sample and the particulate matter was determined and it was compared with the initial parameters of the test sample. Particle size analysis occurred by sieving for the coarse fraction and by laser diffraction for the dust/fines fraction. A more detailed description of the particle sizing techniques employed is presented in the following paragraphs.

The final step of the experimental methodology involved the mineralogical characterisation of the particulate fraction. Once more, this was done by x-ray diffraction analysis and scanning electron microscopy (SEM). The mineralogical composition of dust collected by the Kennecott copper ore and the lamproite ore was quantified using the mineral liberation analyser (MLA).

The results obtained through the various experimental steps were analysed and conclusions were made upon the potential of the involved mechanisms to generate

dust, as well as the particular characteristics of the dust/fines fraction. The same experimental methodology was followed for all ores including the limestone, talc, iron ore, lamproite and copper ore.

4.3.Mineralogy – Analytical techniques and procedures

The mineralogy of the primary rock samples (prior to dustiness testing) and the dust was identified by X-ray diffraction and scanning electron microscopy. The principles behind each analytical technique and the procedures followed are presented in the following paragraphs.

4.3.1.Mineralogy by X-ray diffraction (XRD)

A mineralogical characterization of the bulk mineral samples took place using the X-ray diffraction technique. X-ray diffraction (XRD) is a basic tool in the mineralogical analysis of the rock samples. In this project the Hiltonbrooks diffractometer was used, which incorporates the following parts:

- A Hiltonbrooks 3kW generator model DG3 - *(operated at 40kV, 20mA)*
- A Hiltonbrooks detector control module
- A Hiltonbrooks step motor drive module

- A Philips PW 1050 goniometer and proportional detector
- A Seifert copper long fine focus X-ray (Cu radiation at 1.5406 Angstroms)
- A Sietronics curved graphite monochromator
- A 35 position sample holder

A schematic representation of the typical geometry of a diffractometer is shown in Figure 24. X-rays are produced at the Seifert X-ray tube, by bombardment of a metal anode, by high energy electrons from a heated filament copper is used as the target element (anode) of the Seifert X-ray tube. The resulting radiation emerges from a thin, beryllium window. The X-rays are first collimated to produce a subparallel beam. The amount of divergence is controlled by the divergent slit. The divergence beam is then directed at the sample, which is motor driven to rotate at a regular

speed in degrees per minute (Hardy and Tucker 1988).The scan rate employed using the Hiltonbrooks diffractometer was of 2 degrees 2-theta per minute, whilst the step size employed was set at 0.05. The Hiltonbrooks diffractometer utilizes the Sietronics 'siehilt' automation software or Hiltonbrooks HBX data collection software (set by default).

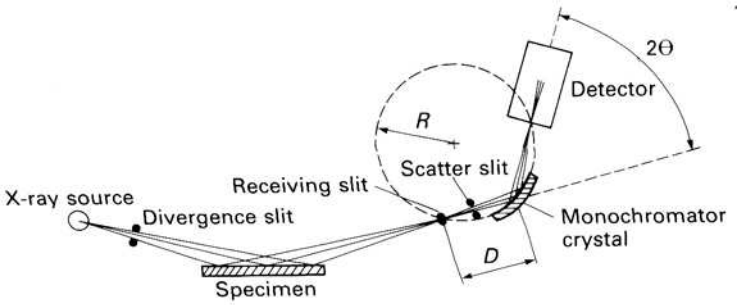

Figure 24: Schematic representation of the typical geometry of a diffractometer (Hardy & Tucker 1988).

Data collected during the measurement steps are extrapolated to the accompanying software and processing of the XRD trace takes place to identify the different mineral phases. The scan processing software used was the Diffraction Technology 'traces v.3' scan processing software.

An XRD analysis of whole rock sample at scan runs from 5 degrees (2-theta) to 65 degrees (2-theta) was conducted. A representative sample (around 150g) of the different rock materials was produced using a riffle, and was then subsequently ground using a mortar and pestle to produce a fine powder. The fine powder sample was further riffled using a rotary micro-riffle to produce a representative small sample used for the preparation of the analysis specimen. For the particulate matter produced by the HSE-WSL test, and the dust/fines fraction produced by the impact test, commonly there was no need for any special sample preparation technique, although sometimes the dust collected from the HSE-WSL test was of very small amounts. Where adequate quantities of sample were available a cavity mount was produced. Hence, the sample was packed in a cavity mount holder. However, when only a small amount of sample was available, a smear mount was prepared by smearing the sample with acetone onto a glass slide. Commonly between five to ten samples of the different rock materials and triplicate samples of the dust/fines fraction were prepared for XRD to make sure that the obtained XRD traces were

reproducible and accurate. Results obtained for the different test samples are presented in Chapters 5 to 9.

4.3.2. Mineralogy by scanning electron microscopy and mineral liberation analysis

Mineralogy by scanning electron microscopy took place using the Mineral Liberation Analyzer system (MLA), which incorporates the FEI Quanta 600 scanning electron microscope (SEM) and EDAX energy dispersive X-ray analysis system. A software suite developed at Julius Kruttschnitt Mineral Research Centre (JKMRC) is combined to the system to provide the facility of a mineral liberation analysis. Scanning electron microscopy was used as a qualitative and quantitative analysis tool, whilst investigations took place for the ores and the particulate matter.

The scanning electron microscope by itself was used for qualitative observations of the particulate matter samples. Parameters like particle shape, homogeneity in terms of particle size and mineralogy of the dust particulates were determined using both the back scattered electron (BSE) and secondary electron (SE) imaging modes. Additional elemental analysis information was made available through the energy dispersive X-ray analysis system (EDAX function). The specimens were used either as they are or mounted in epoxy resin. Results obtained using the SEM, are presented in chapters 5 to 9.

4.3.2.1.*Mineral liberation analysis*

As it has been noted in the previous paragraph, the MLA system comprises a specially developed software package that can provide mineral liberation analysis data. The on-line program of this software package controls the SEM, captures sample images, performs image analysis and acquires energy dispersive X-ray microanalysis spectra unattended. Up to 100 images (containing up to 10,000 particles) can be taken for each sample block. Within one batch up to 14 sample blocks (30mm diameter) can be measured. The MLA off-line program processes all the raw data (particle images and X-ray data) and produces particle mineral maps as well as bulk liberation data (Gu 2003). The measurement of the samples using the Mineral Liberation Analysis system was performed by qualified technical staff of the

School of Chemical, Environmental and Mining Engineering of University of Nottingham.

For this project, the liberation analysis application aimed to identify and quantify the mineralogical differences between the bulk feed samples and the dust/fines fraction, for both principal testing procedures (WSL test and impact test). Analysis was performed for only two of the ores, which exhibited a greater variety of minerals. These were the Kennecott copper ore and the Arglyle lamproite. Results reveal any particular patterns and characteristics of the dust generation potential of the ores under different mechanisms. The mineral liberation analysis has not been used in the past for quantitative mineralogical analysis of mineral dust and therefore experimentation with the copper ore and the lamproite aimed additionally to justify if the technique could be applicable to this research area.

The sample in the form of fine particles (i.e dust or <150μm of bulk feed sample) was mounted in epoxy resin, and polished to produce a polished block. The epoxy resin block was prepared by mixing an epoxy resin with a resin hardener in a ration of 7.5:1 by volume. The epoxy resin was subsequently poured to the block cavity and the fine particles were added and mixed all together. For the bulk samples a representative fraction was obtained using initially a riffle to reduce its amount to a few tenths of grams and subsequently a micro-riffle to produce a sample of a few grams. The whole quantity of the particulate matter was used during the preparation of polished blocks. Sample blocks were coated with carbon before presented to the system. The first step of the process was to set the scanning electron microscope conditions such as the accelerating voltage, the alignment of the gun, the spot size and X-ray parameters, the contrast and brightness in appropriate levels that will allow a clear picture to emerge. All these parameters are controlled through the software of the Quanta 600 scanning electron microscope (SEM)

After the SEM parameters were established, the automated de-agglomeration function was used to detect any agglomerated particles, which were separated accordingly. Particle shape parameters used by the de-agglomeration function evaluated the state of particles and if needed went through the de-agglomeration process. The de-agglomeration process is of great importance as it assists the minimisation of biased results. Prior to de-agglomeration using batch processing, the de-agglomeration parameters need to be calibrated. Using the ParticleTool2000 software program, frames to be included in the de-agglomeration calibration stage are selected and saved. Subsequently, by selecting the de-agglomeration option from

the software menu, the previously selected frames are de-agglomerated. The particles are inspected to make sure that all of them have been de-agglomerated and if not the process is repeated. Once the de-agglomeration parameters have been adjusted correctly, then the entire file can be de-agglomerated by batch processing. Inspection and manual de-agglomeration are the last steps of this process to confirm that all particles have been de-agglomerated successfully (JKMRC 2005a). Mineral phase boundaries within a particle were determined and outlined by regions of grey levels by the image segmentation function. Using the back scattered electron channel, averaged grey values were related to certain minerals of unique average atomic number (AAN). Then, the MLA system performs one X-ray analysis for each grey level region in a particle. For minerals with the same average atomic number are handled using the particle X-mapping method (Gu 2003;JKMRC 2005c). The MLA software utilizes seven basic measurement modes, which correspond to different sample types and mineralogy related requirements. More information on the different measurement modes are given elsewhere (Gu 2003;JKMRC 2005c).

Table 17: List of data generated by XBSE measurements (JKMRC 2005b)

Data obtained from XBSE measurements	
Colour- keyed particle images	✓
Modal mineralogy	✓
Particle density distribution	✓
Calculated assay	✓
Elemental distribution	✓
Mineral association	✓
Mineral locking data	✓
Mineral grain size distribution	✓
Particle size distribution	✓
Grade recovery data	✓
Mineral liberation data	✓

The measurement mode used within this research work was the Extended BSE liberation analysis (XBSE). The XBSE method is a more advanced method that collects an X-ray spectrum for each mineral grain. Hence the XBSE measurement can discriminate between common mineral pairs which have similar average atomic numbers. The data generated by the XBSE method are shown in Table 17 (JKMRC

2005b). An overview of the data processing steps followed by the XBSE method is presented in appendix I.

4.4.The Warren Spring Laboratory (HSE-WSL) test

As has been presented in section 4.2 the Warren Spring Laboratory rotating drum test (HSE-WSL) was used to assess the dustiness of the test samples. The HSE-WSL dustiness test was developed by Warren Spring laboratory with funds made available by the UK Health and Safety Executive (1992).

The selection of this particular test was due to several reasons. First of all, the HSE-WSL method is very well documented and the Health and Safety Executive (U.K.) recommends it for the gravimetric determination of dust. This project investigated the potential of different rock samples to generated dust. The rolling action of the tumbling mill was thought to simulate well many processes of mineral workings, especially the ones that involve mechanisms of abrasion and attrition, like conveyor belts, mixers, grinders, haulage roads, sieves and others. Also, apart from the gravimetric determination of dust, the HSE-WSL test classifies dust in the health related fractions defined by the ISO-CEN working group. Finally, the size of the rotating drum test permits the use of a range of material fractions (granular, powders etc.) and masses, whereas operational parameters can be altered and their effect can be investigated.

The main difference of this method in comparison to the old WSL test, was the adoption of a different particulate size selection stage, which separated and captured the particulates into the health related fractions (Lyons et al. 1992). The new sampling procedure aims to assist occupational health related research to get a better understanding of the adverse implication of generated dust. The results obtained through experimentation with the various materials used in this study and presented in Chapters 5 to 9, will identify any deficiencies of the sampling stage. Nevertheless, the objective of this project does not include the characterisation of dust with relation to human health impacts, therefore analysis and presentation of such results are presented only as a reference source.

4.4.1. Description of the HSE-WSL test method

The HSE-WSL dustiness test used in this project was constructed within the workshops of the School of Chemical, Environmental and Mining Engineering of University of Nottingham (Figure 26). The HSE-WSL drum dustiness apparatus was constructed and commissioned following the specifications and protocols established in the literature (Health and Safety Laboratory 1996;Lyons and Mark 1994). The apparatus comprises of two sections; the dust generator and the dust sampling method. Detailed information on the rotating drum test, the testing procedure and the reporting of the results is given in the following paragraphs.

4.4.1.1. *The dust generator*

The dust generator comprises a stainless steel drum of 0.3m diameter with conical ends. The length of the cylindrical drum body is 0.228m and the length of each conical end section is 0.13 m. Eight vanes are eccentrically mounted on the inside of the cylindrical body of the drum, to promote the lifting and falling action on the material (Figure 27). The drum rotates on a pair of rollers mounted on a support frame. The rotation of the rollers and hence drum are driven by a variable speed motor, normally set at 30rpm. A PLC (programmable logic controller) controller was installed and programmed to allow changes of the rotation speed of the drum. The maximum level of rotation speed allowed by the motor was set to 35 rpm. Air is drawn through the drum, typically at a flow rate of Q=40 l/min. The volume of air sampled is measured by a calibrated airflow meter. The dust generated by the tumbling material and entrained in the airflow is captured by a series of three filters positioned in series and inline with the air exhaust outlet to the drum. A schematic representation of the HSE-WSL dustiness test is shown in Figure 25, whilst a photo of the apparatus and the inner of the drum can be seen in Figure 26 and Figure 27.

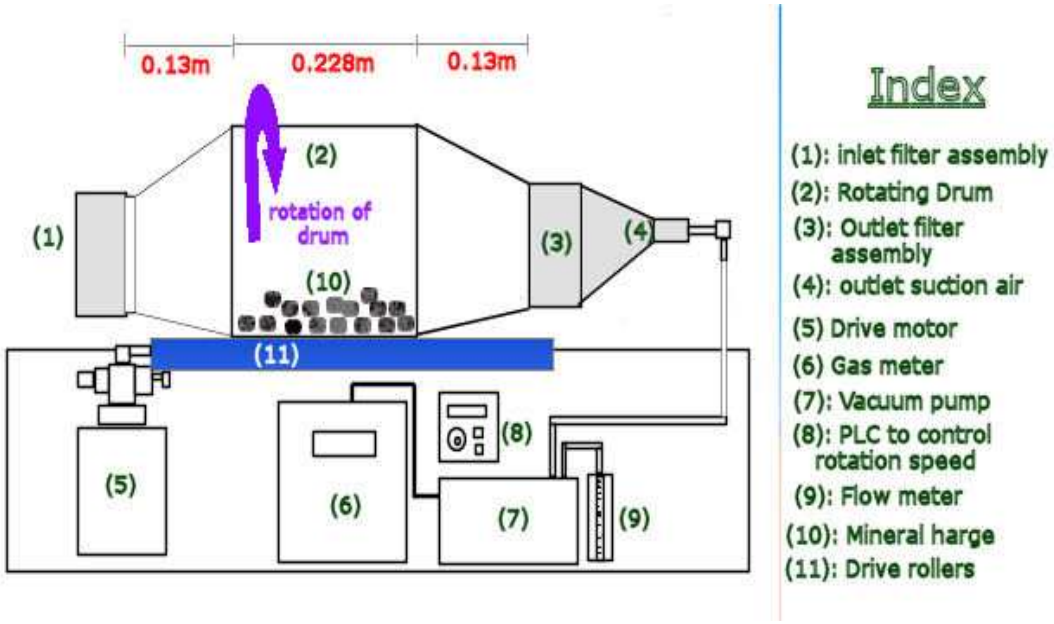

Figure 25: Schematic representation of the HSE-WSL rotating drum test and components (Lyons & Mark 1994).

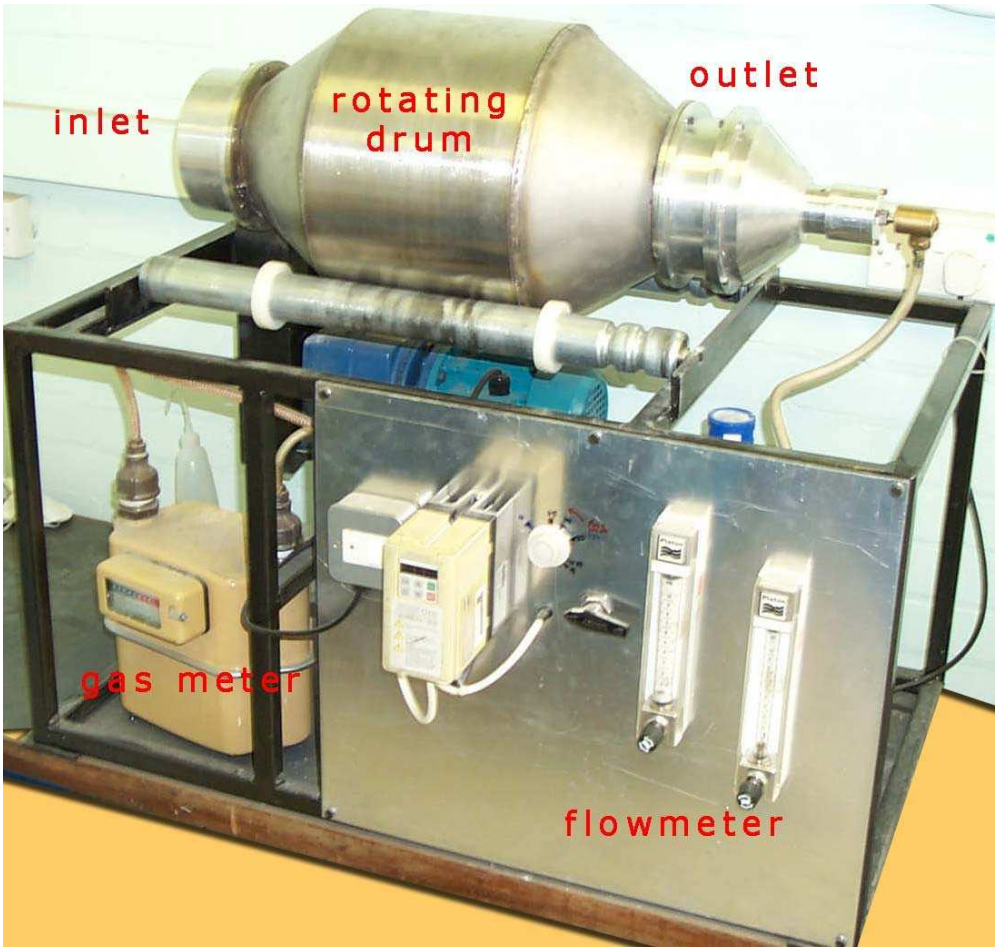

Figure 26: The HSE-WSL rotating drum apparatus constructed within the workshops of the School of Chemical, Environmental and Mining Engineering of University of Nottingham.

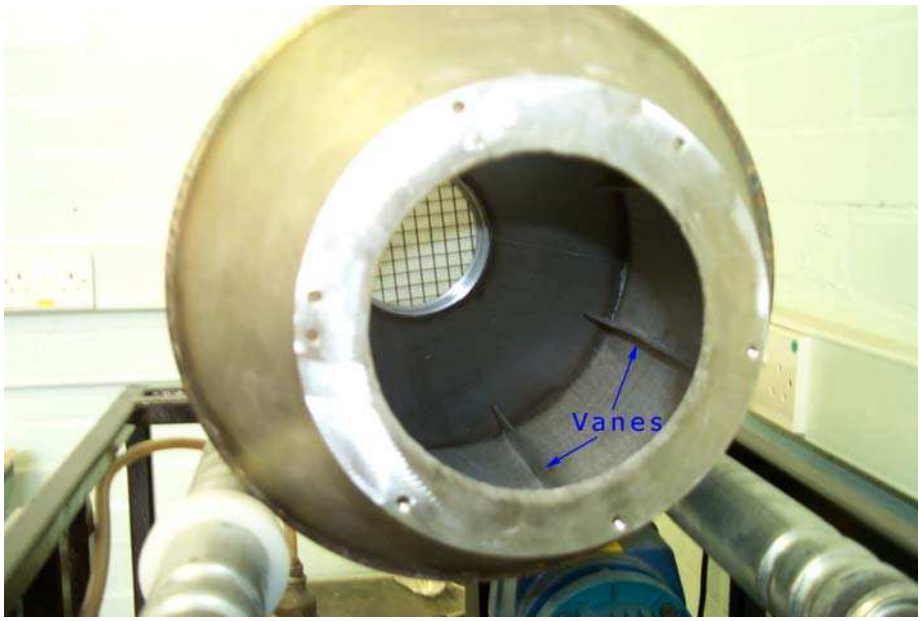

Figure 27: The inner surface of the drum. Vanes are attached on the drum walls. The diameter of the drum is 0.304m.

4.4.1.2. *The dust sampling procedure*

A three-stage dust sampling system consisting of two pre-weighed size–selective foam filters and single fibreglass back up filter was employed to collect the airborne particulates (Figure 28). The two size-selective filters are cylindrical plugs (0.15m diameter, 0.025m thick) of 30 and 90 pores per inch (ppi) polyester foam. These porosity sizes were chosen as previous studies have confirmed that they successively collect the thoracic and respirable fractions, respectively, as defined by the International Standards Organisation (ISO) (Health and Safety Laboratory 1996;ISO. 1995;Lyons & Mark 1994). The different porosities of the foam filters can be seen in Figure 29. A glass fibre filter (0.15m diameter, GF/A Whatman filter, 0.6μm median pore size) was used to collect the particles that penetrate the 90 ppi foam filter. The mass of collected dust was determined by weighing the two foam and glass fibre filters before and after the test. The weight measurement precision was kept to 4 decimal points. An identical set of foams and filter was positioned at the inlet of the drum, which served as a control by taking account of the weight changes due to the passage of air through the foams and filter (Health and Safety Laboratory 1996).

4.4.1.3.*The HSE-WSL rotating drum apparatus testing procedure*

Prior to the performance of each test the inside of the rotating drum was thoroughly cleaned first with a brush and then with acetone to remove any fine material deposited on the drum walls. A series of representative test samples were prepared from the bulk material using a sampling riffle. The sample was spread evenly along the bottom of the drum. A series of clean filters were pre-weighed and fixed in the outlet and inlet stages. An additional paper filter was positioned on the inlet to the drum to prevent contamination of the control stage. The way filters are assembled in inlet and the outlet of the drum is shown in appendix I. The vacuum pump was switched on and the flow rate adjusted to 40 lpm. The rotational speed of the drum was set to maintain a constant rate of 30 rpm. At the conclusion of each test the inlet and outlet filters were carefully removed from either ends of the drum and reweighed. The weights of the filters were taken to a four significant figure accuracy. In order to minimise the risk of loss and contamination the filters were handled very carefully.

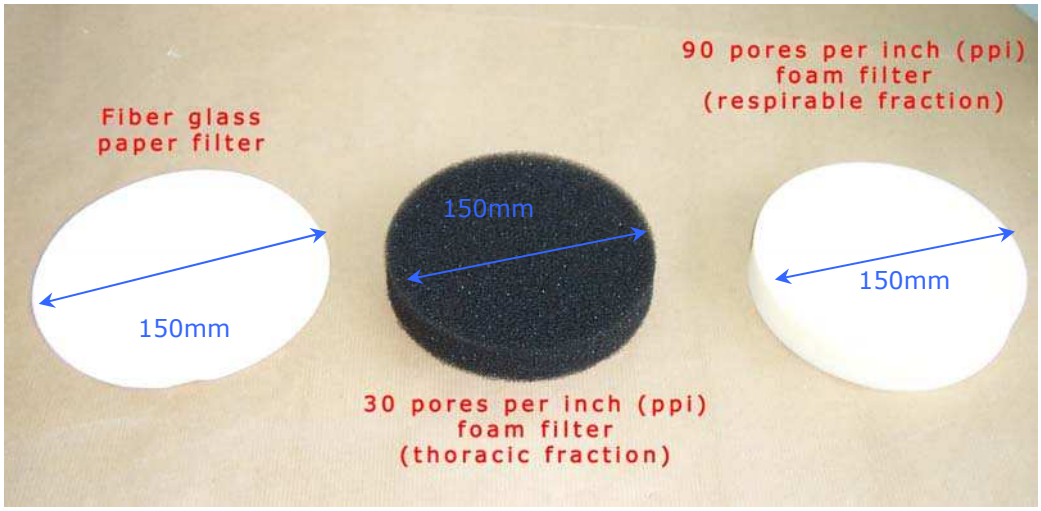

Figure 28: The three-stage filters employed at the HSE-WSL test.

The protocol established by the Health and Safety Laboratory was followed to achieve weighing consistency of the filters (Health and Safety Laboratory 1996). The weight of both the control and test foam filters was taken 30 seconds after the specimen was placed on the balance pan and the balance door closed.

For this research work a series of three size fractions and two sample masses of test material were investigated. A summary of the matrix of tests conducted for the various combinations of size fractions, sample masses and operating conditions is

shown in Figure 30. For the limestone only, an extra single size fraction (10mm) was tested. The dustiness of the single limestone fraction was determined, because the 10mm size fraction was used during further investigation of the mechanisms of dust generation in the tumbling mill using a high speed video system and a discreet element modelling technique. The two different testing procedure presented in Figure 30, were established after preliminary testing using the limestone. Preliminary testing aimed to investigate the dependency of the test operating conditions on the dustiness levels produced. Results obtained from primary examination indicated the use of an additional testing procedure. More information on the findings of primary examination is reported in Chapter 5. Each test was repeated three times and the dustiness values were correlated to confirm the reliability of the test results. If the obtained results from the triplicate tests were unsatisfactory, that is dustiness results fluctuated significantly, then they were discarded and the test was repeated so as to produce three dustiness values from one sample. Often in Chapters 5 to 9, a median dustiness value of the triplicate tests is presented together with a standard deviation and relative standard deviation. For the majority of the materials used there is no previous reference of expected values of relative standard deviation, and for this reason it is not possible to determine an upper limit above which dustiness results will be considered unsatisfactory.

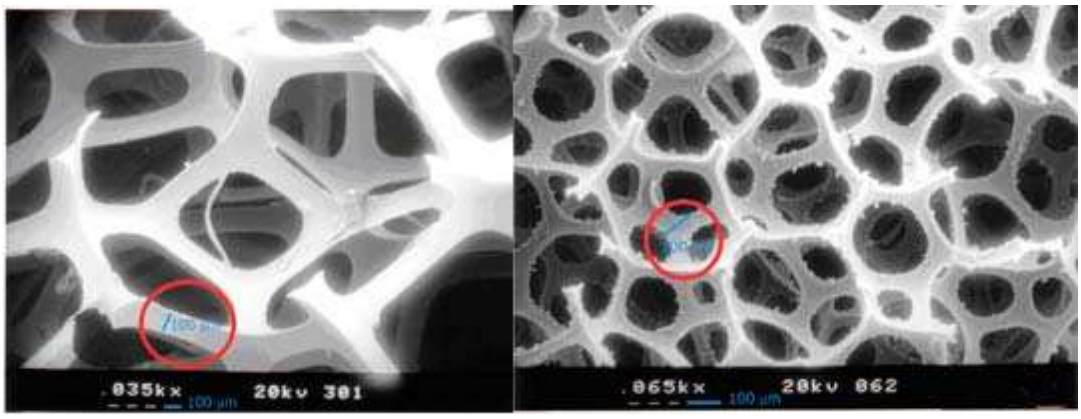

Figure 29: Scanning electron microscopy photomicrographs of the foam filters, (a) left photo corresponds to the 30 ppi foam filter; magnification X350, scale 100μm,(b) right photo corresponds to the 90 ppi foam filter; magnification x 65, scale 100μm.The 30 ppi filter was clean, whereas the 90 ppi filter shows small dust particles attached on the edges of the foam. The open pores structure is presented as well.

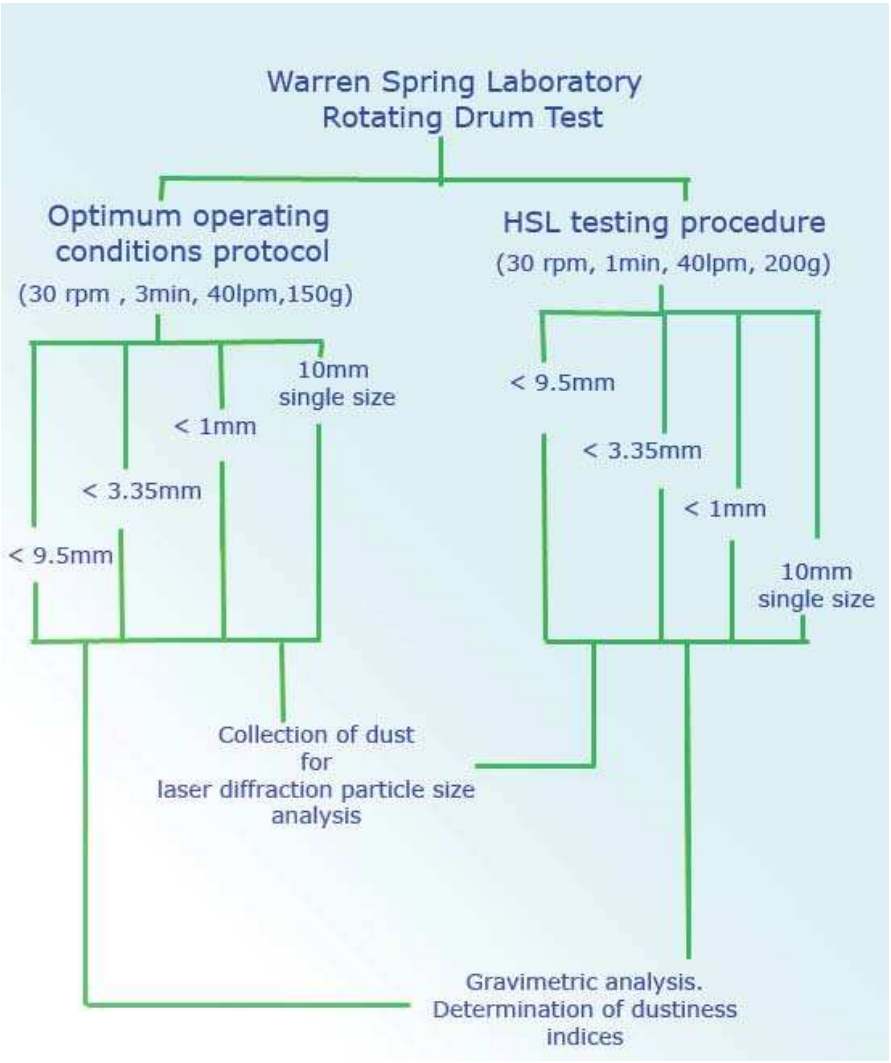

Figure 30: Schematic representation of the experimental steps followed using the HSE-WSL dustiness test.

4.4.1.4.*Recovery of the airborne fraction*

A separate series of experiments were conducted using the WSL rotating drum, following a modified sampling method. The core structure of the testing procedure remained similar to the one described in paragraph 4.4.1.4. The aim of this additional series of tests was to recover the particulate matter fraction for further experimentation (i.e particle size analysis, mineralogical characterisation). During these experiments the airborne fraction was collected on filter paper (Whatman – GF/A type, median pore size 0.6μm, diameter 0.15m). This type of glass fibre filters can adequately collect even the very fine fractions produced. To eliminate any loss of the airborne particles from the edges of the outlet cone, a larger diameter filter was positioned at the back of the main filter media. To increase the cohesiveness of the filter surface, it was slightly sprayed with distilled water, without being saturated. The purpose of these tests was to collect the dust fraction, thus no weighing process

was involved. After the completion of the test, the filters were removed and dried at 60 ^{o}C for one hour. The collected particulate matter fractions were stored and used later on for further analysis.

4.4.1.5. *Reporting of results*

The weight of the dust captured in the size-selecting stages is calculated from (equation 4):

(Equation 4) $D_n=(T_{fn} - T_{in}) – (C_{fn} – C_{in})$

where:

D_n = Weight of dust captured on the n^{th} stage (g)

T_{fn} = Final weight of the n^{th} test stage (g)

T_{in} = Initial weight of the n^{th} test stage (g)

C_{fn} = Final weight of the n^{th} control stage (g)

C_{in} = Initial weight of the n^{th} control stage (g)

The n^{th} stage corresponds to either the 30 ppi foam filter, the 90 ppi foam filter or the backup filter. This process allows for any weight changes in the foams and filters during the test to be corrected

The dustiness of the test sample is reported in terms of the inhalable (D_I), thoracic (D_T) and respirable (D_R) dust fractions as defined by the ISO and CEN standards (ISO. 1995). Extended information on the ISO classification can be found in Chapter 2.

The dustiness values of each fraction are calculated using the Equation 5, Equation 6 and Equation 7:

(Equation 5)

$$D_i=\frac{weight\ gain\ in\ two\ test\ \ foam\ \ filter + weight\ gain\ in\ backup\ \ filter}{weight\ of\ \ test\ sample} x100(\%)$$

(Equation 6)

$$D_t = \frac{weight\ gain\ in\ 90\ ppi\ \ foam\ \ filter + weight\ gain\ in\ backup\ \ filter}{weight\ in\ two\ test\ \ foams + \quad backup\ \ filter} x100(\%)$$

(Equation 7)

$$D_r = \frac{weight\ gain\ in\ backup\ \ filter}{weight\ in\ two\ test\ \ foams + \quad backup\ \ filter} x100(\%)$$

Where D_i = the dustiness value of the inhalable dust fraction (%);

D_t = the dustiness value of the thoracic fraction and (%);

D_r = the dustiness value of the respirable fraction (%).

Dustiness results obtained for each ore are presented and discussed in the corresponding chapters for each individual material.

4.5. The Impact Test

The impact test was used to assess the dust/fines generation potential of a range of ores that they were exposed on impact events. The test aims to simulate the impact levels found in common mineral related processes for example stockpiling, transfer points, tipping and others. The initial idea for the development of this test came from single particle breakage apparatus used for breakage characterisation purposes in comminution research. The impact test is a modified version of the JK drop weight test, although it does not represent a single particle breakage test. It was built on a JK drop weight tester and it uses the operating facilities the JK test provides. A review of the JK drop weight tester and the impact test is presented in the following paragraphs.

4.5.1.The JK Drop Weigh test

The JK drop weight test, developed by the Julius Kruttschnitt mineral research centre (JKMRC), determines the ore parameters derived through the use of single particle impact breakage testing. It aims to characterise rocks in the context of comminution. The breakage data obtained by the JK drop weight tester is used for modelling and simulating mineral comminution processes such as rod and ball mills, AG and SAG

mills and crushers. However, comminution modelling was not of interest in this project. Specific parts of the JK test were borrowed at the development stage of the impact test. These were the drop weight device and the theoretical background upon which testing parameters were set, and they are described below.

The JKMRC drop weight apparatus consists of a steel drop weight mounted on two guide rails and enclosed in Perspex as shown in Figure 31 (Napier-Munn et al. 1996). The weight is released by a pneumatic switch and falls under gravity to crush a single particle placed on a steel anvil (Napier-Munn et al. 1996). The drop weight device is fitted with a 20 Kg mass, which can be extended to 50 Kg. The range of drop heights available is from 0.05 – 1 m and represents energy levels from 0.01 to 50 KWh/t based on 10-50 mm particles (Bearman et al. 1997).

Based on the required specific input energy (*Eis*) for each test, the release height of the drop weight test is determined as shown in the equation below (equation 8) (Bearman et al. 1997):

Equation 8 $$hi = \frac{\overline{m}Eis}{0.0272Md}$$

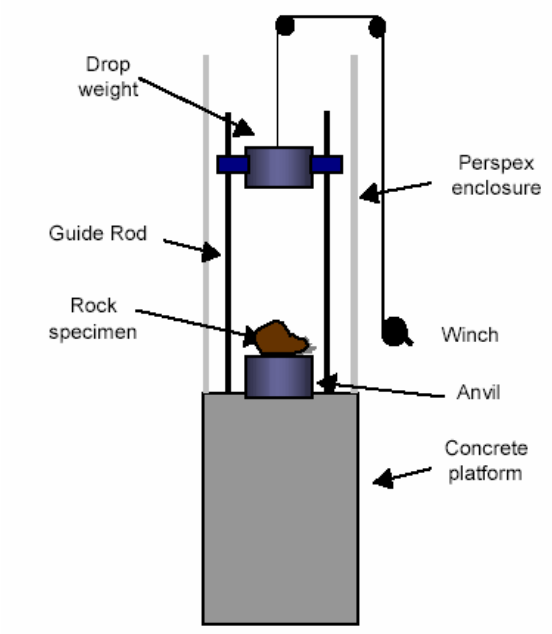

Figure 31: Schematic presentation of JK Drop weight tester (JKMRC 2003).

where *hi* is the initial height (cm) from which the drop weight is released, and Md is the mass of the drop weight (kg) and $\overline{m}$ the mean mass of each set of particles (g). When the particle is broken the drop weight test is brought to rest at a distance above the anvil due to presence of the broken particle (Napier-Munn et al. 1996). Ten to thirty particles are required in each size fraction for each energy level, depending on particle mass. Typically fifteen size/energy combinations are selected. The input energy levels for a particular test are designed to suit ore hardness. The actual applied energy *Eis* is calculated for each group of particles (equation 9) (*hf* is the average offset) (Napier-Munn et al. 1996).

Equation 9 $$Eis = \frac{0.0272 Md (hi - hf)}{\overline{m}}$$

The specific comminution energy *Ecs* (kWh/t) is equal to the specific input energy *Eis* (KWh/t) as long as the drop weight test does not rebound. The breakage products of all particles for each size/energy combination are collected and sized (JKMRC 2003).

4.5.2. Design of the impact test

The impact test was designed on an already available JK drop weight tester, so as to make use of the main operational characteristics like the weight lifting and releasing process. The impact test is shown in Figure 32, Figure 33 and Figure 34. The difference between the developed impact test and the drop weight test is that the first one uses a bed of particles to perform testing, whilst the collection of the broken particles is easy and accurate.

To allow testing using a bed of particles instead of a single one, but also in order to achieve accurate collection of the dust/fines fraction modifications were made on the existent JK drop weight test rig. A steel cylindrical holder designed to accommodate the test samples, was screwed over a steel anvil (Figure 32), so as to secure its position when impact occurred. The dimensions of the components of the impact test are given in Figure 33. The impact surface was the inner circular base of the sample holder. The thickness of both the anvil and the base of the cylindrical holder were chosen carefully so as to sustain the impact. The volume of the cylindrical holder allowed a range of fractions and sample bulk volumes to be used. The head weight of the original drop tester was modified as well. The impact test made use only of the heavy head compartment of the drop weight tester. This is because the heavy head

allows a range of weight to be utilized and therefore a variety of energy input levels to be achieved. The modified head weight consisted of a solid steel cylinder which is fixed onto the heavy weight holder. The dimensions of the solid extension of the head weight were such that during release it fitted well into the sample holder without leaving gaps, which could result to lose of fine material. Moreover, a rubber flange attached on the solid cylinder of the head weight sealed any gaps between the sample holder and head weight after impaction.

The impact test is versatile enough to permit testing not just on a confined bed of particles, but on single particles as well. One of the major advantages of the impact test is the accurate collection of the dust/fines fraction. It has to be noted here that the impact test did not collect the particulate matter fraction on the airborne state. Any particulate matter produced due to impact settled down in the sample holder and subsequently collected.

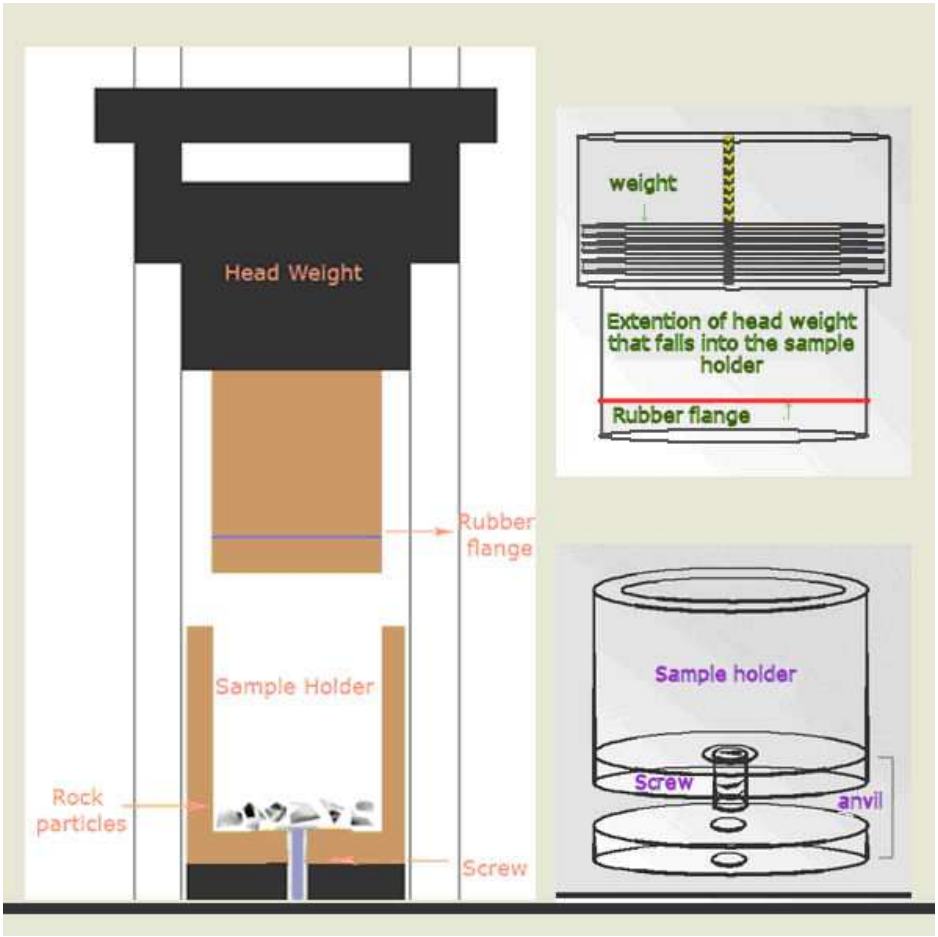

Figure 32: Schematic representation of the impact test. The sample holder and head weights are also presented in a 3D format.

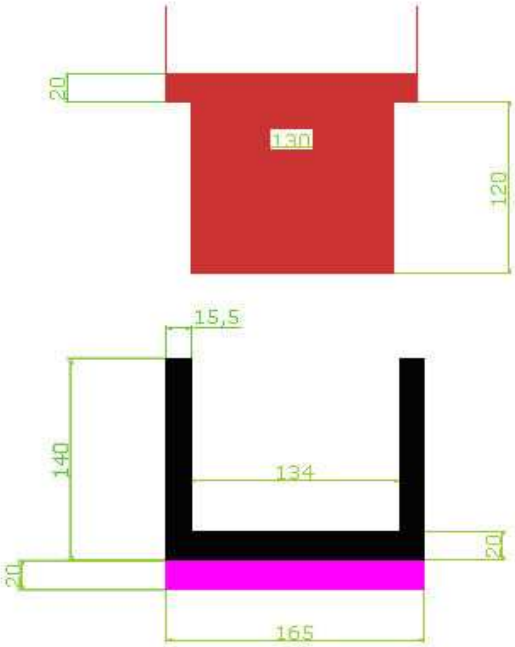

Figure 33: The dimensions of the impact test are presented. They correspond to a millimetre scale.

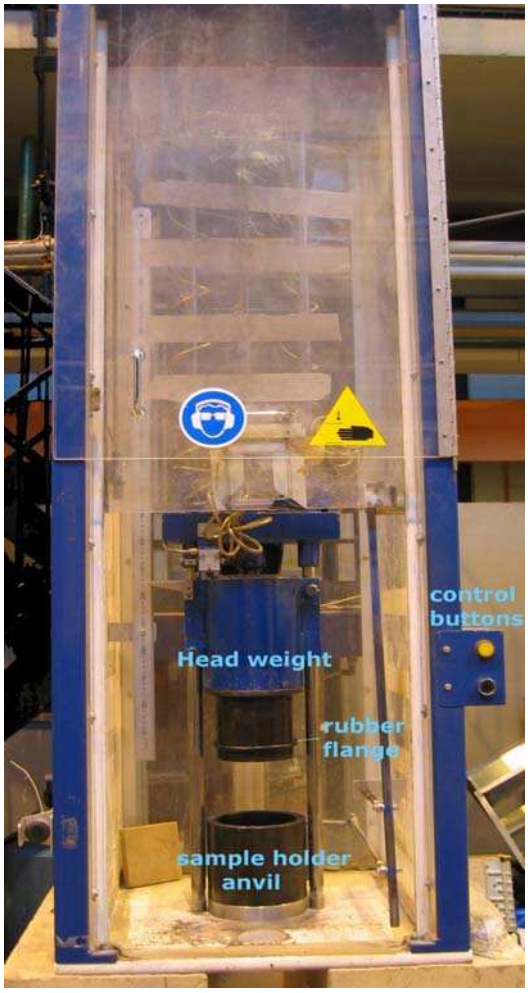

Figure 34: The impact test.

4.5.3.The applied testing methodology using the impact apparatus

The impact testing procedure was followed for all participating ores. A variety of particle fractions, energy levels and sample bulk volumes were selected to be investigated. A graphical illustration of the testing route is shown in Figure 35.

4.5.3.1.*Sample preparation*

Four different single fractions were prepared from each ore. These were the:

- -16 +13.2 mm
- -8 +6.7 mm
- -4 +3.35 mm
- -2 +1.7 mm

Preparation of the single fractions took place through several stages of crushing (use of a jaw crusher and roll crusher) and sieving to achieve the adequate quantities. Single fractions were preferred over mixtures so as to minimize attrition and abrasion effects produced during packing of the particles in the sample holder. If the test samples comprised of fractions with wider particle size distributions, then finer particles would preferentially pack between the coarse ones. Impaction would have forced the fine particles to abrade with the coarse particles, which would potentially have produced excess dust and fines. Also it would have been difficult to monitor the impact effect in relation to particle size. An action like this could make it very difficult to distinguish what is the dominant mechanism that is liable for the generation of dust/fines. Single fractions were carefully chosen so as to ensure that meaningful results could be obtained over the relationship of particle size and dust/fines generation potential.

The quantity of each test sample was determined by its bulk volume. Two bulk volumes were selected for each fraction (Figure 35). The bulk volume values corresponded to the percentage of the sample holder that it was occupied by particles. For instance, test samples of the -16+13.2 mm fraction were prepared for sample holder bulk volumes equal to 10% and 20%. Likewise the test samples of the smaller fractions equaled the 5% and 10% of the sample holder bulk volume. Bulk volume values used for each particle size fraction are presented in Table 18.

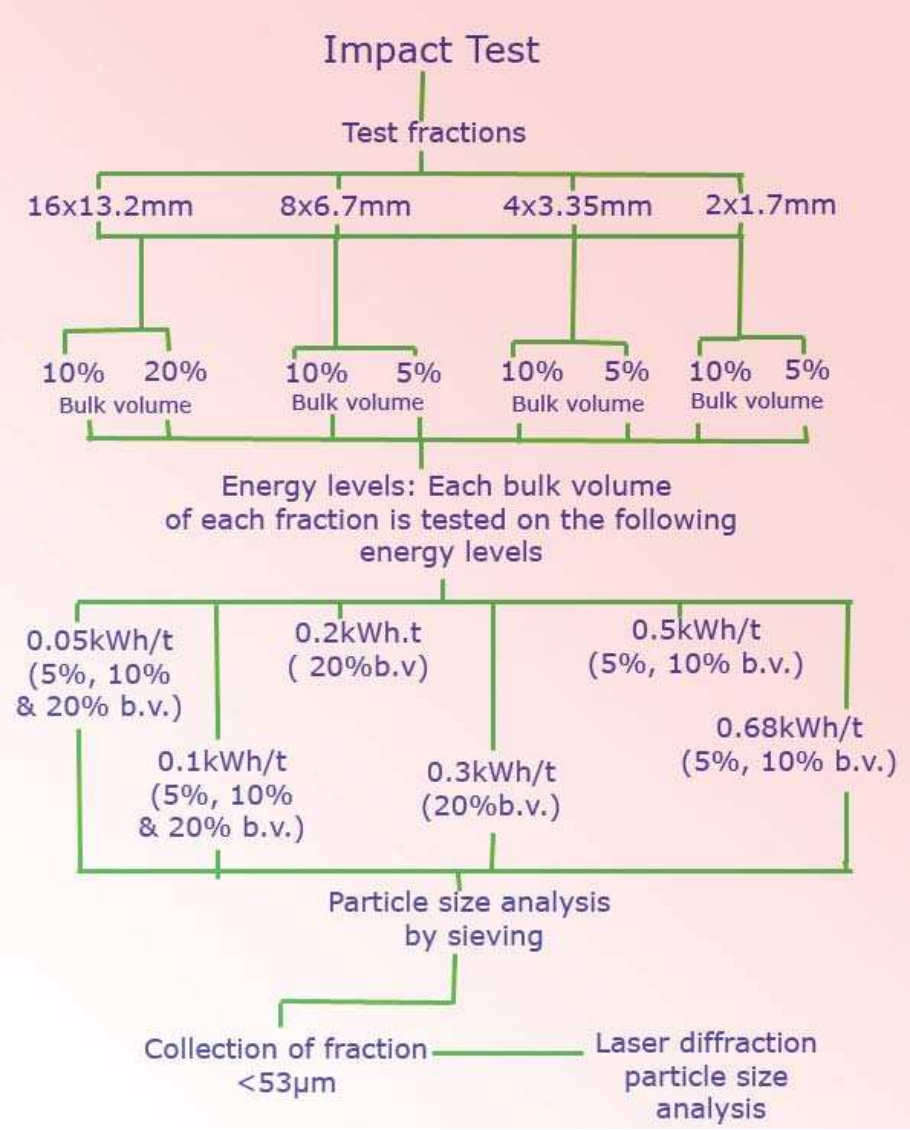

Figure 35: A graphic representation of the testing procedure followed for the impact test.

The bulk volume percentages were carefully selected to reflect certain changes in the confined bed. For example the 10% value of the sample holder bulk volume for the -16 +13.2mm corresponded to a single layer of particles at the bottom of the cylinder, whereas the 20% of bulk volume represents more than one layer.

Similarly, the 5% of the cylindrical holder bulk volume is occupied only by one layer of particles of the -8+6.7 mm fraction. For the fractions -8+6.7mm, -4+3.35mm and -2+1.7mm the same sets of bulk volume percentages were utilized, so as to make the comparison of the results possible. Bulk volume percentages of the different test samples were measured using a measuring cylinder (500 ml or 1000 ml).

Table 18: Bulk volumes used for each particle size fraction

% of sample holder bulk volume	20% (332 cm^3)	10% (166 $cm^{3)}$	5% (82 $cm^{3)}$
-16 +13.2 mm	✓	✓	
-8 + 6.7 mm		✓	✓
-4 + 3.35 mm		✓	✓
-2 + 1.7 mm		✓	✓

It has to be noted that loose bulk volume values were determined. After measurement of the appropriate bulk volume percentage the weight of the sample was recorded and the loose bulk density was calculated using Equation 10. Triplicates of each test sample were prepared and the variation in bulk density was recorded. These results reported the repeatability of the sample preparation method. The results are presented in Chapters 5 to 9 alongside with the experimental results of the individual ores.

$$\text{(Equation 10)} \quad d_b = \frac{m}{V_b}$$

Where d_b is the bulk density (g/cm^3), m is the mass of the test sample (g) and V_b is the bulk volume of the test sample (cm^3).The bulk density results were used to assess the reproducibility of the sample preparation procedure. They also provided a measure of the influence of physical properties (i.e particle size and shape, composition) upon bulk density for the different ores and particle fractions.

Four energy input levels were selected for each bulk volume – particle fraction pair. The range of energy input levels used for the different test samples are shown in Figure 35 and Table 19. Energy levels were chosen to simulate a variety of processes found in the mineral industries. Very low energy levels could correspond to small transfers of material in a mineral processing plant, whereas higher energy levels could describe specific processes that require higher energy input (i.e tipping). The selected energy input levels correspond to drop heights (of the head weight) within the range of 15cm to 100cm. In general low energy levels were preferable, because they better replicate common handling processes.

The upper energy level was limited by the operational capabilities of the impact test, namely the combination of height/weight that determined the energy input (Equation

8). Nevertheless this was not an obstacle for this research work, because much higher energy levels would simulate processes such as comminution which was not the objective of the testing. Therefore, each test sample had a specific identity, described by a particle fraction - bulk volume – energy level set.

Table 19: Combinations of energy levels – bulk volumes – and particle fractions used for testing.

Bulk volume (%)	20%				10%				5%			
Energy level (kWh/t)	0.05	0.1	0.2	0.3	0.05	0.1	0.5	0.68	0.05	0.1	0.5	0.68
16x13.2mm	✓	✓	✓	✓	✓	✓	✓	✓				
8x6.7mm					✓	✓	✓	✓	✓	✓	✓	✓
4x3.35mm					✓	✓	✓	✓	✓	✓	✓	✓
2x1.7mm					✓	✓	✓	✓	✓	✓	✓	✓

The required specific input energy for each test is determined by the release height of the impact test and the selection of the head weight. For the chosen energy levels two head weight combinations were applicable, shown in Table 20. The weight combination H1 represents the head weight without any weight additions, whereas the H2 combination uses all additional weights provided. The release height was determined similarly to the drop weight test by solving Equation 9 in terms of the initial height (Equation 11), where h_i (cm) is the initial height, E_{is} (kWh/t) is the energy input, M_h (kg) is the mass of head weight, m is the sample mass (g) and h_f is the average offset (cm).

Table 20: Head weight combinations used to achieve the required energy levels

Bulk volume (%)	Energy level (kWh/t)	Head weight (kg)
10%, 5%	0.05	H1 = 22.61 kg
	0.1	H1 = 22.61 kg
	0.5	H2 = 57.63 kg
	0.68	H2 = 57.63 kg
20%	0.05	H1 = 22.61 kg
	0.1	H1 = 22.61 kg
	0.2	H2 = 57.63 kg
	0.3	H2 = 57.63 kg

Equation 11 $$h_i = \frac{E_{is} m}{0.0272 M_h} + h_f$$

The average offset was determined by preliminary testing using the limestone samples. More information on preliminary testing is given in Chapter 5.

4.5.3.2. *Testing procedure and reporting of results*

Prior to testing the sample holder, the head weight and the rubber flange were thoroughly cleaned with acetone. The cylindrical holder was fixed on the steel anvil and it was filled with the test sample. At that point, it was made sure that particles were horizontally leveled into the cylinder without creating a cone or pile.

The head weight was set at an appropriate height, calculated using Equation 9, the safety switches were liberated and the Perspex door of the apparatus enclosure was shut. Afterwards, the head weight was released and it was impacted on the particles. The offset left due to particles presence was recorded by a ruler, which is fixed by the side of the impact test (Figure 34). Subsequently the head weight was lifted and secured at a position over the sample holder using the safety switches. The cylindrical holder was unscrewed and the test sample was carefully recovered. To remove and collect all the fine particles the sample holder, rubber flange and head weight were rinsed with acetone. The acetone – fines mixture was left to dry and the fine particles once more were recovered. The same procedure was followed for all different ores and test samples. Triplicates of each sample were tested to monitor results reproducibility. The testing procedure described here was set after experimentation with the limestone samples. Hence, extra tests were performed using the limestone. The results of the initial examination steps are presented in Chapter 5.

Recovered samples were sieved to obtain the fines/dust fraction (<53μm). The particle size distribution of one of the three repeatable tests was determined by sieving. A $\sqrt{2}$ sequence of sieve apertures was used. The sieve series used for the classification of the different particle fractions are presented in Table 21. The particle size distribution results of the broken test samples provided knowledge on the breakage profile of the ores. The fine fraction (< 53μm) was analysed by laser diffraction particle size analysis using a Malvern Mastersizer – S. Information on the laser diffraction particle sizing technique is given in the following paragraphs.

Results obtained using the impact test, are presented in chapter 5 to 9. Discussions are made upon the rock – dust relationship, whilst the potential of the different ores to generate dust/ fines under impact mechanisms is evaluated.

4.6.Particle size measurement techniques

Particle size classification took place by two main techniques, sieving and laser diffraction analysis. Sieving was used to measure the particle size of the coarse fractions produced during impact breakage or to define the feed samples particle size distributions used in the HSE-WSL test, whereas laser diffraction determined the particle size of the airborne particulate matter and the fine fraction below 53μm collected using both the HSE-WSL dustiness test and the impact apparatus.

4.6.1. Particle size analysis by sieving

Sieving was utilized both for the preparation of samples and after test analysis. For example, prior to testing fractions used in the WSL rotating drum test were sieved to determine their particle size distributions. Also fractions tested using the impact test, were classified by sieving. The sieving procedure was specified by British standard BS 1796-1:1989 (BSI 1989), whilst all sieves used comply with the technical requirements of the British standards BS 410-1:2000 and BS 410-2:2000 (BSI 2000a;BSI 2000b).

Commonly a $\sqrt{2}$ definite sequence of sieve apertures was utilized. Two different diameter sieves were used, the 450mm (large) and the 200mm (small) diameter sieves. The apertures of the used screens can be seen in Table 21.

Table 21: Apertures of used sieve sequence

	APERTURE (mm)
Large Sieves	13.2
	9.5
	6.7
	4.75
	3.35
Small sieves	2.36
	1.70
	1.18
	0.850
	0.600
	0.425
	0.300
	0.212
	0.150
	0.106
	0.075
	0.053
Pan	<0.053

4.6.2.Particle size analysis by laser light scattering

The laser light scattering method was applicable to the particulate matter fraction (airborne and non-airborne) and was used to measure its full particle size distribution of the -53µm. The particle size of the dust collected by the WSL rotating drum test and the impact test was determined using a low angle laser light scattering based particle sizer, the Malvern Mastersizer – S.

The next paragraphs describe the principles behind the low laser light scattering technique, the particular characteristics and steps followed during analysis by the Malvern Mastersizer – S, as well as the testing procedure employed for this project.

4.6.2.1. *The low angle laser light scattering method*

The low angle laser light scattering method has become the preferred standard in many industries for characterization and quality control. An ISO standard (ISO 13320) describes the basic principles of low angle laser light scattering (ISO 1999). The laser diffraction technique is based on the phenomenon that particles scatter

light in all directions with an intensity pattern that is dependent on particle size. All present light scattering instruments assume a spherical shape for the particles (ISO 1999). The principal requirement of the technique is that each phase must be distinct optically from the other and the medium must be transparent to the laser wavelength. In practice this means that the refractive index of the material must be different from the medium in which it is supported (Malvern Instruments 1994).

The scattering pattern of a group of particles within certain limits is identical to the scattering patterns of all particles present. By using an optical model to compute scattering patterns for unit volumes of particles in selected size classes and a mathematical deconvolution procedure, a volumetric particle size distribution is calculated, the scattering pattern of which fits best with the measured pattern (ISO 1999). For non-spherical particles, an equivalent sphere size distribution is obtained because the technique uses the assumption of spherical particles in its optical model (ISO 1999).

Typically, laser diffraction instruments consist of a light beam (i.e a laser beam), a particulate dispersion unit, a detector for measuring the scattering pattern and a computer for both control of the instrument and calculation of the particle size distribution (ISO 1999). A graphic illustration of the main components of the Malvern Mastersizer-S is shown in Figure 36. One of the drawbacks of the laser diffraction technique is that it is not possible to distinguish if the scattering corresponds to a single particle, an agglomerate or an aggregate (ISO 1999). Therefore dispersion of the sample prior to measurement is of great importance as the size distribution of the primary particles is commonly of interest (ISO 1999).

Two forms of optical configuration are employed by the Mastersizer. These are the optical method called “conventional Fourier optics” and the “reverse Fourier optics” that allow the measurement size range to be extended down to 0.05μm. A low power Hellium – Neon laser is used to form a collimated and monochromatic beam of light (maximum diameter 18mm). This laser beam represents the analyser beam, so any particles present will scatter the laser beam (Malvern Instruments 1994). The light scattered by the particles and the unscattered remainder are incident on a receiver lens also known as the range lens.

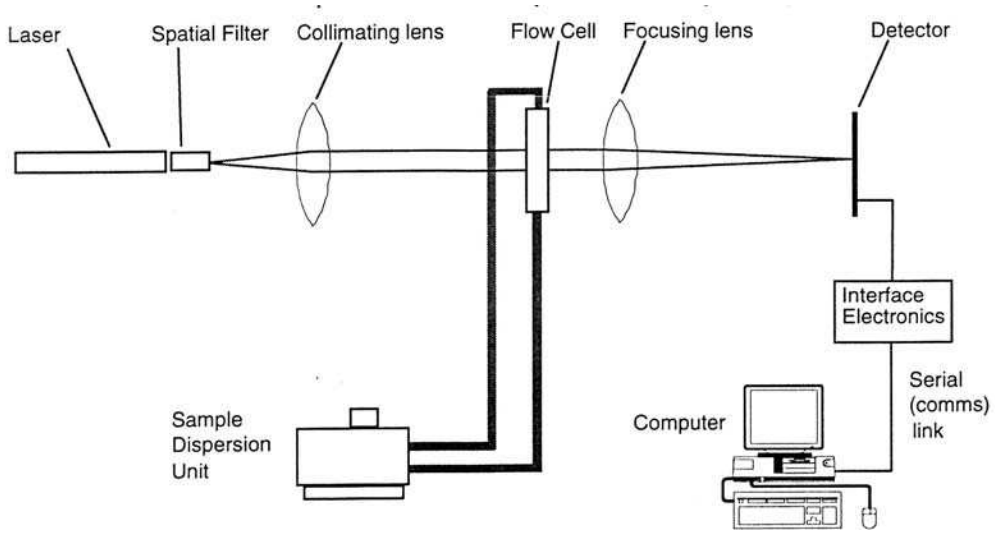

Figure 36: Schematic representation of the Malvern Mastersizer-S components (manual) (Malvern Instruments 1994).

This operates as a Fourier transform lens forming the far field diffraction pattern of the scattered light at its focal plane. The unscattered light is brought to a focus on the detector and passes through a small aperture in the detector and out of the optical system. The total laser power passing out of the system in this way is monitored allowing the sample volume concentration to be determined (Malvern Instruments 1994). In the reverse Fourier optics configuration, the laser beam does not form a collimated analyser beam. The output beam is focused to a point in the plane of the detector. The cell is placed at a distance from the detector plane in this converging analyser beam. The detector still measures the effective far field diffraction pattern. In the reverse Fourier configuration, the scaling factor becomes the cell-detector distance and not the focal point. The benefit of such a configuration is in the measurement of small particles, which scatter at large angles, typically greater than 10 degrees. The Mastersizer allows both optical methods to be used minimising errors that can be caused by using one technique over the other (Malvern Instruments 1994).

Many particles are present simultaneously in the analyser beam. Hence, the system inherently measures the integral scattering from all particles present in the beam. The measurement taken is a time averaged observation of the scattering as the material continuously passes through the analyser beam. By making many measurements of the detector readings (sweeps) and averaging over many such sweeps of the detector, it is possible to build up an integral light scattering characteristic based on millions of individual particles (Malvern Instruments 1994). For particles in the size range 10μm and upwards, the scattering with angle, is

largely independent of the optical properties of the material or the suspension medium. In the range below 10μm refractive index dependence becomes significant, because the light coupled into a small sized particle is not completely attenuated and can emerge as a refracted ray. Therefore, for particles sizes above 0.05μm the optical properties of the material must be considered. To overcome this problem, Mastersizer makes use of the full "Mie theory" model for scattering (Malvern Instruments 1994).

The computer predicts the scattering signal received from a wide range of materials at a given size. It contains a table that characterises how a unit volume of material of a range of sizes throughout the working range scatters light. Then the computer using these theoretical data deduces the volume size distribution that gives rise to the observed scattering characteristics. The construction of the volume size distribution is achieved by a process of constrained least squares fitting of the theoretical scattering characteristics to the observed data (Malvern Instruments 1994).

4.6.2.2. *The Mie and Fraunhofer approximation*

Malvern Mastersizer-S allows the user to choose between two different optical models. These are the Fraunhofer and Mie approximations. The Fraunhofer approximation was the basis for the first optical model for particle size measurement. Certain assumptions are employed by this optical model. Hence, the approximation applies to particles larger than the light wavelength (diameter at least 40 times the wavelength of the light). This also means that the same scattering pattern is obtained as for thin two-dimensional circular disks (i.e. silts, disc shaped particles). The second assumption made is that scattering occurs only in low angles ($<10^{o}$), in the near forward direction (ISO 1999). The Fraunhofer approximation does not take into account the optical properties of the material. Therefore its use is recommended for opaque particles, or particles with a high refractive index and mixtures of materials. However for small particles with a low refractive index, errors occur in the volume based diameter measurement. This is caused because the Fraunhofer approximation does not predict that for small particles the intensity of scattering falls more rapidly than the geometric cross – section would predict (ISO 1999).

To summarise, the Fraunhofer optical model can result to incorrect answers when measurements are performed with small particles (< 50μm) where the scattered

angles become large and secondary scattering occurs and when the relative refractive index (refractive index of the particle n_p relative to the refractive index of medium $n_{m)}$ is small normally below 1.1.

To overcome all these obstacles the Mastersizer makes use of another optical model, the Mie approximation (Figure 37). The Mie solution is the complete formal proof of Maxwell's equation for the incidence of a plane wavefront on a particle. The mathematical details of the theory are too extensive and can be found elsewhere (Bohren and Huffman 1983). The Mie theory can probably be described as a computational black box, where the particle properties can be input and the scattering pattern output. Necessary parameters that need to be determined in order to calculate the light scattering pattern are the complex refractive index of the sample material, the refractive index of the suspending medium, the particle size and the wavelength of light being scattered (Washington 1992). The complex refractive index is given by Equation 12, where N_p is the particle refractive index and n_m the refractive index of the dispersion medium (ISO 1999). The refractive index of a particle (N_p) consists of a real (n_p) and an imaginary (k_p) (absorption) part and can be calculated by Equation 13 (ISO 1999). The essential parameters are then combined into two dimensionless parameters, the relative refractive index and the size parameter x that is given by Equation 14, where a is the particle radius (μm) and λ the wavelength of scattered light (nm) (Washington 1992).

The Mie theory is valid for all sizes of particles, wavelengths and scattering patterns. According to ISO specifications this approximation provides the best solution for particles smaller in size than about 50μm. For medium size particles with a relative refractive index higher than 1.1 (k_p >0.05) the Fraunhofer approximation can also find use. Whenever the Mie theory is used, the optical properties of the particle and dispersion medium need to be considered (ISO 1999). The determination of the refractive indices values is not always straight forward and sometimes it is difficult to be defined. An example of the influence the selection of the appropriate optical model and the optical parameters (for Mie theory) can have at the experimental results is presented in Figure 38. It is observed that the diameter values D10, D50 and D90 are different when the Fraunhofer or Mie approximations are used, whereas slightly different optical properties (refractive index R.I.) cause to some extend changes to the diameter values.

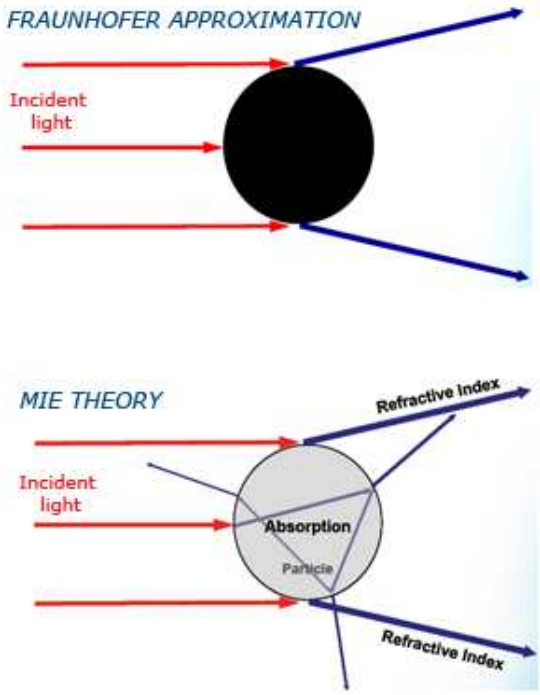

Figure 37: The Fraunhofer and Mie approximations (Malvern Instruments, 2005c).

(Equation 12) $$m = \frac{N_p}{n_m}$$

(Equation 13) $$N_p = n_p - ik_p$$

(Equation 14) $$x = \frac{2\pi m\alpha}{\lambda}$$

For the purposes of this project the selection of the Mie approximation was considered suitable, as the laser diffraction techniques was used to determine the particle size of the particulate matter. Commentary analysis on the optical properties chosen for each ore is given on the respective Chapters (5 to 9).

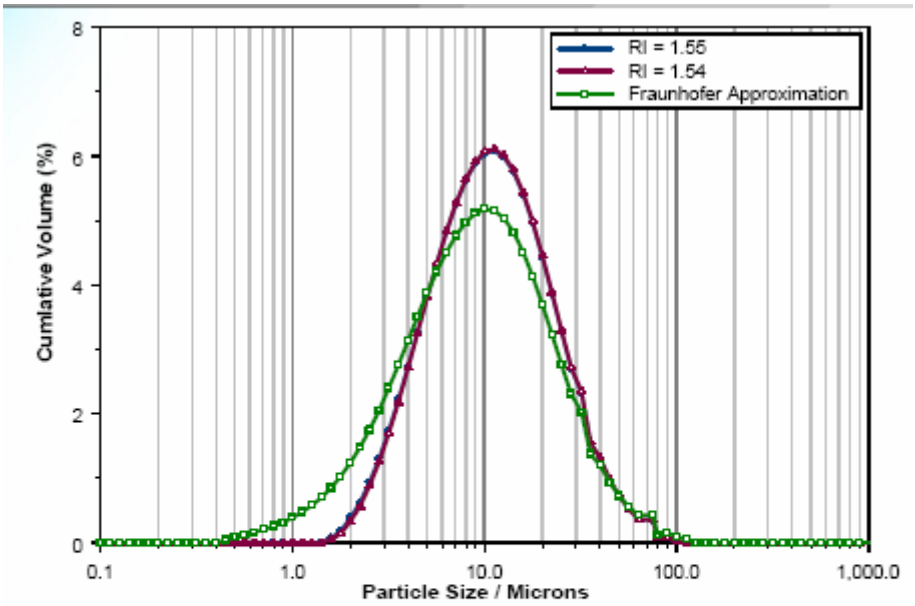

Model	Dv10	Dv50	Dv90
RI=1.54	3.96	10.17	26.22
RI=1.555	4.02	10.23	26.30
Fraunhofer Approximation	2.56	8.73	25.68

Figure 38: The influence that optical models and parameters have upon the particle size distribution results for a pharmaceutical powder.

4.6.2.3.*The Mastersizer-S measurement procedure*

Measurement of particle size using the Mastersizer followed a sequence of steps, which are presented in Figure 39. The measurement-analysis steps of the process were guided by the supported software of Malvern Mastersizer-S, version 2.19.

Firstly, the sample under examination was prepared. Two different preparation procedures were followed. Commonly a paste was formed with the test sample adding water.

The paste sample was well mixed with a spatula. The consistency of the paste avoided segregation errors. The preparation method followed the ISO recommendations (ISO 1999). A second method was employed for the particulate matter fraction collected by the WSL rotating drum method due to its very low quantity, which did not allow the preparation of a paste. In this occasion a pulp was created adding water and mixed using a power mixer. The pulp was mixed for 5

minutes so as to break any agglomerates and aggregates present in the sample. Occasionally some samples that had the tendency to aggregate were treated using an ultrasound bath for a few seconds, in between of the mixing process.

After the sample was prepared a measurement was setup. During the setup process firstly the hardware properties were defined, namely the range of the instrument, the active beam length and the sample unit. The range of the instrument corresponds to the range lens fitted. In this project the 300RF lens were used and their range was from 0.05μm to 900μm. The active beam length was set to 2.4 mm, which reflect the cell thickness. As sample unit it was used the small volume sample dispersion unit (MS1). At the setup analysis window the analysis model was chosen to be the polydisperse. This is the most common applicable model as it does not make any assumptions about the form of the results.

At the final setup window the presentation of the measurement was selected. The presentation represents the optical model of the subsequent measurement. The Fraunhofer or Mie approximation could be chosen. In this project only the Mie approximation was used, hence various presentations were prepared to reflect the optical properties of the different rock samples (refractive index of the particle, the suspension medium and the imaginary part). In detail discussion of each prepared presentation is given at the following chapters along with the presentation of the results obtained.

Following the various setup steps, the details of the test sample were documented and the automatic alignment procedure of the optics was started. The dispersion unit was filled with clean water and the stirrer was set to a medium rotation speed. Then, the alignment button was pressed, which centred the detector on the laser beam. The alignment of the optics is an essential step to achieve a good measurement.

After the optics was aligned a background measurement was taken. This was an essential step before each measurement, which measured the background light scattered from the clean dispersant. The background measurement was a two stage process. The first stage measured the electrical offset of the detector amplifiers, which was then subtracted from all subsequent measurements. The second stage measured the scattering with no sample in the dispersant. The measure window showed the scattering with the electrical offset subtracted.

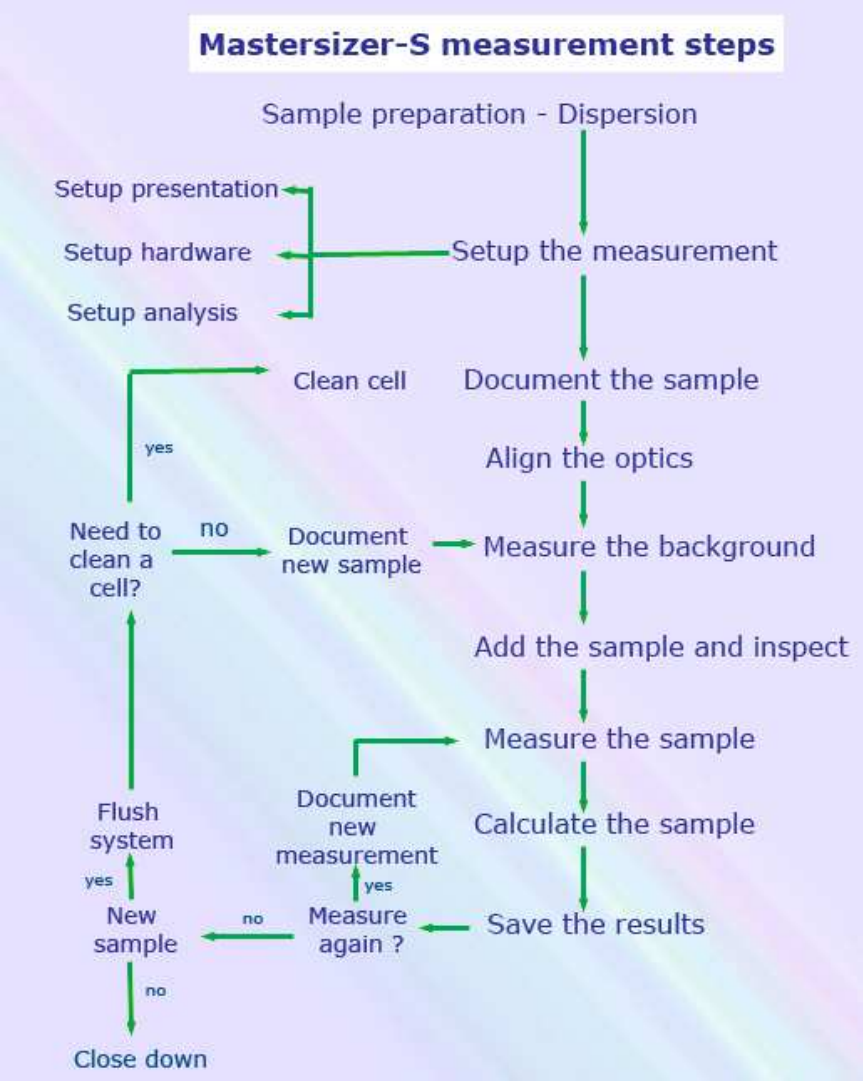

Figure 39: The particle size measurement sequence followed using the Mastersizer-S.

Subsequently the sample was added to the dispersion unit. The amount of added sample was determined by the online obscuration value. According to ISO specifications and the proposed testing procedure of Malvern Instruments for the Mastersizer-S (wet dispersion unit), the obscuration value should be kept between 10 to 15%. The inspect-measure window showed the light scattered from the sample with the background subtracted, as well as the results of a quick analysis of the data. The data was analysed to form a result, hence the relative distribution of particle volume by size was calculated. The result was saved on disk as a record in a sample file. Two extra repeats of the measurement procedure for the same sample in the dispersion unit were taken to check and increase accuracy. During these repeatable measurement the background was not calculated again as the sample unit was full with the analysis sample. Furthermore, every sample was measured two or three times, depending on the sample, namely two to three proportions of the same sample were tested following the whole measurement procedure as described above.

Similar to the first measurement for every subsequent measurement with fresh material from the same sample, the last step was repeated twice. This way the particle size results of a sample was verified, whereas the fluctuation in particle size observed between different repeats was examined. Unsatisfactory measurements were discarded, whilst during the interpretation and analysis steps a median particle size distribution was produced from the replicate tests of a sample. Commonly the repeatability of the measurements taken with a single feed was good, resulting to a relative standard deviation below 1%. When fresh sample was about to be introduced, the sample unit was thoroughly cleaned and flushed with water several times. The results obtained from every run were saved and exported in a Microsoft excel spreadsheet for further interpretation and analysis. Particle size measurement results obtained by the laser diffraction technique are presented in Chapters 5 to 9.

4.7. Summary of Chapter 4

The contents of this chapter referred to the mainstream experimental procedure that had been decided for the completion of this project. Experimentation aimed to identify and quantify the dust generation potential resulting from different industrial process and thus different mechanisms. Furthermore, the relationship between rock and dust was examined. A closer examination at industrial processes mechanisms that exhibit high liability to emit particulate matter revealed that dust is generated due to impact or abrasion-attrition forces or the combination of them. The experimental procedure followed by this project held on to this statement and it was developed accordingly. Two tests were used, which aimed to simulate common processes found in mineral workings, implementing the impact and abrasion-attrition mechanisms. These were the Warren Spring Laboratory rotating drum test and the Impact test. The outcome of these two tests was the determination of the dustiness potential resulting from different processes. Dustiness had not been attributed a single value descriptor, but it was explored from many-sides. Quantitative results of the airborne particulate matter and the generated dust and particle size analysis were some of the employed tools to verify dustiness.The relationship that exists between rock samples and the dust fraction had been established through the use of mineralogical characterisation practices. These steps provided in depth understanding of the rock degradation process. Also it worked as an identification stage of the hazardous potential of dust. The utilized experimental techniques were investigated in detail for a variety of operational set up combinations, rock samples and test fractions. The results obtained are presented in the following chapters.

Chapter 5. Experimentation with Tunstead quarry limestone

5.1. Introduction

The production of aggregate materials, which include sand and gravel and crushed rock, is now the largest extractive industry in the United Kingdom with over 200 million tonnes being extracted each year. By their very nature quarry operations involve drilling, blasting, handling and movement of significant quantities of often dry material. At almost all stages of extraction and processing there is the potential to produce and emit dust to the atmosphere. In some situations this dust can contain harmful substances such as quartz and this clearly requires special attention. The dual concern of occupational health and air quality near quarry sites requires careful management. For quarries operating in dry or windy environments, the issue is especially challenging.

From visits to Tunstead Quarry we had the opportunity to evaluate the sensitivity of the location of the quarry, to discuss with employees about any problematic areas with high dust emission rates, to valuate the mitigation techniques already used and to review the environmental policies and monitoring methods implemented by Tunstead works. Tunstead Quarry is located on the boundaries of Peak District National Park, thus particulate emissions from mineral works become a major issue.

This chapter refers to the experimental practices that took place for Tunstead Quarry limestone (Buxton, Derbyshire), while trying to assess its propensity to generate dust through various mechanisms that simulate numerous handling, processing and transport operations of the quarrry.

5.1.1. Experimentation steps

The structure of this chapter is outlined below and deals with the research findings relevant to limestone. A brief background to Tunstead works is given in the following paragraphs. The steps followed to assess the limestone samples are:

- Mineralogical characterisation of the rock samples by X-ray diffraction analysis and scanning electron microscopy.
- Determination of the dust propensity of limestone using the Warren Spring Laboratory (HSE-WSL) rotating drum test. Preliminary testing investigated the effects of the operational parameters of the test to the dust generation process. Initial testing allowed the establishment of routine experimental procedures.
- Collection of the dust fraction produced by the HSE-WSL rotating drum test and measurement of the dust particle size distribution by laser diffraction analysis using the Malvern Mastersizer - S.
- In depth determination of the breakage mechanisms involved in the HSE-WSL test. The breakage process within the tumbling mill was modelled using the discreet element modelling practices, whereas the tumbling action was investigated using a high speed camera.
- Determination of the dust propensity of limestone using the modified JK impact test. Preliminary testing using the limestone established a specific experimental procedure applicable to all rock samples and this is presented here. The relation between dustiness and specific comminution energy input was investigated.
- Collection of the fine particulates fraction produced by the impact test by sieve analysis and measurement of the impact test particulates by laser diffraction analysis using the Malvern Mastersizer-S.
- Mineralogical characterisation of limestone particulates produced by the tumbling mill test and the impact test by X-ray diffraction analysis and scanning electron microscopy.

Most of the work described further on, in the following chapters, is based on the knowledge gained by testing the limestone samples. Limestone was chosen to be the material that initial testing will take place, due to its homogeneity and simplified mineralogy, in comparison to the other samples used. The simplified composition assisted initial experimentation by reducing the parameters that can produce variation in testing, and thus making possible the establishment of an optimised experimental procedure.

5.2.Tunstead Quarry - History and industry

Tunstead quarry is located near Buxton in Derbyshire, within the Peak District Area and due to its production capacity and size it has been characterized as a superquarry (British Geological Survey 2005).

Tunstead is now part of the Tarmac Group, which in turn is owned by Anglo American plc. Large deposits of high-purity limestone were found at Tunstead, which is used both in construction and the chemical industry. The reserves of the quarry approach the 260 million tonnes (James 2004). The quarry along with the Old Moor quarry produces 6 million tonnes of limestone annually (British Geological Survey 2005;James 2004)

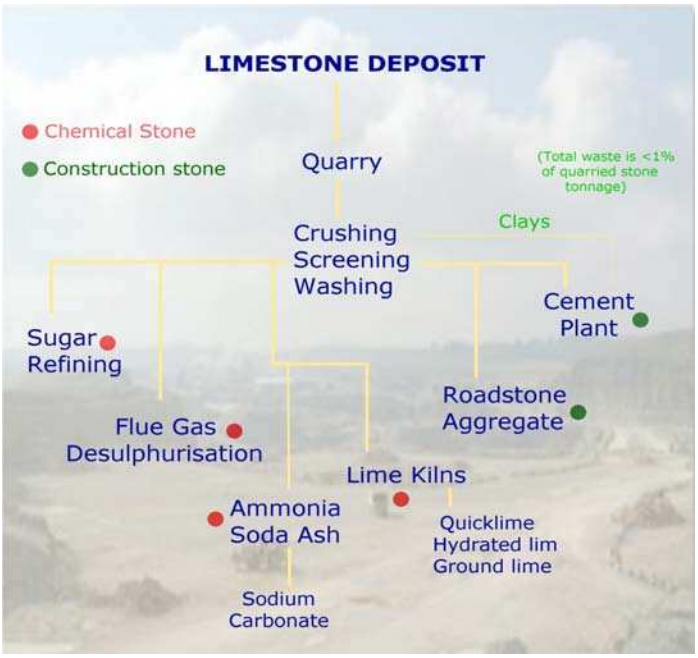

Figure 40: Industrial applications of Tunstead quarry limestone (modified by (James 2004).

Tunstead limestone consists of over 95% calcite (calcium carbonate-$CaCO_3$). Limestone finds numerous applications, some of which are shown in Figure 40. Lower grades of limestone (of dolomitic nature) are used as road stone aggregate, whereas the cement plant utilizes most of the waste produced during the processing of limestone for roadstone. A new cement plant started to operate during 2004, which will provide improved environmental performance. According to Tarmac Central, the new plant will reduce (in total tonnes per annum) the particulate emissions by 70% and the oxides of nitrogen and sulphur by 9% and 60% respectively. It will also improve energy efficiency and visual appearance of the quarry due to removal of old cement works and restoration of the site (James 2004).

5.2.1. The geology of Tunstead limestone Quarry

Tunstead works are located in the White Peak area, which is made up of limestone with pale grey outcrops. Limestone here is thickly – bedded, of Carboniferous age and forms a sequence of strata up to two kilometres thick, although only the uppermost 600m are exposed at the surface. They were deposited around 350 to 325 million years ago, on a shallow platform in a tropical sea, which was surrounded by much deeper water. The geological profile of Tunstead quarry is shown in the map of Figure 41. Two main formations are present in both the Tunstead quarry and Old Moor quarry. These are the Bee Low limestone and the Woo Dale limestone formation. Volcanic rocks occupy the boundaries of the Tunstead works as well as they comprise the basement rocks (British Geological Survey 2005).

Boreholes conducted by Tarmac Central in Old Moor quarry revealed that Bee Low limestone is exposed at the surface and according to location the thickness of the bed can vary from 60 to 115 metres. Woo Dale limestone is located in higher depths between 60 to 141 metres. In Tunstead quarry, boreholes show that the northern part consists mainly of Bee Low limestone with a bed thickness between 12 and 118 metres, whereas in the southern part the Bee Low limestone formation is followed by the Woo Dale limestone. The bed thickness of the Bee Low limestone in the southern part can vary from as little as 8 meters to up to 118 metres. Woo Dale limestone according to location is found between 8 and 134 metres in depth (Tarmac Central 1996).

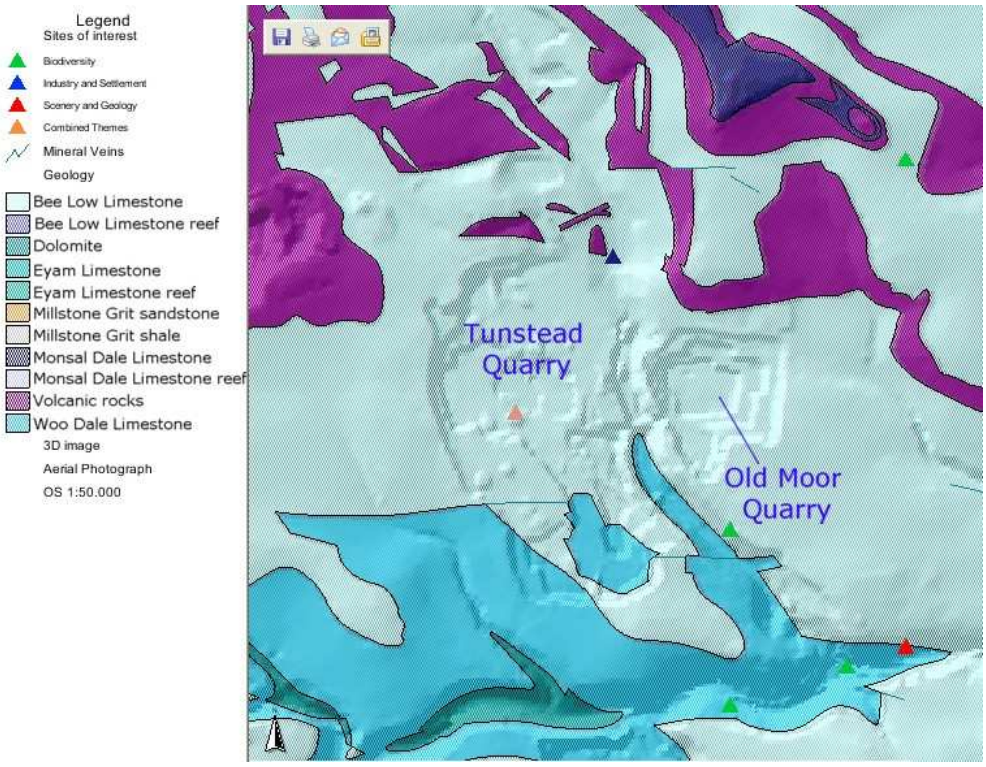

Figure 41: Geological map of the Tunstead works area. Apart from the geological formations, a 3D –image and an aerial photograph are also presented making possible to distinguish the Old Moor Quarry and Tunstead Quarry (British Geological Survey 2005)}.

Bee Low limestone is of high chemical purity (> 95% calcite). This limestone is composed of shell derbis, predominantly made of the mineral calcite (British Geological Survey 2005). Woo Dale limestone is of lower chemical purity and of a dolomitic composition, implying higher magnesium (Mg) content. Boreholes have justified both of these statements (Tarmac Central 1996).

5.3. Tunstead quarry mining processes and particulate matter emissions

Limestone is mined through drilling and blasting and the produced material is transferred by trucks to the crushing plant. Subsequently, limestone undergoes processing through a series of steps and a variety of grades for different industrial applications are produced. A detailed representation of the processing stages can be seen in the flow sheet in Figure 42. The processing plant consists of three connected sub-plants, the crushing plant, the washing plant and the roadstone plant. The crushing plant is where primary rock preparation takes place. Crushed material undergoes further secondary, tertiary and sometimes quaternary crushing and screening operations in the washing and roadstone plants to produce the required

grades. The material is generally transported between different units of plant by conveyors. Surplus material may be deposited onto a surge pile and will be loaded back onto conveyors via vibrating feeders, feed hoppers or by hydraulic shovels.

Several visits were made to the Tunstead works, which allowed observations and discussions to be carried out with quarry engineers about problems relevant to particulate matter emissions. The existent dust control practices were also reviewed.

Although, dust emissions from Tunstead quarry were not at very high levels and some mitigation practices were already in use, the position of the quarry, which is set within the boundaries of the Peak District national park, demands that maximum protection to be taken. Except from the national park limitations, nearby inhabited areas require nuisance dust levels to be kept to a minimum.

Mining processes such as drilling, blasting, loading of blasted material to dumpers and transfer to the primary crusher, crushing, screening and conveying, as well as the production of stockpiles were some of the potential identified dust sources. In general, it was recognized that the disturbance and movement of material could result to the production of dust and fines.

The mitigation techniques currently used for dust control were enclosures and water sprays. All crushing-screening stages were enclosed, as well as most of the conveyor belts. This way dust emissions were minimised quite effectively. Some haulage roads were wetted during dry periods to ensure that fine material will not be entrained into the airborne state. Water sprays were utilized during tipping of material from conveyor belts. In terms of monitoring, there was no specific implemented monitoring plan and only a few ambient air monitors were set at the boundaries of the quarry for air quality evaluation.

However, it was observed that mitigation practices did not adequately control the dust produced, resulting in fugitive and nuisance particulate matter concentrations. This was due to a plethora of reasons such as the underestimation of the dust generation levels from certain processes, the limited use of control practices (i.e use of only a few water sprays), the incorrect planning, implementation and maintenance of specific mitigation techniques, the lack of a well established monitoring plan, as well as atmospheric conditions (i.e. local microclimate). For instance, some of the

water sprays used at tipping points did not manage to control the dust cloud resulting in fugitive dust.

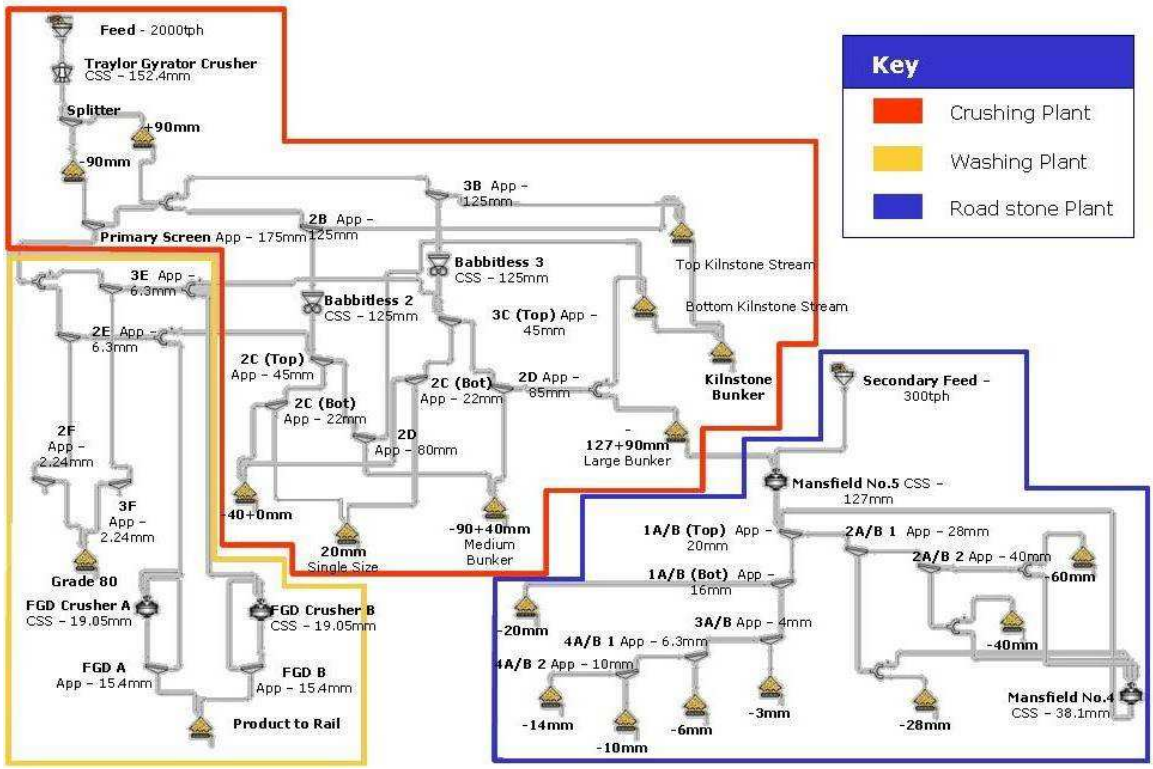

Figure 42: Flow sheet of the processing plant of Tunstead works.

Also stockpiles of different product grades were left uncovered. Some of these stockpiles comprise fine material, for example the industrial grade dust (< 3mm), thus permitted the wind to move fine material away. In the enclosed washing plant, the emissions of particulate matter were high, even making visibility impossible. This was due to dry screening, where no dust prevention methods were implemented. Even though the plant did not require the continual presence of human operators, several employees had to walk everyday through the plant to enter the plant control room. Blasting took place on a daily basis and generated great amounts of dust instantaneously. Blasting was considered a problem from the quarry engineers, because wind often transferred particulate matter emissions outside the quarry boundaries and into the national park. The use of trucks to transfer the ore from the quarry to the primary crusher also generated dust. Another parameter that played an important role in the dust emission potential was the atmospheric conditions. The area around Tunstead works exhibit a microclimate, which makes estimation of weather conditions (i.e winds direction) very difficult. Hence, the correct selection of control practices that could effectively reduce dust levels becomes more complicated. Appendix II presents some examples from Tunstead and Old Moor quarry.

Further research work is required to assess the production of particulate matter by qualitative and quantitative means. The different mining operations produce dust due to the effect of the various mechanisms of these processes. For instance, during sieving dust is produced by the abrasion – attrition of the ore particles with the sieve mesh or with other particles. During stockpiling particulates are generated because limestone is dropped from height. The experimental procedure followed by this project intends to identify how dust is produced from such processes by simulating their principle mechanisms using the HSE-WSL drum test and the modified JK impact test. In addition qualitative analysis of dust takes place by determining its particle size and the mineralogy. The combination of these results could provide alternative routes to approach the dust generation problem.

5.4.Mineralogical characterisation of limestone

The limestone used in this project was a high – purity material containing over 97% calcium carbonate. Some typical chemical analysis values can be seen in Table 22. The presented results were provided by Tarmac group and they correspond to the high purity limestone used in the chemical industry.

Table 22: Chemical analysis results for the pure limestone rock samples. (Tarmac Central, 2003)

Chemical composition	% of total concentration
Calcium carbonate ($CaCO_3$)	97.5 (min)
Magnesium as $MgCO_3$	1.0 (max)
Iron (Fe_2O_3)	0.10 (max)
Silica (SiO_2)	0.75 (max)
Aluminium (Al_2O_3)	0.15 (max)
Fluorine (F)	50 ppm (max) (100ppm in lime)
Lead (Pb)	7 ppm (max)
Arsenic (As)	2 ppm (max)

The limestone samples were collected from stockpiles and supplied by Tarmac. The mineralogy of the host rock samples prior to testing was determined by X-ray diffraction whole-rock analysis. The XRD traces of a range of different samples can be seen in Figure 43. More than one limestone rock sample was pulverised and riffled to produce five representative samples that reflected the exact mineralogical identity of

the limestone deposit. The XRD patterns appear to be identical. Limestone comprises of one main mineral phase that corresponds to calcite ($CaCO_3$), whilst for some of the samples a second minor mineral phase has been identified, that of quartz. The chemical analysis results also showed some quantity of dolomite ($MgCO_3$), silica, iron and aluminium. Nevertheless, their participating concentrations were very low (<5%), thus they were undetectable by the XRD technique.

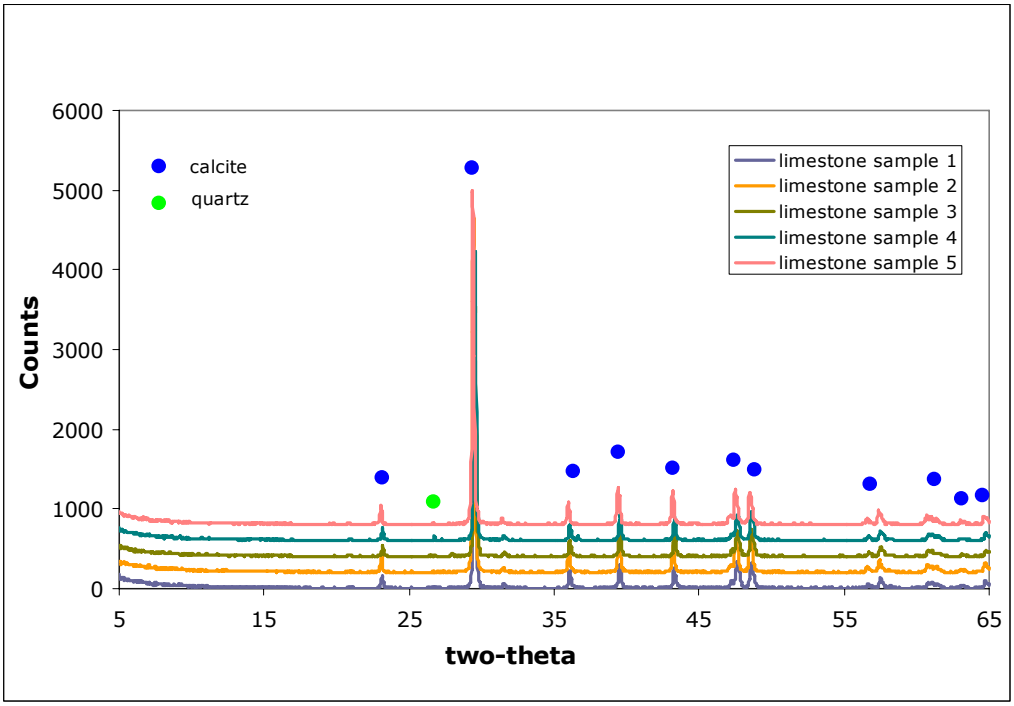

Figure 43: The XRD traces of the limestone rock samples (whole-rock analysis).

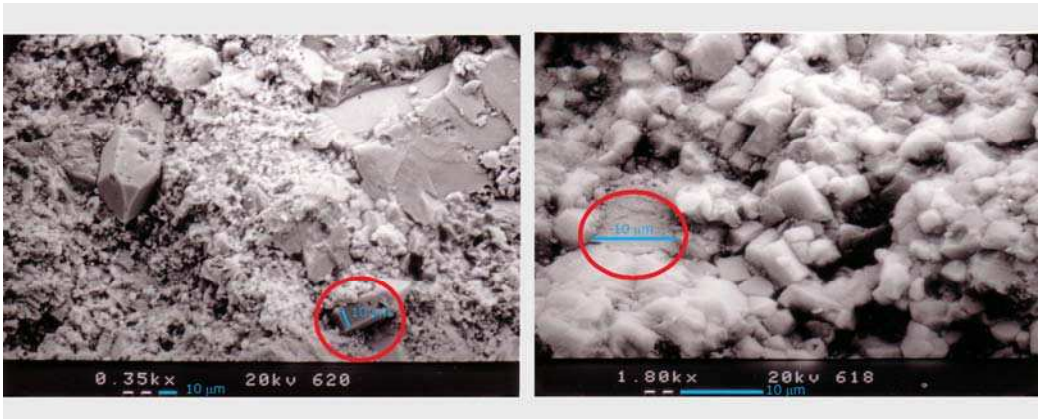

Figure 44: Scanning electron microscope photos of the limestone samples; (a) the left photo presents two quartz crystals in the limestone matrix (magnification X350, scale 10μm); (b)the right photo shows the rhombohedral calcite crystals (magnification X1800, scale 10μm)

The limestone rock samples were also observed using a scanning electron microscope. In the limestone rock matrix, calcite appears in rhombohedral crystals,

whereas a few quartz crystals were also found. The particle size of the calcite crystals varies but in most cases it was below 10μm.

5.5. Determination of the dustiness of limestone using the HSE-WSL rotating drum test

The dustiness of limestone under the effect of the abrasion mechanisms was evaluated using the HSE-WSL test. Preliminary testing investigated the effect of the operating parameters of the tumbling drum upon limestone. These initial steps of experimentation allowed the determination of a standard experimental procedure. Following preliminary testing, a variety of limestone feed samples were tested and their dustiness values were recorded. The results obtained from preliminary testing and dustiness testing, are presented in the subsequent sections.

5.5.1. Preliminary testing using the HSE-WSL rotating drum test

The evaluation of the effects of the test parameters upon material dustiness was one of the main points of interest for many researchers (Breum 1999;Cowherd and Grelinger 1992;Heitbrink 1990;Lyons et al. 1996;Schneider and Hjemsted 1996). All alterations to test parameters influence the amount of dust and the size distribution of dust generated during such tests. It has been concluded that test parameters need to be carefully controlled in order to have reproducible dustiness results (Breum 1999;Heitbrink 1990). Hence, the dependence of the operating parameters on the dustiness of the limestone samples was quantified. Preliminary testing was thought to provide the operating limits where consistent measurements could be made and allow the optimum operating conditions for limestone to be defined. The parameters explored were:

- The weight stability of the foam filters
- The dust dispersion in relation to the flow rate through the drum
- The dust dispersion time
- The dust dispersion in relation to the mass of test material

The weight stability of the 30 pores per inch (ppi) and 90 pores per inch (ppi) foams under atmospheric conditions was determined by weighing them on a balance against a standard weight of limestone sample. Ten foam plugs of the 30 and 90 ppi foams were weighed three times and the weights were recorded. The effect of air drawn

through the foam plugs was also explored by running a blank test in the WSL drum. During the blank test the rotating drum was not loaded with any sample. A set of clean 30 ppi and 90 ppi foam filters were placed on the outlet (test foams) and inlet (control foams) of the rotating drum and air was drawn at a flow rate of 35 l/min over a period of 1 min. The foam filters were weighed both before and after the test and subsequently every hour over a period of four hours. A last measurement was taken 15 hours after the cessation of the test.

Air flow rates of 20, 30, 35 and 40 l/min were used to determine the variability of the limestone dustiness measured in relation to the change in airflow rate. A charge of 100 g of limestone (–3mm fraction) was tested at a rotational speed of 30 rpm and at a dispersion time of 1 minute.

The dispersion time was varied from 5 to 300 seconds in intervals of 5, 20, 60, 120, 180, 240, 300 seconds and the resultant limestone dust yield determined. A charge of 100 g of limestone (-3mm) was tested at a flow rate of 40 l/min and a rotation speed to 30 rpm.

The effect of input mass charge on the limestone dust yield was determined by varying the mass of the input material from between 25 to 400 g in steps of 25, 50, 100, 125, 150, 200, 300 and 400 g. Tests were carried out at an air flow rate of 40 l/min, for a duration of 1 min and a rotational speed of 30 rpm.

5.5.1.1. *Results of the weight stability of the foam filters*

The weight of the 30 ppi foam filters were found to vary with an average weight of 8.2 mg, whereas the weight of the 90 ppi foam filters changed on average by 4.2 mg. The average variation in the rock sample weight was 1.9 mg. Nevertheless, the 30 ppi foam can vary up to 22mg, whilst the 90ppi filter can change up to 14 mg. Lyons and Mark (1994) found similar results for the weight variation of foam filters with a mean change of up to 20 mg (Lyons and Mark 1994). Due to the weight fluctuation the use of control filters was considered essential. The applicability and effectiveness of control filters have been assessed during a blank experiment with the HSE-WSL test, where air was drawn through the test filters. The control filters were placed in the outlet of the drum.

The results of the effect of drawn air through the foam filters are shown in Figure 45. The weight of the test foam both for the 30ppi filter as well as the 90 ppi filter is presented in contrast to the control foam.

In this experiment the average weight of the 30 ppi control and test foams showed an average variation of, 9.6mg and 10.6mg respectively. The 90 ppi control and test foam filters presented a lower average weight variation in comparison to the 30 ppi foams of of 3.2mg and 2.7mg.The variation of the 30 ppi filters (test and control) was not that different from the variation previously determined when air was not drawn through the filters and similar were the results for the 90ppi foam. The use of control filters eliminated a large amount of the variation in measured weights, reducing the effective variation to 1.2 mg for the 30 ppi foam and to 0.5 mg for the 90 ppi filter. Lyons and Mark (1994) reported a lower variation of 0.5 mg for both the 30 and 90 ppi foam, when control filters were considered in their experiments (Lyons & Mark 1994). This might be due to the different atmospheric conditions (temperature, humidity) on this work. According to Vaughan et al (1989), the masses of dust on filters must be at least three times higher than the background variation of the mass of blank filters (Vaughan et al. 1989). Therefore the detection limit of the mass collected on the foam filters was set at 3.6 mg for the 30ppi foam and 1.5 mg for the 90 ppi foam filter. The results of Figure 45 have also shown that foam tends to change weight continuously. This is due to the porous, open structure of the foam, which allows air to travel through, making it difficult to stabilise its weight. In order to provide a consistent weighing procedure, it was decided to record the foam weight 30 seconds after it was placed on the balance and the enclosure doors were shut. This weighing procedure was proposed by Health and Safety Laboratory (Health and Safety Laboratory 1996).

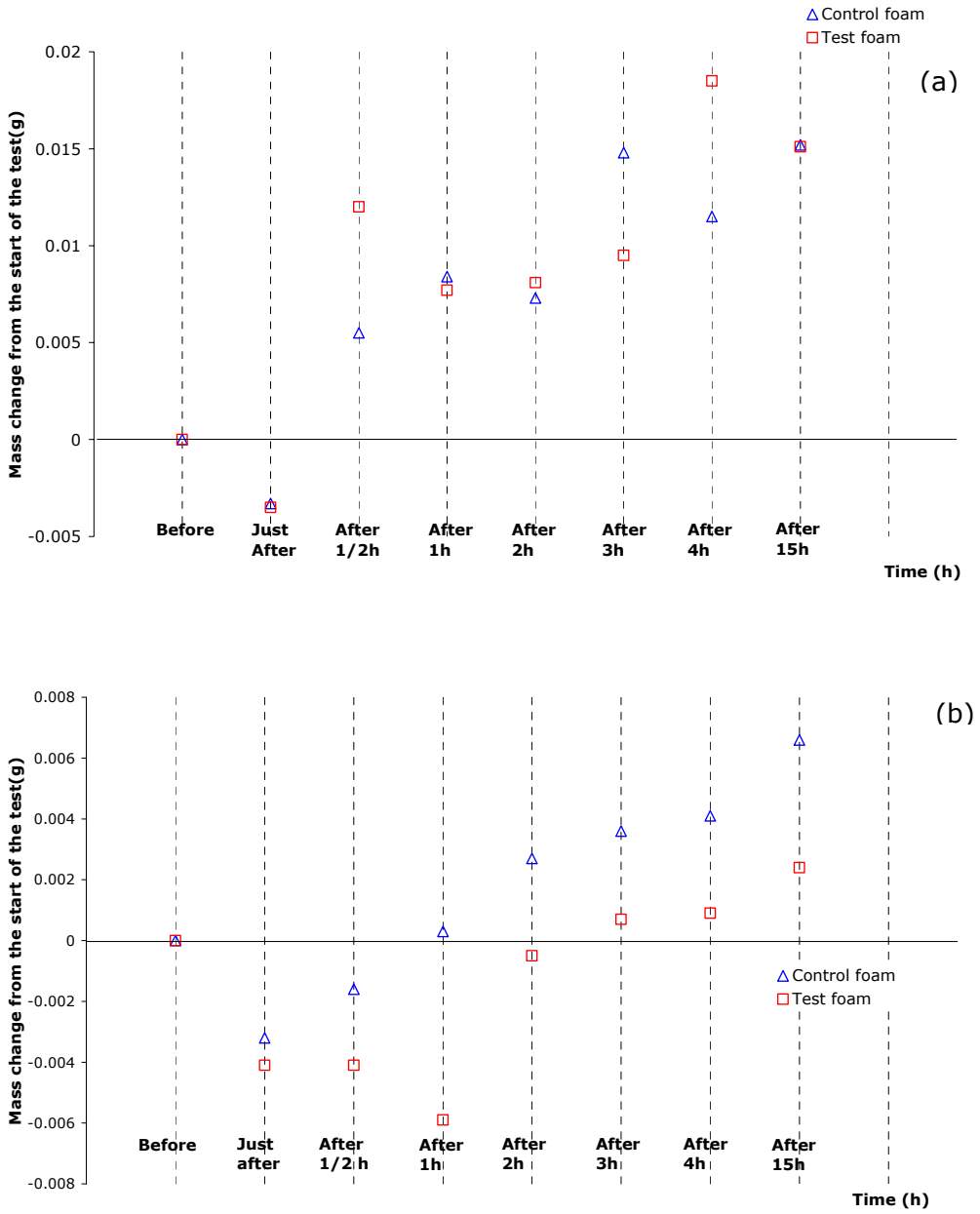

Figure 45: Weight foam stability results for the (a) 30 pores per inch and (b) 90 pores per inch foam filters. The test foam results are plotted against the control and blank foam. Measurements were taken for a period of 15 hours (h). The "just after" measurement corresponds to the values recorded directly after the test.

5.5.1.2. *Results of flow rate variation versus the dust yield*

The results obtained from the study of the total dust yield with variation in airflow rate are presented in Figure 46 and in appendix II. An examination of the results shows that the dust yield increases linearly with flow rate. Hence, higher flow rate values correspond to higher total dust yields. Airflow rates higher than 40 l/min had not been tested as they were not within the capabilities of the air pump in the

apparatus. Higher airflow rates will require a larger open area of foam, which will also not be practical. A similar linear relationship has been reported by the Health and Safety Laboratory during testing of an Aloxite F360 sample at the same flow rate levels (Lyons & Mark 1994).

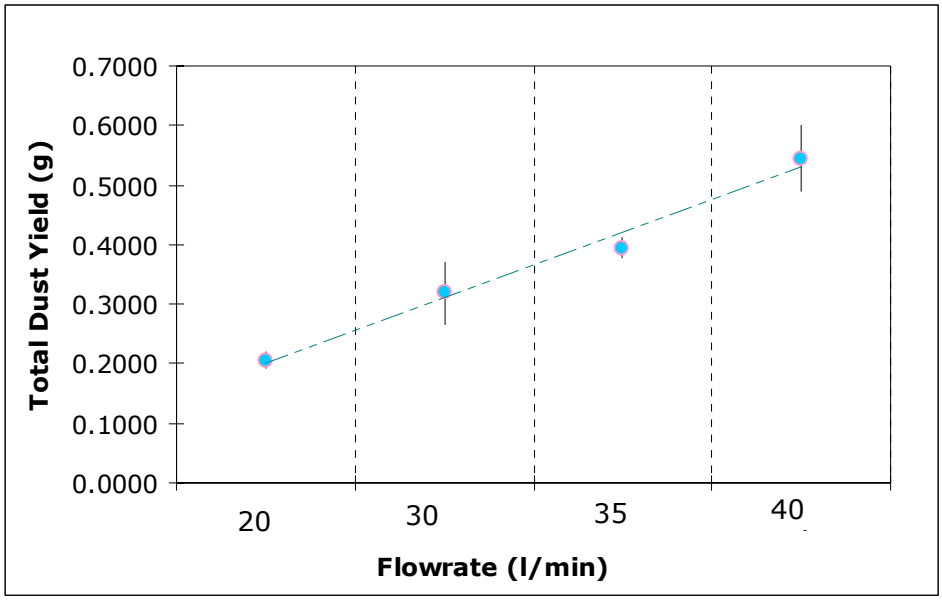

Figure 46: The effect of the variation of airflow rate to the dust yield of limestone (Feed: 100g <3mm limestone, 30rpm, 1 min). The error bars represent one standard deviation from the mean of triplicate tests.

Using a different rotating drum method, the Heubach dustiness tester, the flow rate variation versus the dust yield was examined, on two different occasions, for a limestone sample and an animal feed sample (Heitbrink 1990). Heitbrink (1990) tested a limestone sample (20g, 300sec) at airflow rate values of 5, 10, 15 and 20 l/min and found that the cumulative mass of dust increases with subsequent increase of the flow rate (Heitbrink 1990). When Carlson et al (1992) tested an animal feed (50g, 5min) at airflow rates of 4, 10, 25, 50 and 75 l/min and concluded that dustiness increased linearly as the airflow rate increased, indicating a greater proportion of bulk material was forming an aerosol (Carlson et al. 1992). To maximise the dust yield, so as to make sure that dustiness values will be above the filter weight variation, during further experimentation the flow rate of 40 l/min was chosen as most appropriate.

5.5.1.3.*Results of dispersion time variation versus the dust yield*

The effect of the dispersion time on the dust yield of the limestone samples can be seen in Figure 47 and in appendix II. The total dust yield was observed to increase in

a linear fashion as the tumbling time was extended. The Health and Safety Laboratory (HSL) whilst performing a similar test using an industrial grade of alumina (Aloxite F360) as a test sample concluded that although dispersion time had been doubled, the dust yield remained at the same levels. (Lyons & Mark 1994). This was due to the agglomeration tendency of the sample and its deposition on the walls of the drum (Lyons & Mark 1994). Hjemsted and Schneider (1996) using the HSE-WSL rotating drum test reported that the dustiness index of alumina increased with sampling time from 3 to 10 minutes (50g or 200g, 40rpm, 50 l/min), except with the test conditions of 50g, 60 rev/min and 80 l/min, where the difference between the 3 and 10 minutes was almost negligible (Schneider & Hjemsted 1996). Previous work of the same researchers on the relationship between sampling time and dustiness index of an animal feed using the old version of the WSL dustiness apparatus concluded that dust is liberated only in the beginning when the drum test rotates, with a decrease in dust generation during the rest of the test period (Hjemsted and Schneider 1993). Breum (1999) tested a range of materials (barite, bentonite, coal) using the HSE-WSL rotating drum tester. Different materials gave different dust yield profiles. However, as a general trend it can be noted that the mass of dust increased with sampling time. Dust generated from some materials (i.e bentonite) was produced almost continuously, while the dust from other materials (e.g. talc) was produced instantaneously. During these experiments it was also observed that from the start of a test there was a delay in the mass of dust arriving at the outlet of the drum (Breum 1999). Finally Heitbrink (1990) concluded that the cumulative dust mass of 20g of limestone (at 10-20 l/min), using the Heubauch dustiness apparatus, increased with higher sampling times (Heitbrink 1990).

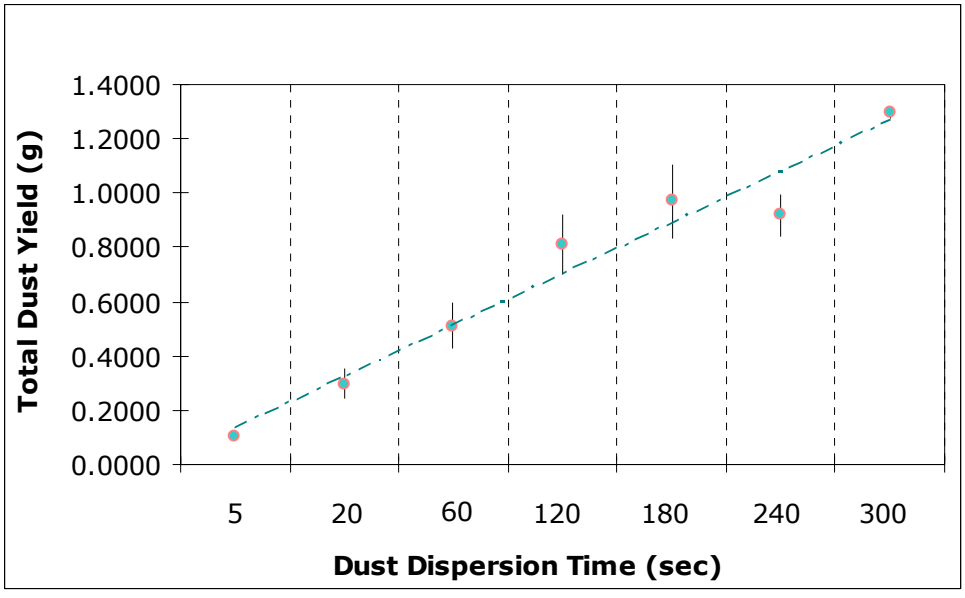

Figure 47: The effect of dust dispersion time to the dust yield of limestone (Feed:100g <3mm limestone, 30rpm, 40l/min). Error bars represent one standard deviation from the mean of triplicate tests.

The limestone sample (< 3.35mm) used in this project, exhibited significant dust yield values within the different sampling time intervals, whilst the deposition on the drum wall was not great. All these results are material specific and they might even be particle size specific (as in feed sample particle size). It is very difficult to define a standard dispersion time as this might underestimate dust emission for some materials and overestimate for others.

From an analysis of these preliminary results it was concluded that two different sampling times should be employed in further tests performed on the limestone samples, namely one and three minutes. The one minute dispersion time is in agreement with the proposed HSL testing procedure (Health and Safety Laboratory 1996), whereas the 3 minutes dispersion time was chosen as a value whereby high limestone dust yield values were achieved.

5.5.1.4.*Results on the sample mass variation versus the dust yield*

The results of mass of dust generated from a variety of sample masses are shown in Figure 48 and in appendix II. It can be seen that increasing the mass of material increases the dust generated from the sample. Lyons and Mark (1994) reported a similar trend while testing a range of masses of aloxite (F360) test sample (25g to 400g) at 40 l/min, 1 min dispersion time and 30 rpm rotation speed. For the limestone a 400g mass of test material, dust yield gave the greatest value. However the dust yield results for masses greater than 150 g present high variations (standard deviation bars, Figure 48). This is probably because a larger mass of test material gives off dust over a longer period of time, so a longer dispersion time is required to achieve coherent results.

Using the same apparatus, Hjemsted and Schneider (1996), investigated the dependency of the mass of alumina on the total dust yield. They found that the weight of dust increased, when the mass of test sample was increased from 50g to 200g and for operational parameters 10 min, 80 l/min and rotation speed 60 rpm. However, when the rotation speed was reduced to 40 rpm, then the dust yield decreased for an increase in sample mass from 50g to 200g. Breum (1999) tested a range of materials (bentonite, talc, coal etc) and concluded that within a material the dustiness was in general positively correlated to the mass of test material. Heitbrink (1990) investigated the effect of the mass of test material (limestone) on dust yield using a different rotating drum test, the Heubauch test and he reported that the amount of dust collected on a filter increases with tester loading until a plateau is

reached. Hence, most previous work reported a positive relationship between the mass of test material and the dustiness levels, as found in this work. However, the dust yield obtained by different samples will increase on different rates accordingly to the particular characteristics and behaviour of the test sample, including the different degradation processes.

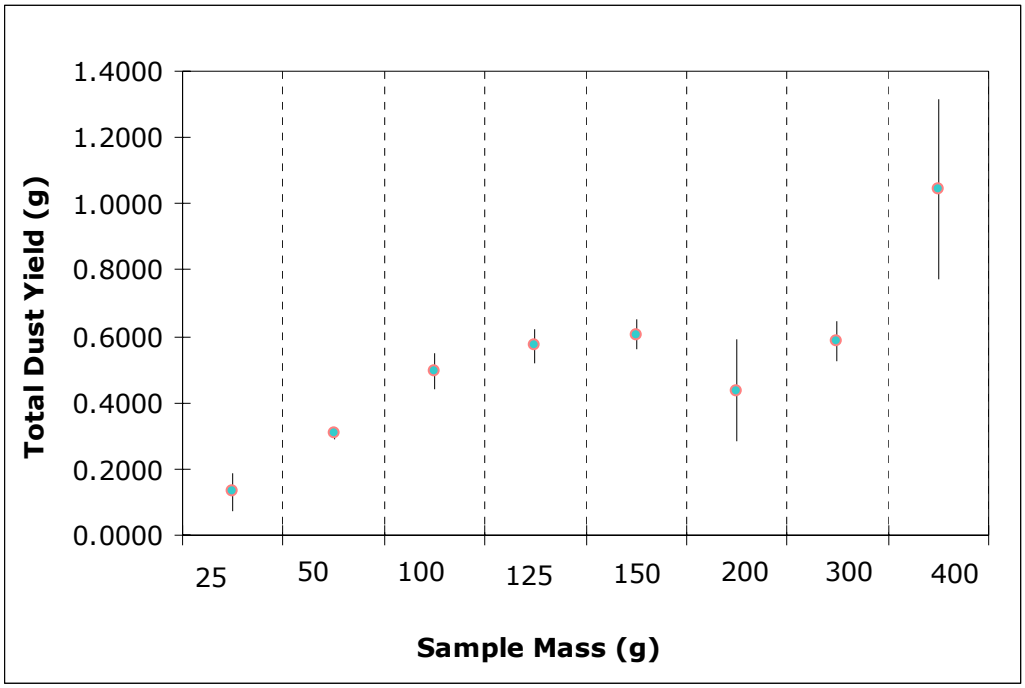

Figure 48: The effect of sample mass variation to the dust yield of limestone. Error bars represent one standard deviation from the mean of triplicate tests (flow rate 40 l/min, tumbling time 1 minute, 30rpm).

The mass of test sample was limited both by the loading-mixing capacity of the drum as well as by the dust capture efficiency of the filters. Also a larger mass of test sample was undesirable as it might convey fine but non-airborne material onto the filters

Two test masses were chosen to further assess the dustiness of limestone 150g and 200g. The 150g sample mass was considered the optimum mass for the limestone sample as it gave a higher value of dust yield with good reproducibility. The 200g of sample mass was chosen in accordance with the HSL proposed testing procedure (Health and Safety Laboratory 1996).

5.5.2.Summary of the preliminary testing results

Preliminary testing took place to identify the dependency of operational parameters upon the dustiness of limestone. The selection of the test material (limestone) was

made based upon its compositional homogeneity. A limestone fraction of <3.35mm was chosen for testing, which comprises fine material, as well as coarser particles.

Results have been obtained for the weight variation of the foam filters, the effect of dust dispersion time, airflow rate and mass of test material, upon dust yield. Experimentation on the weight variation of the foam filters allowed the setting of detection limits of the mass collected on the filters, at 3.6 mg for the 30ppi foam and 1.5 mg for the 90 ppi filter. For limestone the total dust yield correlates positively with the air flow rate, the dust dispersion time and the sample mass. The preliminary testing results were also considered to be influenced by material related properties, such as particle size and shape, density, moisture content. To overcome this obstacle, a range of fractions were tested during dustiness measurements, whilst properties like the moisture content were explored.

Optimum operational parameters produced by preliminary testing were used for dustiness testing of limestone, as well as the rest of the rock samples. The optimum operational parameters were described by an airflow rate of 40 l/min, a sampling time of 3 minutes and a sample mass of 150g. Dustiness results obtained by this set of operational parameters were compared against the experimental procedure recommended by the Health and Safety laboratory.

Preliminary results revealed trends that could be observed in limestone quarry operations. For instance, the effect of tumbling time upon dust yield could equally reflect the dust generation process on an industrial operation such as stockpiling or tipping, or the degree of handling to limestone ore. Thus, according to laboratory findings, increasing the time that stockpiling takes place could result to higher dust levels. Likewise, an increase on material mass, for example in material transfer processes, could subsequently increase the dust yield.

Dustiness results obtained for the limestone samples are presented in the following paragraphs.

5.5.3. Dustiness measurements

Two different testing procedures based upon two different sets of operational parameters were used to test a range of limestone size fractions. According to the

MDHS 81 procedure (Health and Safety Laboratory 1996) 200g of sample were tested at a flow rate of 40 l/m, the tumbling period being 1 minute. The protocol developed from the initial control experiments concluded that 150g of samples should be tested at a 40 l/m for a dispersion period of 3 minutes. In the following paragraphs and chapters the HSL testing procedure is addressed by the abbreviated form of HSL-TP, whereas the optimum operating parameters testing procedure as OPT-TP.

Dustiness indices were determined for limestone particles below 9.5mm, 3.35mm, and 1mm as well as for 10mm single size particles. The particle size distributions of the test samples determined by sieving are shown in Figure 49.

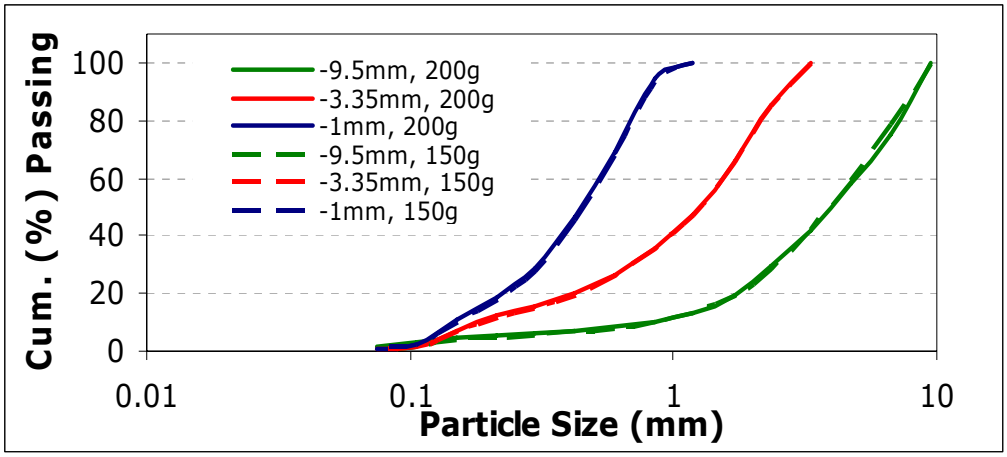

Figure 49: Particle size analysis results obtained by sieving for the limestone test samples.

5.5.3.1. *Analysis and presentation of limestone samples dustiness measurement results*

The dustiness results for the limestone samples tested are shown in Table 23, in appendix II and describe the percentage of the mass of total dust emitted as a function of the mass of test sample. From examination of these results it is concluded that there is a wide spread of dustiness values derived from the tested material fractions ranging from 0.04 to 0.9 %. Results show that the highest dustiness values are obtained over the OPT-TP rather than the HSL-TP. The dustiness values achieved by the OPT-TP and for the majority of the samples, are about three times greater than the ones measured by the HSL-TP, despite the use of a smaller sample mass (150g). These results imply that the tumbling time has a greater effect on the derived dustiness of limestone than the mass of sample tested.

The reproducibility of the dustiness measurements was determined by calculating the standard deviation and relative standard deviation of triplicate tests, which can be reviewed in Table 23. These statistical analysis results concluded that an average standard deviation of 0.03 and an average relative standard deviation of 9.66% should be expected during dustiness testing with limestone. The dustiness indices determined for the various limestone fractions in both tests followed a similar pattern of dustiness, with the highest dustiness values produced corresponding to the <3.35mm and the <1 mm fraction followed by the <9.5 mm and the 10 mm limestone fractions.

Table 23: Dustiness values for the different limestone samples and testing procedure (HSL-TP; OPT-TP). The standard deviation and the relative standard deviation (% RSD) reflect the reproducibility from triplicate tests.

Limestone fractions	HSL procedure			Optimum operating parameters procedure		
	Dustiness (%)	Standard deviation	(%) RDS	Dustiness (%)	Standard deviation	(%) RSD
10mm single size	0.0440	0.013	29.08	0.1207	0.008	6.02
< 9.5mm	0.0514	0.016	3.14	0.2037	0.003	1.55
< 3.35mm	0.2974	0.035	11.83	0.9215	0.144	15.69
< 1mm	0.1307	0.003	2.00	0.2134	0.017	8.02

The effect that the very fine fraction (below 75 μm) of the test sample has on its dustiness levels is shown in Figure 50. The 150g of <3.35mm and the <1mm limestone samples, and the 200g of <9.5mm sample consist of greater percentages of particles below 75 μm. For the <3.35mm and <1mm fractions a higher concentration of fine material corresponds to a higher dustiness value. This is not the case though for the coarser sample (< 9.5mm). However, this might be due to the lower tumbling time (1 minute), thus increasing the rotation time may reverse the existing result between dustiness and fine particles concentration. Both the dispersion time and the concentration of fine particles are critical parameters to the dust emission levels of the test sample.

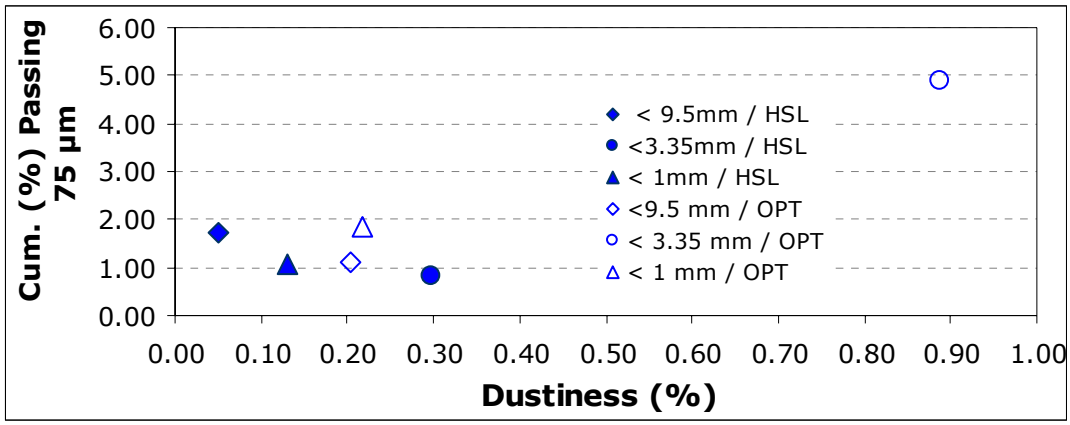

Figure 50: The dustiness of limestone versus the proportion of fines (<75µm) included in the various test sample.

5.5.3.2. *The effect of moisture content upon limestone's dustiness*

Measurement of the moisture content of the various limestone fractions took place, so as to identify how it affects dustiness. Previous research had explored the effect of additives (i.e water, chemicals, oil etc) and hence the moisture content upon dustiness for dust control purposes (Higman 1986). For this project, the moisture content represents a physical property of the test material, which might influence the dust generation process.

The measurement procedure followed was that of the British standard BS812-109:1990 (BSI 1990). According to this procedure, 1000g of the <9.5mm limestone sample and 500g of the <3.35mm and <1mm limestone were placed in a pre-weighed container and left in a ventilated oven set at a temperature of 105 ^{O}C, for 24 hours. At the end of the 24 hours the container with the test sample was removed from the oven and left to cool in atmospheric conditions for half an hour. The weight of the container plus the test sample was weighed before and after the drying process. The moisture content was calculated by Equation 15, where M1 is the weight of the container, M2 is the weight of the container and the test sample before drying and M3 is the weight of the container and the test sample after the drying process.

The results obtained are presented against the dustiness values for both testing procedures in Table 24. The moisture content of the <3.35mm limestone fraction exhibited an increased value of moisture content in comparison to the <1mm fraction, whilst the highest dustiness value of the <3.35mm sample, corresponded to higher moisture content percentages. The difference, between the moisture content measured for the <1mm fraction and <3.35mm was very small. Therefore the effect

of moisture content is not considered a critical parameter to explain the difference in dustiness values obtained from different sample fractions. Nevertheless higher moisture content values could affect the dustiness of limestone and result into reduced dust emissions.

Table 24: The moisture content (%) of the limestone test fractions in relation to dustiness (%) (average values) from the two testing regimes.

Sample	Moisture content (%)	Dustiness (%) HSL testing procedure	Dustiness (%) Optimum parameters procedure
<9.5mm	0.04	0.0514	0.2037
<3.35mm	0.10	0.2974	0.9215
<1mm	0.06	0.1307	0.2134

(Equation 15) $$moisture\ content = \frac{M_2 - M_3}{M_3 - M_1} \times 100\,(\%)$$

5.5.3.3. *Determination of the health based dustiness indices*

The health related dustiness indices are presented in Table 25 and in appendix II. The definition of the health based dustiness indices was given in Chapter 4. The dustiness index of the inhalable fraction equals to the values discussed in the previous sections, shown in Table 23. As an example, the inhalable dustiness value of the <3.35mm – 150g sample is 0.9% implying that 0.9% of the 150g of the mass of test sample will become airborne with a possibility to be inhaled through the nose and mouth. The Dt (thoracic fraction dustiness index) value for the same sample is 29%, which means that 29% of the total dust might penetrate beyond the larynx. Equally the Dr, respirable fraction dustiness index, value is 0.64%, so 0.64% of the total dust might penetrate to the gas exchange region of the lung.

The dustiness index of the thoracic fraction ranges from 5% for the <9.5mm-200g sample up to 67% for the <1mm-200g sample, whereas the dustiness index of the respirable fraction varies from 0.03 % for the 10mm single size – 150g sample to 4.7 % for the 10mm single size – 200g sample. Both the D_t and D_r values of the HSL proposed testing procedure, for the majority of samples, are higher than the ones obtained through the optimum operating conditions testing procedure. So the dustiness indices of the thoracic and respirable fraction are not necessarily proportional to the dust yield of the test sample. For example the dustiness values for the <1mm – 200g is 0.1307% and the D_t and D_r values respectively are 67% and

2.4%. The dustiness value of the <1mm – 150g sample is 0.2134% and the D_t and D_r values are 24% and 0.6%. Even though the total dust yield for the 150g sample is double than for the 200g sample, the health related dustiness indices do not behave in the same way.

Table 25: Health based dustiness indices obtained for the different limestone samples and testing protocols. One standard deviation has been calculated from triplicate tests.

HSL protocol	Limestone fractions			
	10 mm single size	<9.5mm	<3.35mm	<1mm
D_t (%)	39.2118	8.0074	28.0877	66.9935
Standard deviation	21.9393	2.0923	1.9135	23.5744
D_r (%)	4.7461	0.8669	0.2831	2.3792
Standard deviation	6.4596	0.6908	0.4904	0.5896
Optimum parameters protocol				
D_t (%)	17.4847	6.8228	29.2681	24.4112
Standard deviation	2.2282	1.9697	2.9433	0.7595
D_r (%)	0.0299	0.2285	0.6430	0.6025
Standard deviation	0.0423	0.848	0.2419	0.2250

The increased tumbling time (3 minutes instead of 1 minute used by the HSL-TP) of the OPT-TP, allows the test sample to generate dust for a longer period. The higher dustiness rates may allow the deposition of particles on others already attached to the filter surface, thus producing the potential to form stacks of particles. The above statement was justified using the scanning electron microscope on the foam filters that carried dust. A SEM photomicrograph is shown in appendix II.

One standard deviation was calculated from the triplicate tests, which in comparison to the inhalable dustiness values are much higher (Table 25). It is difficult to determine the exact reasons for this variation. However, the mobility characteristics of the airborne fraction might be the most critical factor. The way airborne particulates travel through foam filters might not be very consistent due to the production of agglomerates on the 30 pores per inch filter surface. Several other parameters might account for this variation such as the handling of the foam filters during the disassembling process from the drum, atmospheric conditions (i.e relative humidity), or physical characteristics of the particulate matter like particle shape and orientation of the particles in the airborne state. It is very likely that the combination of all the above parameters of influence could represent the source of error

Earlier work by the Health and Safety Laboratory while performing a round robin test using 30 different test samples revealed that there was no clear evidence as to the effect that atmospheric conditions have upon dustiness indices (Lyons et al. 1996). Nevertheless, it was believed that atmospheric conditions do influence the measurement process and further examinations was required (Lyons et al. 1996). Standard deviation values calculated by the different laboratories were variable some exhibiting very high values and others good reproducibility. The observed variability was mainly attributed to human errors, such as handling of the foam filters, rather than deficiencies of the method. The standard deviations calculated after testing with the limestone fractions lay within the lower values observed by earlier researchers (i.e.(Lyons & Mark 1994)).

The health based classification of the HSE-WSL test aims to simulate the effect of dust on human exposure. The penetration of particles in human bodies does not always follow the same pattern and even for one individual, several parameters such as fatigue or atmospheric conditions or breathing rates could increase or decrease the effect of particulate matter. When assumptions are made for a plethora of individuals then the examination process complicates even further. Hence, it is difficult to set a lower and upper limit for each health related dustiness index which will ensure accuracy.

5.5.4. Summary of the dustiness results analysis

Experimental testing on limestone was carried out using two different testing regimes the HSL proposed testing procedure (HSL-TP) and the optimum operating procedure protocol (OPT-TP), which resulted from preliminary testing. The main difference between the two regimes was the established operational parameters and in particular the mass of test material and the sampling time. Four different limestone fractions were tested using these protocols. Three of the fractions comprise mixtures of a range of limestone particles with the <9.5mm limestone representing a coarser particle size distribution, followed by the <3.35 mm sample, whilst narrower and finer particle size distributions were represented by the <1mm limestone. The fourth fraction consisted of single sized particles of 10mm.

The <3.35mm limestone produced the highest dustiness index followed by the <1mm fraction, which in turn was followed by the <9.5mm fraction and 10 mm particles. The single sized particles in contrast to the rest of the samples produced dust only due to abrasion mechanisms within the tumbling drum and not due to the presence of fine liberated particles, therefore, produced dustiness levels were low.

Dustiness results revealed that the concentration of fine material (<75μm) in the test sample positively correlates to the dust generation potential of a sample. In terms of the operational parameter, rotation time has the greatest effect upon dustiness, as the uppermost dustiness values were produced by the OPT-TP for all fractions. It has to be noted here that the optimum parameters regime used a lower sample mass. The same trend was observed by preliminary testing.

According to the Health and Safety Laboratory the inhalable dustiness results of materials can be classified within the five categories shown in Table 26 (Chung and Burdett 1994). Following the proposed description the limestone test samples are categorised accordingly in Table 27.

Table 26: HSL proposed classification on the basis of the inhalable results of materials (Chung & Burdett 1994).

Descriptor	Dustiness level
Not dusty	Percentage of inhalable fraction <0.01%
Slightly dusty	0.01%< percentage of inhalable fraction <0.1%
Dusty	0.1%<percentage of inhalable fraction<1%
Very dusty	1%< percentage of inhalable fraction <10%
Extremely dusty	Percentage of inhalable fraction >10%

Table 27: Classification of the dustiness results for the limestone samples as proposed by HSL

Testing procedure	Limestone fractions	Dustiness (%)	Classification
HSL procedure	10mm single size	0.0440	slightly dusty
	< 9.5mm	0.0514	slightly dusty
	< 3.35mm	0.2974	dusty
	< 1mm	0.1307	dusty
Optimum operating parameters procedure	10mm single size	0.1207	dusty
	< 9.5mm	0.2037	dusty
	< 3.35mm	0.9215	dusty
	< 1mm	0.2134	dusty

Calculations of the health based indices also took place, even though the application of dustiness testing to the prediction of human exposure was not within the objectives of this project. However, it was thought useful to present these results as the HSE-WSL drum enabled health based classification of dust. The HSL-TP gave for most of the samples higher dustiness values of the thoracic and respirable fractions implying that lower total dustiness rates enable particulate matter to travel through the whole filter sequence and not just the first (30ppi) foam filter. In the case of the

OPT-TP there is the possibility that the first filter gets saturated by dust particulates forming stacks of particles, which do not allow the finer ones to penetrate to the next stage. Also, greater tumbling time could enable coarser particles to pass into the airborne state. Other parameters that may account for this difference are the mobility characteristics of the airborne fraction. Nevertheless, investigation of the dust emission process is beyond the scope of this project. Particle size analysis results on the particulate matter fraction will allow elucidation of the main differences between the two testing regimes. For this project, health related classification of the dust fraction is used to outline only general trends.

Measurement of the moisture content of the different limestone fractions showed that there was not great a discrepancy between the values recorded from various feed samples, therefore the influence of moisture content upon dustiness was considered minimal (under the used testing conditions).

According to the research findings so far, it is obvious that dustiness depends upon several parameters such as material properties and characteristics (i.e particle size distribution of feed sample) and operational parameters (airflow rate, mass of test sample, sampling time). Therefore it becomes difficult to attribute a single value that can reflect the dust generation potential of a material such as limestone independently of material properties and operational parameters.

However certain trends were identified such as the positive dependency of fines to dustiness levels as well as sampling time to dust yield, which exhibited a similar profile for all different fractions and operational parameters. In industrial processes the dust generation potential of limestone could be reduced if optimisation steps take place, which aim to minimise the production of fines and the consumption of time in operations that are liable to generate dust. The mass of processed materials should also be considered in such optimisation attempts, as preliminary testing showed that the higher the limestone mass used, the greater the dust yield. For instance, optimisation of the comminution steps of a mineral preparation plant regarding the residence time of the ore, or the sample mass used or a change to the closed size setting of a crusher that could result to lower amounts of fines could greatly reduce the production of dust. Similarly, the transfer of material by a well designed conveyor belt network, which operates for shorter time scales, could enable the reduction of particulate matter emissions. Such alternative solutions to the problem of dust generation that incorporate optimisation steps would also be cost beneficial, as it would result to less dust control requirements and energy consumption.

5.6. Investigation into the mechanisms of dust generation in the HSE-WSL test

One of the major issues that arose during experimentation on dustiness of the limestone samples was to identify what are the exact mechanisms taking place in the tumbling drum that are liable for the production of particulate matter. In common grinding mills, such as autogenous mills, there are various mechanisms that take place, which result to breakage of particles. During tumbling, particles are lifted to the top of the mill and subsequently move perpendicular to the plane of contact, impacting on other particles or on the drum walls, which produces breakage (appendix II). At the same time, part of the charge comprises a series of layers, which slip over one another and promote abrasion and attrition breakage due to interparticle contacts and particle-wall contacts (Napier-Munn et al. 1996). Mineral processing engineers often investigate the breakage patterns found in grinding mills so as to optimise their performance (i.e minimise energy consumption, and fines concentration) and to increase throughput (Napier-Munn et al. 1996).

Similar investigation steps can take place in the HSE-WSL dustiness test, so as to determine if the breakage or attrition of the test particles is liable for the generation of dust and to identify what are the principle mechanisms acting on the particles of this particular test that contribute to the production of particulate matter. In addition, in depth understanding of the dust generation process of the tumbling test can allow critical comparisons to be made upon the simulation of industrial handling processes by the WSL test.

The mechanisms of dust generation in the tumbling mill were investigated using both experimental and computational steps. Experimentation took place through two different procedures. Initially the kinetics of the tumbling action were explored for a variety of single sized limestone fractions, by conducting the WSL test for a range of tumbling times and surveying the effect the tumbling time has on the sample. The specific rate of breakage of each fraction was calculated and conclusions were drawn regarding the probability of the limestone fractions breaking and generating dust. The behaviour of the limestone particles in the drum during the rotating action was further investigated and recorded using a high speed video system. The high speed camera assisted the understanding of the motion of the limestone charge in the tumbling mill, whilst the participating breakage mechanisms were identified. In addition, the tumbling mill was simulated through computational steps using a discreet element modelling (DEM) method. The DEM method was used to predict

particle motion and fragmentation as well as energy distribution in the tumbling mill. Experimental and computational results are compared and conclusions are made regarding the generation of dust and the effectiveness of the WSL rotating drum test to simulate common processes from mineral sites with high dust production potential.

5.6.1. Kinetics of the HSE-WSL drum

The rate of breakage in the tumbling drum was initially investigated by exploring the effect that tumbling time has upon single sized limestone particles. Four different single fractions of 150g of limestone were tested at various tumbling time intervals as shown in Table 28.

Table 28: Single fractions of limestone and tumbling time intervals used to investigate the kinetic dynamics of the WSL mill.

Limestone fractions	Tumbling Time (minutes)
3.35x2.36mm 2.36x1.7mm 1.7x1.18mm 1.18x0.85mm	1 2 3 4 5 7 9 15

At the end of each experiment the limestone particles and fine material were recovered from the mill and sieved using a $\sqrt{2}$ sequence of sieves from the top size of the feed down to 53μm.

The breakage process of the tumbling mill was modelled on the basis of the specific rate of breakage and the breakage distribution functions. The specific rate of breakage S_j, is the probability of a particle of size j being broken in unit time (specific tumbling time interval) (Rhodes 2003). The breakage distribution function b(i,j) describes the size distribution of the product from the breakage of a given size of particle (Rhodes 2003). The modelling of the tumbling mill breakage process is based on the hypothesis that the disappearance rate of particles in a given size interval can be proportional to the amount of that size remaining (Tangsathitkulchai 2002). The breakage process can be modelled on the basis of first order kinetics using Equation 16. The population balance equation states that the production rate of a material of size *i* must be equal to the summation of the production of material of all larger sizes, minus the rate of breakage to size i and smaller sizes (Austin et al. 1984).

(Equation 16) $\frac{dw}{dt} = -S_i w_i(t) + \sum_{j=1}^{i-1} b_{i,j} S_j w_j \quad (i \geq j+1)$

Where w_i is the mass fraction of all particles in the tumbling drum that fall into size class *i*, S_i the breakage rate of particles in size class *i,* and $b_{i,j}$ is the breakage function , which refers to the breakage of size interval *j* relative to the size class *i*. If only the top size fraction is considered then equation 2 can be rewritten to a more simplified format shown in Equation 17.

(Equation 17) $\frac{dw_i}{dt} = -S_i w_i$

The integration of Equation 17 gives Equation 18.

(Equation 18) $\ln \frac{w_i(t)}{w_i(0)} = -S_i t$

Where $w_i(0)$ is the relative amount of material of size *i* in the mill at time zero. The breakage selection function S_i is calculated by plotting the natural logarithm of the relative amount of material greater than a size *i* against the cumulative grinding time. Figure 51 presents the particle size distribution of the -3.35+2.36mm fraction after different tumbling times. Figure 52 shows a plot of the mass retained against the cumulative tumbling time. Figure 53 presents the approximation of the data to first-order kinetics and the specific rate of breakage values (S_i) obtained for the different single size fractions. The particle size distribution results show that greater tumbling time results in finer particle size distributions. The impact that tumbling time had on particles, was particularly intensive at smaller sizes (i.e below 1.7mm for the -3.35+2.36mm fraction). Hence increasing the tumbling time causes an increase in the concentration of fines, implying that mainly surface breakage occurs due to the wear of particles on its surface by abrasion and chipping.

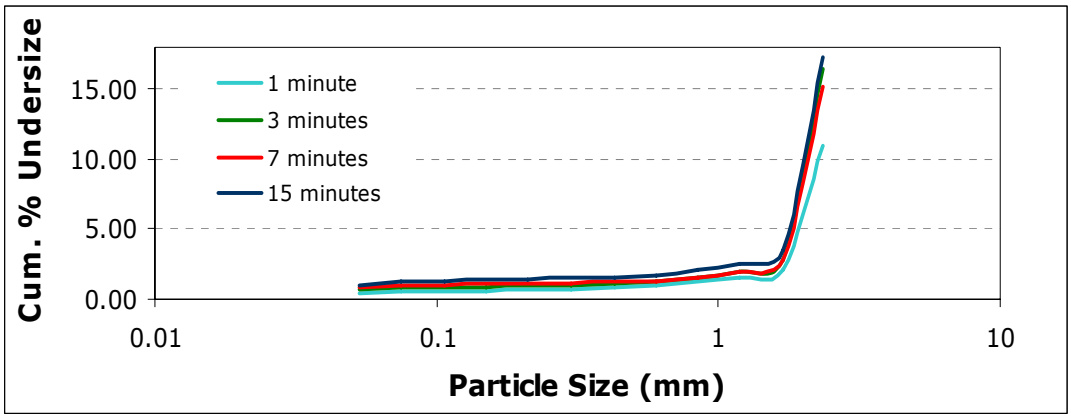

Figure 51: The particle size distribution of the -3.35+2.36mm fraction produced for tumbling times 1, 3, 7 and 15 minutes and at rotation speed 30rpm.

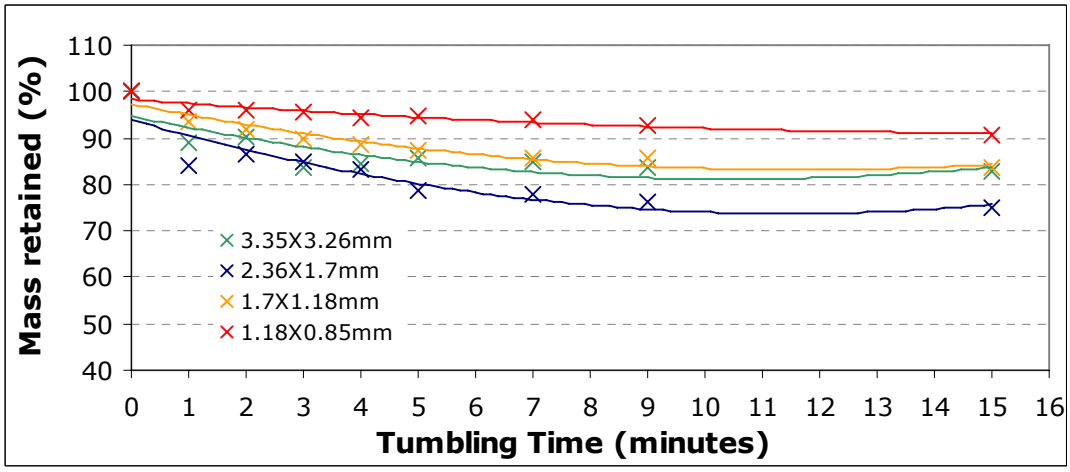

Figure 52: Percentage of mass retained against tumbling time for all tested single fractions at a tumbling speed of 30rpm.

The specific rate of breakage values obtained for the -2.36+1.7 mm and -1.7+1.18 mm fraction, were higher that the coarser fraction -3.35+2.36mm, which signifies that these two fractions have a greater potential to break, thus limestone exhibits selective breakage. The -1.18+0.85 mm presents the lower specific breakage rate. A similar trend has been observed when the percentage of mass retained was plotted against the tumbling time. Figure 53 shows that the disappearance rates are more rapid initially and for tumbling time up to 4 minutes, whilst for increasing times, past 4 minutes, the rate of breakage is lower. For tumbling times greater than 9 minutes no further breakage occurs.

The values of the breakage distribution function b(i,j) were used to describe the size distribution of the breakage product. Some of these results are presented in Table

29. In addition the specific rate of breakage and the breakage distribution function were used to predict the product size distribution of a limestone feed <3mm (150g). The product size distribution was also determined by sieving and the results were compared with the predicted ones. Both the feed and measured product size distributions are expressed as fractions of the mass retained at a particular particle size interval to the total mass of the sample. The product size distribution was predicted using Equation 19, which results from a modification of Equation 16. Since wi=yiM and wj=yjM, where M is the total mass of feed material and yi is the mass fraction in size interval i, then we can write a similar expression for the rate of change of mass fraction of material in size interval, i with time (Equation 19) (Rhodes 2003). The results obtained are presented in Table 30.

$$\text{(Equation 19)} \quad \frac{dy_i}{dt} = \sum_{j=1}^{j=i-1} \{b(i,j) S_j y_j\} - S_i y_i$$

Table 29: The specific rate of breakage and breakage function for the tumbling mill and tumbling time 3 minutes.

Interval (mm)	3.35x2.36	2.36x1.7	1.7x1.18	1.18x0.85
Sj	0.0088	0.0149	0.01	0.0053
b(1,j)	0	0	0	0
b(2,j)	0.83	0	0	0
b(3,j)	0.05	0.84	0	0
b(4,j)	0.02	0.05	0.71	0

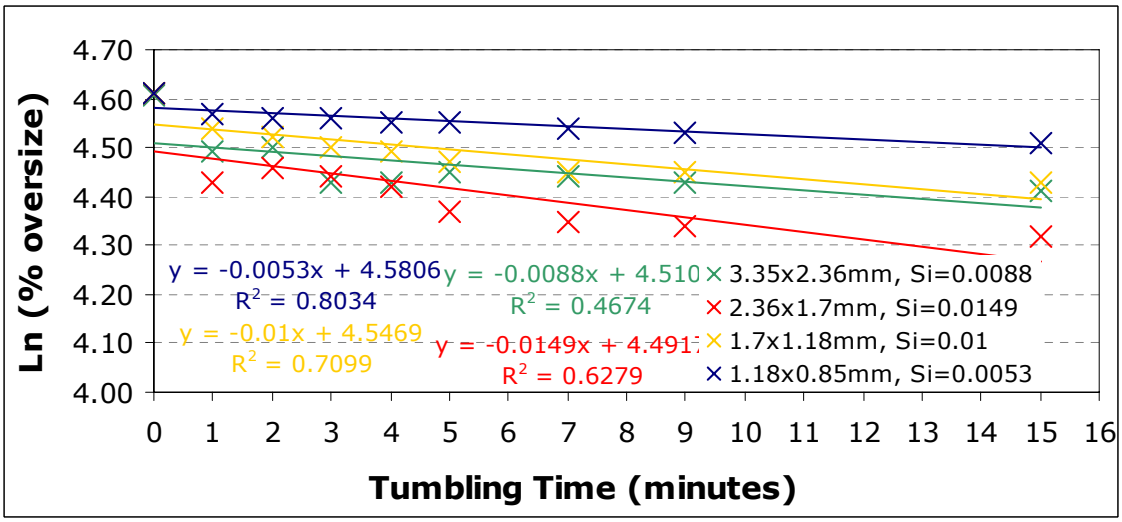

Figure 53: Natural logarithm of the percentage oversized against tumbling time for the limestone single fractions 3.35x 2.36mm, 2.36x1.7mm, 1.7x1.18mm and 1.18x0.85mm and for tumbling speed 30rpm.

As can be seen from Table 30, the predicted and measured product size distributions present very good agreement. Similar results were obtained for all tumbling times and they can be reviewed in appendix. Thus, with a set of specific rate of breakage and breakage function values for a given feed material, the product size distribution after a given time in the WSL mill may be determined.

Table 30: Prediction of the product size distribution of a limestone <3mm feed, 150g, tumbling time 3 minutes. The product size distribution is also determined by sieving (measured product).

Interval (mm)	3.35x2.36	2.36x1.7	1.7x1.18	1.18x0.85
Interval No j	1	2	3	4
Feed				
Fraction	0.21	0.18	0.15	0.1
Prediction for product				
Fraction	0.19	0.17	0.15	0.1
Measured product				
Fraction	0.25	0.19	0.13	0.09

Earlier studies, exploring the effect of tumbling time (1 to 5 minutes) on dust yield (for a limestone sample of 100g, <3.35mm), revealed a linear relationship, where an increase in tumbling time corresponds to an increase in dust yield. The dust yield increased rapidly for tumbling times up to 3 minutes. Also dustiness results for a single size limestone fraction (10mm particles) showed that increasing the tumbling time from 1 minute to 3 minutes doubled the dust yield. This result is in good agreement with the disappearance rates observed for the single size fractions of limestone, which also increase with extended tumbling times up to 4 minutes.

The breakage process of the tumbling mill has successfully been modelled on the basis of first-order kinetics. As a result the HSE-WSL drum test can be considered to simulate well attritive handling processes. Also the product size distribution of limestone has been accurately determined, which indicates that the accumulation rates of fine material in the mill are predictable and as a result the potential dust to be generated could be estimated. Tests such as the ones described in this paragraph, could prove good predictors of materials behaviour under certain processes and its dependency with dustiness levels. Industrially these observations suggest that optimisation of certain processes can result in lower dust emissions.

5.6.2. Recording of the tumbling mill using a high speed camera

The tumbling motion of the particles in the WSL drum was recorded using a Kodak EM high speed video system provided by EPSRC engineering instrument pool. The Kodak EM (electronic memory) system records high speed events and provides immediate slow-motion playback. The system consists of a Kodak ektapro hi-spec processor, a Kodak ektapro hi-spec imager, a monitor, light sources and a PC. To permit an inside view of the rotation of the particles, the conical ends of the drum were covered by perspex discs. The imager was set in parallel to one of the conical ends as well as the main light sources. Additionally, a pair of spot lights was set at each conical end which improved the image detail. The system recorded directly to solid state memory for 20 seconds at 1000 frames per second. The full picture size had a definition of 240 pixels horizontal, 200 pixels vertical and 625 pixels grey levels. The system was also fitted with a Kodak interface, which allowed the recorded images to be downloaded to a 300 MHz Pentium II personal computer, which was supplied as part of the system. The experimental set up can be seen in Figure 54.

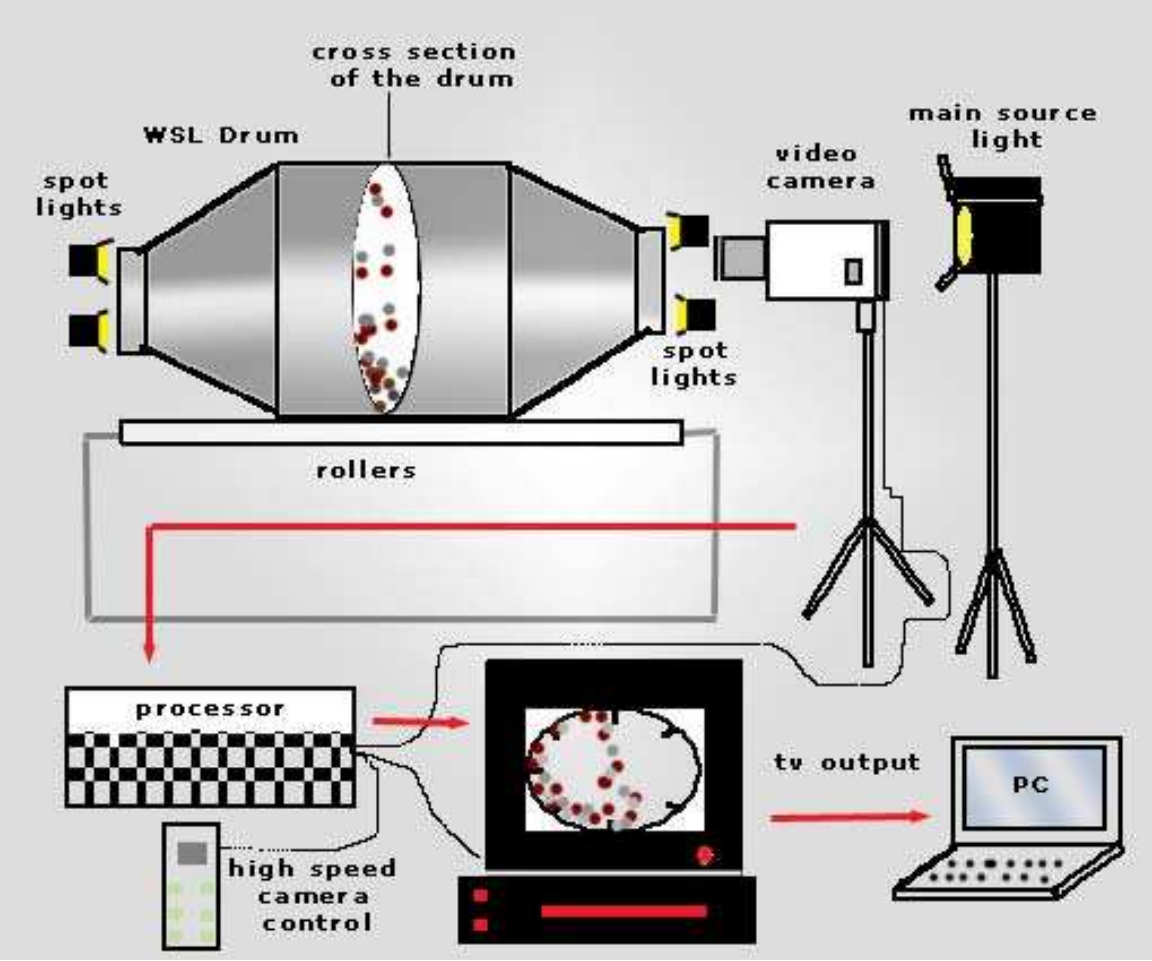

Figure 54: The experimental setup of the recording of the tumbling drum.

For this work, limestone particles of 10mm single size were used at masses of 150g, 200g and 400g. The rotation speed of the mill was kept constant at 30rpm. The tumbling action was recorded till the memory of the system was filled. A certain amount of frames (up to 500) were downloaded to the personal computer for further image processing, which enabled the production of a movie.

5.6.2.1. *Experimental observations using the high speed video system*

Recording of the tumbling process showed that limestone particles were transferred with the help of the lifter bars to the top of the drum, where they were allowed to follow a free fall and eventually impacted at the bottom of the drum. The same process continued several times until the test was completed.

The size of the limestone particles was smaller than the lifter bars (25mm), therefore the particles were attached to the inner edge of the blades and released only when found at a position in the drum where the influence of gravity was greater than any other applied force, normally at a position close to vertical. This behaviour resulted to impaction of particles in discreet events and not continuously for sample masses below 400g. During the impaction it was shown that particles did not break and fragmentation did not occur, implying that dust was not generated due to impact breakage of particles. Also, particle to particle interaction was low for small masses of limestone (i.e 150g and 200g). Particle to particle interactions were present due to sliding of particles caused by the rotation of the mill as well as due to impaction of particles over others during the free fall motion, although the second was observed at higher rates, for sample masses greater than 200g. These observations explain the dependency of dustiness with sample mass, found during preliminary testing, where higher masses resulted to higher dustiness values.

Particles diminished their size only due to abrasion during frictional sliding and interparticle contacts. Consequently, abrasion is the only mechanism present that is liable for the generation of dust.

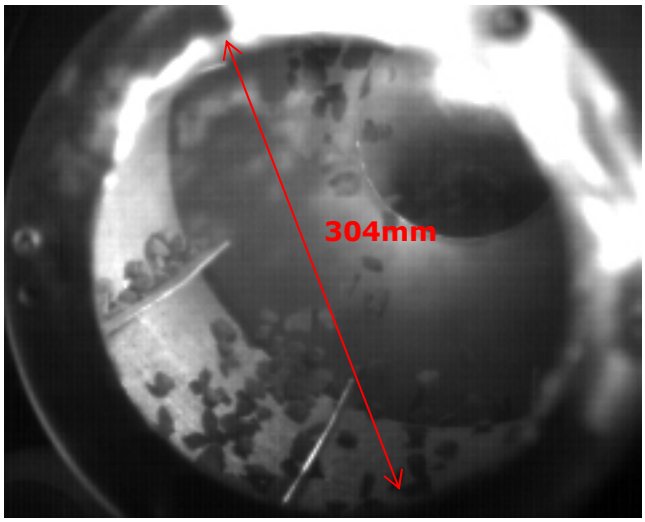

Figure 55: The tumbling action of the 10 mm limestone particles in the HSE-WSL mill as recorded using the high speed video system. The diameter of the mill is 304mm.

The kinetic energy of the particles in the mill is closely related to the probability of breakage. If breakage does not take place, then the particles do not generate sufficient kinetic energy. The kinetic energy of the particles was determined by tracking the trajectories of individual particles on a frame by frame basis from the top of the mill to the impact point. A single particle was tracked by marking its initial position with a reference mark. The reference mark location is presented with an X on the monitor. Subsequently, the new position of the particle (x,y), after a couple of frames, relatively to the initial one is noted. The particle is tracked down till it reaches the impact point. The velocity (v in m/sec) of the particles was calculated from the change in horizontal (dx) and vertical (dy) distances as a function of time (dt) (Equation 20).

(Equation 20) $$v = \sqrt{\left(\frac{dx}{dt}\right)^2 + \left(\frac{dy}{dt}\right)^2}$$

The kinetic energy of the particles is given by Equation 21, where m is the mass of test sample (i.e 150g or 200g) and v (m/sec) is the velocity of the particles.

(Equation 21) $$E_k = \frac{1}{2}mv^2$$

The particles (150g, 10mm) reached their maximum velocity, thus their uppermost kinetic energy, close to impaction. The particle velocity was 1.59 m/sec, whilst the kinetic energy was 0.001 Joules. The velocity and kinetic energy results represent average values from repetitive tests. The experimental results for the kinetic energy of the limestone particles are compared with discreet element modelling data, whereas the minimum kinetic energy requirements for fragmentation to occur are calculated and presented on the following paragraphs.

The coefficient of restitution (c.o.r) was also calculated, because it provided a measure of the energy loss during impact. The coefficient of restitution represents the ratio of the height of the particle during release to its rebound height. The release height of the particle was equal to the diameter of the mill. The Kodak EM system was used to record the impaction of a single particle on a steel surface, whilst the trajectory of the particle was tracked down frame by frame so as to get an accurate measurement of the rebound height. The experiment was repeated three times and an average value equal to 0.31 represented the coefficient of restitution. In a perfect elastic collision scenario, the particle should return to its initial release height resulting to a coefficient of restitution value equal to 1. Nevertheless, this is not the case for the limestone particles as the end value is 0.31, which implies that the impact of the particle results to kinetic energy dissipation (i.e particles spin) or transformation of the kinetic energy to other energy forms (i.e heat or sound). As found in the tumbling drum test, fragmentation did not occur. Therefore, only a small proportion of the kinetic energy released during impact was absorbed by the particle, but was not sufficient to break it.

Figure 56: The limestone particle highest position from rebounding to the steel surface.

Experimentation using the high speed video system concluded that the HSE-WSL test simulates well industrial processes (i.e where impact breakage does not occur), where dust is generated due to abrasion of the rock particles such as conveyor belts, screens, haulage roads and other.

5.6.3. Computational modelling of the tumble mill

Computational modelling of the tumble mill was undertaken to provide a greater understanding of the mechanisms of dust generation that were observed within the mill and also to identify the mill parameters that affect the volume of dust produced. The modelling was undertaken using the distinct element modelling code PFC^{3D} Version 3.0 produced by Itasca (Itasca Consulting Group Inc 2003). Although the DEM method was developed in 1979 (Cundall and Strack 1979) it was only around 1990 that Mishra and Rajamani (Mishra B.K. and Rajamani R.K. 1992) adapted the scheme to solving tumbling mill problems as prior to this the method was too demanding for the computational technology at the time. DEM has now been adopted as an established method for predicting particle motion and energy distributions in tumbling ball mills (Djordjevic 2003;Mishra and Cheung 1999;Morrison and Cleary 2004). More recently application of the DEM technique have modelled power draw demonstrating that the numerical approach produced results that were close to monitored values and comparable with the results obtained using empirical based models (Cleary 2001;Djordjevic 2003). The discrete element modelling method was used as a black box to investigate the mechanisms taking place in the tumbling mill. The simulations were performed and provided by Dr. David Whittles.

5.6.3.1. *Numerical Modeling of the Tumble Mill*

The tumble mill simulation can be considered to comprise of two components which were namely the mill itself and the mass of particles inside the mill. The sub-angular equate shaped limestone particle used in the laboratory experiments was represented as a bonded agglomerate of six spherical elastic particles. A picture of a typical particle is shown in Figure 57.

The friction angle of the wall/particle contact was obtained by undertaking a simple tilt test whereby a single particle was placed on a flat sheet of stainless steel which was tilted until the particle started to slide.

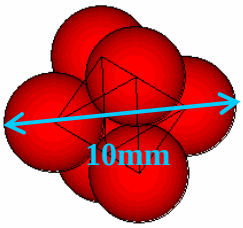

Figure 57: PFC^{3D} Particle Formed by Clump Logic. The diameter of the particle equals to 10mm.

The angle of sliding was measured to provide an estimate of the friction angle. This simple experiment was repeated several times and the average friction angle determined using this method was 21°. To ensure that the friction angle produced the correct trajectory of the particle in the mill, the trajectory of a single particle around the drum was compared to that derived from the video of the tumble drum. It was considered that if the particle traced a similar trajectory to a particle in the actual mill the frictional parameters for the walls and particles would be correct (Figure 58). The trajectory of the particles traced in the actual mill correlates well with the modelled particle track.

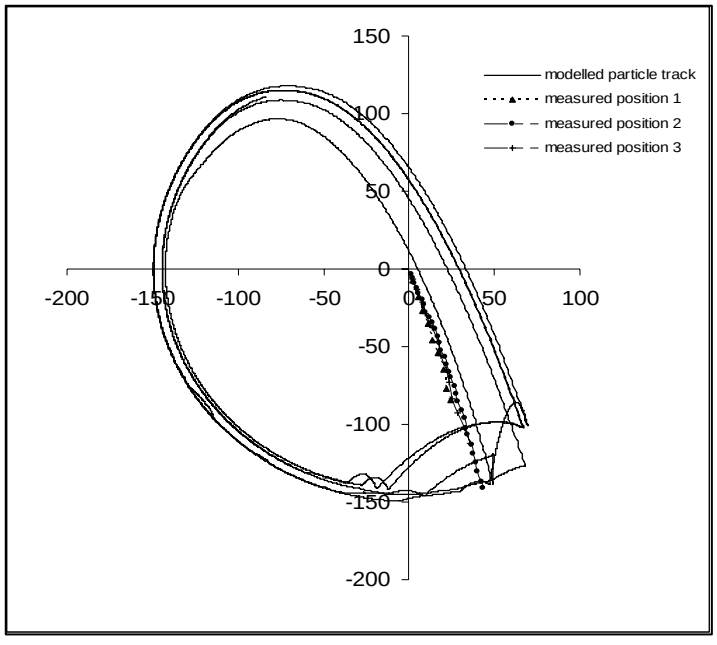

Figure 58: Comparison between the trajectory measured in laboratory test and DEM model

The model of the tumbling mill consisted of a complex polygonal assembly of rectangular walls. The walls act as boundary conditions on the particle assembly. If

contact is detected between a particle and the wall then a contact logic is used to determine the nature of the interaction. The parameters that define the wall and govern its interactions with contacting balls are the normal stiffness, shear stiffness and frictional coefficient. The physical system consists of a series of walls representing the mill (Figure 59).

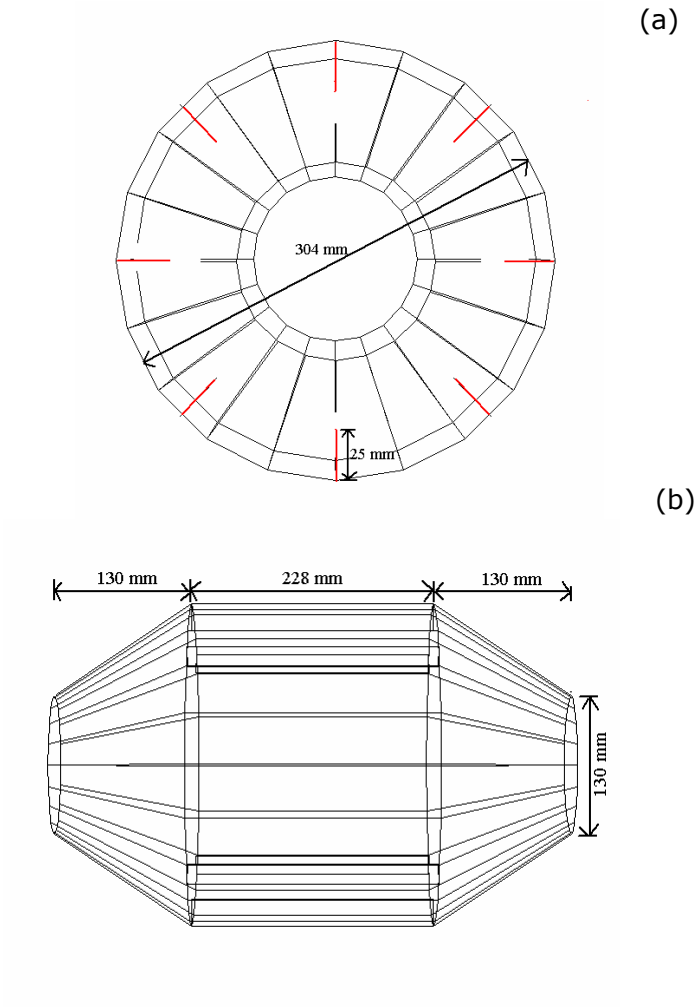

Figure 59: (a) End View of the Drum and (b) Side view of the tumbling mill

The particle properties that were used for the simulations are shown in Table 31. The coefficient of restitution was previously discussed and determined by experiment to be 0.31. The normal and shear stiffness were selected from those previously used for the modelling of particles in a tumble mill (Mishra and Cheung 1999). The stiffness and frictional parameters of the walls were assumed to be equivalent to the parameters of the particles and are given in Table 32.

Table 31: Details of the properties of the particle used within the simulation. Particle stiffness properties were provided by the literature (Mishra and Cheung 1999).

Density (t/m^3)	Coefficient of friction	Coefficient of restitution	Particle stiffness (kNm^{-1})	
			Normal stiffness	Shear stiffness
2800	0.5095	0.31	4e5	3e5

Table 32: Stiffness and frictional parameters of the drum walls (Mishra and Cheung 1999)

Stiffness (kNm^{-1})		Friction coefficient
k_n	k_s	μ
4×10^5	3×10^5	0.5095

5.6.3.2. *Numerical Modelling Programme*

The computer simulations of the mills can be divided into two sets. The first set was undertaken to investigate the effect of particle mass on the generation of dust within the tumble mill, whilst the second set was undertaken to asses the affect of rate of rotation of the mill on the characteristics of dust generation in the mill whilst keeping the particle mass constant.

Four simulations of the laboratory experiments were undertaken but with different particle masses. The four simulations are summarised in Table 33 below and represent particle masses of 150 grams, 200 grams, 300 grams and 400 grams.

Table 33: Number of Particles Simulated for Each mass Fraction

	Total mass (grams)	Number of particles
Model 1	150	180
Model 2	200	264
Model 3	300	396
Model 4	400	528

The speed of revolution of the mill for this set of simulations was 32 revolutions per minute, equivalent to that used in the laboratory tests. To determine the critical velocity of the model mill, the position of a single particle was tracked whilst incrementally increasing the rotational velocity of the mill. The velocity was increased

until the tracked position indicated that the particle was in complete contact with the side of the mill during revolution. In this way the critical velocity of the computer simulation of the mill was determined to be 66 revolutions per minute. Thus the modelled speed represented approximately 48% of the critical speed. The method adopted involved firstly the generation of the clumped particles in the centre of the mill. The particles were then allowed to settle under gravity at the base of the drum prior to the commencement of the revolutions. The stable time step was 6.58×10^{-6} sec and each model was run for 3,000,000 steps representing 19.74 seconds of rotation. During the simulation, the frictional energy, kinetic energy and the boundary energy were logged at 1000 step (0.00658 second) intervals.

5.6.3.3.*Effect of sample Size on Energy Used for Attrition Processes*

Figure 60 shows the amount of energy dissipated due to frictional sliding, the identified mechanism of dust generation. Again the energy rate due to frictional sliding, increased according to approximate linearly relationship with mass of particles in the mill at the rate of 0.0009 joules/sec/gram. The increase of the energy absorption rate due to frictional sliding with increasing mass predicts that production of fines should increase with mass of material within the mill. The increase in the volume of fines produced would be expected to generate a greater volume of dust produced. This conclusion has been justified by earlier experiments based upon the dependency of the mass of material to the dust yield, for a limestone sample (Figure 48). Also a positive correlation between fines accumulation in the mill and dustiness levels has been observed (Figure 50). Dustiness measurements are normally influenced by several parameters such as material properties (i.e particle size, moisture content) and operational parameters (tumbling time, flowrate). Therefore it is with caution that the modelling prediction of increasing frictional energy with mass should be used to infer the increased dust production in the tumble mill.

The percentage of energy drawn from the tumble mill that was used in frictional sliding is shown in Figure 60. The modelling indicates that with increasing mass the amount of energy that is utilised for frictional sliding increases from 23.5 % of power draw for 150 grams of mass to 30 % for 400 grams of material.

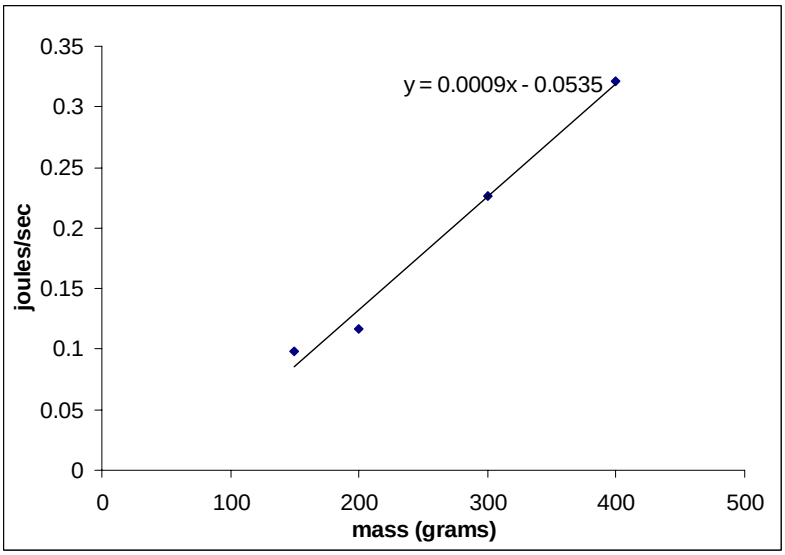

Figure 60: Simulated rate of energy dissipation due to frictional sliding as a function of total mass

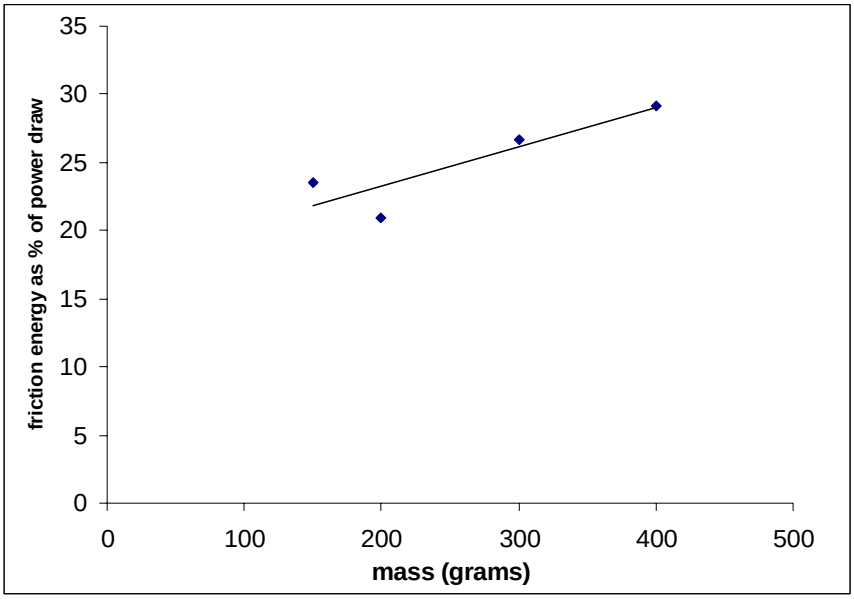

Figure 61: Simulated friction energy utilisation as a percentage of power draw against mass of sample

Figure 61 indicates that a greater degree of the power draw from the mill is used to produce abrasion and therefore dust. This was attributed to the greater degree of particle to particle collisions that occur with a higher mass of material and hence a greater number of particles in the mill. The modelling also indicates that the total amount of energy used in frictional sliding will be directly proportional to the tumble time i.e. it would be expected that the dust generated would increase as a linear function of time. This was also inferred in the testing where it was found that an increase in testing time corresponded to a roughly linear increase in the volume of dust generated (Figure 47).

5.6.3.4. *Influence of mill rotational velocity on dust generation and power draw.*

A further set of simulations were undertaken for a particle mass of 200 grams whereby the effect of the rotational velocity of the mill on power draw and dust production was investigated. The general methodology was the same as for the first set of models with each simulation representing 19.75 seconds of rotation. However the rotational velocity of the drum was varied to simulate critical velocities of 20 %, 35%, 48 %, 65%, 73 %, 90% and 99%. The trajectories of a single particle for each of these velocities are shown in Figure 62.

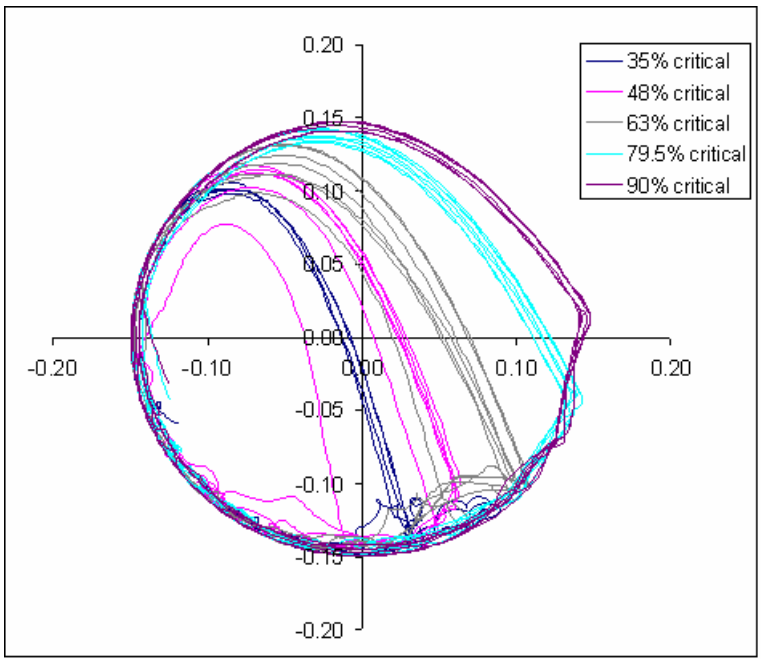

Figure 62 Single Particle Trajectories

The influence of the mill rotational velocity was investigated in terms of net power draw, frictional energy dissipation and the ratio between frictional energy rate and power draw. Figure 63 shows that affect of rotation speed on power draw and indicates that the maximum power draw occurred at approximately 63% critical velocity.

Misra and Cheung (1999) undertook PFC^{3D} simulations of a 2 metre diameter mill with a 45% filling level. They found that the power drawn was a function of the mill speed with speeds between 70 to 85% critical velocity drawing the most power. This can be compared to the HSE-WSL models where the maximum power draw was at approximately 63%. In Misra and Cheung's model the critical mill speed at maximum

power draw was also found to be dependant on the coefficient of restitution and the friction angle of the mill walls. The differences in the predictions between Misra and Cheung's results and the modelling of the HSE-WSL rotating drum may be due to the different sizes of the drum, the amount of particles within the drum and also on the different mechanical properties of the tumble mill and particles. However in both cases it is predicted that power draw is dependant on mill speed and that there exists a mill speed, less then critical velocity, where power draw is at a maximum.

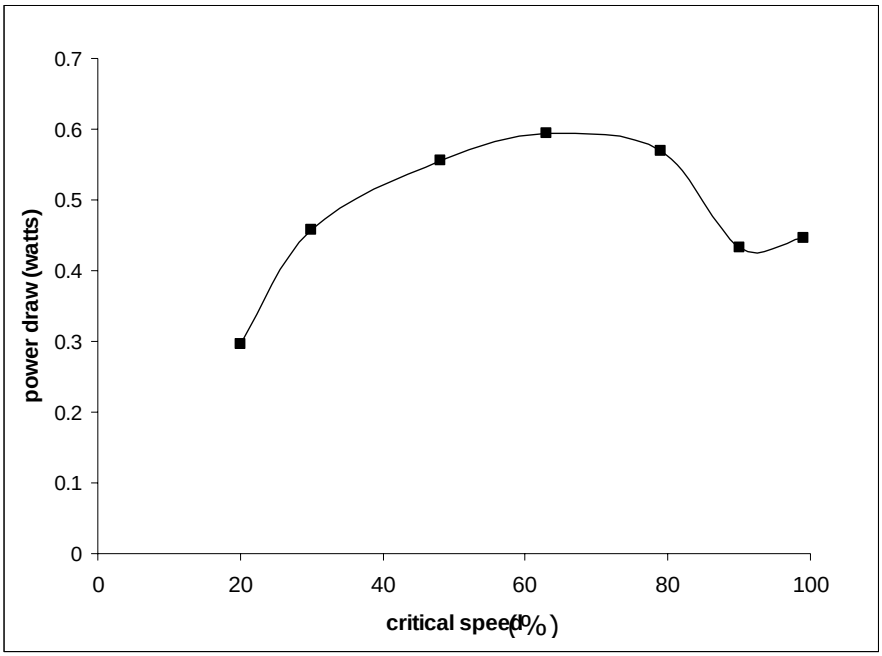

Figure 63: Affect of rotation speed on power draw.

The rate of energy loss due to frictional sliding at the various mill velocities is shown in Figure 64. Although there is a degree of scatter in the data the graph shows a general trend of increasing rate of energy loss due to frictional sliding with mill speed.

The frictional energy loss as a percentage of the power drawn from the mill is shown in Figure 65. This figure clearly indicates that the minimum occurs at approximately 63% of the critical velocity of the mill.

However, although the maximum power draw is predicted to occur at approximately 63% critical velocity the amount of the power draw that is used for frictional abrasion, and therefore dust generation, is at a minimum at this velocity (Figure 65). This indicates that if the drum was of a sufficient size for fragmentation to occur,

optimum fragmentation with minimal dust production due to abrasion would occur at approximately 63% critical mill speed.

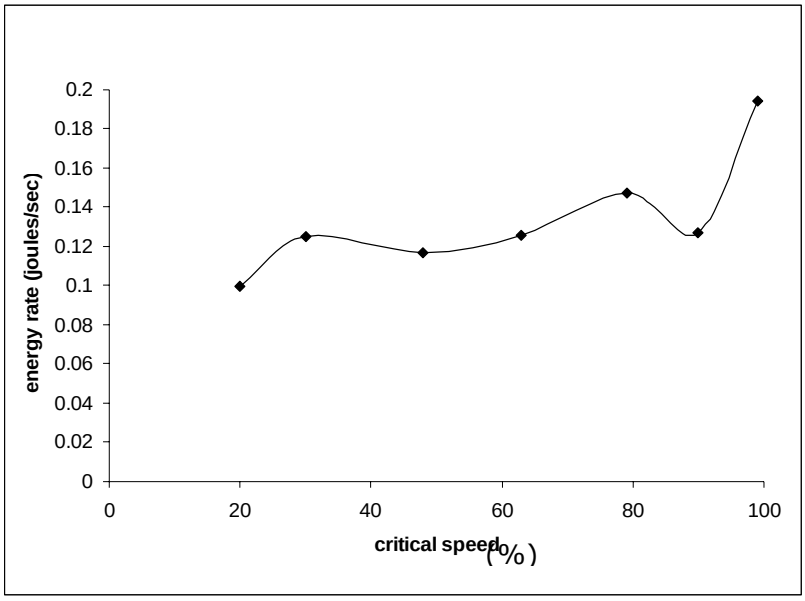

Figure 64: Energy loss due to frictional sliding against mill velocity.

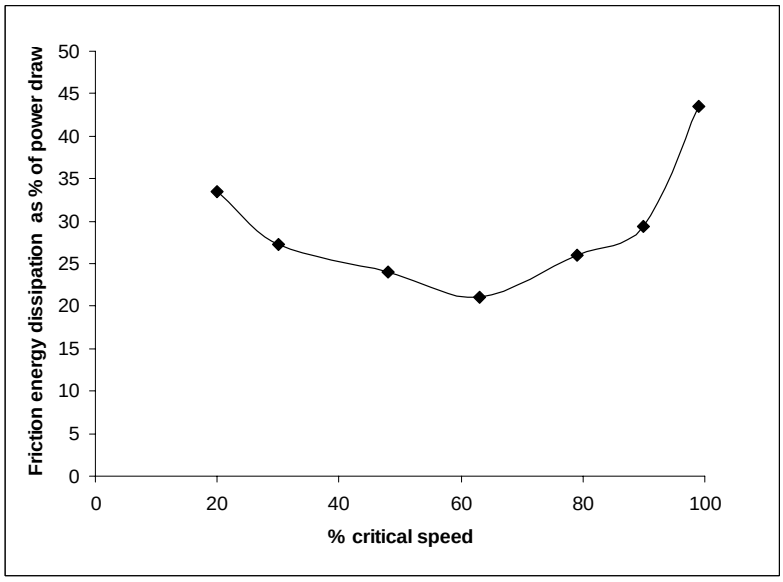

Figure 65: Energy dissipation as a percentage of power draw against mill velocity.

5.6.4. Conclusions of the investigations into the mechanisms of dust generation

Both experimental work and computational simulations have shown that dust generated in the tumbling mill is solely due to one mechanism, that of abrasion,

which is caused by the frictional sliding of particles on the drum walls and over other particles.

The breakage process of the tumbling mill follows first order kinetics, which implies that the mechanisms of the tumbling mill can be predictable, whereas the HSE-WSL drum can find application in the simulation of common handling processes, which cause dust formation by attrition alone.

The experiments and simulations show that for the mill size used, the particles would not have sufficient kinetic energy as a result of impact for fragmentation to occur. Two sets of PFC^{3D} models of the mill were created. The first set investigated the affect of mass of sample on dust production and power draw and indicated that there was a linear relationship between power draw and mass of particles in the mill. The amount of energy dissipated due to frictional sliding also increased linearly with particle mass. It was conjectured that the amount of dust production would be directly related to energy used in sliding and it was therefore seen that there was a positive relationship between the dust yield produced and particle mass at a fixed rotation speed. The second series of models investigated the effect of mill velocity on dust production. This set of models indicted that power draw was a maximum at approximately 63% critical speed but the ratio between energy loss to frictional sliding and power draw was a minimum at this speed. It was concluded that if the mill was of a sufficient size for fragmentation to occur optimum fragmentation with minimal dust production due to abrasion would occur at approximately 63% of critical speed.

The findings of this work indicate that the dust generation potential of industrial processes that they produce dust mainly by abrasion is analogous to the operational parameters of the process (i.e rotational speed). Optimisation of the parameters that have the greatest influence upon the process can result in dust reduction. For instance, optimising the velocity of conveyor belts or the velocity of vehicles in haulage roads could minimise the generation of particulate matter. The results obtained through the investigations of the mechanisms involved in the tumbling mill are in good agreement with the dustiness results produced hence they can be used to predict trends and evaluate the impact of specific events upon industrial processes.

5.7. Particle size analysis of the limestone particulate matter fraction produced by the HSE-WSL test

The particle size of the dust fraction, which has been collected using the WSL-HSE mill, was determined by laser diffraction analysis using a Malvern Mastersizer-S. The dust particle size distribution was measured for all participating test fractions and testing protocols.

5.7.1. Selection of optical properties for the limestone particulate matter

As presented in Chapter 4, the accuracy of a measurement made by particle size laser diffraction is greatly influenced by the selection of optical model and optical properties, namely the Mie or Fraunhofer approximation and the refractive index of the particulate matter as well as the refractive index of the dispersion medium. Due to the very small particle size of dust, the Fraunhofer approximation was disqualified as it does not take into account the optical properties of the test sample. Therefore the Mie approximation was selected. Detailed information of the differences of the two approximations was discussed in Chapter 4. The Mie approximation incorporates the optical properties of the material under test as well as the dispersion medium. The suspension medium used for this work was water. The refractive index of water is known to be 1.33. The mineralogical analysis of the limestone samples showed that the rock sample consists mainly of calcite, implying that the correct optical properties should represent the range for calcite. However, the refractive index of calcite can be any value from 1.486 to 1.77 (Malvern Instruments 1994). To explore the effect that the refractive index of calcite had during measurement of the particulate matter, a range of presentations with different values of refractive indices were prepared using the presentation software of the Malvern Mastersizer. Subsequently such presentations were applied to the measurement taken for the dust fraction of the <3.35mm limestone (OPT-TP). The selected refractive indices values are shown in Table 34, whereas the results are presented in Figure 66 and Table 35.

As shown in Figure 66 and Table 35, changing the optical properties of the particulate matter alters the particle size distribution result. The effect is particularly obvious for the very fine particle sizes, namely the dust particles below 2.5μm. For instance, the cumulative percentage passing 2.5μm when the presentation RI Comb.4 was selected equals to 25.43%, whilst when the presentation changed to the RI Comb.1 the percentage increased to 41.97%. Similar trends are observed on the median

diameters d_{50} and d_{90}. The minimum observed at 1μm for the presentations RI Comb.1 and RI Comb 2 could also be attributed to the poor selection of optical properties. The appearance of a second peak at particle sizes below 1μm has also been observed by Malvern Instrument, when the selected optical properties did not match well the real ones (Malvern Instruments 2004).

Table 34: Optical properties of the presentations prepared for the limestone particulate matter

	Refractive index of particulate matter (R.I.)		
Presentation Code	Real part (n_p)	Imaginary part (K_p: absorption)	Dispersion Medium Refractive Index
RI Comb.1	1.486	0.1	1.33
RI Comb.2	1.57	0.1	1.33
RI Comb.3	1.66	0.1	1.33
RI Comb.4	1.77	0.1	1.33

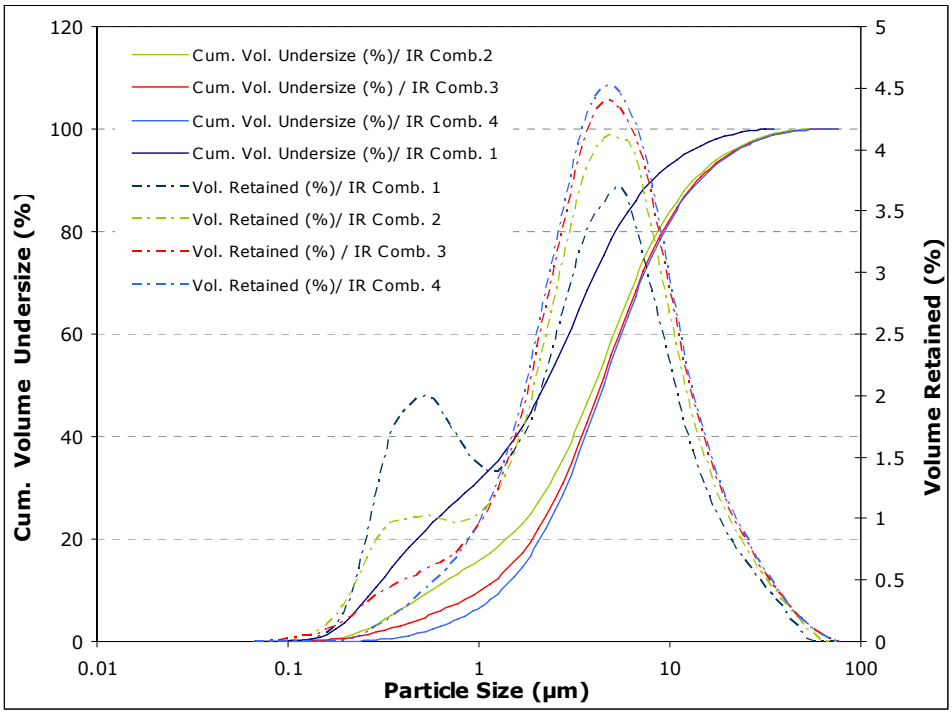

Figure 66: The effect that different presentations have on the particle size distribution of limestone dust (corresponds to a feed of <3.35mm, 150g).

During this study only the real part of the refractive index varied. Changes in the imaginary part of the refractive index might also influence the end particle size distribution. Further investigations into the effect of the imaginary refractive index are presented in the following paragraphs.

Table 35: The cumulative percentages passing 10μm and 2.5μm and the diameters d_{50} and d_{90} as resulted from the different optical properties presentations

Presentation code	Cum.% passing 10μm	Cum. % passing 2.5μm	D50	D90
R.I. Comb.1	86.59	41.97	3.28	11.96
R.I. Comb.2	83.99	32.57	4.02	13.32
R.I. Comb.3	82.61	27.72	4.35	14.02
R.I. Comb.4	82.05	25.43	4.49	14.28

The fluctuations in the volume concentrations of the fine particulate matter cannot be considered negligible, especially when particle size measurements are performed for regulatory or standardisation purposes, such as the production of an occupational health limit for a certain substance. Therefore, the determination of the correct optical properties of the dust samples is crucial. Similar problems account for most light scattering techniques where Mie theory is applicable.

However, the influence of the optical properties varies for different materials, and it needs to be explored separately. Methods that are normally employed to determine the refractive index of a solid sample include the following (Malvern Instruments 2004):

- Index matching fluids: A range of immersions fluids with different refractive indices can be used to suspend the test material. The particles become invisible when suspended in material of identical refractive index.
- Becke line: This technique requires the use of optical microscopy. The technique can determine if a particle has a greater or less refractive index than the medium it suits in.
- Large crystal-gem refractometer: Commonly used by gemmologists. A refractometer cannot measure the refractive index of a rough unpolished surface.
- Two miscible dispersants of different refractive index: A range of refractive indices are used from the miscible liquids. During measurement using the Malvern Mastersizer, a minimum obscuration is achieved when the refractive index is correct.

When the test sample does not consist of only one material, as happens with most rock samples, the determination of the refractive index becomes even more complicated. In a case such as this, the most appropriate techniques for optical

properties determination are the use of immersion fluids or the use of miscible dispersants. The first technique is quite expensive and most of the time a few samples of each immersion fluid would be required. A trial had been undertaken to determine the refractive index of the limestone particulates using the technique of two miscible dispersants. In addition, the selection of optical properties was confirmed using a second technique which involved volume concentration matching. The experimental procedures of both of these techniques were according to Malvern Instruments through personal communication.

5.7.1.1. *Determination of the refractive index of limestone using the two miscible liquids method*

The test sample used into this initial step of experimentation was limestone particles below 53 μm, which simulate the dust fraction. Two miscible liquids of different refractive indices were used to determine the refractive index of rock particles. These were:

- Isopropyl alcohol with a refractive index of 1.38, and
- Methyl naphthalene with a refractive index of 1.62.

A wide range of different mixtures can be created of which the refractive index is known (Table 36). For example, 40% of IPA and 60% of methyl naphthalene produces a mixture that has a refractive index equal to:

(Equation 22) $RI= 1.38*0.4+1.62*0.6=1.52$

To these an equal weight of sample should be added and a Mastersizer measurement performed. By plotting the obscuration against refractive index the point of minimum obscuration can be easily determined. This is not always zero as if the material has a non-zero imaginary refractive index it will scatter even when immersed in a liquid of equal refractive index. If the material being dealt with is a mix of different substances and their refractive indices and proportions of the materials are known, the refractive index of the mixture can be assumed to be a weighted average.

The experimental procedure described above, followed through a series of steps for the limestone <53μm.

The small sample dispersion unit of the Mastersizer was filled with 100ml of IPA and the stirrer started to operate at a medium speed. A measurement was taken using 0.047g of limestone to check if the obscuration levels were within the recommended instrument levels (10 to 15%) and subsequently to determine an adequate sample weight that can be used for further experiments. It was found that a sample mass of 0.02g of limestone would satisfy these expectations.

A range of mixed solutions using the isopropyl alcohol (IPA) and methyl naphthalene (MN) with different concentrations and thus a variety of refractive indices were prepared to be used as the dispersant media of the particle size determination test. During these experiments the Fraunhofen optical model was chosen. The Mie approximation could equally be applied since the observed parameter is obscuration which is independent of the selection of optical model. Each measurement was carried out twice to assess consistency of the results.

The results obtained can be seen in Figure 67, where the obscuration has been plotted against the refractive index. From the plot of Figure 67 a minimum obscuration was reached for a dispersion medium refractive index equal to 1.62, which indicated that the refractive index of the limestone sample was higher or equal to 1.62. The refractive index of limestone could be higher than 1.62 as the measured obscuration value could reduce further, possibly giving a value lower than 8.3%. Nevertheless, it was impossible to explore what the relationship between obscuration and refractive index would be for higher refractive indices, as the two miscible liquids cannot produce a value higher than 1.62. If a material has got a refractive index between the limits of isopropyl alcohol and methyl naphthalene, then this method could be successfully used to estimate its optical properties.

Table 36: Mixed solutions (IPA – MN) concentrations and their refractive indices

Limestone sample mass (g)	IPA	Methyl naphthalene (MN)	R.I.
0.0210	100	0	1.38
0.0214	80	20	1.428
0.0206	60	40	1.476
0.0219	40	60	1.524
0.0209	20	80	1.572
0.0207	0	100	1.62

For the limestone sample, as it has been noted above the refractive index can be higher than the upper limit of the optical properties of the dispersion medium, therefore it is difficult to assign a specific value. Further work using a second method, which might help confirm the optical properties of limestone particulates have been adapted, and it is presented in the following paragraph.

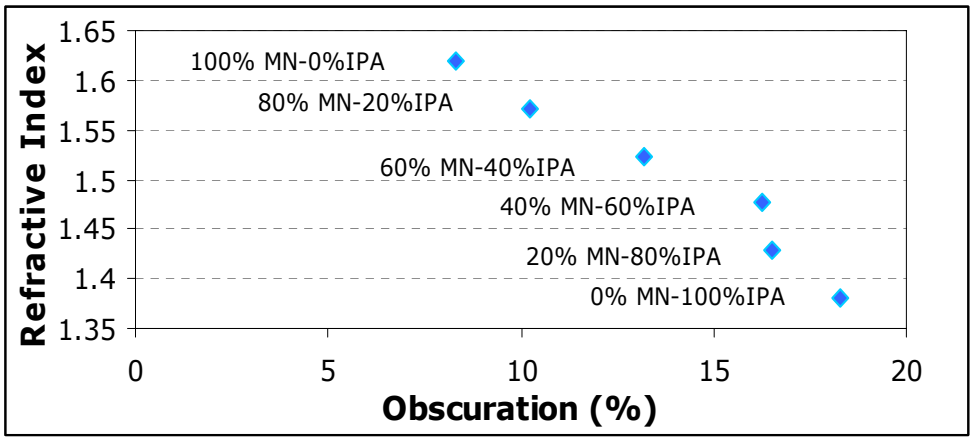

Figure 67: The refractive index of the dispersion medium versus the measured obscuration values that were obtained for the limestone sample (<53μm). The participating concentration of each liquid is also presented.

5.7.1.2. *Determination of the optical properties of limestone using the volume concentration matching method*

It has been shown by (Lips et al. 1992) that the true phase volume of a system of suspended spherical particles whose scattering extinction efficiencies have been correctly predicted by Mie theory can be measured correctly. Experiments confirmed that suspensions of known pre-determined phase volume were correctly reported by the Mastersizer. In addition to the size distribution, the Mastersizer takes a zero angle turbidity measurement that can be used to calculate the volume concentration of particles present. By combining the Mie theory of light scattering with the Beer-Lambert law the following equation is obtained (Malvern Instruments 1994).

$$c = \frac{100 \log_e (1 - \text{Obscuration})}{\frac{-3}{2} b \sum \frac{V_i Q_i}{d_i}} \qquad \text{(Equation 23)}$$

where c is the concentration (%), b is the beam length (m), V_i is the volume in size band I (m^3), Q_i is the extinction coefficient of size band I (m^{-1}) and d_i is the mean

diameter of size band I (m). The extinction coefficient is a measure of how efficient a particle of a particular size is at scattering light. Equation 23 shows the relationship between volume concentration and the obscuration measured as part of a normal experiment. This is used by the machine to calculate a theoretical concentration.

For a stable size distribution (with no multiple scattering), comparison of the real and calculated concentrations can be used to establish that an appropriate R.I. has been used. The Mastersizer calculates the theoretical volume concentration using Equation 23.

The experimental volume concentration was calculated following the procedure presented below. The weight of the sample used for the measurement was divided by the specific gravity of the material and divided again with the volume of the dispersant liquid used in the measurement. This result was multiplied by 100 to give the result as a volume %. The specific gravity of limestone was calculated on the basis of Archimedean displacement and it was found to be 2.79. Hence, the closest volume concentrations (real and theoretical) obtained corresponded to the correct refractive index.

Six different mass weights of limestone (<53μm) were used as test samples and their particle size distributions were determined using the Malvern Mastersizer. The theoretical volume concentration (%), was recorded, whilst the real volume concentration was calculated using the method described above. The presentation used during the measurements was described by a real refractive index equal to 1.596 and an imaginary part equal to 0.1, whereas the suspension medium was water with a refractive index equal to 1.33. The volume of the dispersant (water) used was 100 ml. A variety of different presentations with different optical properties for both the refractive index and the imaginary index were prepared and applied to the measurements and the theoretical volume concentration was recorded. For each one of the different optical profiles the theoretical volume concentration was plotted against the calculated one and their fit was investigated. Some of the results obtained can be seen in Table 37, Figure 68 and in appendix II.

From the results obtained, it was observed that for any presentation with a stable imaginary index equal to 0.1, the theoretical volume concentration matched quite well to the calculated one. However, when the imaginary part of the refractive index was changed to 1 or 0.01 then the theoretical volume concentration diverged from the measured volume concentration (Table 37). Therefore the imaginary refractive

index for the limestone sample was determined to be 0.1. For this imaginary index, changes to the real part of the refractive index affected only slightly the theoretical volume concentrations, making it difficult to decide which one reflects better the properties of limestone. The use of sample weights 0.0354g and 0.0592g resulted in increased obscuration values, which are undesirable as they can cause multiple scattering. Considering the experimentation with the two miscible liquids, where was concluded that the refractive index of limestone should be higher than 1.62, as well as the observed changes in the particle size distribution caused when different values were selected (Figure 68), the real part of the refractive index was chosen to be equal to 1.7.

Table 37: The theoretical and calculated volume concentration results that correspond for a range of optical profiles

	Sample Mass (g)					
	0.0014	0.0053	0.0114	0.0198	0.0354	0.0592
Obscuration (%)	0.8	3.6	7.6	14.1	23.3	35.7
Calc.Vol.Conc.(%)	0.0005	0.0019	0.0041	0.0071	0.0127	0.0212
Theor. Vol. Conc. (%) Presentation(1.596, 0.1 in 1.33)	0.0004	0.0018	0.0037	0.0072	0.0118	0.0183
Theor. Vol. Conc. (%) Presentation(1.62, 0.1 in 1.33)	0.0004	0.0018	0.0038	0.0073	0.012	0.0185
Theor. Vol. Conc. (%) Presentation(1.7, 0.1 in 1.33)	0.0004	0.0019	0.0039	0.0075	0.0124	0.0191
Theor. Vol. Conc. (%) Presentation(1.7, 1 in 1.33)	0.0003	0.0013	0.0027	0.0054	0.0086	0.0129

Based upon this, any further particle size measurements of limestone particulate matter by light scattering used a presentation with a refractive index equal to 1.7, an imaginary refractive index equivalent to 0.1 and a dispersion medium refractive index of 1.33, as only water was used. Even though several techniques have been developed through the years that determine the refractive index of materials, there are still issues to be explored in particular when handling mixtures of materials, where the identification of optical properties is complicated. The techniques described in this chapter can only provide a confirmation of the choice made. However if the optical properties of the material are completely unknown and there is not any sort of reference that could produce an upper and lower limit of them then the use of other techniques should be considered.

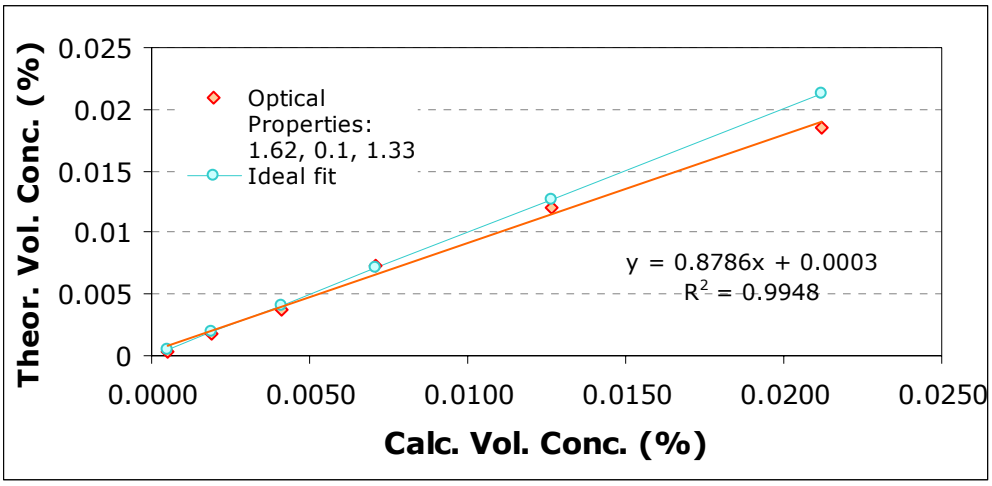

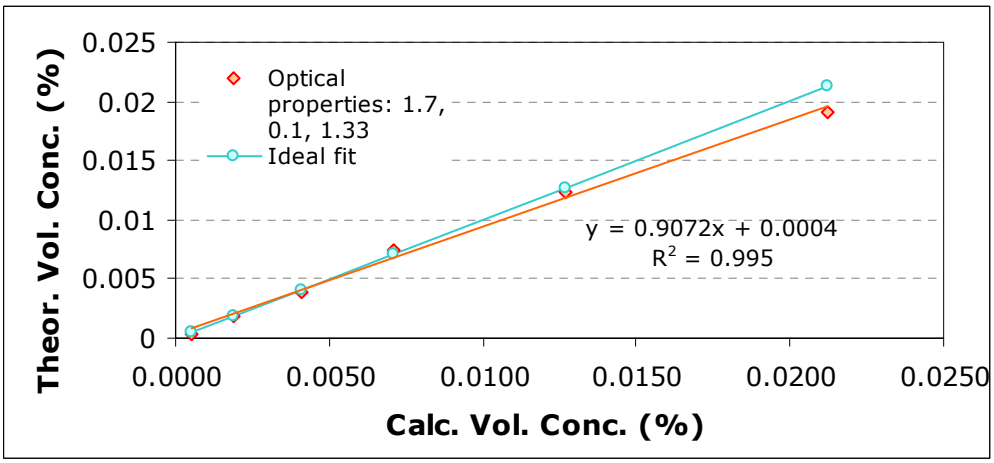

Figure 68: The theoretical versus the calculated volume concentration (%) for (a) a refractive index of 1.62, imaginary index 0.1 and dispersion medium refractive index 1.33 and (b) a refractive index of 1.7, imaginary index 0.1 and dispersion medium refractive index 1.33.

5.7.2.Particle size analysis results

The particle size of the dust fraction collected during testing with the HSE-WSL dustiness test was determined using the Malvern Mastersizer-S. The dust fraction was collected on paper glass-fibre filters following the procedure described in chapter 4 and for the limestone test samples < 9.5mm, <3.35mm and <1mm. Triplicates from each sample were collected using the HSE-WSL test, which were analysed using the Mastersizer.

Each time a sample was introduced to the Mastersizer, a measurement was taken, which repeated three times and if good results were obtained then an average particle size distribution was produced. Fresh feed from the same sample was

introduced to the Mastersizer more than once, if adequate quantities of the dust fraction were available. Afterwards, the same steps were followed for the remaining two samples of the triplicate set. The reproducibility of the measurements is presented in Table 38 by a standard deviation and a relative standard deviation value (RSD %) and in appendix II. The standard deviation and relative standard deviation values in Table 38 describe the reproducibility of the measurements acquired from the triplicate sets of the dust samples. As it can be seen, the reproducibility of the particle size measurements was very good with an average standard deviation of the d_{50} diameter (for all fractions) equal to 0.031 and an average relative standard deviation of 0.67%.

Table 38: The median values of the diameters d_{10}, d_{50} and d_{90} of the limestone particulate matter produced using the HSE-WSL test, from a range of sample fractions (OPT-TP). The standard deviation and relative standard deviation values were calculated from the results obtained by the triplicate samples.

Sample Fraction	D_{10}	Stdev	RSD(%)	D_{50}	Stdev	RSD(%)	D_{90}	Stdev	RSD(%)
-9.5 mm	1.22	0.011	0.94	4.63	0.047	1.01	17.54	0.36	2.07
-3.35 mm	1.17	0.011	0.98	4.42	0.026	0.60	14.14	0.27	1.9
-1 mm	1.22	0.015	1.25	4.96	0.02	0.42	15.82	0.31	1.84

The dust particle size distributions determined through the laser diffraction method are expressed in terms of the equivalent volume diameter (dv). The presented results correspond to the average values obtained from a sequence of consecutive tests. Figure 69 reports the particle size distribution of the limestone particulate matter produced through the two different testing regimes. Both the cumulative volume percentage passing and the volume percentage remaining versus size are presented. The particle size distributions of the particulate matter produced from the <1mm and <9.5mm limestone fractions and for any testing protocol, are similar, whilst the dust particle size distribution of the <3.35mm limestone fraction is slightly different and appears finer for both testing regimes.

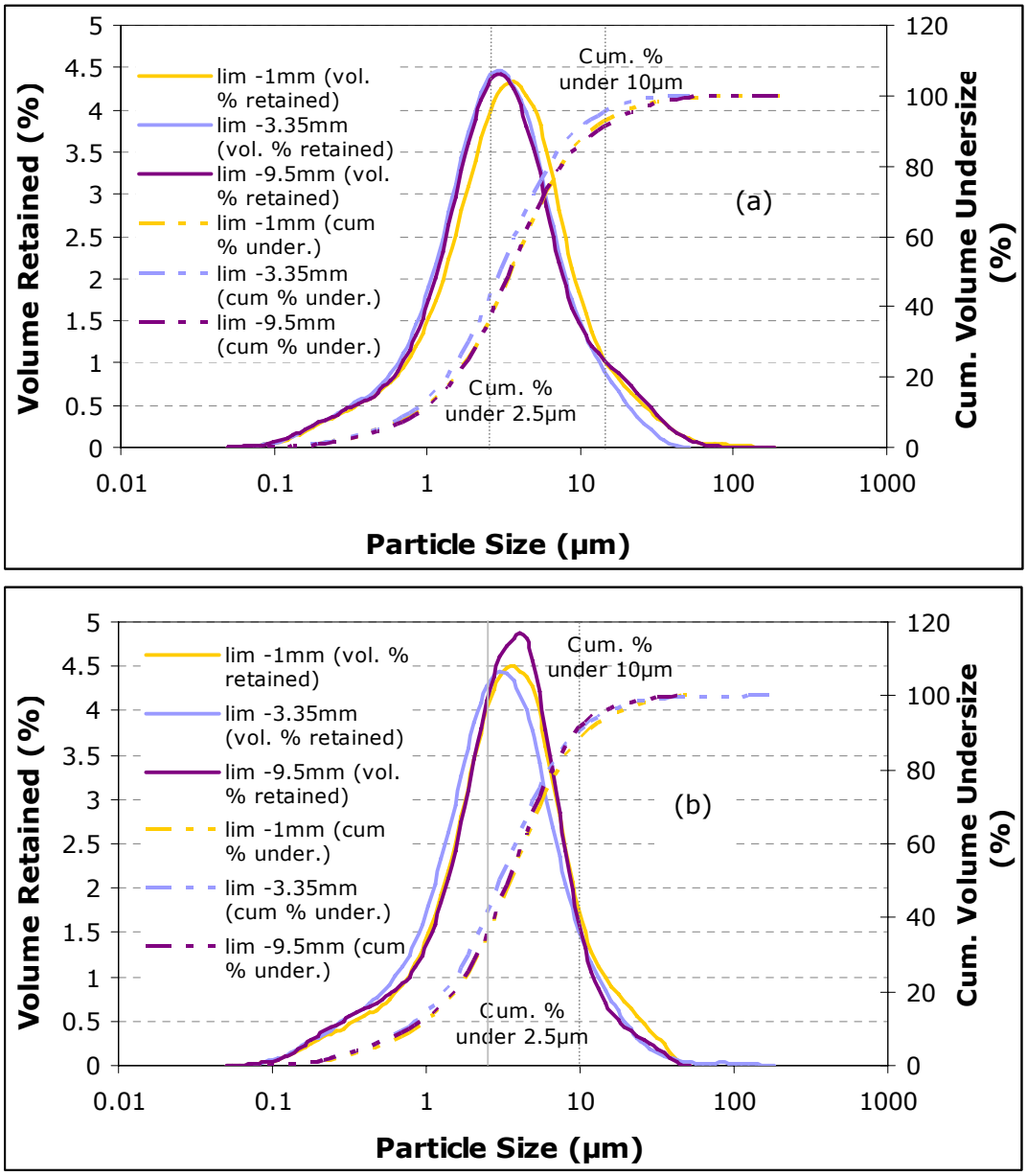

Figure 69: Particle size distribution of the limestone particulate matter produced through (a) the OPT-TP and (b) the HSL-TP. The presented results correspond to average values of repeatable tests.

A summary of the cumulative percentages passing 10μm and 2.5μm, as well as the d_{80} values (80% of the particles are found below this size) are displayed in Table 39. The cumulative percentage passing 10μm and 2.5μm and the diameter (d_{80}) results, for all samples, do not suggest great discrepancies. The d_{80} values of the particulate matter that corresponds to the <9.5mm limestone are slightly lower, but again the difference cannot be considered significant. Also the dust particle size distributions of the two testing protocols do not present great differences. An example is given in Figure 70 for the particulate matter produced from limestone <1mm. The profiles of the two particle size distributions are identical. Similar results were obtained for the dust particle size distributions of the other limestone fractions and they can be reviewed in appendix II.

Table 39: Cumulative percentages passing 10µm and 2.5µm and the d_{80} values for all samples and testing regime ((1): corresponds to the OPT-TP; (2) corresponds to the HSL-TP)

Limestone fractions	Cum. % passing 10µm	Cum. % passing 2.5µm	D_{80}
-9.5mm (1)	79.58	25.03	10.16
-9.5mm (2)	84.5	25.3	12.4
-3.35mm (1)	82.34	26.55	14.14
-3.35mm (2)	79.15	23.54	15.63
-1mm (1)	79.94	25.35	15.82
-1mm (2)	81.36	24.94	14.64

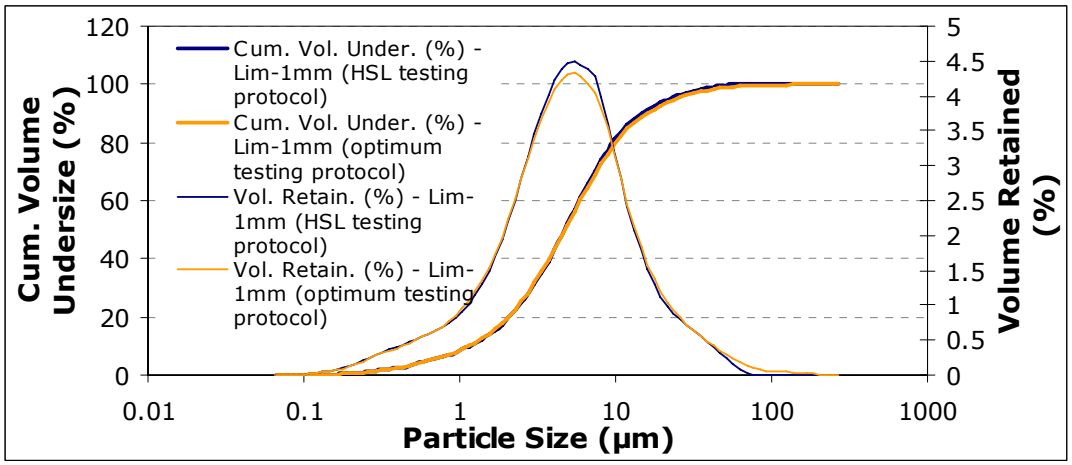

Figure 70: Particle size distribution results of the particulate matter produced by a limestone feed fraction below 1mm and both testing protocols.

Even though the concentrations of fine material in the test samples and the dustiness levels differ within the different fractions, the size distributions of the airborne particulates exhibit similar profiles without substantial differences. To summarize, the dust size distributions produced from the <3.35mm feed samples were slightly finer. For instance 82.34% and 26.55% of the dust particles produced from the <3.35mm sample (OPT-TP) were found with a size below 10µm and 2.5µm respectively, in comparison to 79.58% and 25.03% of the <9.5mm sample and 79.94% and 25.35% of the <1mm sample (Table 39). The dustiness levels of the <3.35mm limestone for both testing regimes were increased in comparison to the rest of the samples, implying that higher dustiness levels might also be associated to smaller particle size for the dust fraction. The d_{80} of all the tested samples was around 10 to 16 µm, whereas around 23% to 27% of the particles have been defined with a particle size below 2.5 µm.

Even though the results presented do not typify aerodynamic diameter values and it would not be correct to directly attribute the PM10 (particles with an aerodynamic

diameter less than or equal to a nominal 10 micrometers) and PM 2.5 (particles with an aerodynamic diameter less than or equal to a nominal 2.5 micrometers), it is suggested that the percentages passing 10 μm and 2.5μm can be used as indicators of the hazardous potential of dust to human health and the environment. The use of aerodynamic diameter is of particular interest to occupational hygienists and aerosol scientists. However this research work does not attempt to characterise particulate matter in terms of its hazardous potential effect to health. Dust comprises the product of certain process routines hence characterisation practices aim to relate process mechanisms with their particulate matter generation potential. Nevertheless, results obtained outline the potential impact of dust to the environment and human health. The volume equivalent diameter data could be transformed into aerodynamic diameter results and the procedure to follow with some outcomes for the limestone dust is presented in appendix II. As a result, industrial processes in the limestone quarry that are simulated well by the rotating drum test, such as transfer of material in conveyor belts, sieving, mixing in drums, haulage roads, will generate dust with comparable particle size distributions.

5.8.Experimentation using the impact test

The impact test aims to simulate industrial processes that operate and produce dust due to impact such as drop from height from conveyor belts, loading and dumping processes, tipping – stockpiling, draglines and others. Similarly to the HSE-WSL test, testing using the limestone samples was used to determine a standard experimental procedure, which was followed during investigation with other ores. Four single fractions, two bulk densities and four energy levels were considered for testing. An analytical presentation of the different testing combinations followed for the impact test has been presented in detail in Chapter 4. The paragraphs to come report the results obtained during experimentation with the impact test for the limestone single fractions.

5.8.1. Determination of the residual height of the limestone particles

Testing using the modified JK impact apparatus relies on the principle that a certain energy input is applied to the test sample, which might or might not cause breakage. The energy input level is determined by the release height and head weight combination as shown in Chapter 4. However during impact, particles tend to leave an offset between the anvil and the head weight, so the specific energy input needs to be normalised to this. Three test samples were prepared from each single fraction, bulk volume and energy input and tested under impact to record the residual height.

The offset is considered the rest position of the head weight after release and it is the height indicated by the pointer attached at the head weight, on the vertical ruler of the apparatus.

Table 40: Average values of residual height for all fractions, energy levels and bulk volumes.

		Residual height (cm)			
Energy input (kWh/t)	Bulk volume (%)	16x13.2mm	8x6.7mm	4x3.35mm	2x1.7mm
0.05	10	0.85	0.6	0.48	0.57
0.1	10	1.00	0.55	0.63	0.70
0.5	10	0.50	0.53	0.27	0.18
0.68	10	0.30	0.45	0.42	0.18
0.05	5	-	0.13	0.02	0.02
0.1	5	-	0.13	0.02	0.00
0.5	5	-	0.00	0.02	0.00
0.68	5	-	0.00	0.00	0.00
0.05	20	1.67	-	-	-
0.1	20	1.65	-	-	-
0.2	20	1.37	-	-	-
0.3	20	1.08	-	-	-

Three repeatable measurements were averaged and subsequently used to accurately determine the release height during experimentation. The averaged values of the results obtained can be seen in Table 40. Results had revealed that the greatest the specific energy input, the lowest the offset. This is particularly obvious for the energy levels between 0.1 kWh/t and 0.5 kWh/t. Also, the smaller the particle size, the lower the offset. The offset left due to particles presence after impact is influenced by many parameters, such as particle shape, particle size, orientation and packing in the sample holder. For instance, smaller particle fractions pack better in the cylindrical holder leaving fewer gaps, hence under impaction they result at a lower offset. Similarly, particles with a round shape will pack differently to particles with an angular or elongated shape. The residual height values obtained for limestone were also used during experimentation with other ores, because the same single particle fractions have been tested. The effect that the use of the limestone particle offset has on other ores is discussed in the appropriate chapters.

5.8.2. The bulk density of the limestone samples

The mass of the single fraction limestone sample used was governed by its bulk volume, which corresponded to the percentage of the sample holder being occupied by particles. The procedure followed to determine the bulk volume of the limestone samples has been referred to in detail in Chapter 4.

Particle properties such as their irregular shape, or the way they stacked in the metric cylinder could result to slight differences of the bulk density values recorded for each test sample. This section presents the differences observed for the limestone test fractions, which they assess the adapted sample preparation method. The bulk density values of the single fraction for all three sets of selected bulk volumes are presented in Figure 72.

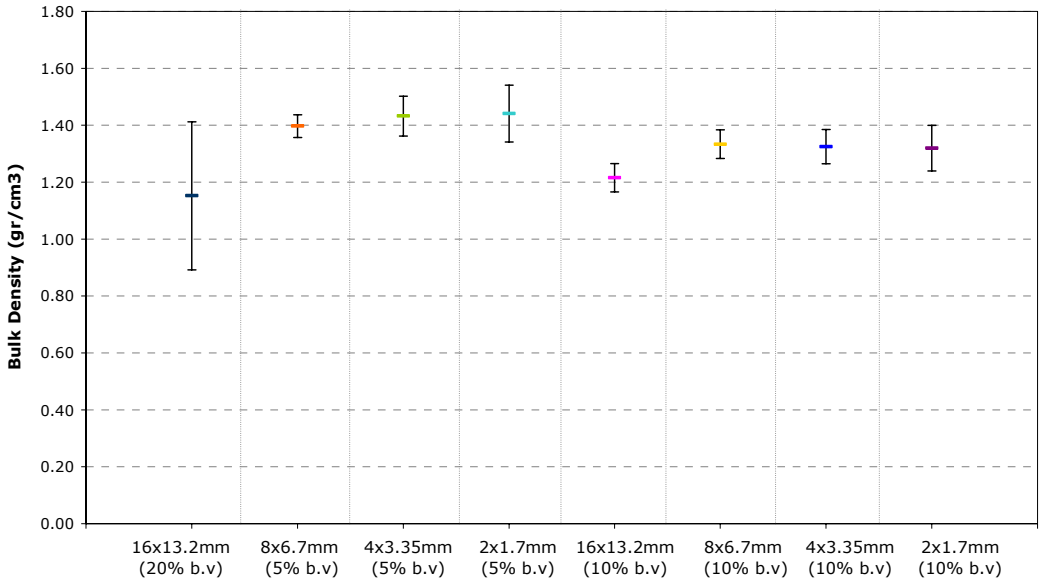

Figure 71: The recorded bulk density values of the limestone single fractions. The vertical bars represent one standard deviation.

The differences in bulk density could be attributed to the less consistent stacking of particles, as coarser ones tend to leave larger gaps between the particle-particle and particle-wall (of metric cylinder) contact points. Likewise, the bulk density of the 16x13.2mm (20% of sample's holder bulk volume) presented a higher standard deviation than any other test sample. Hence, orientation of the particles and the way they are set in the sample holder is of great importance for the coarser particles.

Nevertheless, the observed variability was very low, which indicated that limestone is considerably homogeneous, whilst the sample preparation method does not introduce large errors to the impact testing procedure.

5.8.3. Impact test – Results for the limestone ore

The prepared limestone samples were placed in the modified JK impact test sample holder and subsequently impacted with a load of specific energy input. The release height of the head weight was normalized by incorporating the residual height results obtained in paragraph 5.8.1, so as to achieve the required energy levels, namely the 0.05 kWh/t, 0.1 kWh/t, 0.5 kWh/t and 0.68 kWh/t as well as the 0.2 kWh/t and 0.3 kWh/t for the case of the 20% bulk volume. For each experiment the actual height used as well as the offset height left due to the presence of the particles was recorded. Afterwards, the height was adjusted once more using the measured residual height and the actual energy achieved was determined. Most of the time the achieved energy levels matched the required ones and only slight differences were observed.

The broken particles were carefully collected and sieved on a $\sqrt{2}$ sequence of sieves. Triplicates of each sample were tested but the whole series sieving analysis took place only for one of the samples. For the remaining two samples only the fraction below 53μm was collected by sieving for further particle size analysis. The particle size distributions obtained can be seen in Figure 72. A general trend is observable, where higher energy input levels increase the amount of broken particles, resulting in a finer particle size distribution, independently of material size fraction and bulk volume.

The effect that an increase or decrease in bulk volume has on particles under impact has also been investigated and it is expressed in the particle size distributions in Figure 72. For the -16+13.2mm fraction the bulk volume of the sample holder has been increased from 10% to 20%. The particle size distributions of these test samples are comparable only for the two lower energy input levels, namely the 0.05 kWh/t and 0.1 kWh/t. Higher energy levels, for the 20% bulk volume sample (0.5 kWh/t and 0.68 kWh/t) require a release height beyond the capabilities of the apparatus.

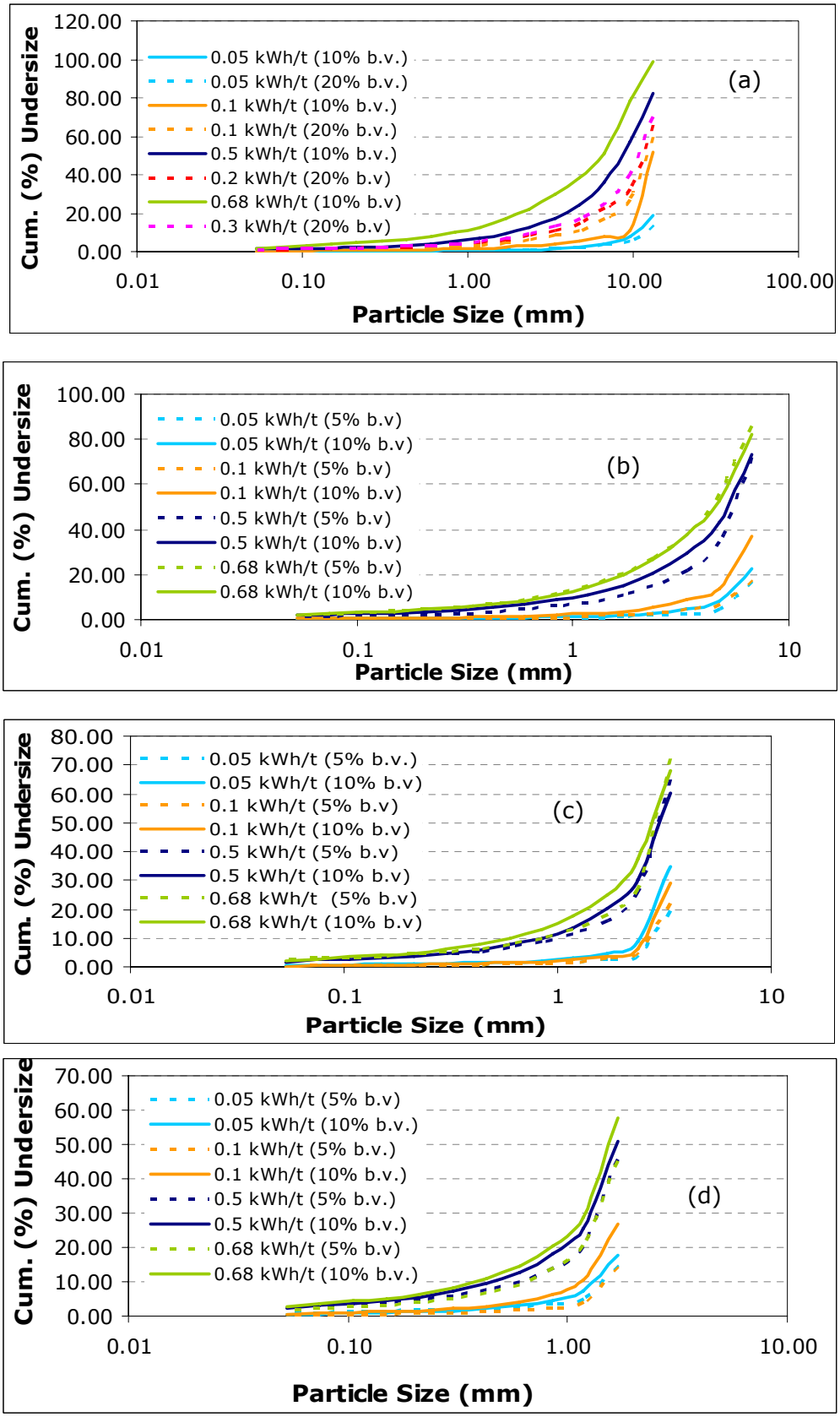

Figure 72: Particle size distribution of the limestone particles after impact for the single fractions (a) -16+13.2mm (10% and 20% bulk volume) and (b)-8+6.7mm fractions (c) -4+3.35mm and (d)-2+1.7mm fractions, (10% and 5% bulk volume).

For 0.05 kWh/t, the particle size distribution of the -16+13.2mm (10% bulk volume) and the -16+13.2mm (20% bulk volume) matched. In view of that, changes in the bulk volume of the -16+13.2mm limestone fraction and for very low energy levels do not alter the particle size of the broken particles. However, when the energy input level was doubled (0.1 kWh/t), then the 20% bulk volume test sample produced a finer particle size distribution than the 10% bulk volume sample.

For the -8+6.7mm single size fraction the bulk volume was reduced from 10% to 5%. For energy input levels (0.05 kWh/t, 0.1 kWh/t and 0.5 kWh/t) the particle size distributions of 5% bulk volume samples were coarser. The highest energy input level (0.68 kWh/t) resulted in similar particle size distributions for both the 10% and 5% bulk volume samples.

For the -4+3.35mm fraction, as well as the -2+1.7mm fractions two different bulk volumes were tested, the 10% and 5%. The particle size distributions of the -4+3.35mm fraction (5% bulk volume) at any energy input level are coarser than the ones produced by the 10% bulk volume samples. The energy input levels, 0.05 kWh/t and 0.1 kWh/t produced similar particle size distributions for both the 10% and 5% bulk volume samples.

Therefore, a greater mass of particles in the sample holder enables more breakage to occur during impact, implying that at a lower bulk volume, energy is dissipated or transformed into other forms (e.g vibration, sound) without causing extra breakage. The two variables, bulk volume and energy input must be governed by an equilibrium relationship, where a certain energy level can cause maximum breakage under impact to a specific mass of test sample and any further increase in the bulk volume will not result in additional volume breakage. An increase in sample mass could result in accumulation of extra fine material produced due to enabled attrition mechanisms caused by particle to particle contacts, which are more frequent for greater masses. For instance, for the -16+13.2mm, -8+6.7mm and -2+1.7mm limestone fractions, the greater breakage discrepancies between the different bulk volume test samples were reported for the 0.1 kWh/t energy input level, where doubling of bulk volume produced a doubling of the mass percentage of particles remaining (on average) at each individual sieve size. For the -4+3.35mm single size fraction a similar trend was observable at the 0.05 kWh/t energy input level. Determining this equilibrium between bulk volume and energy input is very important not just for energy and process optimization purposes, but also because the generation of fine particulate matter could be controllable and kept to a minimum level for high process

performance. The relationship between bulk volume and energy input will be possibly influenced by a variety of parameters such as the composition of the material, the hardness and brittleness of the test sample, its particle size, shape and orientation during testing and others. The results presented in this paragraph with different single size fractions of limestone have justified that particle size does affect the end particle size distribution results. Nevertheless, experimentation took place for a range of other ores with different material properties, and theses results will be presented in subsequent chapters.

5.8.4. The effect of impact upon the generation of fines from the limestone ore

This project is particularly interested in the effect that process parameters and mechanisms have on the generation of fines.

Figure 73 presents how the test sample particle size, the bulk volume and energy input can influence the production of fine material (below 53μm). The cumulative mass percentages of fine particulates below 53μm are closely related to the energy input levels. Hence higher energy inputs result in larger quantities of fines, which in turn have a greater potential to entrain into the airborne state. The above statement is satisfied by any single size limestone fraction and for any bulk volume. The test sample -4+3.35mm (0.68 kWh/t, 5% bulk volume) produced the highest concentration of fine particles (below 53μm) followed by the -2+1.7mm (0.68 kWh/t, 10% bulk volume and 0.5 kWh/t, 10% bulk volume).

For the -16+13.2 mm single fraction the greatest concentration of fines was achieved by the 0.68 kWh/t – 10% bulk volume test sample. For the comparable energy input levels (0.05 kWh/t and 0.1 kWh/t) the larger bulk volume sample produced a higher concentration of particles below 53μm.

The -8+6.7mm fraction exhibits the greater accumulation of particulate matter for the sample of 5% bulk volume and 0.68 kWh/t energy level. The second highest values correspond to the 10% bulk volume sample and on energy input of 0.5 and 0.68 kWh/t. At lower energy inputs the 10% bulk volume sample resulted to higher concentrations of fine particulates.

Likewise, the high energy input levels (0.5 and 0.68 kWh/t) of the 5% bulk volume sample, of the -4+3.35mm fraction, gave the highest mass percentages of fines.

These results indicate that despite the particle size distributions (5% bulk volume) appearing coarser than the corresponding ones for the 10% bulk volume sample, the concentration of fine material behaved in an opposite manner to the above statement.

The higher concentration of fine particulates for the -2+1.7mm fraction was achieved by breakage at 0.68 and 0.5 kWh/t from the 10% bulk volume samples. For the 5% bulk volume sample, the highest mass percentage of particles below 53μm corresponded to the 0.5 kWh/t test sample, whereas the 0.68 kWh/t produced a lower percentage. This might be due to particles being differently orientated in the sample holder during testing with the higher energy level, which resulted to lower concentration of fines.

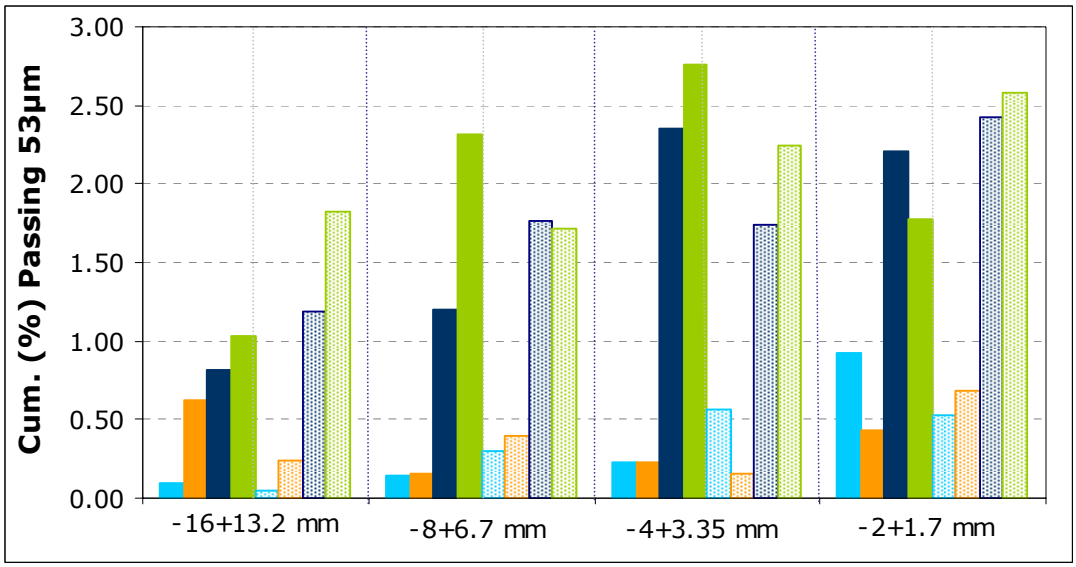

Figure 73: The cumulative percentages passing 53μm for the single limestone particle fractions. The *textured columns* represent the samples of 10% bulk volume, whereas the *saturated coloured columns* represent the 20% (for the 16x13.2mm fraction) or 5% bulk volume samples. The different colours represent different energy levels : • = 0.05 kWh/t, • = 0.1 kWh/t, • = 0.5 kWh/t or 0.2 kWh/t (for the 16x13.2mm, 20% bulk volume) and • = 0.68 kWh/t or 0.3 kWh/t (for the 16x13.2mm, 20% bulk volume).

In general, for the smaller single size fractions (4x3.35mm, 2x1.7mm) and energy input levels equal to 0.5 and 0.68kWh/t, the differences at mass percentages of particles below 53μm, were very close and only slight differences were present. For the coarser size fractions this difference was more obvious, whereas of great importance were the concentration of fines recorded for any sample, at energy levels between 0.1 and 0.5 kWh/t. Smaller particles left smaller gaps during packing in the

sample holder, which signified that the interparticle contacts were greater. Under impact, particles were squeezed and broken, whilst the ones in contact abraded. For larger test size fractions, the particles in contact are less, hence after impact the attrition rates are lower. In addition smaller particles have a higher mobility potential, meaning that particles could more easy slide over others during impact than larger ones. All these reasons could account for the higher concentrations generated from smaller test size fractions.

5.8.5.Summary of the impact test results

Prior to testing, the residual height of the single fraction was determined, so as to accurately calculate the energy input levels used during testing. Higher energy levels as well as smaller particle size, was found to result to a smaller offset.

Impact testing revealed that the dust/fines generation process was influenced by the test sample particle size, which indicates that in industrial processes every case has to be investigated separately. Some general trends were identified, hence, the higher the energy input, the finer the particle size distribution. This statement is satisfied by any particle size fraction and bulk volume sample. Also the concentration of fines (<53μm) increased, when energy levels increased. The difference in the mass percentages of fine particulates between the low and high energy levels is particularly distinct for the 0.1 kWh/t and 0.5 kWh/t.

The highest amounts of fines (below 53μm) have been reported for the top energy level of the -4+3.35mm fraction (5% bulk volume), followed by the -2+1.7mm fraction (10% bulk volume). In general, the smaller single size fractions resulted to higher mass percentages of fines. This might be attributed to the interparticle interactions that take place in the sample holder, which are more frequent for smaller particles, hence they abrade resulting to generation of fines.

For the -16+13.2mm, -8+6.7mm and -2+1.7mm limestone fractions, the greater breakage discrepancies between the different bulk volume test samples were reported at energy input level of 0.1 kWh/t, whereas for the -4+3.35mm sample high breakage rates have been found at energy input of 0.05 kWh/t. For both energy levels (the 0.05 kWh/t and 0.1 kWh/t), the accumulation of fines was low in comparison to higher energy input. Hence, for industrial processes, where breakage steps are incorporated such as comminution, knowledge of the sample mass-energy

input equilibrium can assist the optimization of the process and minimization of waste (i.e fines, dust). However, these results could also find application for processes, where breakage is not essential, such as stockpiling of an end product. The correct selection of energy input and bulk volume could result to the reduction of breakage and minimisation of fines.

The impact test does not collect the airborne dust fraction. Particulate matter is allowed to settle in the sample holder. The attached rubber flange on the head weight avoids effectively dust escaping. Dustiness testing using the HSE-WSL drum has proved that the concentration of fines in the test sample positively relates to the dust yield. Consequently, higher mass percentages of fines produced during impact testing would have a greater potential to generate dust, with higher dust yield values.

Impact testing was used to simulate common industrial processes that usually give rise to a high probability to produce particulate matter (under impact), such as drop from heights, haulage roads, draglines, stockpiling operations and others. It has been shown that process parameters (i.e energy input levels, bulk volume) and material properties (i.e particle size) influence the dust generation potential of limestone, whereas careful investigation and control upon them can help reduce dust as well as optimize process performance.

5.9. Particle size analysis results of the fines produced from limestone by the impact test

Fine particles below 53μm produced during impact testing were collected by sieving and their particle size distribution was determined using the Malvern Mastersizer–S. Triplicates of the fraction below 53μm from the same sample were produced during impact testing and they were tested by the light scattering technique to make sure that reproducible as well as representative results were achieved. As for the procedure followed for particle size analysis of the particulate matter produced from the HSE-WSL test, the Mie approximation has been selected as well as the optical properties determined for the limestone particulates (refractive index:1.7, imaginary refractive index:0.1, dispersion medium refractive index:1.33).

The measurement procedure using the Mastersizer followed the same steps as during experimentation with the dust fraction of the HSE-WSL test. Most of the time, the reproducibility of the results was good, therefore no more than two repeats on the same sample were needed. The quantity of the particulate matter collected during impact testing was greater than the dust collected using the HSE-WSL test, which permitted replicate measurements of the same sample to take place. The relative standard deviation of replicate measurements with the same feed was commonly below 1%. Table 41 presents the median values of the diameters d_{10}, d_{50} and d_{90} (10%, 50% and 90% of the particles are found below this size) together with the standard deviation and relative standard deviation values, which have been calculated after measuring the particle size of the triplicate sets of particulate matter. Results in Table 41 relate to the fine fractions (below 53μm) collected from the 10% bulk volume samples. Subsequent results from the different bulk volume samples are presented in detail in appendix II. The particle size distributions of the volume percentage retained, which are shown in appendix II, incorporate one standard deviation (error bars) calculated from replicate tests.

Table 41: The median values of the diameters d_{10}, d_{50} and d_{90} of the limestone fines produced using the impact test. The standard deviation and relative standard deviation values correspond to replicate measurements of triplicate sets of test samples. Only the results obtained for the 0.05 kWh/t (E1) and 0.68 kWh/t (E4) are shown.

		D_{10}	Stdev	RSD (%)	D_{50}	Stdev	RSD (%)	D_{90}	Stdev	RSD (%)
16x13.2 mm 10% b.v.	E1	5.67	0.50	8.85	32.89	0.95	2.90	70.73	1.39	1.96
	E4	2.28	0.11	4.91	11.62	0.54	4.62	40.48	2.95	7.29
8x6.7 mm 10% b.v	E1	1.81	0.06	3.11	9.58	0.81	8.41	41.40	4.10	9.91
	E4	1.93	0.10	5.39	10.90	0.42	3.84	37.72	0.75	1.98
4x3.35 mm 10% b.v.	E1	1.44	0.03	1.96	7.19	0.05	0.69	30.41	0.45	1.46
	E4	2.12	0.03	1.61	12.82	0.35	2.72	42.68	0.92	2.15
2x1.7 mm 10% b.v.	E1	1.90	0.08	4.39	11.96	0.69	5.74	46.17	1.05	2.28
	E4	1.91	0.04	2.30	11.04	0.35	3.21	38.59	0.60	1.56

The median values of the diameters measured by the Mastersizer demonstrate significant differences for the range of single size fractions and energy input levels, whilst a similar trend has been observed for the other bulk volume samples. The standard deviation values of replicate tests can vary from as little as 0.02 to up to 4.10 and the relative standard deviation could fluctuate from below 1% to up to 10%. Commonly, high relative standard deviation values have been observed for the particulate matter produced by coarse single size fractions, namely the -16+13.2mm and -8+6.7mm. This could be attributed to the way particles pack in the sample holder, which is less consistent for the coarse particles, whilst their orientation in the sample holder is also a determinant of the end particle size distribution.

The particle size distributions of the particulate matter produced from the 10% bulk volume samples are presented in Figure 74 and Figure 75. The graphs display both the cumulative volume percentage undersize and the volume percentage retained curves.

Results obtained for the different bulk volume samples can be reviewed in detail in appendix II. All particle size distribution graphs represent average values obtained from measurements of the triplicate sets.

For the particulate matter produced from the -16+13.2mm fraction, a positive gradation of the particle size distributions in respect of the energy input level is demonstrated. Hence, low energy input result in coarser particle size distributions than high energy levels.

The cumulative volume percentages passing 10μm and 2.5μm for all the different size fractions are displayed in Table 42. For the -16+13.2mm fraction, the percentages passing 10μm are classified according to the energy input level.

It can be seen that for the 0.05 kWh/t, the cumulative percentage below 10μm was 14.85%, whilst for the 0.68 kWh/t this was 45.16%, indicating that the extra energy input for this fraction has a significant effect on the fine particulate matter. The percentages below 2.5μm for the different energy levels are very close and only the 0.05 kWh/t produces a lower volume concentration.

The particle size distribution of the particulate matter of the -4+3.35mm-10% bulk volume sample is displayed in Figure 75. For energy input levels between 0.1 kWh/t and 0.68 kWh/t it appears that the lower the energy input the coarser the particle size distribution. Overall however, the finer particle size distribution corresponds to the sample of 0.05 kWh/t. At lower energy levels, breakage due to impact is low hence fines are generated mainly due to friction caused by interparticle contacts, which produces a much finer particle size distribution than impact alone

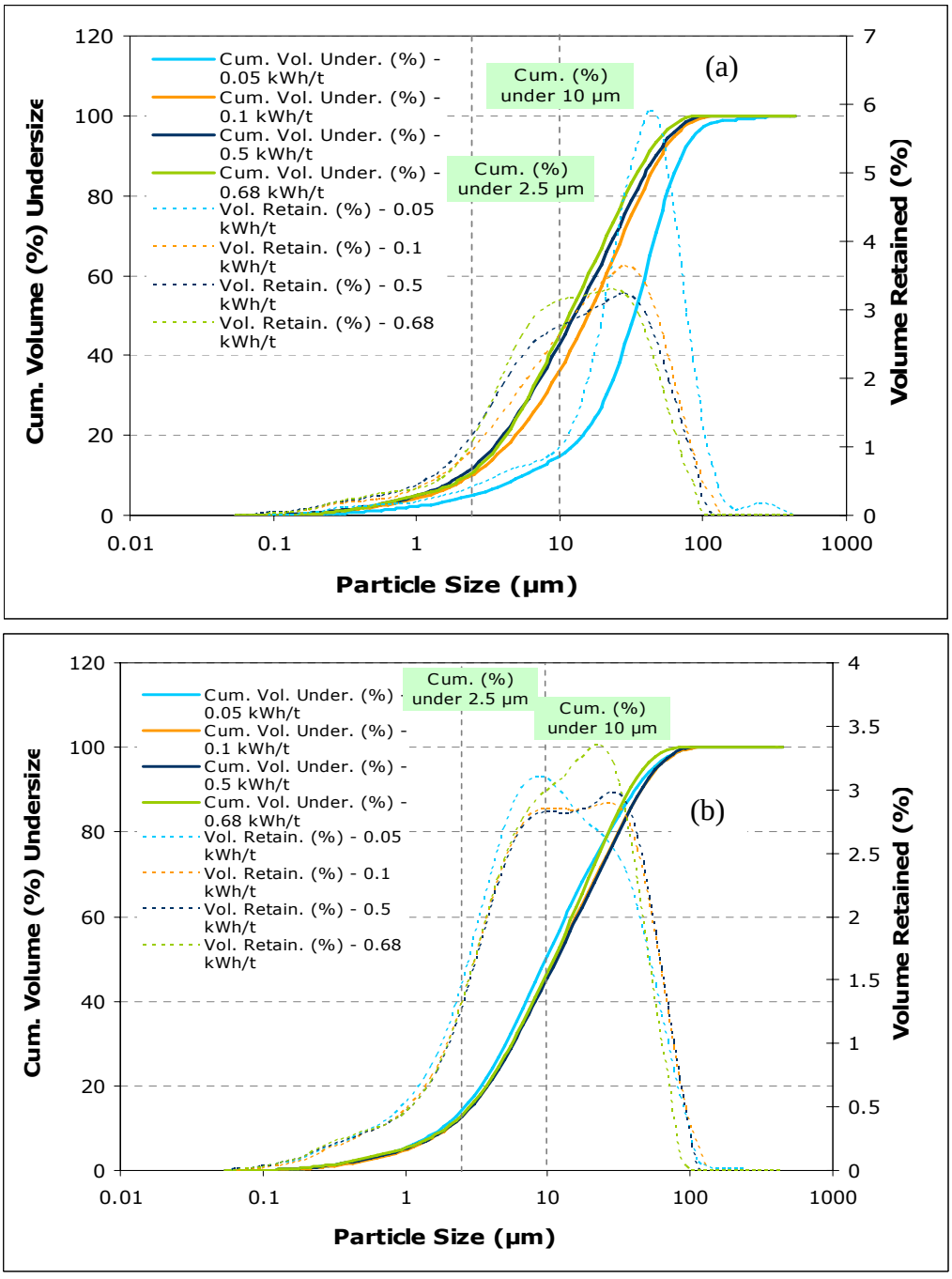

Figure 74: Particle size distributions of the limestone particulate matter fraction generated by the impact test of a) the -16+13.2mm fraction – 10% bulk volume and b) the -8+6.7mm fraction – 10% bulk volume.

The cumulative volume percentages below 10μm and 2.5μm for energy inputs equal to 0.05 kWh/t were also increased in comparison to any higher energy input level (Table 42).

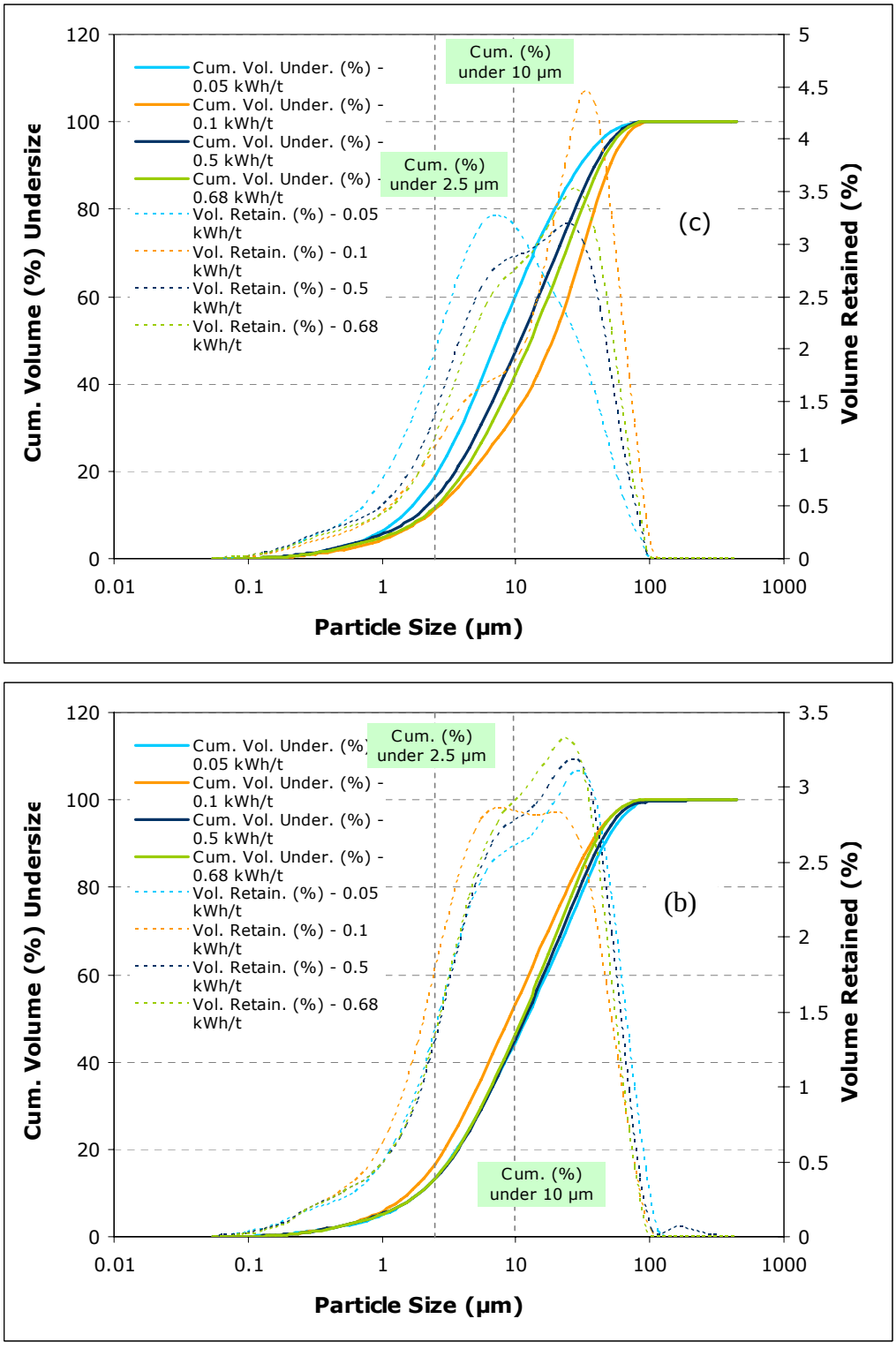

Figure 75: Particle size distributions of the limestone particulate matter fraction generated by the impact test of a) the -4+3.35mm fraction – 10% bulk volume and b) the -2+1.7mm fraction – 10% bulk volume.

The particle size analysis results that correspond to the -2+1.7mm-10% bulk volume sample revealed that the variable energy input levels do not influence the particle size distributions of the particulate matter, therefore they appear very similar. The only exception comprises the particle size distribution of the 0.1 kWh/t, which is slightly finer. The concentrations below 10 and 2.5μm present a similar profile.

The particle size distribution of the 5% and 20% bulk volume samples presented again different profiles from the ones obtained for the 10% bulk volume samples (appendix II). In Table 42 the cumulative volume percentage below 10 and 2.5 μm as well as the median values of the diameter d_{80} describe the particle size of the 5% and 20% bulk volume samples.

Table 42: The cumulative volume percentages below 10μm and 2.5μm of the limestone particulate matter generated by impact testing of a range of single fractions and bulk volumes. The median diameter d_{80} is shown as well.

Size fraction	Energy level (kWh/t)	Cum. % <10 μm	Cum. % <2.5μm	D_{80}
16x13.2mm-10% b.v.	0.05	14.85	5.01	55.44
	0.68	45.16	11.02	28.77
8x6.7mm-10% b.v	0.05	51.34	14.31	27.22
	0.68	47.32	13.16	26.98
4x3.35mm-10% b.v.	0.05	60.82	19.08	19.59
	0.68	42.73	11.87	31.22
2x1.7mm-10%b.v.	0.05	45.17	13.54	32.63
	0.68	47.01	13.41	27.67
16x13.2mm-20% b.v.	0.05	42.76	12.78	31.26
	0.3	48.82	14.41	30.09
8x6.7mmc-5% b.v	0.05	42.84	12.95	17.92
	0.68	48.77	13.71	29.31
4x3.35mm-5% b.v.	0.05	52.57	15.47	26.55
	0.68	53.55	18.43	26.70
2x1.7mm-5%b.v.	0.05	50.05	20.77	32.03
	0.68	41.97	14.13	37.49

For instance, the volume concentration of particles below 10μm and 2.5μm for the -16+13.2mm-20% bulk volume sample is much higher than the one measured for the -16+13.2mm-10% bulk volume sample. Also, the diameter (d_{80}) of the -8+6.7mm-5% bulk volume sample is significantly smaller than the d_{80} of the -8+6.7mm-10% bulk volume sample. For the same sample, the volume percentages below 10μm fluctuate for different energy input levels, while for the -8+6.7mm-10% bulk volume sample only slight differences have been observed.

Generally, particle size analysis of the particulate matter fraction collected during impact testing has revealed that fines do not follow the patterns that have been outlined for the breakage product. Even though a clear positive relationship between energy input and particle size has been determined for the breakage product, where increasing the energy input levels result to finer particle size distributions and higher concentrations of fines (below 53μm), this relationship was not reflected in the particle size distribution of the -53μm samples. On the contrary, the particulate matter behaves independently of energy input and particle size of the test sample. However some general trends are evident. Thus, for the majority of the samples tested, particle size distributions did not exhibit substantial differences. Only small fluctuations were present for both the median diameters and the cumulative volume percentages below 10 and 2.5μm. Therefore, on average 50% of the particulate matter volume exhibits a particle size below 10μm, whilst 80% of the particles are below 30μm. Particle size analysis on the dust fraction collected using the HSE-WSL test had also not found significant differences within a variety of samples. The increased concentration of fine particles (below 30 and 10μm) testifies the dust generation potential of the limestone particulate matter, as well as its possible adverse impact to human health and the environment if entrained in the air.

5.10. Mineralogical characterisation of the limestone particulate matter

The mineralogy of the particulate matter captured using the HSE-WSL test, as well as the modified JK impact test was identified by X-ray diffraction analysis and scanning electron microscopy. As it has already been mentioned at the beginning of this chapter, the limestone used was of high purity hence the X-ray diffraction patterns of the particulate matter (Figure 76) do not exhibit any differences in comparison to the rock sample. Again one main mineral phase is present, that of calcite, whereas for some of the dust samples a small quantity of quartz was identifiable as well.

The dust particles were examined using scanning electron microscopy (Figure 77). In the limestone rock matrix, calcite appears in rhombohedral crystals. Airborne particulates do not retain the same degree of crystallinity. They would better be described as sub-rhombohedral calcite crystals. Large particles (>10μm) exhibit a sub-angular shape, whereas smaller particles display a sub-rounded shape. A wide spread of particle sizes are shown ranging from sub-microns to up to a few tens of microns.

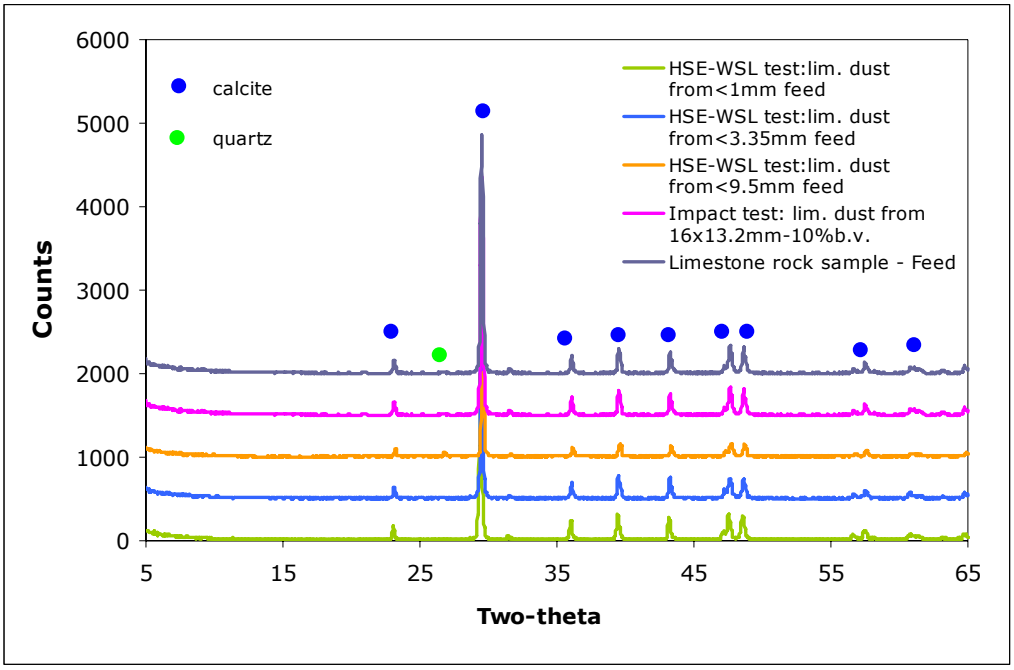

Figure 76: XRD traces of the limestone dust/fines fraction collected by the dustiness test and the impact test. The x-ray diffraction pattern of a rock sample (feed) is presented as well.

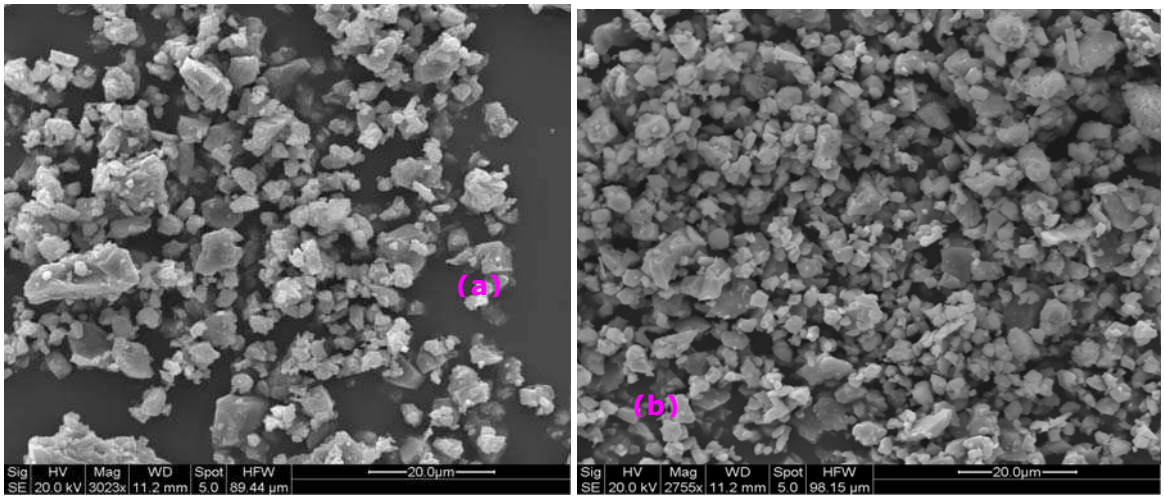

Figure 77: Scanning electron microscope (SEM) photomicrographs of the limestone airborne particulates produced from a feed of -3.35mm/150g;(a) Magnification x3023, scale 20 µm. Calcite particles are present ;(b) Magnification x2755, scale 20 µm. Calcite particles are present.

5.11. Summary of Chapter 5

The dust generation potential of limestone from Tunstead quarry, due to abrasion and impact mechanisms was evaluated through the use of two laboratory based tests, the HSE-WSL dustiness test and the impact test. The two tests simulated the mechanisms involved in a variety of industrial processes that are liable to produce

dust, such as drilling, loading and tipping of material, crushing and screening, stockpiling, conveying etc. Most of these processes have been identified as potential dust sources in Tunstead quarry. In addition the dust fraction was collected and characterised in terms of mineralogy and particle size distributions.

Experimentation with the dustiness test took place on a variety of limestone size fractions, whilst preliminary testing investigated the dependency of the operational parameters of the apparatus to the dust yield of limestone produced. Preliminary results revealed that a positive relationship exists between tumbling time and sample mass with the total dust yield. These results reflect trends that could be present in mining operations. Hence increasing the operation time of a certain process i.e tipping would increase the potential of higher rates of dust to be generated. Also, an increase on material mass, for example in material transfer processes, could give rise to an increase in dust yield.

During dustiness testing, two different testing regimes were used, the HSL proposed testing procedure (HSL-TP) and the optimum operating procedure protocol (OPT-TP), which resulted from preliminary testing. Four different limestone fractions were tested using these protocols, the <9.5mm, <3.35mm, <1mm and 10mm single size fraction. The <3.35mm limestone produced the highest dustiness index followed by the <1mm fraction, which in turn is followed by the <9.5mm fraction and 10 mm particles. Also, the OPT-TP always gives the greatest dustiness values. Dustiness results revealed that the concentration of fine material (<75μm) in the test sample positively correlates to the dust generation potential of a sample, whereas the rotation time has the greater effect upon dustiness, than any other operational parameter. In general limestone is classified as a "dusty" material with dustiness levels between 0.1% to 1%.

The mechanisms of dust generation in the tumbling mill were identified by experimental tests and computational simulation. Firstly, the effect of tumbling time on a range of single size fractions of limestone was investigated. Then the tumbling mill was modelled on the basis of the specific rate of breakage and the breakage distribution function. It was found that the breakage process of the tumbling mill follows first order kinetics, which implies that the mechanisms of the tumbling mill can be predicted, whereas the HSE-WSL drum can find application on the simulation of common handling processes. Subsequently, the exact mechanisms taking placing during the tumbling action were identified with the use of a high speed video camera and discreet element modelling steps. It was shown that dust generated in the

tumbling mill is solely due to one mechanism that of abrasion, which is caused by the frictional sliding of particles on the drum walls and over other particles. Also the computational modelling results regarding the dependency of operational parameters (i.e tumbling speed, sample mass) have shown a good agreement with the dustiness results hence they can be used as prediction for industrial processes.

Particle size measurements on the dust fraction of the HSE-WSL drum has shown that there are no substantial differences between the particle size distributions from different feed test samples. Also it was found that 80 % of the particles have a size between 10 to 16μm, which implies that limestone dust could cause adverse implications to human health and the environment.

Impact testing revealed that there is a close correlation between the energy input levels and the particle size distribution of the broken product. Hence the higher the the energy input, the finer the particle size distribution. This statement is satisfied by any particle size fraction and bulk volume sample. Also the concentration of fines (<53μm) increased, when the energy levels increased. The difference in the mass percentages of fine particulates between the low and high energy levels is particularly distinct for input energies of 0.1 kWh/t and 0.5 kWh/t. The highest accumulation of fines were found for the smaller single size fractions of test sample, which could be attributed to the particle – particle interactions that take place in the sample holder, which are more frequent for smaller particles. The impact test does not collect the dust fraction in the airborne state, however dustiness testing using the HSE-WSL drum has proved that the concentration of fines in the test sample positively relates to the dust yield. Consequently, higher mass percentages of fines produced during impact testing would have a greater potential to generate dust, with higher dust yield values. Impact testing simulated industrial processes such as drop from heights, haulage roads, draglines, stockpiling operations and others. It has been shown that process parameters (i.e energy input levels, sample mass rates) and material properties (i.e particle size) influence the dust generation potential of limestone, whereas careful investigation and control upon these parameters can help reduce dust as well as optimize process performance.

Particle size analysis of the particulate matter fraction collected during impact testing has revealed that fines do not follow the same trends that have been outlined for the breakage product. Thus, particulates behave independently of energy input and particle size of the test sample. Only small fluctuations were present for both the median diameters and the cumulative volume percentages below 10 and 2.5μm.

Therefore, on average, 50% of the particulate matter volume exhibits a particle size below 10μm, whilst 80% of the particles are below 30μm. If the cumulative volume percentages below 10μm and 2.5μm of the dust and fines produced from the HSE-WSL test and modified JK impact test respectively, are compared then it is observed that the latter are significantly lower. This is probably because with the impact test the airborne fraction was not collected separately. However, similarly to the HSE-WSL test, particulates exhibit only slight differences in size, for different test samples. Once again, the increased concentration of fine particles (below 30 and 10μm) testifies the dust generation potential of the limestone particulate matter, as well as its possible adverse impact to human health and the environment if entrained in the air.

Finally the mineralogy of the dust and fines produced from the HSE-WSL test and the impact test was identified by X-ray diffraction analysis. The limestone used for this study was of high purity therefore the particulate matter presents similar mineralogical profile with the host rock. Conclusively, one major mineral phase is present that of calcite, whilst some of the samples include a minor quantity of quartz.

Looking back at the processing plant of Tunstead quarry, dust generation could be minimised in areas such as the tipping process to the gyratory crusher, the sieving steps of the roadstone plant, or the stockpiling of limestone products, by optimising theses processes. For instance decreasing the residence time of the limestone ore in conveyor belts (i.e by reducing the length of conveyor belts after careful design) could minimise the effect of abrasion upon the ore and thus reduce the generation of dust. Also the reduction of energy input, namely the drop height, during tipping, stockpiling or loading and dumping activities could minimise the production of fines that result due to impact breakage, which could cause the emission of particulates. Finally adjusting the bulk volume of ore involved in processes that require drop from height, so as to produce lower amounts of fines could equally minimise dust.

Chapter 6. Experimentation with ore from Talc de Luzenac

6.1. Introduction

Talc is one of the most important industrial minerals as finds application in a wide range of markets. Talc is the softest mineral known, and it is commonly extracted by surface mining techniques. Due to talc's softness, as well as its platy and often acicular particle shape, dust is a major issue in talc mining and processing, with high potential to cause adverse effects to the environment and human health. Human exposure to talc can give rise to various types of pulmonary diseases, such as talcosis and talc pneumoconiosis (National Occupational Health and Safety Commission 2005). Low grades of talc ore can contain quartz or tremolite (an amphibole asbestos), which can also negatively impact human health. In addition, deposition of talc in fields can be a major issue due to high colour contrast and it can effect the surrounding environment, the plants and woodlands. Therefore, occupational health and air quality concerns associated with the mining activities of talc have to be careful managed and controlled.

The talc used in this project came from Trimouns mine (Pyrenees) in France. The company that operates the talc mine is called Talc de Luzenac and it belongs to the international Luzenac Group that produces, ships and sells in excess of 1.4 million tonnes of talc from 11 mines and 20 processing plants in Europe, North and Central

America and Asia-Pacific. The Luzenac Group is member of the Rio Tinto group (Luzenac Plc. 2005).

The objective of this chapter was to evaluate talc's potential to generate dust from various mechanisms. Experimental work was aimed at investigating which industrial processes might present a greater liability to produced particulate matter.

6.1.1. Experimentation steps

The structure of this chapter is outlined below. A brief introduction on Talc de Luzenac mine is given at the start of the chapter, which reviews general information associated with the Trimouns mine

Experimentation took place through the following steps:

- Mineralogical characterisation of the rock samples by X-ray diffraction analysis and scanning electron microscopy.
- Determination of the dust generation propensity of talc using the Warren Spring Laboratory (HSE-WSL) rotating drum test. Collection of the dust fraction produced by the HSE-WSL rotating drum test.
- Measurement of the dust particle size by laser diffraction analysis using the Malvern Mastersizer-S.
- Determination of the dust propensity of talc using the impact test. The relation between dustiness and specific comminution energy input was investigated. The particulates fraction below 53µm was collected by sieving for further investigations.
- Measurement of the particle size of the fines collected by the impact test by laser diffraction analysis.
- Mineralogical characterisation of talc dust produced by the HSE-WSL test and impact test using the X-ray diffraction analysis technique and the scanning electron microscope.

The results obtained through the different experimentation steps allowed conclusions to be drawn regarding the dust generation potential of talc for a range of industrial and handling processes.

6.2. Talc de Luzenac- History, geology and industry

The talc deposit lies in the French Pyrenees, close to the French borders with Andora. The company operates several pits responsible for Talc de Luzenac's production, but Trimouns is the most important as it yields 60% of the total production (Kennedy 1988). It is the only operating talc mine in France and maintains its leading position despite the fact that it can only operate between May and October, due to the severity of the winter weather. Over the winter months, all mining machinery is housed in garages on the mountaintop. However, the plant in the valley continues processing stockpiled material (Crossley 2002).

Luzenac produces 430,000 tpa of talc product from the Trimouns mine. There are 66 finished talc grades and more than 200 products (Crossley 2002). The largest single volume market for talc from Trimouns is in the paper industry, where it finds application as a filler (Crossley 2002). The next biggest application is in plastics, where it is used as filler. Other industrial applications of talc is in the paint industry, for the manufacturing of ceramic bodies (tableware, tiles, sanitaryware, technical) and for refractory applications (chlorite rich types), in food and personal care industry and elsewhere (Kennedy 1988;Luzenac Plc. 2005).

6.2.1. Mining and processing of talc

The ore mined at Trimouns is a mixture of talc and chlorite, and chlorite can represent a 5% to 60% of the ore. There are 18 types of talc ore in the Trimouns mine, and reserves for over 100 years (Crossley 2002). Trimouns talc deposit is an open pit mine. Due to the heterogeneous nature of the ore, sorting takes place even on this stage. The ore is sorted according to its talc content and brightness and techniques used include hand sorting, state –of the art-laser and image analysis technology (Luzenac Plc. 2005).

The different ore grades are jaw crushed and then stockpiled at the mine to await transfer to the processing plant by aerial cable transporter (Figure 78) (Crossley 2002). Crude talc is dried at 150^{o} C in five rotary dryers before moving to the milling unit (Crossley 2002).

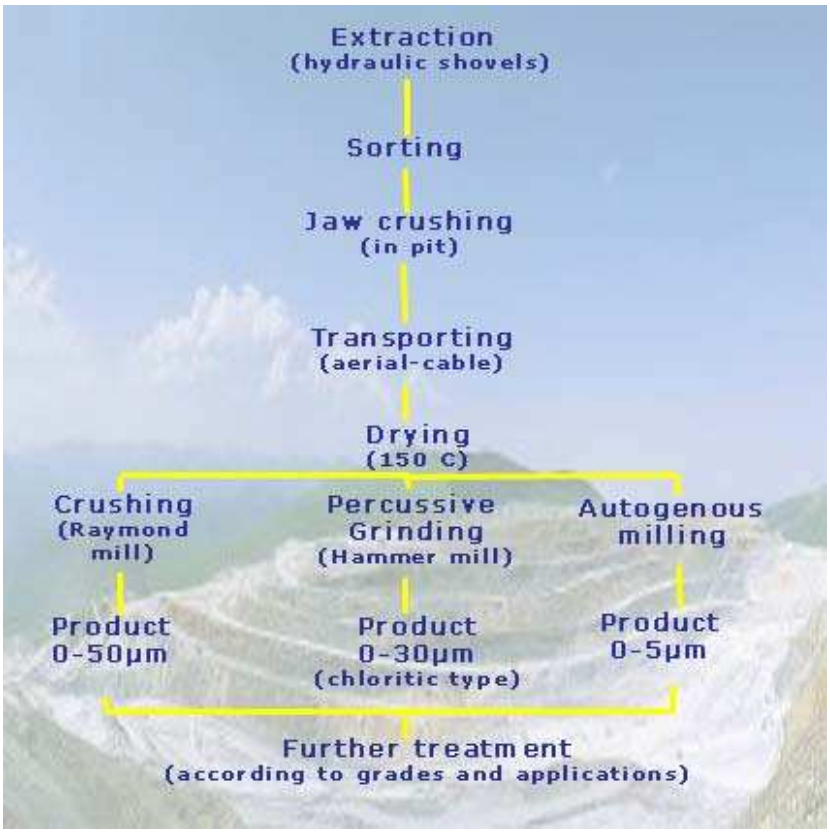

Figure 78: Processing steps followed for talc in Trimouns mines.

At the processing plant the talc is crushed and ground to a range of particle size distributions, suitable for any of the end uses. To achieve exactly the right particle size distribution and top cut for a given application, several techniques are used including compressed air and impact milling (Luzenac Plc. 2005). Crushing, grinding and selection has two purposes to alter the relative sizes of the talc and chlorite flakes and to allow talc, chlorite, dolomite, and quartz separation (Kennedy 1988). Talc is dry crushed in Raymond- type mills and it is impacted in autogenous or hammer mills. The use of Raymond- type mills allows liberation of individual talc flakes. The ground particles are drawn into a rising air current and graded in a 'Whizzer' (Kennedy 1988). Larger particles return into the grinding mill. The resulting grain size varies between 0 to 50 μm. Percussive grinding makes it possible to obtain a product with a grain size between 0 to 30 μm. This type of grinding is suitable to hard particles, because talc tends to bend under impact and retain its original shape, thus it is mainly used to chloritic types of ore (Kennedy 1988). Quartz, which occurs in small quantities, is particularly associated with chloritic varieties. Autogenous grinding, where particles are forming the grinding media, enables very fine grain sizes (0 to 5 μm) to be produced. A schematic representation of the processing steps discussed before for talc is shown in Figure 78.

6.2.2.Talc de Luzenac – Geology and Mineralogy

The Trimouns talc ore occur along the boundary between a basement of high-grade metamorphic rocks and migmatites of the St Barthelemy massif and an overthrust cover of lower grade metamorphic rocks of upper Ordovician to Devonian age (Evans 1993). The deposit is 3 miles long and is worked over a distance of one mile (Kennedy 1988). The main ore body is 10 – 80 metres thick, dips eastwards at 40° – 80° and reserves of at least 20 Mt are present (Evans 1993). During the overthrusting, intense shearing of the dolomites, schists and other rocks permitted extensive hydrothermal circulation, which produced talc rich ore (80 – 97%) in the dolomites and chlorite rich ore (10 – 30% talc) in the silicate rocks (Evans 1993). The talc mineralization contains varying quantities of chlorite, which are distributed between principal and minor veins located mainly in the footwall. The elongated crushed dolomitic crystals are associated with chlorite and also frequently with pyrite (Kennedy 1988). The lower part of the hanging wall rocks, contains discontinuous dolomitic lenses 5 – 80 metres thick overlying, but also intercalated with mica schists in which small bodies of cross cutting leucogranites, aplites, pegmatites and quartz veins occur (Evans 1993).

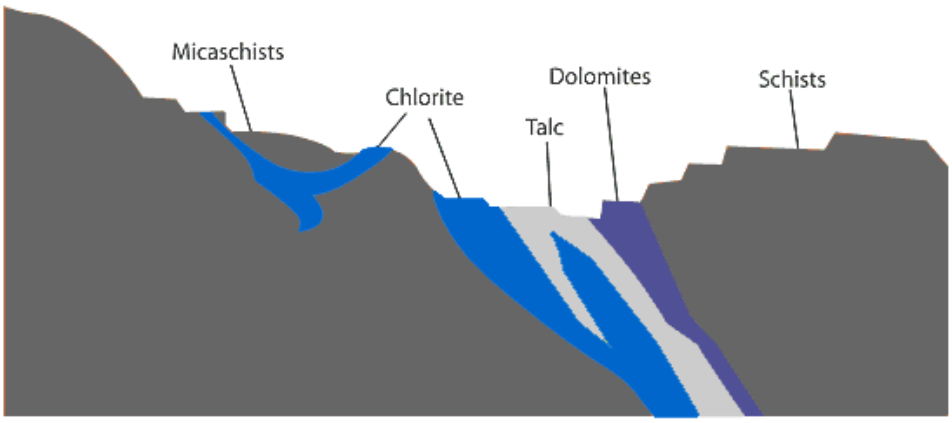

Figure 79: A cross sectional representation of the geology of the Trimouns talc deposit (Luzenac Plc. 2005)

Although talc and chlorite are the main mineralogical phases, other minerals like calcite, quartz, graphite, pyrite, pyrrhotite, and chalcopyrite, dolomites, rare earth carbonates, phosphates and cassiterite are present as well. The better grade talc is associated with dolomites and therefore occurs in the hangingwall. Chlorites are prominent and abundant in chloritic schists, varying from greenish-grey to dark grey (Kennedy 1988).

6.3. Particulate matter emissions from talc mining and processing

According to the air pollution (AP-42) emission factors documentation produced by the U.S. Environmental Protection Agency, in talc processing, particulate matter is emitted from drilling, blasting, crushing, screening, grinding, drying, calcining, classifying, materials handling and transfer operations and packaging and storage (US EPA 1995). A typical schematic diagram of talc processing steps is shown in Figure 80. Most of these processing steps are taking place in Trimouns mine, so they represent potential dust sources of the plant.

The mitigation techniques used by Talc de Luzenac to minimise dust include wetting the mine haulage roads, covering stockpiles to prevent wind blow and water spraying of trucks before they go on public roads. In the processing plants, dust is captured by high efficiency filters (i.e fabric filters) and suction systems and recycled through the production process. In addition, continuous assessment and monitoring takes place to ensure that dust levels are maintained below legal requirements. In particular for Trimouns mine, the talc ore is transported from the mine to the processing plant by cableway rather than by truck, which minimizes significantly emissions due to truck transfer (Luzenac Plc. 2005). Talc de Luzenac implements a screening testing protocol to certify that talc does not contain asbestos, based on analytical methods. In terms of health and safety practices, exposure to workers is assessed by monitoring through a series of epidemiological studies (Wild 2000;Wild et al. 2002).

Unfortunately it was not made possible to visit the Trimouns mine so as to assess the effectiveness of the dust control techniques utilized by Luzenac. However, due to the friability and softness of talc, dust can easily be generated by inappropriate handling and processing, resulting to fugitive emissions. For instance, talc's hydrophobicity could reduce the efficiency of water suppression systems, allowing dust to escape capture. Processing of talc requires several steps of comminution and grinding in dry conditions, and although mills are enclosed, particulate matter can be produced during feeding the raw material to the mill or transfer of the product. The end product size is very small, normally below 50 μm, therefore can easily entrain into an airborne state. The aerial transfer system even though it reduced emissions that could be caused from truck transportation, it can generate dust due to wind blow as talc is not completely enclosed. Finally, talc particulates are associated with serious

impacts on human health, consequently it is essential to minimise emissions as much as possible.

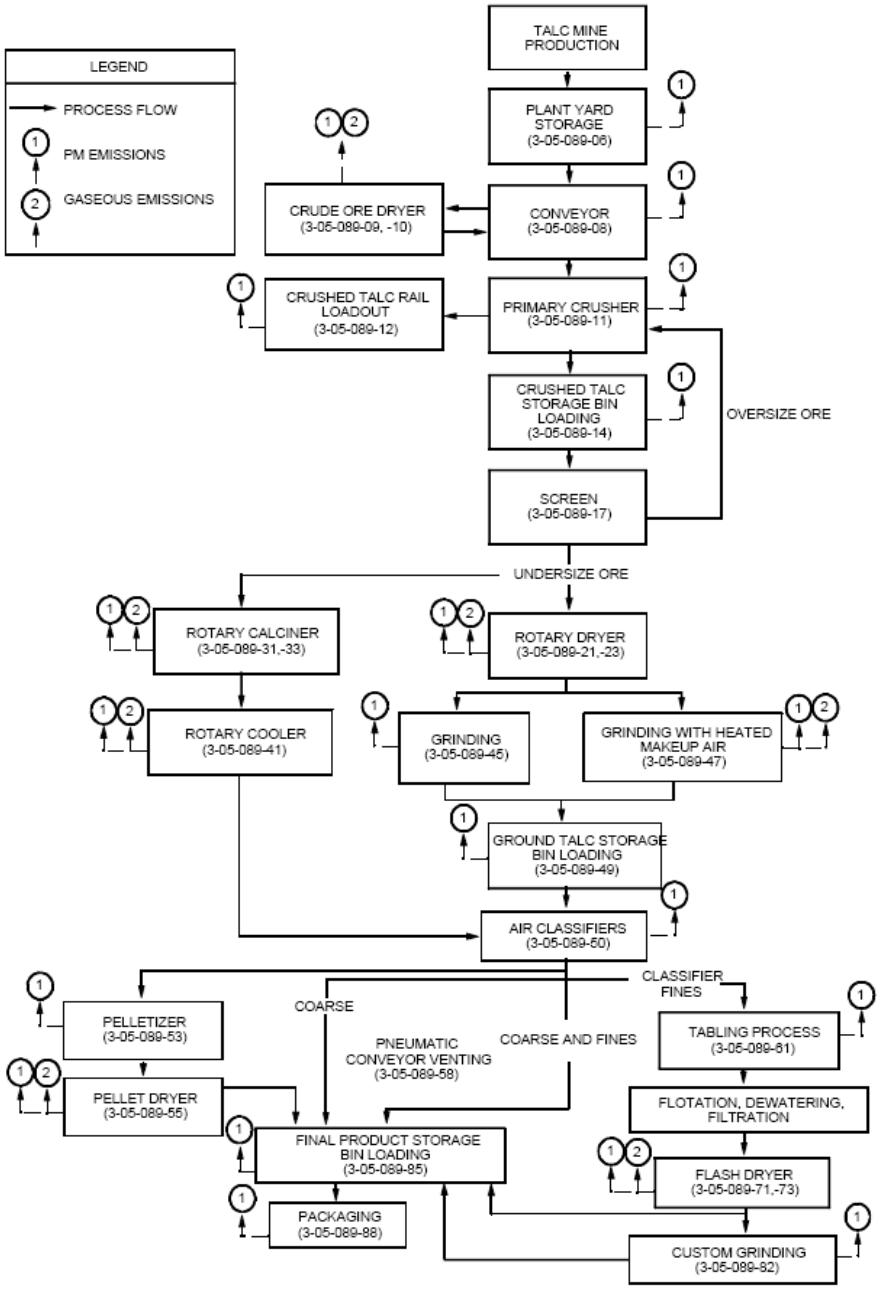

Figure 80: Process flow diagram for talc processing (US EPA 1995).

This project aimed to determine the dust generation potential of talc resulting from different industrial processes, and therefore different mechanisms, and to evaluate if some steps could be implemented to reduce dust generation without implementing additional dust control practices.

6.4.Mineralogical characterisation of the talc ore

Talc is a member mineral of the phyllosilicate group and it is described as a hydrous magnesium silicate, which is theoretically characterised by the formula, $Mg_3Si_4O_{10}(OH)_{12}$ (Dana 1998). Talc from Trimouns mine tends to occur in a lamellar – platy form. Its colour varies from white to pale green and grey. The differences in colour are mainly due to the presence of chlorite, which varies in composition according to location in mine. As previously mentioned, the chlorite content can vary from 5 to 60%.

The mineralogy of the talc rock samples was identified by X-ray diffraction whole rock analysis. Fifteen different representative samples of 5 g were prepared following the procedure shown in Chapter 4. The XRD traces of all the prepared samples were identical. Several of them can be reviewed in Figure 81.

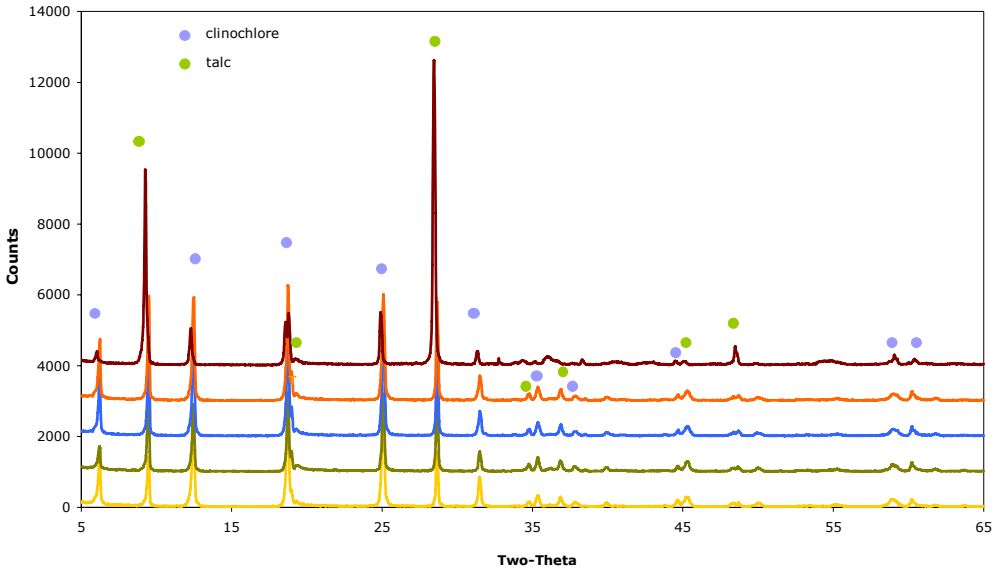

Figure 81: The XRD traces of the talc rock samples (two-theta, whole rock analysis).

It can be seen that talc consists of two main mineral phases, the minerals talc and clinochlore. The clinochlore is a common chlorite group mineral with a theoretical formula of $Mg_{3.7}5Fe_{2+1.2}5Si_3Al_2O_{10}(OH)_8$. Both the talc and chlorite minerals present strong XRD patterns, which imply that they participate as major minerals to the rock composition. The mineralogy of the rock samples is compared with the particulates composition to explore if any differences are present. These results are presented later in the chapter.

6.5. Determination of the dustiness of talc using the HSE-WSL rotating drum test

The next step of experimentation included the use of the HSE-WSL dustiness test, which assessed the dustiness of talc under abrasion. A variety of size fractions were selected for analysis. Detailed presentation of the experimental steps followed as well as the results obtained is presented in the following sections.

6.5.1. Dustiness measurements

Following the testing procedures established after experimentation with limestone, two different testing protocols (HSL-TP and OPT-TP) based on two different sets of operational parameters were used to assess the dustiness of the talc samples.

The dustiness of three different size fractions of talc (<9.5mm, <3.35mm, and <1mm) was determined following both testing procedures. Prior to testing the particle size distribution of the talc feed (<9.5mm, <3.35mm, <1mm) was measured by sieving and the results are presented in Figure 82. As expected the coarser particle size distribution correspond to the fraction below 9.5mm, followed by the fractions below 3.35mm and below 1mm.

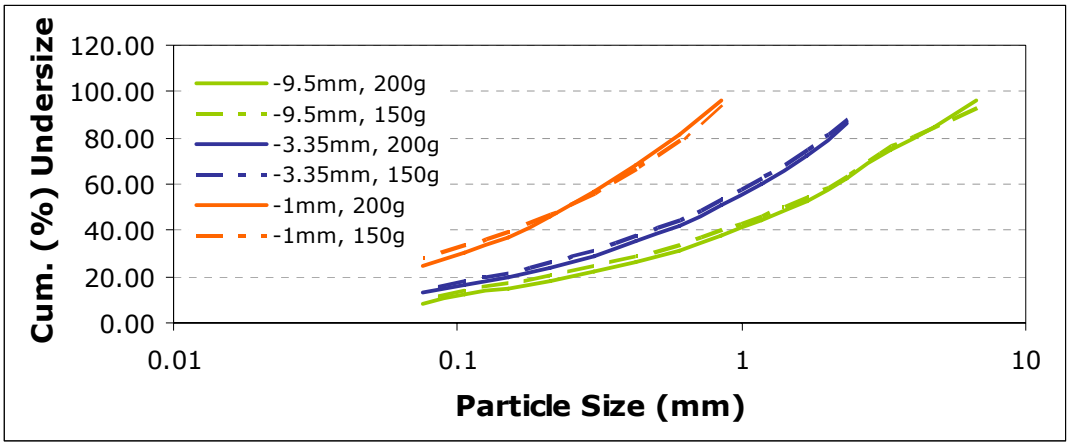

Figure 82: Particle size distributions of the talc feed samples.

6.5.1.1. *Presentation and analysis of the dustiness measurement results*

The dustiness values of the talc test samples can be reviewed in Table 43 and in appendix III. The dustiness results shown in Table 43 correspond to average values resulted by triplicate repeats of a test. The standard deviation of the replicate tests is reported in Table 43 together with the relative standard deviation values. Statistical analysis results have shown that an average standard deviation of 0.02 and a relative standard deviation equal to 8.66% should be expected during testing with talc.

Table 43: Dustiness values of the talc samples obtained for both testing protocols. The standard deviation and the relative standard deviation (% RSD) reflect the reproducibility of the replicate tests.

Talc fractions	HSL procedure			Optimum operating parameters procedure		
	Dustiness (%)	Standard deviation	(%) RDS	Dustiness (%)	Standard deviation	(%) RSD
< 9.5mm	0.2070	0.046	22.08	0.3592	0.036	10.15
< 3.35mm	0.1828	0.007	4.06	0.3440	0.033	9.57
< 1mm	0.2402	0.0004	0.16	0.4123	0.024	5.92

The two different testing protocols produced a range of dustiness values from the talc samples, varying from 0.18% to 0.41%. The HSL-TP always produced lower dustiness results than the optimum operating parameters protocol. On average the optimum parameters procedure resulted to dustiness values 1.8 times higher than the HSL protocol.

For the HSL-TP, the highest dustiness value is obtained from the < 1mm test sample, followed by the <9.5 mm and the <3.35mm samples. Nevertheless, dustiness values of the different size fractions of the test sample do not fluctuate by a great degree. The dustiness results derived by the OPT-TP exhibit a similar gradation with the values of the HSL-TP. Hence, the <1mm test sample presents the highest dustiness, followed by the <9.5mm sample, whereas last on the dustiness scale comes the <3.35mm sample. Similar to the results obtained by the HSL-TP, the dustiness values of the various talc size fractions show small differences. The extended tumbling time in the mill during the OPT-TP produced much higher dustiness results, despite the lower sample mass usage (150g for the optimum conditions instead of 200g for the HSL procedure). A similar trend has also been observed during experimentation with limestone.

In Chapter 5, it was determined that the concentration of fines in the test sample is another factor that can affect the final dustiness values. The relationship of the fines content in the talc test samples with dustiness is shown in Figure 83.

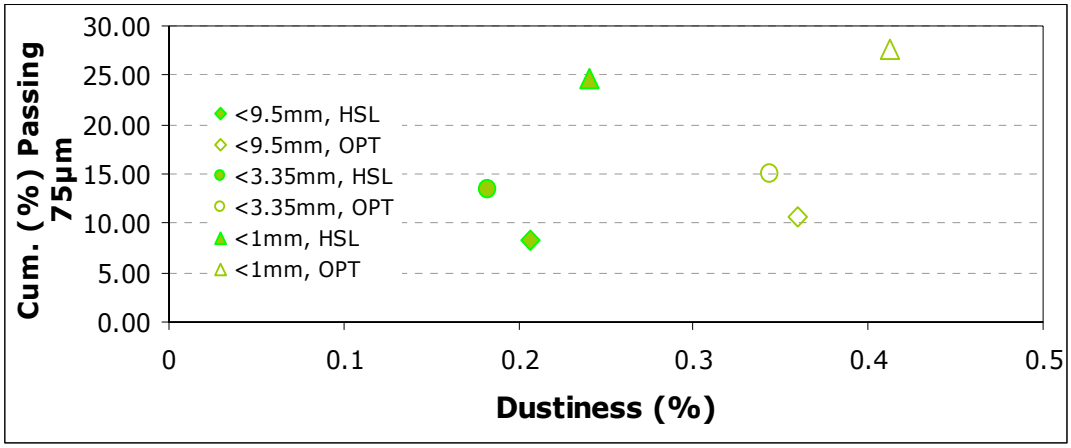

Figure 83: Dustiness result of the talc fractions versus the proportion of fines in the test sample (HSL: corresponds to the HSL testing procedure, OPT: represents the optimum operating parameters protocol)

The <1mm sample contained the highest proportion of particles below 75µm and it produced the highest dustiness values. This is not the case for the <3.35mm samples, which although they contain a greater mass proportion of particles below 75µm than the <9.5 µm samples, their dustiness is lower. Nevertheless, differences in dustiness between the <9.5mm and <3.35mm samples are very small. Even the dustiness of the < 1mm sample does not differ that much from the <3.35mm and <9.5 mm samples. This indicates that under specific testing conditions (i.e HSL protocol) the dustiness of talc samples, consisting of a range of particles with different sizes, is independent of the particle size distribution of the test sample. The concentration of fines (below 75µm) in the test sample will affect the dustiness values obtained only if they exceed a minimum limit where some significant differences in dustiness can be observed. According to Figure 83, this limit for the <1mm, <3.35mm and <9.5mm could be defined as the cumulative percentage passing 75µm being above 20%. Also, the discrepancy in dustiness for a specific sample (i.e <1mm) observed by the different testing protocols could not be attributed to the higher concentration of fines, but to the greater tumbling time. Talc is a friable and soft material and abrasion, attrition rates therefore increase with tumbling time resulting in larger dust yield.

6.5.1.2.*The effect of moisture content upon talc's dustiness*

The moisture content of the talc samples was determined to allow examination of the relationship with dustiness. The measurement procedure followed British standard BS812-109:1990 (BSI 1990) and is presented in detail in Chapter 5 together with the moisture content results for limestone. For all the talc samples (<1mm, <3.35mm, <9.5mm) the moisture content was found to be the same and equal to 0.16%, which indicates that it does not influence the dustiness results. As mentioned in previous paragraphs, talc is a hydrophobic material hence it was expected that the moisture content will not be a property which significantly influences dustiness.

6.5.1.3.*Determination of the health based dustiness indices*

The HSE-WSL test enables the determination of health related dustiness indices. Although the objective of this project was not to characterise dust in terms of an occupational hazard, it was thought important to provide an indication of the particulate's adverse impact to human health. The dustiness indices of the talc samples are presented in Table 44. The standard deviation values for the data in Table 44 have been determined by triplicate tests.

Table 44: Health based dustiness indices of the talc samples (both testing protocols). One standard deviation has been calculated from replicate tests.

HSL protocol	Talc fractions		
	<9.5mm	<3.35mm	<1mm
D_t (%)	1.2992	2.1844	1.7009
Standard deviation	0.0053	0.0217	0.0070
D_r (%)	0.0173	0.3066	0.0486
Standard deviation	0.0003	0.0046	0.0008
Optimum parameters protocol			
D_t (%)	1.0011	0.7524	1.5782
Standard deviation	0.0042	0.0065	0.0107
D_r (%)	0.0499	0.0100	0.0732
Standard deviation	0.0009	0.0001	0.0013

The different testing protocols used resulted to a range of dustiness values. Hence, the thoracic fraction dustiness index can vary from 0.7524% to 2.1844% and the respirable fraction dustiness index ranges from 0.0100% to 0.3066%. The inhalable fraction dustiness indices represent total dust and they have been discussed in paragraph 6.5.1.1.

The HSL-TP produced higher values of the thoracic dustiness index than the OPT-TP, whereas the latter resulted in slightly greater dustiness indices of the respirable fraction of the <9.5mm and <1 mm samples. The maximum dustiness index of the thoracic and respirable fractions correspond to the <3.35mm test sample (HSL testing procedure).
The gradation of the dustiness indices of both the thoracic and respirable fractions for the optimum operating conditions protocol follows the general trend observed for dustiness in paragraph 6.5.1.1. Consequently, the uppermost value corresponds to the <1mm test sample followed by the <9.5mm and <3.35mm samples. For the HSL testing procedure, the higher values of the respirable and thoracic fractions were obtained for the <3.35mm sample, while second in turn being the <1mm sample and third the <9.5mm test sample. It is difficult to explain what is the exact reason that accounts for the high variation in the dustiness indices (thoracic and respirable fraction) of the <3.35mm sample between the two different testing procedures. However, it is possible that the fine fraction of the test sample used by the HSL protocol comprises of a greater number of particles with a size that falls within the thoracic and respirable fraction.

The dustiness indices of the <9.5mm and <1mm samples do not present significant differences for the different testing protocols. A general conclusion that can be made according to the findings of the health based classification of talc particulates is that only a small mass proportion (normally below 2%) of particles can be found in the thoracic and respirable fractions, whereas the majority of the particulates exhibit a coarser particle size.

6.5.2. Summary of the dustiness results analysis

Higher dustiness values of the talc samples were recorded by the OPT-TP rather than the HSL-TP. The <1mm sample produced the highest dustiness levels, followed by the <9.5mm and the <3.35mm samples, for any of the testing protocols.

Dustiness results indicated that tumbling time is the parameter that has the greater effect upon dustiness of talc, as an increase in dust yield has been observed for the 3 minutes rotation time (OPT-TP), even though a smaller mass of test sample has been used. Thus, in industrial scale operations correct planning of the time scales of processes could decrease dust levels.

The correlation of dustiness levels with the concentration of fines in the test samples has shown that talc particulates behave independently of the particle size distribution

of the test sample. This is why dustiness of the different test fractions, does not exhibit substantial differences, under the same testing regime. The above statement implies that a limit value of the mass percentage of fines included in the test sample exists, below which dustiness will not be affected by the particle size distribution of the test fraction. On the contrary, above that limit dustiness will positively correlate with the proportion of fines in the test sample. In talc processing operations such as the transfer of materials with conveyor belts, comminution, sieving, mixing, grinding and others, dustiness could be controlled by identifying this limit value of the concentration of fines, where dust levels will remain in steady state. Further decrease of dust could be achieved through optimisation steps of the processes involved, by reducing the residence time in talc processes that involve the application of abrasion.

Several other researchers assessed the dustiness of talc using the HSE-WSL drum. Breum (1999) reported that the dustiness of 25g-50g of talc was 0.4% (air flow rate of 50 l/min, tumbling time of 3 minutes and rotating speed 40 revs/min), whereas an increase in sample mass (100g to 200g) resulted in higher dustiness levels, equal to 3 to 4% (Breum 1999). Hjemested et al. (1996) concluded that the dustiness of 50 g of talc was 0.8% (flowrate: 50 l/min, tumbling time: 3 minutes, rotation speed: 40 revs/min), whilst for a larger sample mass (200g) and different operational parameters (flowrate: 80 l/min, tumbling time: 10 minutes, rotation speed: 60 revs/min) only a minor increase in dustiness was found equal to 1% (Schneider and Hjemsted 1996). Chung et al. used the HSL testing procedure and determined that talc dustiness was 4.102% (Chung and Burdett 1994). All these results gave greater dustiness levels than the ones obtained within this project. Nevertheless, previous research findings looked at the dustiness of powder grades of talc and unfortunately none of them report any information relevant to the particle size characteristic of the test samples in use. In addition most of them experimented with different operational settings. A general trend that can be outlined from the above results is that dustiness of fine powder samples is greater than the ones reported from sample mixtures which consist of granular and fine talc particles. This is because powders comprise such high concentrations of fine particles (<75μm) that can affect the dustiness levels of talc.

The health related classification of the talc fractions <9.5mm, <3.35mm and <1mm indicated that only a small percentage (below 2%) of the particulate matter falls within the thoracic and respirable fractions.

According to the Health and Safety Laboratory the dustiness of materials can be classified within five different categories ranging from not dusty to extremely dusty

(Chung & Burdett 1994) (Table 26). The classification steps have been presented in Chapter 5. Following the proposed description talc samples are categorised accordingly in Table 45.

The results of the various talc fractions and testing protocols, expressed in dust yield per filter, including a standard deviation from replicate tests can be reviewed in appendix III.

Table 45: Classification of the dustiness results for the talc samples as proposed by HSL

Testing procedure	Talc fractions	Dustiness (%)	Classification
HSL procedure	< 9.5mm	0.2070	dusty
	< 3.35mm	0.1828	dusty
	< 1mm	0.2402	dusty
Optimum operating parameters procedure	< 9.5mm	0.3592	dusty
	< 3.35mm	0.3440	dusty
	< 1mm	0.4123	dusty

6.6. Particle size analysis of the talc particulate matter fraction generated by the HSE-WSL test

The particle size of dust collected using the HSE-WSL mill, was determined by laser diffraction analysis using the Malvern Mastersizer-S and the results are presented in the following paragraphs.

6.6.1. Selection of the optical properties of the talc particulate matter

During experimentations with limestone particulates using the Malvern Mastersizer-S, it has been shown that the Mie approximation relies on the accurate selection of the optical properties of the material under investigation. If the selected optical properties do not represent well the test material, then the particle size distribution results will be less accurate. In order to explore the effect that different optical parameters (refractive index of the test material and dispersion medium) have upon particle size results, a range of presentations have been prepared and applied to the measurement taken for the talc dust fraction <9.5mm (HSL-TP). The presentations have been prepared using the presentation software of the Malvern Mastersizer – S and they are presented in Table 46.

The mineralogy of talc ore comprises two main mineral phases, that of talc and clinochlore. Therefore the optical properties and in particular the refractive index of the test sample should correspond to the refractive indices of the included minerals. The refractive index of talc ranges within 1.57 to 1.6, whilst the refractive index of clinochlore can vary form 1.57 to 1.67.

Table 46: Optical properties of the presentations prepared for talc particulates

	Refractive index of particulate matter (R.I.)		
Presentation Code	Real part (n_p)	Imaginary part (K_p: absorption)	Dispersion Medium Refractive Index
RI Comb.1	1.567	0.1	1.33
RI Comb.2	1.60	0.1	1.33
RI Comb.3	1.62	0.1	1.33

The particle size distribution results obtained for the different presentations are displayed in Figure 84. In Table 47 the cumulative volume percentages below 10μm and 2.5μm as well as the median values of the diameters d_{50} and d_{90} provide some extra information on the acquired particle size analysis results.

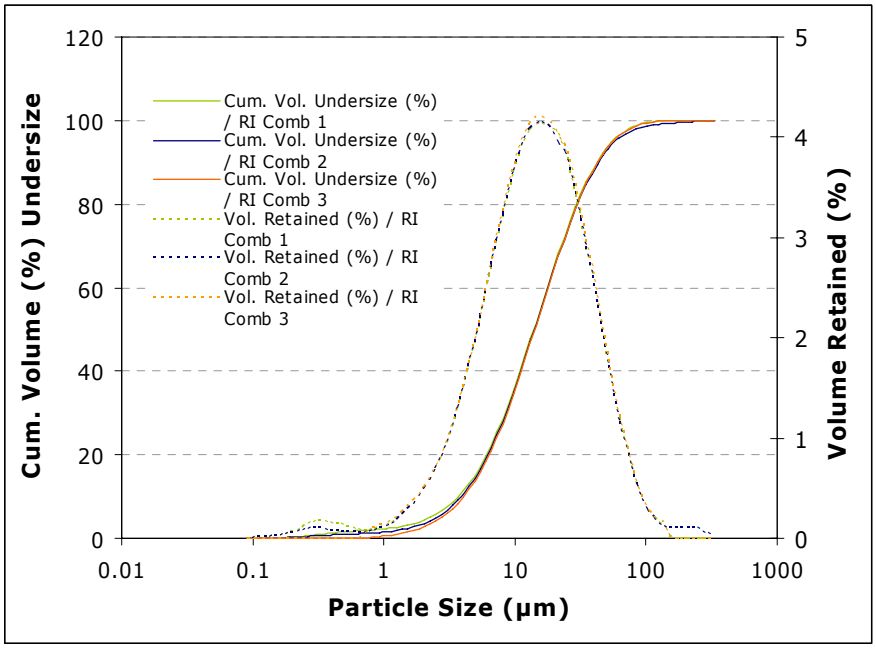

Figure 84: Particle size distribution of the dust collected for the talc test sample <9.5mm (HSL protocol) for various presentations.

Table 47: The cumulative percentages passing 10μm and 2.5μm and the diameters d_{50} and d_{90} as resulted from the different optical properties presentations

Presentation code	Cum.% passing 10μm	Cum. % passing 2.5μm	D50	D90
R.I. Comb.1	36.51	5.74	13.91	42.12
R.I. Comb.2	35.9	4.99	14.09	43.35
R.I. Comb.3	35.4	4.16	14.19	42.57

The changes in optical properties do not influence the particle size distribution results significantly. Only small differences are observed for the very fine particles, below 1μm. This is also justified by the results of Table 47, as no significant variation is displayed. An exception is the cumulative volume percentages below 2.5μm, which presents a slightly higher discrepancy. The incorrect optical model can be identified by the appearance of an extra peak at the bottom end of the size distribution. According to Malvern Instruments (2004) when wrong optical properties have been selected then the light scattering data at higher angles (smaller sizes) will start to be badly fitted and a second peak will become visible, in the volume (%) retained curve, with a peak at 0.2 to 0.3μm and a minimum around 1μm (Malvern Instruments 2004). This is the case for the talc particulate particle size measurements and it has also been observed during experimentation with limestone. For a refractive index equal to 1.62 the second peak disappears, therefore this value has been chosen as appropriate for particle size measurements with talc.

The imaginary part of the refractive index was kept at 0.1 as it fitted well with the results obtained for talc particulates. According to the instructions of the Malvern Mastersizer, for milled or irregular shaped transparent particles an imaginary index of 0.1 is likely to be correct (Malvern Instruments 1994). This can be evaluated further during measurement by looking at the raw data and the fit of the optical model (appendix III). If the fit line is higher than the data line then the imaginary refractive index is too high, if it is lower, then the imaginary index is too low. Nevertheless, for talc particulates the data line matched very well with the fit line, which indicates that a correct index has been chosen.

Consequently, particle size measurements of the talc particulates used a real refractive index of 1.62, an imaginary index of 0.1 and a dispersion medium index of 1.33 as only water was used.

6.6.2. Particle size analysis results

The particle size distribution results for the dust fractions collected from the various talc test samples and both testing regimes are displayed in Figure 85. They represent average results obtained from replicate tests. The reproducibility of the measurements made on triplicate samples is described by the median of the diameters d_{10}, d_{50} and d_{90} and with the standard deviation and relative standard deviation values shown in Table 48. In addition the standard deviation resulting from triplicate tests can be reviewed in the volume (%) retained particle size distributions of the test samples in appendix III. The repeatability of a measurement taken for one sample was very good with a relative standard deviation below 1%. The reproducibility of the particle size measurements taken from triplicate tests was also good with an average standard deviation of the median d_{50} diameter (for all fractions) equal to 0.43 and an average relative standard deviation of 3.19%.

Table 48: The median values of the diameters d_{10}, d_{50} and d_{90} of the talc particulate matter produced using the HSE-WSL test, from a range of sample fractions (optimum conditions testing protocol). The standard deviation and relative standard deviation values were calculated from the results obtained by the triplicate samples.

Sample Fraction	D_{10}	Stdev	RSD(%)	D_{50}	Stdev	RSD(%)	D_{90}	Stdev	RSD(%)
-9.5 mm	4	0.15	3.82	13.63	0.45	3.17	40.8	2.88	7.07
-3.35 mm	4.19	0.03	0.68	14.06	0.12	0.85	41.14	0.50	1.22
-1 mm	3.74	0.31	8.39	13.08	0.73	5.57	45.32	4.04	8.92

The particle size distributions of talc particulates that were collected during the OPT-TP and for any test size fraction are very similar. The same trend was also observed for the particle size analysis results of the HSL testing procedure.

The cumulative percentages under 10μm and 2.5μm (Table 49) recorded for any test sample and testing procedure also present small discrepancies. For instance, the lower cumulative percentage under 10μm corresponds to the <1mm sample (HSL testing protocol), whereas the uppermost percentage has been measured by the <1mm sample (optimum conditions protocol). In general, slightly higher percentages below 10μm and 2.5μm have been measured for the particulate matter produced by the optimum operational parameters procedure, although the difference is not considered significant. Finally no substantial variation in the particle size distribution results exist for a specific test sample (i.e <1mm) within the different testing regimes. An example is given in Figure 86 for the particulate matter produced from

the talc <3.35mm fraction, where it can be seen that the profiles of the two particle size distributions are identical. Similar results were obtained for the dust particle size distributions of the other talc fractions and they are presented in appendix III. The health based dustiness indices of the thoracic and respirable fractions produced by the different dustiness testing protocols did not present such similarities, which justifies that health related classification of dust using the dustiness tests should only be considered for occupational health testing.

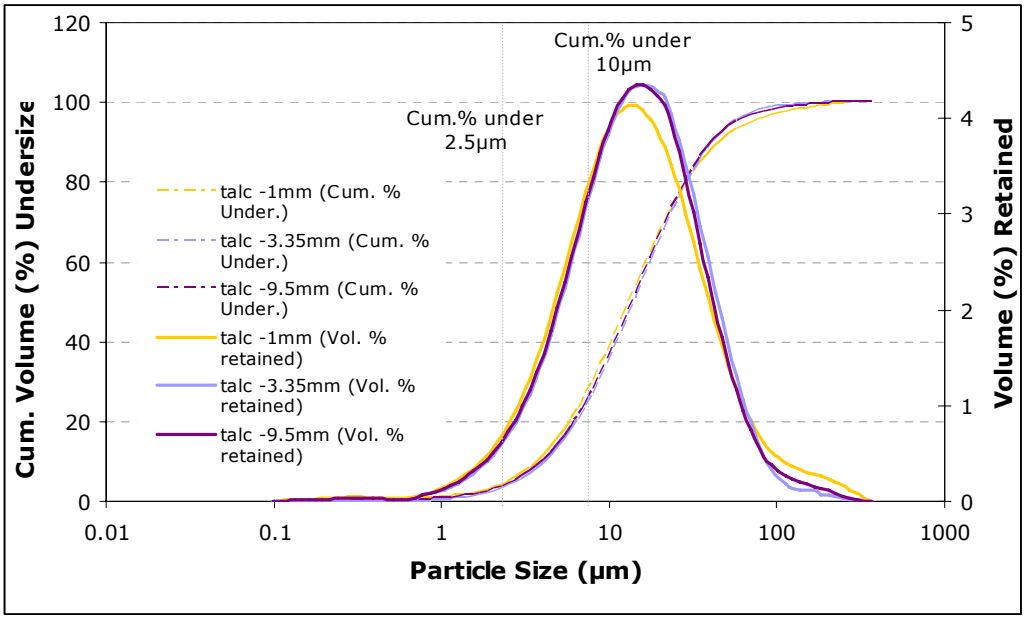

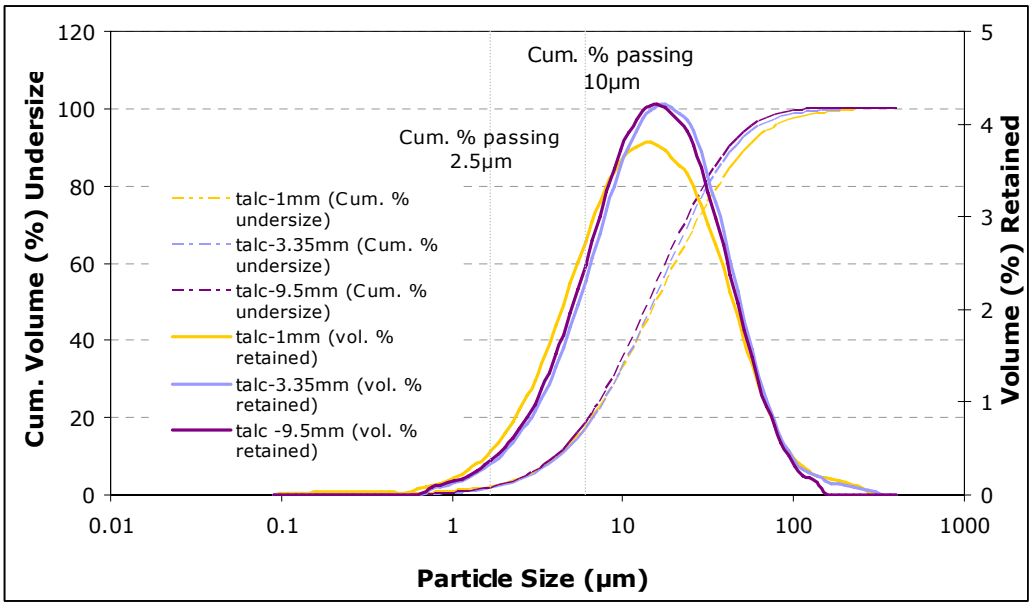

Figure 85: Particle size distribution of the talc particulate matter produced through (a) the OPT-TP and (b) the HSL-TP. The presented results correspond to average values of repeatable tests.

Although the optimum operating parameters protocol resulted in higher dustiness values than the HSL testing procedure, the particle size distributions within the different testing regimes appear very similar. Also, the dust particle size distributions from the various talc sample fractions presented only slight discrepancies. According to the particle size analysis results, under abrasion dust from the talc ore follows a specific particle size distribution profile, which is not influenced by the operational parameters and the ore characteristics (i.e particle size). Such a result is very important for legislative purposes (i.e development of standards or occupational health limits) because it certifies that the dust generation process for talc follows a specific pattern hence upper and low limits could be established. Dust control planning could also be assisted and optimised to minimise and collect particulates within the specific limits that correspond to talc. Around 35% of the talc dust particles have been measured with a particle size below 10μm, which indicates the hazardous potential of talc particulates to human health and the environment.

Table 49: Cumulative percentages passing 10μm and 2.5μm and the diameter d_{80} values for all samples and testing regime ((1): corresponds to the OPT-TP; (2) corresponds to the HSL-TP)

Talc fractions	Cum. % passing 10μm	Cum. % passing 2.5μm	D_{80}
-9.5mm (1)	36.62	4.4	28.12
-9.5mm (2)	35.4	4.16	29.89
-3.35mm (1)	35.35	3.8	28.86
-3.35mm (2)	32.87	3.73	31.83
-1mm (1)	38.78	4.99	28.95
-1mm (2)	32.77	4.21	36.33

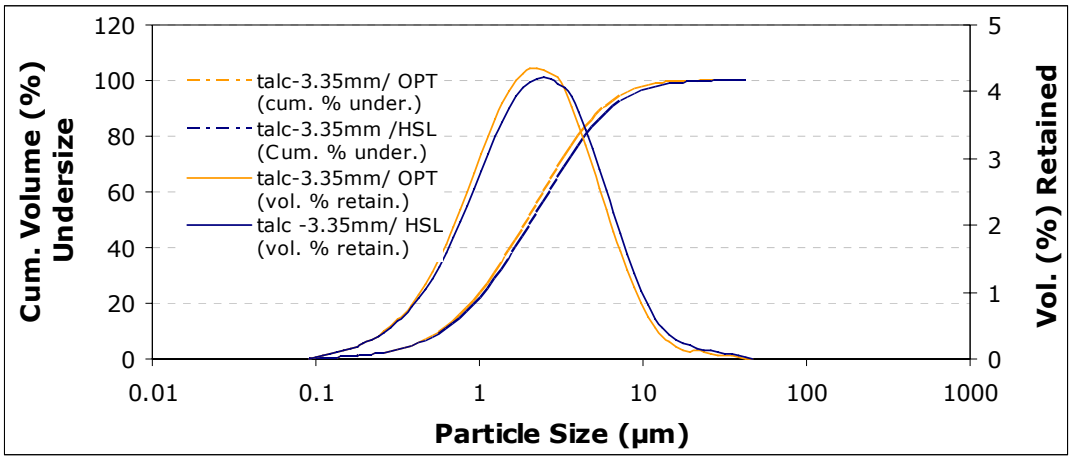

Figure 86: Particle size distribution results of the particulate matter produced by a talc feed fraction below 1mm and both testing protocols.

6.7.Experimentation using the impact test

The impact test has been used to assess the propensity of talc to generate dust under impact mechanisms. The test simulates industrial processes which involve dropping of particulates from heights (i.e conveyor belts) loading and dumping, tipping and others, which will potentially produce dust due to impaction of particles over others or on surfaces.

6.7.1. Determination of the residual height of the talc particles

During the use of the impact test, the offset left by unbroken or partly broken particles has been recorded and it is presented in. For the low bulk volume samples (10% and 5% bulk volume) and the high energy input levels (0.5 and 0.68 kWh/t) all particles were broken hence the residual height was zero. As expected the greater offset was left by the larger bulk volume sample (20% bulk volume- 16x13.2mm). Also the larger particle size fractions resulted in higher offsets. The energy input levels for the talc samples were calculated using the offset values recorded for limestone during primary investigation. Therefore the residual height values presented in this paragraph correspond to the final outcomes of the impact test. The differences in residual height for the limestone and talc samples are displayed in Table 50.

Table 50: The offset of limestone and talc particles. Limestone residual height has been used for the calculation of the release height for the talc samples.

	Residual height (cm)							
	16x13.2mm		8x6.7mm		4x3.35mm		2x1.7mm	
10% bulk volume	Talc	Lim.	Talc	Lim.	Talc	Lim.	Talc	Lim.
0.05 kWh/t	0.42	0.85	0.20	0.60	0.22	0.48	0.15	0.57
0.1 kWh/t	0.25	1.00	0.15	0.55	0.17	0.63	0.10	0.70
0.5 kWh/t	0.00	0.50	0.00	0.53	0.00	0.27	0.00	0.18
0.68 kWh/t	0.00	0.30	0.00	0.45	0.00	0.42	0.00	0.18
20% bulk volume								
0.05 kWh/t	1.28	1.67						
0.1 kWh/t	1.05	1.65						
0.2 kWh/t	0.93	1.37						
0.3 kWh/t	0.80	1.08						
5% bulk volume								
0.05 kWh/t			0.07	0.13	0.00	0.02	0.00	0.02
0.1 kWh/t			0.02	0.13	0.00	0.02	0.00	0.00
0.5 kWh/t			0.00	0.00	0.00	0.02	0.00	0.00
0.68 kWh/t			0.00	0.00	0.00	0.00	0.00	0.00

Limestone particles were more resistant to impact and they left larger offsets than the talc particles. However during back calculation of the required drop height using the offset left by talc, only a small discrepancy from the used height was observed. These results can be reviewed in appendix III. Thus using the residual height of limestone particles to calculate the release heights and energy input levels was a good approximation.

6.7.2.The bulk density of the talc samples

Three different bulk volumes were selected for testing and the talc test samples were prepared accordingly. For each test sample, its bulk density was calculated with respect to bulk volume and subsequently an average value and standard deviation were calculated to determine the reproducibility of the preparation method. Results are shown in Figure 87, where it can be seen that the bulk density of the talc samples does not vary significantly for a specific bulk volume percentage. Also the reproducibility for the majority of the single fractions, resulting from replicate samples, was very good as very small standard deviation values were recorded. The only exception comprises the -16+13.2mm (20% bulk volume sample) which presents a greater variability than the rest of the samples. A larger mass of coarse particles would increase the influence of the physical properties of particles such as shape and orientation in the sample holder resulting to higher variation.

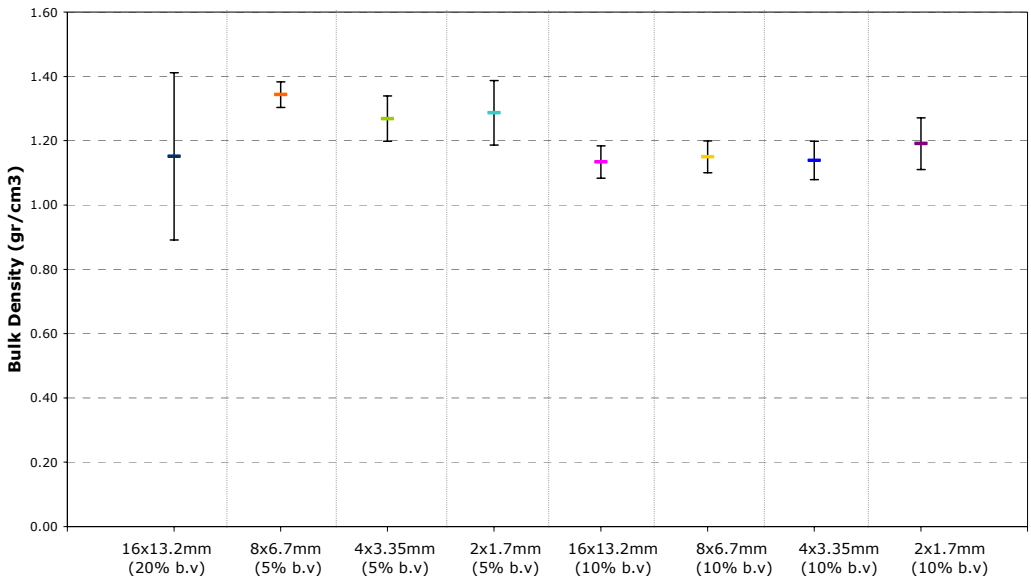

Figure 87: The recorded bulk density values of the talc single fractions. The vertical bars represent one standard deviation from replicate tests.

6.7.3. Impact Test – Results for the talc ore

The effect that impact has upon talc is expressed by the particle size distributions shown in Figure 88. These results correspond to sieving data from the broken talc particles. For a specific bulk volume (i.e B2), it is observed that the higher the energy input, the finer the particle size distribution. For the single fractions 8x6.7mm, 4x3.35mm and 2x1.7mm the two highest energy levels (0.5 and 0.68 kWh/t) produced very similar particle size distributions. Most of the time, the higher energy input levels caused compaction of the talc particles in the sample holder, which reduced the effectiveness of impact as the properties of the test sample had been altered.

As increase in energy input from 0.1kWh/t to 0.5 kWh/t produced a distinct difference to the particle size distributions of the samples, resulting to smaller particles.

For the 16x13.2mm fraction, increasing the bulk volume of the test sample caused more breakage to occur. The particle size distributions of the 20% bulk volume test samples appear finer than the respective of smaller bulk volume. The same trend is observed for the smaller single fractions, where the bulk volume has been reduced from 10% to 5%. Therefore for talc, the sample mass used in an operation can influence the degradation process, even at very low energy levels. The coarser particle size distributions obtained for smaller bulk volumes indicate that energy is dissipated or transformed to other forms without breaking the particles. To some extend and in particular the fine part of the particle size distribution, can be influenced by attrition caused due to interparticle contacts or particle wall contacts. Interparticle contacts are more frequent for high bulk volumes of particles resulting to greater proportions of fines in the test sample. The changes in rates of fines accumulation observed for different test samples and operation conditions are discussed in detail in the following paragraph.

The lower bulk volume test samples (5% bulk volume) of the 8x6.7mm, 4x3.35mm, 2x1.7mm, produced coarser particle size distributions than the higher bulk volume test samples, but retained a positive correlation with energy input. Consequently the lower the energy input, the less the breakage.

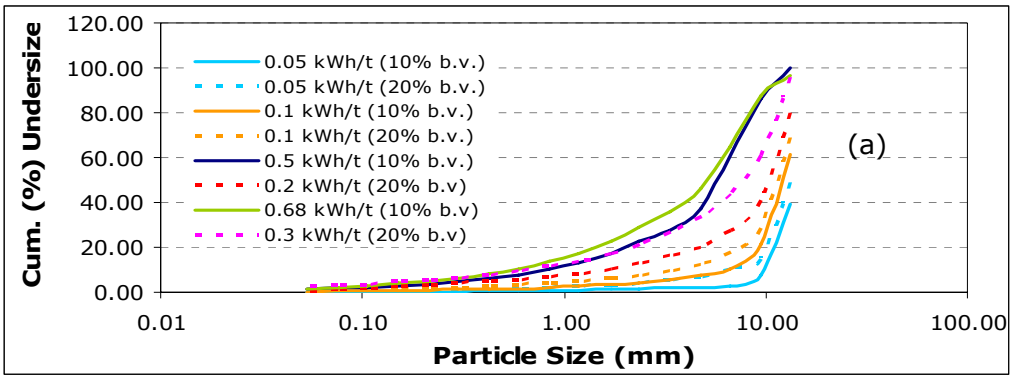

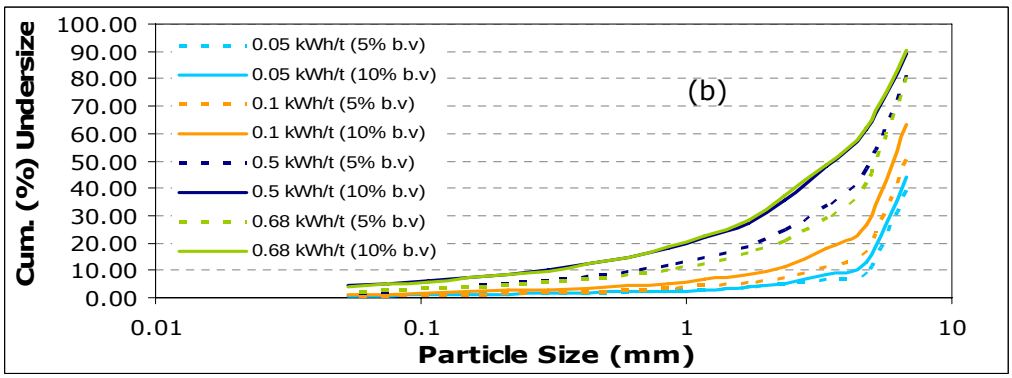

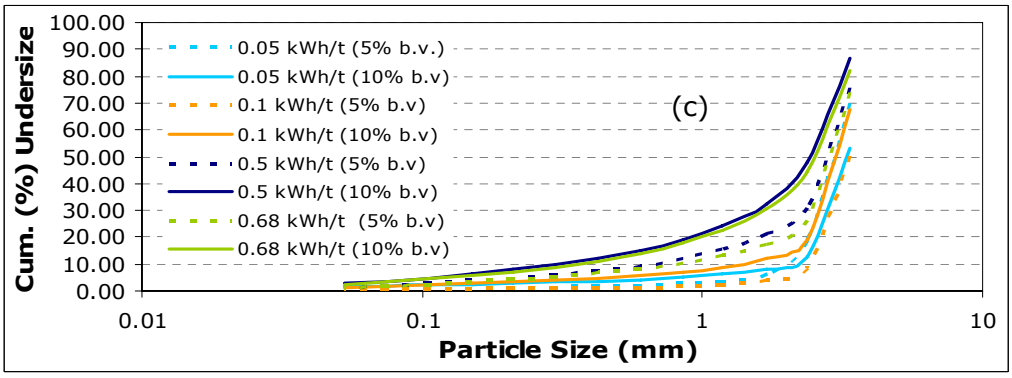

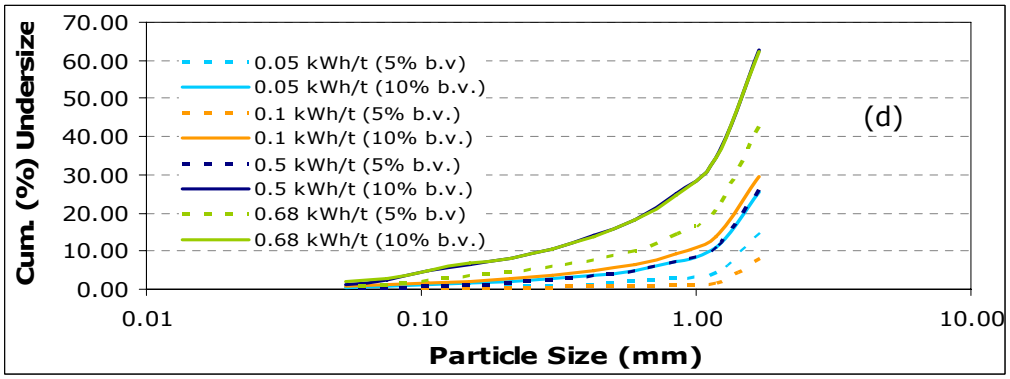

Figure 88: : Particle size distribution of the talc particles after impact for the single fractions (a) -16+13.2mm (10% and 20% of sample's holder bulk volume) and (b)-8+6.7mm fractions (5% and 10% of sample's holder bulk volume) (c) -4+3.35mm (10% and 5% of sample's holder bulk volume) and (d)-2+1.7mm fractions (10% and 5% of sample's holder bulk volume).

For a single size fraction, the particle size distributions of the different bulk volume test samples have shown significant variations, which are attributed to the different degree of breakage taking place. For instance, the 2x1.7mm fraction showed the higher discrepancy in the particle size distribution of the 10% and 5% bulk volume samples at energy input level 0.1 kWh/t and 0.5kWh/t. The average ratio of the cumulative percentages undersize of the 10% and 5% bulk volume samples was six to one at energy input 0.1 kWh/t and 4 to 1 at 0.5 kWh/t. Hence, the increase in bulk volume (from 5% to 10%) allowed more breakage to occur on the talc ore particles at a lower energy input, which suggests that for a lower bulk volume energy is dissipated (in sound, vibration) without affecting further the particles. Likewise, for any of the single fractions, equilibrium within energy input and sample mass exists, where maximum breakage can be achieved without unnecessary increase in energy.

6.7.3.1. *The effect of impact upon fines generation for the talc ore*

The generation of fines caused by impact has also been explored as it reflects the dust production potential. The results are presented in Figure 89.

The various test fractions generate different percentages of fines, whereas the sample mass used during testing also influences the fines production process. For the majority of the samples higher energy input results in greater production of fines (below 53μm).

The 16x13.2 mm fraction produced more fines when the bulk volume of the test sample was increased. The same trend was observed in the other single fraction. For the 5% bulk volume test samples, uppermost concentrations of fines were generated by the 8x6.7mm fraction followed by the 4x3.35mm fraction, whilst the 2x1.7mm sample generated the lower rates. The order of samples according to fineness for the 10% bulk volume tests is more complicated. Therefore, at low energies (0.05 and 0.1 kWh/t) the 4x3.35mm sample produced the highest percentages of fine particulates followed by the 2x1.7mm and the 8x6.7mm samples, whereas at higher energies (0.5 and 0.68 kWh/t) the 8x6.7mm sample comes first in the sequence followed by the 4x3.35mm and the 2x1.7mm samples. The 16x13.2mm (10% bulk volume sample) always generates lower rates of fines.

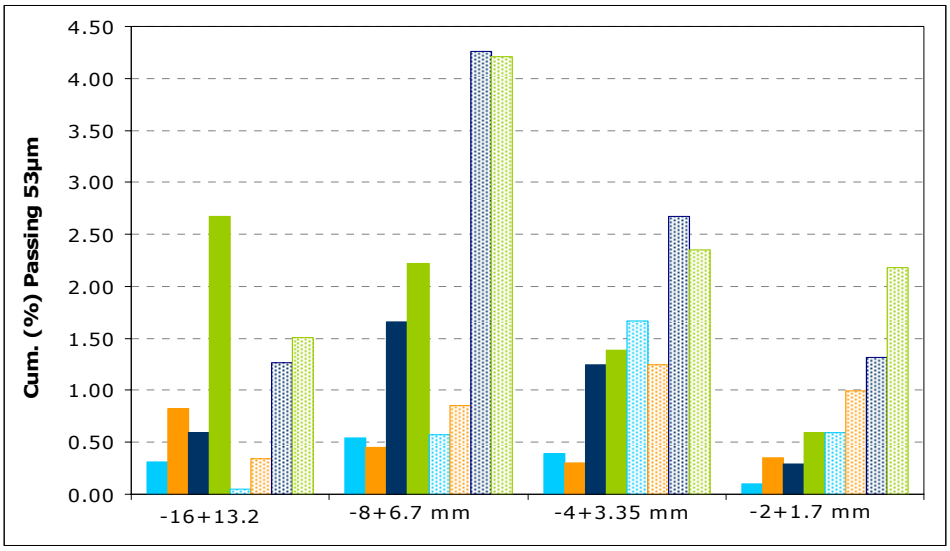

Figure 89: The cumulative percentages passing 53µm for the single talc particle fractions. The textured columns represent the samples of 10% bulk volume, whereas the saturated coloured columns represent the 20% (for the 16x13.2mm fraction) or 5% bulk volume samples. The different colours represent different energy levels : • = 0.05 kWh/t, • = 0.1 kWh/t, • = 0.5 kWh/t or 0.2 kWh/t (for the 16x13.2mm, 20% bulk volume) and • = 0.68 kWh/t or 0.3 kWh/t (for the 16x13.2mm, 20% bulk volume).

Dustiness testing has shown that the concentration of fines in the test sample (above a certain value) could influence the emission rates of particulates. Therefore it is possible that the 8x6.7mm fraction, which comprises higher concentrations of fines, could result to a larger dust yield in comparison to the rest of the samples. Further work however is required to prove this.

6.7.4. Summary of the impact test results

The dust generation potential of talc under impact is influenced both by operational parameters, such as the energy input and the sample mass, as well as by the particle size of the test sample.

Results have shown an analogy between energy input and the generation of fines. For any of the test fractions an increase in impact load resulted in a finer particle size distribution and higher concentration of fines production. Hence materials processed under increased impact forces will yield more dust. The mass of sample used in an operation could also affect the dust generation rates of talc as impact testing on single fractions has confirmed that larger masses will give rise to greater proportions of fine particulates (<53µm). The particle size of the test sample under use is another factor, which has proved to influence the liability of talc to produce dust. Overall, the concentration of fines produces highest value for the 8x6.7mm sample (10% bulk volume) and energy input levels between 0.5 to 0.68 kWh/t, whereas at

lower energy input (0.05 to 0.1 kWh/t) the 4x3.35mm fraction (10% bulk volume) produces higher rates of fines.

Impact testing has been used to quantify how talc will behave under industrial processes which involve the application of impact, such as drop from heights during stockpiling or tipping, draglines, haulage roads and others. Results suggest that the dust generation process could be controlled or even minimised after careful considerations of the particle size and volume of sample practical in use, as well as control of the energy input levels. In addition, the results obtained by the impact test could be used to identify potential dust sources, to optimise existent dust control practises or implement extra mitigation methods. For instance, a process such as tipping which involves drop from heights could become less hazardous by reducing the energy input levels or by reducing the talc mass in use. On other occasions, where both energy levels and mass of talc are kept low, dust could be generated due to the use of a specific product size (e.g. 4x3.35mm). Knowledge that the 4x3.35mm talc sample is liable to produce high rates of particulates, even under these conditions, could assist the identification of a potential dust source, which otherwise could result to fugitive emission.

6.8. Particle size analysis results of the talc particulates produced by the impact test

During sieving of the broken particles produced by impact testing, the <53μm fraction was collected and further analysed by laser diffraction analysis using the Malvern Mastersizer – S. Triplicates of each sample were tested with the impact apparatus and the <53μm fraction of all these samples was collected and analysed. Likewise with the talc particulates produced by the HSE-WSL test, the <53μm samples made use of the optical properties defined previously. Hence, the refractive index used was set to 1.62, the imaginary refractive index was equal to 0.1 and the dispersion medium index was 1.33. The reproducibility of the measurements taken for the triplicate samples is presented through the median values of the diameters d_{10}, d_{50} and d_{90} and their standard deviation and relative standard deviation values in Table 51.

In appendix III, the repeatability of the replicate tests is displayed by the error bars, representing one standard deviation, in the volume (%) retained particle size distributions of the various samples.

According to Table 51, the reproducibility of the particle size measurements from the triplicate tests was good with an average standard deviation of the diameter d_{50} of 2.54 and a relative standard deviation of 7.27%.

The particle size distribution of the <53µm fraction produced by the 10% bulk volume samples are shown in Figure 90 and Figure 91. The particle size distributions of the fine particulates collected by the 20% and 5% bulk volume feed samples can be reviewed in appendix III. They display both the cumulative volume (%) undersize and the volume (%) retained. For the particulates from the -16+13.2mm test sample, it can be seen that the low energy input levels (0.05 and 0.1 kWh/t) produced a coarser particle size distribution than the higher energy levels (0.5 and 0.68 kWh/t). However for the smaller single fractions, there is no relationship between energy input and particle size and the particle size distributions appear very similar. The particle size distributions of the particulates <53µm that correspond to the 5% and 20% bulk volume samples are shown in appendix III.

Table 51: The median of the diameters d_{10}, d_{50} and d_{90} of the talc particulate matter produced using the impact test. The standard deviation and relative standard deviation values correspond to replicate measurements of triplicate sets of test samples. Only the results obtained for the 0.05 kWh/t (E1) and 0.68 kWh/t (E4) are shown.

		D_{10}	Stdev	RSD (%)	D_{50}	Stdev	RSD (%)	D_{90}	Stdev	RSD (%)
16x13.2 mm 10% b.v.	E1	4.61	0.19	4.34	23.14	2.06	4.79	58.85	1.98	3.48
	E4	3.78	0.19	4.95	15.85	3.70	10.90	46.46	4.17	8.97
8x6.7 mm 10% b.v	E1	3.88	0.12	3.14	14.63	1.59	5.10	43.03	2.23	5.18
	E4	3.77	0.10	2.61	15.42	2.40	7.24	45.80	3.08	6.72
4x3.35 mm 10% b.v.	E1	3.83	0.12	3.07	14.74	2.78	8.64	45.18	4.11	9.09
	E4	3.84	0.08	1.96	15.85	2.44	6.98	48.31	3.28	6.80
2x1.7 mm 10% b.v.	E1	3.90	0.22	5.74	15.26	3.28	9.81	46.82	3.90	8.32
	E4	3.72	0.11	3.07	14.67	1.49	4.69	44.09	2.32	5.26

This is shown also in Table 52 by the cumulative percentages below 10 and 2.5 μm and the d_{80} values. Only slight differences are observed for the cumulative volume percentage below 10μm. Only slight differences are observable for the cumulative volume percentages below 10μm, whereas the cumulative percentages below 2.5μm and the d_{80} values fluctuate less. Table 52 also presents the cumulative volume percentages below 10 and 2.5μm and the d_{80} values of the particulates collected by the lower bulk volume samples (5% bulk volume) of the 8x6.7mm, 4x3.35mm and 2x1.7mm fractions as well as the higher bulk volume samples of the 16x13.2mm fraction (20% bulk volume).

Table 52: The cumulative volume percentages below 10μm and 2.5μm of the talc particulate matter generated by impact testing of a range of single fractions and bulk volumes. The median diameter d_{80} is shown as well.

Size fraction	Energy level (kWh/t)	Cum. % <10 μm	Cum. % <2.5μm	D_{80}
16x13.2mm-10% b.v.	0.05	24.14	4.60	44.92
	0.68	33.76	5.42	33.91
8x6.7mm-10% b.v	0.05	35.37	4.67	31.07
	0.68	34.23	5.28	33.20
4x3.35mm-10% b.v.	0.05	35.43	4.90	32.17
	0.68	33.59	5.13	34.86
2x1.7mm-10%b.v.	0.05	34.69	4.75	33.48
	0.68	35.60	5.32	31.73
16x13.2mm-20% b.v.	0.05	32.92	5.41	35.96
	0.3	37.89	5.61	30.59
8x6.7mmc-5% b.v	0.05	35.43	5.42	32.91
	0.68	34.43	5.36	33.77
4x3.35mm-5% b.v.	0.05	36.63	4.70	31.48
	0.68	31.85	4.85	35.16
2x1.7mm-5%b.v.	0.05	36.94	5.16	33.97
	0.68	34.52	5.50	35.42

Some discrepancies in the cumulative volume percentages below 10μm are shown. Hence for the -16+13.2mm fraction (20% bulk volume) the lower the energy input, the lower the amount of particles below 10μm. The particulates (cumulative %) under 10μm of the 8x6.7mm, 4x3.35mm and 2x1.7mm fractions do not follow the same pattern. Each one exhibits a distinct sequence in respect to energy input level, although values vary very little. Consequently it is concluded that the particle size of the fine fraction (<53μm) is not influenced by changes in operational parameters such as the energy input level and the mass of sample in use. In general, for the majority of the samples, the cumulative volume percentages below 10μm ranges

between 30 to 38%, the cumulative percentage below 2.5µm varies between 4.6 to 5.6%, whilst the d_{80} is found to be between 31 to 35 µm.

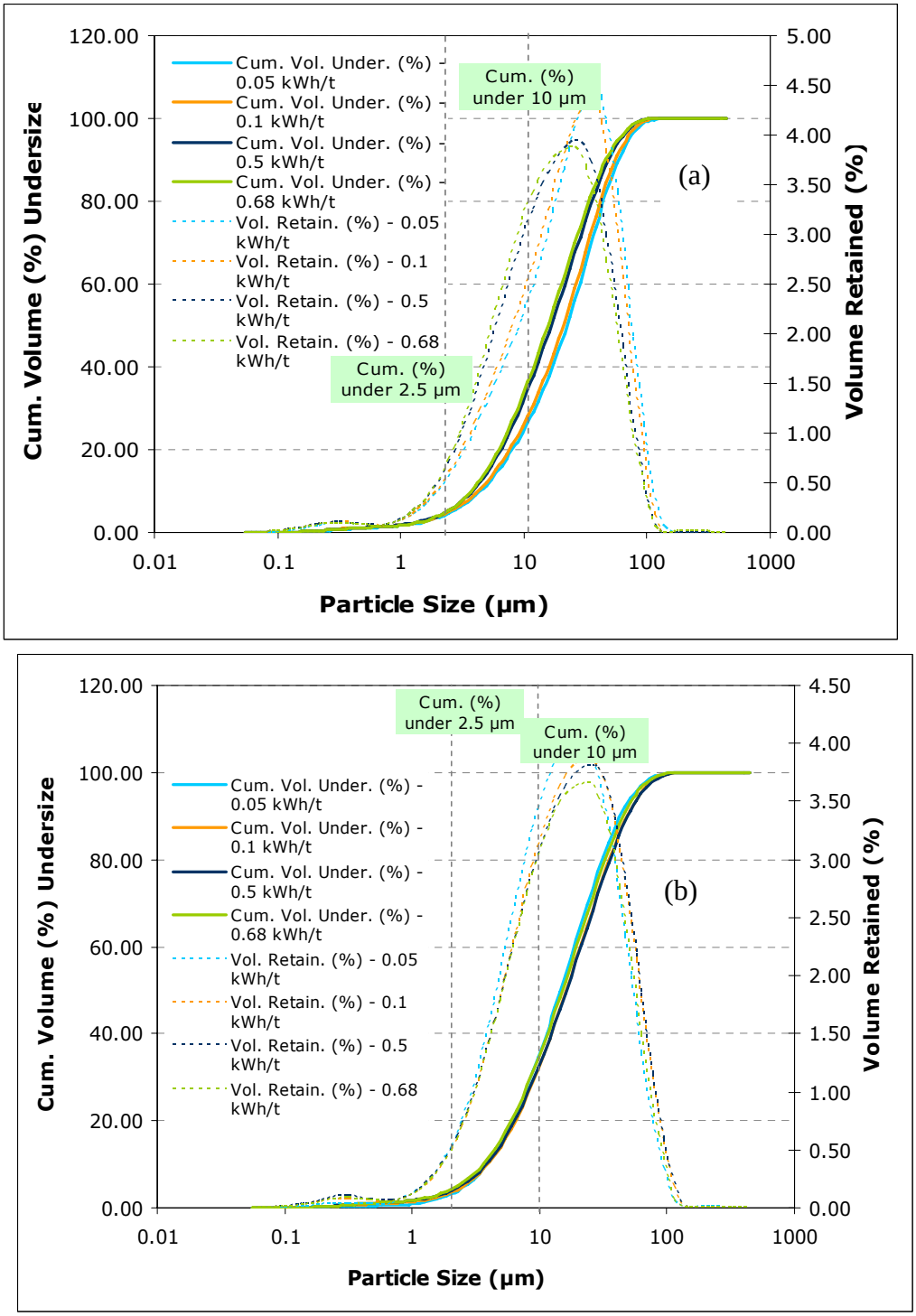

Figure 90: Particle size distributions of the talc particulate matter fraction generated by the impact test of a) the -16+13.2mm fraction – 10% bulk volume and b) the -8+6.7mm fraction – 10% bulk volume.

A similar trend has been found during particle size analysis of the particulate matter collected using the HSE-WSL test, as various testing regimes and sample fractions produced identical particle size distributions. Also if the cumulative percentages

below 10 and 2.5µm of the dust captured during the HSE-WSL test are compared with the equivalent of the impact test, then it can be noticed that differences are minor, even though during impact testing measurements were not performed on the airborne particles.

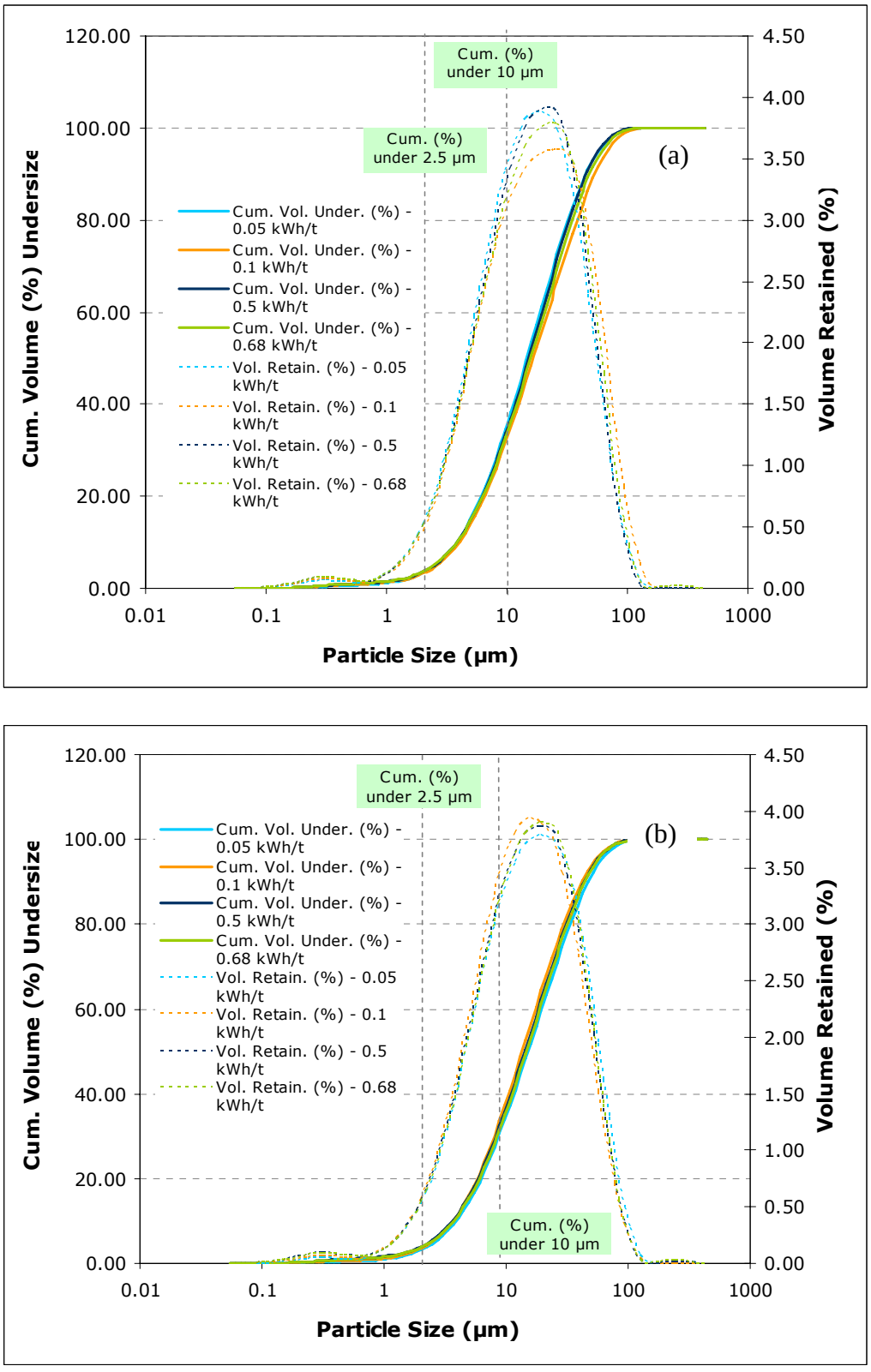

Figure 91: Particle size distributions of the talc particulate matter fraction generated by the impact test of a) the -4+3.35mm fraction – 10% bulk volume and b) the -2+1.7mm fraction – 10% bulk volume.

According to particle size analysis results for talc it becomes clear that it is possible to set standards and produce a well designed dust assessment plan, because talc particulates produce very similar particle size distributions either under the effect of impact or abrasion mechanisms. In addition, in average 35% of the particles are below 10μm, which indicates that talc particulates can affect human health and the environment.

6.9. Mineralogical characterisation of the talc particulate matter

The mineralogy of the talc particulates collected during the HSE-WSL test and the impact test was examined by X-ray diffraction analysis and scanning electron microscopy. The X-ray diffraction traces produced from the particulate matter of the HSE-WSL test and the impact test are displayed in Figure 92 against the pattern of the feed.

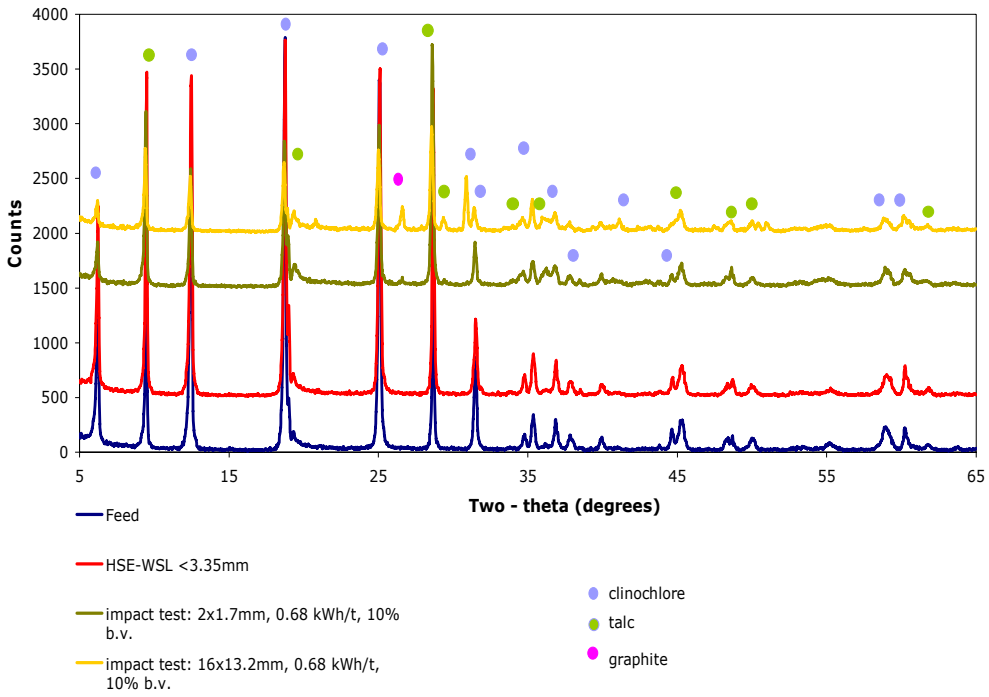

Figure 92: XRD traces of the talc dust/fines fraction collected by the dustiness test and the impact test. The x-ray diffraction pattern of a rock sample is presented as well (whole rock analysis – two theta).

In all cases, the X-ray diffraction patterns are very similar and they show that two main mineral phases are present these of talc and clinochlore. Both minerals are considered as major constituents, because they have produced multiple peaks with

high intensities, which indicate that they participate in large quantities. However the XRD traces of the impact test particulates exhibit one extra mineral phase, this of graphite (C). Graphite is a mineral commonly found in Trimouns talc and it was a known inclusion of the samples used in this project. Nevertheless, during mineralogical characterisation of the rock samples or the airborne particulates, graphite was not detected by X-ray diffraction analysis, whereas during impact testing it has been identified as a minor mineral phase. This is attributed to the variability of the feed samples and not the impact process taking place.

Mineralogical investigation also made use of scanning electron microscopy. Only the airborne particulates captured by the HSE-WSL test were observed by scanning electron microscopy. Particles were mounted on a sticky pad, as well as in epoxy resin during the preparation of polished blocks. Polished blocks allowed the use of the energy dispersive X-ray microanalysis system for compositional analysis purposes. Some of the SEM photomicrographs taken can be seen in Figure 93 and Figure 94. Figure 93 represents the dust particles on a sticky pad, whereas Figure 94 corresponds to an image taken by a polished block. It can be seen that particles exhibit a flaky shape and various sizes.

The mixture of particle sizes is particularly obvious in Figure 93, where coarse particles (i.e 500μm) and very fine ones (i.e a few microns) are presented. X-ray microanalysis on individual grains of the polished block determined that the majority of the particles correspond to talc or clinochlore, whilst some other minerals have been identified in minor quantities such as titanite ($CaTiO(SiO_4)$) and calcite ($CaCO_3$). More photos taken on the talc samples can be reviewed in appendix III.

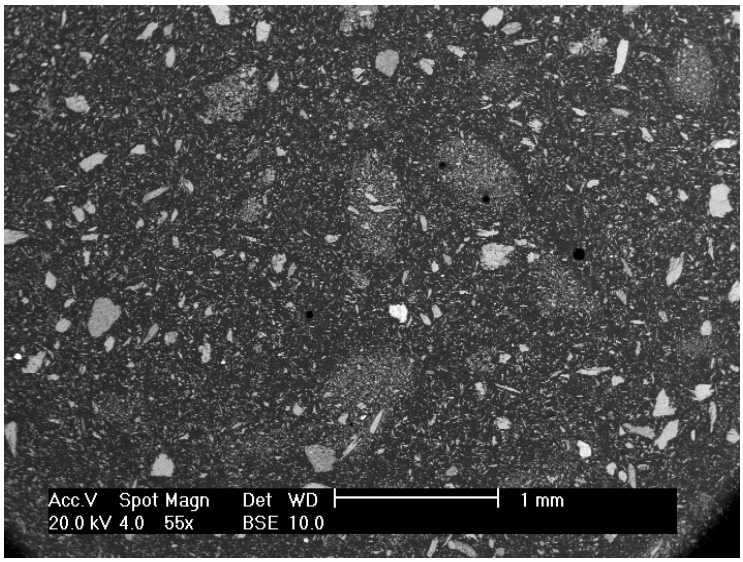

Figure 93: Scanning electron microscope (SEM) photomicrograph of the talc airborne particulates produced from a feed of -3.35mm/150g prepared in a polished block. Magnification x 55, scale 1mm.

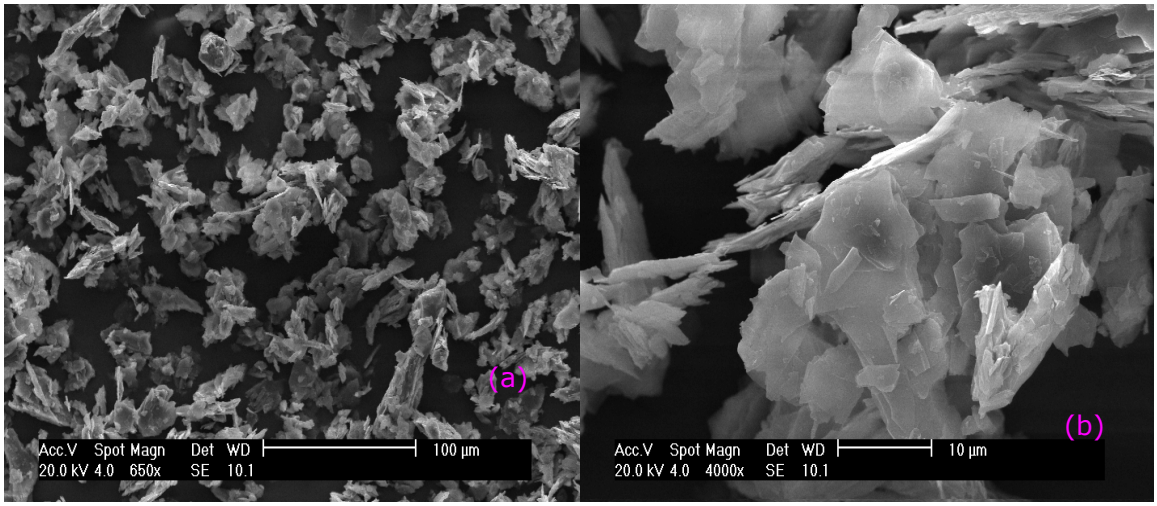

Figure 94: Scanning electron microscope (SEM) photomicrographs of the talc airborne particulates produced from a feed of -3.35mm/150g.(a) Magnification x 650, scale 100 µm. Talc and chlorite particles are present ;(b) Magnification x4000, scale 10 µm. Talc and chlorite particles are present.

6.10. Summary of Chapter 6

The use of the HSE-WSL test and the impact test enabled the evaluation of the dust generation potential of talc under abrasion and impact mechanisms. According to the processes taking place for talc and as presented in Figure 78, particulate emissions can be produced through all crushing, grinding and screening processes, during drying, sorting and classifying and transfer by conveyor belts and aerial-cable transport.

Investigations into the dustiness potential of talc using the HSE-WSL test took place with various size fractions using two different testing regimes. The <1mm sample exhibited the highest dustiness levels, followed by the < 9.5mm and the <3.35mm samples, for any of the testing protocols, although the differences in dustiness are not significant. Tumbling time is the parameter which has the greatest effect upon dustiness of talc, as an increase in dust yield has been observed for the optimum conditions testing protocol. Hence, if operations which involve abrasion mechanisms, such as grinding and drying, then control the residence time, could allow dust generation to be reduced. Although the concentrations of fines in the talc feed samples varied for the different fractions, dustiness was not influenced by its value. For concentrations of fine particulates (<75μm) below 25% (cumlulative % undersize), dustiness levels did not change for the different talc fractions. However for higher percentages of particles below 75μm it is believed that dustiness positively correlates with the concentration of fines. The dust yield of talc produced due to abrasion is not influenced greatly by the particle size of the material in the process, and the parameters that could affect dustiness levels are the time spent in an operation and the contained fines if they exceed a certain limit value. Thus control and reduction in dust are achievable through optimisation stages of the time scales of operations and the use of well implemented mitigation practices that can efficiently capture the dust levels defined for talc. In addition when particles of a millimetre scale are used, the dust yield could be controlled by minimising the production of fines so as not to influence dustiness and subsequently reduce the emissions further through the use of dust control practices

Particle size measurements on the dust fraction from the HSE-WSL drum have shown that talc particulates produce identical particle size distributions, independent of the particle size of the feed sample and the operational parameters of the test. Such a conclusion can be of great help to legislative parties because it justifies that it is possible to produce limit values for talc which they will reflect the correct particle size and dust levels of talc produced by abrasion mechanisms. Dust control planning could also be assisted and optimised to minimise and collect particulates within the specific limits that correspond to talc. Finally it was found that around 35% of the talc dust particles have been measured with a particle size below 10μm, which indicates the hazardous potential of talc particulates to human health and the environment.

Impact testing results have shown that when energy levels increase then the particle size distribution of the broken particles become finer, and the generation of fine particulates increases as well. This trend has been followed by all the tested single

fractions and for all the bulk volume values. The bulk volume of the samples used in an operation could also affect the dust generation process of talc. Results have shown that usage of larger bulk volumes produced greater amounts of fine particulates (<53μm). Also the particle size of the test sample can influence the dust generation potential of talc. Overall, the 8x6.7mm sample (10% bulk volume) and energy input levels between 0.5 to 0.68 kWh/t presented the highest amounts of fines, whereas at low energy input (0.05 to 0.1 kWh/t) the 4x3.35mm fraction (10% bulk volume) produced higher concentrations of fines. Impact testing was used to simulate industrial processes such as drop from heights, haulage roads, draglines, stockpiling operations and others. The impact test results suggest that the dust generation process could be controlled or even minimised after careful considerations of the particle size and volume of sample in use, as well as of the energy input levels. Finally results could be used to identify potential dust sources, to optimise existent dust control practises or implement extra mitigation methods.

Particle size analysis of the particulate matter fraction collected during impact testing has shown that the particle size distributions of the various samples presented only slight differences, which indicates that talc follows specific particle size distribution patterns under impact independently of operational parameters (energy input, bulk volume) and feed sample properties (i.e particle size, volume). On average 35% of the particulate matter volume exhibits a particle size below 10μm, whilst 80% of the particles are below 35μm. These results are in very good agreement with the outcomes of the HSE-WSL test which has also revealed similar average percentages of particles below 10μm.

The mineralogy of the particulate matter captured using the HSE-WSL test, as well as the impact test has shown that it does not present great differences for the different tests and it is also in good agreement with the mineralogy of the talc ore. Two major mineral phases were found, these of talc and clinochlore, whereas the particulate matter collected from the impact test consisted also of a minor quantity of graphite, which is commonly associated with the talc ore. Talc and chlorite particles exhibited a flaky shape and a large variety of sizes.

Chapter 7. Experimentation with Hamersley Iron Ore

7.1. Introduction

The demand for iron ore has increased significantly over the past decade, mainly in response to China's demand for pig iron. Hamersley iron ore is located in the Hamersley province in Western Australia and it is owned by Rio Tinto Group. The company is considered one of the world's leading producers of iron ore and mining is extended within the 80,000 km^2 Hamersley iron province (Hamersley Iron 2005a). Due to the size of the operations taken place, dust is a major issue and accordingly any steps possible that could assist to the reduction of dust levels should be taken to ensure that emissions do not adversely affect the environment, welfare and amenity of peoples and land in use (Hamersley Iron 2005a). Human exposure to iron particulates is associated with a plethora of diseases, starting from simple allergies to very important ones such as siderosis, which is a kind of pneumoconiosis (Banks and Parker 1998).

The iron ore utilised in this project comes from the Brockman iron formation and this chapter refers to the experimental practices taken for this material to assess its propensity to produce dust through various mechanisms. These mechanisms simulate common mining processes, which are liable to generate dust. The Hamersley iron ore

samples were provided by the industrial sponsor of this project Rio Tinto Technology Group.

7.1.1. Experimentation steps

The structure of this chapter is outlined in the bullet points below. Prior to presentation of results, a brief introduction is given to Hamersley mining operations, the geology, the processing route as well as the environmental issues relevant to particulate matter emissions in this area of Australia.

Experimentation was carried out based on the following steps:

- Mineralogical characterisation of the rock samples by X-ray diffraction analysis.
- The dustiness was quantified using the HSE-WSL dustiness test. Collection of the dust fraction also took place.
- Measurement of the dust particle size collected during the use of the HSE-WSL test by laser diffraction analysis.
- Determination of the dust propensity of iron ore using the impact test. The relation between dustiness, energy input and sample mass was quantified.
- The fine fraction (below 53μm) produced by the impact test was collected and its particle size was measured by laser diffraction analysis.
- Mineralogical characterisation of produced dust during testing with the HSE-WSL apparatus and impact test by X-ray diffraction analysis.

Conclusions were drawn upon the dust generation potential of iron ore for a range of industrial applications and handling processes.

7.2. Hamersley iron ore- History, geology and industry

Hamersley Iron Pty Limited is owned by Rio Tinto and it operates in the north west of Western Australia (Figure 95), in Pilbara region. The mining operations began in 1966. Iron ore is mined from six operations in the Pilbara region. These are Mount Tom Price, Paraburdoo/Channar, Brockman/Nammuldi, Marandoo, Yandicoogina and the Eastern Range. In 2004, more than 76 million tonnes of ore were produced and exported across Asia and Europe (Hamersley Iron 2005b).

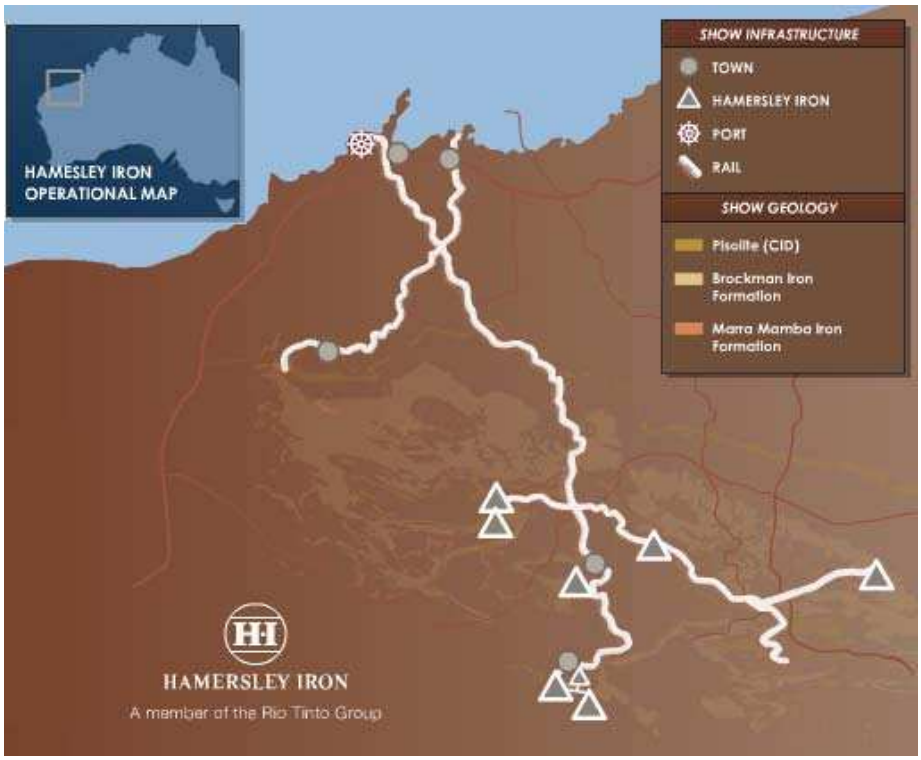

Figure 95: Hamersley iron operational map (Hamersley Iron 2005b).

Hamersley Iron produces several distinct iron ore products, which include blended lump ore (-31.5+6.3mm) and blended fines (-6.3mm). The product is carried from the mine by a rail network operated by Pilbara Rail Company to the port at Dampier, where it is shipped to customers. Iron ore is blended prior to ship loading in the nine live-blending stockpiles at Parker point and fourteen further stockpiles at the East Intercourse Island (EII) facility.

7.2.1.Mining and processing of Hamersley iron

Mining of iron ore from the six mines in Pilbara region takes place in precisely planned open pits. The mines are operating as "one mine" and each mine runs to a planned production schedule. Mine resources, equipment and manpower are managed centrally and moved around and between sites. Ore from all mines is treated as feed for making a single product during blending at the port (Hamersley Iron 2005b).

Ore initially follows the drilling-blasting sequence and it is subsequently loaded into haul trucks for transporting to the crushing plant. Here, crushing and screening steps take place. Lump and fines are then blended into separate stockpiles. Samples used in this project came from Brockman mine and for this material the applied processing

steps are shown in Figure 96. For Brockman ore, the proved reserves at the end of 2002 were 117 million tonnes. Crushing is done in two stages through the use of the primary and secondary crushers, lump and fines are then blended onto separate stockpiles by travelling stackers (Hamersley Iron 2005a).

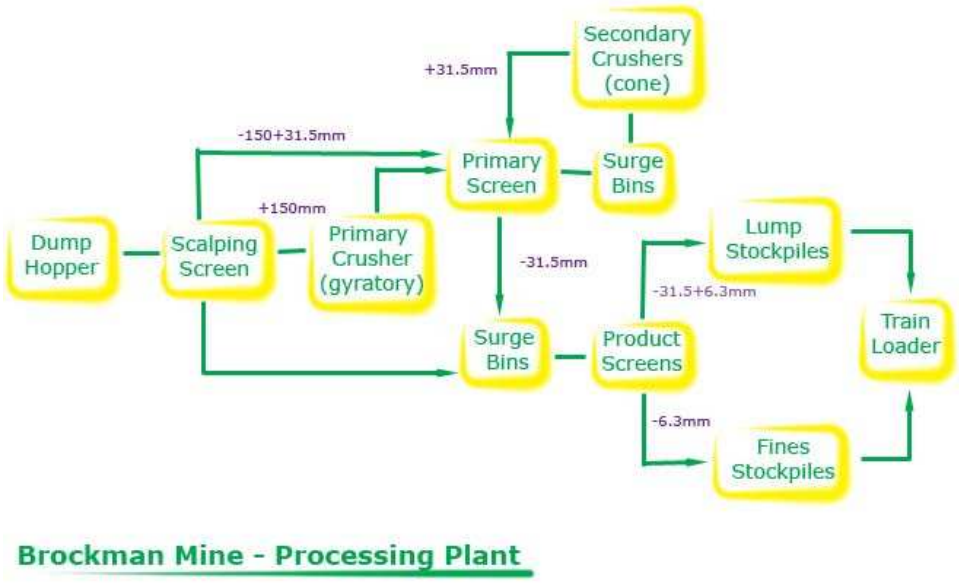

Figure 96: Processing steps followed for iron ore in Brockman Mine (Hamersley Iron 2005a).

7.2.2. Hamersley Iron Ore – Geology and Mineralogy

Rocks in the Hamersley iron province were formed about 2,500 million years ago (late Archaean to early Protezoic) mostly by chemical sedimentation, after a phase of basic volcanism (basalts) and clastic sedimentation (i.e. sandstones) in the older Fortescue Group. The Hamersley group is approximately 2.5km thick and it contains several large units of Banded Iron Formation (BIF), which comprises rock with bands of iron minerals such as magnetite and hematite as well as gangue minerals, mostly carbonates, silicates and chert. Typically the banded iron formation contains about 30% iron by weight (Ramanaidou et al. 2003) and three distinct types of deposits are identified:

- the banded iron formation (BIF), which consists of hematite and the hematite-goethite bedded iron deposits
- the minor hematite-goethite detrital iron deposits and
- the goethite-hematite channel iron deposits (CID).

The bedded iron ores have been formed by natural enrichment of banded iron formation (parent rock). In some places bedded iron deposits (Marra Mamba iron formation, Brockman iron formation) have been enriched to form high grade ore with more than 60% iron content (Fe) (Hamersley Iron 2005b). The channel iron deposits are also called pisolites. They are iron-rich fluvial deposits and their principal characteristic is their pisolitic texture, which comprises rounded hematitic 'pea stones' (5mm or less in diameter) rimmed and cemented by a geothetic matrix (Hamersley Iron 2005a;Ramanaidou et al. 2003). The detrital iron deposits are present where weathering has eroded iron orebodies and deposited fragments of ore in traps (usually drainage channels) (Hamersley Iron 2005b). The different iron ore formations can be reviewed on the geological map in Figure 97.

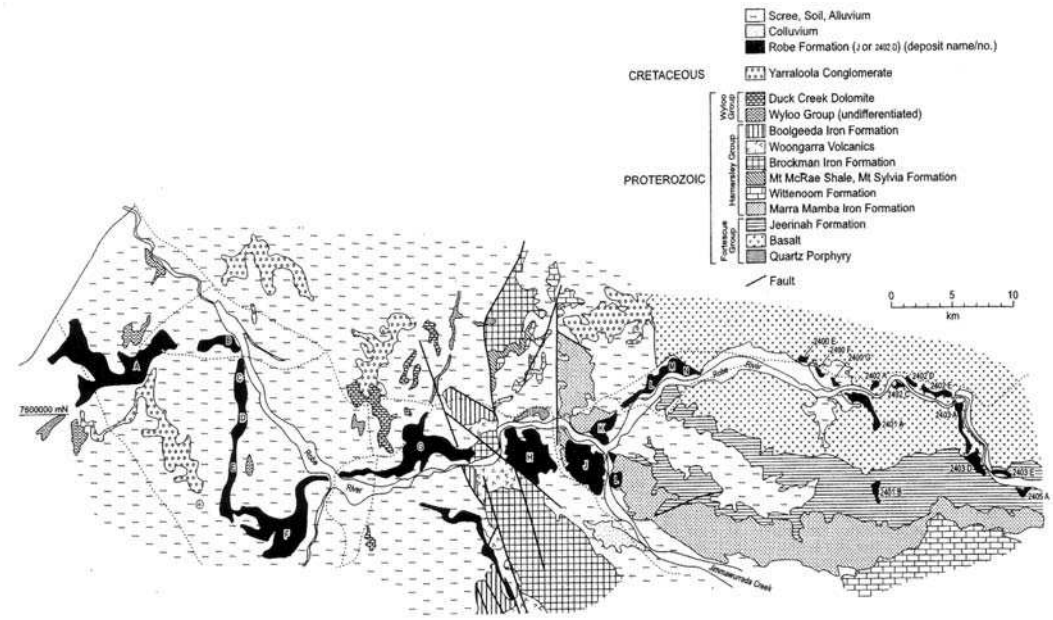

Figure 97: Geological map of the Hamersley group iron formations (Ramanaidou et al. 2003).

The samples used for this project correspond to the bedded iron deposits (Brockman iron formation) and their mineralogy is described by the presence of hematite and goethite. Other possible inclusions can be alumina (Al_2O_3), silica (SiO_2) (both at moderately low concentrations), as well as phosphorus (at 0.05 to 0.1 weight %). The iron content of the majority of mined ores is above 58% and in certain cases it can exceed the 64%.

7.3.Particulate matter emissions from iron ore mining and processing

Particulate matter emissions from mining and processing activities of iron ore are considered a major issue, mainly due to the vast size of operations taking place, therefore Hamersley Iron has established several procedures to minimise and control dust.

Dust is generated during construction work, mining (drilling and blasting), ore handling (loading and unloading, transporting), ore processing (crushing, screening, stockpiling, blending) and ore transport activities. In addition, the existing environment is an arid area and normally high background dust levels are present. Background levels of airborne dust in some areas (Pilbara) can reach close to or higher than the National Environmental Protection Measure standard (NEPM) (Hamersley Iron 2005a). Also some of the ores (i.e Brockman ore) have low moisture contents, which imply that they have a greater potential to generate dust. Mining works take place in an isolated area, where there are no nearby inhabitants, nevertheless particulate emissions can be an occupational hazard to the employees of Hamersley Iron, it can affect the environment (flora and fauna) and it can adhere to equipment causing wear and minimising their performance.

In order to reduce and control dust Hamersley Iron uses dust management measures, which include the implementation of mitigation methodologies and monitoring practices. Dust suppression techniques, haul road watering and enclosed processing areas are commonly used. Most of the crushing plants are enclosed and fitted with a dry bag house type dust collection system. Conveyor belts and transfer points are enclosed as well, whereas spills of product around transfer points are cleaned and the moisture content of the ore is maintained at favourable levels, which minimise dust. To reduce dust levels during mining, blasting activities are planned with favourable weather conditions. Employees are encourages to maintain speed limits on unsealed roads and rehabilitation takes place to minimise the total area remaining exposed. Visual inspections regularly asses the generation of dust as well as the functionality of dust control techniques (Hamersley Iron 2005a;Hamersley Iron 2005b). Dust monitoring takes place periodically so as to quantify the significance of dust emissions and to determine ambient dust levels. Commonly, real time and high volume dust monitoring and sampling is used and the total suspended particulate as well as the PM10 and PM2.5 emissions are determined (Hamersley Iron 2005a).

All these mitigation practices manage to minimise dust levels. Nevertheless, particulate matter emissions are still an issue for Hamersley Iron due to the high background dust levels (plus fugitive emissions) and the continuous mining as well as expansion of the mines in response to the increased global demand for iron ore. Iron ore is a relatively soft and friable material and can generate dust easily. The use of dust suppression techniques, even though they minimise dust levels, require vast amounts of water. However, weather conditions, which are often hot and dry, diminish the effectiveness of dust suppression, requiring even higher rates of water consumption, plus additional dust control techniques thus substantially increase the cost for dust management.

The objective of this research is to assess the dust production potential of iron ore under different mechanisms, which simulate typical industrial processes and to expose certain factors (i.e. material properties, operational parameters), which could minimise the generation of particulates and reduce the number of mitigation techniques used.

7.4.Mineralogical characterisation of iron ore

Macroscopic investigation of the received iron ore identified that the minerals included belong to the iron oxide group. Due to the sedimentary formation of the ore, it exhibits a dark red to brown colour and an earthy luster, whilst lumps are composed of fine particles.

The mineralogy of the iron ore has been determined using X-ray diffraction whole rock analysis. Ten different representative samples of 5g were prepared from a bulk following the procedures described in Chapter 4. The X-ray diffraction traces of the various samples were identical and several are displayed in Figure 98. Two major mineral phases have been identified, hematite (Fe_2O_3) - goethite (FeO(OH)), which belong to the iron oxide group. Hematite and goethite have been produced during the enrichment of the original banded iron formations, where they have replaced magnetite and chert respectively. X-ray diffraction analysis did not identify any other mineral inclusions, although they might be present in minor quantities, but not within the detection limits of the apparatus.

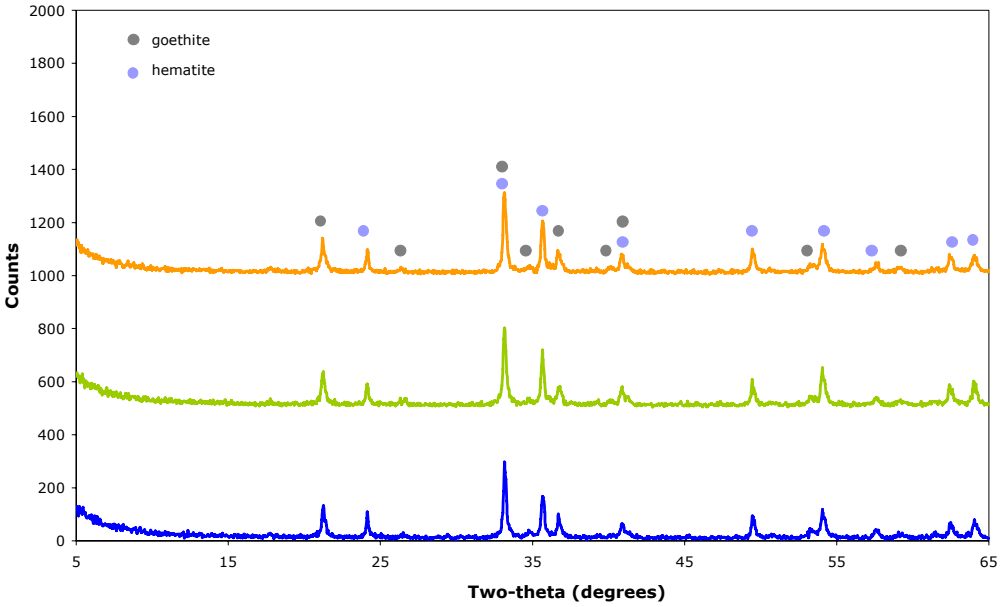

Figure 98: The XRD traces of the iron ore rock samples (two-theta, whole rock analysis).

7.5. Determination of the dustiness of iron ore using the HSE-WSL rotating drum test

The dustiness of iron ore under abrasion conditions was assessed using the HSE-WSL dustiness test. Two different testing regimes (HSL-TP and OPT-TP) and various test size samples were used and are presented in the following sections.

7.5.1. Dustiness measurements

Dustiness measurements were performed for three different size fractions of iron ore, namely for particles below 9.5mm, 3.35mm and 1mm. These samples were tested in both testing regimes. Prior to testing the particle size distribution of the iron ore feed (<9.5mm, <3.35mm, <1mm) was measured by sieving and the results are presented in Figure 99. The particle size distribution of the <9.5mm is the coarser followed by the <3.35mm and <1mm test samples that showed a finer profile.

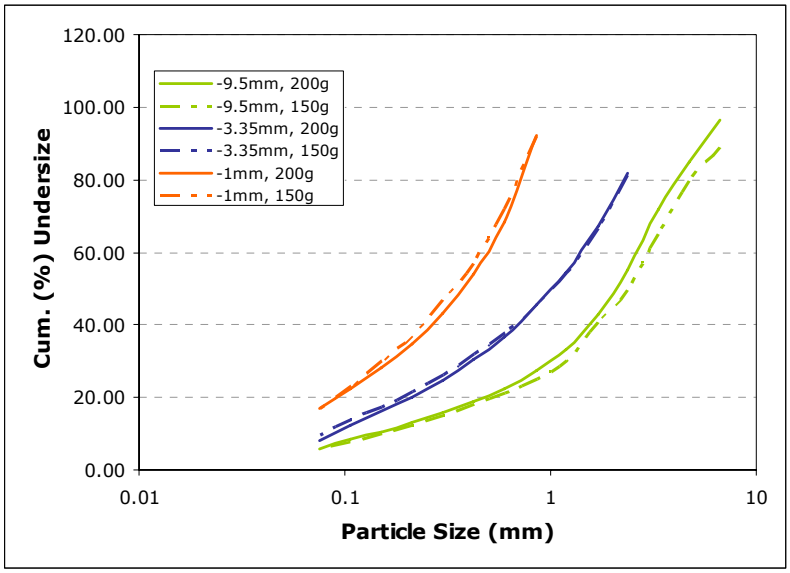

Figure 99: Particle size distributions of the iron ore feed samples produced by sieving using a $\sqrt{2}$ sequence of sieve apertures.

7.5.1.1. *Presentation and analysis of the dustiness measurements results*

The results obtained by dustiness measurements using the HSE-WSL test are reviewed in Table 53 and in appendix IV and they correspond to average values of triplicate tests. The reproducibility of the replicate tests has been assessed by calculation of the standard deviation and relative standard deviation values (Table 53).

Statistical analysis has shown that during dustiness testing with iron ore an average standard deviation of 0.009 and a relative standard deviation of 6.56% should be expected. There are no previous records of the "safe" dustiness limits that should be followed for iron ore. However past research on a large variety of materials has shown that the coefficient of variance of dustiness indices from replicate tests was found to be between 10% and 30% (Lyons et al. 1996). Therefore the iron ore dustiness results are considered reproducible.

The two different testing regimes produced a spread of dustiness values for iron ore, ranging form 0.0591% to 0.2258%. The OPT-TP produced higher dustiness results than the HSL-TP and the dustiness patterns of the two testing regimes were not the same. During experimentation with the HSL-TP, dustiness was highest for the <9.5mm test sample, followed by the <1mm and <3.35mm samples. When the OPT-TP was used, the higher dustiness value was produced again by the <9.5mm test

sample, but this time it was followed by the <3.35mm sample, whilst last in dustiness scale was the <1mm sample.

Table 53: Dustiness values of the iron ore samples obtained for both testing protocols. The standard deviation and the relative standard deviation (% RSD) reflect the reproducibility of the replicate tests.

Iron Ore fractions	HSL procedure			Optimum operating parameters procedure		
	Dustiness (%)	Standard deviation	(%) RDS	Dustiness (%)	Standard deviation	(%) RSD
< 9.5mm	0.1185	0.0178	15.05	0.2258	0.009	4.10
< 3.35mm	0.0591	0.0004	0.74	0.1747	0.007	4.14
< 1mm	0.0903	0.0067	7.45	0.1618	0.013	7.88

On average the OPT-TP and for the test samples <9.5mm and <1mm resulted in dustiness values of 1.85 times higher than the HSL-TP. The effect that the OPT-TP has upon the <3.35mm test sample is even greater, thus dustiness appear 2.9 times higher that the measurements taken during the HSL-TP. The presentation of higher dustiness values for all the samples during the OPT-TP indicates that the tumbling time and not the sample mass is the principal factor affecting the dust generation potential of iron ore. This is because the rotation time utilized for the OPT-TP is 3 minutes and the sample mass 150g instead of 1 minute tumbling time and 200g of sample mass used during the HSL-TP. However the use of sample masses much higher than 200g could also positively relate to dustiness, as it has been shown during testing with limestone in Chapter 5.

Figure 100 presents the cumulative weight percentage passing 75μm, versus the average dustiness values of the various test samples and testing procedures. The concentration of fines in the test sample correlates inversely proportionally to dustiness. That is to say the coarser fraction (<9.5mm), which exhibits the highest dustiness value for any of the testing protocols, contains the lowest percentage of fines. Dust might be generated at higher rates from the <9.5mm sample for two reasons. Firstly, the abrasion mechanisms taking place in the drum due to frictional sliding of particles with the drum walls or over other particles might have a greater effect upon coarser particles. Secondly, the moisture content of the <9.5mm samples could be much lower than any of the other samples hence enabling the fine particles to entrain easier into the airborne state. The moisture content was determined and results are presented in the following paragraph. For the OTP-TP the <1mm sample, which consists of higher percentages of particles below 75μm yielded less dust. For

the HSL-TP the percentages of fines (<75µm) of <1mm and <3.35mm samples positively relate to dustiness.

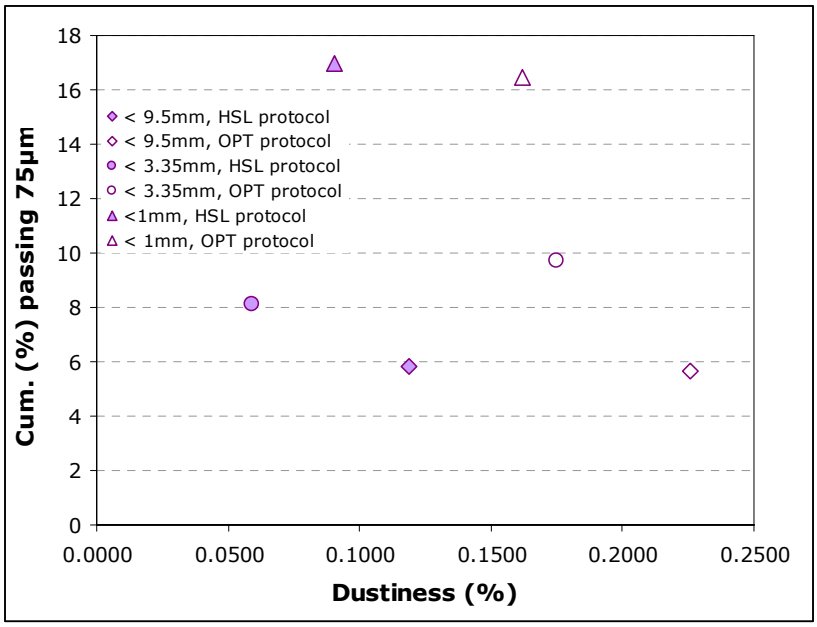

Figure 100: Dustiness result of the iron ore fractions versus the proportion of fines (<75µm) in the test sample (HSL: corresponds to the HSL-TP (40l/min, 1min, 30 rpm, 200g), OPT: represents the OPT-TP (40l/min, 3min, 30rpm, 150g)

In general, for longer tumbling times all of the test fractions receive higher dustiness values, and also are inversely proportional to the percentage of particles below 75µm contained in the feed. Hence it is suggested that abrasion significantly affects the iron ore particles (from the coarser to the finer fraction) resulting in dust production. The abrasion mechanisms at lower tumbling time, still affect the <9.5mm sample, but not the finer test fractions. In conclusion, the combination of abrasion and increased tumbling time are critical to the dust production potential from iron ore. Industrial processes such as conveyor belts, grinding mills, mixers, sieves, could minimise the generation rates of particulates by optimising their operational time as well as equipment parameters that can ensure lower abrasion rates (i.e sieves design -use of rubber apertures, optimise the speed of conveyor belts or the rotation speed of mixers and mills).

7.5.1.2.*The effect of moisture content upon iron ore dustiness*

The moisture content of the iron ore test samples used for testing with the HSE-WSL mill was determined following British Standard BS812-109:1990 (BSI 1990). The experimental procedure can be reviewed in detail in Chapter 5. The results obtained are presented in Table 54. For both testing regimes the lowest moisture content was

measured for the iron ore fraction (<9.5mm), which resulted the highest dustiness values. Nevertheless the moisture content of the <9.5mm sample is not that different from the <1mm sample, which indicates that abrasion mainly accounts for the discrepancy observed in the dustiness values. For the HSL testing regime, it can be seen that the lower the moisture content, the higher the dustiness. For the optimum parameters procedure, this is also the case for the <9.5mm and <1mm samples, whilst the <3.35mm fraction, although it exhibits a greater moisture content, presents a dustiness value higher than the <1mm. The greater dustiness values of the optimum parameters protocol, suggests that at increased operational time, the moisture content of the samples has to be kept high, in order to reduce or control dust.

Table 54: The moisture content (%) of the iron ore test fractions in relation to dustiness (%) (average values) from the two testing regimes.

Sample	Moisture content (%)	Dustiness (%) HSL testing procedure	Dustiness (%) Optimum parameters procedure
<9.5mm	0.24	0.1185	0.2255
<3.35mm	0.30	0.0591	0.1747
<1mm	0.25	0.0903	0.1618

7.5.1.3.*Determination of the health based dustiness indices*

As for limestone and talc, the health based dustiness indices of the inhalable (Di), thoracic (Dt) and respirable (Dr) fractions have been determined during testing with the HSE-WSL test. The inhalable fraction dustiness index corresponds to the total dust yield and these results are presented in detail in the above paragraph. All results are displayed in Table 55 and in appendix IV. The reproducibility of the health based dustiness indices is expressed by the standard deviation values in Table 55, which were calculated based on triplicate tests. The two testing protocols produced a variety of dustiness indices thus the thoracic faction ranges from 0.1099% to 0.0458% and the respirable fraction varies from 0% to 0.0181%.

It is difficult to distinguish a specific pattern from the health based indices of the thoracic and respirable fractions that correspond to any of the testing regimes. The various test fractions behave individually, under different operational conditions. For instance the <9.5mm test sample produced the highest dustiness indices for the thoracic and respirable fraction under the HSL-TP. The <3.35mm and <1mm test samples yielded higher dustiness indices of the thoracic fraction by the OPT-TP,

whilst for the <1mm sample the respirable fraction dustiness index was greater after testing with the HSL procedure.

The proportion of particles found in the thoracic and respirable fraction, for any of the test samples, was very small, which suggests that the impact to human health might be low. Nevertheless, the health based classification provided by the HSE-WSL test might be affected by many factors such as the motion dynamics of particulates, atmospheric conditions, the collection efficiency of the filters, as well as testing related parameters such as the loss of dust during removal of filters from the apparatus. If the purpose of the experiment is to classify dust, then particle size analysis is a much better approach. However if testing takes place to identify the impact of dust on human health then the proposed health based classification might be more appropriate.

Table 55: Health based dustiness indices of the iron ore samples (both testing protocols). One standard deviation has been calculated from replicate tests.

HSL protocol	Iron ore fractions		
	<9.5mm	<3.35mm	<1mm
D_t (%)	0.0890	0.0000	0.0831
Standard deviation	0.0297	0.0000	0.0478
D_r (%)	0.0181	0.0000	0.0026
Standard deviation	0.0203	0.0000	0.0027
Optimum parameters protocol			
D_t (%)	0.0458	0.0564	0.1099
Standard deviation	0.0047	0.0076	0.0356
D_r (%)	0.0018	0.0014	0.0008
Standard deviation	0.0016	0.0013	0.0015

7.5.2. Summary of the dustiness analysis results

Two testing regimes, which make use of different operational parameters have been used to assess the dustiness of iron ore samples of size < 9.5mm, <3.35mm and <1mm. The OPT-TP yielded the highest dustiness for all fractions, whilst the <9.5mm test sample generated more airborne particulates during both the HSL and optimum parameters procedures.

Tumbling time is considered the parameter that mainly affects the dust generation potential of this iron ore, because highest values where achieved during the OPT-TP, despite lower sample mass have been used. In particular the <3.35mm sample

produced a greater discrepancy between the various testing procedures and a higher dustiness ratio.

For longer tumbling time (OPT-TP) the concentration of fines (cumulative weight percentage below 75µm) in the test sample relates inversely proportional to dustiness. Thus, the coarser fraction (<9.5mm), which contained less fines (<75µm) produced the highest dust levels, which suggests that the abrasion mechanisms that take place in the drum affect the iron ore and increase the potential of particulates to be liberated.

There is no previous reference of dustiness results for iron ore. According to the Health and Safety Laboratory the dustiness of materials can range from not dusty to extremely dusty (Chung and Burdett 1994) (Table 26). The iron ore samples are categorised accordingly in Table 56.

Table 56: Classification of the dustiness results for the iron ore samples as proposed by HSL

Testing procedure	Iron ore fractions	Dustiness (%)	Classification
HSL procedure	< 9.5mm	0.1185	dusty
	< 3.35mm	0.0591	slightly dusty
	< 1mm	0.0903	slightly dusty
Optimum operating parameters procedure	< 9.5mm	0.2258	dusty
	< 3.35mm	0.1747	dusty
	< 1mm	0.1618	dusty

The results of the various iron ore fractions and testing protocols, expressed in dust yield per filter, including a standard deviation from replicate tests can be reviewed in appendix IV.

Conclusively, in industrial processes (i.e handling processes) the abrasion rates in combination with the time consumed in an operation will determine the dust generation level. In order to minimise the production of particulates, optimisation steps should be taken, which will reduce abrasion as well as minimise the process duration.

7.6. Particle size analysis of the iron ore particulate matter fraction generated by the HSE-WSL test

The particle size analysis results for the iron ore dust fractions collected by the HSE-WSL test are presented in the following paragraphs. Prior to presentation of the results, the selection of the optical properties used during measurements, is discussed.

7.6.1. Selection of the optical properties of the iron ore particulate matter

Iron ore particulates are opaque thus their refractive index is much higher than those of limestone and talc. For instance, hematite, which is one of the main mineral phases in iron ore, has a refractive index of 2.94. According to ISO specifications, for opaque particles and particles that have a high contrast with the refractive index of the dispersion medium, the Fraunhofer approximation could be used (ISO 1999). However due to the small size of the particulates tested, it was considered a better approach to make use of Mie theory optical model. The ISO standards suggest that for particles below 50μm, even opaque ones, interference between the particulates and the laser beam might be observed (ISO 1999).

The Mie approximation requires the use of optical properties and for iron ore several presentations with different optical parameters were prepared and used. Some of them are displayed in Table 57. If incorrect optical properties are applied to the measurement, which for example might be applicable for transparent particles (RI Comb 3), then particle size analysis will not be accurate. An example of this is given in Figure 101.

Table 57: Optical properties of some of the presentations prepared for iron ore particulates

	Refractive index of particulate matter (R.I.)		
Presentation Code	Real part (n_p)	Imaginary part (K_p: absorption)	Dispersion Medium Refractive Index
RI Comb.1	2.94	0.1	1.33
RI Comb.2	None – Fraunhofer optical model		
RI Comb.3	1.53	0.1	1.33
RI Comb.4	2.59	0.1	1.33

The selection of a refractive index that is not appropriate for iron ore increases the concentration of fines below 1μm giving a second peak in the volume (%) remaining size distribution, with a distinct minimum at 1μm (Figure 101). A similar pattern has been observed during experimentation with talc and limestone when incorrect optical properties have been used as well as (Malvern Instruments 2004).

In Figure 101 the particle size distribution resulting by the use of Fraunhofer optical model is also shown, which does not present high discrepancy from Mie theory when the correct optical properties have been selected. Hence the Fraunhofer optical model would not be a bad approximation for iron ore. Several other presentations with refractive indices between 2.39 to 2.99 have been applied, which do not affect the particle size distribution of the iron ore samples (Figure 101 – RI Comb1, RI Comb4). In Table 58 the cumulative volume percentage below 10μm and 2.5μm as well as the diameters d_{50} and d_{90} provide some extra information about the characteristics of the particle size distributions resulting from the various optical properties and models. For instance, it can be seen that the cumulative volume percentages below 10μm and 2.5μm for the presentation RI Comb3 (incorrect profile) are increased in comparison to other selected optical properties. Considering that the cumulative volume percentages below 10μm and 2.5μm can be used for the determination of occupational exposure limits or an ambient air standard, it becomes clear that the selection of correct optical properties during laser diffraction particle size measurements is critical.

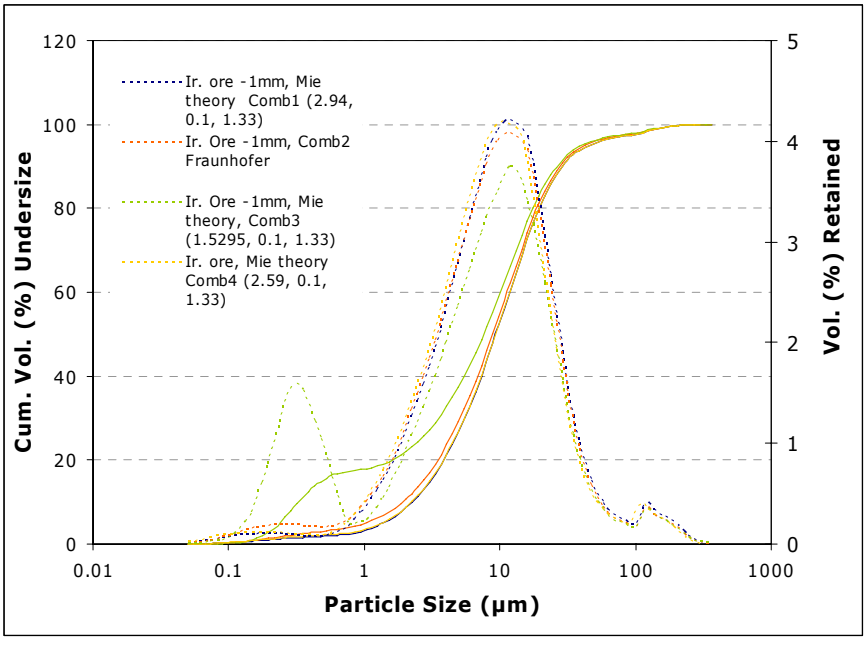

Figure 101: Particle size distribution of the dust collected for the iron ore sample <1mm (HSL-TP) for various presentations.

Table 58: The cumulative percentages passing 10μm and 2.5μm and the median diameters d_{50} and d_{90} as resulted from the different optical properties presentations

Presentation code	Cum.% passing 10μm	Cum. % passing 2.5μm	D50	D90
R.I. Comb.1	52.82	11.44	9.36	28.93
R.I. Comb.2	54.92	13.55	8.87	27.57
R.I. Comb.3	59.6	24.40	7.61	26.32
R.I. Comb.4	52.88	11.61	9.34	28.91

Conclusively, particle size analysis results, which are presented in the following paragraph, as well as during experimentation with the impact test will use as optical properties a refractive index of 2.94 (real part- corresponds to hematite) an imaginary index of 0.1 and a dispersion medium index of 1.33 (water).

7.6.2. Particle size analysis results

The dust particle size distributions for the various iron ore factions tested during the two different testing regimes are displayed in Figure 102. They correspond to average values obtained by triplicate tests. Commonly several measurements were performed for each sample with the same or fresh feed. The measurement steps have been described in detail in Chapters 4 and 5.

To assess the reproducibility of the particle size measurements taken, the standard deviation and relative standard deviation of the median of the diameters d_{10}, d_{50} and d_{90} have been calculated and results can be seen in Table 59. The standard deviation of the triplicate tests can also be seen in the volume (%) retained particle size distributions of the test samples shown in appendix IV. The measurements taken for one sample exhibited very good reproducibility with a relative standard deviation below 1%. When triplicate tests were measured the standard deviation and relative standard deviation values were higher and for the median diameter of d_{50} equal to 0.71 and 5.51% respectively. The data of Table 59 represents the expected standard deviation and relative standard deviation values of iron ore particulates for the method in use as no previous reference is available.

In Figure 102 (a) the particle size distributions of the dust fraction of the <9.5mm, <3.35mm and <1mm samples show distinct differences. Hence the dust particle size distribution of the <9.5mm sample is coarser than the <3.35mm and <1mm

samples, whereas the particulates of the <1mm fraction appear to have a smaller particle size.

Dustiness results however have shown that the <9.5mm sample generated the highest dust levels followed by the <3.35mm and the <1mm test samples. It is clear from the OPT-TP that dustiness and dust particle size present a inverse relationship, where samples of high dustiness (i.e <9.5mm sample) produce a coarser dust particle size range than samples with a low dust yield. A similar outcome was obtained from the health based classification of dust and in particular for the dustiness index of the thoracic fraction.

Table 59: The median diameters d_{10}, d_{50} and d_{90} of the iron ore particulate matter produced using the HSE-WSL test, from a range of sample fractions (optimum conditions testing protocol). The standard deviation and relative standard deviation values were calculated from the results obtained by the triplicate samples.

Sample Fraction	D_{10}	Stdev	RSD(%)	D_{50}	Stdev	RSD(%)	D_{90}	Stdev	RSD(%)
-9.5 mm	3.4	0.23	6.66	17.66	1.39	7.89	53.39	1.42	2.66
-3.35 mm	2.60	0.12	4.60	9.43	0.52	5.53	24.19	1.45	5.98
-1 mm	1.68	0.01	0.84	7.10	0.22	3.11	22.30	1.07	4.79

The dust particle size distributions (Figure 102 – b) collected after the HSL-TP did not show the same discrepancies as for the case of the optimum parameters protocol, however they appear very similar. Some differences are observable for the coarse part of the particle size distributions, namely for particles above 10μm. At this particle size region, the dust fraction of the <9.5mm sample produced the coarser size distribution.

In Table 60 some extra information regarding the dust particle size distributions shown in Figure 103 is given, which include the cumulative volume percentage passing 10μm and 2.5μm as well as the median of the diameter of d_{80}. For the particulate matter produced after the HSL testing procedure, the cumulative volume percentages below 10μm and 2.5μm are very similar and equal to an average value of 53.57% and 11.46% respectively. The median values of the d_{80} diameter that corresponds to the <3.35mm and <1mm samples (HSL testing procedure) are similar with an average size of 18.57μm, whilst the d_{80} of the <9.5mm sample is higher and equal to 26.48μm.

For the samples produced by the OPT-TP, the cumulative volume percentages under 10μm and 2.5μm and the d_{80} values follow the same sequence with the particle size distributions of Figure 102.

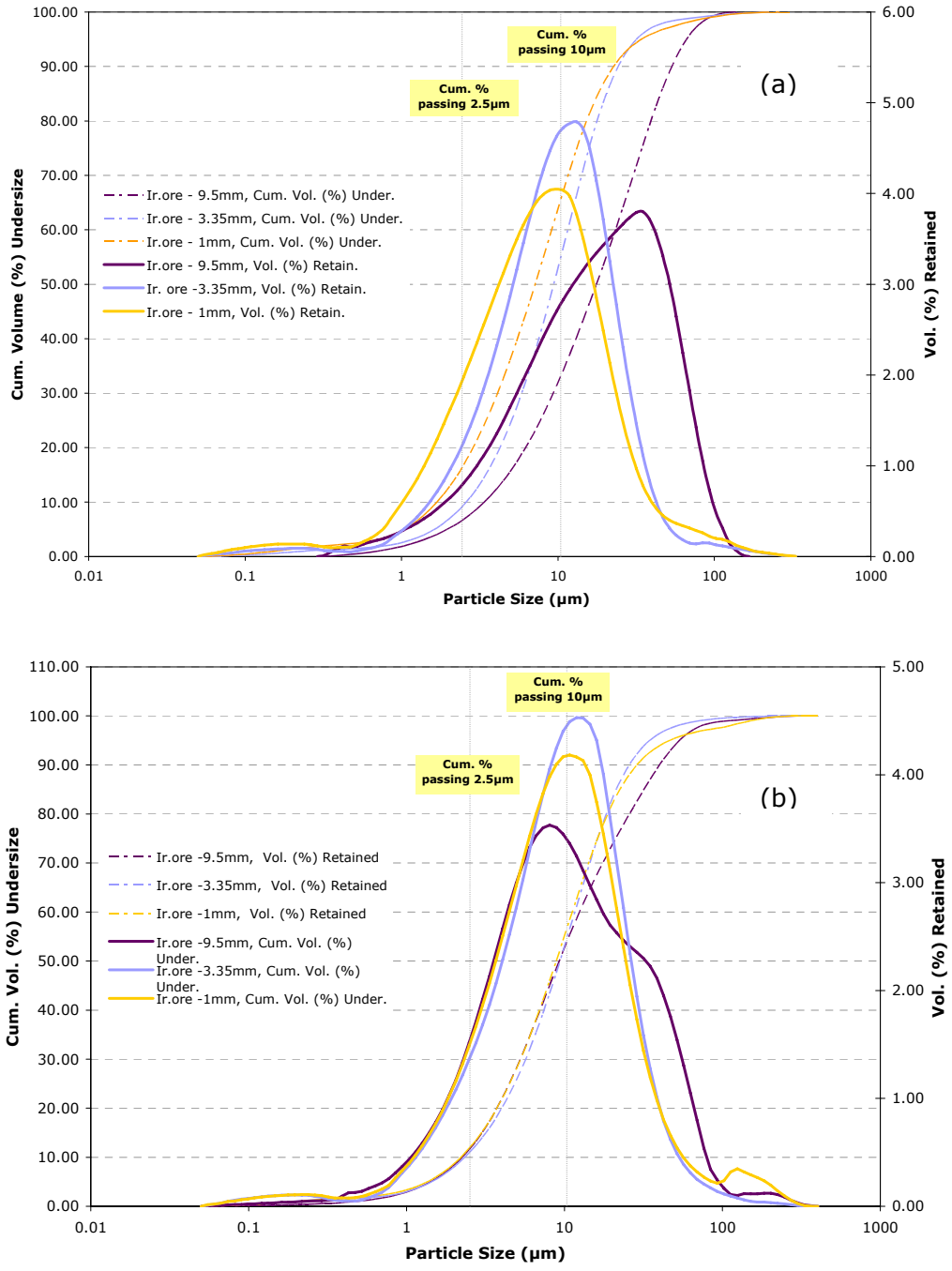

Figure 102: Particle size distribution of the iron ore particulate matter produced by the HSE-WSL test through (a) the optimum operating conditions testing protocol and (b) the HSL testing protocol. The presented results correspond to average values of repeatable tests.

Table 60: Cumulative percentages passing 10μm and 2.5μm and the median diameter d_{80} values for all samples and testing regime ((1): corresponds to the OPT-TP; (2) corresponds to the HSL-TP)

Iron ore fractions	Cum. % passing 10μm	Cum. % passing 2.5μm	D_{80}
-9.5mm (1)	31.93	6.58	39.36
-9.5mm (2)	52.68	11.60	26.48
-3.35mm (1)	52.92	9.47	17.79
-3.35mm (2)	52.93	10.94	18.41
-1mm (1)	63.80	16.90	15.39
-1mm (2)	55.10	11.85	18.73

The effect the two testing protocols had on the particulates of a specific test sample (e.g <1mm) are shown in Figure 103 and in appendix IV. It is clear that the additional tumbling time of the optimum parameters regime produced a finer dust particle size distribution.

According to the results presented in this paragraph, around 51.56% and 11.22% (average values) of the dust particles were found to give a size below 10μm and 2.5μm respectively. Consequently, the particle size of iron ore dust generated by abrasion indicates that it might have adverse implications to human health and the environment

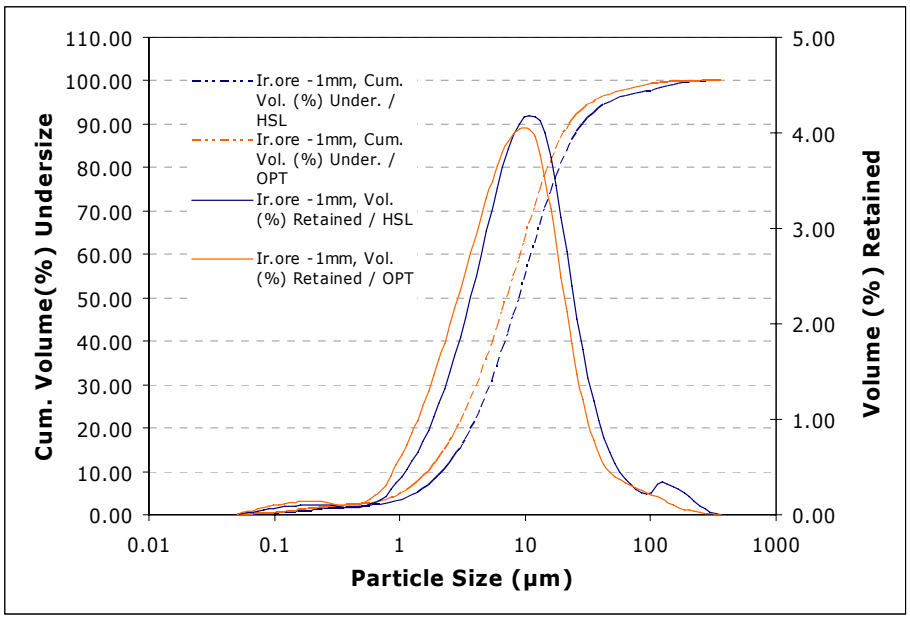

Figure 103: Particle size distributions of the particulate matter produced by the HSE-WSL test from an iron ore feed fraction below 1mm (both testing protocols).

7.7.Experimentation using the impact test

Many industrial processes require the transfer or drop of materials from heights such a transfer points in conveyor belts, the loading, tipping or stockpiling of ore, the use of draglines, where dust is liable to be generated due to impaction of particulates over surfaces or on other particles. The propensity of iron ore to produce dust under impact mechanisms was assessed using the impact test. The experimental procedure followed during testing has been described in detail in Chapters 4 and 5. The following sections present the results obtained during testing with this iron ore.

7.7.1. Determination of the residual height of iron ore particulates

The residual height of the iron ore particles left after impact is presented in Table 61 and in appendix IV. For a specific energy level, the larger the size of the test sample, the higher the offset remaining (Table 61). Also for a single fraction (i.e 16x13.2mm) the increase in bulk volume gave rise to higher residual height values. For example, the residual height left by the 8x6.7mm test sample – 10% bulk volume at an energy level (Eis) equal to 0.05 kWh/t was 0.68 cm, whilst for a lower bulk volume (5%), the offset was 0.3 cm. Hence the reduction in bulk volume to half resulted to a respective reduction of the residual height.

As found for the talc samples, the energy input levels were calculated using the offset values recorded for limestone during the initial investigations. The results displayed in Table 61 correspond to the final values recorded after impact testing and they are presented against the limestone offsets. For the 20% bulk volume samples, iron ore produced slightly lower residual height values, whereas for the 5% bulk volume samples, the remaining offsets were higher than the ones reported for limestone. In order to assess what effect the above offset differences between iron ore and limestone had on energy input, back calculation of the energy levels using the values recorded for iron ore took place. These calculations suggested that energy levels are not affected by the residual height difference. Thus using the residual height of limestone particles to calculate the release heights and energy input levels of iron ore was an acceptable approximation.

Table 61: The offset of limestone and iron ore test fractions (in cm). Limestone residual height has been used for the calculation of the release height for the iron ore samples.

	Residual height (cm)							
Test fraction	16x13.2mm		8x6.7mm		4x3.35mm		2x1.7mm	
10% bulk volume	Ir. Ore	Lim.	Ir. Ore	Lim.	Ir. Ore	Lim.	Ir. Ore	Lim.
0.05 kWh/t	0.85	0.85	0.68	0.60	0.47	0.48	0.33	0.57
0.1 kWh/t	0.85	1.00	0.60	0.55	0.57	0.63	0.37	0.70
0.5 kWh/t	0.38	0.50	0.23	0.53	0.38	0.27	0.13	0.18
20% bulk volume								
0.05 kWh/t	1.28	1.67						
0.1 kWh/t	1.05	1.65						
0.2 kWh/t	0.93	1.37						
5% bulk volume								
0.05 kWh/t			0.30	0.13	0.08	0.02	0.10	0.02
0.1 kWh/t			0.40	0.13	0.02	0.02	0.10	0.00
0.5 kWh/t			0.15	0.00	0.10	0.02	0.05	0.00
0.68 kWh/t			0.15	0.00	0.13	0.00	0.07	0.00

7.7.2.The bulk density of the iron ore samples

The preparation of the iron ore samples was based not just on particle size, but on bulk volume as well. For each singe size fraction, two different bulk volumes were selected, as discussed in Chapter 4. With respect to bulk volume, the bulk densities of the test samples were calculated and these are presented in Figure 104.

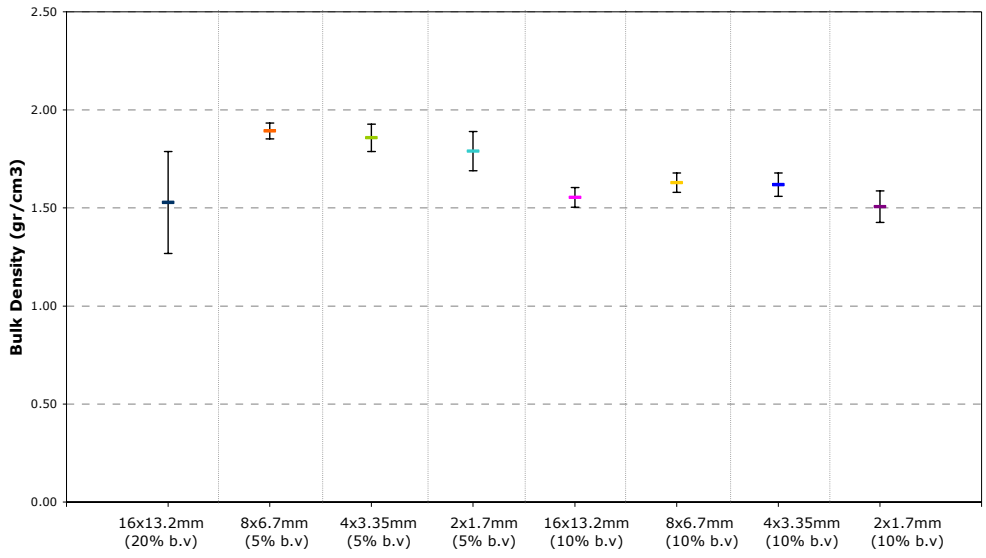

Figure 104: The recorded bulk density values of the iron ore single fractions. The vertical bars represent one standard deviation.

These values represent averages of the triplicate prepared samples, whilst their variance is expressed by the standard deviation (error bars). The bulk density of the various single size fractions and for a specific bulk volume did not vary significantly. Thus for the bulk volume percentages 5%, 10% and 20%, the bulk density of iron ore was 1.85 g/cm^3, 1.58 g/cm^3 and 1.53 g/cm^3 respectively. Higher bulk volumes tend to increase not just the sample mass, but also the gaps left within particles, as well as the influence of the physical properties of particles (i.e shape, orientation in the sample holder). Therefore for the bulk volume percentages of 10% and 5%, bulk density exhibits a higher variation than for the bulk volume percentages of 10% and 20%.

7.7.3. Impact Test - Results

The effect that impact has upon single size fractions of iron ore is expressed by the particle size distributions displayed in Figure 105. These results present sieving data for the broken iron ore particles. The single size fraction of iron ore at bulk volumes of 10% and 20% were tested at three energy input levels instead of four used for talc and limestone. This is because the bulk density of iron ore is higher than that of talc and limestone thus to achieve the upper energy input level of 0.68kWh/t a release height beyond the capabilities of the apparatus was required. For any of the test samples (e.g 16x13.2mm – 10% bulk volume) it is observed that increasing the energy input results to a finer particle size distribution.

For any of the single size fractions of the 10% bulk volume samples, the increase in energy input from 0.1kWh/t to 0.5kWh/t produced a significant difference in the size distribution of the iron ore particles resulting in further breakage and a much finer particle size distribution.

When the sample mass of the 16x13.2mm fraction was increased (from 10% to 20% bulk volume) it was shown that only for 0.1kWh/t did a finer particle size distribution occur. For 0.05 kWh/t the increase in bulk volume did not influence the breakage of the iron ore particles under impact thus similar particle size distributions were generated.

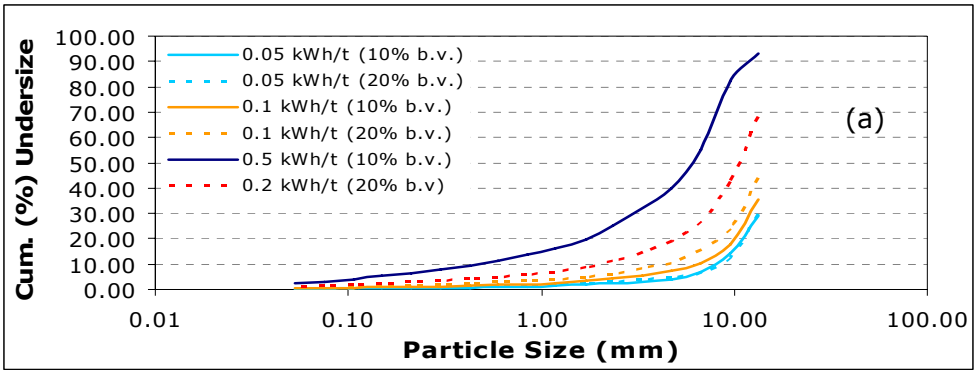

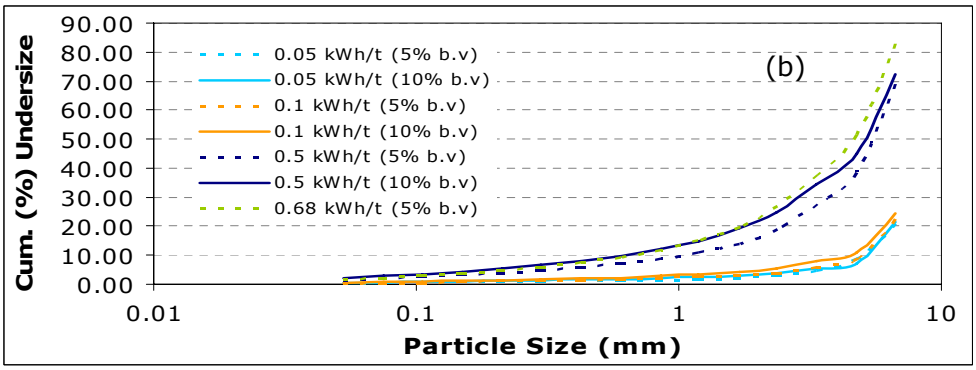

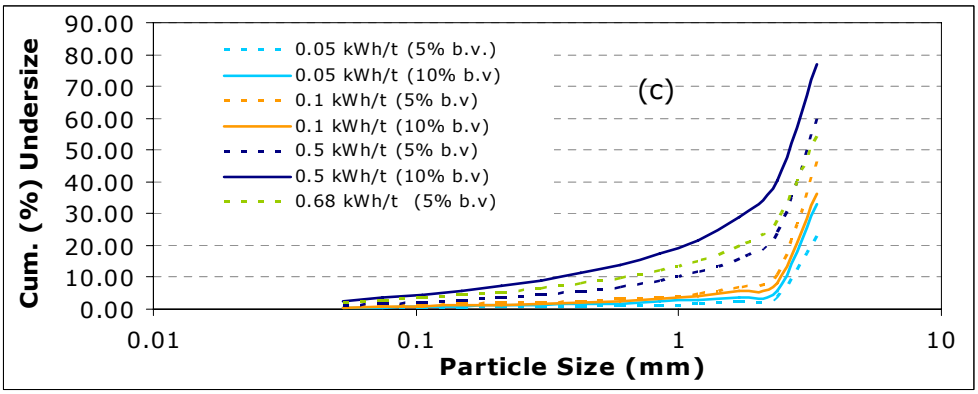

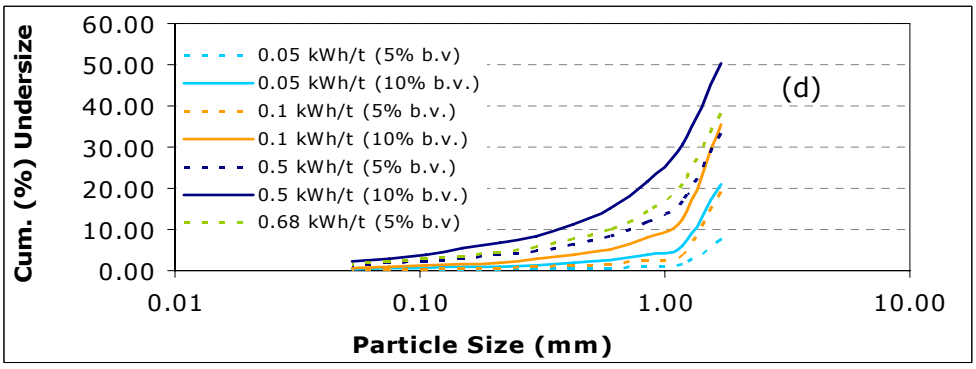

Figure 105: : Particle size distribution of the iron ore particles collected and sieved after impact of the single fractions (a) -16+13.2mm (10% and 20% bulk volume), (b)-8+6.7mm, (c) -4+3.35mm and (d) -2+1.7mm (5% and 10% bulk volume).

For the 8x6.7mm, 4x3.35mm and 2x1.7mm single size fractions the sample bulk volume was reduced from 10% to 5%. The reduction in bulk volume resulted in lower

breakage rates and coarser particle size distributions. Nevertheless, even the lower bulk volume samples retained the positive correlation with energy input, whereas once more greater breakage was achieved within the energy levels of 0.1kWh/t and 0.5kWh/t. The coarser particle size distributions obtained for smaller bulk volumes (e.g 5% bulk volume) indicates that energy is dissipated or transformed to other forms, vibration or noise for example, without breaking the particles.

The particle size distributions of the 10% and 5% bulk volume samples produced from the 2x1.7mm fraction and for energy input levels of 0.05kWh/t and 0.1kWh/t gave the highest breakage. Hence the ratio (average) of the cumulative percentage undersize of the 10% and 5% bulk volume sample at 0.05kWh/t and 0.1kWh/t is 3 to 1, whilst at 0.5kWh/t this is 1.6 to 1.

7.7.3.1. *The effect of impact upon fines generation for the iron ore*

The generation of dust from the impact test is closely associated with the production of fines under impact. Results to illustrate this association are presented in Figure 106.

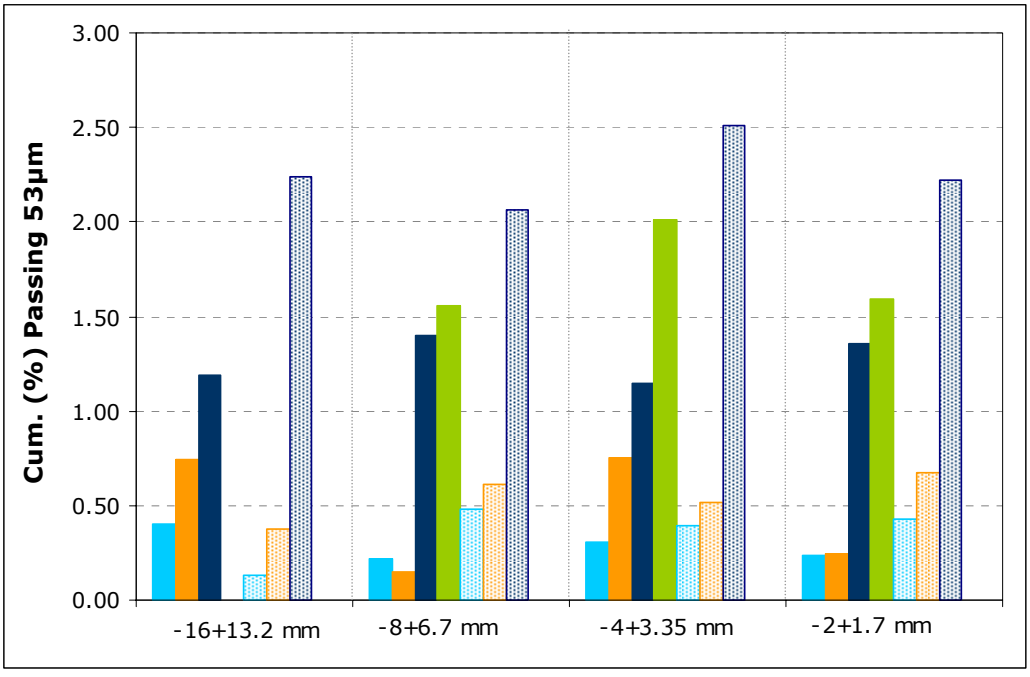

Figure 106: The cumulative percentages passing 53µm for the single iron ore particle fractions. The textured columns represent the samples of 10% bulk volume, whereas the saturated coloured columns represent the 20% (for the 16x13.2mm fraction) or 5% bulk volume samples. The different colours represent different energy levels : • = 0.05 kWh/t, • = 0.1 kWh/t, • = 0.5 kWh/t or 0.2 kWh/t (for the 16x13.2mm, 20% bulk volume) and • = 0.68 kWh/t or 0.3 kWh/t (for the 16x13.2mm, 20% bulk volume).

Results have shown that the concentration of fines (below 53μm) increases proportional to the energy input level, independently of the characteristics of the test sample (i.e bulk volume, particle size).

The 16x13.2 mm test sample generated greater quantities of fines (<53μm) at low energy levels (0.05kWh/t and 0.1kWh/t) for the high bulk volume sample (20%), whilst the higher percentage of particulates was produced at an impact energy of 0.5kWh/t and at the lower bulk volume (10%). The increased production of fines at low energy levels for the 20% bulk volume sample is attributed to attrition caused by interparticle contacts as particle to particle interactions being more frequent for the higher mass samples.

For the 8x6.7mm, 4x3.35mm and 2x1.7mm size fractions, the larger volume samples (10% bulk volume) resulted in greater concentration of fines (<53μm). The 8x6.7mm and 4x3.35mm size fractions of 10% bulk volume and at low energy inputs (0.05 and 0.1 kWh/t) produced higher concentrations of fines due to attrition caused by interparticle contacts than the respective 5% bulk volume samples. At higher energy input further breakage occurred for the 10% bulk volume samples, which resulted to greater quantities of particulates below 53μm. This is clear in the particle size distributions of Figure 105. Similar is the case for the 2x1.7mm size fraction of 10% bulk volume, which resulted to greater amounts of fines than the 5% bulk volume sample due to further breakage. The only exception was the results obtained for the 4x3.35mm sample at an energy input of 0.1kWh/t, which generated more fines for the smaller sample bulk volume.

Overall the higher concentrations of particulates <53μm have been generated by the 4x3.35mm fraction (10% bulk volume) at 0.5kWh/t, followed by the 16x13.2mm, the 2x1.7mm and the 8x6.7mm fractions (10% bulk volume), which also generated uppermost percentages of fines at 0.5kWh/t. At low energy levels (0.05kWh/t and 0.1kWh/t) the 16x13.2mm – 20% bulk volume sample and the 4x3.35mm – 5% bulk volume samples produced the higher quantities of fines, whilst the 16x13.2mm – 10% bulk volume sample produced the lower.

Dustiness measurements have shown that under abrasion dust relates inversely proportional to the concentration of fines in the test sample. The above statement although satisfactory for mechanisms that involve abrasion gives an indication of how

iron ore particulates entrain into the airborne state. Thus even the single fractions that generate low concentrations of fines could result in high dustiness levels.

7.7.4. Summary of the impact test results

The propensity of iron ore to generate fine particulates from processes that involve impact mechanisms was assessed using the impact test. Four different single size fractions at two different bulk volumes and three or four energy input levels (depending on the utilized bulk volume) were tested. Results have shown that increasing the energy input level produced a finer particle size distribution and larger quantities of fines below 53μm. Also, it was clear that the generation of fines was affected by the sample mass and particle size. Therefore the highest percentages of particles below 53μm were recorded for the 4x3.35mm-10% bulk volume sample at high energy input levels (0.5kWh/t), whereas the lowest proportion of fine particulates was produced by the 16x13.2mm – 10% bulk volume sample at 0.05kWh/t.

The above results suggest that processes which involve the application of impact (i.e drop from heights, haulage roads, loading and dumping etc) could minimise the propensity of iron ore to generate dust by appropriate selection of the particle size and bulk volume of sample utilized at a certain operation, as well as by adjusting the energy levels so as to reduce the fines production. Changing the particle size of iron ore that undergoes processing could not always be technically feasible, as product specifications, customer requirements or even the current comminution practices might discourage such an action. However, if none of the above limitations exist, then it could be possible by altering the characteristics of comminution equipments (e.g. closed size setting (CSS)) to reduce the production of specific size fractions or fines that might be liable to generate more dust. The bulk volume of the iron ore in use could be adjusted by using equipments that they handle and process lower quantities of ores.

These results could be used as prediction tools to identify potential dust sources, or as indicators which could help optimise existent dust control practises or implement extra mitigation techniques. Thus reducing the energy input levels during loading or dumping operations could prove beneficial to the minimisation of dust. Moreover the use of an appropriate bulk volume of iron ore, which do not lead to the generation of higher quantities of fines, could reduce the potential of dust to be produced.

Dust is not only a major issue when found airborne, but also when it is generated and travels with the product during processing. This is because fine particles can deposit on equipment producing wear, reducing the efficiency of a specific process taking place or even minimising the quality of end product by adhering to the surface of particles. Also these fine particles might not be emitted when produced but afterwards during a subsequent processing step. Consequently any steps that can reduce the production of fines are essential to ensure that the generation of dust will be minimised.

7.8. Particle size analysis results of the iron ore particulates produced by the impact test

The particulates below 53μm produced during impact testing were collected by sieving and further analysed by laser diffraction particle size analysis using the Malvern Mastersizer-S. Triplicates of each sample were measured on the basis of Mie theory, using the optical properties selected previously. The optical properties defined for iron ore are described by a refractive index (real part) of 2.94, an imaginary index of 0.1 and a dispersion medium refractive index of 1.33.

The reproducibility of the measurements taken for the triplicate samples is expressed by the standard deviation and relative standard deviation values of the median diameters d_{10}, d_{50} and d_{90} displayed in Table 62. Additionally, in appendix IV the repeatability of the replicate tests can be seen in the volume (%) retained particle size distributions, the error bars representing one standard deviation. In Table 62 it can be seen that for the median diameter d_{50} of the iron ore replicate samples, an average standard deviation of 1.36 and a relative standard deviation of 5.54% should be expected.

Figure 107 and Figure 108 show the particle size distributions of iron ore particulates that correspond to the 10% bulk volume samples. These figures show the cumulative volume (%) undersize, as well as the volume (%) retained. The equivalent particle size distributions of the 20% and 5% bulk volume samples are shown in appendix IV. For the particulates produced from the 16x13.2mm and 8x6.7mm test samples the differences in particle size distributions are minor and in both cases the higher energy input (0.5 kWh/t) produced a slightly coarser particle size distribution than the lower energy levels (0.05 and 0.1 kWh/t) (Figure 107). Conversely, the

particulates of the smaller size test samples (4x3.35mm and 2x1.7mm) have shown that higher energy input resulted to a significantly finer particle size distribution in comparison to lower energy levels (Figure 108).

Table 62: The median of the diameters of the values of d_{10}, d_{50} and d_{90} of the iron ore particulate matter produced using the impact test. The standard deviation and relative standard deviation values correspond to replicate measurements of triplicate sets of the test samples. Only the results obtained for the 0.05 k Wh/t (E1) and 0.5 kWh/t (E4) are shown.

		D_{10}	Stdev	RSD (%)	D_{50}	Stdev	RSD (%)	D_{90}	Stdev	RSD (%)
16x13.2 mm 10% b.v.	E1	3.58	0.22	6.25	23.28	2.31	9.93	56.19	2.70	4.80
	E4	4.74	0.31	6.62	25.37	1.41	5.58	57.39	1.88	3.27
8x6.7 mm 10% b.v	E1	3.90	0.41	10.47	23.87	2.14	8.97	58.79	2.62	4.46
	E4	3.98	0.39	9.84	24.67	1.19	4.82	59.49	3.03	5.09
4x3.35 mm 10% b.v.	E1	5.11	0.41	8.02	27.88	0.48	1.72	60.63	2.07	3.41
	E4	3.41	0.37	10.99	22.19	1.34	6.04	58.03	1.26	2.17
2x1.7 mm 10% b.v.	E1	6.58	0.39	5.99	30.07	1.15	3.84	63.39	1.74	2.74
	E4	4.06	0.25	6.20	25.40	0.86	3.39	61.71	1.24	2.02

In Table 63 the cumulative percentage below 10 and 2.5 μm as well as the d_{80} values of the fines are presented for a low (0.05 kWh/t) and high (0.5kWh/t) energy input for each of the single fractions that participated during the investigations with the impact test. The median value of the diameter d_{80} ranges between 43 to 52μm, although the majority of the samples exhibit an average d_{80} diameter of around 45μm. The cumulative volume percentage below 10μm and 2.5μm for the 10% bulk volume samples justifies the conclusions presented above for the particle size distribution results (Figure 107 and Figure 108). Consequently for the 16x13.2mm and 8x6.7mm test samples, slightly greater percentages of particulates below 10μm and 2.5μm are recorded for the low energy input (0.05 kWh/t) than the high energy level. The reverse relationship is observed for the particulate matter produced from the 4x3.35mm and 2x1.7mm samples.

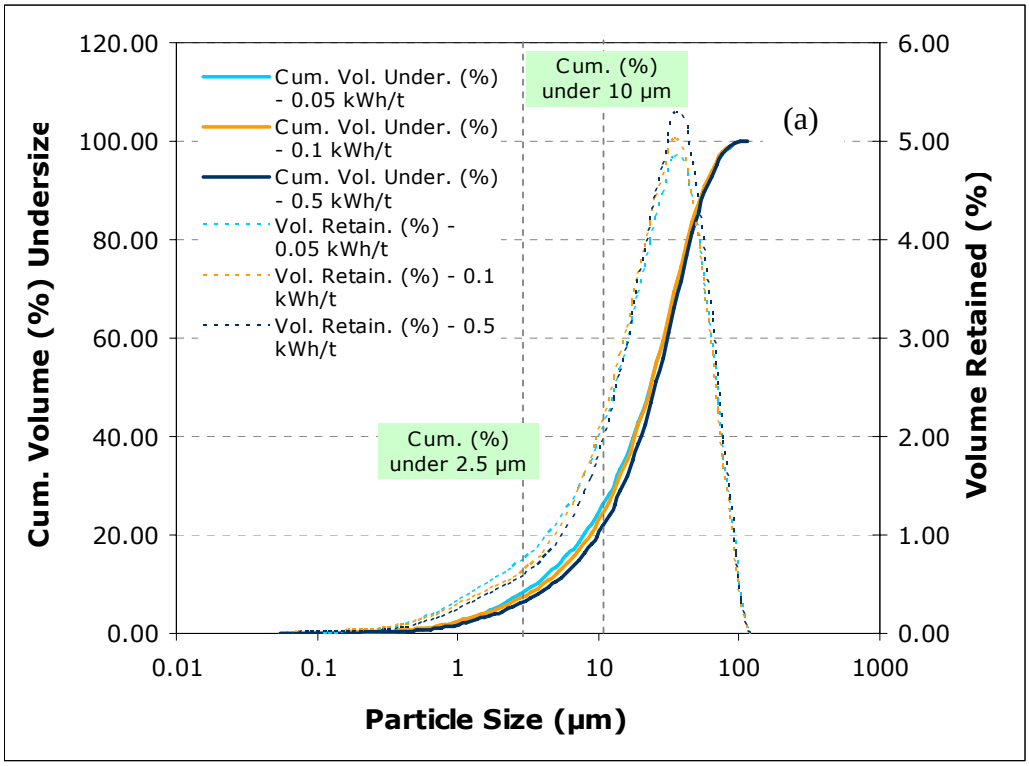

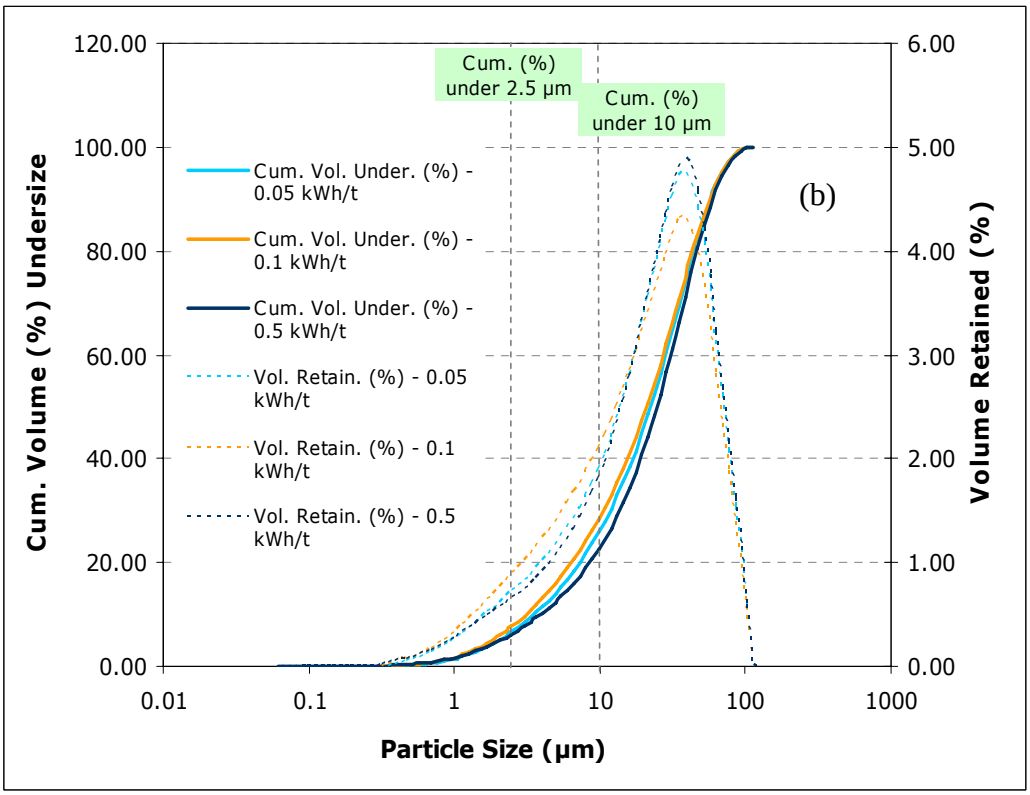

Figure 107: Particle size distributions of the iron ore particulate matter fraction generated by the impact test of a) the -16+13.2mm fraction – 10% bulk volume and b) the -8+6.7mm fraction – 10% bulk volume.

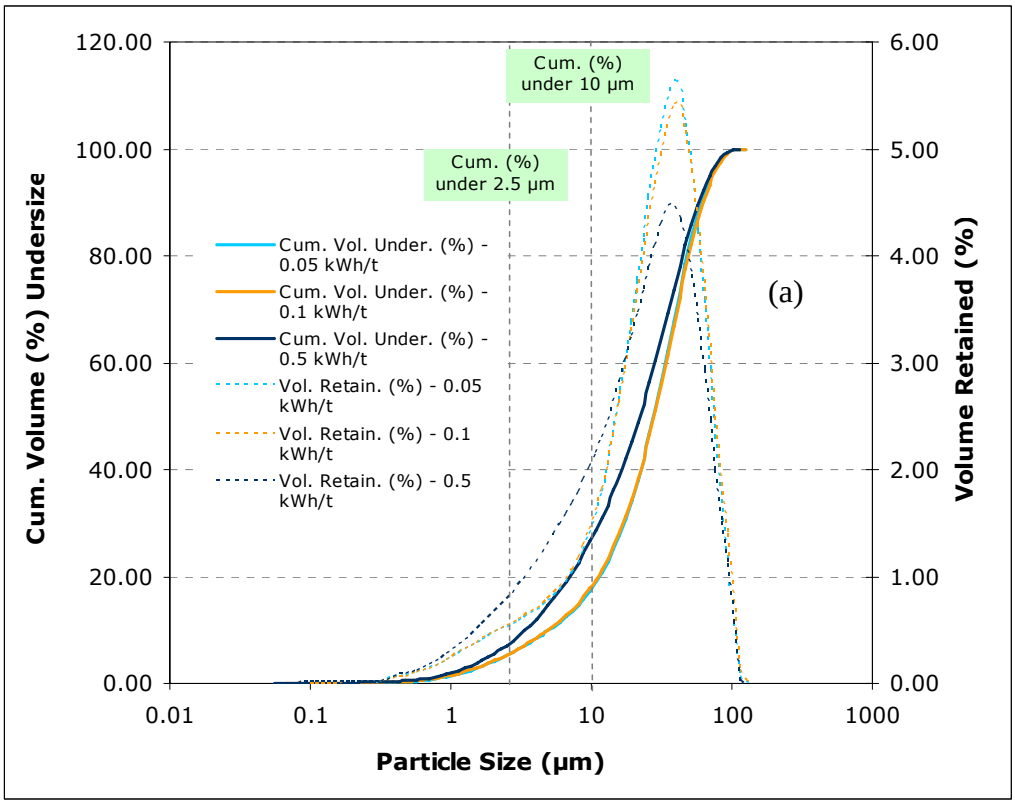

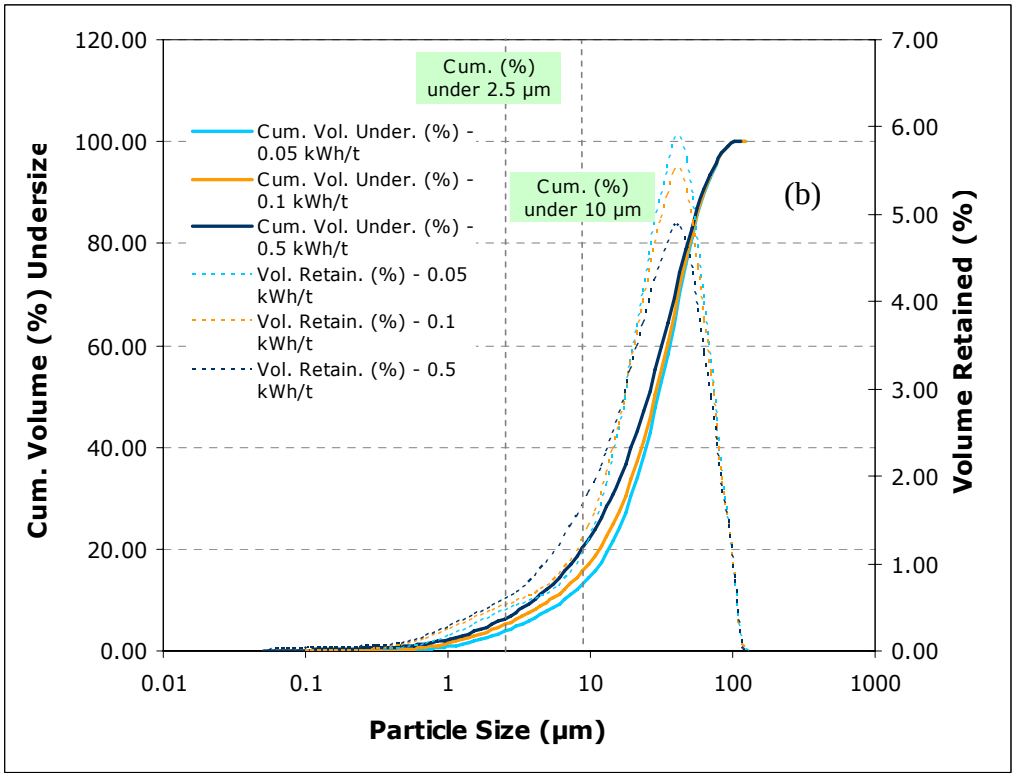

Figure 108: Particle size distributions of the iron ore particulate matter fraction generated by the impact test of a) the -4+3.35mm fraction – 10% bulk volume and b) the -2+1.7mm fraction – 10% bulk volume.

The iron ore particulates from the 16x13.2mm – 20% bulk volume and 8x6.7mm and 4x3.35mm – 5% bulk volume fractions produced lower percentages of particles less

than 10µm and 2.5µm at low energy inputs, whilst the 2x1.7mm (5% bulk volume) generated a smaller concentration of fine particles (<10, 2.5µm) at 0.5 kWh/t.

Overall the higher and lower cumulative volume percentage of particles below 10µm is associated with the 2x1.7mm test fraction at 0.05 kWh/t and for bulk volumes of 5% and 10% respectively. Hence the volume difference of the test sample influenced the particle size of dust. Conclusively the influence of operational parameters such as the energy input or the bulk volume of a sample on the particle size distribution of the particulates fraction will be greater for iron ore particles of a few millimetres (e.g. 4x3.35mm, 2x1.7mm) than for coarser particles. On the contrary, the particle size distribution of the fines generated by coarser iron ore fractions (16x13.2mm or 8x6.7mm) is not influenced by operating parameters. This suggests that for the 4x3.35mm and 2x1.7mm test fractions lowering the energy input of an industrial process that involves the impaction of iron ore particles will result not just to a lower quantity of fines, but also to a coarser particle size distribution of the particulates fraction.

Table 63: The cumulative volume percentages below 10µm and 2.5µm of the iron ore particulates generated by impact testing and for a range of single fractions and bulk volumes. The median diameter d_{80} is shown as well.

Size fraction	Energy level (kWh/t)	Cum. % <10 µm	Cum. % <2.5µm	D_{80}
16x13.2mm-10% b.v.	0.05	24.36	7.16	43.79
	0.5	20.19	5.49	45.33
8x6.7mm-10% b.v	0.05	24.13	6.13	45.59
	0.5	22.93	3.98	46.36
4x3.35mm-10% b.v.	0.05	17.59	5.24	48.17
	0.5	26.93	7.15	44.46
2x1.7mm-10%b.v.	0.05	14.64	3.86	50.65
	0.5	22.42	6.38	48.00
16x13.2mm-20% b.v.	0.05	24.70	6.98	45.04
	0.5	26.64	7.91	43.82
8x6.7mmc-5% b.v	0.05	23.64	6.11	45.85
	0.5	28.89	7.86	43.32
4x3.35mm-5% b.v.	0.05	15.35	3.28	52.40
	0.5	23.17	5.95	48.10
2x1.7mm-5%b.v.	0.05	33.30	10.97	42.78
	0.5	28.26	7.89	44.20

7.9. Mineralogical characterisation of the iron ore particulate matter

The particulate matter collected by the HSE-WSL test and the impact test was examined by X-ray diffraction analysis and scanning electron microscopy to identify its mineralogy. Several of the resultant X-ray diffraction traces are displayed in Figure 109 against the XRD pattern of the rock sample (feed). The mineralogy of the dust was found to be not different to their of the iron ore. Hence two main minerals dominate the composition of iron ore particulates and these are hematite (Fe_2O_3) and goethite (FeO(OH)).

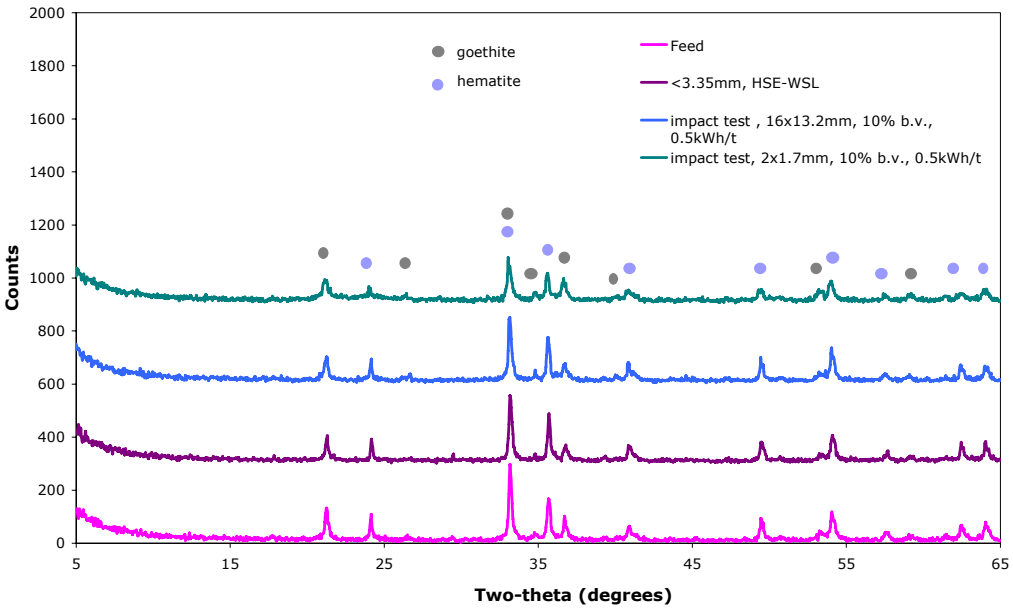

Figure 109: XRD traces of the iron ore dust/fines fraction collected by the dustiness test and the impact test. The x-ray diffraction pattern of a rock sample is presented as well (two-theta, whole rock analysis).

The airborne iron ore particulates collected by the HSE-WSL test were also examined by scanning electron microscopy (SEM). Dust particles were mounted on a sticky pad as well as forming the basis of polished blocks, which allowed the use of the energy dispersive X-ray microanalysis system for compositional analysis. Figure 110 and Figure 111 show some of the SEM photos taken. Figure 111 (a) presents the dust particles on a sticky pad and in the first SEM photomicrograph (low magnification) it can be seen that iron ore particulates exhibit a tendency to form aggregates. Exactly the same trend is observable in the second photomicrograph (Figure 111 (b)) as well. Even though a higher magnification was used individual particles could not easily be distinguished due to the agglomeration. The samples consist mainly of iron oxides

(hematite and goethite), whilst the hematite particles exhibit a platy particle shape as shown in the second photomicrograph of Figure 111. Figure 110 shows a SEM photomicrograph of the dust particulates mounted in epoxy resin and it presents overgrowths of goethite (medium grey) on hematite (light grey). Several other minor minerals were identified using the x-ray microanalysis facility of scanning electron microscope such as talc, quartz and clinochlore (a chlorite group mineral in needle like particles).

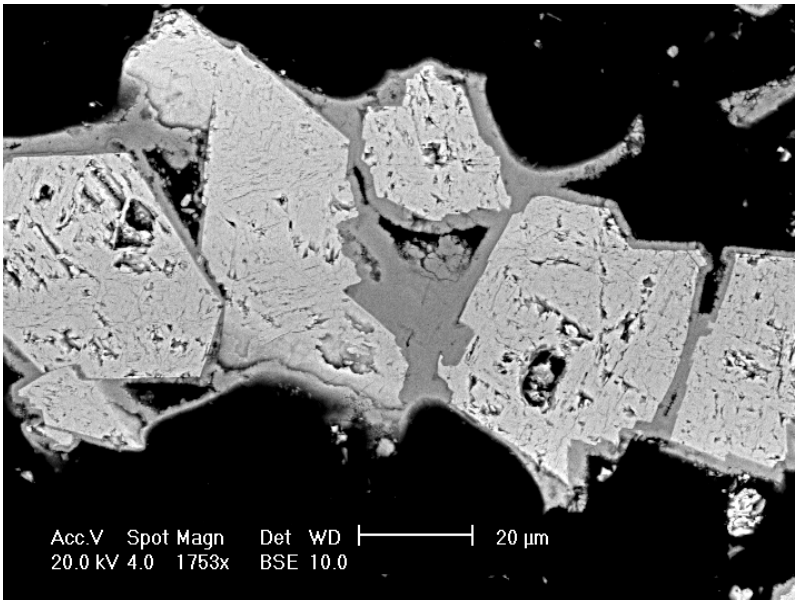

Figure 110: Scanning electron microscope (SEM) photomicrograph of the iron ore airborne particulates produced from a feed of -3.35mm/150g prepared in a polished block. Magnification x 55, scale 1mm.

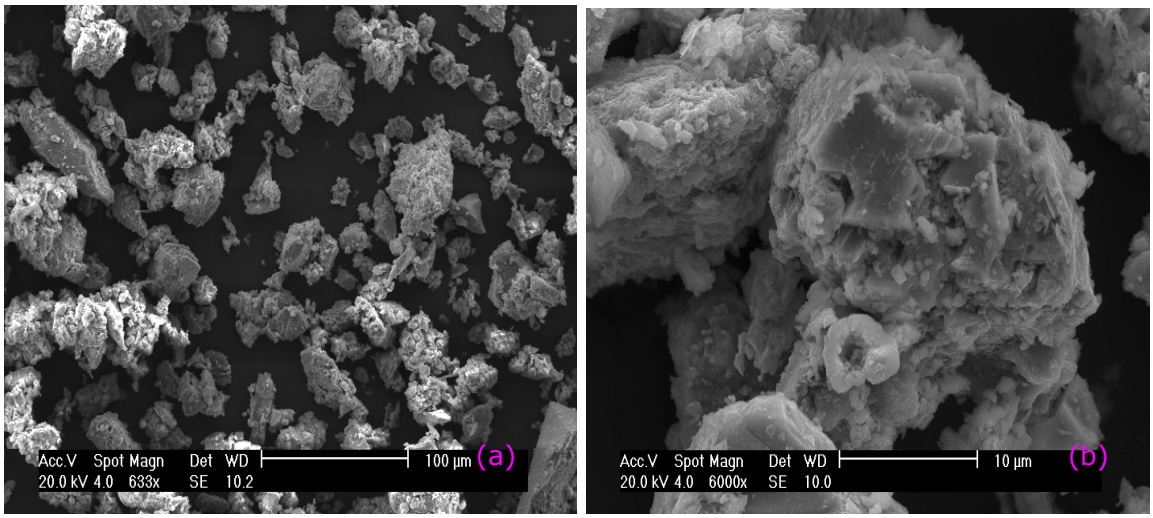

Figure 111: Scanning electron microscope (SEM) photomicrograph of the iron ore airborne particulates produced from a feed of (a) -9.5mm/150g, Magnification x 633, scale 100 µm. Iron oxide aggregates are present ;(b) -3.35mm/150g, Magnification x6000, scale 10 µm. Platy hematite particles are shown.

7.10.Conclusions

The dust generation potential of iron ore produced under abrasion and impact was assessed using the HSE-WSL test and the impact test. These two experimental techniques aimed to simulate common processes found in Hamersley Iron works, which could generate high rates of dust such as drilling and blasting, loading and unloading (i.e tipping, stockpiling), transporting activities (conveyor belts, haulage roads), comminution and others.

Dustiness testing took place for two testing protocols, which used different operational parameters and for various test fractions (<9.5mm. <3.35mm and <1mm). The OPT-TP yielded higher dustiness for all of the test samples with the coarser fraction (<9.5mm) resulting in the highest dustiness levels during both testing regimes. Tumbling time was considered the parameter that has the most influence on dustiness with a positive correlation. Also it was concluded that high concentrations of fines in the test sample resulted in lower dustiness, which suggests that abrasion mechanisms taking place in the drum influence the iron ore increasing its potential to generate dust.

The moisture content measurements indicated that when higher abrasion rates and operational times are utilised a greater dust yield is produced. It is possible therefore that increasing the moisture of iron ore could reduce the emission potential of particulates. Namely, dust control as well as water and energy consumption will have to be increased to minimise dust. However, it is possible to minimise the generation of particulates by reducing abrasion in processes such as conveyor belts, sieves, haulage roads and mill as well as the time consumed in an operation through alternative equipment design and optimisation practices. This solution could be beneficial for the processing of iron ore, as it will reduce the production of fine material and the mitigation practices in use.

The particle size distribution results for the dust fractions collected by the HSE-WSL test have shown that for the optimum parameters regime dust particle size and dust yield behave inversely proportional. Therefore the <9.5mm sample which resulted in higher quantities of particulates produced a coarser particle size than the lower dustiness index samples. For the HSL testing protocol, the various iron ore fractions produced similar dust particle size distributions. According to the results, around 51.56% and 11.22% (average values) of the dust particles were below 10μm and

2.5μm which suggests that the particle size of iron ore dust generated by abrasion might have adverse effects on human health and the environment

Experimentation with the impact test took place for a range of single size fractions of iron ore, sample masses (bulk volumes) and energy input levels. Results indicate that an increase in the energy input gives rise to a finer particle size distribution and a higher accumulation of fines below 53μm. Also, the generation of fines was affected by the sample mass and the particle size of the test sample. Hence the use of a larger volume of sample always produced greater percentages of fine particulates (<53μm), whilst the various test fractions exhibited a different propensity to generate fines at different energy input levels. The impact test outcomes indicate that industrial processes such as drop from heights, haulage roads, loading, stockpiling and others, which can generate dust due to impaction, could reduce or keep particulates in a safe limit by adjusting the sample volume and the energy input so as to reduce the production of fines.

Particle size measurements on the fine fraction (<53μm) produced by impact, revealed that the particle size distributions from the coarse test fractions are identical. On the other hand the particle size distribution for the smaller size test samples (4x3.35mm and 2x1.7mm) and at high energy input levels are found to be significantly finer. Sample mass also influenced the particle size of the fine particulates produced although the differences were not significant. The particle size of the <53μm particles produced by the impact test were coarser than the results obtained by the HSE-WSL test. However, the impact test did not capture the airborne dust fraction.

The mineralogy of the dust fraction was found to be similar to the feed iron ore consisting mainly of hematite and goethite. The generation of high dust rates are associated with loss of valuable material, whereas human exposure to iron ore particulates could cause serious illnesses such as pneumoconiosis (siderosis).

Chapter 8. Experimentation with Argyle Diamonds lamproite

8.1. Introduction

The diamondiferous lamproite ore is located in Kimberley area of Western Australia. Each year approximately 80 million tonnes of ore are extracted and processed to recover the diamonds, which do not exceed the 6 tonnes leaving a substantial quantity of waste rock. As a rock, lamproite comprises a quartz rich ore (more than 60% weight content) that during the mining and processing is liable to produce particulates. Also the generation of large volumes of waste material could result in secondary sources of dust and fines as well as to fugitive emissions. The high silica content of lamproite could be potentially hazardous to human health as the exposure to airborne particulate matter may cause silicosis, various other pneumoconiosis or cancer. In addition, dust could cause adverse effect to the soil, air and ecology of the area, whilst fines or silica rich dust could deposit on machinery causing wear.

This chapter explores the dust generation potential of lamproite under various mechanisms, which simulate the various industrial processes taking place during lamproite mining and processing. The lamproite samples were made available from the industrial sponsor of this project, Rio Tinto Technology group.

8.1.1. Experimentation steps

This chapter presents an analysis of the experimental results obtained during the assessment of the lamproite ore. The presentation and analysis of the results follows the experimental stages performed on the ore samples, which have been discussed in detail in Chapter 4 and are summarised below. Prior to results a brief review of the Argyle Diamonds geology, mining, processing, industrial applications and environmental practices is given.

Summary of the experimental processes followed.

- Mineralogical characterisation of the original rock samples by X-ray diffraction analysis. In addition the Mineral Liberation Analyser (MLA) was used to identify the modal mineralogy of the rock sample by quantitative means.
- The dust propensity (dustiness) of the lamproite ore was determined using the Warren Spring Laboratory (HSE-WSL) rotating drum test. During a specific run of the test, the dust fraction was collected for further analysis.
- The particle size of the dust fraction collected during the rotating drum test was measured by laser diffraction analysis using the Malvern Mastersizer – S.
- The dust generation potential of the lamproite ore was also assessed using the modified JK impact test. The relationship between the dustiness and the energy input was established.
- The fine fraction (below 53μm) produced during impact testing was collected by sieving and its particle size was determined by laser diffraction analysis using the Malvern Mastersizer-S.
- The mineralogical profile of the particulates produced by the HSE-WSL test and the impact test was identified by X-ray diffraction analysis, whilst the modal mineralogy of the dust fractions by quantitative means was determined using the Mineral Liberation Analyser (MLA).

Following an analysis of the results obtained from the above experiments, conclusions were drawn upon the propensity of lamproite to generate dust under various mechanisms, which simulate the various transport and processing operations taking place at Argyle Diamonds mine.

8.2. Arglyle lamproite - History, geology and industry

The Argyle (AK1) diamond pipe and its associated alluvial deposits are located in the East Kimberley region of Western Australia, 100 km south of Kununurra (Harben and Bates 1990). The Argyle mine was established and started working in 1985 (Argyle Diamonds 2005;Karpin 1993).

Each year approximately 80 million tonnes of material is extracted. The plant processes approximately 10 million tonnes of ore and it produces around 30 million carats (equivalent to 6 tonnes) of diamonds. Good quality diamonds are used as gem stones, whereas less pure diamonds are used in industrial applications. (Argyle Diamonds 2005).

The Argyle diamond pipe is elongated in plan, 2 km long and 150 to 1500 m wide (Boxer and Jaques 1990). The pipe consists of a thick series of nearly flat-lying sedimentary and volcanic rocks that were deposited between 1.6 to 1.9 billion years ago, which form the Kimberley plateau. The basement of the pipe comprise of crystalline igneous and metamorphic rocks, which are not exposed on the surface of the plateau (Argyle Diamonds 2005;Boxer & Jaques 1990). The Argyle host rock is a lamproite, which is defined as a potash and magnesia rich lamprophyric rock or volcanic of hypabyssal origin belonging to the ultrapotassic rock series (Harben & Bates 1990). The lamproite ore is bluish grey and it is composed of variable amounts of lapilli and ash fragments of olivine lamproite set in a matrix of lamproite ash and abundant (up to 80% in volume) well rounded quartz grains and fine lithic fragments of disaggregated country rock (Argyle Diamonds 2004). Common minerals present in lamproite include quartz, altered olivine (now mainly talc), clinopyroxenes (diopside), phlogopite, orthopyroxene, sanidine as well as clay minerals, produced due to weathering, such as chlorite, serpentine, and talc (Boxer & Jaques 1990;Harben & Bates 1990).

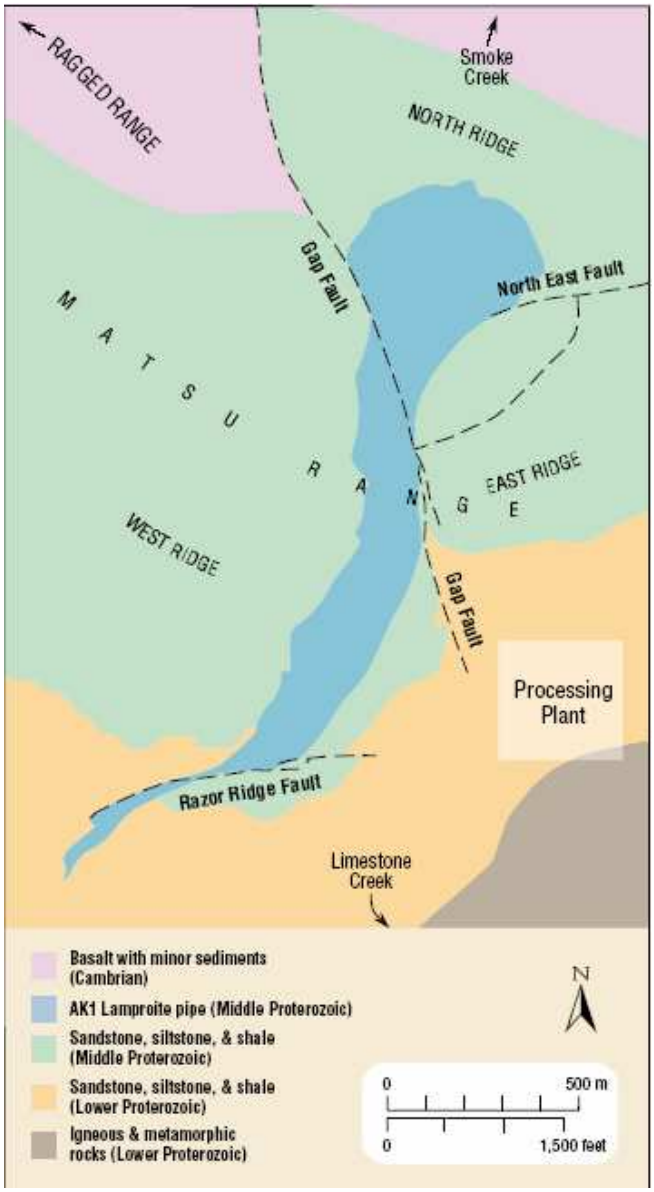

Figure 112: The Argyle (AK1) diamond pipe (Argyle Diamonds, 2004)

8.2.1. Mining and processing of lamproite

Mining of the lamproite ore takes place in open pit mines. Ore is broken by the use of explosives and excavators load the rock into haul trucks (average capacity of 200 tonnes). Subsequently, the diamond bearing ore is transported 2.5 km to a primary crusher. The unwanted overburden is deposited on the perimeter of the pit and represents almost 7 times the volume of the diamondiferous ore. The remainder (about 60% of the volume excavated) is returned immediately to the area being mined. At the alluvial plant, ore is scrubbed, screened and gravity-separated. The resulting concentrate is then transported to the AK1 process plant for final diamond recovery (Argyle Diamonds 2005;Karpin 1993).

Argyle also mines alluvial stone which tends to be a higher quality ore than those from the open pit, as the transport processes can break up lower quality diamonds. An excavator removes diamond bearing gravel from the alluvial mining face, which is directly screened into a mobile screening unit. The reduced volume is then hauled to the alluvial processing plant for additional treatment (Argyle Diamonds 2005;Reeves 1993).

Processing of the ore takes place into three principal steps, the feed preparation, the heavy medium separation and the diamond recovery (Hutton 1993). The mined ore from the open pit goes through the primary crusher, which is reduced to a size below 250 mm. An average of 2,500 tonnes of ore is tipped into the primary crusher each hour. Crushing continues through a secondary crusher and the broken material is then conveyed to the 10,000 tonnes capacity primary stockpile. Subsequently the ore is transferred to a high pressure roll crusher where its maximum size is reduced to 30mm. Ore then undergoes through several scrubbing and screening steps, where it is separated into three sizes. The oversize material (above 18 mm) is further reduced, whereas the undersize material (<3mm) is rejected to tailings dump. The -18+3mm is conveyed to a heavy media separation plant feed stockpile. The lamproite ore is then passed through a hydrocyclone separations plant, where the lamproite ore is separated from the heavy minerals and diamonds, which they sink to provide a diamond rich concentrate. The diamond concentrate passes through a series of custom designed X-ray sorters. Diamonds are detected by sensors as they fluoresce when exposed to X-rays, which are collected through an air blowing system. Subsequently the diamonds are acid-cleaned, washed, weighed and transferred to the final sorting and sale facility in Perth (Argyle Diamonds 2005;Hutton 1993). The processing of lamproite can be reviewed in detail in Figure 113.

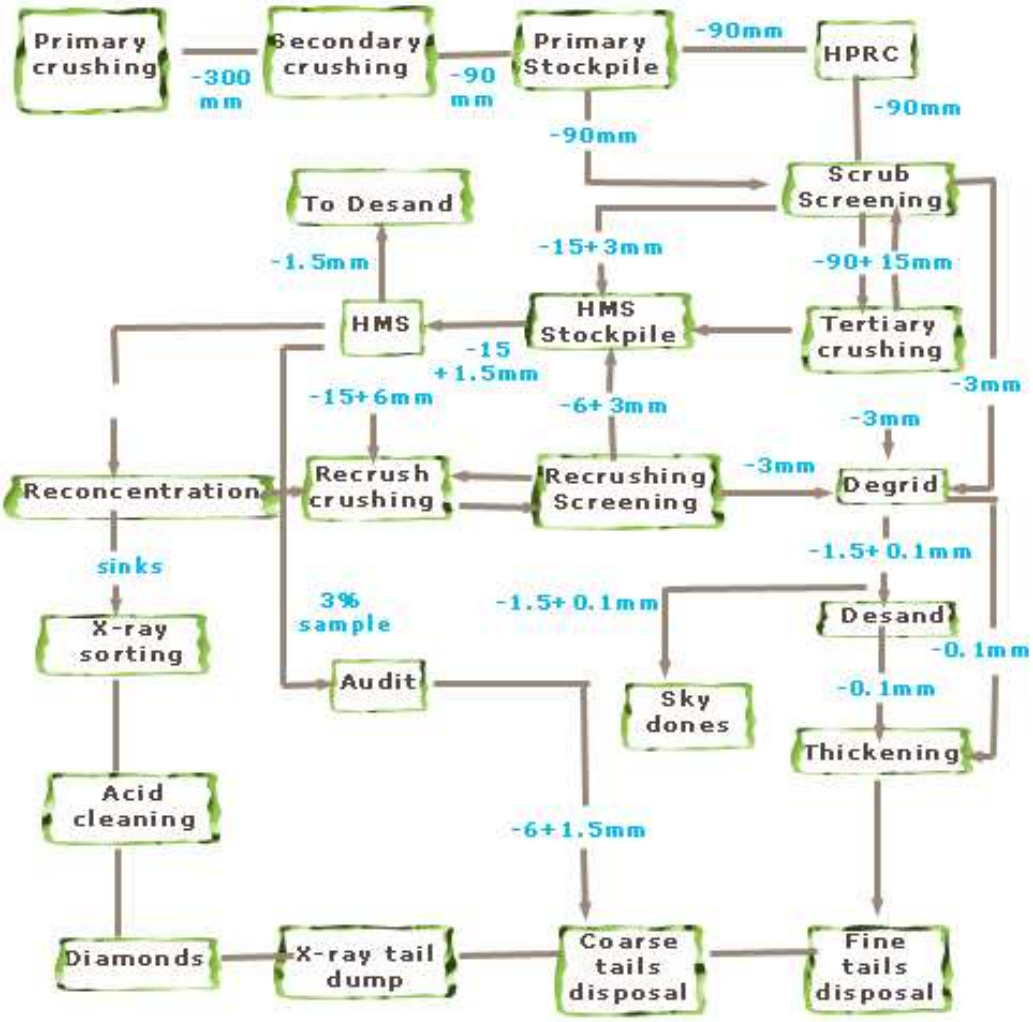

Figure 113: Processing steps followed for the lamproite from Argyle mine (Argyle Diamonds, 2004).

8.3. Particulate matter emissions from lamproite mining and processing

Dust is a constant environmental, and health and safety problem within the Argyle diamond mining and processing operations (Stanton-Hicks and Newman 2005). The continuous mining process, as well as the scale of the operation, are some of the main reasons for the particulate matter emissions.

Dust is generated by drilling and blasting, loading and dumping, transporting, crushing, screening and stockpiling. The very dry and hot weather conditions during

the summer months produce high background emissions that can overcome upper levels and they reduce the capacity of the mitigation techniques in use. Also the vast amount of waste rock deposited in stockpiles in the periphery of the mine can potentially comprise a secondary dust source, as they generate particulates by air blowing.

In order to reduce and control dust, mitigation and monitoring techniques are employed such as dust suppression, haulage roads watering, enclosures and dust collection systems. As being part of Rio Tinto Group, it utilizes their internal air quality standards, whereas monitoring takes place to quantify ambient dust levels. Argyle diamonds recognises innovation and a good example relevant to dust was the suggestion that molasses produced during the sugar making process could be applied to haulage roads to eliminate airborne emissions. Currently environmental monitoring takes place to ensure than no adverse effects result. This innovation is believed to reduce the cost in water and chemicals used for dust suppression.

By employing the implemented mitigation and innovation practices they manage to minimise dust levels. Nevertheless, dust emissions remain an issue for Argyle, whilst mitigation practices increase the cost of processing and mining. Airborne emissions can affect the human health and the environment. Therefore, any alternative suggestions that can reduce the generation of dust are considered. This research project intends to make alternative solutions that can result to the reduction of dust.

8.4.Mineralogical characterisation of the lamproite

The mineralogy of the lamproite rock samples was identified by X-ray diffraction analysis, as well as by mineral liberation analysis. This latter method comprises a quantitative analysis tool of the modal mineralogy of the sample.

X-ray diffraction – whole rock analysis of the lamproite ore took place for 10 different representative samples prior to the performance of the dustiness test, which was produced following the procedure described in Chapter 4. The XRD traces were identical for each of the samples and an example of two of them can be seen in Figure 114. It was concluded that the lamproite consists of several different minerals including quartz, clinochlore (a chlorite group mineral), illite (a clay group mineral), orthoclase (a K-feldspar), ankerite and sericite (a fine grained mica). According to

the resultant intensities patterns, quartz was the most dominant mineral in each of the samples, but for any of the other minerals it was difficult to determine from the XRD patterns, whether they comprise a major or minor phase.

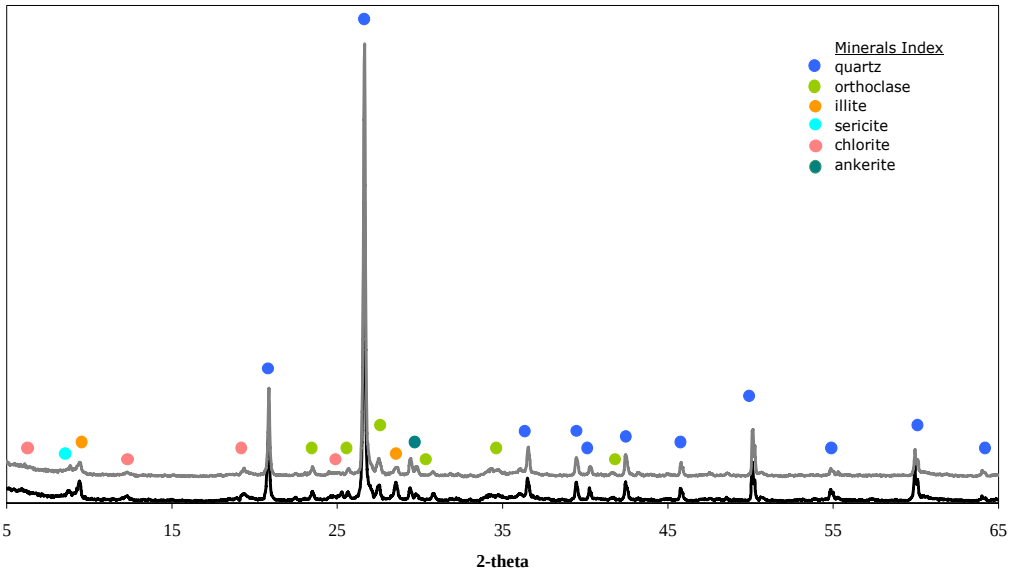

Figure 114: The XRD traces of the lamproite rock samples (two-theta, whole rock analysis).

In order to determine the participation percentages of each mineral in the composition of the whole sample, the mineralogy of the lamproite ore was quantified using the Mineral Liberation Analyser system of the scanning electron microscope and energy dispersive X-ray microanalysis system. Two fine-grained samples of the lamproite ore were prepared in polished blocks following the method presented in Chapter 4. The measurement mode used for this research project was the Extended BSE (XBSE) liberation analysis, which collects an X-ray spectrum for each mineral grain. Further information of the measurement steps of the XBSE liberation analysis method can be reviewed in Chapter 4.

From each polished block an average of 15,200 particles were measured and the various different mineral phases were identified. The modal mineralogy of lamproite ore expressed in mineral weight percentages is displayed in Table 64. The minerals quartz, illite and chlorite participate in considerable quantities in the matrix of lamproite, subsequently they represent the major minerals, whereas sphene, ankerite, sericite, orthoclase and pyrite are less significant and they comprise the minor mineral phases of the ore. Quartz participates in a weight percentage approximately equal to 50%, whereas illite which is the second more common

mineral in lamproite is associated with the quartz grains, representing its alteration product (Figure 115). The two different samples (feed 1 and feed 2) produced very similar results, which indicate the reproducibility of the measurement. Figure 115 displays one of mineral liberation analysis frames that correspond to the lamproite particles including reference to the different mineral phases. In detail presentation of the modal mineralogy results can be reviewed in appendix V.

Table 64: The modal mineralogy results of the lamproite ore obtained by the mineral liberation analyzer system (XBSE analysis method).

Mineral list	Mineral weight (%) Feed 1	Feed 2
Sphene	3.77	3.04
Quartz	47.73	48.47
Pyrite	0.32	0.11
Ankerite	1.94	2.19
Chlorite	16.01	16.43
Sericite	1.85	1.37
Orthoclase	1.35	1.13
Illite	27.03	27.25
Total	100.00	100.00

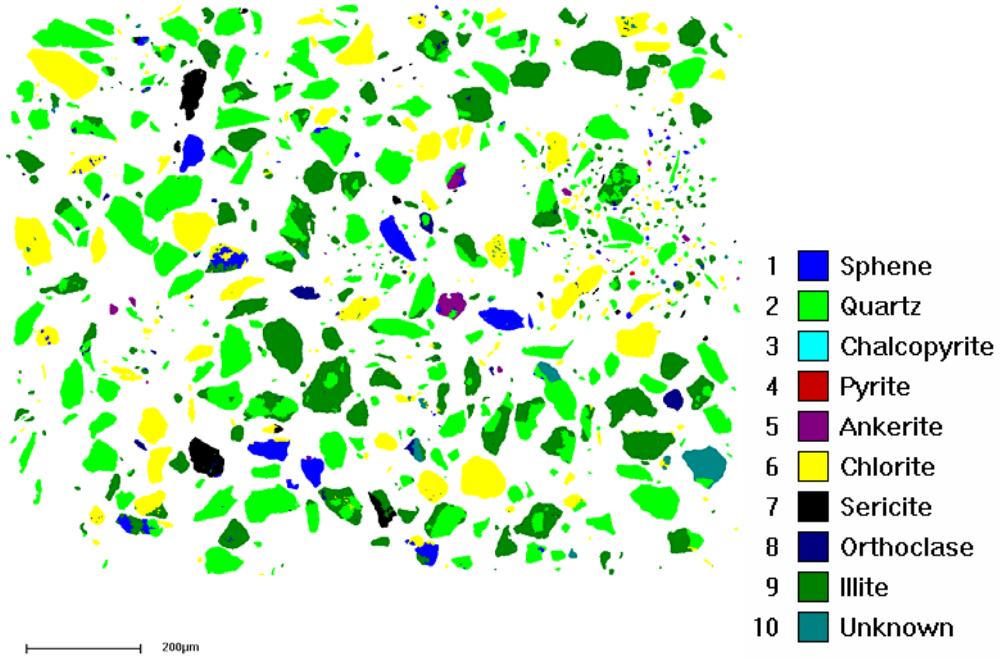

Figure 115: A frame of the mineral liberation analysis results obtained using the XBSE method. The various minerals of the lamproite are presented with different colours. In many cases a particle consists of more than one mineral phases. Magnification X350, scale 200µm

8.5. Determination of the dustiness of lamproite using the HSE-WSL rotating drum test

The dust generation potential of lamproite under abrasion mechanisms was evaluated using the HSE-WSL rotating drum dustiness test. The abrasion mechanism produced by this test simulates many common handling and mining processes, such as transfer processes in conveyor belts, grinding mills, mixers, haulage roads, sieves and other. Experimentation took place using two different testing regimes and various size fractions and the results are presented in the following paragraphs.

8.5.1. Dustiness measurements

The dustiness was determined for three different size fractions of the lamproite ore, namely for particles of size ranges less than 9.5mm, 3.35mm and 1mm. The particle size distributions of the lamproite feed samples (200g and 150g) of the <9.5mm, <3.35mm and <1mm were determined by sieving and the results are presented in Figure 116. The particle size distribution of the fraction below 9.5mm exhibits the coarser profile followed by the fractions below 3.35mm and below 1mm.

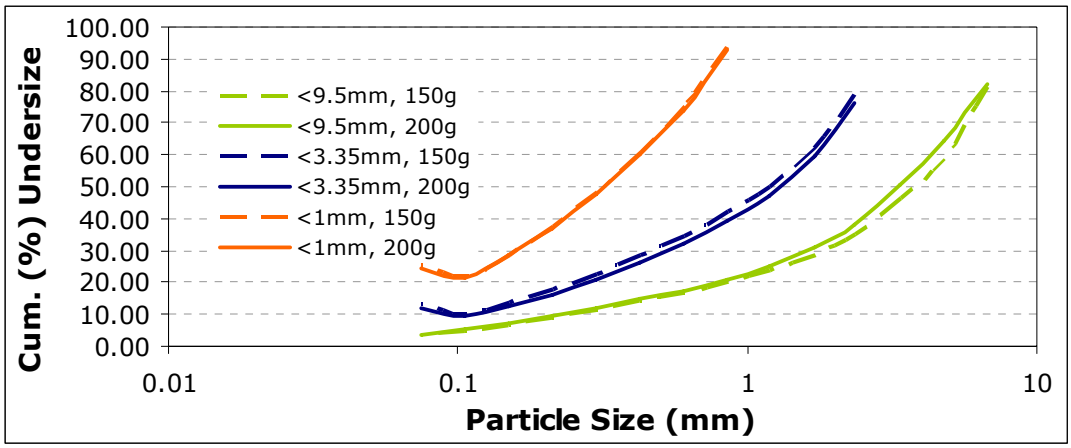

Figure 116: Particle size distributions of the lamproite feed samples <9.5mm, <3.35mm and <1mm.

8.5.1.1. *Presentation and analysis of the dustiness measurements results*

The dustiness results obtained for the lamproite ore during testing with the HSE-WSL test can be reviewed in Table 65 and in appendix V. The results presented in Table 65 correspond to average values of triplicate tests. The reproducibility of dustiness

measurements is reflected by the standard deviation and relative standard deviation values (Table 65).

Table 65: Dustiness results of the lamproite samples obtained for both testing protocols. The standard deviation and the relative standard deviation (% RSD) reflect the reproducibility of the replicate tests.

Lamproite fractions	HSL procedure			Optimum operating parameters procedure		
	Dustiness (%)	Standard deviation	(%) RDS	Dustiness (%)	Standard deviation	(%) RSD
< 9.5mm	0.1024	0.013	12.70	0.2460	0.028	11.50
< 3.35mm	0.1160	0.010	8.77	0.2653	0.026	9.66
< 1mm	0.1383	0.011	7.97	0.2074	0.019	9.20

In respect with the statistical analysis results displayed in Table 65, during experimentation with the lamproite ore an average standard deviation of 0.018 and a relative standard deviation of 9.97% should be expected.

The two different testing protocols employed, produced a wide spread of dustiness values which range from 0.1024% to 0.2653%. The OPT-TP gave greater dustiness values for any of the test fractions tested, (on average 2.1 times higher than the HSL testing regime).

An analysis of the HSL-TP data concluded that the highest dustiness values were achieved for the <1mm sample followed by the <3.35mm and <9.5mm samples. Hence, the finer the sample fraction is, the higher the dustiness. For the OPT-TP, the <3.35mm sample produced the higher dustiness value followed by the <9.5mm and the <1mm sample. Thus, when tumbling time is extended from 1 (HSL-TP) to 3 minutes (OPT-TP), then the dustiness ranking of the samples exhibits a different profile. As a general conclusion, the extended tumbling time of the OPT-TP produced a greater quantity of airborne particulate matter, although the mass of lamproite used for testing was less (150g instead of 200g).

The concentration of fines in the test sample might be a parameter of influence of the dust generation process. Figure 117 displays the cumulative weight percentage of particles below 75μm versus the dustiness values of the various test fractions. During testing with the HSL-TP, the proportion of fine particles in the test sample correlate positively to dustiness. For instance the highest concentration of fines in the test sample was found in the <1mm sample, which also produced the greatest dustiness value.

However for longer tumbling times (OPT-TP), the above statement is not true. For these tests, the higher concentration of fines was again found to be for the <1mm sample, which produced the lower dustiness value. The highest dustiness value was determined for the <3.35mm sample, which comprise a lower cumulative percentage of particles below 75μm in comparison to the <1mm sample (13.01% instead of 25.70%). These results suggest that for longer tumbling times, the abrasion mechanisms taking place in the drum affect the particle fractions <3.35mm and <9.5mm, producing finer particulates and hence higher dustiness values. This is not the case though for the <1mm sample, as smaller size particles requires greater amounts of energy to degrade them, which the tumbling mill does not provide.

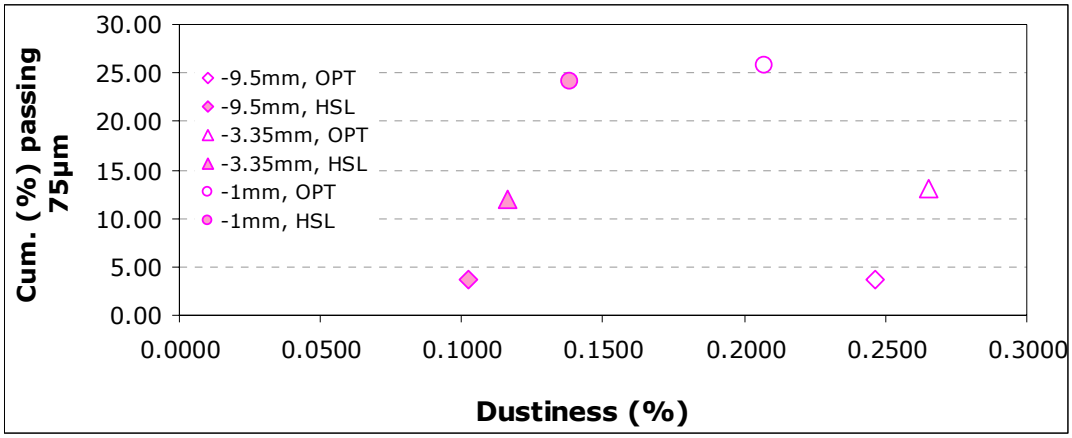

Figure 117: Dustiness result of the lamproite fractions versus the proportion of fines in the test sample (HSL: corresponds to the HSL-TP, OPT: represents the OPT-TP)

Consequently the dust generation potential of lamproite in processes that involve abrasion mechanisms (i.e the use of conveyor belts) will depend upon the time the operation runs for, whereas extended time consumed in a process will tend to produce higher dustiness levels as ore particles will start to be affected by abrasion.

8.5.1.2.*The effect of moisture content upon lamproite's dustiness*

The moisture content of the lamproite ore test fraction was determined following the British standard BS812-109:1990 (BSI 1990). The experimental steps can be reviewed in Chapter 5. The moisture content of the finer fraction (<1mm) exhibited the lower value equal to 0.32%, whilst the <9.5mm sample produced the higher value equal to 0.67%.

For the HSL-TP, samples with low moisture content produce high dustiness. Hence the <9.5mm sample that exhibits uppermost moisture content (0.67%) generated

the lowest dustiness level (0.1024%). However, during testing with the optimum parameters procedure dustiness behaves independently of the moisture content and this is why for instance the high moisture content sample produced uppermost dustiness. In order to minimise or control the generation and emission of particulates at increased operational times the moisture content of the lamproite ore should be kept in higher levels.

Table 66: The moisture content (%) of the lamproite ore test fractions in relation to dustiness (%) (average values) from the two testing regimes.

Sample	Moisture content (%)	Dustiness (%) HSL testing procedure	Dustiness (%) Optimum parameters procedure
<9.5mm	0.67	0.1024	0.2460
<3.35mm	0.58	0.1160	0.2653
<1mm	0.32	0.1383	0.2074

8.5.1.3. *Determination of the health based dustiness indices*

The health based dustiness indices of the inhalable (Di), thoracic (Dt) and respirable (Dr) fractions for the lamproite ore were also determined using the HSE-WSL test. The inhalable fraction dustiness index is equivalent to the total dustiness values presented in the previous paragraph. The determination of the thoracic and respirable dustiness indices are displayed in Table 67 and in appendix V. In addition to the derived health based dustiness indices, Table 67 also presents the standard deviation values, which have been calculated from a set of three independent sample tests. A variety of dustiness indices have been determined, thus the thoracic fraction (Dt) ranges from 4.6945% to 11.3630%, whilst the respirable fraction (Dr) vary from 0.0866% to 1.7860%.

Following an analysis of sample data obtained from the ore of the optimum parameters protocol it was concluded that the test fractions <3.35mm and <1mm produced higher dustiness indices of the thoracic and respirable fractions. Namely the increased dustiness levels achieved during testing with the OPT-TP, also resulted in producing higher concentrations of dust in the thoracic and respirable fraction. This is not the case for the <9.5mm test sample, which produced the highest thoracic and respirable dustiness indices during experimentation using the HSL-TP.

For the HSL–TP the dustiness index of the thoracic fraction of the <9.5mm and <3.35mm samples is higher for the finer fraction (<3.35mm), whereas the <1mm

sample exhibits the lowest index. The respirable dustiness index obtained uppermost value for the <9.5mm sample, followed by the <1mm and <3.35mm samples.

For the OPT-TP the dustiness indices of the thoracic and respirable fraction increase in respect to the fineness of the test sample. Therefore the <9.5mm sample produced the lower thoracic and respirable fraction dustiness index, whereas the <1mm sample produced the highest values.

Table 67: Health based dustiness indices of the lamproite samples (both testing protocols). One standard deviation has been calculated from replicate tests.

HSL protocol	Lamproite fractions		
	<9.5mm	<3.35mm	<1mm
D_t (%)	5.9642	6.4797	5.2640
Standard deviation	2.243	0.3571	1.499
D_r (%)	1.7860	0.1341	0.2411
Standard deviation	0.411	0.061	0.118
Optimum parameters protocol			
D_t (%)	4.6945	7.0170	11.3630
Standard deviation	1.820	1.233	2.458
D_r (%)	0.0866	0.2569	0.3422
Standard deviation	0.042	0.117	0.148

In general the proportion of particles that fall within the thoracic and respirable fraction for some of the test samples (e.g. <1mm/ OPT-TP) is significant, which suggests that the lamproite particulates could pose a threat to human health. The health based classification method of the HSE-WSL test represents a valuable tool when the research interest focuses on the adverse effects of dust to human health. However, classification of dust can be more accurate and detailed by particle size analysis.

8.5.2. Summary of the dustiness analysis results

The dustiness of lamproite ore was assessed by two different testing procedures (HSL-TP and OPT-TP) and for various test fractions, namely for samples below 9.5mm, 3.35mm and 1mm.

Dustiness testing with the HSE-WSL apparatus showed that higher values were recorded using the OPT-TP, which suggests that tumbling time is the parameter that mainly affects the dust generation potential of lamproite.

It is concluded that the greater the proportion of fine particles (<75μm) in the test sample, during testing using the HSL-TP, the higher the dustiness index. However, the application of the OPT-TP, namely the longer tumbling time, alters the above relation. This is because increased abrasion mechanisms are enabled during longer tumbling of the lamproite particles in the mill. In particular for the coarse test fractions (<9.5mm, <3.35mm), this results in higher concentrations of fine particulates and dust. For the fine test sample (<1mm) greater energy levels would be required to degrade the sample, which are not provided by the HSE-WSL mill, concluding to lower dustiness.

The UK Health and Safety Laboratory scales the dustiness of materials from not dusty to extremely dusty (Chung and Burdett 1994) (Table 26). The lamproite ore samples were categorised using this scale and the results are presented in Table 68. In detail, the outcomes of the various lamproite ore fractions and testing protocols, expressed in dust yield per filter, including a standard deviation from replicate tests can be reviewed in appendix V.

Table 68: Classification of the dustiness results for the lamproite samples as proposed by HSL

Testing procedure	Lamproite fractions	Dustiness (%)	Classification
HSL procedure	< 9.5mm	0.1024	dusty
	< 3.35mm	0.1160	dusty
	< 1mm	0.1383	dusty
Optimum operating parameters procedure	< 9.5mm	0.2460	dusty
	< 3.35mm	0.2653	dusty
	< 1mm	0.2074	dusty

In conclusion, the lamproite is liable to generate dust due to abrasion, whilst operational parameters, such as the utilized operational time intervals could also affect the dustiness profile of the ore. Therefore minimisation or control of the dust generation process could be achieved by reducing or optimising the abrasion rates and time the ore spends in a particular operation or industrial processes such as conveyor belts, sieves, mills and others.

8.6. Particle size analysis of the lamproite ore particulate matter fraction generated by the HSE-WSL test

The particle size of dust collected using the HSE-WSL mill, was determined by laser diffraction analysis using the Malvern Mastersizer-S and the results are presented in the following paragraphs.

8.6.1. Selection of the optical properties of the lamproite particulate matter

Similar to any of the ores presented so far, the Mie approximation was selected as the appropriate optical model for particle size analysis using the laser scattering method. The effect that different optical properties have upon the particle size distribution results of lamproite can be seen in appendix V. So far the optical properties of the ores were determined through comparative studies. Nevertheless, the selection of the optical properties for the lamproite ore followed a different route. The mineralogical profile of lamproite has been quantified using the mineral liberation analyzer. The mineral weight percentages as well as the refractive index of each mineral can be combined to calculate a bulk refractive index (real part) of the ore. This calculation follows a similar logic to that presented in Chapter 5, where the two miscible liquids method was used to determine the optical properties of limestone particulates.

For many of the minerals the refractive index is not a specific value but a range of values. In that case a median value of the refractive index has been used. The refractive indices of the participated minerals and their mineral weight percentages measured earlier by the mineral liberation analysis are displayed in Table 69. The bulk refractive index was calculated by (Equation 24.

(Equation 24) $$RI_{(bulk)} = \sum RI_{(i)} x w_{(i)}$$

Table 69: The refractive indices of the lamproite ore minerals, as well as the mineral weight percentages determined by mineral liberation analysis.

Mineral	Refractive Index ($R.I_{(i)}$)	Mineral weight (%) ($w_{(i)}$)
Sphene	1.97	3.77
Quartz	1.54	47.73
Pyrite	1.81	0.32
Ankerite	1.63	1.94
Chlorite	1.63	16.01
Sericite	1.58	1.85
Orthoclase	1.53	1.35
Illite	1.57	27.03
Total		100.00

Hence the refractive index of the lamproite ore equals to the sum of the refractive index of each participating mineral multiplied by its mineral weight percentage. Consequently, the real part of the refractive index was calculated to be 1.59. The imaginary part of the refractive index was kept at 0.1 as it fitted well with the results obtained for the lamproite particulates. Thus any particle size analysis results presented later in this chapter utilized as optical properties of the lamproite particulates a real refractive index of 1.59, an imaginary index of 0.1 and a dispersion medium index of 1.33 (for water).

8.6.2. Particle size analysis results

The particle size distributions of the lamproite dust fractions collected by various size fractions of test sample and testing protocols are presented in Figure 118. These results correspond to average values that have been calculated by triplicate samples and following several repeatable measurement steps. The measurement sequence has been described in detail in Chapters 4 and 5.

The reproducibility of the measurements taken is assessed by the variation of the standard deviation and relative standard deviation values of the diameters d_{10}, d_{50} and d_{90} shown in Table 70. Additionally, the standard deviation of the triplicate tests can be reviewed in the volume (%) retained particle size distributions of the test samples shown in appendix V. Repeatable measurements taken for one sample (same feed) produced very accurate measurements with a relative standard deviation below 1%. For the triplicate samples, the reproducibility of the particle size measurement results was higher producing an average standard deviation of the d_{50}

diameter (for all fractions) equal to 0.35 and an average relative standard deviation of 4.99%.

Table 70 : The median values of the diameters d_{10}, d_{50} and d_{90} of the lamproite particulates produced using the HSE-WSL test, from a range of sample fractions (OPT-TP). The standard deviation and relative standard deviation values were calculated from the results obtained by the triplicate samples.

Sample Fraction	D_{10}	Stdev	RSD(%)	D_{50}	Stdev	RSD(%)	D_{90}	Stdev	RSD(%)
-9.5 mm	1.33	0.01	0.61	6.62	0.29	4.45	32.08	1.91	5.96
-3.35 mm	1.64	0.04	2.15	7.54	0.65	8.66	29.78	1.89	6.33
-1 mm	1.42	0.01	1.00	6.54	0.12	1.85	25.26	1.15	4.56

Figure 118 (a) displays the dust particle size distributions obtained during testing with the OPT-TP. The particle size distributions of the different test fractions do not present great discrepancies, although the results of the particulates collected by the <9.5mm and <1mm are slightly finer than the <3.35mm. Figure 118 (b) presents the particle size distribution of the dust fraction collected during testing with the HSL -TP. Hence the particulates of the <1mm sample exhibit the finer size distribution, followed by the results that correspond to the <9.5mm and the <3.35mm samples. The <3.35mm test sample in both testing procedures produced the coarser dust particle size distribution, whilst for the HSL-TP the sample that produced the higher dustiness levels, the <1mm, also possessed a finer particle size distribution.

The cumulative volume percentages under 10 and 2.5 μm of Table 71 exhibit similar trends with the above statements. Also they show that the OPT-TP for any of the test fractions resulted in higher volume concentrations of particles below 10 and 2.5μm and smaller particle size, as the d_{80} values are smaller. This is also justified by the dust particle size distributions resulted from the OPT-TP, which can be reviewed in Figure 119 and in appendix V. Therefore the higher tumbling time utilized by the OPT-TP as well as the increased abrasion rates produces not just higher dustiness, but finer particle size distributions, which could pose a threat to human health and the environment.

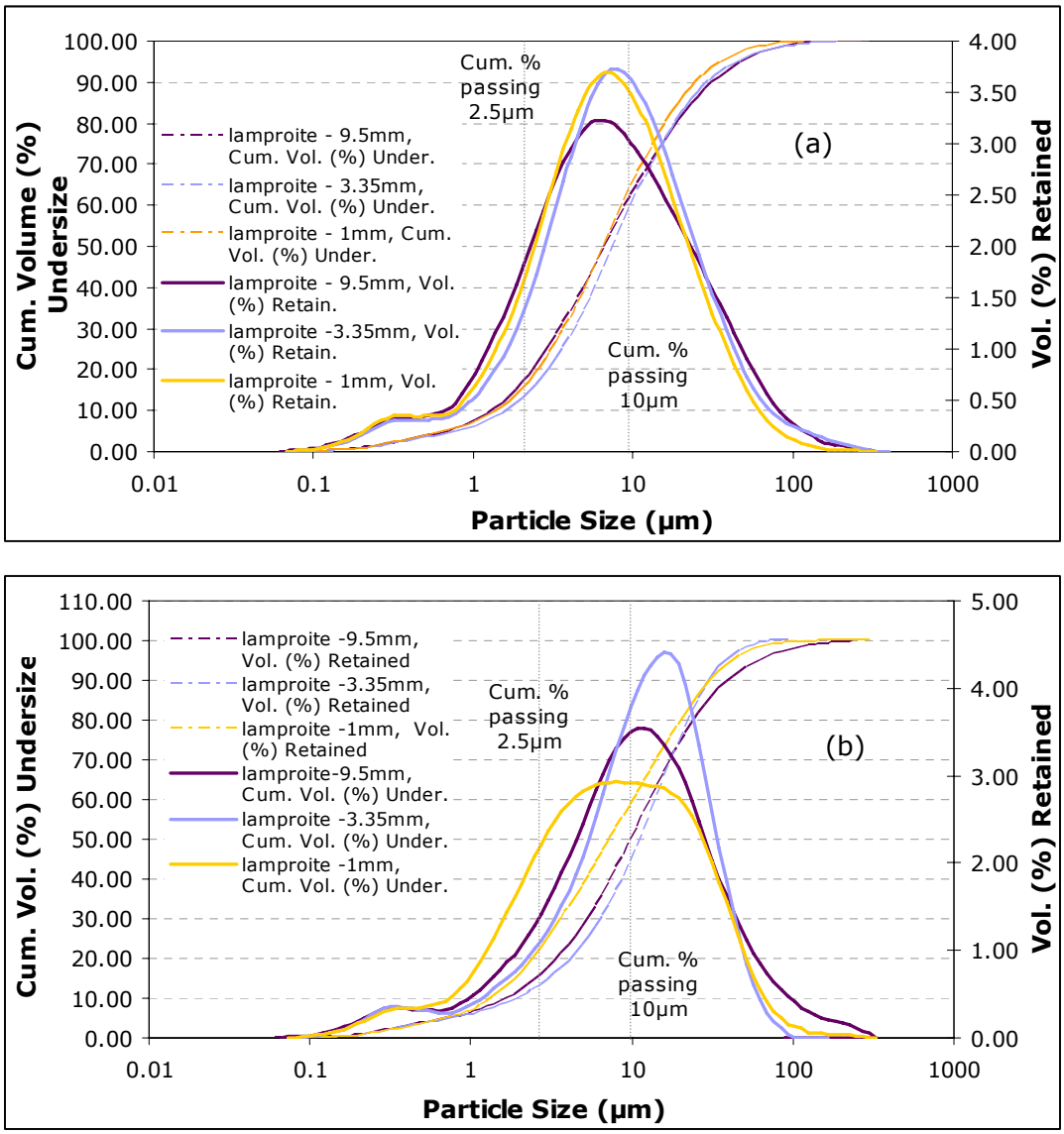

Figure 118: Particle size distribution of the lamproite particulate matter produced through (a) the OPT-TP and (b) the HSL-TP. The presented results correspond to average values of repeatable tests.

Table 71: Cumulative percentages passing 10μm and 2.5μm and the values of the diameter d_{80} for all samples and testing regime ((1): corresponds to the OPT-TP; (2) corresponds to the HSL-TP)

Lamproite fractions	Cum. % passing 10μm	Cum. % passing 2.5μm	D_{80}
-9.5mm (1)	63.18	20.97	18.96
-9.5mm (2)	50.57	14.55	24.33
-3.35mm (1)	60.73	16.19	18.40
-3.35mm (2)	45.34	12.39	22.31
-1mm (1)	65.63	19.25	15.93
-1mm (2)	59.30	20.46	20.41

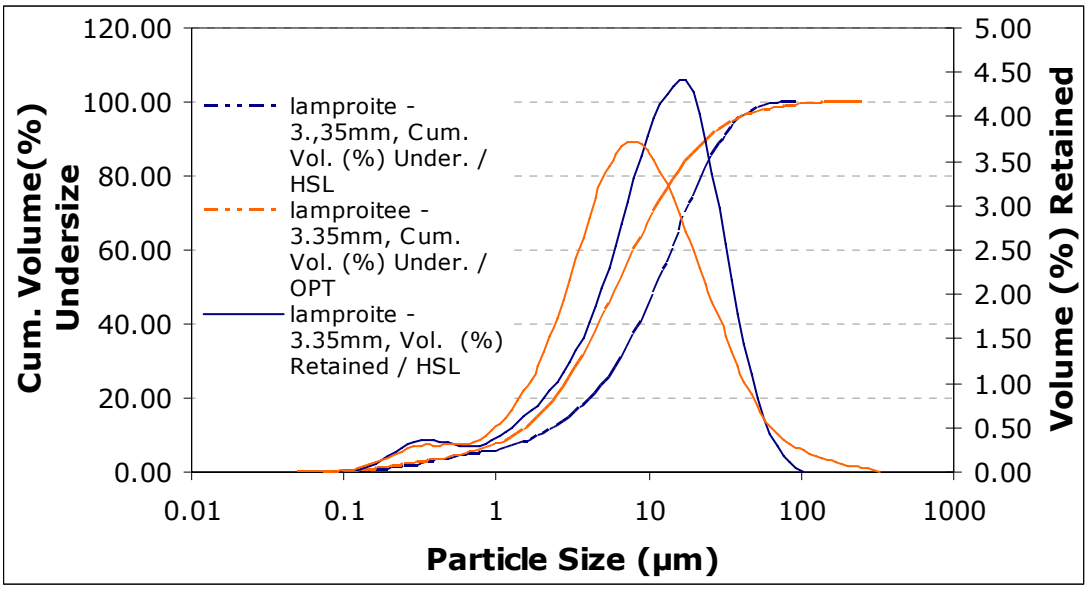

Figure 119: Particle size distribution results of the particulate matter produced by a lamproite feed fraction below 3.35mm and both testing protocols.

8.7.Experimentation using the impact test

The impact test was used to investigate the propensity of lamproite to generate dust and fines from industrial processes that require drop from heights such as loading and dumping, tipping, stockpiling and other. The results obtained are presented in the paragraphs to come

8.7.1. Determination of the residual height of lamproite particulates

The residual height of the lamproite particles left after impact is presented in Table 72. For any of the single size lamproite fractions, the lower the energy input, the larger the residual height (Table 72). Also for a specific energy level, the larger the size of the test sample, the higher the offset left (Table 72). The increase in bulk volume for a single fraction, for instance the increase of the 16x13.2mm fraction from 10% to 20% resulted to a greater offset value. This is the case for any of the single size lamproite fractions.

Similar to any of the ores presented so far, the required energy input levels were calculated on the basis of the residual height values recorded for limestone during primary investigations.

Table 72 displays the residual height values of limestone as well, whilst the lamproite offset values correspond to the final ones recorded after performing an impact test. The lamproite ore residual values obtained from the 20% bulk volume test sample is lower than that recorded for the corresponding limestone samples, whereas the 5% bulk volume test samples produced higher offsets. The required drop height for the lamproite ore was back calculated using the residual height values resulted after impact testing to determine the degree of discrepancy with the limestone offset values. These results can be reviewed in appendix V. Only very small differences in the required drop height values were observed, which indicates that the use of the limestone offsets gave a good approximation.

Table 72: The offset of limestone and lamproite particles; Limestone residual height has been used for the calculation of the release height for the lamproite ore samples.

	Residual height (cm)							
	16x13.2mm		8x6.7mm		4x3.35mm		2x1.7mm	
10% bulk volume	lamproite	Lim.	lamproite	Lim.	lamproite	Lim.	lamproite	Lim.
0.05 kWh/t	0.95	0.85	0.55	0.60	0.42	0.48	0.40	0.57
0.1 kWh/t	0.90	1.00	0.52	0.55	0.38	0.63	0.52	0.70
0.5 kWh/t	0.40	0.50	0.23	0.53	0.28	0.27	0.22	0.18
0.68 kWh/t	0.33	0.30	0.28	0.45	0.17	0.42	0.07	0.18
20% bulk volume								
0.05 kWh/t	1.19	1.67						
0.1 kWh/t	1.17	1.65						
0.2 kWh/t	1.16	1.37						
0.3kWh/t	1.13	1.08						
5% bulk volume								
0.05 kWh/t			0.20	0.13	0.20	0.02	0.10	0.02
0.1 kWh/t			0.30	0.13	0.20	0.02	0.05	0.00
0.5 kWh/t			0.10	0.00	0.10	0.02	0.10	0.00
0.68 kWh/t			0.10	0.00	0.20	0.00	0.10	0.00

8.7.2.The bulk density of the lamproite samples

For each single size lamproite test sample, two different bulk volumes were selected. The bulk densities of the test samples were determined and are displayed in Figure 120. The results correspond to the average values of three independent samples and the error bars represent one standard deviation (Figure 120). The bulk density of the various single size fractions exhibits slight changes for the different bulk volume percentages. Hence the bulk density of the 5%, 10% and 20% bulk volume test samples is 1.39 g/cm^3, 1.18 g/cm^3 and 1.19 g/cm^3. The bulk density of the 5% bulk volume samples is higher than any of the other samples because the smaller mass leaves fewer gaps between the particles. The preparation of three independent test samples resulted to small standard deviation values (<0.11), which suggests that the preparation method was adequate.

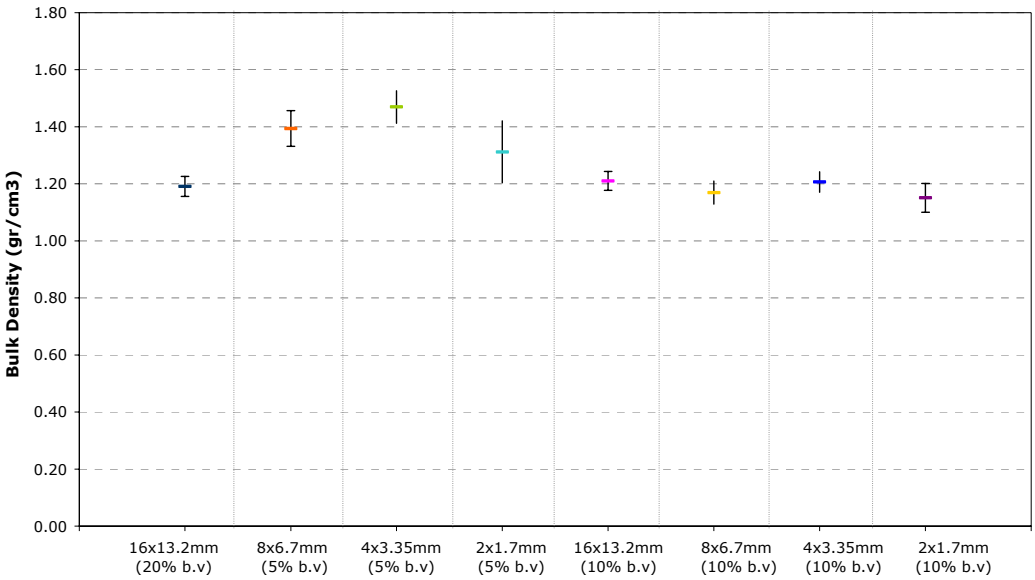

Figure 120: The recorded bulk density values of the lamproite single fractions. The vertical bars represent one standard deviation.

8.7.3. Impact Test - Results

Four different single size fractions (16x13.2m, 8x6.7mm, 4x3.35mm, 2x1.7mm) of the lamproite ore were tested using the impact test. The resultant particle size distributions are displayed in Figure 121. These results were obtained by performing sieve analysis on the broken lamproite particles. For any of the single size fractions and bulk volume percentages, an increase in the energy input produced a finer particle size distribution. The greatest difference in particle size distributions is noticed for energy levels 0.1 and 0.5 kWh/t, which exhibit the largest divergence than any of the other sequential energy inputs (Figure 121).

Following an analysis of the individual single size fractions, for the 16x13.2mm test sample, it was concluded that the increase in bulk volume from 10% to 20% did not produce any distinct differences to the particle size distribution of the comparable energy inputs, namely the 0.05 and 0.1 kWh/t. The decrease in bulk volume from 10% to 5%, for the 8x6.7mm, 4x3.35mm and 2x1.7mm test samples for any energy level, resulted in coarser particle size distributions. This suggests that during testing with the 5% bulk volume test samples energy is dissipated or transformed to other forms (i.e heat, sound) without causing further breakage to the particles. In addition the coarser particle size distributions indicate that interparticle contacts are fewer and thus attrition rates are lower for the 5% bulk volume test samples.

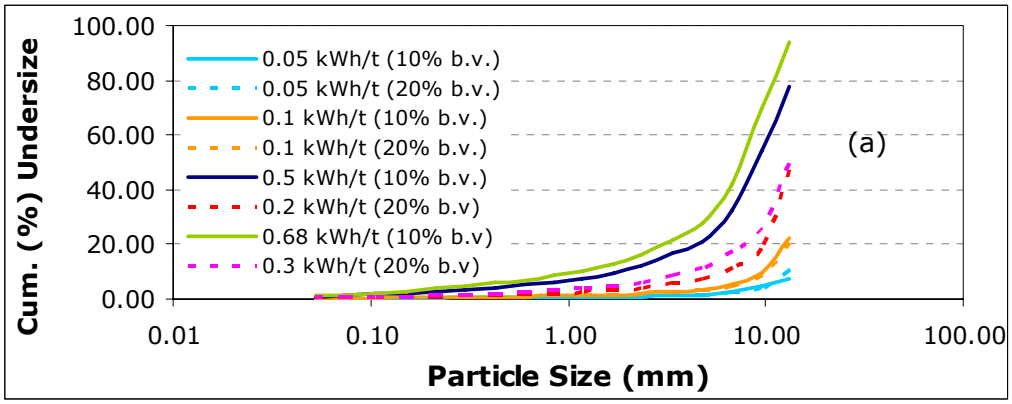

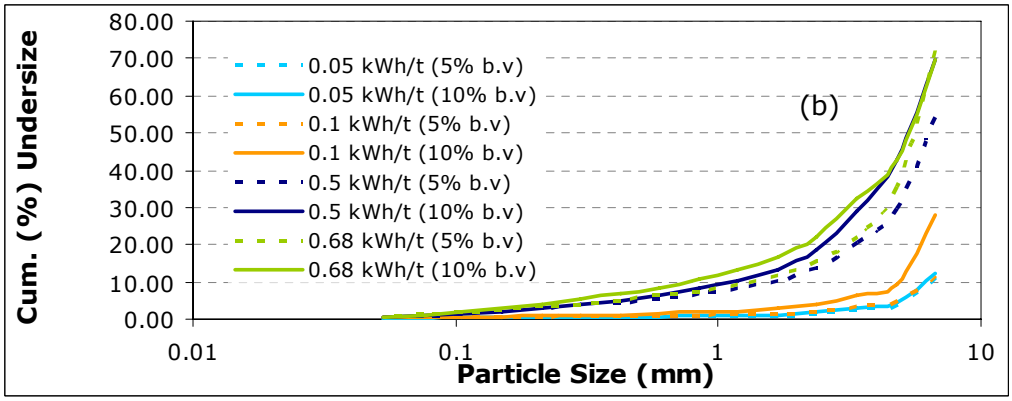

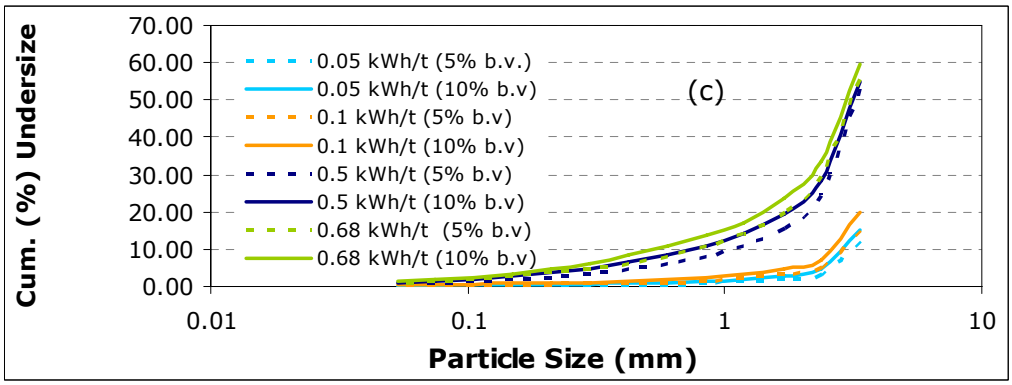

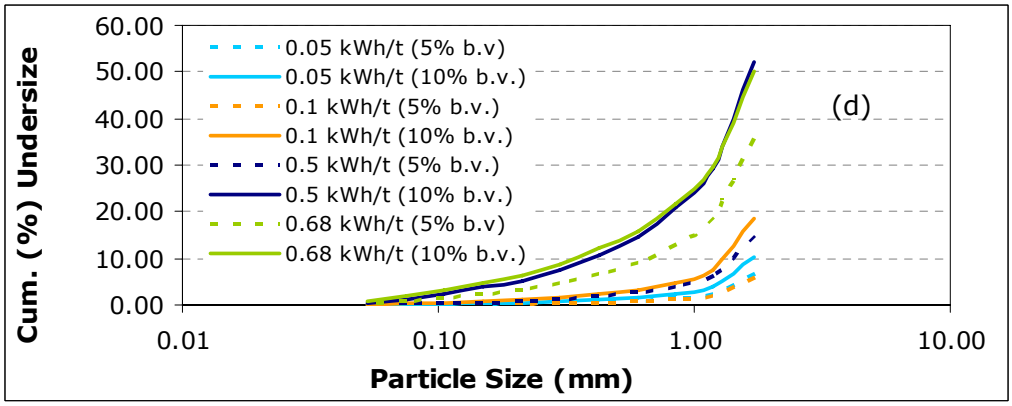

Figure 121: : Particle size distribution of the lamproite particles after impact for the single fractions (a) -16+13.2mm (10% and 20% bulk volume), (b)-8+6.7mm fractions (c) -4+3.35mm holder bulk volume) and (d)-2+1.7mm fractions, (10% and 5% bulk volume).

The greatest difference in the form of the particle size distributions measured for the different bulk volume test samples, correspond to the 2x1.7mm fraction and energy level 0.1 kWh/t and 0.5 kWh/t (Figure 121). The average ratio of the cumulative percentages undersize of the 10% and 5% bulk volume samples at 0.1 kWh/t and 0.5 kWh/t is 4.5 to one and 5.5 to one respectively, whilst at energy level 0.68 kWh/t this ratio is 1.8 to one. Consequently, breakage was increased for the 2x1.7mm fraction during the increase of bulk volume at energy levels 0.1 and 0.5 kWh/t. The other single size fractions did not exhibit such distinct differences in breakage for the various bulk volumes and energy levels used. Nevertheless, small discrepancies are present which indicate that slightly higher breakage rates could be achieved without unnecessary increase of energy and possibly with lower concentrations of fine particulates.

8.7.3.1. *The effect of impact upon fines generation for the lamproite ore*

The dust generation potential of lamproite under impact from the single size fractions is closely associated to the production of fines. The results obtained by sieve analysis permit the determination of the generation rates of particulates below 53μm, which possess a high potential to be liberated to air. These results are presented in Figure 122.

Figure 122 exhibits a wide spread of values of the cumulative percentages below 53μm for the various single size fractions and bulk volumes. For any of the test samples the proportion of fines (<53μm) correlates positively to the energy input level. Hence, the uppermost energy of the 0.68 kWh/t results to the higher cumulative percentage of particles below 53μm, whilst at the 0.05 kWh/t energy receives its lower value.

For the 10% bulk volume test sample the greater percentage of fine particulates (<53μm) was generated by the 4x3.35mm fraction and for energy input 0.68 kWh/t, which equates to 1.28% followed by the 16x13.2mm fraction – 0.68 kWh/t and the 2x1.7mm fraction – 0.68 kWh/t. Whilst, last in the sequence comes the 8x6.7mm fraction – 0.5 kWh/t with a cumulative percentage of fines equal to 0.60 %. The lowest percentage of fine particulates (<53μm) of the 10% bulk volume test samples was achieved at 0.05 kWh/t by the 16x13.2mm fraction and it was 0.03%.

At lower bulk volume (5%) and for the single size fractions 8x6.7mm, 4x3.35mm and 2x1.7mm, the maximum concentration of fine particulates was recorded at 0.68 kWh/t by the 4x3.35mm fraction, followed by the 8x6.7mm and 2x1.7mm fractions. The lowest amount of particles below 53µm corresponds to the 2x1.7mm fraction at 0.05 kWh/t.

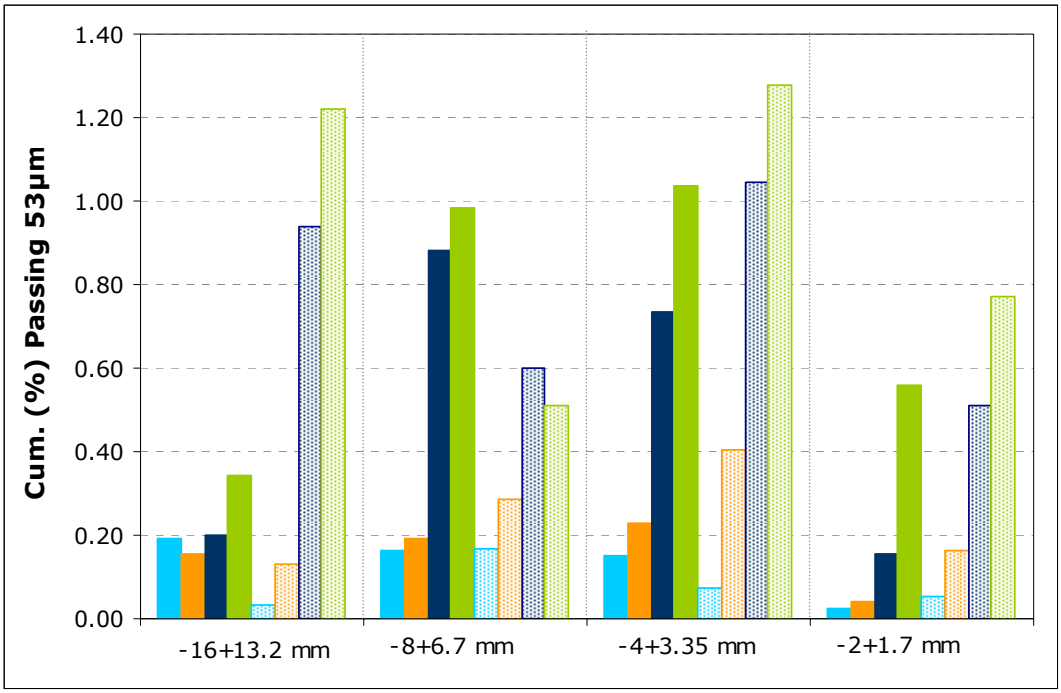

Figure 122: The cumulative percentages passing 53µm for the single lamproite particle fractions. The textured columns represent the samples of 10% bulk volume, whereas the solid coloured columns represent the 20% (for the 16x13.2mm fraction) or 5% bulk volume samples. The different colours represent different energy levels : • = 0.05 kWh/t, • = 0.1 kWh/t, • = 0.5 kWh/t or 0.2 kWh/t (for the 16x13.2mm, 20% bulk volume) and • = 0.68 kWh/t or 0.3 kWh/t (for the 16x13.2mm, 20% bulk volume).

The 16x13.2mm fraction generated higher percentages of fine particles at the low energy inputs (0.05 and 0.1 kWh/t) for the 20% bulk volume test samples. The 8x6.7mm fraction of the 5% and 10% bulk volume samples, produced similar percentages of fines (<53µm) at 0.05kWh/t whereas at higher energy levels, namely at 0.5 and 0.68 kWh/t the 5% bulk volume sample generated more fines. The 4x3.35mm fraction produced a lower concentration of fines for the smaller bulk volume samples (5%), apart from the energy level of 0.05 kWh/t, which produced a higher. The low bulk volume (5%) of the 2x1.7mm fraction generated less fines than the higher sample mass (10% bulk volume).

8.7.4. Summary of the impact test results

Particulates from the lamproite ore can be generated by impact in any industrial process that includes drop from heights (i.e tipping, loading) or compression (i.e haulage roads). Particulates are not dangerous only when found in airborne state, but also when they remain as fines and they travel through the subsequent processing steps, because they might diminish the effectiveness of operations (i.e cause wear) and they might result to secondary or fugitive dust emissions.

Experimentation using the impact apparatus took place for various single size fractions, sample masses and energy input levels. Results have revealed that the dust generation potential of lamproite under impact is influenced both by operational parameters, such as the energy input and the sample mass, as well as by the particle size of the test sample.

A positive relationship between energy input and the particle size distributions as well as the cumulative percentages of fines below 53μm of the various test samples has been shown. Additionally the samples of higher bulk volume were observed to generate finer particle size distributions and greater quantities of fines. The only exception to this observation was for the 8x6.7mm fraction, which generated higher percentages of particulates below 53μm, when a smaller mass was used. The way the particle size of the lamproite feed sample influences the potential of dust/fines to be generated follow a more complicated pattern. Hence highest amounts of fines were recorded for the 4x3.35mm sample and the 16x13.2mm sample (10% bulk volume), whereas the use of 2x1.7mm and 8x6.7mm fraction (10% bulk volume) produced less fines.

All the above conclusions suggest that several steps can be followed by processing engineers to ensure that the dust generation potential of lamproite ore is kept in minimum levels. For instance adjustments of the energy input of processes such as draglines, by reducing the drop from height could minimise the generation of fines, thus the possibility of dust to be emitted and it could also decrease the need for dust control practices (i.e use of water sprays). Also the utilization of a smaller mass load of ore in trucks could minimise the impaction of particles in haulage roads, which will allow them to keep a coarser size and so they will exhibit a lower potential to become airborne. In conclusion, this work provides an alternative proposal and under correct implementation it could assist to reduce the generation of fines and dust from mining

processes as well as the associated risks to the environment and the health and safety of the employees.

8.8. Particle size analysis results of the lamproite particulates produced by the impact test

The particulates below 53μm collected during the performance of the modified JK impact test was further analysed by laser diffraction particle size analysis using the Malvern Mastersizer – S. Triplicates of each sample were measured using as optical model the Mie approximation and the optical properties determined earlier during analysis of the dust fraction collected by the HSE-WSL test. Hence, the refractive index used was set to 1.59, the imaginary refractive index was equal to 0.1 and the dispersion medium (water) index was 1.33. The reproducibility of the measurements taken on triplicate samples is expressed by the median values of the diameters d_{10}, d_{50} and d_{90} and their standard deviation and relative standard deviation values (Table 73). In appendix V, the repeatability of the replicate tests is displayed by the error bars, representing one standard deviation, in the volume (%) retained particle size distributions of the various samples. The reproducibility of the particle size measurements of the lamproite particulates resulted to an average standard deviation of the diameter d_{50} equal to 1.49 and a relative standard deviation of 7.86% (Table 73).

Figure 123 and Figure 124 presents the particle size distributions of the lamproite particulates that correspond to the 10% bulk volume test sample. They exhibit both the cumulative volume (%) undersize and the volume (%) retained. The particle size distributions of the particulates produced by the 5% and 20% bulk volume samples can be reviewed in appendix V.

The particle size distributions of the particulates generated by the 16x13.2mm test sample were not influence by energy input resulting to identical results (Figure 123 (a)).

The particulates of the 8x6.7mm test sample produced the finer particle size distribution at energy input 0.05 kWh/t, whilst the coarser particle size resulted at 0.1 kWh/t followed by the size distribution obtained at 0.5 and 0.68 kWh/t (Figure 123 (b)). In Figure 124 (a) the particulates generated by the 4x3.35mm test sample

has shown that the higher energy input levels (0.5 and 0.68 kWh/t) resulted to coarser particle size distributions than the lower energy levels. The particle size distribution curves of the particulates produced at 0.05kWh/t and 0.1 kWh/t are almost identical as well as the equivalent at 0.5 and 0.68 kWh/t. The particle size distributions of the fines generated by the 2x1.7mm test (Figure 124 (b)) sample exhibited a similar trend to the one discussed for the 4x3.35mm fraction. The finer particle size distribution was produced at 0.1 kWh/t, whereas the 0.5 and 0.68 kWh/t produced the coarser particle sizes.

Table 73: The median values of the diameters d_{10}, d_{50} and d_{90} of the lamproite particulate matter produced using the impact test. The standard deviation and relative standard deviation values correspond to replicate measurements of triplicate sets of test samples. Only the results obtained for the 0.05 kWh/t (E1) and 0.68 kWh/t (E4) are shown.

		D_{10}	Stdev	RSD (%)	D_{50}	Stdev	RSD (%)	D_{90}	Stdev	RSD (%)
16x13.2 mm 10% b.v.	E1	1.74	0.24	13.95	19.20	2.37	12.35	42.93	3.02	7.04
	E4	1.50	0.17	11.56	19.35	0.62	3.22	59.41	1.14	1.92
8x6.7 mm 10% b.v	E1	1.63	0.08	5.12	15.53	1.13	7.30	51.77	2.25	4.35
	E4	1.27	0.11	8.52	18.04	2.02	11.19	58.96	1.97	3.34
4x3.35 mm 10% b.v.	E1	1.59	0.06	3.66	15.09	1.00	6.65	53.81	1.51	2.81
	E4	2.33	0.35	14.91	25.26	2.31	9.16	64.43	1.61	2.50
2x1.7 mm 10% b.v.	E1	1.63	0.05	3.30	16.47	0.87	5.29	58.34	1.32	2.27
	E4	1.63	0.23	13.85	21.32	1.65	7.72	61.06	2.67	4.38

Overall the particle size distributions of the fines (<53μm) obtained by the impact apparatus are influenced both by the particle size of the sample (single size fractions) used for testing as well as by the energy input.

However, these results differ from the sieve data in the way they correlate to energy input, except from the particulates collected from the coarse single size fraction (16x13.2mm). Any of the subsequent test samples resulted in a finer particle size distribution at low energy inputs rather than high. This is believed to happen, because fines at low energy levels are primarily produced due to attrition and not due

to breakage, whilst when energy increases and higher breakage rates are achieved then fines produce a coarser particle size, but also much higher concentrations.

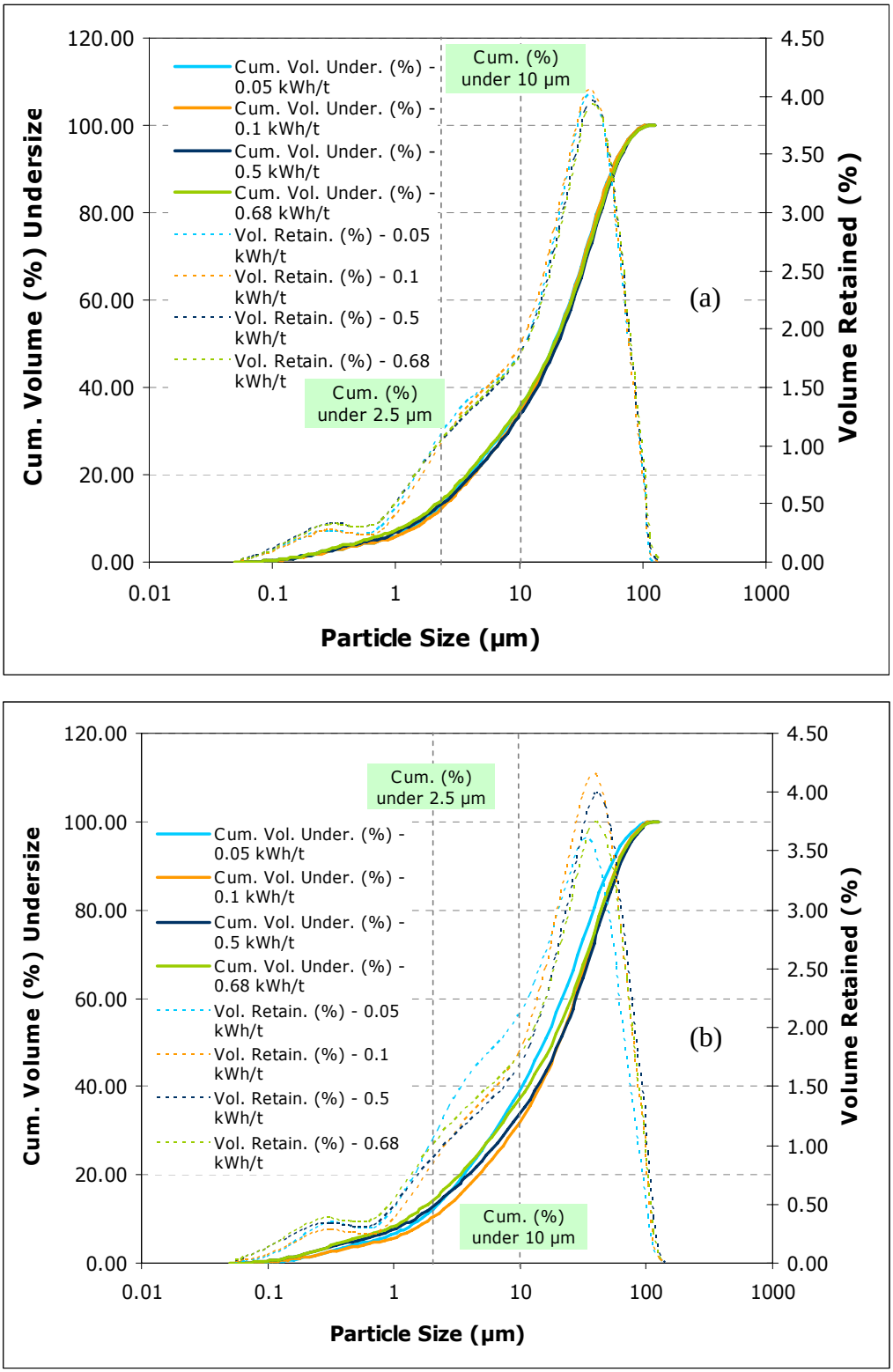

Figure 123: Particle size distributions of the lamproite particulate matter fraction generated by the impact test of a) the -16+13.2mm fraction – 10% bulk volume and b) the -8+6.7mm fraction – 10% bulk volume.

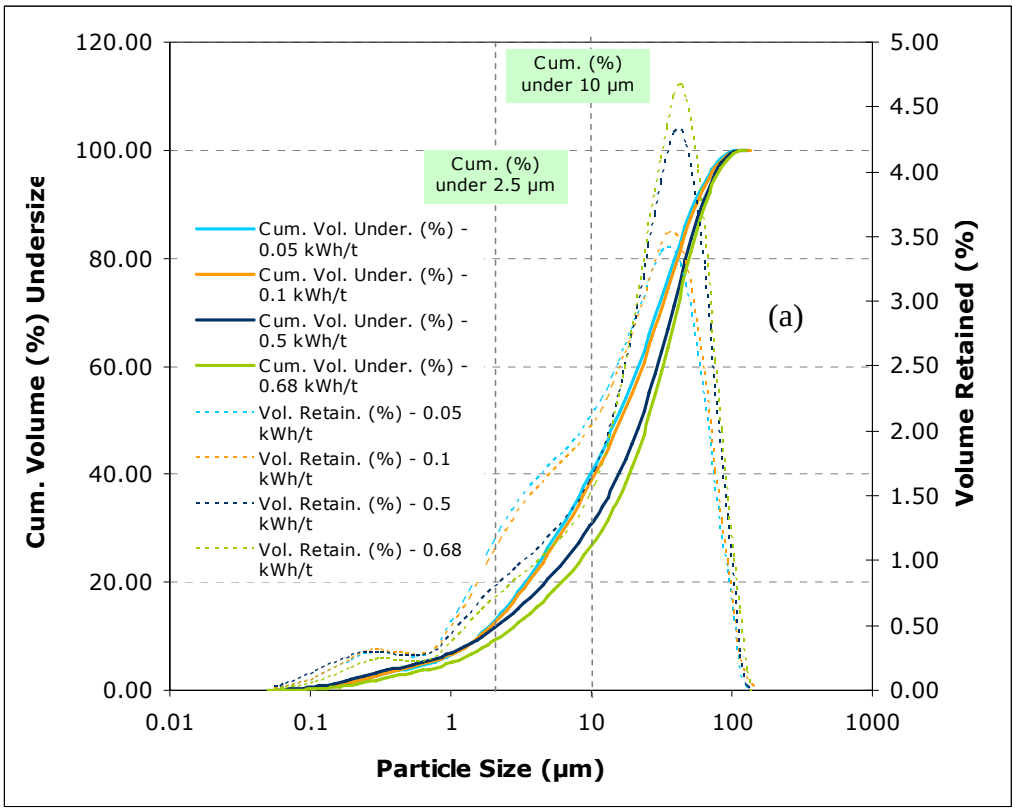

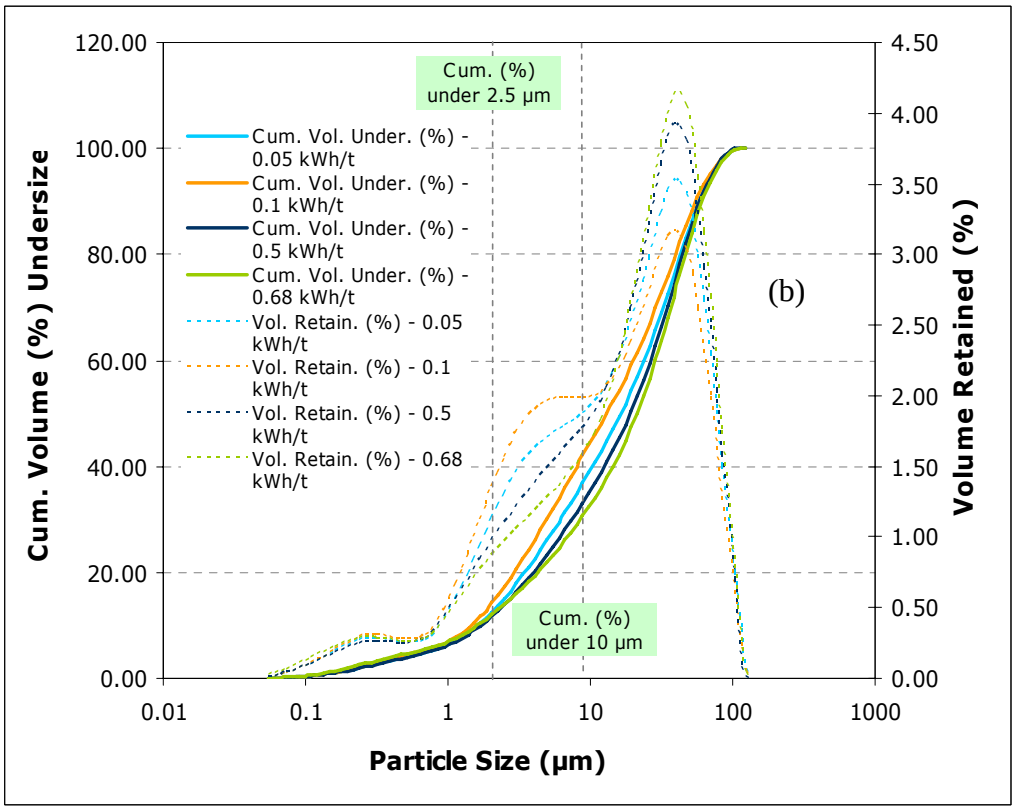

Figure 124: Particle size distributions of the lamproite particulate matter fraction generated by the impact test of a) the -4+3.35mm fraction – 10% bulk volume and b) the -2+1.7mm fraction – 10% bulk volume.

The cumulative volume percentages below 10 and 2.5µm displayed in Table 74 of the 10% bulk volume samples justify the discussion and statements made from the particle size distributions of Figure 123 and Figure 124. Hence the percentages of the 16x13.2mm fraction are higher for the uppermost energy level, whereas the 8x6.7mm, 4x3.35mm and 2x1.7mm samples exhibit higher concentrations below 10 and 2.5µm at 0.05 kWh/t. The 20% bulk volume of the 16x13.2mm sample produced slightly higher percentages at low energy levels. The low bulk volume samples (5%) of the 8x6.7mm, 4x3.35mm and 2x1.7mm fractions generated more particulates below 10 and 2.5µm at the 0.68 kWh/t. The diameter d_{80} of the majority of the samples was smaller for the particulates produced at low energy input. An exception comprises the 2x1.7mm and 4x3.35mm which produced the smaller particle size at 0.68 kWh/t. The cumulative volume percentages below 10 and 2.5µm of the dust fraction collected by the HSE-WSL test were higher and the median diameter d_{80} much smaller than the values obtained by the impact test. However the impact test did not collect the airborne fraction of the lamproite particulates, which makes difficult direct comparisons to be made.

Table 74 : The cumulative volume percentages below 10µm and 2.5µm of the lamproite particulate matter generated by impact testing of a range of single fractions and bulk volumes. The median diameter d_{80} is shown as well.

Size fraction	Energy level (kWh/t)	Cum. % <10 µm	Cum. % <2.5µm	D_{80}
16x13.2mm-10% b.v.	0.05	35.06	14.03	42.93
	0.68	35.28	15.03	44.71
8x6.7mm-10% b.v	0.05	40.23	15.46	39.04
	0.68	26.66	10.75	49.81
4x3.35mm-10% b.v.	0.05	39.20	15.10	42.94
	0.68	32.63	13.95	46.51
2x1.7mm-10%b.v.	0.05	39.20	15.10	42.94
	0.68	32.63	13.95	46.51
16x13.2mm-20% b.v.	0.05	37.92	15.01	39.57
	0.3	35.38	14.67	44.21
8x6.7mmc-5% b.v	0.05	28.31	10.00	46.63
	0.68	29.89	11.58	47.23
4x3.35mm-5% b.v.	0.05	31.67	11.54	46.53
	0.68	35.83	15.23	45.69
2x1.7mm-5%b.v.	0.05	22.41	7.60	59.72
	0.68	28.98	12.06	49.58

A general conclusion that can be drawn is that high concentrations of fine lamproite particulates produced at high energy levels do not necessarily suggest that they will have a particle size lower than the smaller concentrations of particles resulted from lower energy input. Thus, even when low rates of fines are achieved some mitigation practices should be implemented to ensure that the dust does not affect the health and safety of the individuals. Approximately 35% of the lamproite particulates are below 10μm and at the same time 80% of the particles have a diameter of 45μm.

8.9. Mineralogical characterisation of the lamproite particulate matter

The mineralogy of the lamproite particulates produced by the HSE-WSL test and the impact test was initially examined by X-ray diffraction analysis, as well as using the Mineral Liberation Analysis system of the scanning electron microscope.

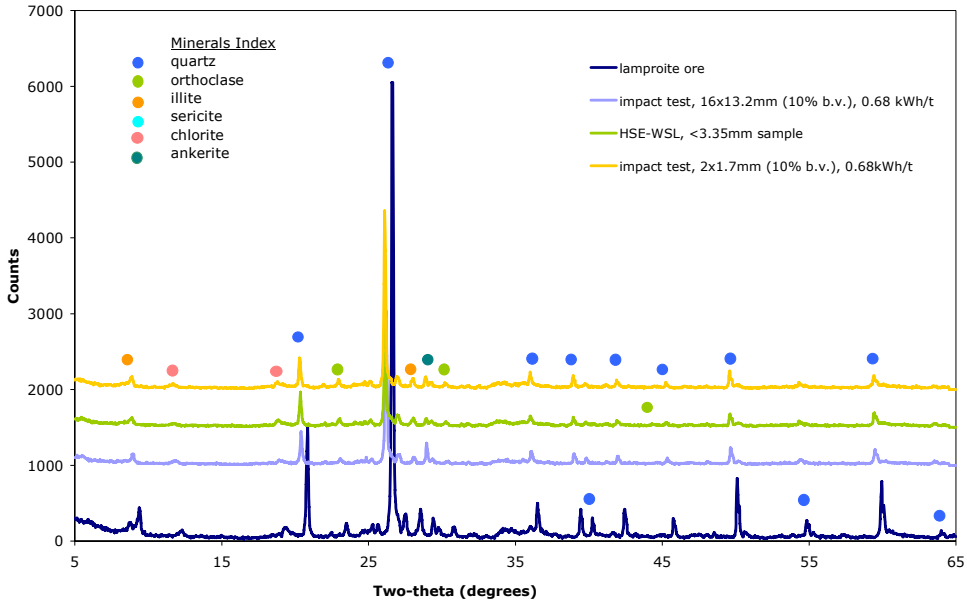

Figure 125: XRD traces of the lamproite particulates collected by the HSE-WSL test and the impact test. The x-ray diffraction pattern of a rock sample is presented as well (two-theta, whole rock analysis).

The X-ray diffraction patterns of the particulate matter were quite similar and some of them are displayed in Figure 125. The identified minerals of the lamproite particulates are similar to the host ore, but many of the peaks that mainly correspond to quartz are lower, which suggests that quartz might be present in lower concentrations. The same samples were quantified using the mineral liberation analyser. From an analysis of the X-ray diffraction data, it is concluded that quartz is

the dominant mineral present in the particulate matter. Nevertheless, it is difficult to determine whether clay or chlorite group minerals participate as major or minor phases, because the whole-rock analysis cannot distinguish such differences.

The modal mineralogy of the lamproite particulates was also determined using the mineral liberation analyser of the scanning electron microscope and energy dispersive X-ray microanalysis system. The dust captured during the HSE-WSL test by the <9.5mm, <3.35mm, and <1mm as well as the fines collected by the single size fractions 16x13.2mm and 4x3.35mm at 0.05 and 0.68 kWh/t and 10% bulk volume, they were mounted in polished blocks following the method detailed in Chapter 4. The Extended BSE (XBSE) liberation mode has been used for analysis, similar to the measurements that took place for the lamproite ore. The XBSE liberation mode was previously discussed in detail in Chapter 4.

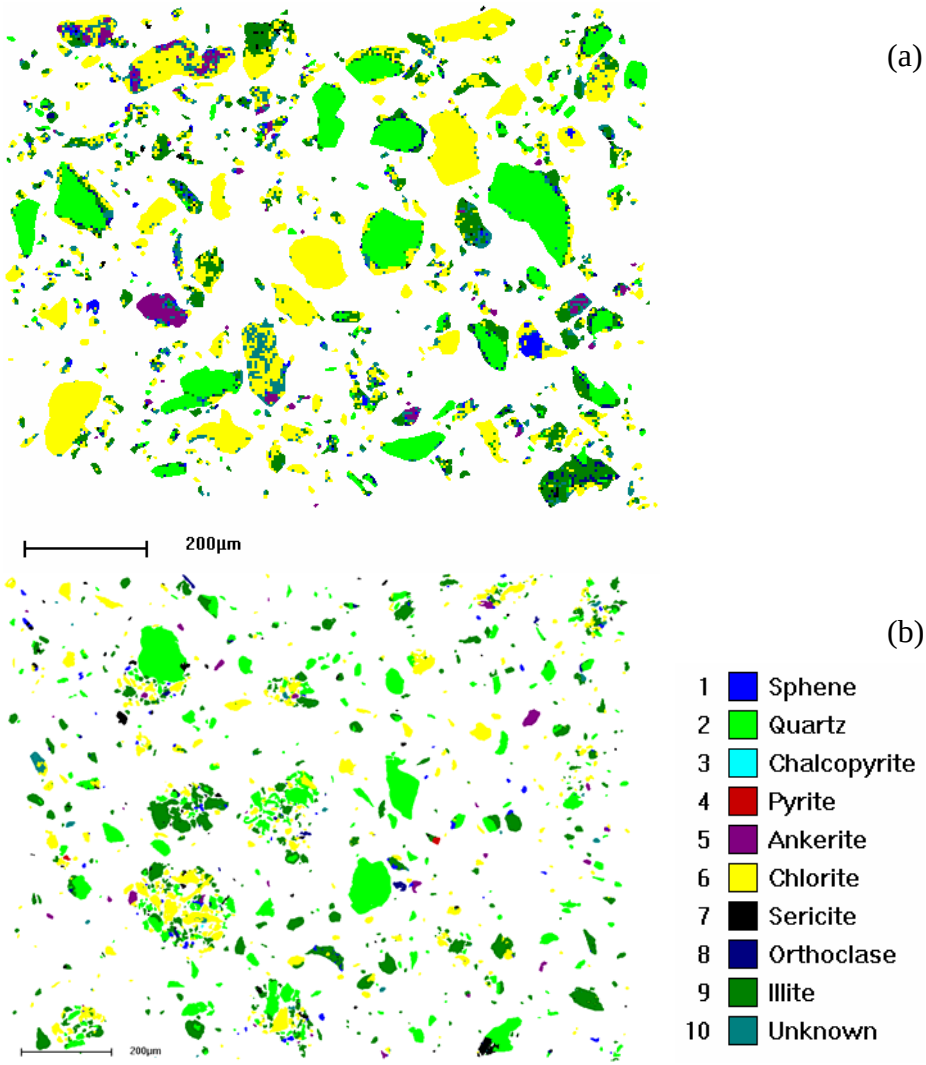

Figure 126: The modal mineralogical profile of the lamproite particulates produced (a) by the HSE-WSL test, from the <9.5mm test sample and (b) by the impact test from the 16x13.2mm -10% bulk volume at 0.68kWh/t sample. The various grain colours correspond to different minerals shown in the mineral list. Magnification x350, scale 200µm.

Approximately 15,000 particles were measured by the XBSE mode, which identified various different mineral phases. The modal mineralogy of the lamproite particulates and the lamproite ore expressed in mineral weight percentages can be seen in Table 75. The major minerals of the lamproite particulates are the chlorite, illite and quartz, whereas the minerals sphene, ankerite, sericite, orthoclase, chalcopyrite and pyrite participate in smaller quantities and they represent the minor phases. Nevertheless, the mineral weight percentages between the lamproite ore and the lamproite particulates are not similar. Approximately 40% by weight of the airborne particulates captured by the HSE-WSL test correspond to chlorite, 25% to illite and 20% to quartz. For the particulates produced by impact around 35% by weight of the sample is quartz, 27% is illite and 25% chlorite. Hence the composition of the dust liberated due to abrasion of the lamproite ore is rich in chlorite and clay group minerals (illite), whereas the concentration of quartz is less than in the host rock samples. The fines generated by the impact test also exhibit lower concentrations of quartz and higher concentrations of chlorite than the host rock samples. Consequently, soft minerals such as chlorite and illite exhibit a higher liability to pass into the airborne and fines fraction. The composition of the particulates produced by the impact test differs from the HSE-WSL test, as they include higher percentages of quartz and lower percentages of chlorite. However, during the impact tests no airborne particulates samples were collected. The concentration of illite as well as most of the minor minerals is similar for the ore and the lamproite particulates. Two frames that correspond to the mineral liberation analysis results obtained by the impact and HSE-WSL test can be seen in Figure 126. A summary of additional data obtained by the mineral liberation analyzer such as in detail presentation of the modal mineralogy results may be found in appendix V.

In conclusion the differences in the mineralogy of the dust fraction and the lamproite ore as well as the substantial variability of the particulates composition resulted from different processes (abrasion and impact) confirms that the analyses performed are essential to determine the hazardous potential of dusts produced at various stages of a transport or processing flowsheet. The mineral liberation analysis system has not been used so far as a method to examine dust. However it has proved to comprise a powerful analysis method as it can provide both mineralogical data as well as high quality quantitative results.

Table 75: The modal mineralogy of the lamproite particulates collected by the HSE-WSL test and the impact test determined by the mineral liberation analysis system (XBSE method). The results obtained for the lamproite ore are also presented.

		HSE- WSL test			Impact Test			
Mineral list	Feed	<9.5mm	<3.35mm	<1mm	16x13.2mm, 10%, 0.05kWh/t	16x13.2mm, 10%, 0.68kWh/t	4x3.35mm, 10%, 0.05kWh/t	4x3.35mm , 10%, 0.68kWh/t
Sphene	3.77	5.33	4.67	3.43	3.88	3.71	4.73	3.06
Chalcopyrite	0.00	0.06	0.01	0.01	0.04	0.23	0.08	0.02
Quartz	47.73	19.78	18.07	26.81	39.42	33.88	25.38	40.11
Pyrite	0.32	0.04	0.04	0.02	0.12	0.44	0.22	0.16
Ankerite	1.94	1.71	3.37	3.01	2.98	3.57	4.20	2.96
Chlorite	16.01	38.82	43.55	42.01	21.94	24.76	33.18	21.50
Sericite	1.85	2.69	1.77	0.82	2.50	2.64	3.22	2.48
Orthoclase	1.35	1.62	1.53	2.88	1.50	1.34	0.93	1.50
Illite	27.03	29.94	27.00	20.99	27.62	29.43	28.06	28.20
Total	100.00	100.00	100.00	100.00	100.00	100.00	100.00	100.00

8.10. Summary of Chapter 8

The dust generation potential of lamproite was assessed using the HSE-WSL dustiness test and the impact test. These two different techniques simulate common processes within the mining industry that produce particulates due to involved abrasion or impact mechanisms. Processes such as crushing, grinding, sorting, handling, transferring, classifying, screening and others they incorporate both abrasion for example due to frictional sliding of the ore and impact (i.e during drop from heights).

The HSE-WSL apparatus tested a variety of lamproite test samples (<9.5mm, <3.35mm and <1mm) under two testing regimes that they made use of different operational parameters. The OPT-TP resulted to higher dustiness values for any of the test fractions in comparison to the HSL-TP. The OPT-TP operates at higher tumbling time (three minutes rather than the one minute used by the HSL procedure) and smaller sample mass (150g instead of 200g utilized by the HSL protocol). This suggests that the time ore is exposed to a particular operation is a critical parameter for the potential of lamproite to generate particulates. Maximum dustiness was recorded for the <3.35mm test sample. During tests performed using the HSL protocol, it has been observed that the proportion of fines (<75μm) is directly proportional to the dustiness. However, for longer tumbling times (OPT-TP) the sample with the higher concentration of fine particles does not correspond to those possessing the maximum dustiness. It is proposed that this is because the abrasion mechanisms taking place in the drum, at longer tumbling times generate more fines for the coarser size fraction, which entrain into the air and they are collected as dust.

Investigations performed to study the motion dynamics of the tumbling mill in Chapter 5 have concluded that it does not generate enough kinetic energy to cause breakage of the particles. Thus lamproite can generate dust even at low abrasion rates. Therefore in order to reduce or control the dust production levels, optimisation steps should be taken, which will reduce the abrasion of the ore as well as they will minimise the time consumed in a process. For instance optimising the transfer of ore using conveyor belts, by adjusting their velocity so as to decrease abrasion could result to a reduced amount of particulates and less demand for dust control.

Particle size analysis of the dust collected by the HSE-WSL test has shown that the particle size distributions of the particulates collected during the use of the OPT-TP did not differ greatly. However analysis of the dust collected by the HSL-TP presented substantial differences. In particular the particulates of the <1mm sample, which produced the maximum dustiness exhibited the finer size distribution, followed by the results that correspond to the <9.5mm and the <3.35mm samples. In conclusion the higher tumbling time utilized by the OPT-TP, combined with the increased abrasion rates produces not only a higher dustiness, but a finer particle size. This has important implications to the hazardous potential of lamproite particulates to human health and the environment.

A variety of single size lamproite fractions, bulk volumes and energy input levels were tested using the impact apparatus. Results have shown that the dust generation potential of lamproite under impact is influenced both by operational parameters, such as the energy input and the sample mass, and the particle size of the test sample. The particle size distributions of any of the single size fractions as well as the cumulative percentages of fines below 53μm relate positively to energy input. Hence, for higher energy levels, particle size distributions become finer whilst the concentration of fines below 53μm increases. Samples of higher bulk volume generated both finer particle size distributions and greater proportions of fine particulates (<53μm). The particle size of the lamproite ore in use influenced its dust generation potential in a more complicated way. Therefore the 4x3.35mm and 16x13.2mm samples (10% bulk volume) generated the maximum concentration of fines, whereas the 2x1.7mm and 8x6.7mm fraction (10% bulk volume) produced less fines (<53μm). Consequently, the production of dust in industrial processes that incorporate impact mechanisms can be reduced or controlled by adjusting the energy input or the bulk volume of the lamproite ore. For instance, during stockpiling reducing the drop from heights will minimise the energy input to the lamproite ore, which will subsequently reduce the generation potential of dust. The utilisation of a

smaller volume of ore in processes that involve drop from heights could also minimise the production of particulates.

The particle size distributions of the particulates generated during impact testing of the 16x13.2mm fraction exhibit a finer size, for higher energy levels. However for the smaller single size fractions and in particular for the 4x3.35mm and 2x1.7mm, the lower energy levels (0.05 and 0.1 kWh/t) produced finer particle size distributions. Although high energy levels generate increased concentrations of particulates, the particle size distribution appears often finer at lower energy input. Around 35% of the lamproite particulates are below 10μm, whereas 80% of the particles have a median diameter of 45μm.

The mineralogy of the particulate matter collected by the HSE-WSL test and impact test was quantified using the mineral liberation analysis system of the scanning electron microscope. An analysis of the quantitative data that represent mineral weight percentages concluded that there were significant differences between mineralogy of the host lamproite ore and the dust. Under abrasion mechanisms, the generated dust mainly consists of chlorite and clay group minerals (illite), whilst the concentration of quartz is low in comparison to the host lamproite ore. Under impact the particulates produced, contained a smaller percentage of quartz and a higher of chlorite than the ore. However, the quartz concentration is higher than that recorded for the airborne particulates of the corresponding HSE-WSL test. These results can be of great importance to occupational hygienists and legislative parties as it proved that the composition of lamproite dust liberated at each stage of a flowsheet can vary considerably from the ore, and within different industrial processes that they incorporate impact or abrasion mechanisms. Therefore the production of standards or occupational health limits should be produced after detailed analysis of airborne emissions from various dust sources. The use of the mineral liberation analysis system is a powerful tool for the determination of the composition of dust as it can provide both mineralogical and quantitative data of high accuracy.

These research findings may be used to investigate alternative flowsheet routes to minimise or control of dust. These could be implemented through optimisation of operational parameters of industrial processes, such as energy input, sample mass, the time scale of an operation and others. These solutions apart from reducing or controlling the production of dust could ensure that less mitigation practices are utilised as well as less energy and dust suppression mediums.

Chapter 9. Experimentation with Kennecott Copper Ore

9.1. Introduction

Kennecott Utah Copper mines the copper rich ore from the Bingham Canyon Mine located near Salt Lake City in Utah, USA. In 2004, Bingham Canyon mined 45.7 Mt of ore with an average copper grade of 0.6% Cu, including also 0.033% Mo, 0.29 g/t Au and 3.049 g/t Ag. The final copper concentrate recovered from the smelter-refinery complex was 247,000 tonnes. Dust generation is a major issue to this large scale mining operation during the blasting, loading, transferring and processing operations. Additionally, the concentration of copper involves several processing stages, which increase the potential of dust to be produced, whilst it leaves large quantities of waste, which can comprise secondary dust sources. The ore mined is rich in quartz and depending on its grade, the silica content can range from 10% to 85%. The high silica content in airborne state is associated with various dangerous illnesses such as pneumoconiosis (i.e silicosis) as well as cancer. Also deposition of dust can affect the environment, close by rural areas and the safety and productivity of the mine.

The objective of this chapter is to investigate the potential of the copper ore to produce particulates from the two major dust generation mechanisms of impact and abrasion, which are commonly associated with processes taking place during mining

and processing of the copper ore The Kennecott copper ore samples were made available from the industrial sponsor of this project, Rio Tinto Technology group.

9.1.1. Experimentation steps

This chapter presents an analysis of the results obtained from the tests performed on Kennecott copper ore. The results are discussed in the chronological order that the experiments were conducted. Prior to analytical presentation and discussion of the research findings a brief introduction to Kennecott copper mine is given.

The experimental steps followed are outlined in the following bullet points:

- The mineralogy of the rock samples was initially identified by X-ray diffraction analysis. In addition the modal mineralogy of the copper ore was quantified using the Mineral Liberation Analyser of the scanning electron microscope.
- The dustiness of the copper ore was determined using the Warren Spring Laboratory (HSE-WSL) rotating drum test. On a separate run of the tests, the copper ore dust was collected for further analysis.
- The dust particle size distribution was determined by laser diffraction analysis using the Malvern Mastersizer – S.
- The potential of the copper ore to generate dust under impact was assessed using the impact apparatus. Conclusions were drawn upon the effect of energy input, bulk volume and particle size on copper ore and its liability to produce dust.
- The particulates fraction (below 53μm) produced by impact was collected, and following sieving and its particle size distribution was further determined by laser diffraction analysis using the Malvern Mastersizer-S.
- The mineralogy of the particulates produced by the HSE-WSL test and the impact test was identified by X-ray diffraction analysis, whilst their modal mineralogy was quantified using the Mineral Liberation Analyser (MLA). Results were compared with the mineralogical data of the host copper ore and conclusions were made upon the compositional differences between dust and the host ore.

The conclusions drawn from an analysis of the experimental allowed suggestions to be made on the dust generation potential of copper ore from common mining

processes that they involve the mechanisms under investigation (impact and abrasion).

9.2. Kennecott Utah Copper - History, geology and industry

The Bingham Canyon mine, Copperton concentrator and Garfield smelter comprise one of the largest and most up-to-date integrated copper operations in the world, located near the Salt Lake City, Utah, USA. At the moment, the Bingham Canyon mine represents the largest man-made surface excavation ever achieved (Kennecott Utah Copper 2006).

The Bingham Canyon ore is characterised by the classic mineralisation of porphyric ore bodies with a fairly uniform distribution of sulphides and mainly chalcopyrite (Landtwing et al. 2005;Mining Technology 2006). The sequence of mineralising porphyries can be reviewed in the geological map of Figure 127. The copper-gold mineralization is associated with the potassic alteration, which occurs in all five porphyric intrusions (Figure 127, zoomed cross section). The copper ore body has a shape of a mushroom cap centred on the quartz monzonite porphyry as its stem. The quartz monzonite porphyry intrusion contains the highest ore grade (Landtwing et al. 2005). As it has been mentioned in the introduction of this chapter, apart from copper, the minerals gold, molybdenite and silver comprise also valuable parts of the ore, which are mined and recovered in parallel with copper (Landtwing et al. 2005;Mining Technology 2006).

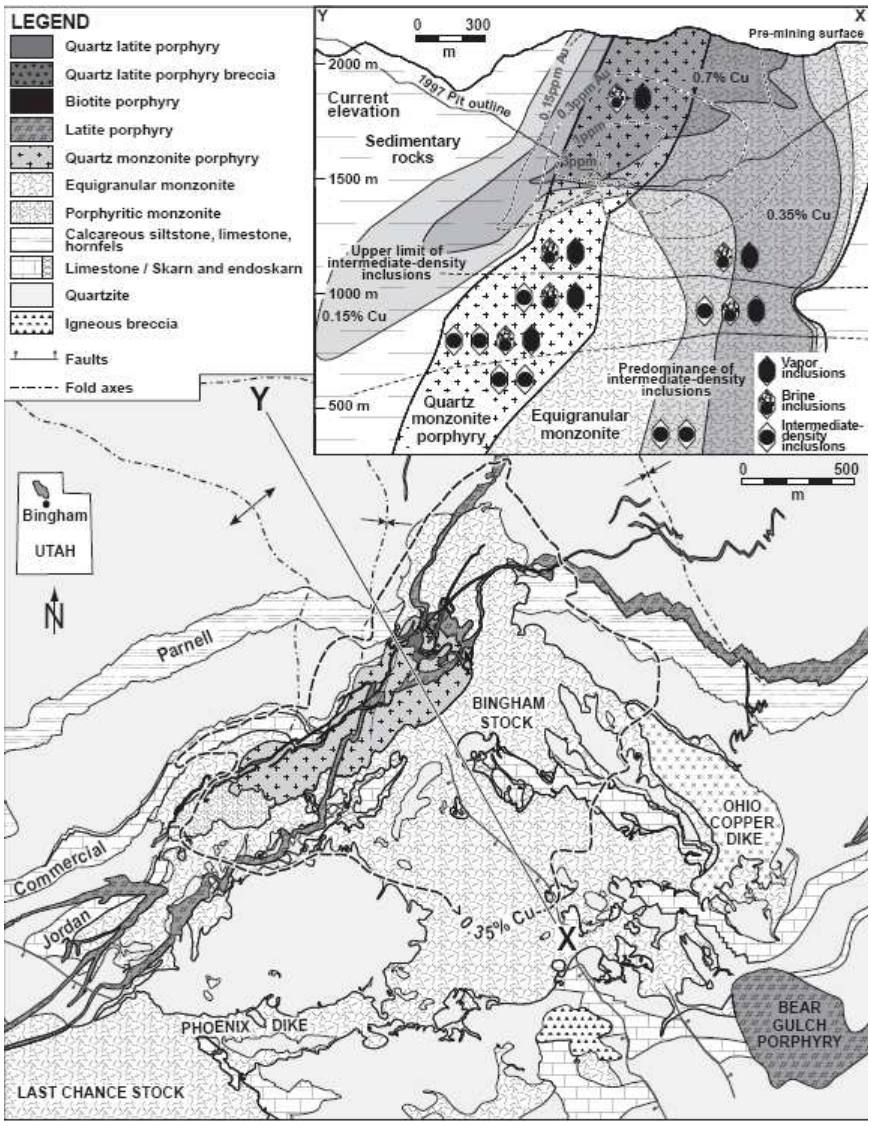

Figure 127: Geological map of the Bingham Canyon porphyric copper ore. The Y-X cross section is presented in detail in the upper right corner of the figure (Landtwing et al. 2005).

9.2.1. Mining and processing of the copper ore

The Bingham Canyon pit is mined through by drilling and blasting of benches. The blasted ore is subsequently loaded by shovels into trucks and crushed by in-pit gyratory crusher. Bench blasting takes place two to four times per day. (Kennecott Utah Copper 2006;Mining Technology 2006).

The semi-mobile (in-pit) crushing unit is linked to the Copperton concentrator by an 8 km conveyor system. The concentrator is fitted with some of the world's largest semi autogenous grinding mills, ball mills and flotation cells. The ore is ground and then a copper concentrate of 28% is produced by flotation. This copper concentrate is transported 17 miles to the smelter via a slurry pipeline for further processing and

production of the cathode copper (Kennecott Utah Copper 2006;Mining Technology 2006). The processing flowsheet of the copper ore is shown in Figure 128

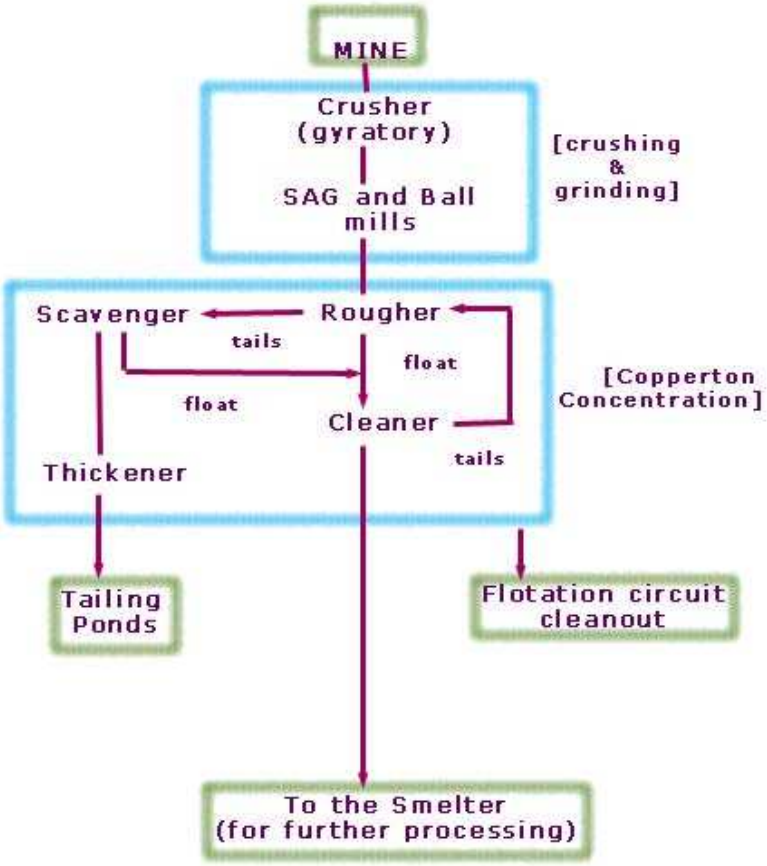

Figure 128: Processing steps of the copper ore (US EPA 2003).

9.3. Particulate matter emissions from copper ore mining and processing

The scale of mining and processing taking place in Bingham Canyon pit, the concentrator and the smelter produce several adverse environmental impacts such as the production of waste, air pollution, water pollution and effects on land and wildlife.

The generation and emission of dust is also a major issue to the mine and it is mainly produced by the drilling and blasting that takes place more than once per day and the loading and transfer by haulage roads of 500,000 tonnes of ore. Additional particulate matter emissions are generated by processing of the ore, namely the

comminution stages and transfer by conveyor belts, as well as from the smelter plant.

Sustainability, environmental awareness, as well as health and safety are strategic objectives of Kennecott Utah Copper. To improve air quality, the company aims to comply with all relevant environmental and safety commitments, law and regulations and to establish practices that promote safe workplaces and reduce pollution. Common mitigation practices utilized are the plant vegetation on barren patches of ground, the use of water sprays to suppress dust produced from haulage roads, the deposition of waste on the periphery of the mine and its wetting with water, the use of latest technologies, update equipment and development of new processes that reduce emissions A good example of their strategy comprises the replacement of trucks that carried 190 tonnes of material with trucks of 250 to 360 tonnes per load, so as to reduce the trips through the mine and minimise the generation rates of dust. Employees are provided with air purifying respirators, which are used by them when the conditions require it. Additionally Kennecott Utah Copper uses internal standards set by Rio Tinto Group such as the standard 10.6 on "Particulate and gas / vapour exposures" or the standard 10.7 on "Occupational Exposure Limits" (Kennecott Utah Copper Corporation 2003;Kennecott Utah Copper Corporation 2004b). In terms of monitoring, meteorological sensors collect data, such as forecast of wind directions on the tailings impoundment, which are combined with operational information, for example surface wetness to estimate dust events. Often monitoring data are utilized in air quality dispersion models. Internal standards are available for monitoring as well, like the Standard 10.9 on "Workplace Monitoring" (Kennecott Utah Copper Corporation 2004a).

The established mitigation practices, standards and regulations they manage to minimise dust considerably. Nevertheless, the continuous mining and processing of ore in such a vast scale require the implementation of alternative techniques that could minimise the generation of dust in a way that will be cost effective. The use of dust control techniques they require the use of large quantities of water, energy, equipment and maintenance, increasing the cost of mining. The research work undertaken for the copper ore aimed to provide a fundamental understanding of the mechanisms of dust generation associated with industrial processes, which will potentially suggest new or improved means of reducing the production of particulates, without requiring extra mitigation practices.

9.4.Mineralogical characterisation of the copper ore

The mineralogy of the host copper ore was initially identified by X-ray diffraction analysis, and subsequently its modal mineralogy was quantified using the mineral liberation analysis system.

Ten different representative samples of the copper ore were prepared and were analysed by X-ray diffraction – whole rock analysis. Examples of the XRD traces of some of the copper ore samples are shown in Figure 129. The patterns were found to be identical mainly consisting of four different minerals. These are the quartz, kaolinite, mica (probably biotite) and chalcopyrite. From the intensities of the peaks we can assume that quartz comprises the major mineral phase, whereas the minerals kaolinite, mica and chalcopyrite participate in smaller quantities and are thus characterised as minor minerals.

The mineralogical composition of the ore was analysed by quantitative means using the mineral liberation analyser system of the scanning electron microscope. Two representative fine-grained samples were prepared in polished blocks. The mineral liberation analyser involves several different measurement modes, but for this work the Extended BSE (XBSE) method was employed.

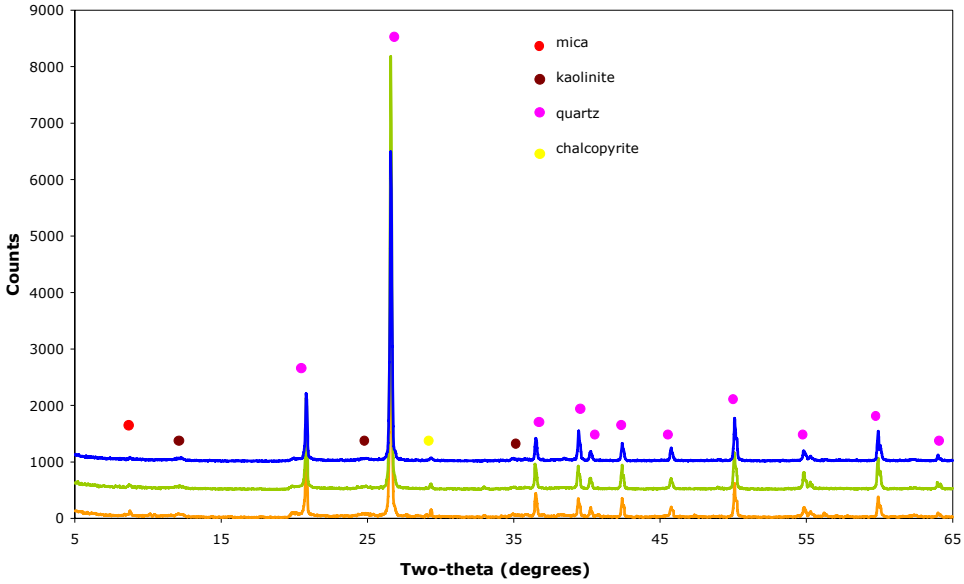

Figure 129: The XRD traces of the copper ore rock samples (two-theta, whole rock analysis).

Table 76: The modal mineralogy results of the copper ore obtained by the mineral liberation analyzer system (XBSE analysis method).

Mineral list	Mineral weight (%) Feed 1	Feed 2
Covellite	0.02	0.02
Quartz	89.32	89.41
Chalcopyrite	1.44	2.09
Pyrite	2.81	3.13
Other	0.32	0.58
Iron	0.09	0.16
Iron 2	0.06	0.07
Titanite	0.02	0.02
Zircon	0.34	0.17
Ankerite	0.07	0.05
Orthoclase	0.28	0.22
Biotite	0.72	0.51
Kaolinite	2.88	2.26
Illite	1.64	1.31
total	100.00	100.00

An average of 15,250 particles were analysed from each polished block, which allowed the identification of all different mineral phases. The modal mineralogy results obtained from the two different samples are displayed in Table 76. According to the quantitative results both of the samples consist mainly of quartz with a mineral weight percentage over 89%, whilst the minerals pyrite, chalcopyrite, kaolinite and illite correspond to the secondary or minor phases. Some additional minerals such as the biotite, titanite, zircon and covellite participate with very small percentages. The two different samples (feed 1 and feed 2) produced very similar mineralogical compositions hence the results can be considered representative. Chalcopyrite is the copper-rich mineral and its weight percentage ranges from 1.44 to 2.09%. The various minerals commonly occupy the whole surface of particles, suggesting that at this size they are liberated. However macroscopic observations of the rock samples have determined that the copper rich minerals, namely chalcopyrite, or covellite, in the ore occur on the outer surface of quartz. Figure 130 shows one frame of the mineral liberation analysis outcomes, where the different mineral phases of the copper ore are represented with different colours. Some additional information regarding the results obtained by the mineral liberation analyzer can be reviewed in appendix VI.

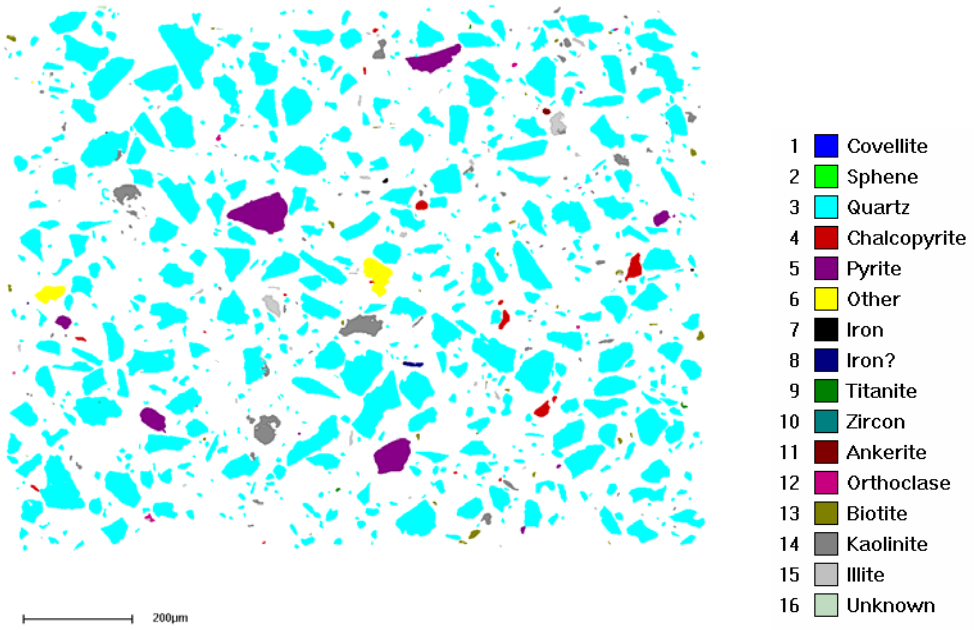

Figure 130: A frame of the mineral liberation analysis results obtained using the XBSE method. The various minerals are presented with different colours. Particles commonly consist of one mineral phase, which suggests that at this size minerals are liberated. Magnification X350, scale 200µm

9.5. Determination of the dustiness of copper ore using the HSE-WSL rotating drum test

Dustiness testing with the Kennecott copper ore made use of the two testing regimes (HSL-TP and OPT-TP) and a variety of feed test samples (<9.5mm, <3.35mm and <1mm).

9.5.1.Dustiness measurements

The particle size distributions of the copper ore feed samples (200g and 150g) of the <9.5mm, <3.35mm and <1mm were determined by sieving analysis prior to testing and results are presented in Figure 131. As expected the particle size distribution of the fraction below 9.5mm exhibits the coarser profile followed by the fractions below 3.35mm and below 1mm.

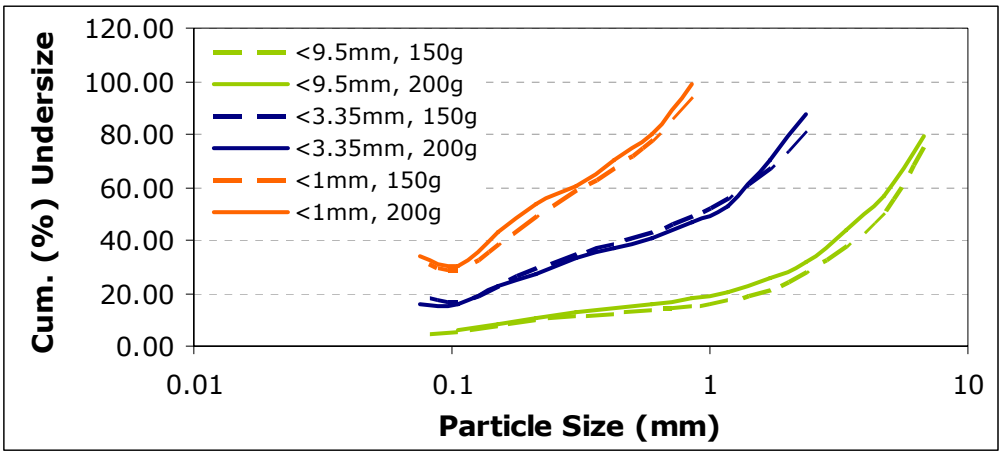

Figure 131: Particle size distributions of the copper ore feed samples <9.5mm, <3.35mm and <1mm and for sample masses of 200g and 150g.

9.5.1.1. *Presentation and analysis of the dustiness measurements results*

The HSE-WSL dustiness results obtained for the copper ore are displayed in Table 77 and in appendix VI. They represent results from the various test fractions and testing protocols, which correspond to average values of three successive tests. The reproducibility of the dustiness outcomes is expressed by the standard deviation and relative standard deviation values shown in Table 77.

Table 77: Dustiness results of the copper ore samples obtained for both testing protocols. The standard deviation and the relative standard deviation (% RSD) reflect the reproducibility of the replicate tests.

Copper ore fractions	HSL procedure			Optimum operating parameters procedure		
	Dustiness (%)	Standard deviation	(%) RSD	Dustiness (%)	Standard deviation	(%) RSD
< 9.5mm	0.1143	0.013	11.68	0.2640	0.020	7.57
< 3.35mm	0.1456	0.023	15.53	0.2870	0.048	17.17
< 1mm	0.0789	0.007	8.75	0.2249	0.022	9.62

The dustiness of the copper ore obtained for any of the test procedures varied from 0.0780% to up to 0.2870% The optimum conditions testing regime produced the highest dustiness values, on average 2.4 times higher, than the comparable test fractions using the HSL test protocol.

For the HSL-TP, the maximum dustiness corresponded to the <3.35mm sample followed by the <9.5mm and <1mm test samples. The same trend in dustiness sequence was recorded for the test performed using the OPT-TP. The extended

tumbling time (3 minutes instead of 1 minute) of the optimum parameters regime produced an increase in the corresponding dustiness values. However as a lower sample mass, 150g instead of 200g is utilised, this suggests that the time scale of an operation is a critical parameter upon the dust generation potential of the copper ore.

The cumulative percentage of particles below 75μm is plotted against the determinant dustiness (%) in Figure 132. The highest concentration of fine particles (<75μm) correspond to the <1mm test sample. However for both testing regimes these samples generated the lowest dustiness values. The <3.35mm fraction, which produced maximum dustiness values consisted of a lower proportion of fine particles (<75μm), than the <1mm test sample. Whereas the <9.5mm sample possessed the lowest percentage of fines below 75μm, but resulted to a higher dustiness value than the <1mm sample. These results suggest that the tumbling action has a greater effect upon the <3.35mm fraction and the <9.5mm fraction than the <1mm sample, allowing more dust to be emitted. Several reasons could be responsible for this result, such as the cohesion of the <3.35mm sample in comparison to the <1mm sample, the abrasion mechanisms taking place in the drum or even the moisture content of the different fractions. It is possible that dustiness is increased for the <3.35mm fraction, because the mixing action in the drum is more effective for this sample thus permitting the fine fraction to entrain into the air. Also abrasion might have a greater influence upon the <3.35mm and the <9.5mm fractions, which could result to higher rates of fine particles that they can easily become airborne. The relation of moisture content and dustiness is discussed in the following paragraph. It is likely that a combination of all these parameters is responsible for the dustiness values obtained.

In conclusion, the dust generation potential of the copper ore in processes that involve abrasion mechanisms is influenced by the particle size of the ore, parameters like the time-scale of an operation, the abrasion rates of the ore particles by friction and also some physical characteristics of the material under investigation, for instance its cohesion. The main aim of this study is to investigate the mechanisms of dust generation, therefore parameters which are related to the dust emission dynamics, like cohesion, which has previously referred, have not been examined. According to the dustiness outcomes, the test fraction <3.35mm exhibits a higher liability to produce dust in processes such as conveyor belts, haulage roads and anywhere else that abrasion occur. Increasing the time spend in a process has shown that could result to higher dust levels, whilst extended abrasion of coarse particle fractions can cause the generation of fine particulates and dust.

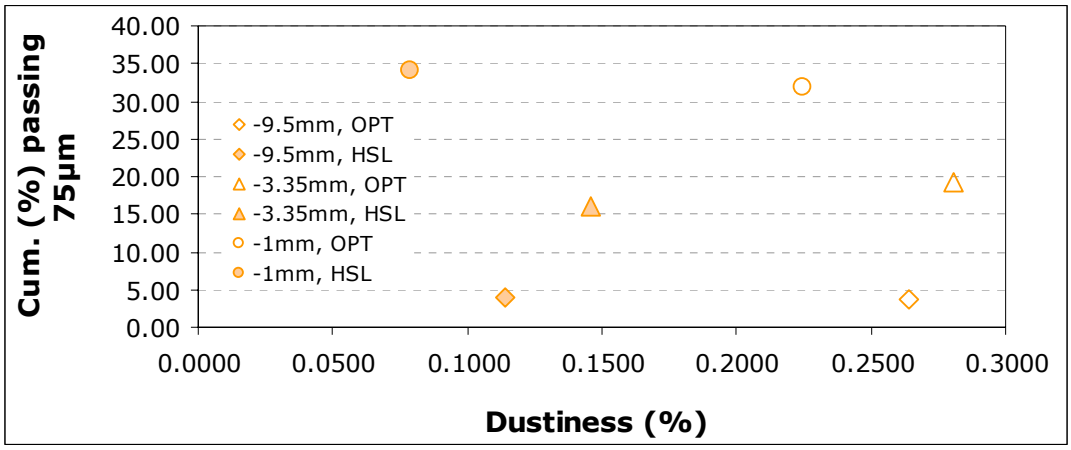

Figure 132: Dustiness result of the copper ore fractions versus the proportion of fines in the test sample (HSL: corresponds to the HSL-TP, OPT: represents theOPt-TP)

9.5.1.2.*The effect of moisture content upon copper ore dustiness*

The moisture content of the copper ore test samples was measured following the British standard BS812-109:1990 (BSI 1990). In detail the experimental procedure can be reviewed in Chapter 5. The finer fraction <1mm exhibited the higher moisture content equal to 0.23%, followed by the <3.35mm sample with a value of 0.22% and the <9.5mm with a value equal to 0.17%.

Table 78: The moisture content (%) of the copper ore test fractions in relation to dustiness (%) (average values) from the two testing regimes.

Sample	Moisture content (%)	Dustiness (%) HSL testing procedure	Dustiness (%) Optimum parameters procedure
<9.5mm	0.17	0.1143	0.2640
<3.35mm	0.22	0.1456	0.2870
<1mm	0.23	0.0789	0.2249

The <1mm sample generated the lowest dustiness and to some extend this might be attributed to the higher moisture content. However, the differences in the moisture content values between the <3.35mm and <1mm samples are not significant enough to explain the discrepancy in the measured dustiness values. This suggests that the <3.35mm sample produced higher dust levels from the <1mm fraction due to extra reasons other than the moisture content such as the increased effect of abrasion upon the coarser particles. The moisture content of the <9.5mm sample is significantly lower than any of the other test samples, which justifies why this

fraction that comprises such a low concentration of fine particulates (<75μm) resulted to a higher dustiness value than the <1mm sample

9.5.1.3. *Determination of the health based dustiness indices*

In addition to the dustiness measurements made using the HSE-WSL apparatus, the health based dustiness indices of the inhalable (Di), thoracic (Dt) and respirable (Dr) fractions of the copper ore were determined. The explanation of what the inhalable, thoracic and respirable fractions represent can be reviewed in Chapter 4. The inhalable index reflects the total dustiness, and these results have been discussed in detail in paragraph 9.5.1.1. The outcomes of the thoracic and respirable dustiness indices are displayed in Table 79 and in appendix VI. Table 79 also includes the standard deviation values, which have been calculate from triplicate repeats of the test. The dustiness indices of the thoracic fraction vary from 3.9566% to 8.4443%, whilst the respirable fraction dustiness indices range from 0.0728% to 0.4240%

During the tests performed using the OPT-TP, the copper ore samples generated higher dustiness indices for the thoracic fraction than that determined using the HSL-TP. The maximum thoracic fraction dustiness index was obtained for the <3.35mm sample, followed by the <1mm and <9.5mm samples. The copper ore fractions tested using the HSL-TP produced exactly the same sequence of results of the thoracic dustiness index values. For both testing regimes the sample that produced maximum dustiness, namely the <3.35mm also generated the highest dustiness indices of thoracic fraction. The <1mm sample, although it exhibited the lowest dustiness, produced a greater thoracic fraction dustiness index than the <9.5mm sample.

The dustiness index of the respirable fraction exhibited higher values, for the majority of the samples, during testing using the HSL-TP. The only exception comprises the <3.35mm sample, which produced a greater value of the respirable fraction dustiness index at the optimum parameters testing protocol. The maximum dustiness index of the respirable fraction using the HSL-TP corresponded to the <9.5mm sample, followed by the <1mm and <3.35mm samples. Therefore the <3.35mm sample that generated the highest dustiness value, produced the lowest respirable dustiness index. For the OPT-TP the uppermost value of the respirable fraction was achieved by the <3.35mm sample, whereas second and third in turn come the <9.5mm and <1mm samples respectively. The sequence of the respirable dustiness index is in good agreement with the one recorded for total dustiness (or inhalable dustiness index).

Hence, according to the health based classification of the dust collected from the HSE-WSL drum, the shorter tumbling time (HSL-TP) although producing lower dust levels, generates dust of finer size. As it has been mentioned in the previous chapters, the classification of dust in the health based fractions should be adopted when the research interest focuses on exposure to humans and not as sizing method. This is because particle size analysis techniques, such as the light scattering method used in this project can provide data of higher accuracy and reproducibility.

Table 79: Health based dustiness indices of the copper ore samples (both testing protocols). One standard deviation has been calculated from replicate tests.

HSL protocol	Copper ore fractions		
	<9.5mm	<3.35mm	<1mm
D_t (%)	3.9566	5.3348	5.2640
Standard deviation	0.735	0.885	1.499
D_r (%)	0.4240	0.1247	0.2411
Standard deviation	0.081	0.025	0.118
Optimum parameters protocol			
D_t (%)	5.7368	8.4443	7.6409
Standard deviation	1.414	1.228	1.324
D_r (%)	0.0951	0.4291	0.0728
Standard deviation	0.016	0.123	0.014

9.5.2. Summary of the dustiness analysis results

The potential of the copper ore to generate dust was assessed using the HSE-WSL apparatus using two different testing procedures (HSL-TP and OPT-TP) and the test fractions, <9.5mm, <3.35mm and <1mm.

From an analysis of the dust collected during the use of the OPT-TP, the dustiness values are higher than the ones obtained with the HSL-TP. For any of the test procedures, the <3.35mm fraction resulted in the maximum dustiness, whereas the <1mm sample produced the lowest dustiness. Thus the extended tumbling time utilized using the OPT-TP is considered a critical parameter upon the dust generation potential of the copper ore.

The proportion of the fine particles already present in the test sample did not present some correlation patterns with dustiness. Thus the <1mm sample which comprised the higher concentration of particles below <75μm it generated the lowest dust

levels. These results suggested that the abrasion mechanisms taking place in the drum as well as properties such as the moisture content and the cohesion of the samples are responsible for the discrepancy in the dustiness values. The effect of abrasion is significant for the coarser fractions (<3.35mm and <9.5mm), and in particular for the <3.35mm fraction, as this sample produced the greater dustiness value although its moisture content was high. The <9.5mm fraction produced higher dustiness than the <1mm sample because its moisture content was significantly lower.

The UK Health and Safety Laboratory scale the dustiness of materials from not dusty to extremely dusty (Chung and Burdett 1994) (Table 26). The copper ore fractions are categorised accordingly in Table 80. In detail, the results of the various copper ore fractions, expressed in dust yield per filter, including a standard deviation from replicate tests can be reviewed in appendix VI.

Table 80: Classification of the dustiness results for the copper ore samples as proposed by HSL.

Testing procedure	Copper ore fractions	Dustiness (%)	Classification
HSL procedure	< 9.5mm	0.1143	dusty
	< 3.35mm	0.1456	dusty
	< 1mm	0.0789	Slightly dusty
Optimum operating parameters procedure	< 9.5mm	0.2640	dusty
	< 3.35mm	0.2870	dusty
	< 1mm	0.2249	dusty

The transport processes conveyor belts or haulage roads, they could reduce the liability of the ore to produce particulates, by decreasing the time consumed to transfer the ore. This could be achieved by either minimising the distance of the transport process, or by increasing the capacity of the conveyor belts or trucks. In addition the optimisation of parameters such as the velocity of the conveyor belts or trucks could reduce abrasion and minimise the dust generation levels. Similar steps could be followed for other processes such as grinding mills, or sieves, mixers and others.

9.6. Particle size analysis of the copper ore particulate matter fraction generated by the HSE-WSL test

The particle size of dust collected by the HSE-WSL apparatus was measured by laser diffraction analysis using the Malvern Mastersizer-S and the results are presented in the following paragraphs.

9.6.1. Selection of the optical properties of the copper ore particulate matter

For the copper ore as well as with any of the ores that experimentation took place so far, the Mie approximation was selected as the appropriate optical model. Hence the optical properties of the ore had to be determined in order to achieve accurate measurements. The variability in particle size caused by different selected optical properties can be reviewed in appendix VI. The optical properties of the copper ore were defined following the procedure described in Chapter 8 for the lamproite ore. This is because for both of these ores the use of the Mineral Liberation Analysis system allowed the collection of quantitative data regarding the mineralogical profile of the samples. A weighted average refractive index was calculated by combining the mineral weight percentages obtained by the mineral liberation analysis with the refractive indices of each individual mineral that participates to the whole composition of the ore. The refractive index of many of the minerals is a range of values and not a specific one and in that case a median refractive index has been used. The refractive indices of the participated minerals and their mineral weight percentages measured earlier by the mineral liberation analysis are displayed in Table 81, whereas the weighted average refractive index was calculated by (Equation 24.

According to (Equation 24, the refractive index of the copper ore was calculated to be equal to 1.55. The imaginary refractive index was kept at 0.1, as it was found that this value provides the best fit. As dispersion medium water was used with a refractive index of 1.33. Any subsequent particle size analysis results made use of the above optical properties.

Table 81: The refractive indices of the copper ore minerals, and the mineral weight percentages determined by mineral liberation analysis.

Mineral	Refractive Index ($R.I_{(i)}$)	Mineral weight (%) ($w_{(i)}$)
titanite	1.97	0.02
Quartz	1.54	89.32
Pyrite	1.81	2.81
Ankerite	1.63	0.07
chalcopyrite	1.82	1.44
Iron	1.51	0.15
zircon	1.97	0.34
biotite	1.61	0.72
covellite	1.83	0.02
kaolinite	1.56	2.88
Orthoclase	1.53	0.28
Illite	1.57	1.64
Total		100.00

9.6.2. Particle size analysis results

The particle size distributions of the copper ore dust fractions collected during testing with the HSE-WSL apparatus of the various size fractions and testing protocols are presented in Figure 133. These results correspond to average size distributions that have been obtained by tests on triplicate samples and after several repeatable measurement steps. The repeatability and reproducibility of the measurements taken on the triplicate samples is expressed by the standard deviation and relative standard deviation values of the diameters d_{10}, d_{50} and d_{90} displayed in Table 82. The results of this table correspond to the dust fraction capture by the OPT-TP, whilst the respective results of the dust collected by the HSL-TP may be reviewed in appendix VI. The repeatability-reproducibility of the multiple measurements can also be reviewed in the volume (%) retained particle size distributions, by the error bars representing one standard deviation, which are shown in appendix VI. Repeatable measurements taken for one sample (same feed) produced very accurate measurements with a relative standard deviation of below 1%. The reproducibility of the particle size measurement results of the triplicate samples was only slightly higher, giving an average standard deviation of the median d_{50} diameter (for all fractions) equal to 0.16 and an average relative standard deviation of 2.00%.

Table 82 : The median values of the diameters d_{10}, d_{50} and d_{90} of the copper ore particulates produced using the HSE-WSL test, from a range of sample fractions (optimum conditions testing protocol). The standard deviation and relative standard deviation values were calculated from the results obtained by the triplicate samples.

Sample Fraction	D_{10}	Stdev	RSD(%)	D_{50}	Stdev	RSD(%)	D_{90}	Stdev	RSD(%)
-9.5 mm	1.51	0.02	1.38	8.03	0.15	1.83	28.44	1.59	5.59
-3.35 mm	1.50	0.04	2.55	8.32	0.33	4.01	28.83	0.74	2.57
-1 mm	1.50	0.01	0.47	8.54	0.01	0.17	32.37	0.40	1.25

Figure 133(a) presents the particle size distribution results of the dust captured using the OPT-TP. The various test fractions produced similar dust particle size distributions and this conclusion is also justified by the cumulative volume percentages below 10 and 2.5μm, as well as by the d_{80} values of Table 83. Approximately 57.20% (in volume) of the dust particles collected using the optimum parameters protocol exhibit a particle size below 10μm and 16.47% of the particulates are below 2.5μm in size, whereas the median diameter d_{80} of dust is 19.20μm.

Figure 133(b) displays the dust particle size distributions that correspond to the HSL-TP. For the <9.5mm and <3.35mm test samples, dust particle size distributions are similar. Nevertheless the <1mm sample exhibits a different profile and a finer particle size. The cumulative percentages passing 10 and 2.5μm and the median diameter d_{80} follow similar trends. Hence in average 30.30% and 9.5% of the dust particles of the <9.5mm and <3.35mm samples and 41.11% and 11.80% of the particulates of the <1mm sample exhibit a size below 10μm and 2.5μm respectively (Table 83). The median diameter d_{80} is around 37.40μm for the particulates of the <9.5mm and <3.35mm test sample and smaller, 34.31μm of the <1mm sample.

For a specific test sample, for instance the <3.35mm, the dust particle size distribution associated with the OPT-TP is finer (Figure 134 and in appendix VI). This is the case for any of the test samples, namely the <9.5mm, <3.35mm and <1mm.

Consequently the longer operational time and higher abrasion rates of the optimum parameters protocol resulted to a finer particle size, whereas the size of the various test samples were identical. At these testing conditions more than 50% of the volume of the particulates are below 10μm, suggesting that the dust generated by the copper ore can be a potential hazard to human health and the environment.

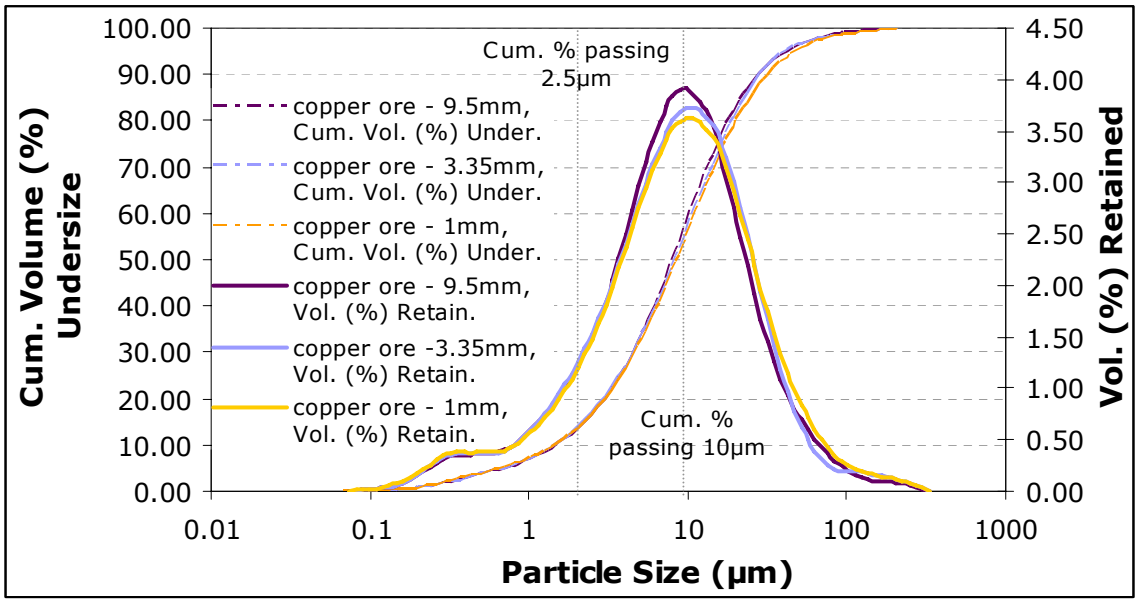

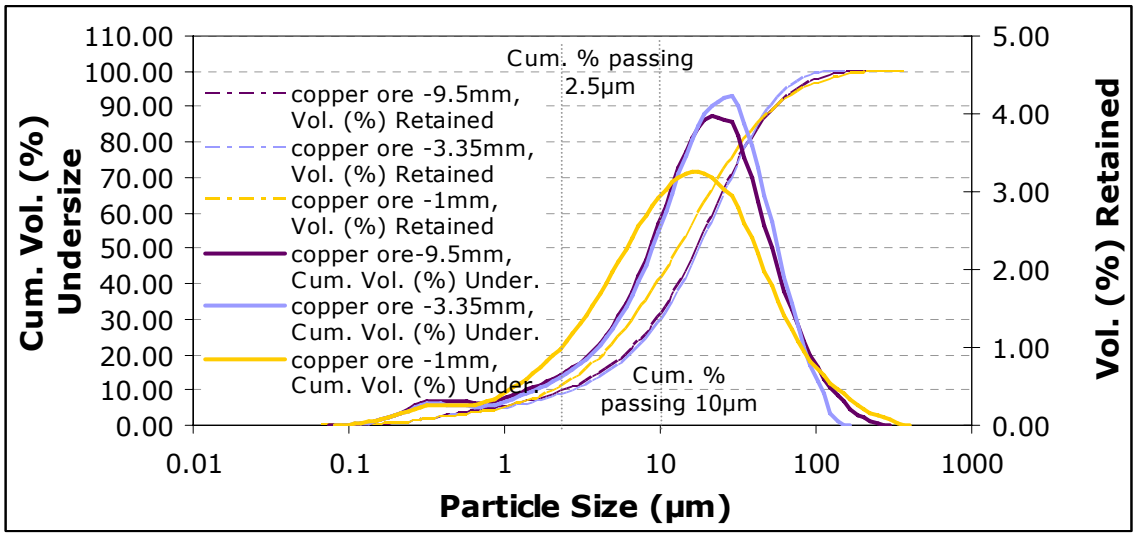

Figure 133: Particle size distribution of the copper ore particulate matter produced through (a) the OPT-TP and (b) the HSL-TP. The presented results correspond to average values of repeatable tests.

Table 83: Cumulative percentages passing 10µm and 2.5µm and the median values of the diameter d_{80} for all samples and testing regime (1): corresponds to the OPT-TP; (2) corresponds to the HSL-TP)

Copper ore fractions	Cum. % passing 10µm	Cum. % passing 2.5µm	D_{80}
-9.5mm (1)	58.77	16.39	18.12
-9.5mm (2)	31.10	10.03	37.56
-3.35mm (1)	56.99	16.68	19.07
-3.35mm (2)	29.51	9.08	37.25
-1mm (1)	55.85	16.35	20.41
-1mm (2)	41.11	11.80	34.31

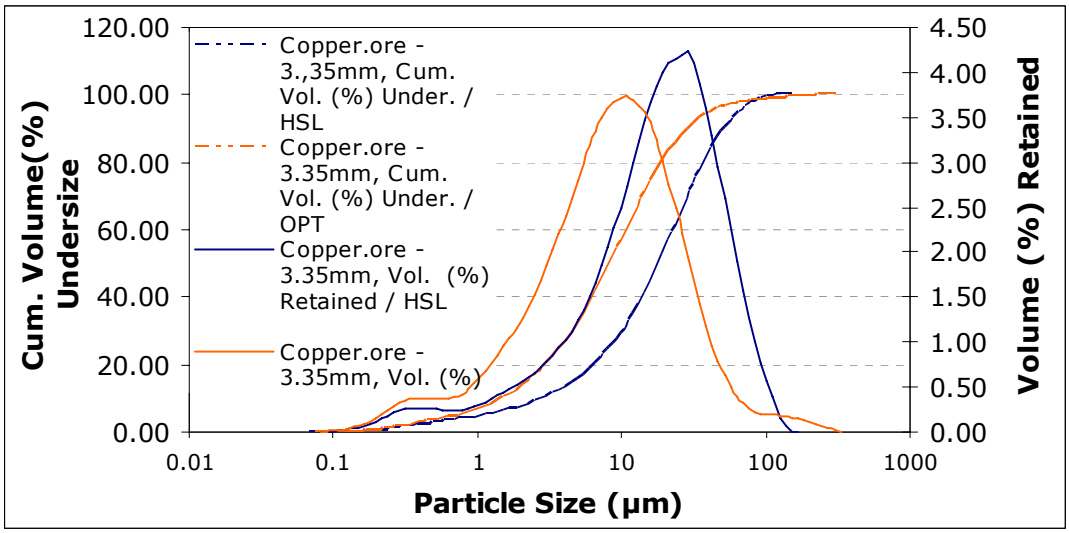

Figure 134: Particle size distribution results of the particulate matter produced by a copper ore feed fraction below 3.35mm and both testing protocols.

9.7.Experimentation using the impact test

The propensity of copper ore to generate fines and dust from industrial processes that involve the impaction of the ore on surfaces or other particles was investigated using the impact apparatus. The experimentation results obtained using the impact test, are presented in the following paragraphs.

9.7.1. Determination of the residual height of the copper ore particulates

The residual height values of the copper ore particles left after impact is displayed in Table 84. For the majority of the copper ore single size fractions the residual height is observed to be inversely proportional to the energy input. Hence, for the lowest energy input, the offset is a maximum value and decreases as the energy input increases. Also at a specific energy level, for example 0.05 kWh/t, the larger size fractions will leave a higher gap between the anvil and the head weight than smaller fractions (Table 84). The increase in mass of a single size fraction, for instance the increase in bulk volume of the 8x6.7mm fraction from 5% to 10% produced a greater residual height, which is observable for any of the copper ore sample tests.

The required energy input levels of the copper ore were calculated using the offset values recorded from limestone during preliminary examination, which are also displayed in Table 84 against the copper ore residual heights. Thus the values that

correspond to the copper ore test samples reflect the final results obtained after impact testing. The offsets recorded for the limestone and the copper ore do not present high discrepancies, although for the 16x13.2mm fraction and 20% bulk volume test sample, the limestone left a larger residual height, whereas for the 5% bulk volume samples slightly higher values were recorded for the copper ore. The required drop height was back-calculated using the residual height that resulted after testing the copper ore to evaluate the degree of difference from the used drop height. These results are shown in appendix VI. Only very small differences were present which suggest that the use of the limestone residual height for the calculation of release height and energy levels were adequate.

Table 84: The offset of limestone and copper ore particles; Limestone residual height has been used for the calculation of the release height of the copper ore samples.

	Residual height (cm)							
	16x13.2mm		8x6.7mm		4x3.35mm		2x1.7mm	
10% bulk volume	copper ore	Lim.	copper ore	Lim.	copper ore	Lim.	copper ore	Lim.
0.05 kWh/t	0.90	0.85	0.57	0.60	0.53	0.48	0.35	0.57
0.1 kWh/t	0.80	1.00	0.48	0.55	0.48	0.63	0.40	0.70
0.5 kWh/t	0.33	0.50	0.30	0.53	0.30	0.27	0.23	0.18
0.68 kWh/t	0.33	0.30	0.32	0.45	0.22	0.42	0.27	0.18
20% bulk volume								
0.05 kWh/t	1.19	1.67						
0.1 kWh/t	1.17	1.65						
0.2 kWh/t	1.16	1.37						
0.3kWh/t	1.13	1.08						
5% bulk volume								
0.05 kWh/t			0.22	0.13	0.12	0.02	0.03	0.02
0.1 kWh/t			0.22	0.13	0.20	0.02	0.07	0.00
0.5 kWh/t			0.18	0.00	0.08	0.02	0.07	0.00
0.68 kWh/t			0.10	0.00	0.10	0.00	0.13	0.00

9.7.2.The bulk density of the copper ore samples

The preparations of the samples used for experimentation with the impact apparatus was based not only on particle size, but also on bulk volume. Each of the single size fractions was represented by two different bulk volumes. With respect to bulk volume, the bulk densities of the test samples were determined and they are displayed in Figure 135. These results correspond to average values of three independent samples, whilst the error bars represent one standard deviation (Figure 135). Only small changes in the bulk densities of the various single size fractions were observed hence for the 5%, 10% and 20% bulk volume test samples the bulk density is 1.40g/cm^3, 1.18 g/cm^3 and 1.14 g/cm^3. The values of the 5% bulk volume samples are higher than any of the other samples because the smaller mass leaves fewer gaps within the particles. The standard deviation of the triplicate test samples was small (<0.06), which confirms that the preparation method is reproducible.

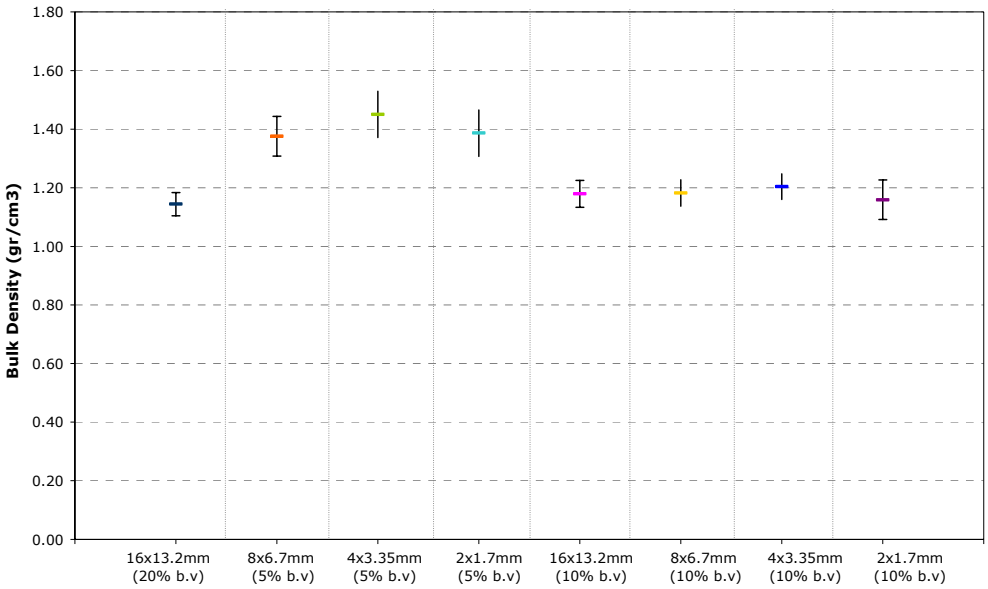

Figure 135: The recorded bulk density values of the copper ore single size fractions. The vertical bars represent one standard deviation.

9.7.3. Impact Test - Results

A series of sample tests using the impact apparatus took place for four different single size fractions of the copper ore, namely the 16x13.2mm, 8x6.7mm, 4x3.35mm and 2x1.7mm. The particle size distribution results of the broken particles were determined by sieve analysis and are presented in Figure 136. It is observed that for any of the test samples, a higher energy input results to a finer particle size distribution even when energy input increases only slightly. The greatest difference between the determined particle size distributions is produced by the samples adjusted to energy levels between the energy levels 0.1 and 0.5kWh/t.

For the 16x13.2mm fraction, the increase in bulk volume from 10% to 20% and experimented at an energy level of 0.05kWh/t, did not produce any distinct difference in the particle size distributions of the fines produced. However, when energy input increased to 0.1kWh/t, then a finer particle size distribution was produced for the 20% bulk volume sample. For the 8x6.7mm, 4x3.35mm and 2x1.7mm fractions the use of a lower bulk volume (5%) produced a coarser particle size distribution. These results suggest that during the testing of lower bulk volume samples, energy is dissipated or transformed to other forms (i.e heat, sound) without further breakage of the particles. Also for a smaller bulk volume sample, the particle-particle interactions taking place during impaction are fewer, and thus the

concentrations of fines should be lower. The relationship between fine particulates to bulk volume and energy input is further discussed in the following paragraph.

For a specific fraction (i.e 16x13.2mm) the average ratio of the cumulative percentages of the two bulk volume samples (i.e 10% and 20%) was calculated to determine under what conditions higher breakage rates were recorded. These ratios do not fluctuate greatly between the various single size fractions. For example, at 0.1 kWh/t the average ratio of the 16x13.2mm sample is 1.57 to one, whilst of the 8x6.7mm, 4x3.35mm and 2x1.7mm is 2.31, 1.43 and 1.56 to one respectively. Overall, only the ratios of the 8x6.7mm fraction are slightly higher, which suggests that more breakage occur in comparison to any of the other samples that their ratios differ only to a small degree.

For any of the single size fractions, small differences in the calculated ratios are observable in respect to energy input. The average ratios of the cumulative percentages undersize for the various bulk volume samples and single size fractions are displayed in detail in appendix VI. There it can be seen that for many of the samples, higher breakage rates are achieved at lower energy levels, which indicates that the increase of energy is not the only parameter affecting breakage, but the sample mass as well. Other parameters that could also affect these results are the orientation of particles in the sample holder and the particle shape.

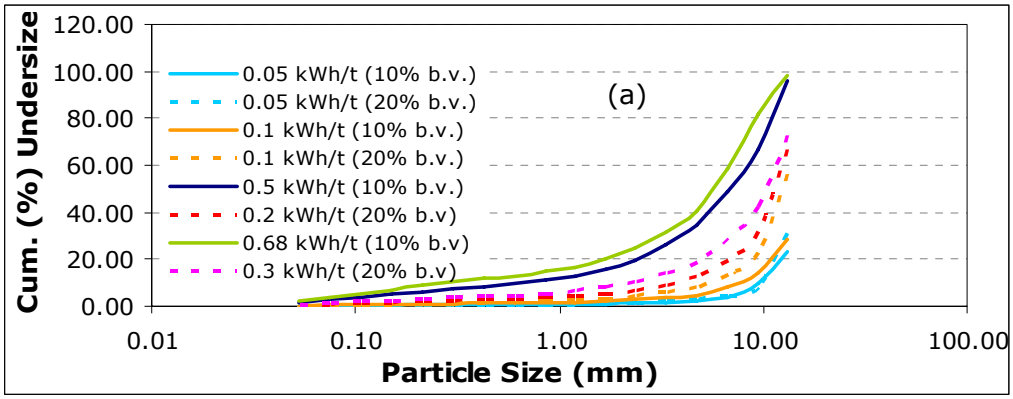

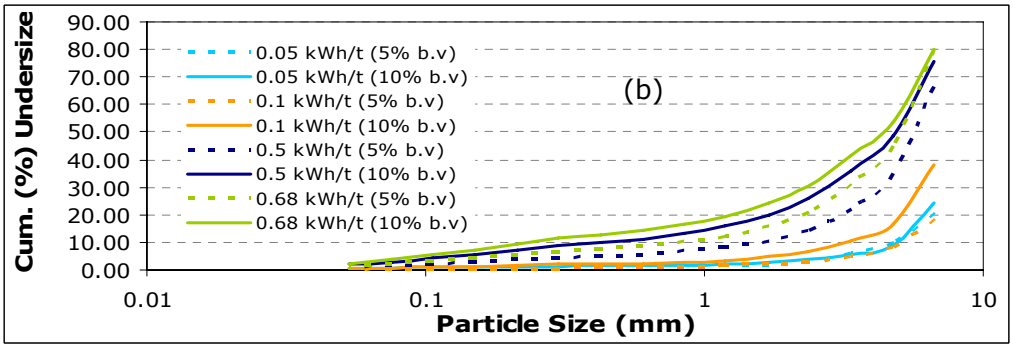

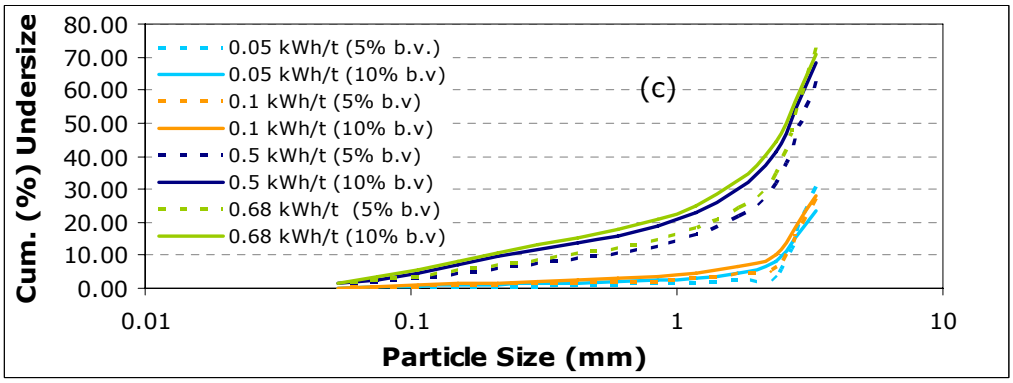

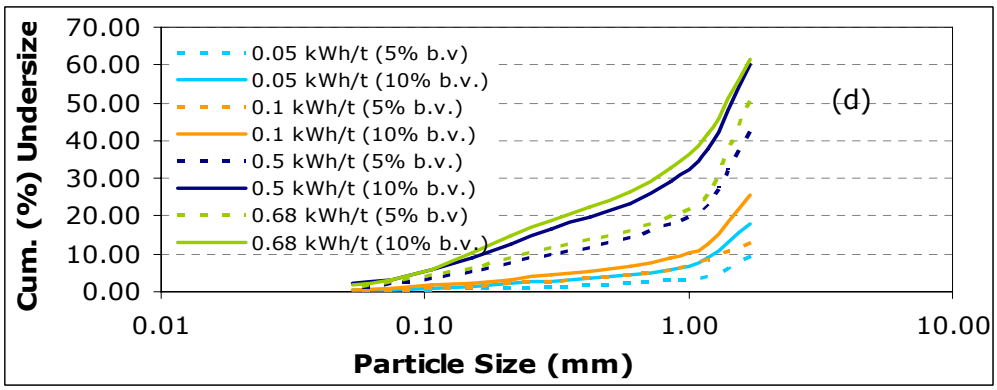

Figure 136: Particle size distribution of the copper ore particles after impact for the single fractions (a) -16+13.2mm (10% and 20% bulk volume) and (b)-8+6.7mm fractions, (c) -4+3.35mm, (d) -2+1.7mm (5% and 10% bulk volume).

9.7.3.1. *The effect of impact upon fines generation for the copper ore*

This paragraph presents a discussion of how the various conditions used during experimentation with the impact test may be related to the generation process of fines. This is of particular interest, as it is during the production of fine particulates that dust is potentially produced. The results presented in Figure 137 describe the cumulative percentages under 53μm collected by sieve analysis from various test samples.

For all test samples the concentration of fines (<53μm) increases as the energy input receives higher values. Consequently, for the majority of the samples, the uppermost energy input of 0.68kWh/t produced the larger concentration of fines, whilst at 0.05kWh/t the lower.

For the 10% bulk volume samples the highest percentage of fine particulates (<53μm) was generated by the 8x6.7mm fraction at 0.68kWh/t, followed by the 16x13.2mm fraction at 0.68kWh/t and the 4x3.35mm fraction at 0.5kWh/t, whereas last in the sequence comes the 2x1.7mm sample at 0.5 kWh/t. At low energy inputs, namely for energy levels of 0.05 and 0.1kWh/t, the 8x6.7mm fraction generated once more uppermost concentrations of fines, followed by the 2x1.7mm fraction and the 4x3.35mm and 16x13.2mm fractions that produced significantly lower percentages of particulates below 53μm.

The increase in sample mass of the 16x13.2mm fraction from a bulk volume of 10% to 20% resulted to an increase in the concentration of fine particulates regarding the comparable energy input levels (0.05 and 0.1kWh/t). On the other hand, the decrease in bulk volume from 10% to 5% for the test fractions 8x6.7mm, 4x3.35mm and 2x1.7mm resulted to smaller percentages of fines (<53μm). For the 5% bulk volume samples, the higher concentrations of particles below 53μm were achieved by the coarser fractions, that is to say the 4x3.35mm and 8x6.7mm, whilst at low energy input (0.05 and 0.1kWh/t) the smaller single size fraction 4x3.35mm and 2x1.7mm generated greater proportions of fines.

In conclusion, the production of fine particulates under impact is governed by the energy input as well as the bulk volume and the particle size of the material. Specific size fractions of the copper ore (i.e the 8x6.7mm) could exhibit a larger liability to

generate dust in comparison to others, whereas the parameters, energy input and bulk volume relate positively to the percentages of fine particulates below 53μm.

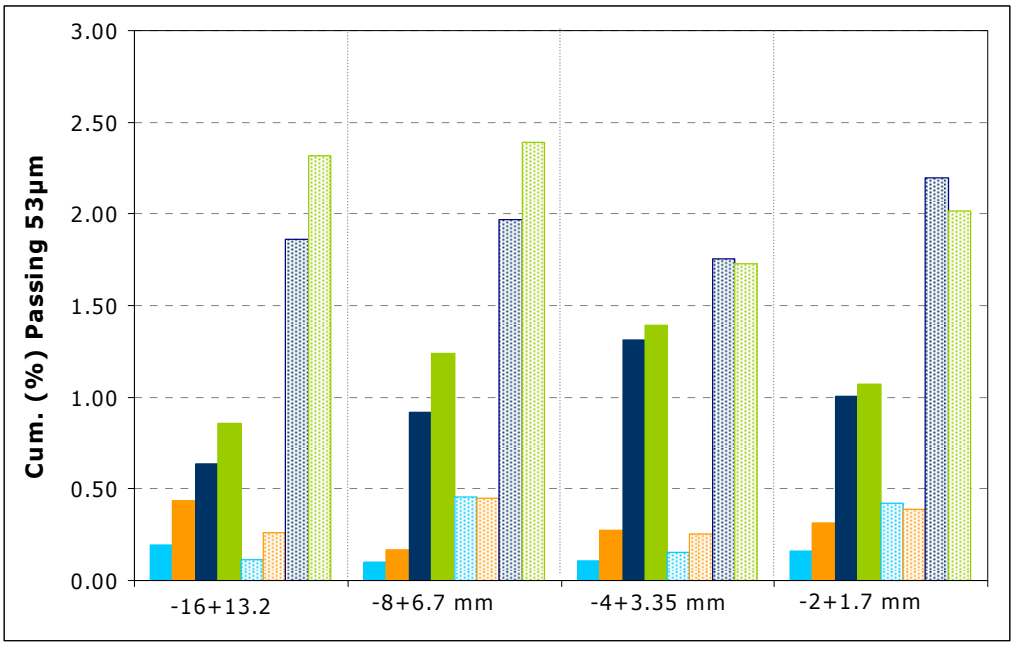

Figure 137: The cumulative percentages passing 53μm for the single copper ore particle fractions. The textured columns represent the samples of 10% bulk volume, whereas the solid coloured columns represent the 20% (for the 16x13.2mm fraction) or 5% bulk volume samples. The different colours represent different energy levels : • = 0.05 kWh/t, • = 0.1 kWh/t, • = 0.5 kWh/t or 0.2 kWh/t (for the 16x13.2mm, 20% bulk volume) and • = 0.68 kWh/t or 0.3 kWh/t (for the 16x13.2mm, 20% bulk volume).

9.7.4. Summary of the impact test results

The copper ore can produce dust from processes that involve the impaction of particles such as drop from heights during tipping, stockpiling, feeding, loading and dumping, as well as due to compression, for instance during the transfer of material with trucks along haulage roads.

Although the impact test did not investigate directly the dustiness of copper ore under impact, that is to say the airborne concentration of particulate matter, nevertheless the use of single size fractions as test samples proclaims that dust would be closely related to the proportion of fine particles produced by impact. Furthermore, particulates of very small size (tens of μm) are not only dangerous when found airborne, because the deposition of them in equipment and products can reduce their effectiveness (i.e due to wear) and quality and additionally they might result to secondary dust sources that can become active during following processing steps.

The effect impact has upon copper ore, was assessed for various single size fractions, bulk volumes and energy input levels and it has been concluded that the dust generation potential of copper ore is influenced by any of these parameters.

Certain trends were observed during the experiments. An increase in energy input resulted to finer particle size distributions and higher percentages of fine particles (<53μm). Also higher bulk volumes produced a smaller particle size and greater concentrations of particulates below 53μm. The particle size of the single fraction influences the breakage of the copper ore and the accumulation process of fines in a more random way. Hence, specific size fractions exhibit a higher liability to break under impact as well as to produce fines. Overall it was found that of the 10% bulk volume samples, the 8x6.7mm fraction generated uppermost proportions of fines, whilst the 4x3.35mm the lowest concentrations.

According to the experimental findings, the mineral flowsheet could be modified in respect to energy input, volume and particle size and to minimise the generation of dust. For example adjusting the energy input in processes that require drop from heights could reduce the generation rates of particulates. Additionally, reducing the bulk volume of the copper ore in use, at such a level that excess quantities of fine particles are not produced would enable the minimisation of dust. Finally taking into account that certain particle sizes (i.e 8x6.7mm) might have a greater potential to produce particulates under impact so as to avoid their use could also prove beneficial for the decrease of fines and dust. If in processes such as loading and dumping, draglines, feeding and other, also the combination of these parameters (energy input, mass and particle size) is taken into account, then further reduction of the generation of particulates could be achieved. The proposed solutions regarding the mitigation of dust produced from the copper ore do not aim to completely replace the existent dust control methodology, but to assist it by providing alternative and cost effective approaches to the problem. The research results have revealed that optimisation practices of processes might improve the current conditions, requiring fewer mitigation practices as well as less water and energy consumption.

9.8. Particle size analysis results of the copper ore particulates produced by the impact test

The fine fraction below 53μm produced by the impact apparatus and collected by sieving, it was further analysed, regarding its particle size using the Malvern Mastersizer – S. Triplicates of each sample were measured adapting the Mie approximation, which made use of the optical properties (refractive indices) discussed earlier in paragraph 9.6.1 and they correspond to a refractive index (real part) of 1.55, an imaginary index of 0.1 and a dispersion medium refractive index of 1.33 (for water). The reproducibility of the measurements taken on triplicate samples is expressed by the median of the diameter of the values d_{10}, d_{50} and d_{90} and their standard deviation and relative standard deviation. In appendix VI, the repeatability of the replicate tests is displayed by the error bars, representing one standard deviation, in the volume (%) retained particle size distributions of the various samples.

According to Table 85, the reproducibility of the particle size measurements from the triplicate tests was good with an average standard deviation of the diameter d_{50} of 2.54 and a relative standard deviation of 7.27%.

The particle size distributions of the copper ore particulates produced by the impact test are shown in Figure 138 and Figure 139. These figures present both the cumulative volume (%) undersize and volume (%) retained that correspond to the fine particles of the 10% bulk volume samples. The particle size distribution of the particulates produced by the 5% and 20% bulk volume sample can be reviewed in appendix VI. The particle size distributions of the particulates generated by the 16x13.2mm did not exhibit substantial differences relative to energy input (Figure 138 (a)). That is to say that the particle size distribution of the particulates produced for energy input of 0.05kWh/t is similar to the one produced for a much higher energy (i.e 0.68kWh/t). The same trend has also been observed for the particle size distributions of the particulates that correspond to the 4x3.35mm and 2x1.7mm samples (Figure 139). A slightly different profile was presented by the particle size distributions of the particulates produced from the 8x6.7mm sample (Figure 138 (b)). Thus the particulates generated at the lowest energy level, namely at 0.05kWh/t, produced a finer particle size distribution, whilst as energy input increases then the particulates resulted to a coarser particle size distribution. At

0.5kWh/t and 0.68kWh/t, the particle size distributions are identical. Nevertheless, the differences in the particle size distributions of the 8x6.7mm sample are small.

Table 85: The median valuesof the diameters d_{10}, d_{50} and d_{90} of the copper ore particulate matter produced using the impact test. The standard deviation and relative standard deviation values correspond to replicate measurements of triplicate sets of test samples. Only the results obtained for the 0.05 kWh/t (E1) and 0.68 kWh/t (E4) are shown.

		D_{10}	Stdev	RSD (%)	D_{50}	Stdev	RSD (%)	D_{90}	Stdev	RSD (%)
16x13.2 mm 10% b.v.	E1	1.91	0.22	11.56	19.29	1.18	6.10	57.27	1.29	2.25
	E4	2.65	0.28	10.55	24.63	0.47	1.90	62.36	2.51	4.02
8x6.7 mm 10% b.v	E1	2.13	0.34	16.02	21.36	2.66	12.46	58.62	2.20	3.75
	E4	3.22	0.13	4.09	26.74	0.95	3.56	63.98	0.41	0.64
4x3.35 mm 10% b.v.	E1	3.01	0.16	5.18	26.27	0.87	3.32	64.53	1.23	1.90
	E4	3.22	0.44	13.77	26.67	0.84	3.13	62.34	2.54	4.07
2x1.7 mm 10% b.v.	E1	2.85	0.31	10.86	24.84	1.38	5.54	61.52	1.18	1.92
	E4	3.19	0.12	3.65	27.04	0.29	1.06	64.55	0.52	0.80

The cumulative volume percentages below 10μm and 2.5μm, and the diameter d_{80} of Table 86 also confirms the particle size distribution profiles of the particulate matter collected by the various impact test samples (Figure 138 and Figure 139). Hence the cumulative volume percentages below 10μm and 2.5μm exhibit only slight fluctuations for the range of test fractions and bulk volume samples. On average 24.9% and 9.2% of the particulates are below 10μm and 2.5μm respectively, whereas 80% of the particles exhibit a size below 48.8μm. For almost all the samples, at low energy input (0.05kWh/t) the cumulative volume percentages below 10μm and 2.5μm presented a small increase in comparison to higher energy levels (0.68kWh/t).

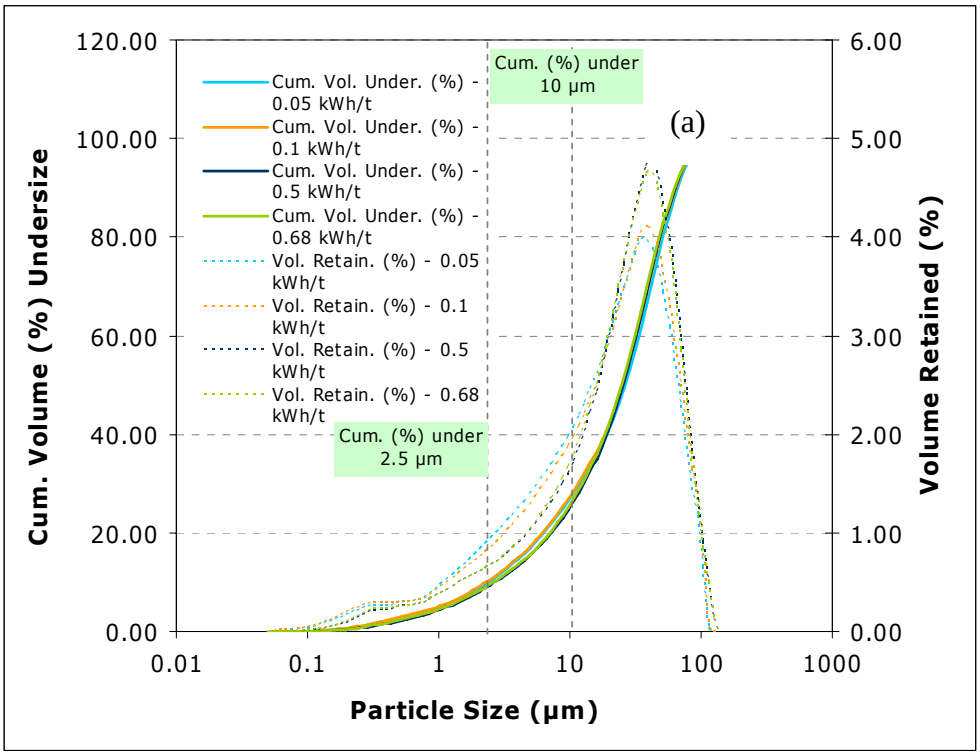

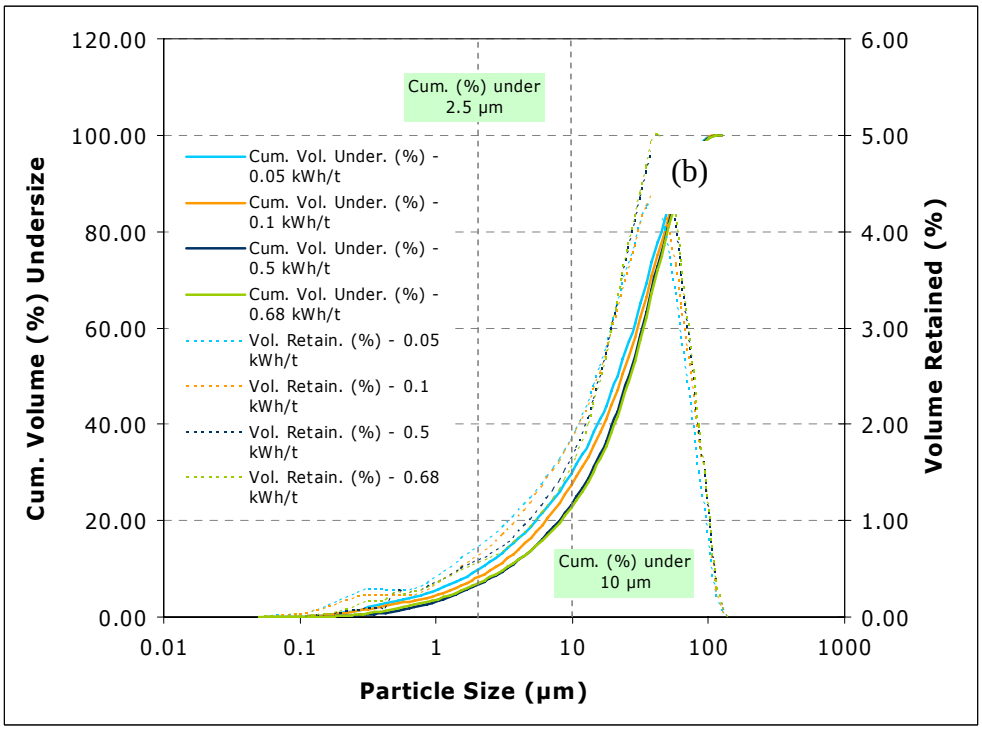

Figure 138: Particle size distributions of the copper ore particulate matter fraction generated by the impact test of a) the -16+13.2mm fraction – 10% bulk volume and b) the -8+6.7mm fraction – 10% bulk volume.

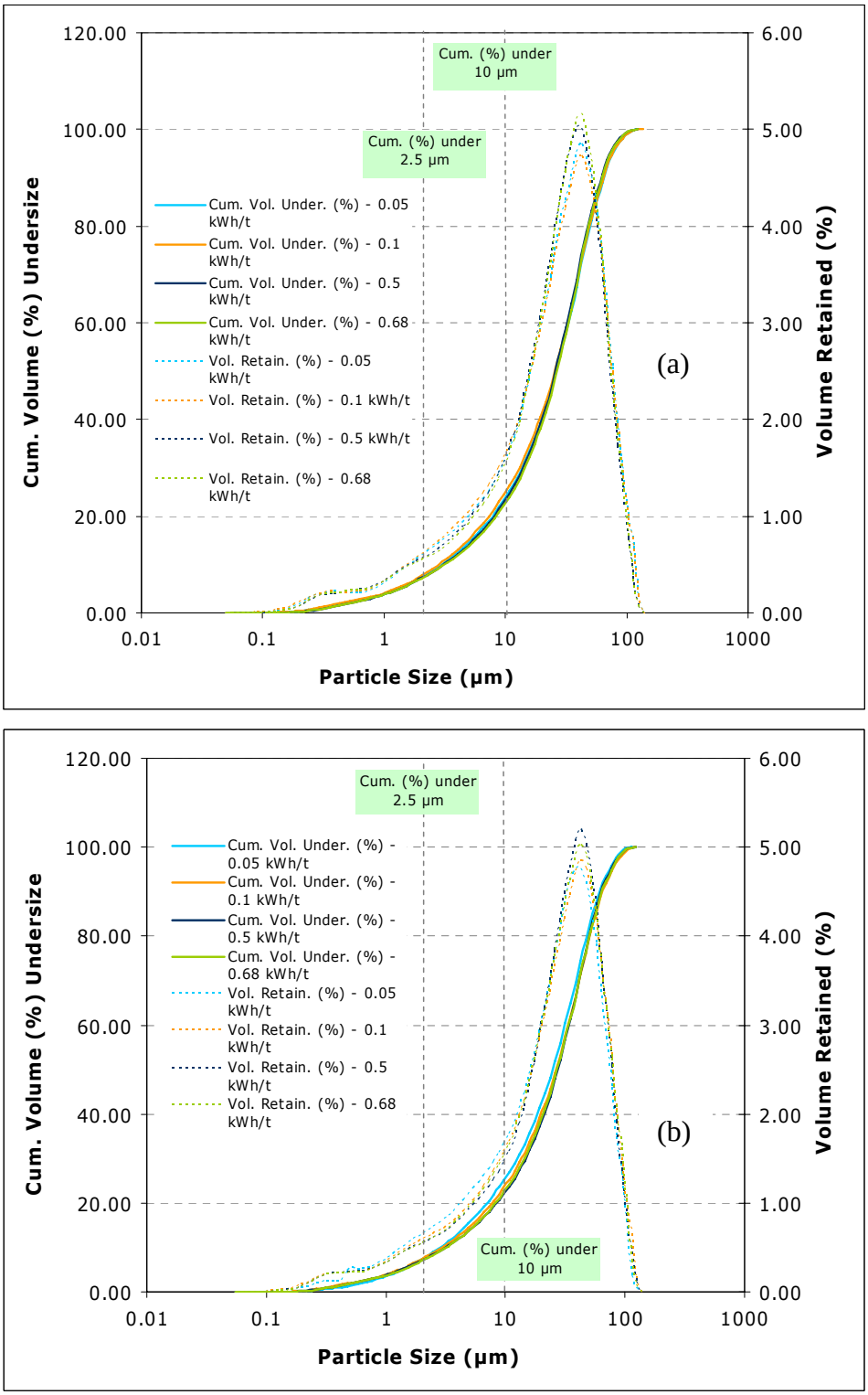

Figure 139: Particle size distributions of the copper ore particulate matter fraction generated by the impact test of a) the -4+3.35mm fraction – 10% bulk volume and b) the -2+1.7mm fraction – 10% bulk volume.

Table 86 : The cumulative volume percentages below 10μm and 2.5μm of the copper ore particulate matter generated by impact testing of a range of single fractions and bulk volumes. The median of the mean diameter d_{80} is shown as well.

Size fraction	Energy level (kWh/t)	Cum. % <10 μm	Cum. % <2.5μm	D_{80}
16x13.2mm-10% b.v.	0.05	33.19	12.46	42.93
	0.68	25.65	9.63	48.24
8x6.7mm-10% b.v	0.05	30.09	11.50	44.55
	0.68	22.76	8.27	49.96
4x3.35mm-10% b.v.	0.05	23.83	8.62	50.14
	0.68	22.64	8.36	49.00
2x1.7mm-10%b.v.	0.05	25.62	8.98	47.81
	0.68	22.91	8.32	50.47
16x13.2mm-20% b.v.	0.05	34.93	14.24	41.87
	0.3	23.86	8.80	49.21
8x6.7mmc-5% b.v	0.05	24.94	8.60	50.79
	0.68	21.99	7.57	51.75
4x3.35mm-5% b.v.	0.05	24.64	8.27	49.88
	0.68	15.58	6.32	52.66
2x1.7mm-5%b.v.	0.05	25.67	9.30	51.07
	0.68	20.27	7.36	50.75

The similar particle size distributions of the particulates generated by the various copper ore test fractions suggest that it is possible to establish a standard or limit value (i.e cumulative volume % below 10μm, 2.5μm) for processes that incorporate the impaction of the ore. This limit will ensure that low quantities of fines are produced, decreasing this way also the potential for airborne particulates to be emitted.

9.9. Mineralogical characterisation of the copper ore particulate matter

The mineralogy of the dust/fines fraction produced during experimentation using the HSE-WSL test and the impact test was defined by X-ray diffraction analysis, as well as using the mineral liberation analysis system of the scanning electron microscope.

An analysis of the X-ray diffraction patterns of the particulate matter shown in Figure 140 indicates that they are identical. The minerals that have been identified earlier during examination of the copper ore were also present in the dust/fines fractions

produced by the HSE-WSL test and the impact test. Hence quartz is the major mineral present, whereas secondary mineral phases comprise the kaolinite, mica and chalcopyrite. The whole-rock analysis of the X-ray diffraction method could not show the differences, if present, for clay minerals, whereas it is difficult to distinguish if the quantities of quartz vary considerably between the various samples.

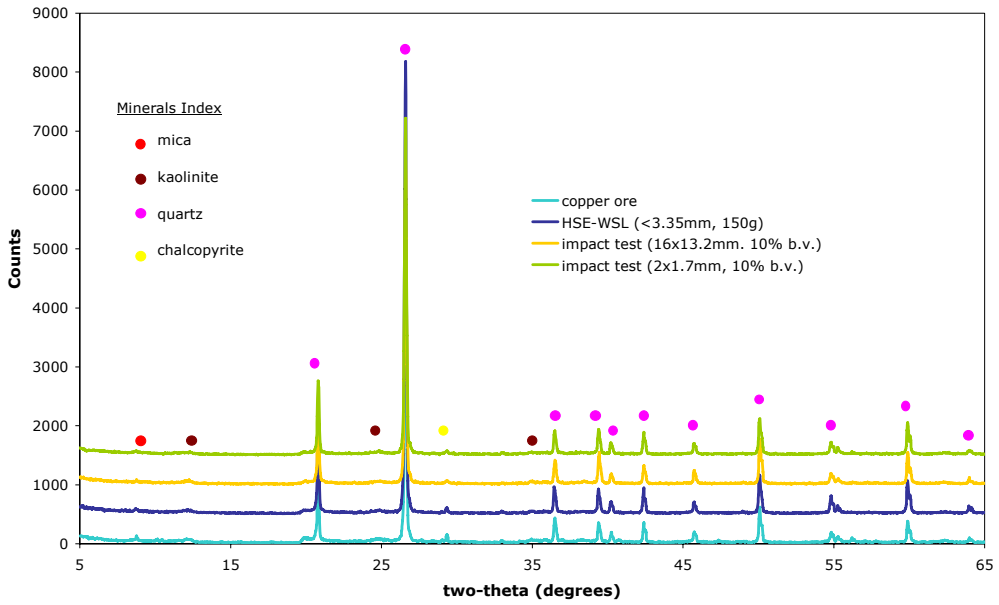

Figure 140: XRD traces of the copper ore particulates collected by the HSE-WSL test and the impact test. The x-ray diffraction pattern of a rock sample is presented as well (two theta, whole rock analysis).

The dust produced by the HSE-WSL test was also examined using the scanning electron microscope and some of SEM photomicrographs are shown in Figure 141. The investigations have shown that the dust fractions consist mainly of quartz particles, but also clay minerals such as kaolinite, which were found in a needle-like form attached on the surface of the quartz particles. These needle-like kaolinite particles are often of a submicron size (width) and quite long exhibiting an aspect ratio that in some cases can be high (i.e 7:1). The acicular shape of kaolinite could comprise a potential occupational health hazard. The presence of clay minerals has been underestimated by the X-ray diffraction analysis, whereas the scanning electron microscopy examination cannot provide bulk quantitative results.

In order to determine accurately what the differences between the dust fraction and the ore are the mineral liberation analyser was employed, which quantified the minerals present by calculating their mineral weight percentages. The dust captured by the HSE-WSL apparatus and the test fractions <9.5mm, <3.35mm, and <1mm as

well as the fines collected by the single size fractions 16x13.2mm and 4x3.35mm at 0.05 and 0.68 kWh/t and 10% bulk volume of the impact test, they were mounted in polished blocks following the procedure presented in Chapter 4. As with the copper ore, the Extended BSE (XBSE) liberation mode has been used for analysis and the details of this method have been discussed in Chapter 4.

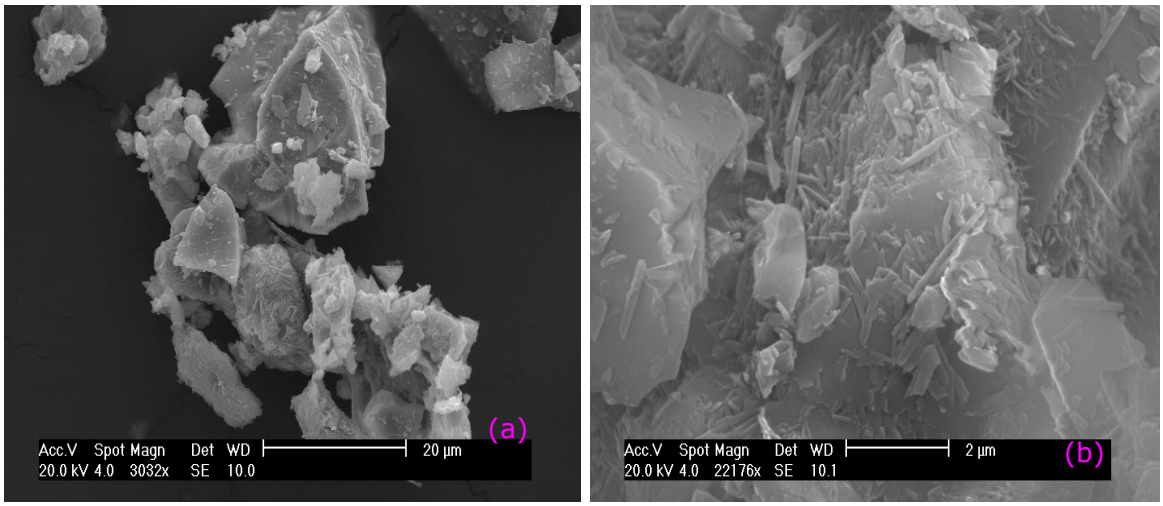

Figure 141: Scanning electron photomicrographs of the copper ore dust produced by the HSE-WSL test from the sample <3.35mm. Quartz particles as well as acicular kaolinite particles are presented (a) Magnification x3032, scale 20μm, (b) Magnification x 22176, scale 2μm.

Approximately 15,300 particles were measured by the XBSE mode, and a variety of mineral phases have been identified. The modal mineralogy results obtained are shown in Table 87, whilst some of the analysis frames are presented in Figure 142. Some further information obtained by the mineral liberation analyzer such as in detail presentation of the modal mineralogy results as well as some SEM photomicrographs can be reviewed in appendix VI.

The mineral weight percentages of the dust/ fines are expressed against the copper ore results. The dust collected by the HSE-WSL test comprises mainly of quartz which corresponds to the major mineral phase, kaolinite, illite and orthoclase that could be described as the second more abundant minerals and biotite, chalcopyrite and pyrite that correspond to the minor minerals phases. The mineral list of Table 87 consists of several other minerals that they participate in very small negligible quantities.

The modal mineralogy of the fines produced by the impact apparatus consist mainly of quartz (major mineral), kaolinite that corresponds to a secondary mineral and

illite, pyrite, orthoclase, biotite, chalcopyrite and iron oxide that participate as minor minerals. Once again several other minerals are present in very small amounts.

Table 87: The modal mineralogy of the copper ore particulates collected by the HSE-WSL test and the impact test determined by the mineral liberation analysis system (XBSE method). The results obtained for the lamproite ore are also presented.

Mineral		HSE- WSL test			Impact Test			
list	Feed	<9.5mm	<3.35mm	<1mm	16x13.2mm, 10%, 0.05kWh/t	16x13.2mm, 10%, 0.68kWh/t	4x3.35mm, 10%, 0.05kWh/t	4x3.35mm, 10%, 0.68kWh/t
Covellite	0.02	0.00	0.02	0.02	0.11	0.02	0.06	0.02
Sphene	0.00	0.04	0.03	0.03	0.02	0.00	0.02	0.00
Quartz	89.32	71.68	72.67	72.34	80.07	86.22	77.84	81.97
Chalcopyrite	1.44	1.86	0.80	0.78	2.16	1.54	2.80	1.94
Pyrite	2.81	1.53	1.40	1.55	4.60	1.73	2.88	1.65
Other	0.32	0.22	0.04	0.04	0.68	0.33	0.58	0.29
Iron	0.09	0.55	0.10	0.08	1.02	0.31	0.18	0.09
Iron 2	0.06	0.07	0.01	0.06	0.01	0.01	0.13	0.00
Titanite	0.02	0.17	0.26	0.23	0.09	0.05	0.09	0.10
Zircon	0.34	0.01	0.02	0.02	0.22	0.07	0.22	0.14
Ankerite	0.07	0.05	0.16	0.08	0.03	0.01	0.05	0.00
Orthoclase	0.28	3.08	4.48	3.76	0.98	0.68	0.53	0.76
Biotite	0.72	1.56	2.01	1.78	1.01	0.96	1.52	1.42
Kaolinite	2.88	14.13	10.86	11.96	5.85	5.39	10.57	8.82
Illite	1.64	5.06	7.17	7.28	3.17	2.70	2.54	2.80
total	100.00	100.00	100.00	100.00	100.00	100.00	100.00	100.00

The modal mineralogy results of the copper ore, the dust fraction of the HSE-WSL test and the fines of the impact test exhibit significant differences. Thus the airborne particulate matter comprises of a lower mineral weight percentage of quartz than the copper ore and the fines produced by the impact test. The minerals kaolinite, illite and orthoclase participate with higher mineral weight percentages in the dust fraction of the HSE-WSL test than in the ore or the impact test fines. On the other hand, the fines produced by impact also exhibit some differences when compared with the copper ore. Hence, the mineral weight percentage of quartz is lower than in the ore, although the discrepancy is not as large as the one recorded between the ore and the HSE-WSL dust. Also the clay minerals kaolinite and illite present higher percentages than the copper ore, but not as high as the measured ones for airborne particulates. For the fine particulates of the impact test, it can be seen that the higher energy input in any of the test fractions (16x13.2mm or 4x3.35mm) resulted to an increase in the quantity of quartz. Also for the 4x3.35mm sample larger mineral weight percentages of kaolinite were recorded in comparison to the 16x13.2mm sample.

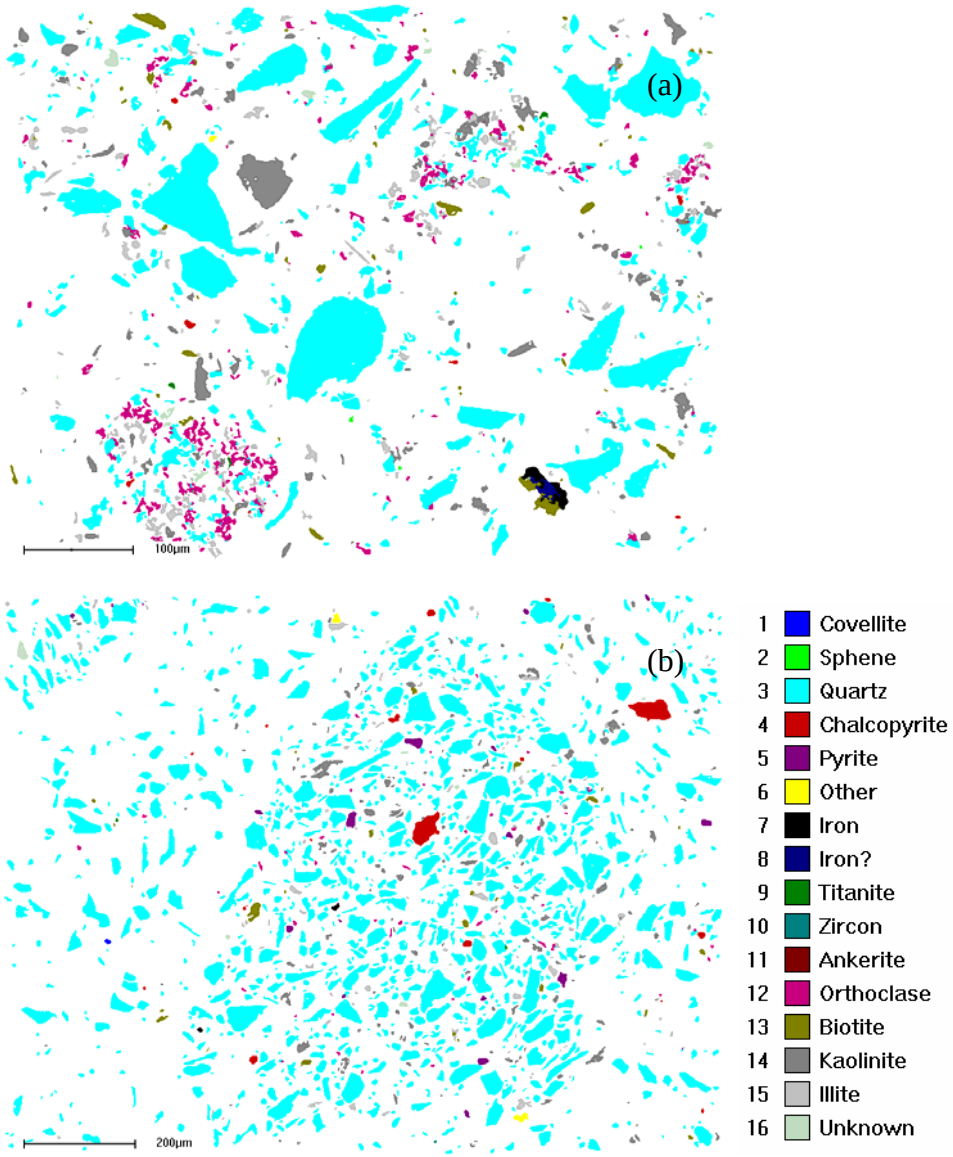

Figure 142: The modal mineralogical profile of the copper ore particulates produced (a) by the HSE-WSL test, from the <9.5mm test sample, magnification X200, scale 100µm and (b) by the impact test from the 16x13.2mm -10% bulk volume at 0.68kWh/t sample. The various grain colours correspond to different minerals shown in the mineral list. Magnification x350, scale 200µm.

Overall it can be said that the dust and fine fraction collected by the HSE-WSL test and the impact test comprise of smaller amounts of quartz and increased amounts of soft minerals such as clays (kaolinite, illite) and feldspars (orthoclase).

The mineralogical profile of dust produced by abrasion was different to that of the fines produced by impact, that is to say that the airborne fraction consists of lower mineral weight percentages of quartz and higher of clays and feldspars. The abrasion mechanism will tend to generate fine particulates due to friction, therefore soft minerals have got a greater potential to be generated under such processes. However, the impact test did not collect the airborne particulate matter thus a direct

comparison is not made. The mineral weight percentage of the copper rich mineral, chalcopyrite is similar for the ore and the dust/fines, which indicates that the generation of dust under abrasion or impact will cause loss of valuable material. In order to estimate the hazardous potential of dust to human health and the environment, analysis steps such as the use of the mineral liberation analyser, are essential.

9.10. Summary of Chapter 9

The effect of the two predominant dust generation mechanisms of impact and abrasion on Kennecott copper ore occur on a variety of mining operation and they were assessed using the impact apparatus and the HSE-WSL test. Typical examples of such operations include the blasting, loading, dumping, preparation stages of ore through crushing, grinding and screening, transferring of ore in haulage roads and conveyor belts, sorting, general handling processes, stockpiling and other.

A variety of copper ore fractions (<9.5mm, <3.35mm and <1mm) were tested under abrasion using the HSE-WSL apparatus and utilizing two testing protocol that are based on different operational parameters. The OPT-TP produced the maximum dustiness, with the <3.35mm fraction receiving the highest value and the <1mm sample the lowest. The results indicated that the increased tumbling time of the OPT-TP is responsible for the difference in dustiness recorded and not the mass. The optimum parameters procedure made use of a lower mass, 150g instead of 200g. It was further concluded that the concentration of fine particles present in the test sample was not related to the dustiness. For instance, the <1mm sample that included the higher proportion of particulates below 75μm, generated the lowest dust levels. Thus, the abrasion mechanism taking place in the drum as well as the moisture content of the test sample, were considered to explain the discrepancy in dustiness observed for the various test fractions. Consequently, in order to reduce or control dust produced from copper ore, optimisation practices should take place regarding the time scale of operations and the abrasion effect on the ore. For example, by reducing the time scale of processes such as comminution, transport and haulage and by optimising their operation to achieve minimum unnecessary abrasion could result to less dust.

The particle size analysis results of the dust collected by the HSE-WSL test has shown that for the OPT-TP the dust particle size distributions of the various sample

fractions are similar, whereas for the HSL –TP the dust of the <1mm sample produced a finer particle size distribution than the <9.5mm and <3.35mm samples that produced similar dust particle size distributions. For a specific test fraction (i.e <3.35mm), the dust particle size distribution produced by the OPT-TP is finer than the one produced by the HSL-TP. Hence the longer operational time and higher abrasion rates of the OPT-TP resulted to a finer particle size.

Testing using the impact test occurred for a variety of single size copper ore fractions and bulk volumes and certain trends were observed. The application of higher energy input and larger bulk volumes of ore resulted to finer particle size distributions and greater percentages of particulates below 53μm. The particle size of the copper ore that comprises the test sample also influences the generation process of fines, but in a more complicated way. For instance, for the 10% bulk volume samples the 8x6.7mm fraction produced uppermost amounts of fines, whereas the 4x3.35mm fraction the lowest. Therefore mining processes that involve impaction of the copper ore, such as drop from heights, could minimise the generation of particulates by reducing the energy levels in impact or the bulk volume of the ore in use. If single fractions are utilised then the use of a particle size that has a lower potential to produce dust (i.e 4x3.35mm instead of 8x6.7mm) could also assist the mitigation plan.

The particle size distribution results of the fine particles produced by the impact test and by various single size fractions and bulk volume samples are very similar and only small discrepancies were present. These results suggest that for processes that involve impaction of the ore particles a limit value could be set (i.e cumulative volume % below 10μm, 2.5μm), which could ensure that low concentrations of fines are produced, reducing this way also the potential for airborne dust to be generated.

The mineralogy of the dust/fines produced by the HSE-WSL test and the impact apparatus was investigated by X-ray diffraction analysis, scanning electron microscopy and using the mineral liberation analysis system. The X-ray diffraction analysis concluded that dust and fines present a mineralogical profile not different from the ore, which implies that the same minerals have been identified. When the airborne dust of the HSE-WSL test examined using a scanning electron microscope, it was found that although the samples mainly consist of quartz, the abundance of kaolinite was also significant. Kaolinite is present in particles of acicular shape with very small size and quite often high aspect ratio, which suggests that it could comprise an occupational health hazard. At the final investigation step the

mineralogy of the dust and fines was accurately determined using the mineral liberation analysis system. The modal mineralogy of the samples was expressed in mineral weight percentages of the participating minerals. Results have revealed that the mineralogy of the ore, the dust produced by the HSE-WSL test and the impact test exhibit substantial differences. Although the same minerals have been identified, the mineral weight percentages were different. Hence, the airborne dust fraction of the HSE-WSL test consists of a lower concentration of quartz, which is the major mineral phase and significantly higher percentages of kaolinite, illite and orthoclase that they correspond to the secondary minerals, than the ore and the fine particulates of the impact test. The fines of the impact test on their turn also exhibit a lower mineral weight percentage of quartz and higher concentration of kaolinite and illite than the copper ore. Therefore the abrasion and impact mechanisms produced different mineralogical profiles, in particular regarding the concentration of clays. The mineral chalcopyrite, which comprises the main copper source of the ore, was present in the dust fraction as well as in the impact test fines, which implies loss of valuable material. The accurate determination of the composition of dust is of great importance to occupational hygienists, environmental and air quality scientists as well as legislative parties and the utilization of the mineral liberation analyzer assisted to the detailed analysis of the particulate matter.

The experimental findings of this chapter, associated with the Kennecott copper ore, do not intend to produce a method that it will confute existent practices. On the contrary it aims to provide additional information and alternative solutions that could be incorporated with the mitigation methods already in use. The suggestions made focus in optimising processes that include the abrasion or impact mechanisms and operational parameters such as energy input, bulk volume, time-scale and particle size so as to achieve low generation of dust and consequently minimise the need for dust control applications.

Chapter 10. Discussion

10.1. Introduction

In Chapter 10 the experimental results obtained from the five different ores are compared on the basis of the same testing technique, in order to identify which dust generation mechanism is prevalent for each material. These comparative studies aim to determine whether a certain ore will exhibit a greater potential to produce particulates in processes that involve either abrasion or impact mechanisms. The comparative results of the dustiness HSE-WSL test and particle size analysis results are presented first followed by the impact test and particle size measurement results. The outcomes of experimentation with each individual ore have been presented and discussed in detail in the corresponding Chapters 5 to 9 where they can be reviewed.

10.2. Discussion of comparative HSE-WSL dustiness measurement results obtained for the various ores

The graphs of Figure 143 and Figure 144 classify the various ores according to their dustiness values, from low to high, and for both testing regimes. Figure 143 shows the dustiness values obtained using the HSL-TP and the graphs (a), (b) and (c) describe the results of the <9.5mm, <3.35mm and <1mm test samples respectively. Figure 144 presents the dustiness of the optimum parameters testing regime, where

the graphs (a), (b) and (c) they also represent the results of the test samples <9.5mm, <3.35mm and <1mm.

If dustiness values are to be presented on a scale where the first in the sequence corresponds to the ore of highest dustiness and the last in place represents the ore of lowest dustiness, then it is observed that such a scale will be influenced by the testing protocol, the particle size distribution of the test sample and mineralogy.

According to the results of Figure 143, it can be seen that the relative dustiness position of ores changes with regard to particle size of the feed sample. For instance, limestone produced the lowest dustiness value than any of the other ores for the feed sample <9.5mm, and the highest for the feed sample <3.35mm (Figure 143). Similarly the coarse feed fraction (<9.5mm), of the iron ore particles produced the second highest dustiness in comparison to other ores, whereas the finer feed fractions produced the lowest

For the results of the OPT-TP, the relative dustiness positions of the various ores presented less dependency with the particle size distributions of the feed samples, therefore it is easier to classify them into a dustiness scale. The operation of the test under longer tumbling time enables attrition-abrasion mechanisms in the mill, which affect the dustiness recordings resulting in higher values. Therefore it is expected that the dustiness of ores will closely depend on rock related characteristics such as hardness and mineralogy. Additionally the sample is allowed to produce dust that results from the quantity of fines in the feed for longer and thus more subjective dustiness profiles of the ores are constructed.

Talc almost in all occasions (various feed samples) produced the highest dustiness index followed by the copper and argyle ores, which in turn is followed by the iron ore that produced the lowest dustiness (Figure 144).

Limestone comprised the only exception and as in the case of the HSL protocol, its dustiness index varied significantly with the particle size of the feed sample. This behaviour of limestone is attributed to the optimisation and control steps that took place during preliminary testing with the HSE-WSL mill.

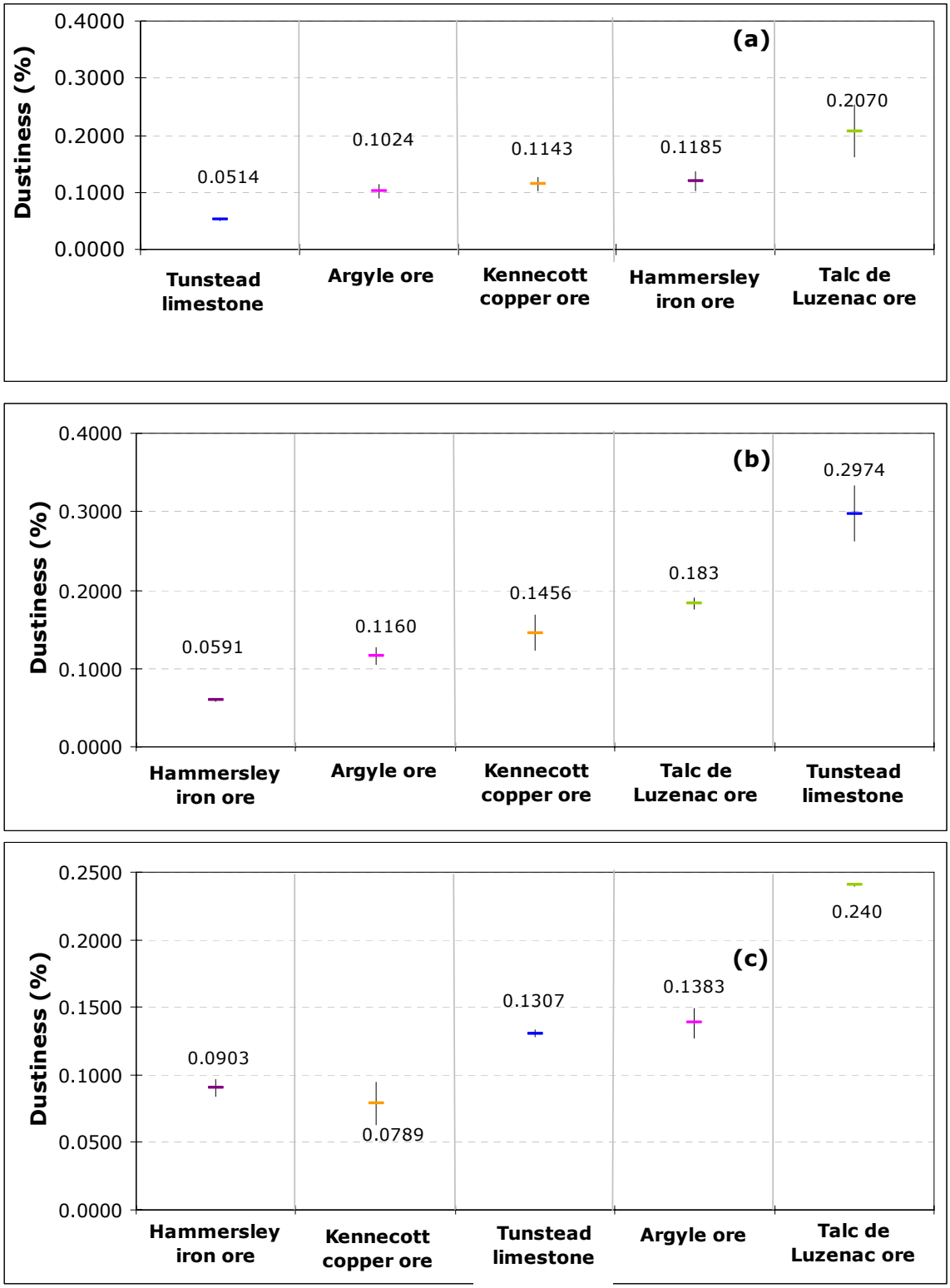

Figure 143: Dustiness results of the various ore samples obtained by the HSL testing protocol for (a) a feed <9.5mm, (b) a feed <3.35mm and (c) a feed <1mm. The presented values correspond to a median dustiness value, whilst the error bars correspond to one standard deviation calculated by triplicate tests.

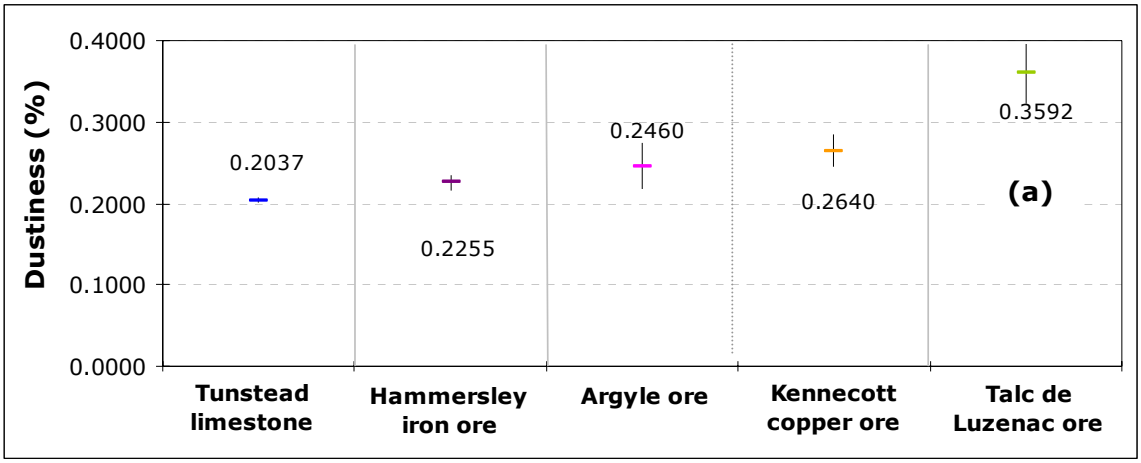

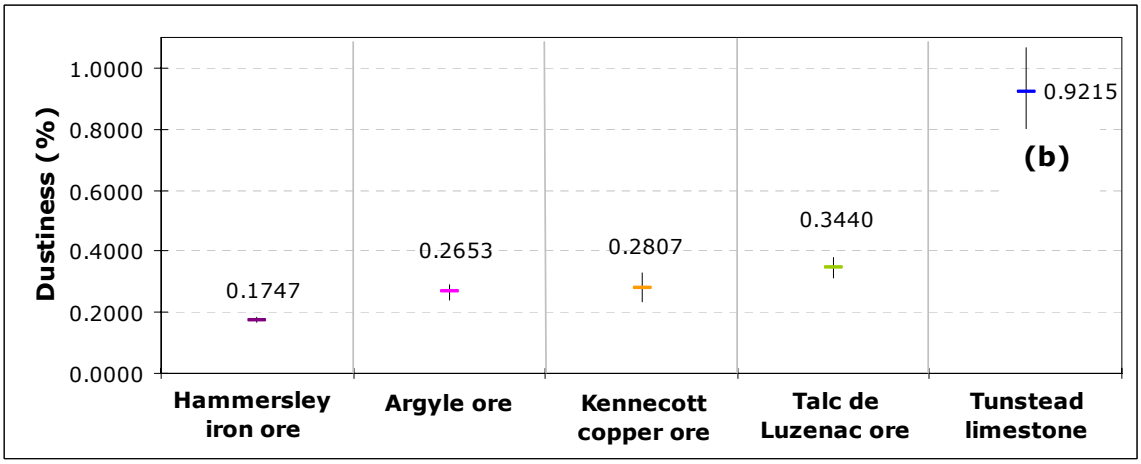

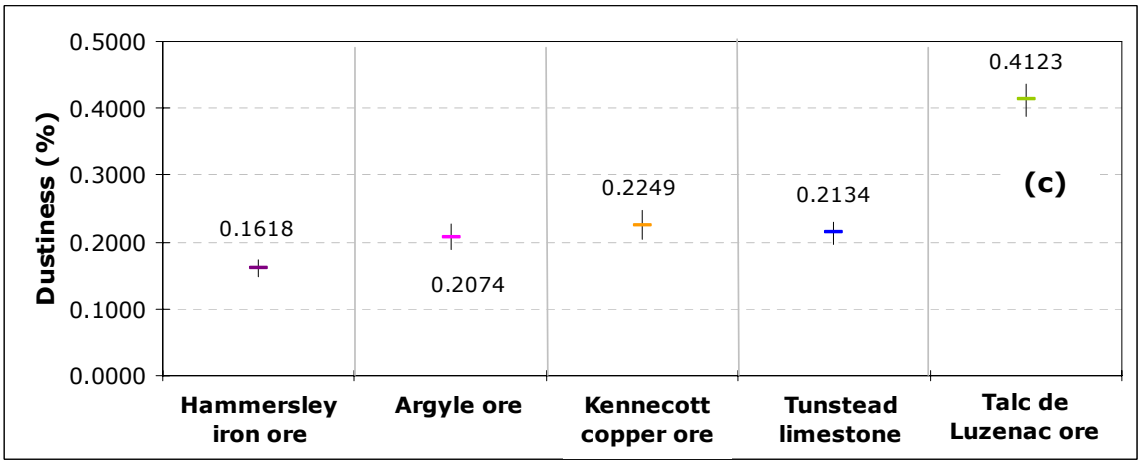

Figure 144: Dustiness results of the various ore samples obtained by the optimum parameters testing protocol for (a) a feed <9.5mm, (b) a feed <3.35mm and (c) a feed <1mm. The presented values correspond to a median dustiness value, whilst the error bars correspond to one standard deviation calculated by triplicate tests.

The OPT-TP made use of these operating conditions (feed sample mass, tumbling time, flowrate) that produce the highest dustiness for the <3.35mm limestone sample, therefore it is not of surprise that the values of the other feed sample fractions (<9.5mm, <1mm) produced very different dustiness. Furthermore the

coarse limestone particles (in <9.5mm sample) tend to be hard as they consist of well compacted fine grained limestone particles, whereas when the limestone is reduced in size it produces high concentrations of fines, which could easily end up as airborne dust.

The effect that the different operating conditions (HSL-TP and OPT-TP) had upon the dustiness of limestone suggests how important is to properly understand their relation with various materials, whilst careful changes (i.e operating time) could have a significant effect (i.e minimisation) upon emitted dust. The above statement could equally be applicable to processes that generate dust by abrasion (conveyor belts, haulage roads, screens). For example, the discreet element modelling findings suggest that the velocity of conveyor belts or of vehicles in haulage roads should be limited in such levels that substantially reduce the effect of friction on the rock particles that produces dust. Also reducing the length of conveyor belts by using an in-pit primary crusher would minimise the initial requirements for transfer of ore and consequently the residence time of rock on conveyor belts, one of the main factor liable for the production of dust as experimentation with the HSE-WSL mill has shown. In screening processes, the generation of dust could be reduced by optimising their operation, for example by investigating the relationship between different inclination angles and friction, or by adjusting the time scale of the process at levels that low abrasion occurs, without diminishing its operational effectiveness . Thus for every material a set of operating conditions should exist, which will result to very high dustiness values under the effect of abrasion and this set of data will greatly depend on material characteristics such as the hardness, mineralogy and particle size.

The almost consistent relative dustiness position of the other four ores for any of the different feed samples (<9.5mm, <3.35mm, <1mm), does not indicate that these are not influenced by the differences in feed's particle size distributions. However these differences are not of the same scale as with limestone. For the iron ore, lamproite, copper ore and talc, the influence of rock related characteristics (hardness, mineralogy) on dustiness is clearly demonstrated. Therefore, talc which comprises the softest material, always results to the highest dustiness values. The iron ore is hard due to the presence of hematite and for this reason its resistance under abrasion is high resulting to low dustiness. The generation of dust from the iron ore is believed that is mainly attributed to the second iron oxide, the goethite which is a softer mineral than hematite. The XRD analysis of the dust fraction showed the presence of both oxides. However it was not possible with X-ray diffraction

analysis to accurately distinguish and quantify the two oxides. The lamproite and copper ores both consist of high quantities of quartz together with some clay-chlorite group minerals. Quartz is a much harder mineral than the clay/chlorite group minerals, therefore in the dust fraction it participates in much lower quantities. Also the quartz grains in the lamproite are finer than in the copper ore (Figure 145), whilst the presence of significant concentrations of chlorite and illite in the lamproite, provides a good cement option for the quartz grains, resulting to a hard and compact rock.

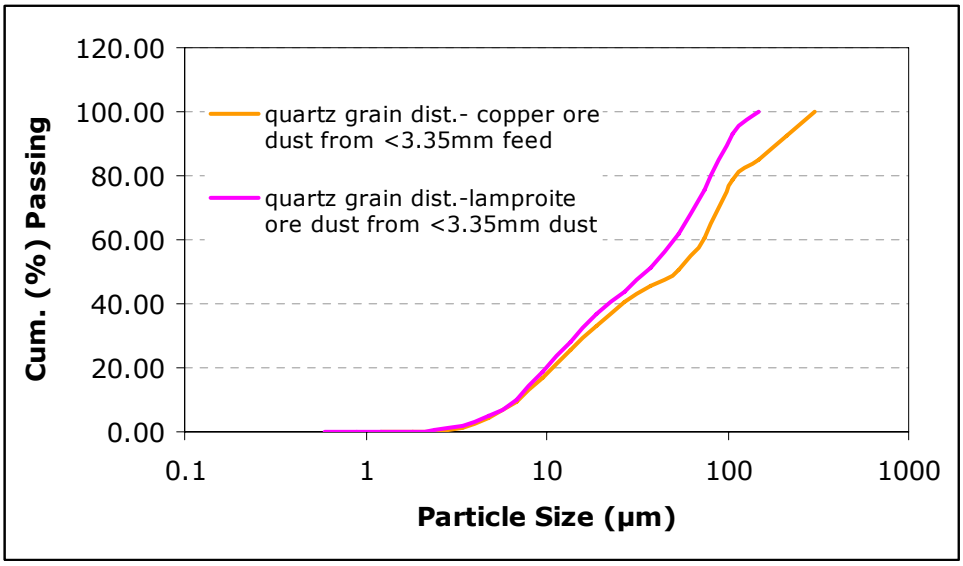

Figure 145: Quartz particle grain distribution of the copper ore and the lamproite ore dust generated by the HSE-WSL test using a feed sample <3.35mm. These results correspond to microscopy observations, which were automatically recorded by the Mineral Liberation Analyser.

The copper ore consists mainly of quartz grains of various sizes that are poorly cemented. Hence the lamproite produced lower dustiness than the copper ore.

The variation in the dustiness indices of the majority of the samples except from talc and limestone (<3.35mm) is within the scale of tens of milligrams. Nevertheless even very small differences might be of great importance for occupational health limits or air quality standards. A classification of materials according to their dustiness values (dustiness scales) could assist engineers to decide on their mitigation strategy and the volume of control approaches needed. Thus, it should be expected that processes such as the transfer of ores through feeders, chutes, conveyor belts or the sieving of talc, will require more mitigation and control practices than the iron ore, because talc is more liable to generate dust under the effect of abrasion mechanism. Nevertheless further work is required to produce a

dustiness classification scheme which will include various materials and it will accurately relate the dust generation potential of ores with mitigation practices.

10.3. Discussion of the particle size analysis results of the HSE-WSL dust

In order to identify what materials produce the finer particulates and whether there is some correlation between dustiness and dust particle size, the particle size analysis results of the various ores were compared. The cumulative volume percentages passing 10μm and 2.5μm of the different ores are presented in Figure 146.

According to these comparative results (Figure 146), talc produced the lower cumulative volume percentage of dust particles below 10μm and 2.5μm than any of the other ores, in almost all occasions, which suggests that dust from talc is coarser than any of the other ores.

On the contrary, limestone produced the higher volume concentration of particles below 10μm and 2.5μm, even for the feed sample (<9.5mm) that is described by a very low dustiness index. This is because limestone rock consists of very small calcite particles (<10μm).

The lamproite resulted to the second higher cumulative volume percentage of particles below 10μm and 2.5μm, which is attributed to the presence of a significant concentration of minerals like illite and chlorite in the dust fraction. One of the main characteristics of these minerals is their very small particle size.

Copper ore dust presented slightly lower volume percentages of particles below 10μm and 2.5μm than the lamproite. The quantitative mineralogy analysis of the copper ore dust using the Mineral Liberation Analyser, has shown that it consists of higher quantities of quartz than the lamproite, whereas the quartz grain size distribution of Figure 145, indicated that the copper ore quartz particles are coarser than the lamproite.

For the iron ore, the particle size distribution of dust presented large differences for the various feed samples. Therefore, the iron ore dust produced by the <9.5mm feed presented very low percentages of particles below 10μm and 2.5μm, even lower than talc, whilst the finer the feed sample was, the finer the dust particle size distribution appeared.

Consequently, ores of high dustiness such as talc produced coarser dust particles than materials of low dustiness such as the lamproite and the iron ore (<1mm, <3.35mm). Therefore, even if the quantity of dust yielded from a specific material is low, depending on its particle size, mitigation practices could be essential to minimise risks against the health and safety of humans or to prevent environmental impacts associated with fugitive dust emission.

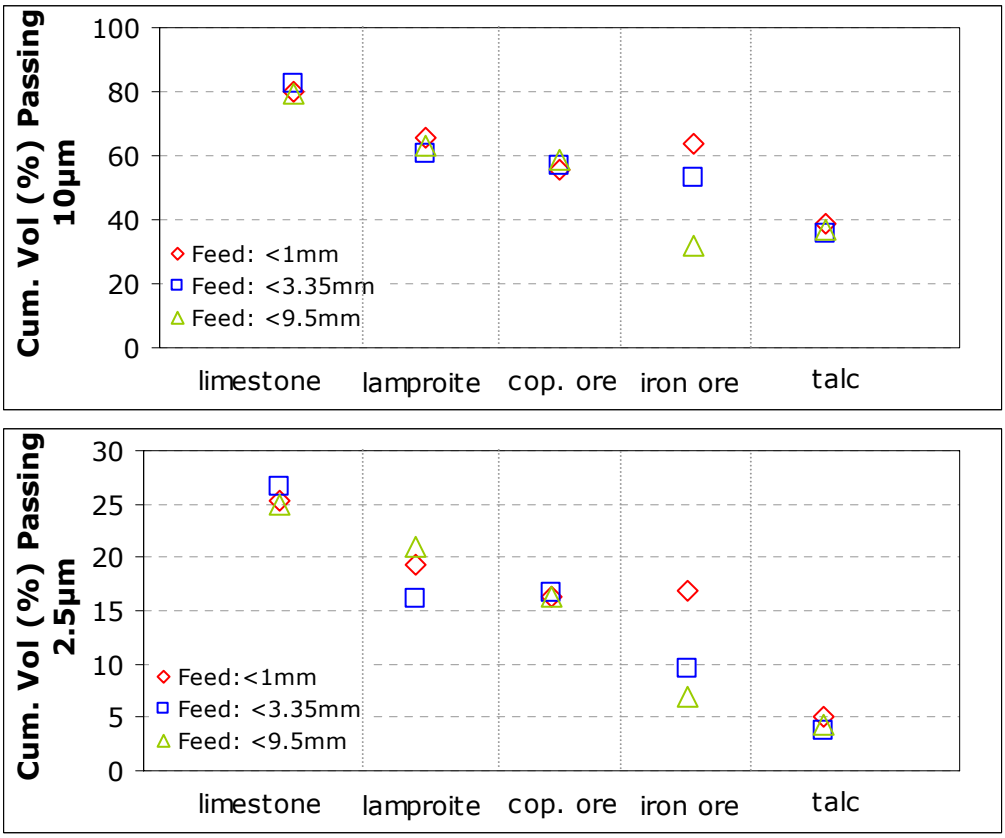

Figure 146: The cumulative volume percentages below (a)10μm and (b) 2.5μm of the various ores as resulted during testing using the OPT-TP and for the different feed fractions (<1mm, <3.35mm, <9.5mm). The results correspond to median values calculated by replicate tests.

10.4. Discussion of the comparative impact test results

The concentrations of fine particulates produced by impact from the various test materials were compared to assess whether certain ores have a greater potential to produce dust/fines than others. The comparative results that correspond to the four single size fraction, 16x13.2mm, 8x6.7mm, 4x3.35m and 2x1.7mm of 10% bulk volume are presented in Figure 147.

A wide spread of values were obtained that vary with respect to rock type, energy input and particle size of the test sample.

At low energy input that is 0.05 kWh/t and 0.1 kWh/t, talc produced the highest quantities of fines than any of the other ores and lamproite the lowest. The cumulative percentages of particles below 53μm that corresponded to the copper and iron ores and the limestone were higher than the respective of lamproite and lower than talc, and fluctuated in a small degree between them. Talc represented the softest rock sample and at low energy input it broke easier than the other samples and therefore generated higher quantities of fine particulates.

At higher energy input, the cumulative percentage below 53μm for the majority of the materials was influenced by the particle size of the feed sample and for that reason comparative results show slight variations. For instance, the 16x13.2mm single fraction of iron ore and copper ore produced the highest quantities of fines, whereas lamproite the lowest.

The lamproite ore produced the lowest amount of fine particulates for any of the particle size fractions of the feed samples. Talc resulted to the highest concentrations of fines for the single fractions 8x6.7mm and 4x3.35mm. Although talc would be expected in any occasion to produce the highest amounts of fines as it comprises the softest test material, this did not happen because often at high energy input levels impaction caused the compaction of the layered structure of talc particles. Thereafter talc particles presented an elastic behaviour, which discouraged further breakage to occur. Iron ore generated some of the highest concentrations of fine particles for any of the single size fractions of the feed sample. The copper ore and limestone produced slightly lower quantities of fines than the iron ore, except from the

2x1.7mm fraction where the limestone produced a greater concentration of particulates.

When the bulk volume of the 8x6.7mm, 4x3.35mm and 2x1.7mm fractions was reduced to 5%, then the highest concentrations of fines (<53μm) were recorded by limestone, followed by the iron ore and the talc, whilst the copper ore and the lamproite produced the lowest concentrations. For the 16x13.2mm fraction, the increase in bulk volume from 10% to 20% resulted to higher quantities of fines (<53μm) from iron ore and talc, whereas the copper ore, the limestone and the lamproite generated fewer fine particulates.

The comparative results derived from the impact test have shown that the propensity of rocks to generate dust/fines cannot be described by a single gradation sequence as the influence of parameters such as the feed particle size, the particle orientation, the hardness, the bulk volume and mineralogy is of major importance.

Nevertheless, a fineness gradation sequence could be produced for selected test materials that are characterised by significant differences in hardness, or resistance under impact and mineralogy. The iron ore and lamproite comprise a good example of the above statement as the first was characterised by low resistance under impact, and the latter by high resistance to impact, whilst the difference in the cumulative percentages of particles below 53μm could be up to 4 times higher for the iron ore. The lamproite comprises a hard compact rock that consist mainly of fine grained quartz cemented on an illite-chlorite matrix, whilst the low resistance to impact for the iron ore is attributed to the presence of goethite, which is a significantly soften mineral than hematite.

The effect of impact mechanism upon any ore in processes that involve drop from heights could be reduced by adjusting the energy input to as low levels as possible, either by lowering the drop height or/and minimising the bulk volume of ore and therefore generating smaller amounts of dust. This could be implemented by utilizing conveyor belts with adjustable booms that would employ the lowest height possible during tipping and stockpiling. Drilling and blasting also produce substantial quantities of dust due to impact. Drilling could be optimised by utilizing energy input levels that suit the particular characteristics such as hardness of each ore, whereas the use of fragmentation modelling during blasting design could prove beneficial for the minimisation of unwanted fractions of rock such as dust and fines.

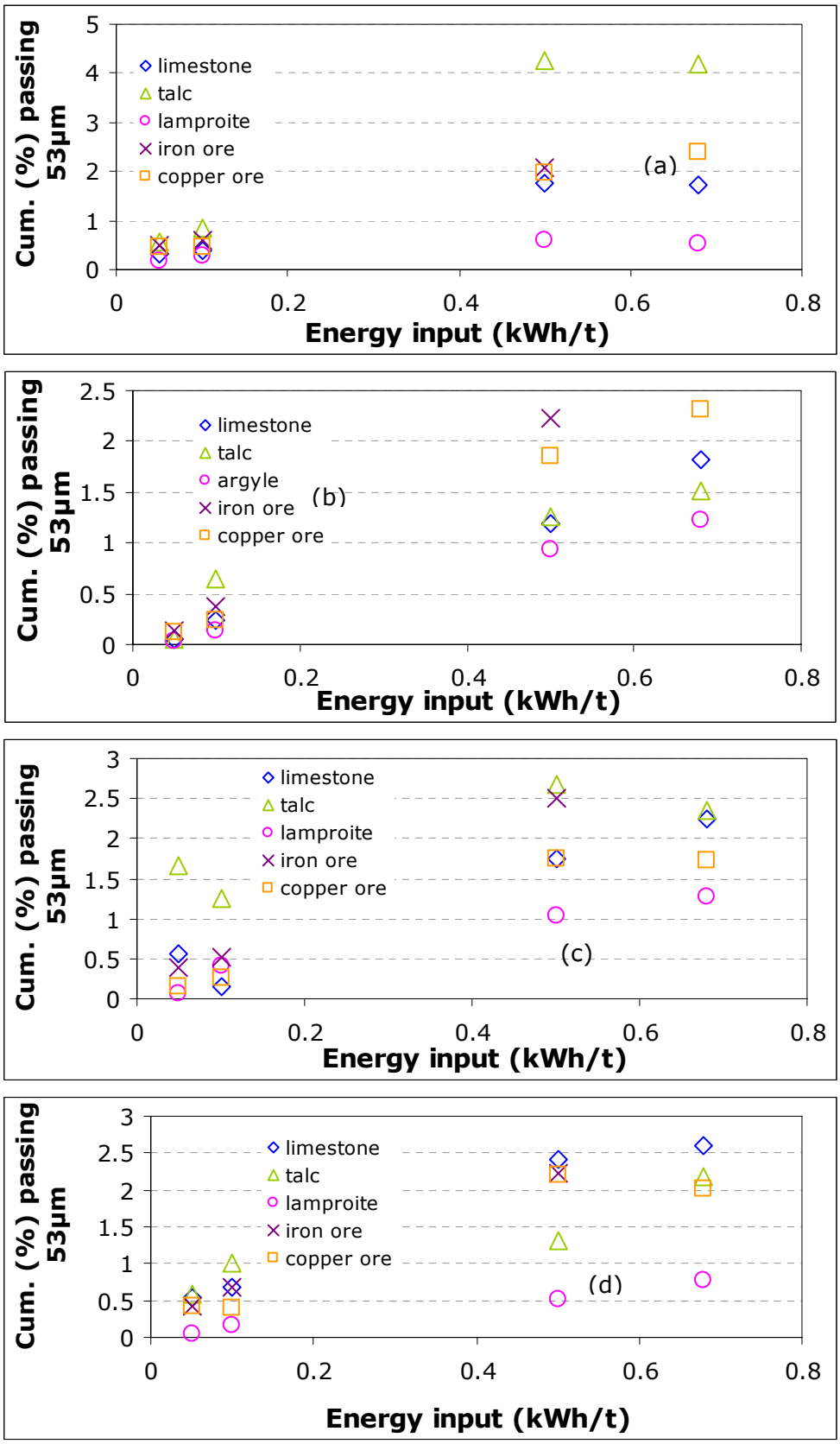

Figure 147: The cumulative percentages passing 53µm versus the energy input of the 10% bulk volume test samples for the various ores and for the single fractions (a) 16x13.2mm, (b) 8x6.7mm, (c) 4x3.35mm, (d) 2x1.7mm.

Consequently if dust is to be reduced from processes that involve the impact mechanism, such as the loading and dumping, or the drop of materials from heights in transfer points between conveyor belts, conveyor belts and feeders, chutes and other, careful consideration of the particular characteristics of the material like hardness, resistance to impact, mineralogy and particle size as well as operating parameters like energy input and bulk volume should be taken into account.

10.5. Discussion of the particle size analysis results of the impact test

The results produced from impact testing of the various ores were compared in order to assess the differences they present. The comparative results of the cumulative volume percentages of the ores below 10μm and 2.5μm are presented in Figure 148.

A wide spread of cumulative volume percentages below 10μm that correspond to the various ores are presented that can range from 15% to 60%, whereas the cumulative volume percentage below 2.5μm varies between 5 to 20%.

For some ores the various feed size fractions and bulk volumes influenced the ores on a greater scale than others and for this reason the cumulative volume percentage below 10μm and 2.5μm presented larger variations. For instance, limestone and copper ore exhibited a greater variation in their cumulative volume percentage values than talc. The particle size analysis results of the individual ores have been discussed in detail in Chapters 5 to 9.

The ores presented a clear, overall gradation sequence for the cumulative volume percentages below 10μm and 2.5μm, which also satisfied the majority of the results from the different feed size fractions and bulk volumes. Therefore, limestone generated the higher cumulative volume percentages below 10μm, followed by the talc and lamproite, the copper ore and final in the sequence is found the iron ore. Consequently, under impact, limestone will produce the finer product, whilst the iron ore the coarser. The gradation sequence of the cumulative volume percentages below 2.5μm is not identical to the one of the percentages below 10μm. Hence limestone produced again the higher cumulative volume percentage below 2.5μm followed by the lamproite, copper ore, iron ore and talc that produced the lowest percentage. Therefore, although talc generates a significant volume percentage of particles below 10μm, only a small proportion of them are below 2.5μm.

According to the impact test results, talc and iron ore in many occasions produced the highest concentrations of fine particles below 53μm. The comparative particle size analysis results have shown that talc produced a significantly high cumulative volume percentage of particles below 10μm and only a small percentage of particles below 2.5μm. Nevertheless, the iron ore produced the lowest cumulative volume percentages below 10 and 2.5 μm than any of the ores. Also the lamproite that generated the lowest quantity of particles below 53μm resulted to high cumulative volume percentages below 10 and 2.5μm, which is explained by the presence of high concentrations of minerals such as illite and chlorite in the fines fraction.

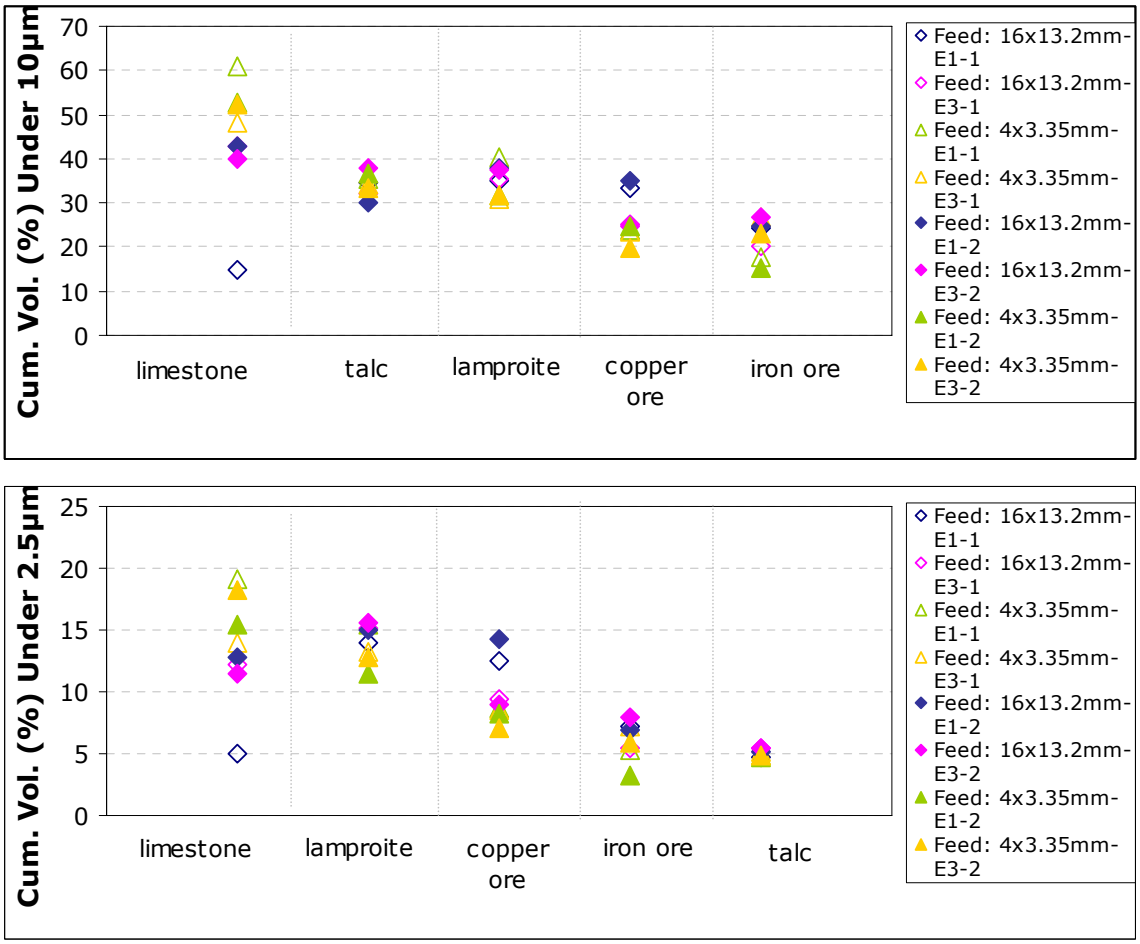

Figure 148: The cumulative volume percentages below (a) 10μm and (b) 2.5μm of the impact test particulates collected by the various ores at energy input levels E1=0.05kWh/t and E3=0.5kWh/t for the 10% bulk volume feed samples (1) and the 20% (only for the 16x13.2mm single fraction) and 5% bulk volume samples (2).

Conclusively ores could be classified according to the particle size of dust/fines generated under impact although depending on the indicators used (i.e cumulative volume percentage below 10μm or 2.5μm) fineness sequences might present significant differences. The fineness sequences did not always match with the impact test a result that is materials which generated large amounts of fines did not

necessarily produced the finest particle size distribution. This is because the particle size of dust and fines is closely related and influenced by the mineralogy of an ore and the softness/ hardness and particle size of these mineral phases that pass into the fines/dust fraction (i.e lamproite). A gradation sequence of dust/fines particle size from various ores produced under impact could prove to be useful to occupational hygienists and engineers, who can use it as a quick reference guide. However such decisions should not be made without accounting quantitative analysis data (mg of dust), as practice has shown that certain materials with low dust yield could still comprise an occupational hazard if their particle size distribution is very fine.

Chapter 11. Conclusions

11.1. Introduction

Following discussion, Chapter 11 summarises the conclusions of this study and makes suggestions that could enable the future development of this research area.

11.2. Conclusions

Reseach undertaken examined the dust generation potential of five different ores, the Tunstead Quarry limestone, the talc from Trimouns mine, the iron ore from Hammersley operations, the lamproite from Argyle operations and the copper ore from Kennecott works. The selection of these five different ores was based on their adverse implications to human health and the environment (i.e talc can cause talcosis, high silica content can cause silicosis etc). Although mitigation practices are in use for all these different mining operations, additional prevention steps are considered essential in order to minimise dust to as low levels as possible and to keep up-to-date with new coming environmental legislation.

The first three chapters presented the technical background associated with the research area of this project. The literature findings in Chapter 2 reviewed what the impacts, the legislative framework and the industry approach (i.e technical background) to dust is. Past research thoroughly investigated and developed dust

control and mitigation techniques for the minimisation of emitted dust. Current trends of legislation however stretch the need for prevention of the generation of dust and if possible the minimisation of control practices that often hides additional environmental impacts due to the continuous consumption of water, chemical additives and energy. Chapter 3 looked at the tools research commonly uses to characterise and analyze dust. Various dustiness tests have been developed in the past, which analyse dust by quantitative means. Very often these tests have been used to describe and understand the dust generation patterns of industrial processes without however providing adequate explanation of how well they relate to them. The research undertaken within this project proposes that the mechanisms taking place in a dustiness test should relate to the mechanisms found in industrial processes. Based on this logic the objective of this research project was to assess the dust generation potential of various ores under the effect of abrasion and impact, namely the principar mechanisms associated with a variety of industrial processes that tend to produce particulates. The outcomes of Chapter 2 and 3 assisted to the development of the experimental procedure of this project.

The dust generation potential of ores was assessed under the mechanisms of abrasion and impact. These mechanisms are associated with numerous industrial processes and it is their effect on ores which results in the production of particulates. The mechanism of abrasion was investigated using the HSE-WSL tumbling drum test. Processes such as the transfer of ore by conveyor belts, screening, haulage roads and mixers produce dust due to friction. The effect of impact mechanism upon ores was assessed using the impact test. Operations that involve drop from heights such as tipping, stockpiling or transfer points, chutes and feeders generate dust and fines due to impact.

Prior to dustiness testing the mechanisms of dust generation, in the tumbling mill, were identified by experimental steps (high speed video recording) and computational simulation (discreet element modelling). Results have shown dust is produced in the mill solely due to one mechanism that of abrasion, which is caused by the frictional sliding of particles in the drum walls and over other particles, whereas fragmentation of particles did not occur. Also energy loss due to frictional sliding was found to increase with mill velocity and sample mass. Therefore the processes that involve abrasion mechanism such as the use of conveyor belts, mills, screens and others could reduce their dust generation potential by optimising the operations to achieve less abrasion and subsequently produce fewer fines.

The dependency of the operational parameters and ore related characteristics upon dust generation was explored. For the HSE-WSL apparatus, two testing protocols were employed, which utilized different operational parameters and also a variety of feed test size distributions. The different operational parameters of the two testing regimes were the tumbling time (1 minute for the HSL-TP/ 3 minutes for the OPT-TP) and the sample mass (a feed sample of 200g fro the HSL-TP and 150g for the OPT-TP). Preliminary testing using the limestone (<3mm fraction) revealed that both the tumbling time and sample mass correlate positively with dust yield. Three different feed particle fractions were selected for dustiness testing, the <9.5mm, <3.35mm and <1mm and results for the various ores revealed that the particle size distribution of the rock samples influences its dust generation potential. Also dustiness testing with the various ores has shown that higher dustiness was recorded during the OPT-TP, hence the increased tumbling time of 3 minutes instead of 1 minute applied by the HSL-TP resulted to greater levels of dust even though a smaller feed sample mass (150g instead of 200g) was used by the HSL-TP. Similar trends were observed for any of the different feed particle size fractions (i.e <9.5mm, <3.35mm and <1mm). Therefore the dust generation potential of ores could be minimised by reducing the time consumed on a particular operation. For example optimisation of the sieving process by critically reviewing the parameters that reduce its efficiency (i.e the process has not been maintained properly or a less efficient sieving technique is in use) could achieve a shorter time scale and less dust. Reducing the length of conveyor belts or the need for transfer of ore using haulage roads by using an in-pit crusher could also minimise the time scale of such operations, the mass of ore processed per unit time and consequently the dust produced. Adjusting the velocity of conveyors and the speed limit of trucks in haulage roads, so as to reduce the friction forces between particles and particle – wall contacts could also reduce the dust generation potential of ores. Finally altering equipment related characteristics such as the screen apertures (i.e by using rubber ones instead of steel apertures) or the closed size setting of crushers and optimising their performance to such levels that reduce the effect of abrasion upon ores could prove beneficial for the minimisation of dust.

The concentration of fine particles (<75μm) in the feed test samples did not correlate positively with dustiness for all the different materials. For instance, the dustiness of limestone under the OPT-TP was higher for greater concentrations of particles below 75μm. For the iron ore the samples with higher concentrations of fines resulted to lower dustiness than the samples with smaller amounts of particles <75μm. Therefore the abrasion mechanism affects the iron ore on a greater scale than the limestone. In the case of iron ore the two main mineral phases the hematite and

goethite present a different hardness profile with the first one being much harder than the second. The resistance under abrasion of the softer mineral, the goethite, will be lower and thus dust will be produced from it. Limestone on the other hand presents a homogeneous minerogical composition.

The AP-42 emission factors produced by the US Environmental Protection Agency to estimate the dust generation profile of materials often utilizes the silt content (particles <75μm) as a parameter of high importance for the prediction of dust. The outcomes of this project however have shown that there is no direct positive correlation between the silt content and the dust generation profile of a material, as the effect of a mechanism associated with a specific process is different for different materials. This is mainly due to the different mineralogy, rock and mineral hardness of the various materials. Hence it is not considered accurate to use the silt content for the determination of the dust generation potential of ores.

For the impact test, the influence of the feed particle size, the feed bulk volume and energy input level was investigated. Energy input was determined by the head weight and the drop height. The impact test has revealed a positive correlation between the energy input levels and the particle size distribution of the broken particles, as well as the concentration of fines. In addition increased bulk volumes appeared to result in higher concentrations of fine particulates. The feed particle size distribution also affected the rock fragmentation processes resulting to different concentrations of particles below 75μm for different single size fractions and ores. The above outcomes suggest that it is possible to reduce dust in processes that require drop from heights and impaction by adjusting the energy input and the bulk volume of ore utilized to as low a level as possible. The stockpiling and tipping processes could be benefited by utilising conveyor belts with adjustable booms, which would allow low drop heights, hence low energy input. Also by reducing the bulk volume of material dropped per unit time the amount of dust produced could be minimised.

According to the experimental findings using the impact test, it is the fragmentation of ore that results to the production of particulates. The way different rocks break under the effect of impact depends both on the mineralogy of the sample and the mechanical properties of the rock such as its strength, elasticity, brittle behaviour, rock mass properties and others. As the project focuses in the very fine fraction of dust, where minerals are commonly liberated, properties such as the hardness and fracture of minerals are also very important. Rock samples like the lamproite that comprises an intact rock with a well cemented fine grained texture and high quartz

content produced always the lowest concentration of fines and dust. On the other hand talc which is characterized by a layered structure and low strength generated always high quantities of dust. In high energy input however, talc presented an elastic behaviour, which often reduced the production of fines in lower levels than other minerals. The iron ore produced high amounts of fine particles under impact due to the presence of two distinct mineral phases of different hardness, the goethite and hematite, with the first one having low resistance under impact and thus passing into the fine fraction.

Dust and fines produced by abrasion and impact were further analysed by particle sizing methods and mineralogical characterisation techniques. The particle size and mineralogy are the physical properties that determine whether dust comprises an occupational, health and safety or an environmental hazard. Also such data can assist engineers to design and introduce mitigation practices that fit the particular characteristics and circumstances of operations. The particle size distributions that correspond to dust/fines of a specific ore and generation mechanism, collected under different operational parameters and from various feed fractions, did not present great discrepancies, which suggest that the dust/fines particle size distributions remain quite consistent. Each ore produced an identical dust particle size distribution profile and almost all the different ores generated cumulative volume percentages of particles below 10μm and 2.5μm that could pose an occupational health hazard, although the operating conditions of both the abrasion and impact tests were considered of low to moderate intensity.

The mineralogy of dust/fines was examined by laser diffraction analysis and by quantitative means, only for the lamproite and copper ore, using the mineral liberation analyser. Experimentation has concluded that the X-ray diffraction method cannot be considered satisfactory to analyse dust, because the minerals found in rock and dust fractions are similar and their quantities cannot be determined to account for any differences present. The use of MLA for the lamproite and copper ore samples allowed the quantitative analysis of the dust/fines and the ore. These results suggested that the mineralogy of dust and rock exhibited significant differences. Thus, the particulate matter consisted of greater weight percentages of minerals such as clays (illite) and chlorites than the rock samples and lower concentrations of quartz which comprised the major mineral phase in both ores. In addition, for the copper ore a significant amount of chalcopyrite has been found in the dust and fines fraction, often equal or higher to the concentrations measured in the rock sample, which indicates that valuable material is lost. Apparently chalcopyrite is liberated at

the particle size of dust and this is why high mineral weight percentages have been recorded. These results suggest that processes such as drilling and blasting in Kennecott copper ore mines will inevitably cause the lose of chalcopyrite, whilst dust collected from various operations during mining and processing should be further processed to collect any valuable fractions. The different dust generation mechanisms also influenced the mineralogy of dust/fines and commonly the composition of the particulates produced by the impact apparatus were closer to that of the rock samples. The generation of dust/fines from the impact test was due to the fragmentation process of the ore particles and not due to surface breakage caused by abrasion as in the case of the HSE-WSL mill. In the case of the abrasion-attrition mechanism, dust and fines are generated due to the effect of friction on particles'' surfaces. Hence it is expected that minerals with lower resistance to impact will potentially be produced. Therefore the dust and fines of the impact test possible consist of a variety of minerals resulted from the breakage of the ore, which might not present high variations from the composition of the rock samples. Furthermore, the impact test did not collect the airborne particulates thus it is difficult to directly compare the impact test and HSE-WSL test results.

Comparative studies of the results obtained for the individual ores have shown that materials could be classified according to their potential to generate dust/fines under the effect of impact or abrasion mechanisms and for specific operating conditions (i.e feed sample, bulk volume, testing protocol). The overall gradation sequence produced from the results of the HSE-WSL test was not identical with the one produced from impact testing, which suggests that some of the ores behave differently under abrasion and impact. Therefore it would be expected that for such materials (i.e iron ore) different dust control approaches would be implemented for processes that involve the abrasion or impact mechanism. The comparative results also revealed the importance of mineralogy and rock mechanical properties such as strength on the dust generation potential of ores, as well as on the dust particle size distribution. For example it has been shown that lamproite will generate low quantities of dust and fines both under abrasion and impact, because it comprises an intact rock, but the particle size distribution of dust and fines will be considerably finer than many of the ores as its mineralogical composition consists of high quantities of illite-chlorite, two minerals with very fine size.

The comparative studies outcomes have shown that the determination of the dust generation potential of an ore and the characterisation of dust should include a combination of analytical techniques, which perform both quantitative and qualitative

analysis. Particle size analysis and mineralogy characterisation are essential to produce an overall view of the dust generation potential of materials and the hazardous impacts of dust to human health and the environment.

11.3. Further work

Several suggestions have been made from the findings of this project, which could assist in the minimisation of dust generation. Most of these proposals recommended steps of optimisation of processes through alteration of operational or ore parameters (i.e specific particle size range) and equipment' design.

These suggestions however have not been validated in real mining sites or by true scale operations. Therefore, further work on this project should justify whether the conclusions made within this PhD thesis agree with field data. Also experimentation with true scale operations should investigate if it is possible to reduce the generation of dust by optimising parameters, such as the time-scale of a process or the energy input levels, the sample mass or the particle size of the ore.

Initially experimentation could focus on a single process, for example the transfer of materials using conveyor belts. The effect of the abrasion mechanism would be explored through the transfer process on the conveyor and any dust generated should be collected by a sampling apparatus (i.e high volume sampler). Trials with different masses of ore, or time-scales, or particle sizes will determine if similar trends with the laboratory findings are obtained. The influence of impact on an ore could be investigated by tipping ore from the conveyor belt and capturing the dust produced with a sampler. Alteration of the height from which tipping takes place would simulate the different energy input levels used by the impact apparatus, whereas the effect of utilisation of various bulk volumes and particle sizes of ores should also be investigated. Analysis of the dust fraction by particle sizing methods and mineralogical characterisation techniques will define if dust produced by abrasion and impact exhibit substantial differences, as well as if the influence of operational parameters affects the particulate fraction. Also it will show whether the laboratory findings of this study agree with data from real operations. The overall results from such investigations will indicate what parameters should be altered to optimise the performance of the conveyor belt transfer process so as to reduce the generation of

dust. They could also be used to indicate dust sources that have not been taken into account before and to re-assess or introduce new dust control methods.

If the trial results compare well with the findings of this study, then the conclusions and recommendations made could be applied to other industrial processes and materials. The laboratory techniques from this thesis could find use as a standard procedure to obtain quick and accurate results. The five different ores used for this project might comprise the start point for further work as laboratory conclusions are available.

Bibliography

Adachi, K. & Tainosho, Y. 2004, "Characterization of heavy metal particles embedded in tire dust", *Environment International*, vol. 30, no. 8, pp. 1009-1017.

Allen, T. 1997, *Particle Size Measurement. Powder sampling and particle size measurement*, Fifth edn, Chapman & Hall, London.

American Conference of Governmental Industrial Hygienists (ACGIH) 2005, TLV®/BEI Resources, Available at: <http://www.acgih.org/TLV/> Access date: [13-5-2005].

Appleton, T., Lowndes, I., Kingman, S., & Silvester, S. 2003, *Cleaner quarries: Optimising environmental performance. Fugitive dust emissions from mines.*, School of Chemical, Environmental and Mining Engineering, University of Nottingham, Nottingham, U.K.

Argyle Diamonds 2004, *AK1 Mine Geology - Visitor's Information*, Argyle Diamonds, Argyle.

Argyle Diamonds 2005, Argyle Diamonds, Available at: <www.argylediamonds.com.au> Access date: [12-12-2005].

Arup Environmental 1995, *The Environmental Effects of Dust from Surface Mineral Workings*, HMSO, London, PECD 7/1/468.

ASOSH 2005, Association of Societies for Occupational Safety and Health (ASOSH) in South Africa, Available at: <http://www.asosh.org/>, Access date: [13-5-2005].

Austin, L. G., Klimpel, R., & Luckie, P. T. 1984, *Process Engineering of Size Reduction: Ball Milling* SME Publishers, New York.

Balkau, F. 1993, *Pollution Prevention and Abatement Guidelines for the Mining Industry*, UNEP IE/PAC, Paris, 2nd Draft.

Banks, D. E. & Parker, J. E. 1998, *Occupational lung disease. An international perspective* Chapman & Hall, London, U.K.

Bearman, R. A., Briggs, C. A., & Kojovic, J. 1997, "The Application of Rock Mechanics Parameters to the Prediction of Comminution Behaviour", *Minerals Engineering Journal*, vol. 10, no. 3, pp. 225-264.

Binzen, W. 1985, "The Integrated approach to dust collection", *Bulk solids handling*, vol. 5, no. 4, pp. 859-864.

Bohren, C. F. & Huffman, D. R. 1983, *Absorption and scattering of light by small particles* Wiley, New York.

Boxer, G. L. & Jaques, A. L. 1990, "Argyle (AK1) Diamond Deposit," in *Geology of the Mineral Deposits of Australia and Papua New Guinea*, F. E. Hughes, ed., The Australasian Institute of Mining and Metallurgy, Melbourne, pp. 697-706.

Breum, N. O. 1999, " The rotating drum dustiness tester: Variability in dustiness in relation to sample mass, testing time, and surface adhesion", *Annals of Occupational Hygiene*, vol. 43, no. 8, pp. 557-566.

British Geological Survey 2005, Foundations of the Peak - Scenery and Geology - Superquarries: Tunstead, Available at: <http://www.bgs.ac.uk/foundation-web/Tunstead.html>, Access date: [5-9-2005].

British Occupational Hygiene Society Technology Committee 1985, *Dustiness Estimation Methods for Dry Materials: Part 1, Their Uses and Standardization; Part 2, Towards a Standard Method*, Science Reviews, UK, Technical Guide No 4.

Brunius, O. & Brunius, M. 1995, "Dust control and prevention of dust explosions in belt conveyor systems", *Bulk solids handling*, vol. 15, no. 2, pp. 265-269.

BSI 1994, *Characterization of air quality - Part 2: Glosssary*, British Standard Institute, Great Britain, BS 6069-2:1994 / ISO 4225:1994.

BSI 1989, *Test sieving. Methods using test sieves of woven wire cloth and perforated metal plate*, British Standard Institute, Great Britain, BS 1796-1:1989; ISO 2591-1:1988.

BSI 2000a, *Test sieves. Technical requirements and testing. Test sieves of metal wire cloth*, British Standards Institute, Great Britain, BS 410-1:2000, ISO 3310-1:2000.

BSI 2000b, *Test sieves. Technical requirements and testing. Test sieves of perforated metal plate*, British Standard Institute, Great Britain, BS 410-2:2000, ISO 3310-2:1999.

BSI 1990, *Testing aggregates. Method for determination of moisture content*, British Standard Institute, U.K., BS 812-109:1990.

Bumiller, M., Carson, J., and Prescott, J. 2005, A preliminary investigation concerning the effect of particle shape on a powder's flow properties, Available at: <www.malvern.co.uk> Access date: [8-9-2005].

Burgess, D. J., Duffy, E., Etzler, F., & Hickey, A. J. 2004, "Particle Size Analysis: AAPS Workshop Report, Cosponsored by the Food and Drug Administration and the United States Pharmacopeia", *The American Association of Pharmaceutical Scientists Journal*, vol. 6, no. 3- Article 20, pp. 1-12.

Carlson, K. H., Herman, D. R., Markey, T. F., Wolff, R. K., & Dorato, M. A. 1992, "A comparison of two dustiness evaluation methods", *American Industrial Hygiene Association Journal*, vol. 53, no. 7, pp. 448-454.

Castor, Wm. & Gray, A. 1990, "Evaluating the dustiness of powders", *Bulk solids handling*, vol. 2, no. 2, pp. 145-148.

CEN 1993, *Workplace atmospheres - Size fraction definitions for measurement of airborne particles*, European Committee for StandardizationBritish Standard Institute, Great Britain, BS EN 481:1993 / BS 6069-3.5:1993.

Chung, K. Y. K. & Burdett, G. J. 1994, "Dustiness testing and moving towards a biologically relevant dustiness index", *Annals of Occupational Hygiene*, vol. 38, pp. 945-949.

Ciba Specialty Chemicals 2006, Dust suppression, Available at: <http://www.cibasc.com/dust-suppression_brochure.pdf>, Access date: [24-3-2006].

Cleary P.W 2001, "Charge Behaviour and Power Consumption in ball Mills: sensitivity to Mill Operating Conditions, Liner geometry and Charge Composition", *International Journal of Mineral Processing*, vol. 63, pp. 79-114.

Commission of the European Communities 2000, *Communication from the Commission. Promoting sustainable development in the EU non-energy-extractive industry*, EC, Brussels, COM(2000) 265 final.

Commission of the European Communities 2005, *Directive on Ambient Air Quality and Cleaner Air for Europe (the "CAFE" Directive) (COM(2005) 447),* European Commision, Brussels, 2005/0183 (COD).

Cowherd, C. & Grelinger, M. A. 1992, "The appropriateness of a dustiness test chamber for representation of natural suspension phenomena", in *PM10 standards and non-traditional particulate source controls*, J. C. Chow & D. M. Ono, eds., Air and Waste Management Association, Pittsburgh, pp. 346-356.

Crossley, P. 2002, "Tour de Force: France's minerals unearthed", *Industrial Minerals*, vol. 420, pp. 28-37.

Cundall P.A. & Strack O.D.L 1979, "A Discrete Numerical Model for Granular Assemblies", *Geotechnique*, vol. 29, no. 1, pp. 47-65.

Dana, J. D. 1998, *Manual of Mineralogy*, 21st edn, John Wiley and Sons, New York.

Davis, B. L. 1984, "X-ray diffraction analysis and source appointment of Denver aerosol.", *Atmospheric Environment*, vol. 18, no. 10, pp. 2197-2208.

DEFRA 2000, *The Air Quality Strategy for England, Scotland, Wales and Northern Ireland,* Department for Environment, Food and Rural Affair (DEFRA), UK.

Department of the Environment - Australian Government 2005, Sustainable Minerals - Dust Control, Available at: <http://www.deh.gov.au/industry/industry-performance/minerals/booklets/dust/index.html>, Access date: [7-3-2005].

Djordjevic N. 2003, "Discrete Element Modelling of Power Draw of Tumbling Mills", *Transactions of the Institute of Mining Metallurgy Canada*, vol. 112, p. C109-C114.

Dorman, R. G. 1974, *Dust Control and Air Cleaning*, First edition edn, Pergamon Press, Oxford.

EC 2005, Occupational Exposure Limits (OELs)., Available at: <http://europa.eu.int/comm/employment_social/health_safety/docs_en.htm#pub4>, Access date: [13-5-2005].

Eckhoff, R. K. 1995a, "Prevention and mitigation of dust explosions in the process industries - Part 1", *Bulk solids handling*, vol. 7, no. 1, pp. 11-21.

EIPPCB 2006, European Integrated Pollution Prevention and Control Bureau (EIPPCB) - Best Available Techniques Reference Documents (BREFs), Available at: <http://eippcb.jrc.es/pages/FAbout.htm>, Access date: [20-3-2006].

Endoh, S., Kuga, Y., Ohya, H., Ikeda, C., & Iwata, H. 1998, "Shape estimation of anisometric particles using size measurement techniques", *Particle and Particle Systems Characterisation*, vol. 15, pp. 145-149.

Environment Australia 2001, *National Pollution Inventory - Emission Estimation Technique Manual for Mineral Sands Mining and Processing*, Environment Australia, Australia.

Eslinger, M. 1997, "Controlling fugitive dust emissions with a foam suppression system", *Ceramic Industry*, vol. 147, no. 7, pp. 3-8.

European Agency for Safety and Health at Work 2005, Preparation of the EU Commission Indicative Occupational Exposure Limit values, Available at: <http://europe.osha.eu.int/good_practice/risks/ds/oel/notes.stm#prep>, Access date: [10-5-2005].

European Commission 1996, Particle Size Distribution. Fibre Length and Diameter Distribution, Available at: <http://www.hse.gov.uk/nons/nonspart.htm >, Access date: [2-4-2006].

European Commission 2005, *Integrated Pollution Prevention and Control - Reference Document on Best Available Techniques on Emissions from Storage*, European IPPC Bureau, Sevilla Spain.

European Commission 2006, The Sixth Environment Action Programme of the European Community 2002-2012, Available at: <http://europa.eu.int/comm/environment/newprg/index.htm>, Access date: [20-3-2006].

European Environment Agency 2006, Emissions of primary particles and secondary particulate precursors (CSI-003) - May 2005 Assessment, Available at: <http://themes.eea.eu.int/IMS/IMS/ISpecs/ISpecification20041001123025/IAssessment1116511151442/view_content>, Access date: [15-2-2006].

Evans, A. M. 1993, *Ore Geology and Industrial Minerals*, Third edn, Blackwell Science, London.

Field, P. 1982, *Dust Explosions* Elsevier Science, England.

Friedlander, S. K. 2000, *Smoke, Dust and Haze. Fundamentals of Aerosol Dynamics*, Second edn, Oxford University Press, Oxford.

Fukasawa, T., Iwatsuki, M., & Tillekeratne, S. P. 1983, "X-ray diffraction analysis of airborne particulates collected by an Andersen sampler. Compound distribution vs. particle size", *Environmental Science Technology*, vol. 17, no. 10, pp. 596-602.

Ganor, E., Levin, Z., & Grieken, R. V. 1998, "Composition of individual aerosol particles above the Israelian Mediterranean coast during the summer time", *Atmospheric Environment*, vol. 32, no. 9, pp. 1632-1642.

Gibor, M. 1997, "Dust collection as applied to the mining and allied industry", *Bulk solids handling*, vol. 17, no. 3, pp. 397-403.

Gill, T. E., Zobeck, T. M., Stout, J. E., & Gregory, J. M. 1999, "Fugitive dust generation in the laboratory", in *Wind Erosion: An International Symposium*, US Department of Agriculture's Wind Erosion Research, USA.

Goldbeck, L. J. & Marti, A. D. 1996, "Dust control at conveyor transfer points: containment suppression and collection", *Bulk solids handling*, vol. 16, no. 3, pp. 367-372.

Gregurek, D., Reimann, C., & Stumpfl, E. F. 1998, "Mineralogical fingerprints of industrial emissions - an example of Ni mining and smelting on the Kola Peninsula, NW Russia.", *The Science of the Total Environment*, vol. 221, pp. 189-200.

Griffiths, W. D., Mark, D., Marshall I.A., & Nichols, A. L. 1998, *Aerosol Particle Size Analysis: Good Calibration Practices* Royal Society of Chemistry, Cambridge.

Gu, Y. 2003, "Automated Scanning Electron Microscope Based Mineral Liberation Analysis. An Introduction to JKMRC/FEI Mineral Liberation Analyser", *Journal of Minerals & Materials Characterization & Engineering*, vol. 2, no. 1, pp. 33-41.

Hamelmann, F. & Schmidt, E. 2003, "Methods of estimating the dustiness of industrial powders - A review", *KONA Powder Science and Technology*, vol. 21, pp. 7-18.

Hamersley Iron, 2005a, Brockman Syncline 4 Iron Ore Project - Public Environmental Review, Available at: <http://www.hamersleyiron.com/pubs_publicenvreports.asp>, Access date: [1-12-2005a].

Hamersley Iron, 2005b, Hamersley Iron Website, Available at: <http://www.hamersleyiron.com> Access date: [1-12-2005b].

Harben, P. W. & Bates, R. L. 1990, "Diamonds," in *Industrial Minerals Geology and World Deposits*, P. W. Harben & R. L. Bates, eds., Metal Bulletin Plc, London, pp. 92-101.

Hardy, R. & Tucker, M. 1988, "X-ray powder diffraction of sediments," in *Techniques in Sedimentology*, M. Tucker, ed., Blackwell Science, UK, pp. 191-228.

Health and Safety Commision 2003, *Proposals to introduce a new occupational exposure limits (OEL) framework*, Health and Safety Executive, UK, Consultive Document (CD).

Health and Safety Executive 1997, *Dust: General principles of protection*, Health and Safety Executive, U.K., EH 44.

Health and Safety Executive 2002, *EH46 Summary Criteria for Occupationals Exposure Limits 2002*, Health and Safety Executive, U.K., EH64.

Health and Safety Laboratories 2000, *General methods for sampling and gravimetric analysis of respirable and inhalable dust*, UK, MDHS 14/3.

Health and Safety Laboratory 1996, *Methods for the Determination of Hazardous Substances 81 (MDHS) - Dustiness of powders and materials*, Health and Safety Executive, UK, MDHS 81.

Heitbrink, W. A. 1990, "Factors Affecting the Heubach and MRI dustiness tests", *American Industrial Hygiene Association Journal*, vol. 51, no. 4, pp. 210-216.

Heitbrink, W. A., Todd, W. F., Cooper, T. C., & O'Brien, D. M. 1990, "The application of dustiness tests to the prediction of worker dust exposure", *American Industrial Hygiene Association Journal*, vol. 51, no. 4, pp. 217-223.

Herrmann, S. & Evensen, J. 1994, "Newly - developed combination products for dust supression in the storage of bulk materials", *Bulk solids handling*, vol. 14, no. 1, pp. 109-112.

Hewson, G. S. & Hartley, B. M. 1990, "Radiation research priorities in the mineral sands industry", *Journal of Radiological Protection*, vol. 10, no. 3, pp. 221-229.

Higman, R. W. "Dustiness testing. A useful tool", in *Ventilation '85, Proceedings of the 1st International Symposium on Ventilation for Contaminant Control. (code 10354)*, Toronto, Ont, Can, pp. 693-702.

Higman, R. W., Schofield, C., & Taylor, M. 1984, "Bulk material dustiness, an important property - its measurement and control. 4th International Environment and Safety Conference", London.

Hinds, W. C. 1999, *Aerosol Technology : Properties, behavior, and measurement of Airborne particles*, 2nd edition edn, John Wiley & Sons, New York.

Hjemsted, K. & Schneider, T. 1993, "Time dependent dust release during dustiness testing", *Journal Of Aerosol Science*, vol. 24, no. Supplement 1, p. S251-S252.

Hjemsted, K. & Schneider, T. 1996, "Dustiness from powder materials", *Journal Of Aerosol Science*, vol. 27, no. Suppl 1, p. S485-S486.

Hume, A. L. 1993, "Assessing and solving the hazard of dust explosions", *Bulk solids handling*, vol. 13, no. 2, pp. 371-372.

Hutton, W. A. 1993, "Diamond recovery from lamproite ore at Argyle Diamond Mines Pty Limited, Argyle, WA," in *Australasian Mining and Metallurgy*, J. T. Woodcock & J. K. Hamilton, eds., AusIMM, Australia, pp. 1458-1463.

ISO. 1995, *Air quality - Particle Size fraction Definitions for Health-related Sampling*, Interantional Organization for Standardization (ISO), Geneva, ISO 7708.

ISO 1999, *Particle size analysis - laser diffraction methods: Part 1: General principles*, International Standards Organization, Geneva, Switzerland, 13320-1.

Itasca Consulting Group Inc. PFC^{3D} (Particle Flow Code in 3 dimensions). [3.0]. 2003. Minneapolis. Ref Type: Computer Program

James, C. 2004, Tarmac Central Overview, Available at: <http://www.angloamerican.co.uk/static/uploads/Tarmac%20Central.pdf>, Access date: [18-3-2006].

Jk Technology Centre 2005, Mineral liberation analyser, Available at: <http://www.jkmla.com/>, Access date: [25-3-2006].

JKMRC 2003, JK Drop Weight Test, Available at: <www.jktech.com.au/LabServices/>, Access date: [25-3-2006].

JKMRC 2005a, *Mineral Liberation Analyser - System User Operating Manual - Module 4 BSE Measurement and Processing*, JKMRC, Australia, Module 4 BSE Measurement and Processing.

JKMRC 2005b, *Mineral Liberation Analyser - System User Operating Manual - Module 5 - XBSE Measurement Processing*, JKMRC, Australia, Module 5 - XBSE measurement processing .

JKMRC 2005c, *Mineral Liberationa Analyser - System User Operating Manual - Measurement Procedures Quick Reference Guide Quanta 600*, JKMRC, Australia, Quick Reference Guide Quanta 600.

Johnson, G. Q. 2003, "Minimizing particle momentum to control dust generation in your process", *Powder and Bulk Engineering*, vol. October, pp. 25-31.

Karpin, D. S. 1993, "Overview of the Australasian diamond and gemstone industry," in *Australian Mining and Metallurgy. The Sir Maurice Mawby Memorial Volume*, Second edn, vol. vol 2 J. T. Woodcock & J. K. Hamilton, eds., Institute of Mining and Metallurgy, Australia, pp. 1437-1452.

Kasparian, J., Frejafon, E., Rambaldi, P., Yu, J., Vezin, B., Wolf, J. P., Ritter, P., & Viscardi, P. 1998, "Characterization of urban aerosols using SEM - microscopy, X-ray analysis and LIDAR measurements", *Atmospheric Environment*, vol. 32, no. 17, pp. 2957-2967.

Kennecott Utah Copper 2006, Kennecott Utah Copper, Available at: <http://www.kennecott.com/index.html>, Access date: [4-1-2006].

Kennecott Utah Copper Corporation 2004a, Kennecott Utah Copper Corporation Safety and Health Standards. Standard No 10.9. Workplace Monitoring, Available at: <http://www.kennecott.com/index.html>, Access date: [4-1-2006a].

Kennecott Utah Copper Corporation 2004b, Kennecott Utah Copper Corporation Safety and Health Standards. Standard No:10.6 Particulate and Gas / Vapor Exposures, Available at: <http://www.kennecott.com/index.html>, Access date: [4-1-2006b].

Kennecott Utah Copper Corporation 2003, Kennecott Utah Copper Corporation Safety and Health Standards. Standard No: 10.7. Occupational Exposure Limits, Available at: <http://www.kennecott.com/index.html>, Access date: [4-1-2006]

Kennedy, A. 1988, "Open pit talc mining in the French Pyrenees", *Mining Magazine*, vol. 159, pp. 488-490.

Kissel, F. N. 2003, *Handbook for Dust Control in Mining*, National Institute for Occupational Safety and Health (NIOSH), USA, IC 9465.

Kousaka, Y., Endo, Y., & Nakai, S. 1998, "A new sizing technique for fine powders dispersed in air", *Powder Technology*, vol. 100, pp. 15-19.

Kupiainen, K., Tervahattu, H., & Raisanen, M. 2003, "Experimental studies about the impact of traction sand on urban road dust composition", *The Science of the Total Environment*, vol. 308, pp. 175-184.

Landtwing, M. R., Pettkea, T., , H. W. E., Heinrich, C. A., Redmondb, P. B., Einaudib, M. T., & Kunzec, K. 2005, "Copper deposition during quartz dissolution by cooling magmatic-hydrothermal fluids: The Bingham porphyry", *Earth and Planetary Science Letters*, vol. 235, pp. 229-243.

Lips, A., Hart, P. M., & Evans, I. D. "Proceedings of the 5th European Symposium in Particle Characterisation", Nurnberg Messe, Nurnberg, p. 443.

Liu, Q. & Katsabanis, P. D. 1992, "Hazard evaluation of sulphide dust explosions", *Journal of Hazardous Materials*, vol. 33, pp. 35-49.

Liu, Z., Wypych, P., & Cooper, P. 1999, "Dust generation and air entrainment in bulk materials handling - A Review", *Powder handling & processing*, vol. 11, no. 4, pp. 421-425.

Luzenac Plc., 2005, Luzenac Talc for the world, Available at: <www.luzenac.com> Access date: [15-08-2006].

Lyons, C. P. & Mark, D. 1992, *An evaluation of the Roaches 'Dust particle apparatus' dustiness testing equipment*, Health and Safety Executive; Warren Spring Laboratory, U.K., 40/1992.

Lyons, C. P. & Mark, D. 1994, *Development and testing of a procedure to evaluate the dustiness of powders and dusts in industrial use*, Health and Safety Executive; U.K., 62/1994.

Lyons, C. P., Adam, M., Mark, D., Fish, J., Chung, K., Brammer, J., Hammond, C. M., Tunnicliffe, R., Fisher, B. T., Keech, S., Rollings, N., Sethi, S., & Chalmers, C. 1996, *Further development and testing of the HSL\WSL health-related dustiness tester*, Health and Safety Executive, U.K., HSE contract research report No. 103/1996.

Lyons, C. P., Mark, D., Chung, K. Y. K., & Burdett, G. 1992, "Application of health-related size fractions to dustiness measurement", *Journal Of Aerosol Science*, vol. 23, no. SUPPL 1, p. S607-S610.

Madler, L., Koch, W., Lange, F., & Husemann, K. 1999, "In situ aerodynamic size classification of aerosols in the size range between 0.1 and 100 mu m for dustiness tests and powder characterization", *Journal Of Aerosol Science*, vol. 30, no. 4, pp. 451-465.

Malvern Instruments 2005a, *Automated particle size and shape measurements using image analysis*, Malvern Instruments, U.K.

Malvern Instruments 2005b, Mastersizer particle size analyzers, Available at: <http://www.malvern.co.uk/LabEng/products/mastersizer/mastersizer_range.htm>, Access date: [3-9-2005b].

Malvern Instruments 2005c, *Particle size analysis*, UK Seminar Presentations, Malvern Instruments, UK.

Malvern Instruments 2004, Optical property determination for laser diffraction particle sizing , Available at: <http://www.malvern.co.uk/common/webcasts/webcasts.htm>, Access date: [24-10-2005].

Malvern Instruments 1994, *Mastersizer-S User Manual*, Malvern Instruments, U.K., MAN0096 - Issue:1.0.

Martin Marietta Corporation 1987, *Dust control handbook for mineral processing*, Bureau of Mines, U.S.Department of the Interior, U.S.A, J0235005 .

Maxwell, A. S. 1999, "Degradation, segregation and dust control of bulk materials", *Bulk solids handling*, vol. 19, no. 3, pp. 399-403.

Mining Technology 2006, Bingham Canyon Copper Ore, Utah, USA, Available at: <http://www.mining-technology.com/projects/bingham/>, Access date: [4-1-2006].

MIRO 2005, Good Quarry, Available at: <http://www.quarry.leeds.ac.uk/goodquarry/index.asp>, Access date: [11-5-2005].

MIRO 2005, Mineral Industry Sustainable Technology (MIST), Available at: <http://www.mi-st.org.uk/>, Access date: [11-5-2005]

Mishra B.K. & Cheung J. 1999, "Particle Motion and Energy Distribution in Tumbling Ball Mills", *Powder Technology*, vol. 105, pp. 222-227.

Mishra B.K. & Rajamani R.K. 1992, "The Discrete Element for Simulation of Ball Mills", *Applied Mathematical Modelling*, vol. 16, pp. 598-604.

Mitchell, J. P. & Nagel, M. W. 2004, "Particle Size Analysis of Aerosols from Medicinal Inhalers", *KONA Powder Science and Technology*, vol. 22, pp. 32-65.

Mohamed, M. A. K., Mutmansky, J. M., & Jankowski, R. A. 1996, "Overview of proven low cost and high efficiency dust control strategies for mining operations", *Mining Technology*, vol. 78, no. 897, pp. 141-148.

Morrison R.D. & Cleary P.W. 2004, "Using DEM to Model Ore Breakage within a Pilot Scale SAG Mill", *Minerals Engineering*, vol. 17, pp. 1117-1124.

Napier-Munn, T. J., Morrell, S., Morrison, R. D., & Kojovic, T. 1996, *Mineral Comminution Circuits. Their operation and Optimisation* Julius Kruttschnitt Mineral Research Centre, Queensland.

National Coal Board 1957, *Laboratory experiments on dust suppression with broken coal*, National Coal Board, UK, MRE No 2083.

National Environment Protection Council 2005, National Pollutant Inventory-Australia, Available at: <http://www.npi.gov.au/>, Access date: [7-3-2005].

National Occupational Health and Safety Commission 2005, National Exposure Standards Database, Available at: <http://www.nohsc.gov.au/OHSInformation/Databases/ExposureStandards/expsearch.asp>, Access date: [13-5-2005].

National Pollutant Inventory 1999, *Emission Estimation Technique Manual for Mining*, National Pollutant Inventory, Australia, Version 2.3.

NIOSH 2005, NIOSH: Databases and Information Resources, Available at: <http://www.cdc.gov/niosh/database.html>, Access date: [13-5-2005].

Office of the Deputy Prime Minister 2003, *Mineral Policy Statement2: Controlling and mitigating the environmental effects of minerals extraction in England* U.K., MPS2.

Office of the Deputy Prime Minister 2005, MPG11: controlling environment effects of minerals extraction - Annex 1: The control and mitigatin of dust at mineral and related workings, Available at: <http://www.odpm.gov.uk/stellent/groups/odpm_control/documents/contentservertemplate/odpm_index.hcst?n=2554&l=2 >, Access date: [11-5-2005].

PEBCO 2006, The Cleveland cascade chute, Available at: <http://www.pebco.com/ProdPgs/cascadechute.html>, Access date: [25-3-2006].

Petavratzi, E., Kingman, S., & Lowndes, I. 2005, "Particulates from mining operations: A review of sources, effects and regulations", *Minerals Engineering*, vol. 18, no. 12, pp. 1183-1199.

Petters, M. D. 2003, The Aerodynamic Particle Sizer, Available at: < http://www-das.uwyo.edu> Access date: [10-5-2003].

Puledda, S., Paoletti, L., & Ferdinandi, M. 1999, "Airborne quartz concentration in an urban site", *Environmental Pollution*, vol. 104, pp. 441-448.

Queralt, I., Sanfeliu, T., Gomez, E., & Alvarez, C. 2001, "X-ray diffraction analysis of atmospheric dust using low background supports", *Aerosol science*, vol. 32, pp. 453-459.

Ramanaidou, E. R., Morris, R. C., & Horwitz, R. C. 2003, "Channel iron deposits of the Hamersley Province, Western Australia", *Australian Journal of Earth Science*, vol. 50, pp. 669-690

Reed, R., Organiscak, J. A., & Page S.J. 2004, "New approach controls dust at the collector dump point", *Engineering and Mining Journal*, vol. July, pp. 29-31.

Reeves, D. 1993, "Alluvial diamond mining and recovery operations at Argyle Diamond Mines Pty Limited, Argyle, WA," in *Australasian Mining and Metallurgy*, vol. Volume 2 J. T. Woodcock & J. K. Hamilton, eds., AusIMM, Australia, pp. 1453-1457.

Rhodes, M. 2003, "Particle Size Reduction," in *Introduction to Particle Technology*, John Wiley & Sons Ltd., England, pp. 241-263.

Schimmelpeennig, M. 2004, "When the dust settles", *Power Engineering*, vol. September 2004, pp. 48-51.

Schimmoller, B. K. 2003, "Coal and ash handling: In search of cost savings", *Power Engineering*, vol. April, pp. 22-27.

Schneider, T. & Hjemsted, K. 1996, "Documentation of a dustiness drum test", *Annals of occupational hygiene society*, vol. 40, no. 6, pp. 627-643.

Sethi, S. A. & Schneider, T. 1996, "A gas fluidization dustiness tester", *Journal Of Aerosol Science*, vol. 27, no. 1, p. S305-S306.

Silvester, S. A., Lowndes, I. S., & Kingman, S. W. 2004, "The ventilation of an underground crushing plant", *Mining Technology - Transactions of the Institute of Mining and Metallurgy: Section A*, vol. 113, no. 4, pp. 201-214.

SIMRAC 2003, *Handbook to reduce the exposure of workers to dust*, Members of the Special Interest Group on Dust and Ventilation, Safety in Mines Research Advisory Committee (SIMRAC), South Africa, COL 027.

Soundararajan R., Amyotte P.R., & Pegg M.J. 1996, "Explosibility hazard of iron suphide dusts as a funcion of particle size", *Journal of Hazardous Materials*, vol. 51, pp. 225-239.

Stanton-Hicks, E. and Newman, P. 2005, Sustainability in Western Australia - Case Studies: Argyle:"Creating a Future", Available at: <http://www.sustainability.dpc.wa.gov.au/CaseStudies/Argyle/Argyle.htm>, Access date: [20-12-2005].

Sturges, W. T., Harrison, R. M., & Barrie, L. A. 1989, "Semi-quantitative X-ray diffraction analysis of size fractionated atmospheric particles", *Atmospheric Environment*, vol. 23, no. 5, pp. 1083-1098.

Sutter, S. L., Johnston, J. W., & Mishima, J. 1982, "Investigation of accident - generated aerosols: releases from free fall spills", *American Industrial Hygiene Association Journal*, vol. 43, pp. 540-543.

Tangsathitkulchai, C. 2002, "Acceleration of particle breakage rates in wet batch ball milling", *Powder Technology*, vol. 124, pp. 67-75.

Tarmac Central, 1996. Geological map of Old Moor Quarry. (from personal communication).

Tarmac Central,2003. Chemical analysis results of limestone. (from personal communication).

Tervahattu, H., Kupiainen, K., Makela, T., Raisanen, M., Aurela, M., and Hillamo, R. 2005, The size distribution and composition of abrasion components in road dust, Available at: <www.ecotraffic.se/pdf/NP2003%20Kaarle%20Kupiainen,%20Envicon.pdf >, Access date: [22-6-2005].

The Council of the European Union 1999, "Council Directive 1999/30/EC of 22 April 1999 relating to limit values for sulphur dioxide, nitrogen dioxide and oxides of nitrogen, particulate matter and lead in ambient air", *Official Journal of the European Communitites*, vol. L 163, pp. 0041-0060.

The Council of the European Union 1996, "Council Directive 96/61/EC of 24 September 1996 concerning integrated pollution prevention and control", *Official Journal*, vol. L257, pp. 0026-0040.

Trade Union Congress 2001, *Hazards at work - TUC Guide to Health and Safety*, Trade Union Congress, U.K.

UK Environment Agency 2005, Environment Agency UK - Air quality, Available at: <http://www.environment-agency.gov.uk/subjects/airquality/?lang=_e>, Access date: [13-11-2005].

UK Environment Agency 2003, *Integrated Pollution Prevention and Control (IPPC) Technical guidance for non-ferrous metals and the production of carbon and graphite*, Environment Agency, UK, IPPC S2.03.

UK Environment Agency 2000, *Monitoring methods for ambient air. Technical Guidance Note M9*, Environment Agency, Bristol, U.K., M9.

Uranium Information Centre 1998, Mineral Sands, Available at: <http://www.uic.com.au/nip25.htm>, Access date: [6-6-2005].

US Department of Energy 2000, Mining industry of the future: Mineral processing technology roadmap, Available at: <http://www.eere.energy.gov/industry/mining/partnerships.html#roadmaps>, Access date: [1-5-2005].

US Department of Labour & Occupational Safety and Health Administration 1998, *Personal Protective Equipment*, OSHA, USA, 3077.

US EPA 2005a, Basic Concepts in Environmental Sciences, Available at: <http://www.epa.gov/eogapti1/module3/collect/collect.htm#gravitational>, Access date: [17-6-2005a].

US EPA 2005b, Compilation of Air Pollutant Emission Factors, AP-42, Available at: <http://www.epa.gov/ttn/chief/ap42/index.html>, Access date: [10-5-2005b].

US EPA 2005c, Factor Information REtrieval (FIRE), Available at: <http://www.epa.gov/ttn/chief/software/fire/index.html >, Access date: [13-5-2005c].

US EPA 2005d, Introduction to Emission Factors, Available at: <http://www.epa.gov/oar/oaqps/efactors.html>, Access date: [10-5-2005d].

US EPA 2003, Mining Industry Profile: Copper, Available at: <http://www.epa.gov/epaoswer/other/mining/techdocs/copper/copper1b.pdf>, Access date: [4-1-2006].

US EPA 1998a, *Guidance for using continuous monitoring in PM2.5 monitoring networks* , United States Environmental Protection Agency, USA, EPA-454/R-98-012.

US EPA 1998b, *Technical assessment paper: Available information for estimating air emissions from stone mining and quarrying operations*, US EPA, USA, Volume II: Chapter 13.

US EPA 1997, *National Ambient Air Quality Standards for Particulate Matter*, Environmental Protection Agency (EPA), USA, 40 CFR Part 50.

US EPA 1995, *Emission factor documentation for AP-42; Section 11.26; Talc Processing*, U.S. Environmental Protection Agency, U.S.A, EPA Contract 68-D2-0159; Work Assignment No. II-01; MRI project No. 4602-01.

US EPA Office of Compliance 1995a, *EPA Office of Compliance Sector Notebook Project. Profile of the Metal Mining Industry*, EPA, USA, EPA/310-R-95-011.

US EPA Office of Compliance 1995b, *EPA Office of Compliance Sector Notebook Project. Profile of the Non-Metal, Non-Fuel Mining Industry*, Environmental Protection Agency (EPA), USA, Sector Notebook Project.

Vaughan, N., Ogden, T. L., & Miller, B. 1989, "Filter weighing reproducibility and the gravimetric detection limit.", *Annals of Occupational Hygiene*, vol. 33, p. 331.

Wagner, G. R. 1996, *Screening and surveillance of workers exposed to mineral dust*, World Health Organisation, Geneva.

Washington C. 1992, *Particle size analysis in pharmaceutics and other industries - Theory and Practice* Ellis Horwood, New York.

Wild, P, 2000, A mortality study in the French talc producing industry, Available at: <www.ima-eu.org/en/wild.pdf>, Access date: [08-07-2005].

Wild, P., Leodolter, K., Refregier, M., Schmidt, H., Zidek, T., & Haidinger, G. 2002, "A cohort mortality and nested case-control study of French and Austrian talc workers", *Occupational and Environmental Medicine*, vol. 59, pp. 98-105.

Wilkinson, H. N., Reed, A. R., & Wright, U. K. 1989, "The cost to U.K. industry of dust, mess and spillage in bulk materials handling plant", *Bulk solids handling*, vol. 9, no. 1, pp. 93-97.

World Health Organization 1999, *Hazard Prevention and Control in the Work Environment: Airborne Dust*, World Health Organization, Switzerland, WHO/SDE/OEH/99.14.

Xu, R. & Di Guida, O. A. 2003, "Comparison of sizing small particles using different technologies", *Powder Technology*, vol. 132, pp. 145-153.